National Library
of Canada

Acquisitions and
Bibliographic Services Branch

395 Wellington Street
Ottawa, Ontario
K1A 0N4

Bibliothèque nationale
du Canada

Direction des acquisitions et
des services bibliographiques

395, rue Wellington
Ottawa (Ontario)
K1A 0N4

Your file Votre référence

Our file Notre référence

NOTICE

The quality of this microform is heavily dependent upon the quality of the original thesis submitted for microfilming. Every effort has been made to ensure the highest quality of reproduction possible.

If pages are missing, contact the university which granted the degree.

Some pages may have indistinct print especially if the original pages were typed with a poor typewriter ribbon or if the university sent us an inferior photocopy.

AVIS

La qualité de cette microforme dépend grandement de la qualité de la thèse soumise au microfilmage. Nous avons tout fait pour assurer une qualité supérieure de reproduction.

S'il manque des pages, veuillez communiquer avec l'université qui a conféré le grade.

La qualité d'impression de certaines pages peut laisser à désirer, surtout si les pages originales ont été dactylographiées à l'aide d'un ruban usé ou si l'université nous a fait parvenir une photocopie de qualité inférieure.

Canada

Impingement and Through Air Drying of Paper

by

Guohua Chen

A thesis submitted to the
Faculty of Graduate Studies and Research
in partial fulfillment of the
requirements for the degree of
Doctor of Philosophy

Department of Chemical Engineering
McGill University
Montreal, Canada

August 1994

ISBN 0-612-00087-7

Abstract

Air drying of paper by pure impingement, pure through flow and by combination of impingement and through flow was studied. For the combined process the inlet and both outlet air flow rates were held constant throughout drying, thereby providing results appropriate for analysis of the complex and interacting kinetics.

Pure impingement drying rate curves were quantified with three parameters which were related to drying process conditions: constant drying rate, critical moisture content and the exponent for a power law relationship over the falling rate period. The Churchill - Usagi asymptotic approach model was tested and found not applicable.

For pure through drying the constant drying rate period disappears at higher drying intensities leaving two drying rate periods, the increasing rate and falling rate periods. A theoretically based exponential relationship was obtained for the increasing rate period, where up to 47% of the drying may occur. Drying rate curves were quantified with no subjective judgements, using five parameters: moisture contents at the end of the increasing rate and constant rate periods, constant drying rate, and exponents for the increasing and falling rate period relations. A universal normalized drying rate curve was obtained. Through drying rates are the same with or without impinging jets.

In combined impingement and through air drying, an adiabatic process, removal of impingement boundary layer humidity by through flow makes both components of the process nonadiabatic. Relative to pure impingement drying, impingement water removal rates are sensitively reduced by through flow. Because critical moisture content is intrinsically lower for through drying than impingement drying, through flow water removal rate curves can be strikingly different from pure through drying, with addition of a unique feature, a secondary increasing rate period when paper temperature is driven up by the falling rate period of impingement water removal. Parameters for quantitative representation were determined, analyzed and related to drying process conditions.

Of two prior models for the combined impingement and through air drying of paper, trends assumed by Randall (1984) are now found contrary to actual rates while the Crotogino and Allenger (1979) model has the trends correct but over predicts the drying rates now measured. Results of the pilot plant work of Burgess et al. (1972) are consistent with the comprehensive model now developed to predict drying time and drying rate for combined impingement and through flow air drying of paper.

Résumé

Nous avons étudié le séchage à l'air du papier uniquement par jets, uniquement par air traversant de même que par le procédé combinant les jets et l'air traversant. Pour le procédé combiné, la conception du montage expérimental permettait de maintenir constants le débit d'entrée et les deux débits de sortie, donnant ainsi une mesure appropriée pour l'analyse cinétique de ces phénomènes complexes et en interaction.

Les courbes de séchage uniquement par jets sont quantifiées par trois paramètres: le taux de séchage constant, la teneur en eau critique et l'exposant d'une relation de puissance dans la période à taux décroissant, lesquels paramètres furent rapportés aux conditions du procédé. Le modèle d'approche asymptotique de Churchill et Usagi fut essayé et trouvé inapplicable à la présente situation.

Pour le séchage uniquement par air traversant, la période à taux constant n'est pas observée aux intensités de séchage les plus élevées, cédant la place à deux périodes de séchage, la premiere à taux croissant, la seconde à taux décroissant. Une relation exponentielle basée sur une analyse théorique fut obtenue pour la période à taux croissant, qui constitue jusqu'à 47% du séchage. Les courbes de séchage furent quantifiées sans jugement subjectif, en utilisant cinq paramètres: la teneur en eau à la fin des périodes à taux croissant et à taux constant, le taux de séchage constant, et les exposants pour les périodes à taux croissant et décroissant. Une courbe de séchage normalisée universelle fut obtenue. Les taux de séchage par air traversant sont identiques avec ou sans l'apport de jets.

Pour le procédé combinant les jets et l'air traversant, un phénomène adiabatique, l'enlèvement de l'humidité dans la couche limite par l'effet de l'air traversant, rend les deux composantes du procédé non-adiabatiques. Par comparaison au séchage uniquement par jets, les taux d'enlèvement d'eau par les jets sont réduits par l'air traversant, de facon très sensible. Comme la teneur en eau critique est intrinsèquement plus basse pour le séchage par air traversant que pour le séchage par jets, les courbes de taux d'enlèvement d'eau peuvent être complètement différentes de celles pour le séchage uniquement par air traversant. Ces courbes comportent une caractéristique unique, une période à taux croissant secondaire, dans laquelle la température du papier augmente à cause de la diminution du taux d'enlèvement de l'eau par les jets. Nous avons determiné, analysé et rapporté aux conditions du procédé les paramètres représentatifs.

Des deux modèles existants sur le séchage combiné par jets et par air traversant, celui de Randall (1984) prédit des tendances contraires à l'observation, alors que celui de Crotogino et Allenger (1979) prédit correctement les tendances observées mais avec des taux de séchage plus élevés que la réalité. Les résultats en usine pilote de Burgess *et al.* (1972) s'accordent avec le modèle compréhensif développé pour prédire le temps et le taux de séchage dans le séchage à l'air du papier par le procédé combinant jets et l'air traversant .

Acknowledgments

The author would like to express his sincere gratitude to the many colleagues and friends who helped him during the course of this thesis.

Thanks must first go to supervisor Prof. W. J. M. Douglas, whose intelligent guidance, detailed training and financial support are deeply appreciated; to Dr. R.H. Crotogino for his constructive advice in the development and use of the experimental equipment, to Drs. J.F. Bond and V. G. Gomes of the research committee for their many help and useful comments during data processing and thesis preparation; to Prof. Weber for consults on various aspects of statistical analysis; to Prof. A.R.P. van Heiningen for his interest in the project and valuable comments in results analysis.

The author would like to take this opportunity to thank Prof. A. S. Mujumdar and Ms. P. Mujumdar for their encouragement and help.

Construction of the apparatus required an unusual range of skills, which were provided by the versatile staff of the machine shops in the Pulp and Paper Research Institute of Canada and the Chemical Engineering Department of McGill University. Thanks to Mr. Jean-Claude Béchet, workshop director of Paprican, who built the major parts of the apparatus and to Mr. A. Krish, workshop superintendent, Mr. L. Cusmich, electronic technician, and machinists Mr. Walter Greenland, Mr. Allan Gagnon and Mr. Charles Dolan of McGill for numerous assistance in the commissioning and use of the apparatus. Thanks also to Mr. Jean Dumont for his cheerful attitude and efficiency in procuring supplies. The help of research assistant Ms. Xiaoxing Wu in literature survey and handsheet preparation is gratefully acknowledged.

The financial support of Paprican fellowships (1987-1990) is also appreciated.

A special word of thanks to many friends and colleagues, especially Mr. Tom Browne, Mr. Ruonan Li, Mr. S.J. Hashemi, Ms. Lijie Wang, Mr. Biao Wang, Dr. J. M. McCall and Dr. M. Berksoy for the many discussions and a friendly working environment.

Special salute goes to the author's parents, Mrs. G. Pan and Mr. H. Chen, first mentor of the author, for their love and encouragement.

Finally, the author would like to thank his wife Yan Hu for her understanding and continuous moral support throughout the project.

Table of Contents

List of figures

List of Tables

Nomenclature

a	slope of CUE asymptote for $X \rightarrow 0$
a_f	correlation coefficient for through drying falling rate data
a_p	interfacial area for heat and mass transfer, m^{-1}
B	paper basis weight, g/m^2
B_w	wet portion of paper below drying front
C	parameter for R_T-X relation in post constant rate periods
C_g	nozzle geometry factor
C_i	Mu_s/St_i
C_{Ri}	coefficient in drying time calculation for increasing rate period
C_{Xi}	coefficient in correlation of increasing rate period extent for CITAD
d	nozzle i.d., mm
D	liquid diffusivity, m^2/s
f	nozzle plate open area ratio, fraction
G	air mass flow rate, kg/m^2s
G_I	for impingement exhaust
G_T	for through flow exhaust
h	convection heat transfer coefficient
H	nozzle exit to paper spacing, mm
I_s	surface drying intensity by Suzuki
I_c	impingement exhaust cross flow interference parameter
K	geometry factor for Martin's correlation
L	paper thickness, m
L_c	maximum distance traveled by impingement spent flow
Mu_s	$\rho_s u_s/\rho_j u_j$
n	exponent of power law R-X relation for impingement falling rate drying
n_i	exponent of R-X relation for through drying over increasing rate period
n_f	exponent of R-X relation for through drying over falling rate period
n_I	exponent for power law R_I-X relationship for falling rate period
n_{Ti}	exponent for R_T-X relation over increasing rate period
N	number of nozzles
P_T	water vapor pressure for through flow air, kPa
P_v	water vapor pressure of paper, kPa
P_v'	water vapor pressure at T_p, kPa
P_v^{as}	water vapor pressure at T_{as}, kPa

ΔP	pressure drop across paper sheet, kPa
q_T	through flow ratio, G_T/G
r	capillary radius, m
r_p	fraction of vapor pressure in the falling rate period
R	drying rate, kg/m^2h
R_c	constant drying rate
R_{cI}	for pure impingement drying
R_{cI}'	value calculated based on the total G for CITAD
R_{cM}	R_c by Martin's correlation
R_{cT}	for pure through drying
R_{cT}'	value calculated based on the total G for CITAD
R_{as}	exhaust saturated at T_{as}
R_I	water removal rate by impingement exhaust, kg/m^2h
R_{Ic}	constant water removal rate
R_{max}	maximum R for through drying
R_T	water removal rate by through flow exhaust, kg/m^2h
R_{Tc}	constant water removal rate
R_{Tm}	maximum value in nonadiabatic drying period
R_{Tas}	exhaust saturated at T_{as}
R	gas constant, 8.314 J/mol K
t	drying time, s
$t_{0.05}$	to X=0.05 kg/kg
T	temperature, °C
T_{as}	at adiabatic saturation
T_e	at exhaust
T_{Ie}	impingement
T_{Te}	through flow
T_j	at nozzle exit
T_p	at paper
T_s	at impingement surface
ΔT	T_j-T_{as}, °C
u	water velocity in capillary, m/s
u_j	jet velocity, m/s
u_s	through flow velocity, m/s
U_j	jet velocity at standard conditions, m^3/m^2s
w	nozzle width, mm

X	moisture content, kg water/kg fibre
X_c	critical moisture content
X_e	equilibrium moisture content
X_i	at end of increasing rate period
X_m	at maximum value of through flow water removal rate, R_{Tm}
X_{Ti}	at end of increasing rate period for through flow water removal
X_o	initial moisture content
X_o^{ic}	with $X_i=X_c$ or $X_{Ti}=X_c$
X_o^{mc}	with $X_m=X_c$
$X(\theta,z)$	moisture content, difference between local and equilibrium values, kg/kg
ΔX	X_c-X_m
$y_o(x)$	asymptote for $x\rightarrow 0$ in Churchill Usagi Equation
$y_\infty(x)$	asymptote for $x\rightarrow \infty$ in Churchill Usagi Equation
z	thickness dimension of sheet, m
α	correlation coefficient
κ	air thermal conductivity, W/Km
λ	latent heat of water, kJ/kg
λ_a	heat of desorption, kJ/kg
θ	drying time measured from the end of constant rate period, s
ρ	density, kg/m^3
σ	standard deviation
Bi	Biot number
Nu	Nusselt number
$\overline{Nu}$	averaged value
Nu_{Ic}	with cross flow interference
Pr	Prandlt number
Re	jet Reynolds number
St	Stanton number
St_i	for impermeable surface
St_p	for permeable surface
ΔSt	$St_p - St_i$, enhancement of St by through flow

Chapter 1 Introduction

1.1 History of papermaking

Papermaking was invented in ancient China and developed in the year 105 AD by Cai Lun of the East Han Dynasty. From that time until the end of the eighteenth century, all paper throughout the world was made one sheet at a time (Clapperton 1967). Rags were washed, beaten and cooked to produce pulp. The papermaking master dipped his mould into the vat of pulp and drew out the fibres from the suspension, allowing the water to drain away through the mesh of the mould, leaving a wet sheet of pulp. This product was dried under the sun, then stacked for use. An improvement found for drying paper was to attach it to the surface of an internally heated brick wall.

The secret of papermaking was learned by the Arabs in 704 and introduced to Europe in 1189 through France, where six centuries later it was modernized. Thus by producing the required machine, Nicolas Louis Robert in 1799 first put into practice the idea of making paper mechanically in long lengths. The real boom of producing paper continuously came after another French invention, the mechanically perfected machine patented in 1804 by the Fourdrinier brothers based on Robert's invention (Butler 1901).

The early machines made by the Fourdrinier brothers consisted of a flowbox which supplied the pulp stock to a moving wire supported between two rolls. The wet web was pressed and accumulated for subsequent drying in sheet form. Since the time of Louis Robert, the Fourdrinier machine has undergone continual change. Figure 1.1 shows a Fourdrinier paper machine integrated into a current paper mill consisting of four major sections: formation, pressing, drying, calendering and reeling. In the formation section, a uniform fibre-water suspension of 0.2-1.0% fibres is supplied from a headbox. This suspension is deposited on a continuously moving mesh where a wet sheet of pulp forms after drainage first by gravity, then by compression under rolls, typically aided finally by vacuum from below. More recently, twin wire formers have been replacing the single wire Fourdrinier design.

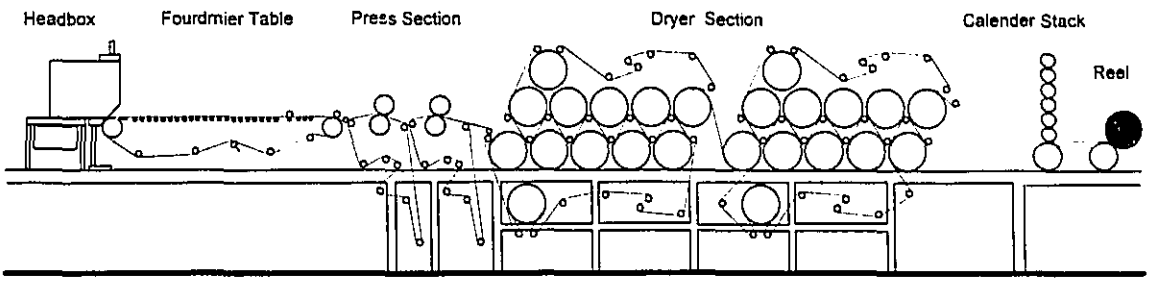

Figure 1.1 Fourdrinier paper machine

This wet web is mostly water, with about 18-23% fibres. About 20% of the water is removed in the next section by the press rolls, from which the paper leaves at about 33-55% fibres. Water is removed in the dryer section to obtain the final product at a moisture content of 6-9%. For most of the world's paper today, drying is achieved by contact heat transfer to the wet sheet from the surface of a series of cylinders (usually 1.5 to 1.8 m diameter) heated internally by condensing steam. The evaporated moisture is carried away by ventilation air. Depending on the grade of paper produced, the efficiency of the dryers and the speed of the paper machine, there are typically more than 40 such cylinder dryers, making the dryer section with its air circulation system a process of impressive size. In the calendering section, the dried paper passes between heavy calender rolls for surface property improvement before it is reeled for shipping.

1.2 Drying paper

In modern paper industry, "the trend toward higher machine speeds, wider machines, and lower grammages has brought about a critical evaluation of the conventional means of drying paper. Not only the water removal capacity of the dryer section, but also the safe passage of the web through the dryer section is growing in significance as a factor limiting the production capacity of high speed paper machines" (Crotogino 1975). In addition, drying consumes almost 75% of the total energy in paper production. In Canada, about $600 million are spent annually on the drying of newsprint alone (Mujumdar 1992). Therefore even a modest improvement in drying technology has

the potential to enable substantial savings in drying cost. Listed in Table 1.1 is the distribution of dryers from McConnell (1980). The drying rate values are from Cui and Mujumdar (1984).

Table 1.1 U.S. Industry Paper Dryer Distribution

	Paper Industry Drying Application					Total	Drying Rate
	Pulp	Tissue	Paper	Board	Coating	%	kg/m²h
	Water removed, %						
	7	6	34	51	2	100	
	Dryer Distribution, %						
Cylinder Dryer	-	15	95	95	35	82.3	10-20
Impingement Dryer	70	-	2	2	50	7.6	100
Yankee Dryer	-	70	-	-	-	4.2	200
Infrared Dryer	-	-	3	3	15	2.8	-
Through Dryer	-	15	-	-	-	0.9	20-140
Flash Dryer	15	-	-	-	-	1.1	-
Vacuum Dryer	15	-	-	-	-	1.1	-

As conventional cylinder drying is restricted to low drying rates by the inherent limitation of low rates of heat transfer from a hot surface to the wet sheet the most promising replacement is some form of air convection drying, with which an order of magnitude higher drying rate can be obtained. Other attractive features of air convection drying are the ease of control provided in the cross machine (CD) direction and relatively low capital cost.

In the tissue industry air convection drying is already the standard, as the Yankee dryer and the through dryer. A Yankee dryer consists of a large diameter (5.5 to 7 m) steam heated cylinder supporting the wet sheet which is dried by a combination of two mechanisms - by contact heat transfer as in cylinder drying, and by convection heat transfer from impinging jets of hot drying air discharging from the nozzle plates of an air hood. The wet sheet is pressed tightly against the highly polished hot surface of the cylinder so that good heat transfer rates are achieved. The impinging jets discharge at nozzle exit velocities around 150 m/s and at nozzle exit temperatures in the range 300-

500 °C (Corboy Jr. 1991). Figure 1.2 (a) shows a schematic diagram of a Yankee dryer employed in a tissue machine.

The through dryer was developed for tissue production not only because of its high drying rate but also because tissue paper of high bulk may thereby be produced. In through drying, figure 1.2 (b), dry air is either pressured or sucked through the permeable wet sheet, producing a much softer product than that produced by a Yankee dryer where the sheet is pressed against a cylinder. In the highly competitive soft tissue segment of the paper industry, a bulkier, lighter product containing less fiber provides an economic advantage (Smook 1986).

Based on pilot plant experiments Burgess and Chapman (1968) patented a convection dryer, which they termed a "Papridryer" , combining the air impingement and air through drying techniques. In this kind of dryer, figure 1.2 (c), part of the high temperature air discharging from nozzles in the hood is withdrawn as an impingement exhaust, as in an impingement dryer, while the remaining part is sucked through the porous wet sheet by applying vacuum inside the cylinder, as in a through dryer. In this process of Combined Impingement and Through Air Drying, referred to here as CITAD for its generic name, part of the water near the impingement surface is evaporated and carried away by the impingement air flow so that, in contrast to through drying, this moisture is transported through only a small part of the sheet. Furthermore, moisture evaporated from the center to the through flow exit side of the sheet need not diffuse to the impingement surface side but can be carried away by the air through flow.

Despite these advantages of the combined impingement and through air dryer, CITAD, and the brief mill demonstration made about 25 years ago, this process did not achieve commercial success. While the reasons for this lack of industrial adoption are complex, the intrinsic advantages of the CITAD technique are such that there remains the possibility of an improved design achieving industrial acceptance in the future. Design improvements may come from a basic understanding of this process, including how the impingement flow affects the through drying, how the through flow affects the efficiency of impingement drying, how the impingement heat transfer interacts with mass transfer

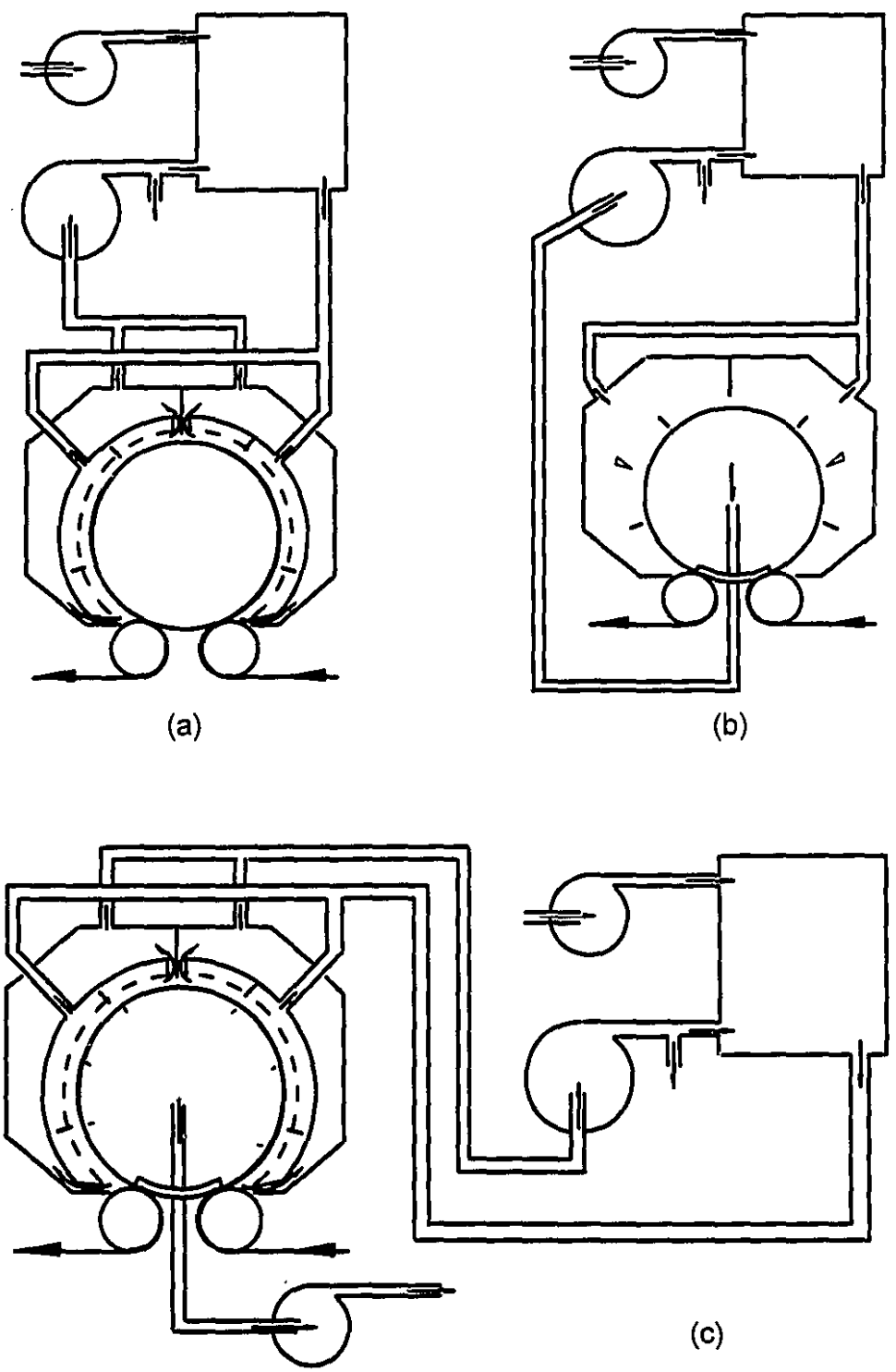

Figure 1.2 Air convection dryers for paper
(a) Yankee dryer (air impingement and surface contact drying)
(b) Through dryer (air through drying)
(c) Combined air impingement - air through dryer

phenomena, what levels of through flow are best at the various levels of paper moisture content from wet to dry, and how to design the nozzle plates for optimum results. The optimum design of such a complex system for industrial use requires an understanding of the fundamental principles, which is the basic motivation of the present investigation.

1.3 Objectives of the present study

The objective of this thesis is to make the first fundamental study of the process of combined impingement and through air drying of paper, including determination of the interaction between these two processes of air convection drying of paper when they occur in combination. The stages towards achievement of this objective are as follows:

(1) Design and construction of a unique experimental facility which enables measurement of the performance characteristics of air impingement drying and air through drying, alone and in combination, under conditions with the key parameters of each process controlled and measured.

(2) Determination of the characteristics of air impingement drying of paper.

(3) Determination of the characteristics of air through drying of paper under impinging jets.

(4) Determination of the characteristics of air convection drying of paper for a combination of air impingement and air through drying, with the proportion of drying varied between the limits of pure impingement and pure through drying.

Chapter 2 Literature Review

2.1 Impingement drying of paper

This review does not treat the much larger topics of impingement flow, heat and mass transfer phenomena as these are available through general reviews such as Gauntner et al. (1970), Mujumdar and Douglas (1972), Martin (1977), Obot (1981), van Heiningen (1982), Polat S. (1993).

As air convective drying by impinging jets takes advantage of very high heat and mass transfer rates it is extensively used to obtain rapid drying in relatively small equipment. Impinging jets find wide application in drying materials in the form of continuous sheets (e.g. tissue paper, photographic film, coated paper, nonwovens, and textiles) or relatively large, thin shapes (e.g. wood veneer, lumber and carpets) or even conveyed beds of granular material (e.g. cat and dog food) (Mujumdar 1987).

Impinging jets are applied in the paper industry for the drying of tissue and toweling by Yankee dryers. This technique consists a large cylinder heated internally by steam, with an impingement air hood for arrays of high velocity air jets impinging on the surface of the wet web. In modern Yankee dryers where air at about 500 °C issues from round nozzle arrays at jet velocities of 150 m/s, the distribution of drying is about 30% by contact heat transfer from the Yankee cylinder heated by steam condensing at about 1 MPa, and about 70% by air impingement heat transfer (Sorrells 1991, Spraker et al. 1969). Thus current Yankee dryer performance is dominated by the air impingement drying component.

In contrast to the extensive studies of impinging jet heat and mass transfer rates, the literature on impingement drying of paper is limited. The few available papers concern mostly dryer performance and deal with energy or engineering aspects, not the fundamentals of impingement drying of paper. This shortage of investigations on the

impingement drying of paper may derive from a perception that for a thin web of fibres, impingement drying is totally externally controlled by the impingement heat transfer rate.

Daane and Han (1961) analyzed the performance of impinging jets using an index of performance for a specific fan power. Based on experimental data of heat transfer they found the index of performance reached a maximum when the fraction of area for the jet nozzles was about 1.5-3% of the area of the nozzle plate or impingement surface. This area ratio is commonly called the "open area ratio" of nozzle plates.

Using an array of round nozzles Allender (1961) studied the impingement drying of paper within the constant drying rate period (up to 70% - 80% solids content). For constant rate period drying, conditions within the sheet are not involved and the findings are simply those of impingement heat and mass transfer.

In his series of publications on paper drying Cirrito (1963, 1964a,b,c) gave a brief analysis of impingement drying in combination with hot surface conduction from internally heated cylinders. Thermal efficiency was found to increase directly with drying air humidity. Recognizing the importance of the falling rate period he suggested increasing the sheet temperature by either increasing the steam pressure inside dryer cans, increasing the air temperature at the impingement side or by adding radiant energy during the falling rate period. He noted that the moisture content at the transition from constant rate to falling rate drying, conventionally called "critical moisture content", is not a paper property but is also affected by drying conditions.

Chance (1974) studied the heat transfer of impinging jets for application in the paper industry, investigating effects of nozzle exit to impingement surface spacing H/d, nozzle open area ratio f, jet pattern and temperature. Heat transfer degradation due to cross-flow resulting from the interference of spent flow on jet flows was successfully correlated with a cross-flow interference parameter proposed, I_c , by Kercher and Tabakoff (1970) as

$$\frac{Nu_{Ic}}{Nu} = 1 - 0.236 I_c \qquad (2.1)$$

for $2 \le H/d \le 8$; $0.012 \le f \le 0.07$; $I_c \le 1.8$; with $I_c = f L_c / d$, where f is the nozzle open area ratio, d the nozzle diameter and L_c the maximum distance traveled by spent flow.

Martin (1977) published an extensive review of the impingement heat transfer research. A general correlation, equation 2.2, was found to predict within ±15% the impingement heat transfer coefficients for a variety of arrays of round nozzles.

$$Nu = K\frac{\sqrt{f}\left(1-2.2\sqrt{f}\right)}{1+0.2\left(H/d-6\right)\sqrt{f}}Re^{2/3}Pr^{0.42} \qquad (2.2)$$

$$\text{with} \qquad K=\left[1+\left(\frac{H/d}{0.6/\sqrt{f}}\right)^{6}\right]^{-0.05}$$

for $2000 \le Re \le 100{,}000$; $0.004 \le f \le 0.04$; $2 \le H/d \le 12$

Wedel (1980) compared slot and round jets for paper drying. Round jets were found to perform better than the slot jets at equal fan power and air flow rate.

Extensive research on impingement drying of paper using superheated steam as the drying medium began in 1984 at McGill University. Cui and Mujumdar (1984) presented a model for a combined impingement and conduction superheated steam dryer. Cui et al. (1985) made preliminary measurements in the constant drying rate period for a superheated steam impingement dryer. Drying rate was found to increase nearly linearly with jet temperature and velocity. The sheet temperature was measured to be that of saturated steam.

Bond (1991) carried out the most comprehensive investigation of impingement drying of paper in both air and superheated steam (Bond et al. 1991, 1992, 1994a,b). The drying rate was analyzed as a constant rate period followed by a falling rate period for which the drying rate was treated as a linear function of paper moisture content. For the constant drying rate period they found that the correlation of Martin (1977) applied. The critical moisture content for both air and superheated steam was found to increase with the constant drying rate.

In a recent patent disclosure Pikulik (1992) reported his findings for drying newsprint by combined hot surface contact and air impingement drying. With his technique the wet web is pressed onto the surface of at least two large diameter cylinders heated to about 120 °C, which provide about half of the drying heat. The other half of the

energy is supplied by convection from the hot jets impinging on the sheet from a hood surrounding the cylinder as in a Yankee dryer. Pikulik claimed a higher drying rate and better paper properties. The nature of his pilot plant study does not provide any drying kinetics.

Thus although impinging air jets are widely used for drying paper, precise documentation is lacking of the critical moisture content and, especially, of the falling rate period of drying which controls dryer size, including the important effect of paper basis weight on impingement drying rate.

2.2 Through drying of paper

As an extensive review on air through drying of paper, the second process of convection drying, was given by Polat O. et al. (1992b), including discussion of the porous structure of paper, flow through porous media and heat and mass transfer in porous media, these aspects are not repeated here. Very high rates can be achieved in through drying paper due to the large area for heat and mass transfer between the air and the paper web when air passes through the sheet. Water vapor must diffuse only on the scale of fibre thickness as compared to sheet thickness in the case of hot surface contact drying or impingement drying. Table 2.1, adapted from Polat O. et al. (1992b), summarizes the studies on through drying of paper.

In their laboratory study Chu and Kuo (1967) constructed a capacitance meter to measure moisture content. As documented subsequently by Bond (1991), this technique has limited accuracy due to the complex relationship of capacitance with moisture content, temperature and geometrical variables. Because of the large through flow rate used, mechanical dewatering occurred at moisture contents as low as 25%. As the experimental technique allowed large changes in through flow rate during drying, quantitative interpretation of their results is not possible.

Walser and Swenson (1968) conducted through drying experiments in the laboratory and a paper mill. A back scatter beta-ray gauge was used to measure the paper

moisture content in their laboratory experimental study, for which a basis weight of 86 g/m^2 was obtained with two plies of 43 g/m^2 . They reported that the air exited from the sheet at the adiabatic saturation condition. Again, because the through flow rate was not controlled during an experiment as much as 100% change in through flow rate occurred during a drying experiment. In their mill trials with intermittent sample collection, a basis weight effect was not detected even though the sheets ranged from 52 - 147 g/m^2.

Table 2.1	Range of parameters in through drying of paper				
Author	Sheet*	B	T	G	X_o
		g/m^2	°C	kg/m^{2}s	kg/kg
Chu and Kuo (1967)	HS	Tissue	21-82	0.8-3.3	1.8
Walser and Swenson (1968)	HS, PM	52-150	60-260	0.05-0.25	2.0
Martin (1972)	HS	100	<250	0.8-6.0	-
Raj and Emmons (1975)	HS	13-64	20, 80	0.3-1.65	3
Rohrer and Gardiner (1976)	PM	16-19	150-350	1.2-3.2	-
Wedel and Chance (1977)	HS, PM	25-50	200	2	2.0
Gummel and Schlünder (1980)	HS	20-23	22-95	0.07-1.8	5-10
Polat O. et al. (1992b)	HS	25-150	20-95	0.09-0.55	1-5
Industrial application	PM	15-40	100-400	0.07-4	2-3

* HS= handsheets, PM= papermachine formed sheets

Martin (1972) measured through drying rates by applying vacuum across a 100 g/m^2 handsheet. As the through flow rate changed three to four fold during each experiment and the drying rate measured was only the overall average value, such results provide no information concerning the drying kinetics.

Raj and Emmons (1975) through dried paper of basis weight 13 - 65 g/m^2 , of porosity as high as 0.86 - 0.89 in ambient temperature air. The accuracy of their measurements, i.e. monitoring the total weight of the sample holder and the sample, was limited by their signal-to-noise ratio of 0.1.

Rohrer and Gardiner (1976) calculated the rate of through drying of paper by modeling the process as one of turbulent flow through ducts. They claimed good agreement between their model prediction and measurements for a mill trial conducted

with highly permeable paper. Shortcomings of this work were pointed out by Polat O. et al. (1992b).

Wedel and Chance (1977) analyzed through flow of air as an external flow over a cylinder. Polat O. et al. (1992b) noted that this model is even further from the reality of the complex structure of air flow through pores in sheet. Wedel and Chance claimed that their calculations agreed well with their experimental measurement, which they did not document. Moreover, they reported that for their experimental conditions the flow exited as saturated air, a condition which makes it impossible to test any drying rate model.

The through drying work of Gummel (1977) and Gummel and Schlünder (1980) was carried out with an infrared analyzer as the air humidity detector, from which complete drying rate curves could be obtained. For their basis weight of paper, 20 and 23 g/m^2, the air exiting the sheet was far from the adiabatic saturation condition, in contrast to the reports of prior researchers. By normalizing the drying rate with respect to the maximum value and moisture content as $(X - X_e) / (X_c - X_e)$, all of their falling rate period drying data collapsed to one curve. An analysis of their data by Polat O. (1989) indicated that leakage at the sample holder probably occurred for all their drying experiments, so their reported values are probably lower than the actual drying rates.

With an improved through dryer design and better instrumentation, Polat O. et al. (1987) carried out a systematic study of through drying with the air mass flow rate held constant during the entire drying. An infrared analyzer was used to monitor the air humidity exiting the sheet, thereby providing the instantaneous value of paper moisture content to associate with the instantaneous drying rate. A relationship between constant drying rate and the process variables (temperature, flow rate, paper basis weight) was obtained. Three distinctive drying rate periods were observed, i.e. an important increasing rate period as well as the constant rate and falling rate periods. It was found that for the highest drying intensity conditions, G=0.55 kg/m^2s, T=88 °C, there was no appreciable constant drying rate period for 25 g/m^2 paper when paper initial moisture content was less than 3 kg water/kg fibre. For these conditions about half of the water was removed during the increasing rate period, half during the falling rate period. A model was constructed in which the controlling factors during the increasing rate and the falling rate periods,

respectively, were the development of transport area and the increase of heat of desorption based on the data of Prahl (1968). The transfer coefficients obtained from the constant drying rate period were applied to the increasing and falling rate periods using the characteristic dimension, d_p , derived from the pressure drop measurements and momentum transfer equation.

This investigation also showed that there is a potential for improvement of through drying even at G=0.55 kg/m^{2}s and T=90 °C, because the air exits a 25 g/m^2 paper sheet at only 50% of saturation, far from the maximum possible through drying rate. In the industrial practice of through air drying of paper as well as with all laboratory through drying studies reported to date, the approach flow of air to the wet sheet has a relatively uniform velocity profile. One possible way of improving the efficiency of through drying would be to have the air approach flow be highly turbulent so that the air would enter the sheet at a higher humidity because of the higher convective heat and mass transfer coefficients at the sheet surface. One way of generating a highly turbulent inlet flow is to provide the approach flow as impinging jets. No investigation of through drying with an impingement approach flow has been reported. Thus the extent to which the rate of through drying of paper may be enhanced by providing the approach flow as impinging jets remains to be determined.

2.3 Enhancement of impingement heat transfer by through flow

For the ideal case of flow of a frictionless fluid of uniform velocity and temperature over a permeable surface of uniform temperature the enhancement of convective heat transfer, represented as the Stanton number, St, due to a uniform through flow is $\Delta St=Mu_s$ where Mu_s is the ratio of through mass flow rate to the mass flow rate at the nozzle exit. In a boundary layer flow, however, the enhancement of heat transfer, ΔSt, is proportional to rather than equal to Mu_s (Polat S. et al. 1991a,b).

Saad (1981) and Saad et al. (1992) studied the effect of through flow on impingement heat transfer with slot jets at H/w=8 and Re values of 10200, 22800 and 29100 for through flow velocities ranging from 0 to 0.3 m/s at a stationary impingement surface. A uniform increase in local heat transfer was observed across the entire impingement surface, i.e. from the jet centerline to the wall jet region. The percentage of enhancement, therefore, varies proportional to the profile of local heat transfer from impinging jet, for example from about 26% to 50% increases at positions 3 and 12 of nozzle widths from stagnation for the case of a through flow velocity of 0.1 m/s (u_s/u_j=0.0074) at Re=10200.

Obot (1982) studied the effect of through flow on average heat transfer coefficients from single confined and unconfined round impinging jets for through flow velocity in the range 0.3% to 0.7% of the nozzle exit velocity. Two values of Re, about 28000 and 51000, were studied with values of the nozzle spacing H/d in the range 2-10. A linear increase in local heat transfer coefficient with through flow rate was observed.

Mickley et al. (1954) and Spalding (1960) independently derived the following relationship for the ratio of local convective heat transfer at a permeable surface with through flow, relative to that at an impermeable surface.

$$\frac{St_p}{St_i} = \frac{-C_i}{e^{-C_i} - 1} \qquad \text{where } C_i = \frac{Mu_s}{St_i} \tag{2.3}$$

At very low throughflow rates, Mu_s<0.01, Moffat and Keys (1968) found agreement between equation 2.3 and their experimental data. With higher through flow their measured Stanton number was, however, always lower than the prediction of equation 2.3. For turbulent impinging jets, equation 2.3 also predicts much greater effect of through flow on heat transfer than that measured by Baines and Keffer (1979), Saad (1981), Saad et al. (1992) and Polat S. et al. (1991a).

The effect of through flow on heat transfer for jets impinging on stationary and high speed impingement surfaces was determined for multiple slot jets by Polat S. and Douglas (1990) and for single slot jet by Polat S. et al. (1991a). Including the results of Saad (1981) for multiple slot jets on a stationary impingement surface, they found the value of the ratio $\Delta St/Mu_s$ for all these cases to be 0.16 - 0.18.

2.4 Combined impingement and through air drying

Burgess et al. (1972a) provided unique results from a pilot plant test of a technique designated by their trade name, "Papridryer", referred to here by the acronym CITAD for the generic name of the process, Combined Impingement and Through Air Drying. The sheet was in contact with a rotating perforated roll covered by a permeable fine wire fabric as the sheet support. Jets of hot air at velocity up to about 100m/s was delivered from an array of slot nozzles in an impingement hood. Air through flow was achieved by applying vacuum inside the roll. For newsprint experiments, never dried sheets from repulped newsprint formed on a laboratory twin-wire former were used. For tests with corrugating medium, never-dried machine formed sheets were obtained from paper mills. Wet pressed paper was fed continuously to the dryer. Sheets moisture contents entering and exiting the dryer were measured with beta-gauge meters.

Subsequent to their pilot plant study a mill trial was carried out at the Trois Rivières, Quebec newsprint mill of the Canadian International Paper Company to evaluate directly in a paper machine the effects of the operating variables, Burgess et al. (1972b). Two cylinder dryers, #34 and #35, out of the 46-cylinder dryer section were replaced by a 1.52 m diameter dryer employing the combined impingement and through air drying technique. The geometric parameters of pilot Papridryer and mill trials are listed in Table 2.2.

Table 2.2 Geometric parameters of pilot plant and mill trial dryers of Burgess et al.

	Pilot plant	Mill trial
Vacuum roll diameter, m	0.38	1.52
Roll width, m	0.406	4.06
Wrap of hood, °	300	270
Total dryer length, m	1.06	3.59
Nozzle opening, mm	0.52	1.3
Nozzle-web spacing, mm	8.4	13-19
Inter-nozzle spacing, mm	38	76
Nozzle open area in hood, %	1.4	1.7

For the pilot plant investigation, two series of tests were performed to determine the influence of operating variables on the drying rate with newsprint, one at fixed jet velocity, the other at fixed initial moisture content of the paper as listed in Table 2.3.

Table 2.3 Experimental conditions for pilot plant test with newsprint

	Series I Jet velocity 96.5 m/s	Series II Paper initial moisture content 1.8 kg/kg	
Jet temperature, °C	149 - 427	260	315
Jet velocity, m/s		0.91 - 97	3.1 - 91
Jet flow rate, kg/m^2s	1.07 - 0.65	0.008 - 0.85	0.025 - 0.72
Through flow rate, kg/m^2s	0.046 - 0.27		
Through flow ratio, %	7 - 41		
Roll vacuum, kPa		17 - 71	1.0 - 41
Initial moisture content, kg/kg	0.25 - 1.95		

The air flow rates were normalized to the effective dryer surface area. Through flow ratio is normalized to the total drying air mass flow rate from the nozzles. For the experiments of series I to determine the effects of through flow rate and jet temperature on drying rate, the wet sheet of initial moisture content about 1.95 kg water/kg fibre was fed in successive passes to the dryer to obtain dry paper at a moisture content of 0.09 kg/kg. The number of passes required ranged from 4 to 7 depending on drying conditions. Representative results were shown as the average drying rate achieved in each successive pass against the corresponding sheet moisture range. The results are summarized in Table 2.4 with the averaged value of drying rate calculated for $1.4>X>1.0$ kg water/kg fibre.

Table 2.4 Results of series I: Effect of jet temperature and through flow rate

Jet velocity, m/s	96.5		
Through flow rate, kg/m^2s	0.22		0.32
Jet temperature, °C	307	427	307
Jet flow rate, kg/m^2s	0.78	0.65	0.78
Through flow ratio, %	28	34	41
Average drying rate, kg/m^2h	148	186	180

At a fixed through flow rate, 0.22 kg/m^2s, an increase of jet temperature from 307 to 427 °C resulted in an 26% increase in drying rate, although the total jet mass flow rate

decreased by about 17% at the constant jet velocity of 96.5 m/s. At constant jet temperature a comparable increase in drying rate was obtained by increasing the through flow rate from 0.22 to 0.32 kg/m^{2}s although the impingement exhaust flow rate would have been correspondingly reduced. These drying rates are of course much higher than the 16 kg/m^{2}h typical for the present hot surface conduction cylinder dryer for paper.

For the four drying rate history curves shown, the drying rate over the first pass is lower than that for the second pass by up to 34% which indicates the existence of increasing rate period derived from through flow. It is amazing, however, to note that only two out of the four curves display a slight drop in drying rate towards the dry end, although sheet moisture content range for the final pass was 0.4>X>0.05 kg/kg. For the flow conditions listed in Table 2.4, through flow is the dominant factor in affecting the total drying rate. According to Polat O. (1989), the critical moisture content for pure through drying is about $0.45X_o$. Hence it is expected that a decrease in drying rate should occur at moisture content around 0.9 kg/kg and a substantial decrease should be found in the final pass for 0.4>X>0.05 kg/kg. There must be other unspecified contributors for the impossibly high drying rate obtained by Burgess et al. at such a low moisture content.

Experiments carried out over the jet temperature range of 140 - 430 °C at jet velocity 96.5 m/s and through flow rate 0.23 kg/m^{2}s established that drying rate was linear with jet temperature. Likewise, a linear relationship was found between drying rate and through flow rate. The slope of this increase, however, is 22% higher at jet temperature of 427 than at 149°C. At jet temperature and velocity of 427 °C and 96.5 m/s the average drying rate calculated for 0.6>X>0.1 kg/kg increased from 70 to 136 kg/m^{2}h when through flow rate increased from 0 to 0.24 kg/m^{2}s.

For experiments of series II at jet temperature of 315 °C, four levels of jet velocity were tested at three levels of vacuum, 10.2, 27.1 and 40.7 kPa. The average drying rate for complete drying was calculated from 1.8 kg/kg down to the final moisture content of about 0.12 kg/kg, as summarized in Table 2.5. As this set of experiments were carried out at fixed values of vacuum, the through flow rate therefore changed substantially from wet to dry paper. Through flow rate was estimated based on the paper permeability given by Burgess et al. (1972a).

Table 2.5 Results of series II: Effect of total and through flow rate				
Jet temperature, °C	315			
Vacuum, kPa	10.2		40.7	
Through flow rate, kg/m^{2}s	0.033 - 0.099		0.13 - 0.39	
Jet velocity, m/s	12	50	12	50
Jet flow rate, kg/m^{2}s	0.096	0.40	0.096	0.40
Through flow ratio, %	34 - 103	8.3 - 25	140 - 406	33 - 98
Average drying rate, kg/m^{2}h	37	97	58	133

Since the paper permeability changed as much as three fold from 0.6×10^{-10} m at a moisture content of 1.8 kg/kg to 1.8×10^{-10} m for a fully dried paper, the through flow mass flow rate changed accordingly. Hence these drying rates are not comparable with those obtained at fixed through flow rate. For the condition of high vacuum and low jet velocity, the through flow ratio was substantially more than 100%, which implies that large amounts of environment air in addition to all of the air from the jet was sucked through the web.

The effect of vacuum was further tested at four levels from 17 to 69 kPa at two levels of jet velocity, as summarized in Table 2.6. The drying rates are simply average values over the range 1.8>X>0.12 kg/kg.

Table 2.6 Results of series II: Effect of vacuum on drying rate		
Jet temperature, °C	260	
Jet velocity, m/s	96.5	
Jet flow rate, kg/m^{2}s	0.85	
Vacuum, kPa	17	69
Through flow rate, kg/m^{2}s	0.06 - 0.18	0.23 - 0.69
Through flow ratio, %	7.1 - 21	27 - 81
Average drying rate, kg/m^{2}h	108	172

The through flow rates were obtained in the same way as those in Table 2.5 as for each sheet the same vacuum was used for all passes. Likewise, as the through flow ratio changed as much as three fold the drying rates cannot be associated with a specific flow condition, hence are of only overall relevance. The results they reported at a very low jet

velocity, 0.9 m/s, have not been shown because their indicated through flow rates were up to 86 times the total inlet air jet flow. As such through flow air would have mostly from the room environment, the drying rate results are impossible to interpret. For the case of high jet velocity, by increasing vacuum from 17 to 69 kPa average drying rate was increased by as much as 60%.

As the drying rates reported by Burgess et al. are based on paper moisture content measurements such rates include that by impingement and through flow air plus hot surface conduction heat transfer from the dryer roll and radiation from the impingement hood. Their reported paper temperature measurements indicate that during each pass the paper temperature increases by about 10 - 15 °C starting from temperature of about the adiabatic saturation value. This increase indicates that the sheet received significant heat from the vacuum roll. As no roll temperatures were reported, the hot surface conduction contribution to their measured drying rate cannot be estimated. In a conventional cylinder dryer section the average drying rate is of the order of 15 kg/m^{2}h. At higher jet temperature, the contribution of radiation is significant. For jet temperature of 427 °C radiation may contribute about 14 kg/m^{2}h.

For trials with corrugating paper of basis weight 140 g/m^2, a similar trend was observed with the drying rates somewhat higher than those achieved with newsprint.

During a brief mill trial, effects of through flow rate, jet temperature as well as total jet flow rate on the average drying rate were investigated similarly to the pilot plant study. The results showed that the mill trial dryer unit approximated the performance determined in the pilot plant, with average drying rate reaching as high as 142 kg/m^{2}h for jet temperature of 430 °C, jet velocity of 85 m/s at nozzle open area ratio of 1.6%, nondimensional nozzle spacing from the sheet of 12 nozzle widths and vacuum of 25kPa with paper of basis weight 52 g/m^2. The paper entered the dryer at a moisture content of 0.4-0.6 kg water/kg fibre and left at 0.02 to 0.2 kg water/kg fibre, and the drying rates reported are average values over that range of moisture content. An empirical relationship without a term for paper moisture content was given which correlated the drying rate with air temperature, jet velocity and through flow velocity.

Two aspects of the report on the pilot plant investigation of Burgess et al. (1972a) lead to reservations concerning the quantitative aspect of their results. They measured both the paper temperature and the temperature of the through flow air exiting the sheet. Their technique for the latter measurement should have provided reliable values. However their measurements indicated that the through flow air exited the sheet at a temperature 5 - 15 °C below the paper temperature. As it is the sheet which cools and humidifies the through flow air, it is of course impossible for the air to exit the sheet at a temperature below the sheet temperature. Secondly, with jet temperature of 307 °C and 427 °C they dried the sheet in four passes, with the corresponding moisture content being approximately 1.8, 1.4, 1.0, 0.5 and 0.05 kg water/kg fibre. Thus they reported four values of average drying rate, one for the moisture content limits of each pass. The surprising feature is that all four values of average drying rate are essentially the same, even the final one for drying from about 0.5 to 0.05 kg/kg moisture content. They concluded that with combined impingement and through flow, "no falling rate zone occurs". All paper drying published research indicates that there will always be a falling rate period. The results of others indicate that for the moisture content range from 0.5 to 0.05 kg/kg, the drying rate would be expected to be only perhaps 1/5 of the maximum drying rate in the moisture content range of about 1.8 - 1.4 kg/kg.

Thus because of the nature of the pilot plant and mill trial tests, the findings of Burgess et al. do not provide insight concerning the detailed performance of this drying process or the interaction between the impingement and through flow. However those were not their basic objectives, and their most valuable investigation revealed the potential of the combined impingement and through air dryer for paper and proved that this technique could be reduced successfully to practice.

Crotogino (1975) concluded that air drying is the only viable alternative to conventional cylinder dryers to meet the trend for increasing paper machine speed and to reduce operating problems such as frequent sheet breaks in existing paper mills with conventional cylinder dryers. A review of factors governing the drying rates attainable with impingement drying was given in terms of jet velocity, jet temperature and nozzle geometries. For through drying, the maximum achievable, i.e. with the adiabatic

saturation condition at the exit was assumed by inference from results of Burgess et al. (1972a). Crotogino discussed the concept of a linear contribution of the two components in combined impingement and through air drying, in order to have a continuous relation of drying rate with through flow ratio from the limits of pure impingement to pure through drying. His analysis of the process employing impingement and through flow by suction identified the benefits to be gained as high drying rate, uniform drying, flexibility and improved paper quality. Moreover, it was noted that these benefits are attainable while the sheet is conveyed through practically the entire dryer section without being subjected to an unsupported draw. The application of air drying in the manufacture of various paper grades, tissue and newsprint was discussed. The similarities in solutions to problems for both grades led to the conclusion that a standard air dryer unit can be built which would be capable of handling a range of types of paper.

Crotogino and Allenger (1979) proposed a model coupling the air impingement and through drying by assuming no interaction between the impingement and through flow drying. Thus they assumed the impingement drying and the through flow drying contributions to be directly proportional to the mass flow rate of the impingement exhaust and the through flow exhaust. For the through drying component they assumed that the maximum drying rate achievable was obtained, i.e. that the through flow air exhaust was saturated at the adiabatic saturation temperature corresponding to the air inlet conditions.

For the falling rate period, the drying rate was considered to be controlled entirely by the decreasing vapor pressure and the increasing heat of desorption of water, with $P_v = P_v' \cdot r_p$ where P_v' is the saturation vapor pressure evaluated at the web temperature, while the fraction r_p was calculated based on the experimental data of Prahl (1968) in the form suggested by Wedel and Chance (1977) as:

$$r_p = 1 - e^{(0.544-14.5 \cdot X)} \quad \text{for} \quad X>0.07 \qquad (2.4)$$

$$r_p = 51.3 \cdot X^{1.86} \quad \text{for} \quad 0.07 \geq X \geq 0$$

The heat of desorption, also taken from Prahl's data, was approximated as:

$$\ln\lambda_a = 7.20 - 17.3 \cdot X \qquad (2.5)$$

Radiation heat transfer from the hood was accounted by

$$q_r = \sigma \bar{F}\left[\left(\frac{T_j + T_e}{2}\right)^4 - T_p^4\right] \qquad (2.6)$$

where σ is the Stefan - Boltzmann constant, $\bar{F}$ the interchange factor, approximated as 0.7, T_j and T_e the jet and air exhaust absolute temperature, and T_p the paper absolute temperature.

Their linear model satisfactorily predicted the performance reported by Burgess et al. (1972a) at conditions of jet velocity of 96.5 m/s, jet temperature 427 °C, through flow mass flow 0.22 kg/m^{2}s, basis weight 52 g/m^2, assuming sheet temperature at 25 °C for paper moisture content $1.8 \geq X \geq 1.4$ and 30 °C for $1.4 > X \geq 0.1$ kg/kg. It also predicted the mill trial results of Burgess et al. (1972b) for the effect of jet temperature, percolation flow rate and jet velocity on drying rate.

Randall (1984) proposed a different model. He separated the impingement and through flow drying, treating the impingement air drying as taking place first, followed by through air drying using part of the impingement exhaust flow. He further assumed that all the nozzle exit air participated in the impingement drying as if there were no through flow. Thus the contribution of impingement drying was taken as constant for a given total nozzle exit mass flow rate. Such an assumption is arbitrary.

Correlations reported by Chance (1974) for impingement heat transfer with round nozzles were used by Randall in predicting the impingement heat transfer coefficient. For calculations of through flow heat transfer coefficient, the approach of Rohrer and Gardiner (1976) was employed. In Randall's model, the warmup as well as the falling rate period was considered. The relation between normalized drying rate, defined as the ratio of drying rate to the constant drying rate, and normalized moisture content, ratio of moisture content to critical moisture content, was adapted from Gottsching and Rhodus (1977) with Randall's own experimental test proof in the falling rate period as:

$$\frac{R}{R_c} = \sqrt{(1 + a_f)\cdot\frac{X}{X_c} - a_f \cdot \left(\frac{X}{X_c}\right)^2} \qquad (2.7)$$

Good agreement was claimed between his model and his experiments on a pure through flow pilot dryer, with no supporting data reported.

For paper basis weight of 49 g/m^2, sheet speed at 18 m/s, hood air temperature at 400 °C, nozzle plate open area ratio of 2%, the minimum energy cost was predicted to occur when through flow water removal is 1/3 of the total drying rate. A roll diameter larger than 5m was recommended from the model prediction in terms of the total energy cost. With the increasing rate period contribution (defined by Randall as the warmup period) and the falling rate period for the sheet entering dryer at moisture of 1.38 kg/kg and leaving at 0.8 kg/kg, an optimal machine speed in terms of drying capacity was found to be at 10 m/s for a cylinder diameter of 4.27m.

Polat S. et al. (1990, 1991a,b) concluded from their experimental heat transfer measurements with a porous heat transfer flux sensor that the impingement heat transfer coefficient increases linearly with through flow rate. As their experiments determined only impingement heat transfer rate and did not involve through drying, those results do not deal with the effect on through drying of the impinging jet approach condition or the effect of through flow on drying rate in combined impingement and through air drying. Thus there are significant differences between the assumptions of the two models, i.e. those of Randall and of Crotogino and Allenger, and it is difficult to relate the experimental findings of Polat S. et al. To the process of combined impingement and through air drying.

Thus to provide sound guidelines for the designer of dryers using combined impingement and through air drying, it remains to be determined by direct measurements how impingement and through flow affect each other and how drying rate can be predicted reliably for the CITAD process.

2.5 Conclusion

Although impingement heat transfer has been extensively studied and impingement drying of paper widely used industrially, basic knowledge of impingement drying remains limited, especially concerning the falling rate period and the point of onset of that key period, the critical moisture content.

All through drying results have been obtained with a uniform flow of air approaching the wet sheet, with no investigation of whether the rate of through drying of paper could be enhanced by providing the inlet air as impinging jets. There is inadequate knowledge of the drying rate - moisture content relations for the complete drying rate curve.

Although the concept of the enhancement of impingement heat transfer by through flow has been thoroughly investigated theoretically and experimentally, the only experimental results concerning combined impingement and through air drying of paper are from an industrial pilot plant and a brief paper mill test which did not lead to an industrial installation of this process. This work provided the crucial confirmation that newsprint could be dried successfully by such a combination of drying techniques. However the scale and nature of this work was not designed to provide fundamental knowledge of the combined process, including the separate role of the components of impingement and through drying, and the interaction between these basic elements of the combined process.

The two models published treat the application of this combination of techniques to drying paper from different approaches. One model assumes no effect from the through flow component on the impingement component. The other model approximates the total drying rate with each component contribution varying directly with the corresponding proportion and assumes the maximum possible through flow contribution, i.e. for the through flow exiting saturated. Thus the question of the mutual interaction of impingement drying and through drying when both processes occur simultaneously remains to be established definitely by experimental measurement.

Chapter 3 Experimental Apparatus

3.1 Overall design concept

An experimental facility was designed and built for the study of the combined impingement and through air drying of paper. The impingement flow was obtained by air jets from arrays of 19 or 61 round nozzles impinging on a 100mm diameter sheet. Nozzles of three diameters were used, 1.59 mm, 2.38 mm and 3.75 mm. The impingement exhaust ports were located between the nozzles so that the cross flow of the impingement exhaust was not a factor. Air through flow was achieved by applying suction downstream of the wet sheet.

Since the prime industrial motivation for this study was to determine the mutual interaction between the impingement and through flows it was therefore essential that the apparatus operate from 100% impingement drying to 100% through flow drying. Because of the high dependence of the permeability of moist paper on its moisture content, the coupled relationship of through flow rate and pressure drop across the sheet is very sensitive to moisture content. Therefore an essential feature of the equipment design was to achieve a constant mass flow rate of all three air flows, i.e. of the total drying air flow at the inlet and at both the through flow and impingement air exhausts. Only in this way can the measured drying rates be associated with the precise flow conditions that produced these drying rates. Of the three flows, the total drying air to the impingement nozzles and the through flow exhaust were instrumented to provide constant flow rates, thereby providing a constant mass flow rate also for the impingement exhaust flow.

The constant inlet mass flow rate was obtained by a pressure regulator in series with a critical flow valve. The pressure regulator ensures that the air from the central supply line is controlled to a fixed pressure of 80 psig (552kPa) upstream of the critical flow valve. With the pressure downstream of this critical flow valve always less than 5 psig, the ratio of absolute pressure downstream to upstream is always less than the value of 0.45 required to achieve critical flow across the valve.

The constant through flow rate was obtained by using vacuum regulators, of range 0 - 14.5 psi, on the through flow exhaust line, in series with another critical flow valve downstream of the vacuum regulators. For the present condition of a fixed mass through flow rate, pressure drop across the sheet can change in a few seconds as much as 15kPa from beginning to end of one experiment. The system performance and the required vacuum regulator specifications were determined in advance by a numerical simulation, which established the feasibility and showed that two vacuum regulators are necessary for a sufficiently fast response. The small system volume, 1.8 liter, from the sheet to the critical valve does not affect the through flow rate significantly. A vacuum pump installed downstream of the critical flow valve maintained the pressure downstream of this valve sufficiently low to maintain critical flow across the valve.

Another aspect of concern was the temperature upstream of the critical flow valve in the through flow exhaust. As critical flow is a velocity effect, a constant flow velocity at such a valve only becomes a constant mass flow rate if the fluid pressure and temperature upstream of the valve remain constant. It was found that although the through flow exhaust air temperature changes by as much as 50 ^{o}C during a drying experiment, the uninsulated exhaust line from the vacuum regulator to the critical valve reduces the temperature variation at the valve to 1° C or less.

Rotameters were used to measure the air flow rates downstream of the critical valves on the air inlet line and on the through flow exhaust line. Calibration of these rotameters was carried out against a dry test meter with error less than 0.1%. Leakage prevention was achieved by having O-rings between each flange connection, by placing the inlet air electrical heaters in a sealed cylindrical housing, and by using special design of sheet insertion mechanism. From a static test, it was determined that leakage was less than 0.05% of the drying air flow rate.

For pure through drying, the through flow can be obtained easily by the pressure drop between the drying chamber and the through flow exit without using the large vacuum pump. The volume from downstream of the critical valve on the inlet line to the drying chamber must be minimized to have a fast system response. For the present apparatus, this volume is less than 7 liter, which requires much less than 1s for the flow to

stabilize at 99% of the set flow rate when paper sample is introduced into the drying chamber. For the subsequent entire drying process, the mass flow rate across the sheet varies less than 1% from the set value for the present experimental conditions.

Accurate measurement of the rapidly changing paper moisture content was another challenge. Paper moisture content was determined by monitoring the air humidity at both the impingement and throughflow exhaust streams with IR analyzers of response time less than 0.25s, which thereby provided the impingement and through drying rates during each experiment. In this way the instantaneous impingement, through flow and total drying rates were all obtained as a function of the instantaneous paper moisture content.

Inlet air temperature was controlled by an electrical heater. To obtain the drying air at a uniform temperature to all parts of the sheet the six units of the heater were installed with a 60^{o} angle between adjacent ones. Each electrical element has an independently controlled variable voltage supply. A perforated plate of 25% open area was placed immediately downstream of the heater to further assure a completely uniform air temperature and air flow velocity. Type-E sub miniature thermocouple probes, of time constant less than 0.1s, were used to document the air temperature at the nozzle exit, impingement exhaust, in the through flow exhaust immediately downstream of the paper. Because of the possible local nonuniformity in through drying due to local nonuniformity in the sheet (Polat O. et al. 1992a) the through flow exhaust temperature was monitored by three thermocouples placed 30 mm downstream of the sheet and at three radial positions - at the center line, 15 mm from the drying chamber wall, and the third one midway between the other two.

Pressure drop across paper during drying was monitored with a pressure transducer. Depending on the experimental conditions, a pressure transducer of range ± 1 psi or ± 5 psi was used. Paper surface temperature at the through flow exit side was also measured for some experiments by attaching to that surface of the sheet a thermocouple of the same type as used for other measurements.

3.2 Equipment description

3.2.1 General Description

Shown in figure 3.1 is the schematic diagram of the experimental apparatus. The supply air pressure was regulated to 80 psig (552kPa) by a pressure regulator, 1 (Norgren R17-801-RNLA), then cleaned with an oil filter, 2 (Norgren F17-800-A3D). A critical flow valve, 3a (Whitley), was used as the regulating valve for the air mass flow rate. The pressure downstream of the critical valve was measured with a mercury manometer, 4. The inlet air flow after the rotameter, 5a (Brooks 1114CL31CMDAA), brought to the desired temperature by an electrical heater, 6. The inlet air flow, 7, passes through a nozzle array, 8, and exhausts via either or both exits, the impingement exhaust, 10, or through flow exhaust, 14 (detailed in figure 3.2). The humidity of the impingement air exhaust was monitored by an IR analyzer, 16a (Foxboro MIRAN 1A CVF). With through flow, the pressure drop of the air flow across the moist paper in the sheet holder, 13 (detailed in section 3.2.3), was measured with a pressure transducer, 9 (either Statham PM6TC±1-350 or PM6TC±5-350). The through flow exhaust mass flow rate was regulated with a critical flow valve, 3b (Whitley), along with two identical vacuum regulators in series, 19a,b (Fairchild 1626). The through flow exhaust rate was metered by a rotameter, 5b (Brooks 1114CL31CMDAA), for the vacuum measured at the rotameter with a vacuum gauge, 20. The critical flow condition through the critical flow valve, 3b, was achieved by suction from the vacuum pump, 23 (Leybold D90A). The humidity of the air of the through flow exhaust was monitored with another IR analyzer, 16b (Foxboro MIRAN 1A CVF). To protect the vacuum pump the moisture in the through flow exhaust was removed by a water vapor condenser, 22 (Leybold A90- 11). A ball valve, 21 (Watts 9214), was installed upstream of the intake of the vacuum pump to maintain high vacuum so as to protect the pump when system is at idle. Signals from the IR analyzers, pressure transducer for pressure drop across the sheet as well as the thermocouples were sent to a dedicated PC (IBM 8086XT). T-valves, 15a,b, were

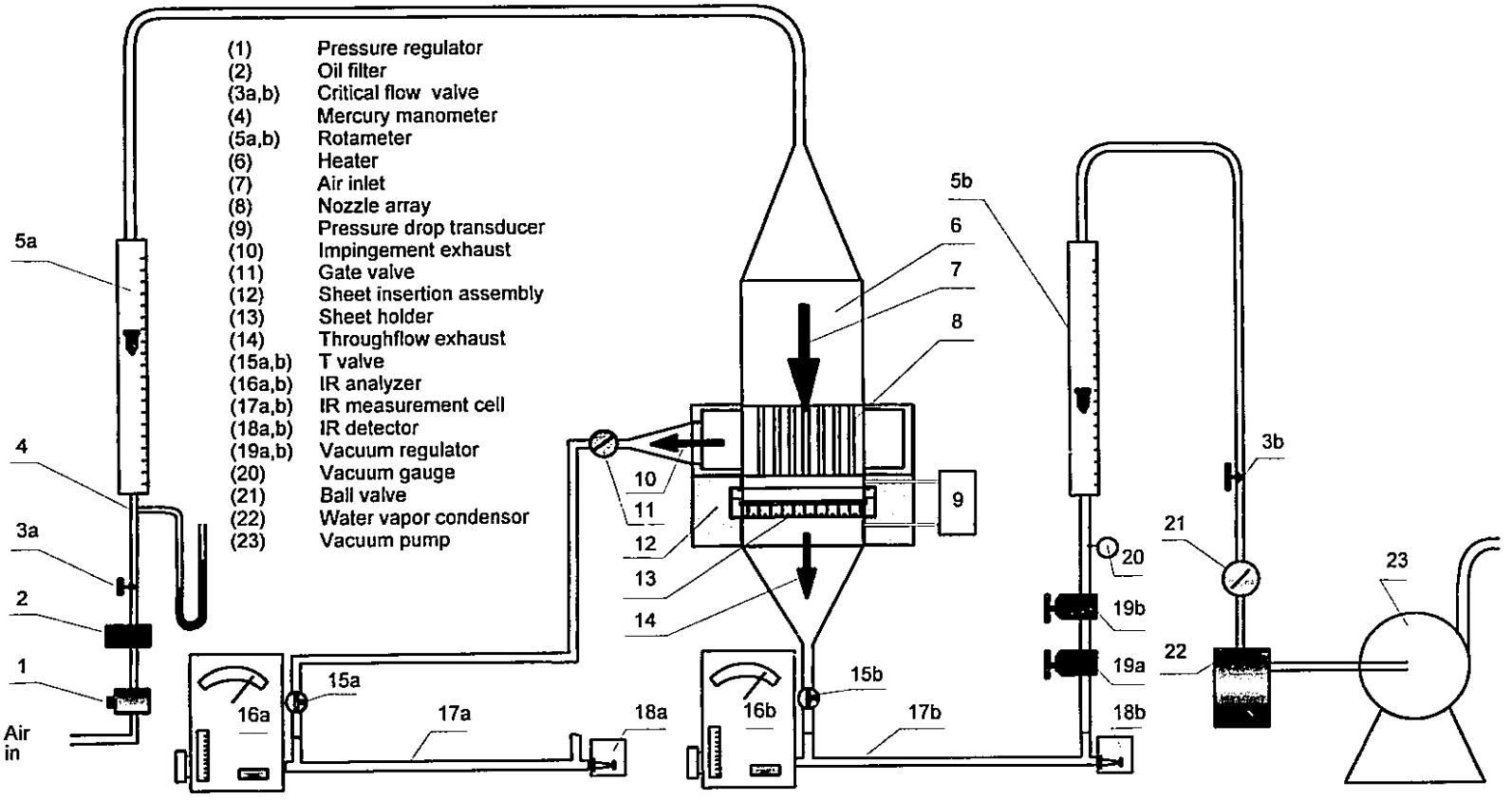

Figure 3.1 Experimental apparatus

used to bypass the air flow from the IR measurement cells, 17a,b, to keep the IR detectors 18a,b, at the ambient environment between drying experiments.

3.2.2 Nozzle geometry

Details of the arrays of multiple round nozzles are provided by Table 3.1 and figures 3.2 and 3.3. All nozzles were made from 45 mm tubing. The equilateral triangle pattern, which is used industrially, was chosen for the layout of nozzle arrays to have a uniform flow distribution from the center to the edges of the I.D.100 mm drying chamber above the sheet.

Table 3.1 Geometry of nozzle arrays

Set #	d (mm)	N	f (%)	H/d
1	2.38	61	3.1	5.0
2	1.59	61	1.4	7.6
3	3.75	19	2.7	8.5

Nozzle sets #1 and #2, fabricated of brass, share the same layout as shown in figures 3.3(a) and (b), having 61 arrays with inside diameter 2.38 mm for nozzle set #1 and 1.59 mm for nozzle set #2, uniformly distributed on an equilateral triangle pattern as shown by the solid circles. Nozzle set #3 of stainless steel, figure 3.3 (c), has 19 round nozzles of inside diameter 3.75 mm. The nozzle diameter was planned to be in the range of 1 - 4 mm with commercially available tube sizes as listed in Table 3.1. The number of nozzles was so chosen that the open area ratio is $1.5\%<f<3\%$, where the performance index reaches maximum value (Daane and Han 1961). The spacing between the nozzle exit and the sheet was planned in the range of $6<H/d<8$ where the heat transfer coefficient from arrays of round nozzles reaches a maximum (Garden and Akfirat, 1966; Martin, 1977). The actual values of H/d are listed in Table 3.1.

The impingement flow exhausts from the ports shown by the open circles around the nozzle exits as well as from the annular spacing between the drying chamber wall and the edge of the nozzle exit plate. The flow area for the impingement exhaust is 4.3 times of the nozzle open area for set #1, 2.9 and 7.2 times the nozzle area for sets #2 and #3.

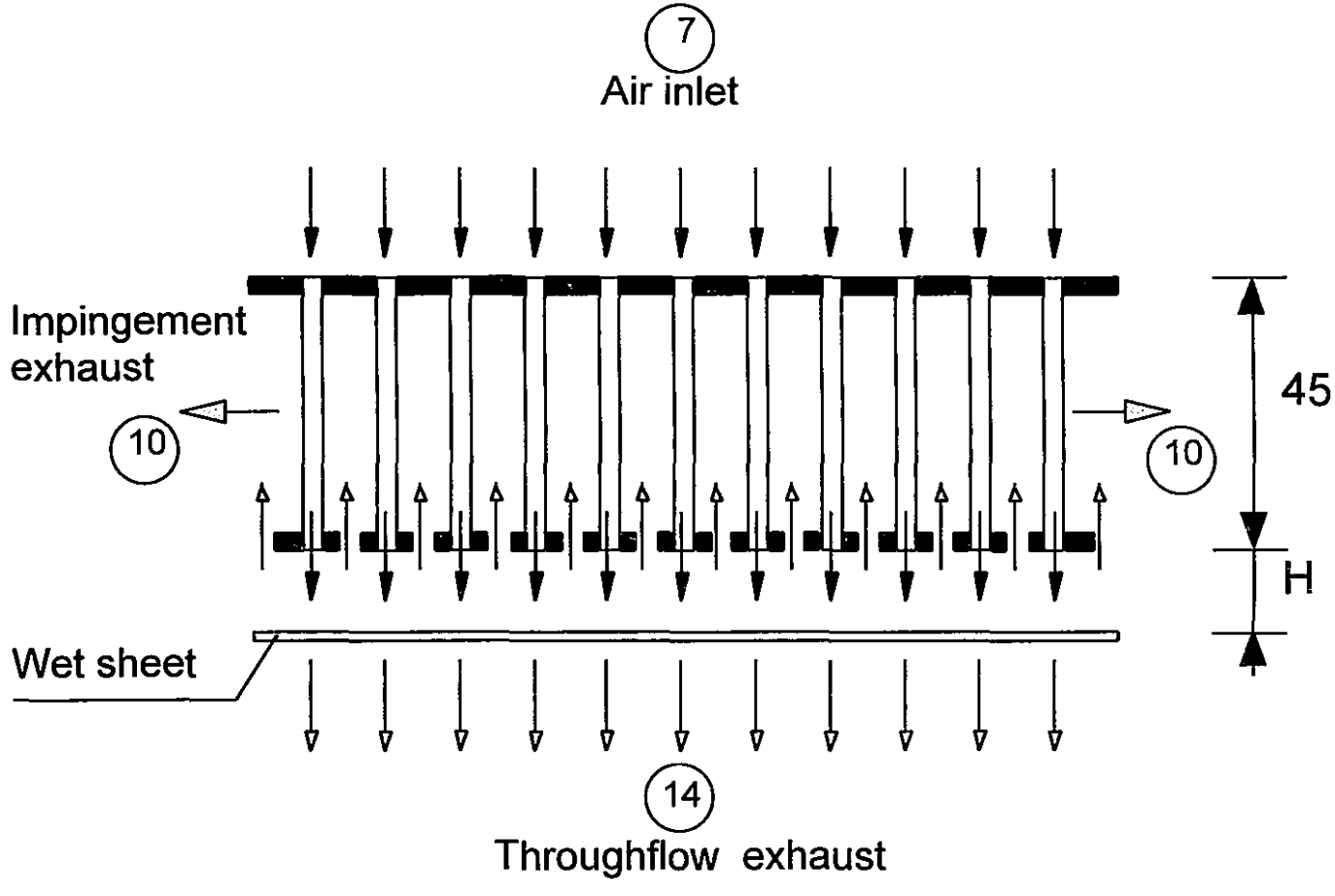

Figure 3.2 Impinging jet nozzle geometry

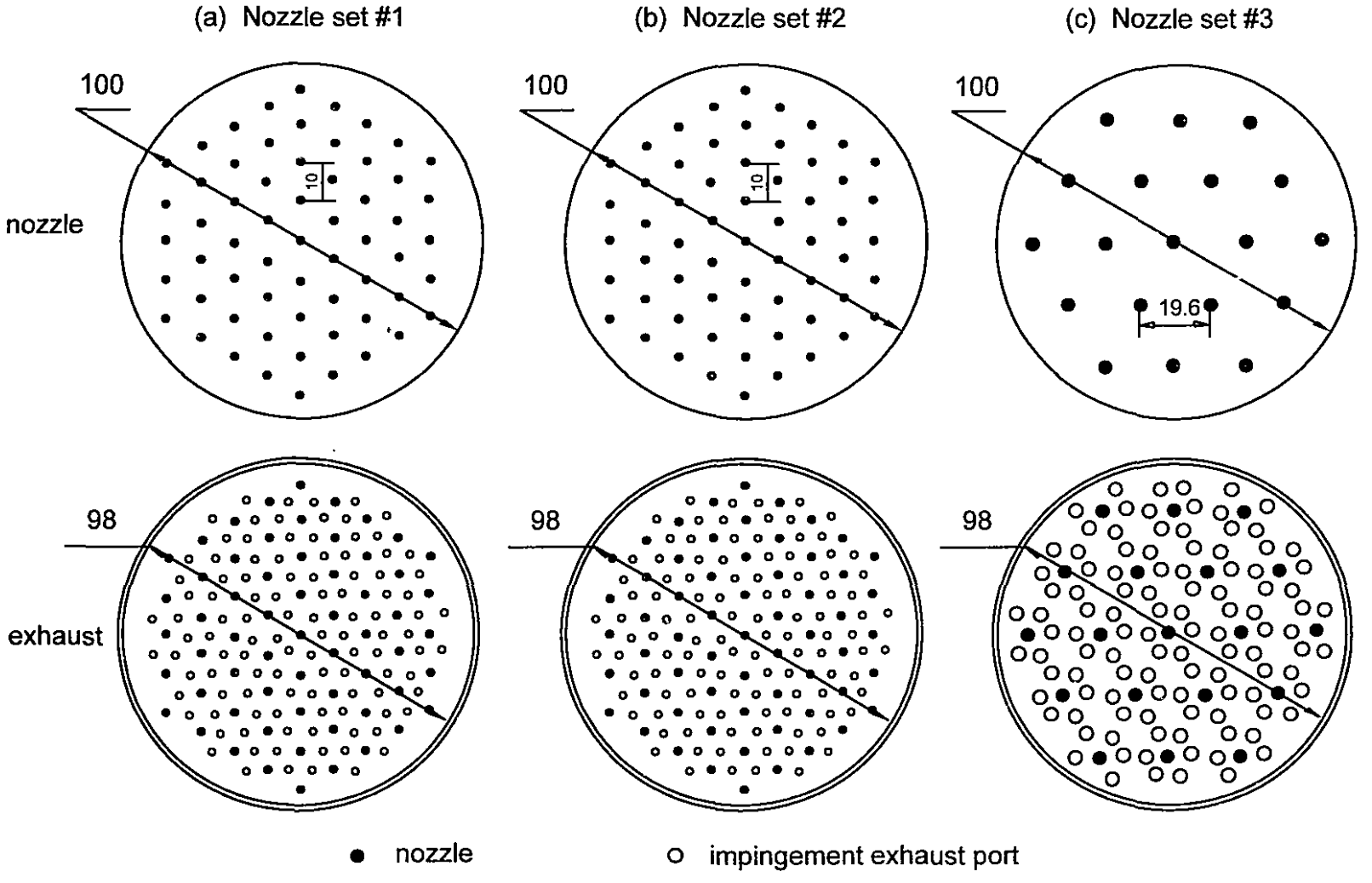

Figure 3.3 Impingement nozzle and exhaust port layout

3.2.3 Sheet holder

The holder for 103 mm diameter sheets consists of two parts, a cover with a 2 mm circular rim, and a base with a matching 2 mm deep notch. The sheet was held on the base by the cover rim. The cover and base was assembled by 6×60° screws. An O-ring was placed on top of the cover to prevent leakage from the drying chamber.

Figure 3.4 shows the detailed design of sheet holder for drying with through flow, whether alone or with impingement drying. The sample rests on #60 mesh supported in turn by honeycomb whose strength was enhanced by a coarse wire screen of 0.8 mm diameter wires on a 6 mm by 6 mm mesh. This screen was sandwiched between two solid Plexiglas rings.

For the sheet holder for pure impingement drying, figure 3.5, the paper rests on a thin insulating sheet of polyester from a standard transparency, selected for its temperature stability and light weight. The plastic sheet rests on honeycomb, mounted on the solid Plexiglas base. A small hole, less than 0.5 mm diameter, through the support enabled insertion of a thermocouple from below to contact the support side of the paper. To minimize heat loss or gain to the sheet the back of the holder was coated with 4 mm foam insulation.

The sheet holder was introduced into the drying chamber with the insertion assembly, figure 3.6. O-rings at the top and side of the lifting support prevented leakage at the movable joints.

3.2.4 Data acquisition

Signals from thermocouples, IR analyzers, and the pressure drop transducer were connected to an IBM-PC microcomputer data acquisition system. Each output was connected to a signal conditioning unit, Data Translation Inc. Model DT6701 or DT6702 depending on the signal voltage level. The signal conditioning unit was equipped with a

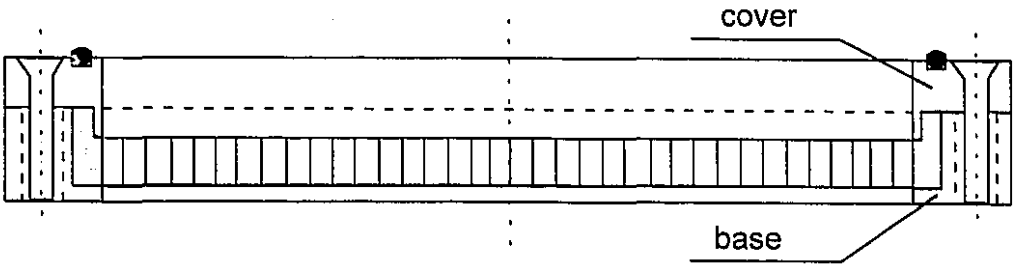

(a) Sheet holder for drying with through flow

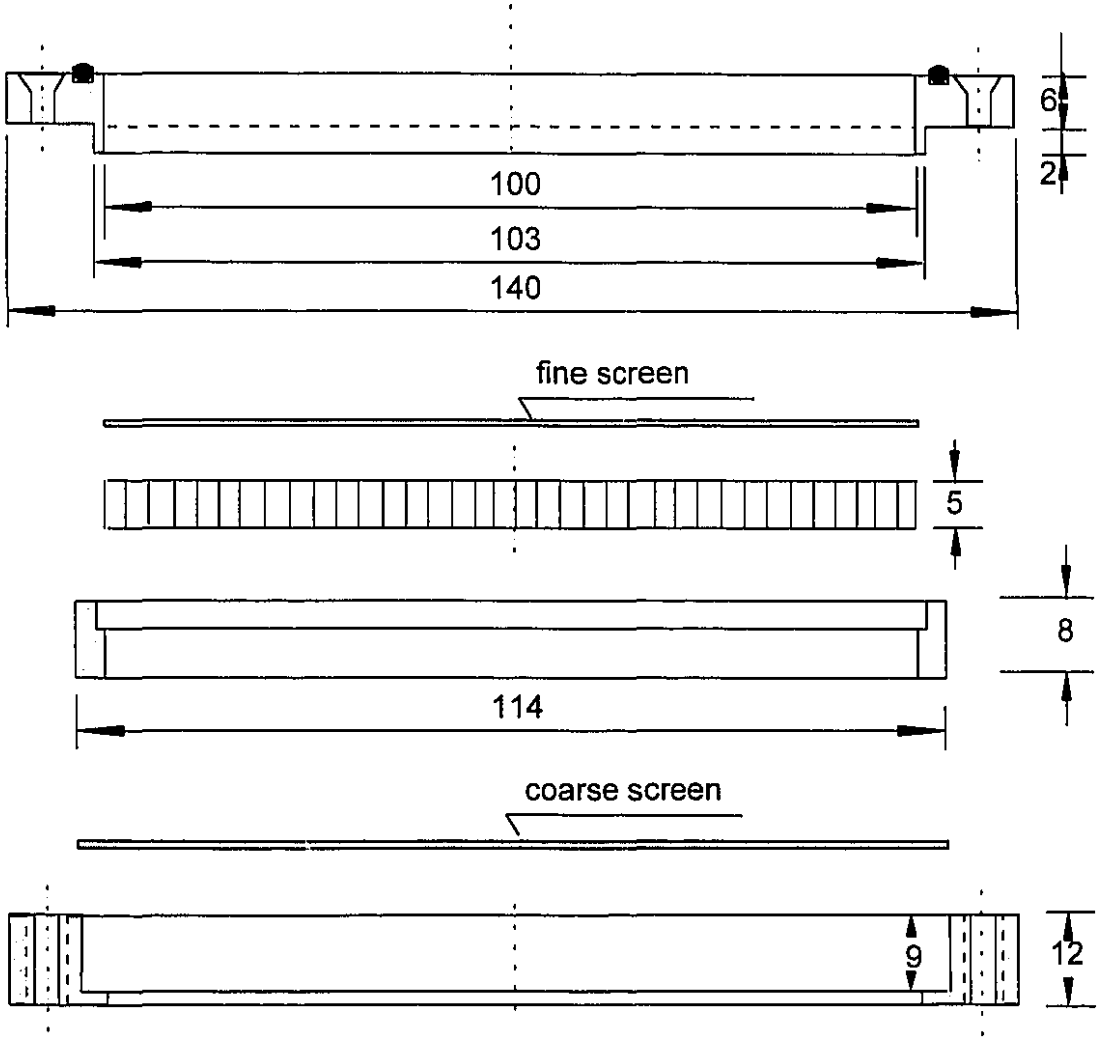

(b) Sheet holder design (dimensions in mm)

Figure 3.4 Sheet holder for drying with throughflow

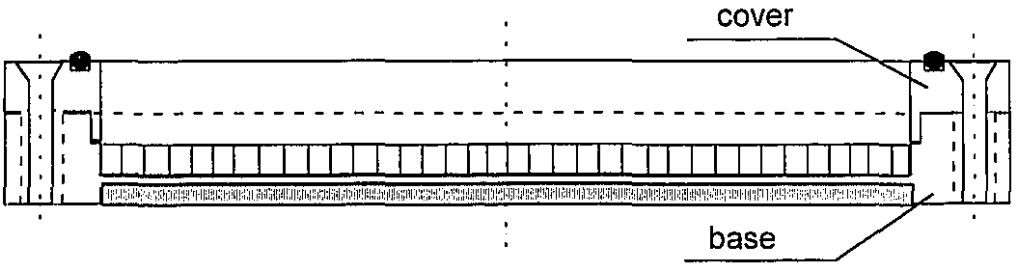

(a) Sheet holder for pure impingement drying

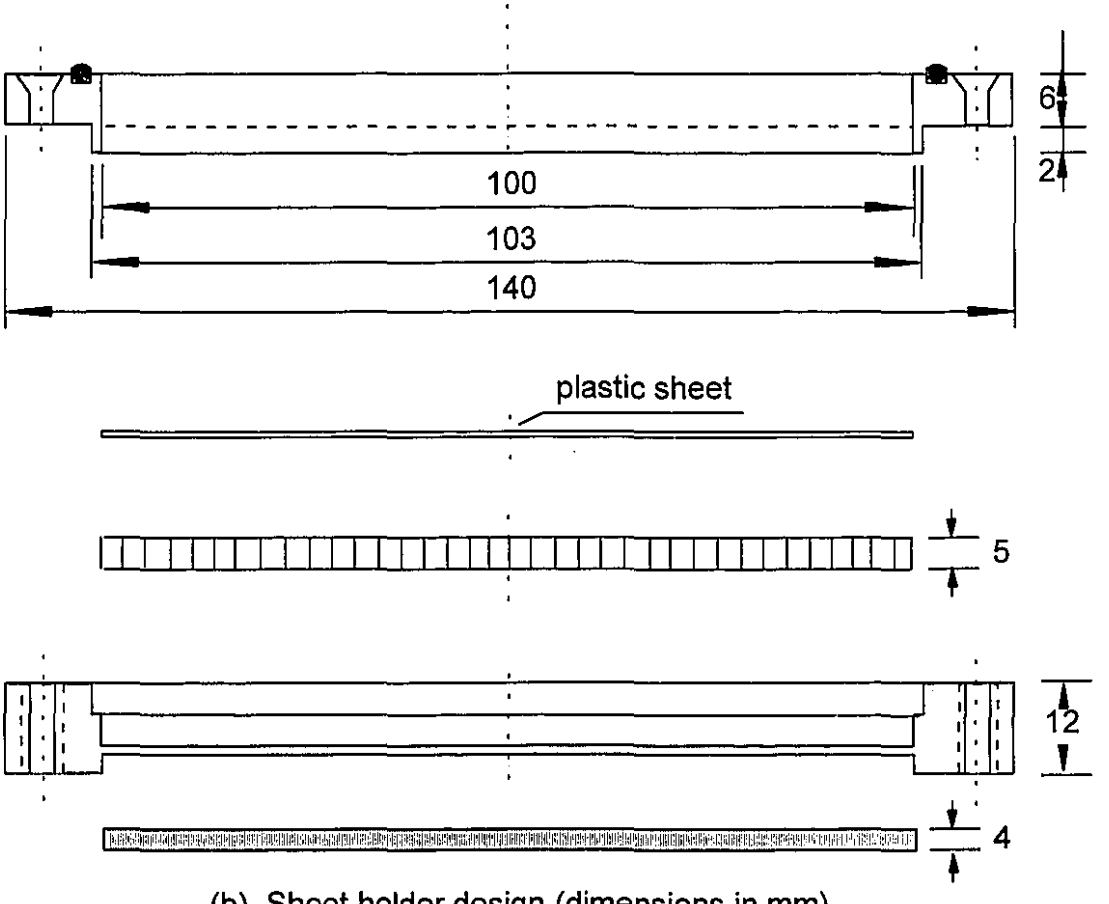

(b) Sheet holder design (dimensions in mm)

Figure 3.5 Sheet holder for pure impingement drying

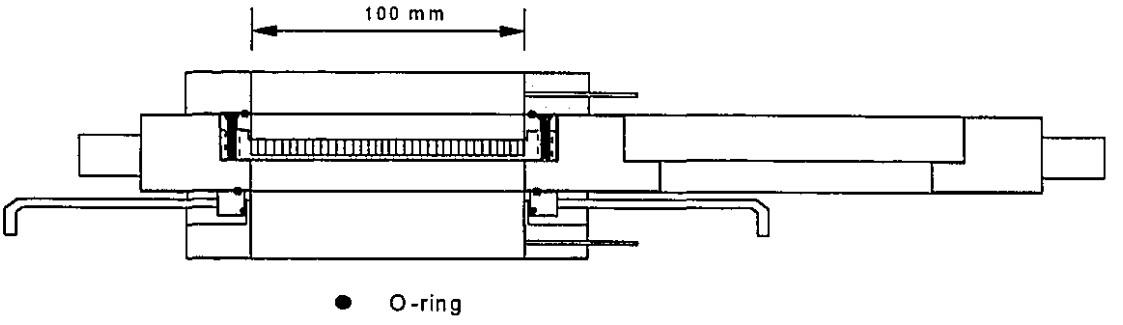

Figure 3.6 Sheet insertion assembly

low-pass filter and gain control unit. The A/D board was Data Translation Inc., Model DT2801-A with 16 single-ended channels.

The sampling frequency, ranging from 0.5 to 10 Hz, was selected in order to have about 250 sets of data for each drying experiment.

A data acquisition program was written in QuickBasic with PC-Lab subroutines used. The program allowed monitoring air humidity, temperature and pressure drop via an on-screen display in real time mode during drying. It saved the raw data as well as preliminary processed data for further treatment. The complete program is given in Appendix A.

3.3 Commissioning of the apparatus

3.3.1 Vacuum regulators performance test

Figure 3.7(a) shows test results for the response of the vacuum regulators with a step change of 13.6 kPa, the pressure drop across a dry blotter of 250 g/m^2. The pressure drop across the sheet and the pressure at the rotameter were measured with pressure transducers. The total inlet air mass flow rate was 1.45 kg/m^{2}s, and the through flow ratio was 34%. The system volume, 1.77 liter, from sheet to upstream of critical valve, 3b on figure 3.1, does not affect the through flow rate significantly. The ratio of the actual

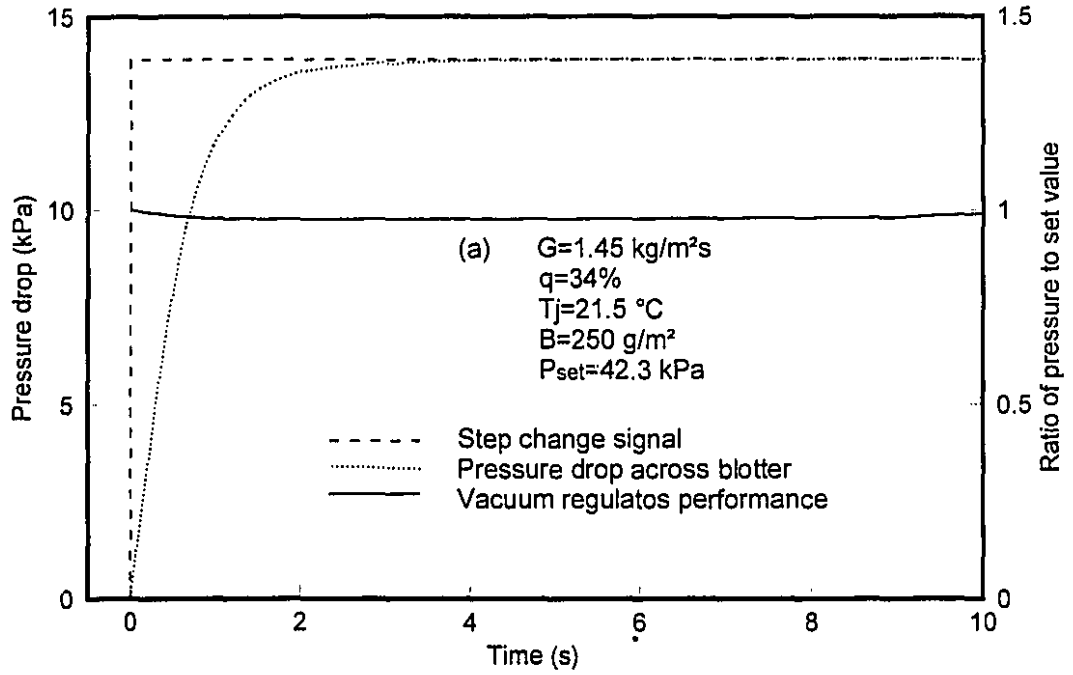

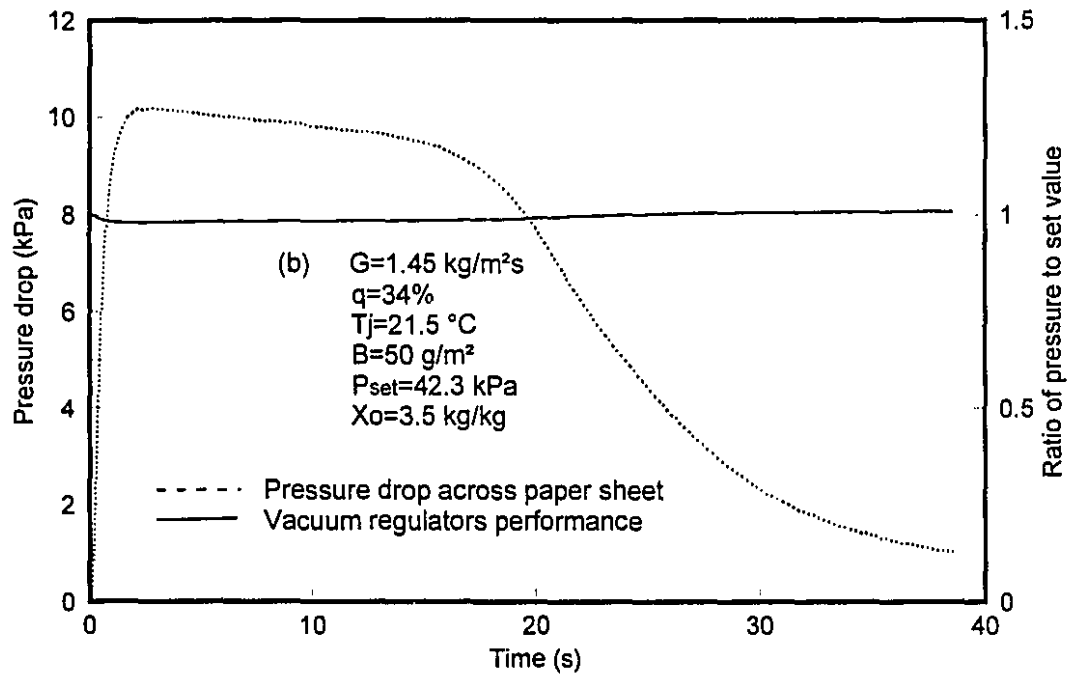

Figure 3.7 Performance check of vacuum regulators

pressure to the set value at the rotameter was found to be 1±0.02. The suction system response time calculated from the pressure drop across the blotter paper was less than 0.6s. Figure 3.7(b) shows the results of pressure at the rotameter for a drying experiment carried out with a 50 g/m^2 kraft handsheet. The inlet air mass flowrate again was 1.45 kg/m^{2}s, of which 34% exited as through flow. The paper initial moisture content was 3.5 kg water/kg dry fibre. Although the pressure drop across the sheet increased sharply from 0 to 10 kPa then gradually decreased to about 1 kPa, the pressure at the rotameter was always less than 2% percent away from the set value at the rotameter, upstream of the critical valve.

3.3.2 Infrared analyzer calibration

The Miran 1-A IR spectrophotometer was adapted for use with a 25.4 mm inside diameter measurement cell of length 550 mm to determine the absorbence of water vapor at a wavelength of 2.70 μm. The cell length is the optimal choice between two opposing factors - the sensitivity of the measurement, which increases in proportion to the cell length, and the time constant, which is inversely proportional to the cell length. Of the five strong IR absorbent bands, 2.55, 2.60, 2.66, 2.70, 2.74 μm excluding the near and far IR regions, 2.70 μm was selected as having the best reproducibility (Polat O. 1989).

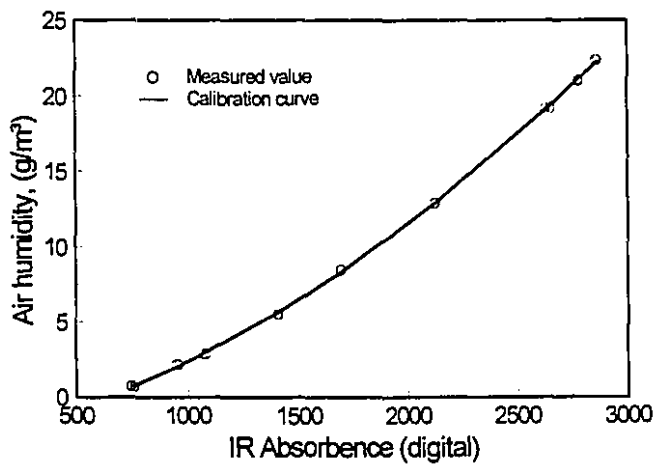

Figure 3.8 IR analyzer calibration curve

The Miran 1-A IR spectrophotometer was chosen for its fast response time and adaptability to the present apparatus. The IR response time was further improved by removal of the C12 capacitor, which reduces its time constant to less than 0.25s. A concave CaF_2 lens of focal length 250 mm was placed at the end of IR source of the

measurement cell, while a plane CaF_2 window was sealed at the IR detector end. The IR analyzer was calibrated against a chilled-mirror type dew point hygrometer, (Model 660, EG&G), using a number of saturated salt solutions of known vapor pressure. Figure 3.8 shows a typical IR analyzer calibration curve. A second-order polynomial was fitted to the data for air humidity, g/m^3, and IR absorbence, digital. Detailed IR calibration procedures and the salt solutions used are given in Appendix B.

3.3.3 Overall performance test

As the equipment operation is more complex and subject to more factors for through drying than for impingement drying, it was tested by replicating a high through flow rate experiment as reported by Polat O. (1989). Thus his exact experimental conditions, including data acquisition and data processing procedures, were replicated prior to the installation of impinging jets. The mass balance for water was 98%. Figure 3.9 shows for drying rate as a function of moisture content the very good agreement obtained between the present measurements and those of Polat O.

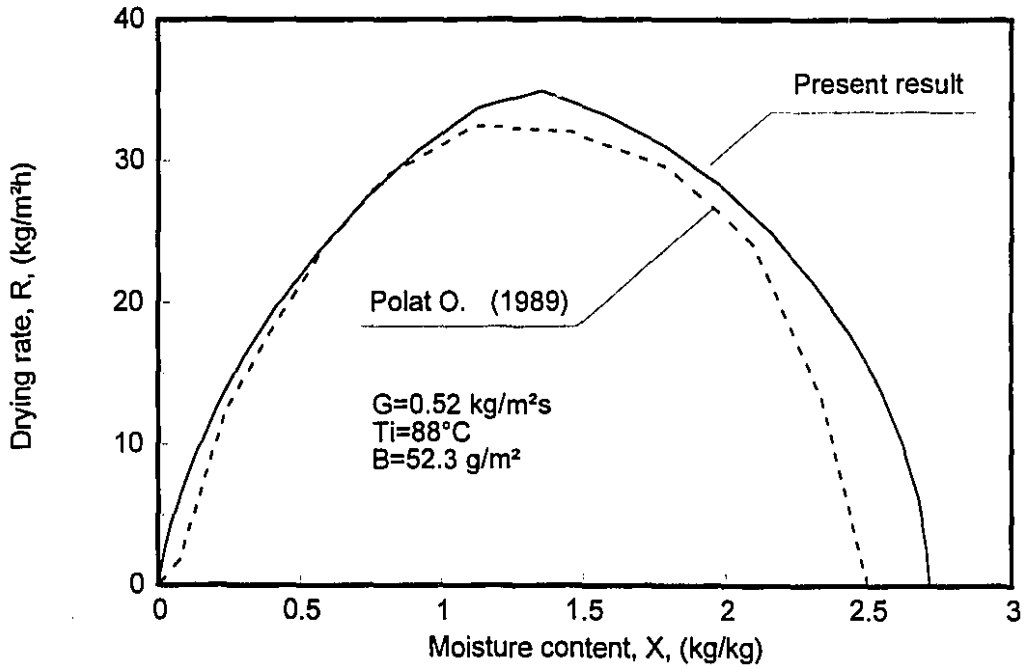

Figure 3.9 Overall performance test of the present apparatus

3.3.4 Demonstration of repeatability

Before the experimental program began a test of the repeatability of the apparatus was conducted at the highest overall flow rate planned, G=1.45 kg/m²s, for two levels of air temperature, 25 °C and 88 °C, the limits for the present study. The through flow ratio q=16.8% was selected to have relatively equal contribution of water removal by the impingement exhaust and through flow exhaust in the constant rate period. Paper of around 50 g/m² basis weight was used to minimize the influence of paper structure on the process.

Figure 3.10 shows the results. The total drying rate sums the impingement and through flow contributions. Its repeatability rests on that of the impingement and through flow components.

For the tests run with ambient temperature air the constant rate period values were replicated within 3% for the through flow exhaust contribution and within 3.5% for the impingement exhaust. The overall drying rate in the constant rate period replicated to within 3.5%. At drying air temperature of 88 °C, the drying rate curves replicated equally well.

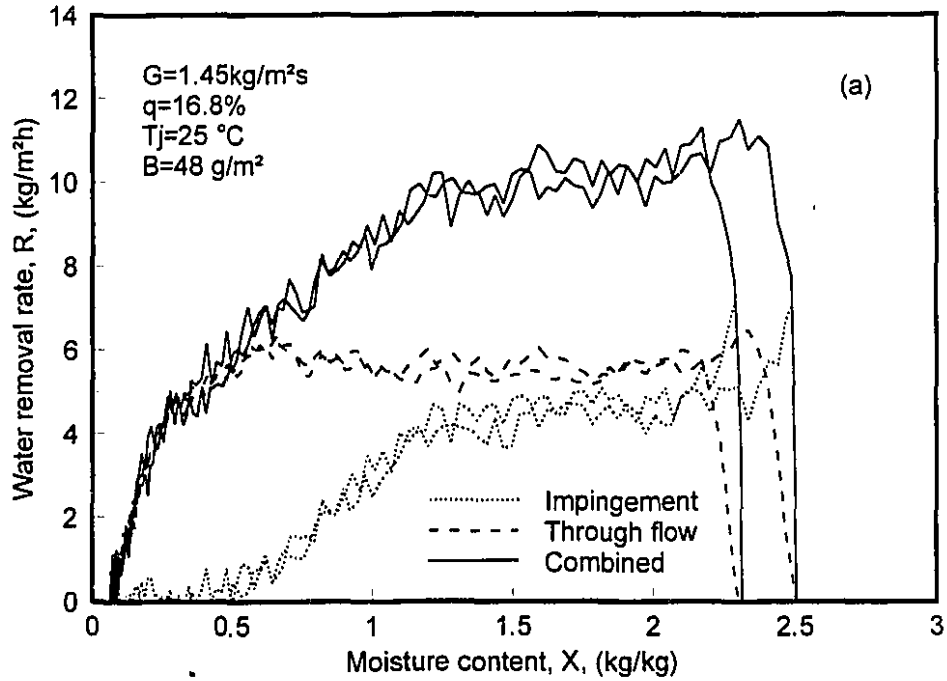

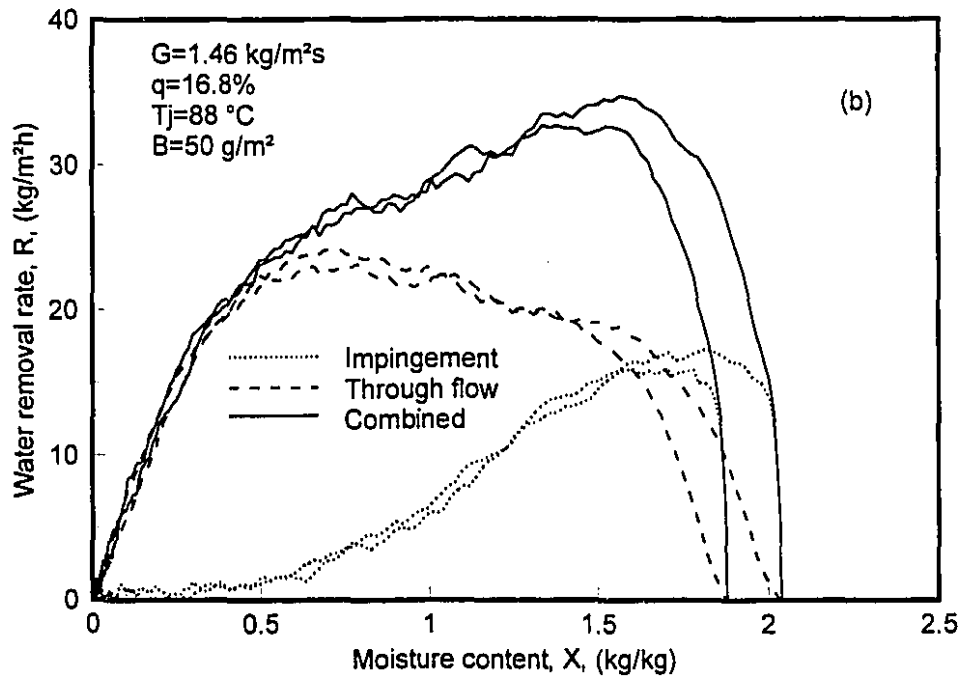

Figure 3.10 Demonstration of repeatability

Chapter 4 Impingement Drying of Paper

4.1 Introduction

Impinging jets are widely used to dry light weight grades of paper, for which they provide the principal drying mechanism in the process known industrially as the Yankee dryer. There is an extensive literature of numerical and experimental studies of pure impingement heat transfer, which is summarized in two reviews, Polat S. et al. (1988) and Polat S. (1993). By contrast, there is little published experimental work on the impingement drying of paper, of which a notable contribution has been by Bond et al. (1991, 1992, 1994a, 1994b). Thus the present study, although undertaken as one element in a research plan for the study of combined impingement and through air drying of paper, also provides measurements supplementing the limited information available on impingement air drying of paper.

4.2 Experimental conditions

The effects of paper parameters and drying conditions were studied through a series of 59 experiments using nozzle set #1, which had a nozzle to paper spacing H/d = 5.0 and nozzle open area ratio f = 3.1%. The effect of nozzle geometry was studied in two supplemental sets of experiments with a single selection of paper parameters and drying conditions but with two nozzle arrays, #2 (H/d = 7.6, f = 1.4%) and #3 (H/d=8.5, f= 2.7%). With nozzle sets #2 and #3, the number of experiments made was 13 and 11, respectively. Each of the 83 drying experiments used a handsheet freshly made from dry unbleached standard laboratory kraft pulp from 100% black spruce, as recorded in Appendix F. Experimental procedures are detailed in Appendix B. Table 4.1 provides the test conditions for jet Reynolds number, Re ; impingement air mass flow velocity, G;

equivalent jet velocity at standard conditions, U_j ; nozzle exit air temperature, T_j ; paper basis weight, B; and paper initial moisture content, X_o .

Table 4.1	Experimental conditions for impingement drying		
	Nozzle set #1	Nozzle set #2	Nozzle set #3
Re	450 - 5300	770-9200	940-11100
G, kg/m^2s	0.125 - 1.45	0.125 - 1.45	0.125 - 1.45
U_j, $Std.m^3/m^2s$	3.13 - 36.3	6.92 - 80.3	3.59 - 41.6
T_j, °C	22, 45, 65, 90	22	22
B, g/m^2	20, 25, 30, 40, 50	50	50
X_o, kg/kg	1.5-3	1.5-3	1.5-3

4.3 Drying history curve

Shown in figure 4.1 is a typical set of curves which show the drying history for impingement air drying of paper with the lowest and highest jet temperatures used, 22 ° and 88 °C. Throughout each experiment paper temperature at the support side, T_p , impingement exhaust temperature, T_e , and air humidity of the impingement exhaust, Y_e , were monitored continuously, which enabled determination of the complete drying rate - paper moisture content relationship. The wet sheet was introduced into the drying chamber at an initial moisture content X_o of 1.78 kg water/kg dry fiber for figure 4.1 (a), 2.96 kg/kg for figure 4.1 (b). As data acquisition frequency was selected in the range of 0.5 to 10Hz, the drying rate curves were obtained in essentially continuous form with instantaneous drying rate R and moisture content X calculated from the Y_e measurement. The drying rate data points obtained experimentally are shown on figure 4.1, but to facilitate visual examination of the results, the temperatures are displayed as straight lines connecting the experimental data. Unless necessary, all subsequent graphs simply show such straight lines rather than the very large number of actual data points.

In figure 4.1 (a) the initial short duration sharp spike on the drying rate curve is accompanied by an equally sharp drop in paper temperature, T_p . This spike in the R - X

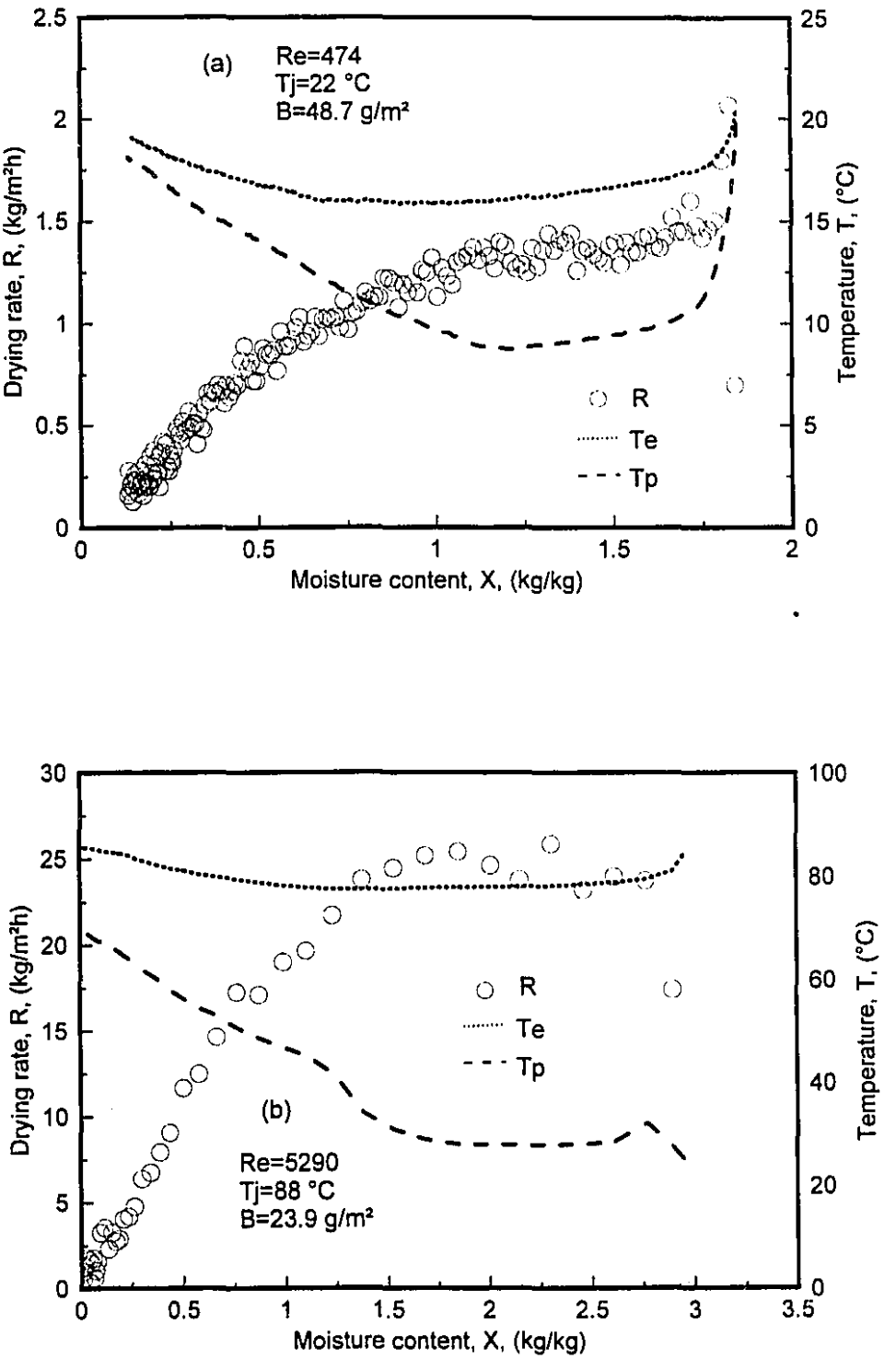

Figure 4.1 Typical drying history curves, nozzle #1

curve results from the initial temperature of the paper, 22 °C, being substantially above the wet bulb temperature, 7.3 °C, to which the paper quickly drops when drying starts, hence the large spike in R until the sheet has cooled to the wet bulb temperature. Thereafter the drying rate remains at R_c, the constant drying rate.

During the constant rate period all conditions remain approximately constant as sheet moisture content decreases. When the paper moisture content decreased to the value of X_c, the critical moisture content, moisture no longer reaches the sheet surface at the rate it can be removed by the impingement flow, at which point the period of falling rate starts. As paper moisture content decreases during the falling rate period the paper temperature, T_p, and the impingement exhaust temperature, T_e, increase to approach T_j while the drying rate R decreases towards zero for fully dry paper. Similar results can be seen from figure 4.1 (b) except that there is no initial spike on the drying rate curve as on figure 4.1 (a) because at the jet temperature of 88 °C the wet bulb temperature is 29 °C, higher than the initial paper temperature of 22 °C. Thus during the initial transient period, T_p and hence R increase quickly to the steady values maintained during the constant rate period with the sheet at the wet bulb temperature of the air jets. For impingement drying of material as thin as paper such transient periods are of very short duration and in general is of negligible importance in the total drying process.

With nozzle set #1 and for paper basis weight of 50 g/m^2, figure 4.2 shows the effect of jet temperature on impingement drying rate curves at two levels of jet Reynolds number, 500 and 2000. With the dry air used, dew point of -20 °C, the jet temperature at which the initial transient period vanishes is about 63 °C, for which the wet bulb temperature is 22 °C. Thus on figure 4.2, large spikes at the start of the R - X curves are seen for the cases of air at ambient temperature, small spikes occur for T_j=46 °C, while there is no perceptible transient period for T_j=66 °C. For the highest value of T_j=93 °C, there is a short transient period of the opposite kind, i.e. the paper warms quickly from ambient temperature to the wet bulb temperature of about 30.3 °C.

Figure 4.3 shows the effect of jet Reynolds number on impingement drying rates with nozzle set #1, paper basis weight 50 g/m^2 and at two levels of temperature, the

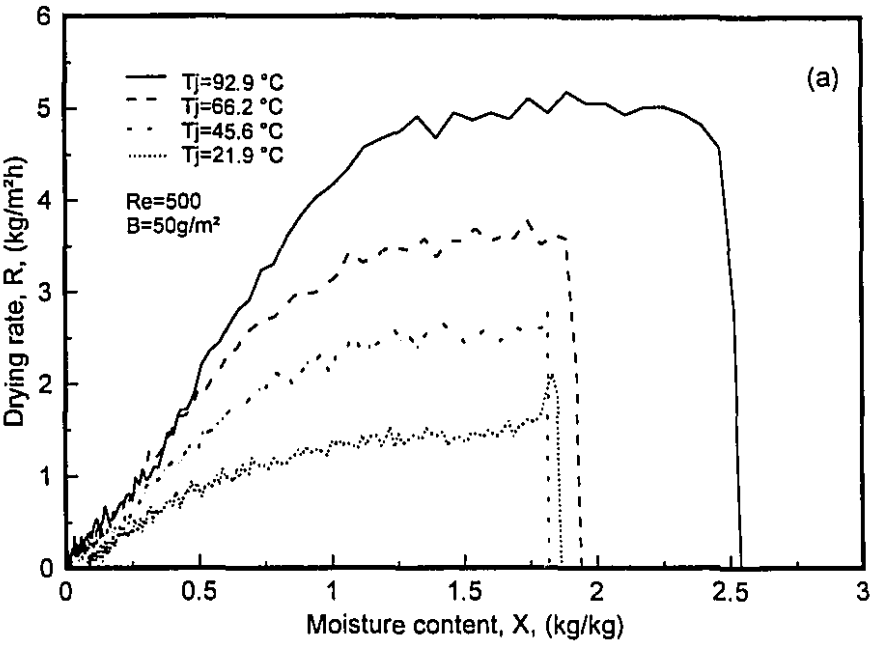

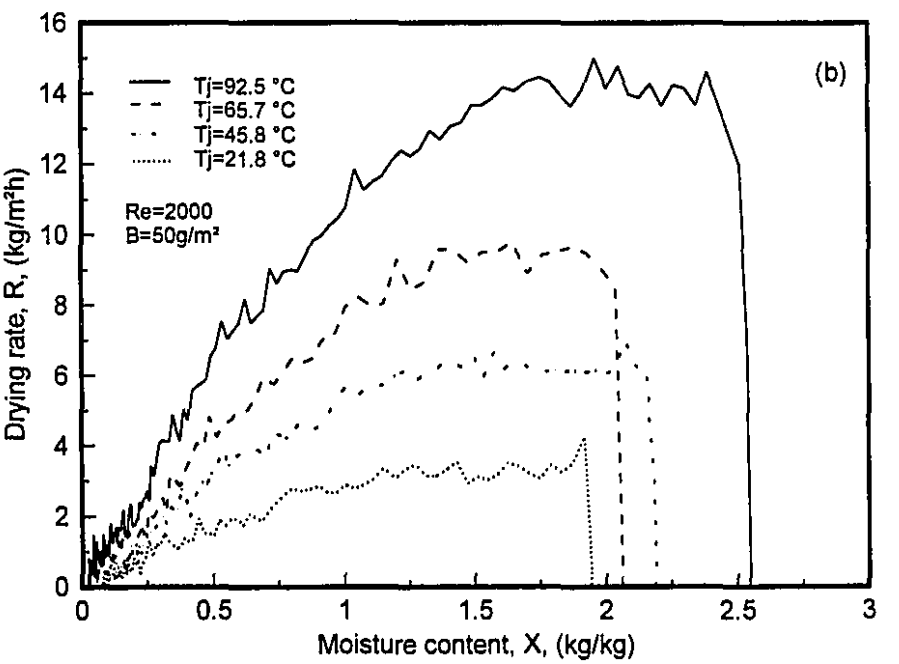

Figure 4.2 Effect of jet temperature on drying rate curves: (a) low Re (b) intermediate Re

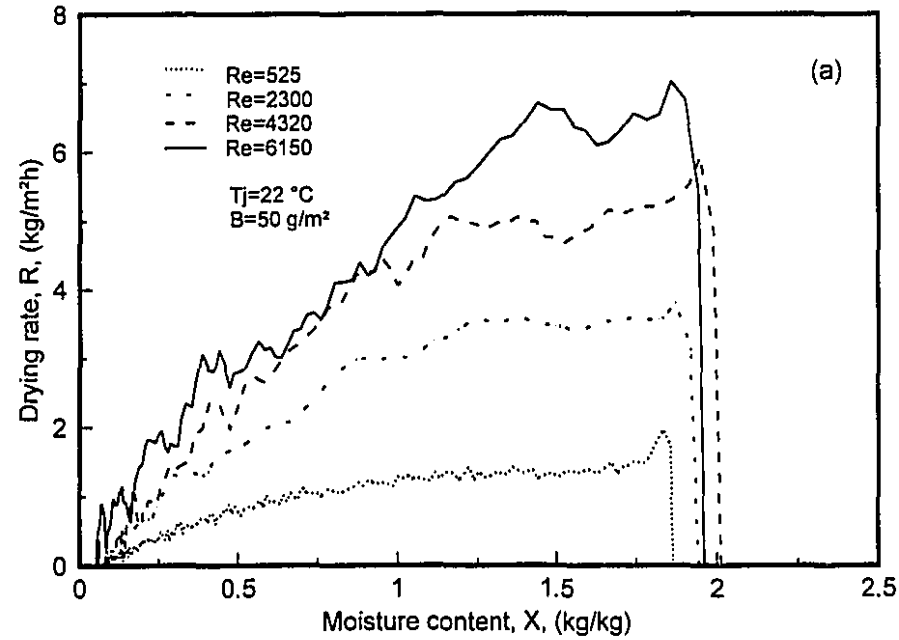

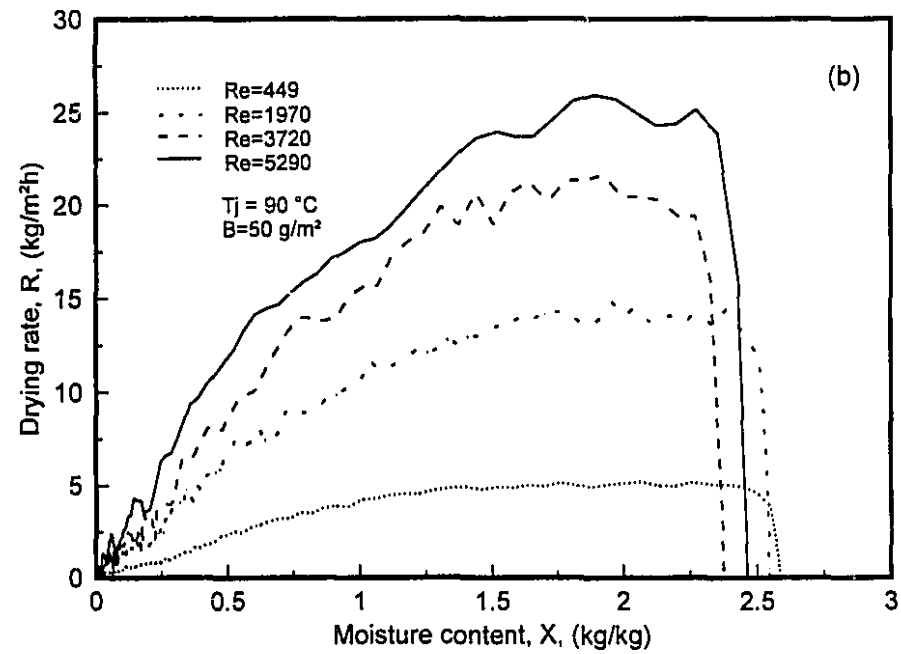

Figure 4.3 Effect of Reynolds number on drying rate curves: (a) low Tj (b) higher Tj

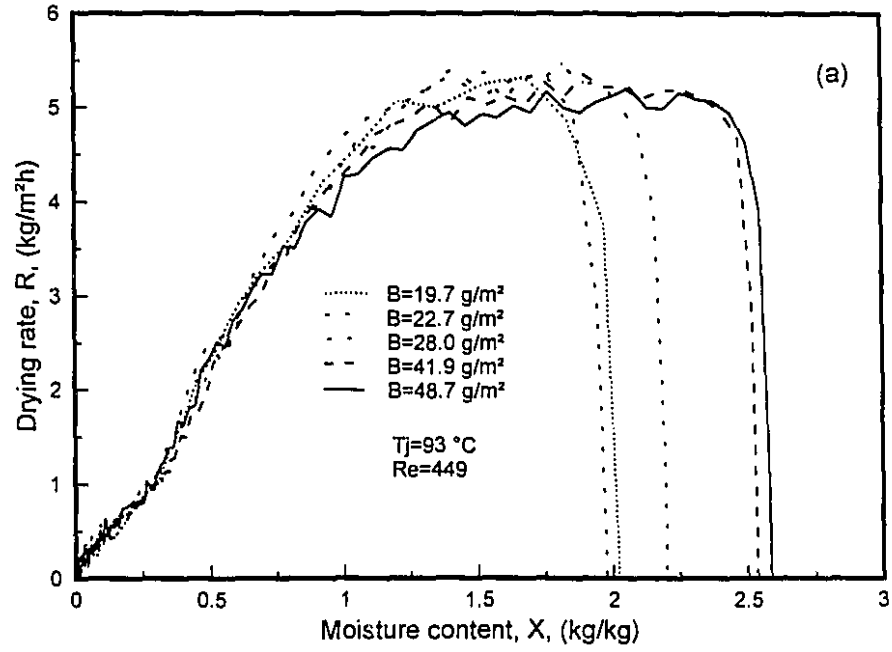

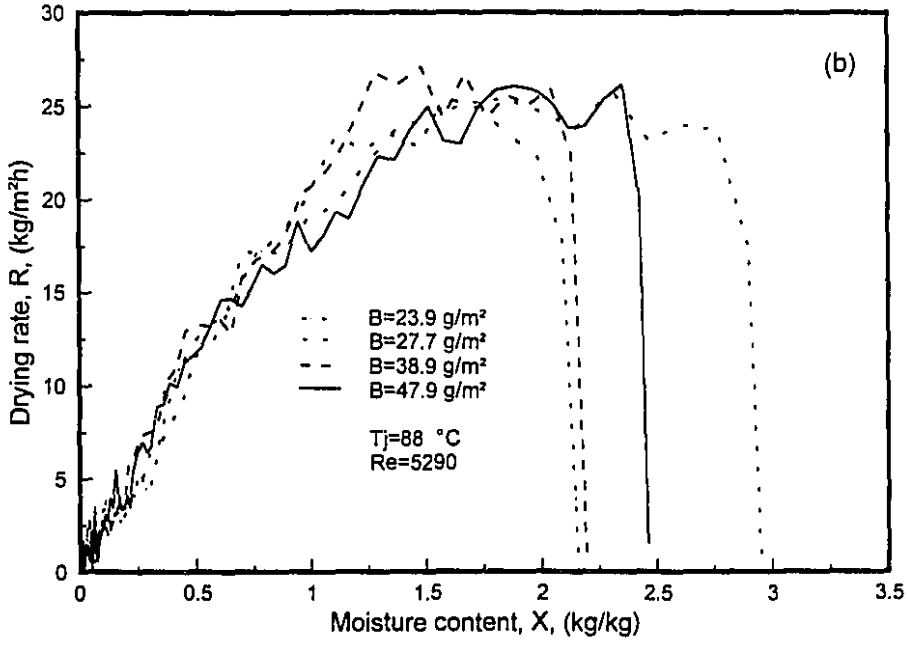

Figure 4.4 Effect of basis weight on drying rate curves: (a) low Re (b) high Re

lowest and the highest for the present study. As Re is increased from 449 to 6150, the extent of constant rate period decreases, i.e. the critical moisture content increases.

For nozzle set #1 and nozzle exit temperature about 90 °C, figure 4.4 shows the paper basis weight effect on impingement drying rate at two levels of jet Reynolds number, 449 and 5290, the lowest and highest used for nozzle set #1 at this jet temperature. During the constant rate period the drying process is determined externally, i.e. completely heat transfer controlled, independent of sheet conditions. The drying rate, therefore, should be independent of paper basis weight, as is seen on figure 4.4. For the lowest B, lowest X_o shown, the drying rate reaches the constant drying rate value only momentarily before the falling rate period starts.

4.4 Quantitative representation of drying rate curves

4.4.1 Conventional treatment

In drying research it has long been general practice (Sherwood 1941, Bagnoli et al. 1963, Porter et al. 1973, Porter et al. 1984) to represent drying rate - moisture content curves by two parameters, R_c, the value during the constant rate drying period, and X_c, the critical moisture content which marks the transition from the constant rate to the falling rate period, with the R-X relationship during the falling rate period conventionally taken as linear. The latter is not just as a convenient empirical approximation but is based on the theoretical analysis of Sherwood (1929). According to Sherwood, when the drying rate at a solid surface is controlled by the rate of internal diffusion of liquid moisture to that surface, the moisture distribution - time relation follows equation 4.1.

$$\frac{\partial X(\theta,z)}{\partial \theta} = D \frac{\partial^2 X(\theta,z)}{\partial z^2} \qquad (4.1)$$

where D is the liquid diffusivity, taken as a constant; z, depth from drying surface; θ, drying time from the start of the falling rate period; $X(\theta, z)$, local moisture content driving force. For the case of a slab drying from one surface with uniform moisture content at

θ=0 and the mass transfer resistance in the adjacent vapor phase negligible relative to the diffusion resistance in the drying material, and assuming the evaporation takes place from the surface at equilibrium, the solution for average moisture content X in the solid is:

$$\frac{X - X_e}{X_c - X_e} = \frac{8}{\pi^2} \sum_{i=1}^{\infty} \frac{e^{-D\left(\frac{\pi}{2L}\right)^2 (2i-1)^2 \cdot \theta}}{(2i-1)^2} \qquad (4.2)$$

where X_c is the critical moisture content; X_e, the equilibrium moisture content; L, the thickness of drying material. Similar results were obtained by Sherwood (1931) for a parabolic moisture distribution X(z) at θ=0, the common case at the end of the constant rate period.

Sherwood (1941) pointed out that because the sum of subsequent terms of equation 4.2 is much smaller than the first, the solution may be approximated by the first term only. Expressed in terms of drying rate, R = - ρL dX/dt , with ρ representing the density of the drying material, it follows that

$$R = \frac{\rho D \pi^2}{4L}(X - X_e) \qquad (4.3)$$

This analysis provides the theoretical basis for the commonly used approximation of the linear R - X relation during the falling rate period. It predicts a linear decline of moisture content with drying time in the constant rate period and an exponential decay of X with t in the falling rate period. Sherwood assumed that moisture movement follows a Fick's law diffusion relation and that capillary and gravitational forces were negligible. However for the case of moisture transport in the solid controlled by capillary moisture movement, i.e. by the Hagen-Poiseuille equation:

$$\Delta P = \frac{2\sigma \cos\theta}{r} = \frac{8\rho\nu u L}{r^2} \qquad (4.4)$$

Porter et al. (1984) reported that the linear relation between drying rate, R, and moisture content, X, remains a fairly accurate approximation despite its limitations (Sherwood and Comings 1933, Hougen et al. 1940). Thus in the conventional representation, drying rate curves pass through the point (X_c, R_c) at the transition from the constant to the falling rate drying period, with a linear R-X relation thereafter towards R=0 at the equilibrium

value of moisture content, X_e , for the drying conditions used. In the present case, X_e=0 effectively.

This procedure has generally been applied without much difficulty because for moderate intensity drying conditions typically used the constant rate period is relatively long and ends with a clearly identifiable critical moisture content, X_c . For example, Wenzel and White (1951) and Chu et al. (1959) observed such a linear falling rate period when drying a bed of sand in a parallel flow dryer with superheated steam. Bond (1991) also used this linear relationship in fitting his drying rate - moisture content measurements for the impingement drying of paper in air and in superheated steam.

This conventional treatment of drying rate curves as two straight lines intersecting at the point (X_c , R_c) is applied to the present study by obtaining the statistical best fit values of the two parameters, R_c and X_c, thereby eliminating subjectivity in R_c and X_c determination. This procedure was carried out using a standard regression package, SYSTAT, to search for the best fit values of these two parameters for representing the data as two straight lines, i.e. $R=R_c$ for $X>X_c$, and a linear R-X relation from $X=X_c$ down to X=0. The results of applying this procedure to four typical sets of drying rate data are shown on figure 4.5. The short initial transient period was excluded in the data processing. Inspection of these four sets of data and drying rate curves shows that the conventional treatment does not provide an adequate representation of the experimental measurements in the falling rate period. This method was therefore rejected for use in the present study.

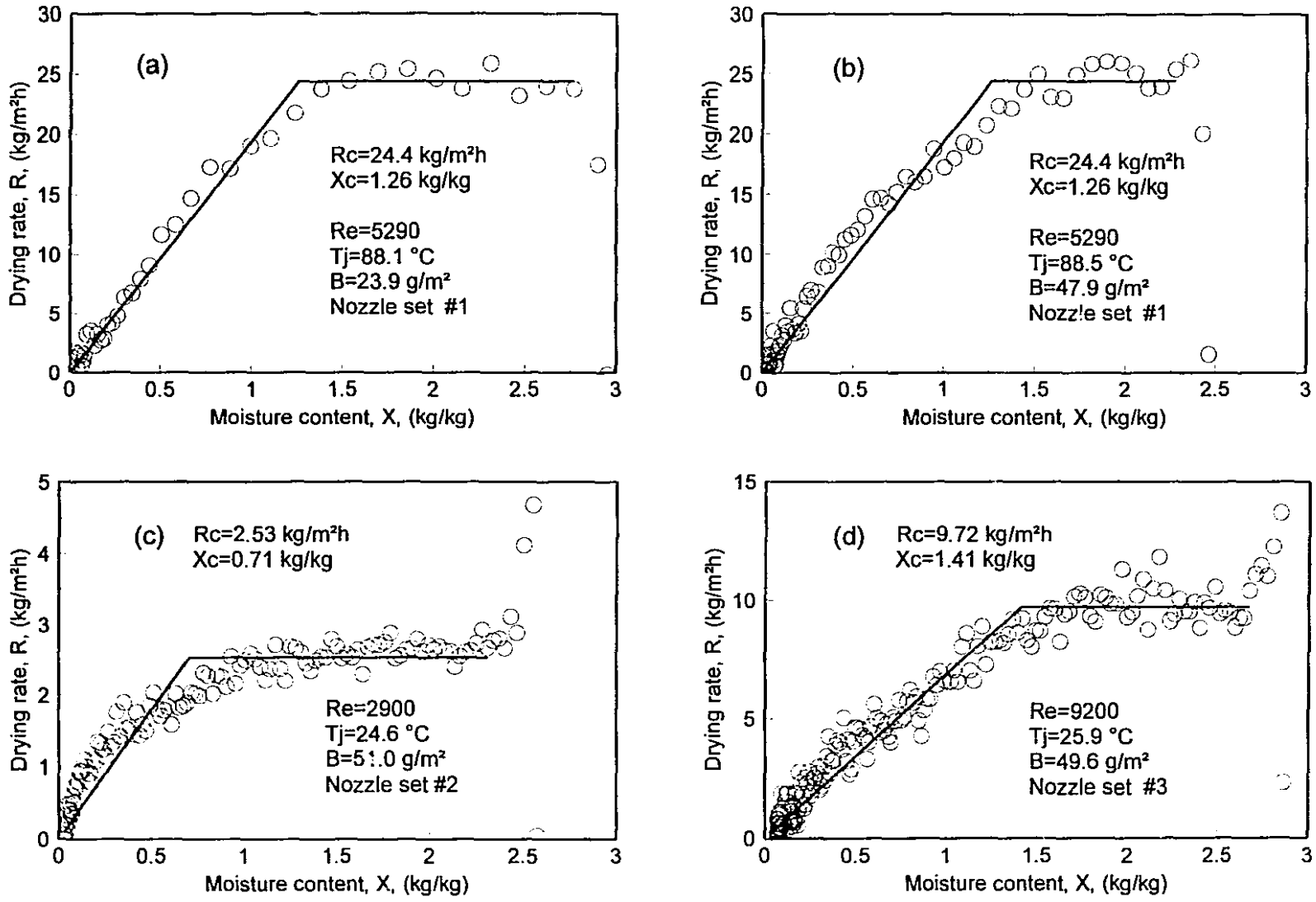

Figure 4.5 Quantitative representation of drying rate curves: conventional approach

4.4.2 Churchill asymptotic treatment

In a series of definitive publications Churchill and associates (1972, 1973, 1974, 1983, 1992) developed a rational, if empirical, procedure for modeling rate data of the type which extend from a region of one asymptotic behavior through a transition region to another asymptotic relation. They tested this concept for a number of systems of transport phenomena, but not for drying. This procedure, often referred to as the Churchill & Usagi Equation, abbreviated as CUE, may be expressed as:

$$y^n(x) = y_0{}^n(x) + y_\infty{}^n(x) \qquad (4.5)$$

where $y_0(x)$ = known asymptote for $x \to 0$

$y_\infty(x)$ = known asymptote for $x \to \infty$

n = an exponent, the only parameter in the CUE approach

The two asymptotes must have a single intersection and the chosen asymptotes be free of singularities.

It is of interest to note that the above equation is in the form of the famous theorem of Pierre de Fermat, which appeared in 1637 in the margin of the French mathematician's copy of Diophantus' *Arithmatic.* Fermat's theorem states that the equation $x^n + y^n = z^n$, where x, y, z and n are positive integers, has no solution if n is greater than 2. Over the past three and half centuries none of the numerous attempts to prove this theorem succeeded. Recently Andrew Wiles, an American mathematician (Cipra, 1993) claimed to have proven this historic theorem. Currently Wiles' proof of approximately 200 pages, which he acknowledges as incomplete, is being examined by leading mathematicians around the world.

Equation 4.5, however, does not depend on Fermat's theorem, but simply states that if the relation is known at two limiting conditions, $y_0(x)$ and $y_\infty(x)$, then there exists an n for the CUE to fit data of $y(x)$ for all the intervening conditions. While this relation applies for $0<x<\infty$, for cases involving negative x, or x in a definite domain, a transformation can always make the CUE applicable. If $y(x)$ is an increasing function of x as $x \to \infty$ then n will be positive; otherwise n is negative. Negative values of n can be

avoided by redefining a variable as $z(x)=1/y(x)$. The parameter n provides a measure of the deviation of the behavior from that of the asymptotes. Thus when n is large, the deviation is small and the region of transition between the asymptotes is small, while for a small value of n the deviation is large, with the large region of transition leaving only a small region of asymptotic behavior.

The CUE approach may be applied to the present drying rate data by considering there to be two linear asymptotic R-X relations, one as X approaches 0, equation 4.6, the other as $X \rightarrow \infty$, equation 4.7. The form of the CUE model for the present case may then be obtained as equation 4.8.

$$R(X) = a\,X \qquad \text{Asymptote for } X \rightarrow 0 \qquad (4.6)$$

$$R(X) = R_c \qquad \text{Asymptote for } X \rightarrow \infty \qquad (4.7)$$

$$R(X) = \left[R_c^{-n} + (a\,X)^{-n}\right]^{-\frac{1}{n}} \qquad \text{CUE form for all values of X} \qquad (4.8)$$

It is important to note that no such parameter as X_c exists in the CUE analysis because equation 4.8 is a smooth curve from the start to the end of drying. With the CUE approach the constant drying rate may either be asymptotically approached at large X or R_c may be predicted to be outside the range of R-X measurements.

The fitting of equation 4.8 to the same four sets of drying rate data was carried out with the same SYSTAT regression package used in fitting the conventional drying model, this time yielding for each drying condition a best fit set of values of the three parameters R_c, a and n. Although Churchill (1993) noted that n could be rounded off to an integer or ratio of integers owing to its insensitivity in affecting the general correlation, here the values of n were not rounded off. As in the conventional treatment, the data in the short initial transient period were excluded from the treatment. The results of the CUE fitting appears on figure 4.6.

While in the previous section the conventional drying model could clearly be rejected on the basis of the fit to the data, the CUE fits are satisfactory. The asymptotic slope, a, of the CUE procedure as $X \rightarrow 0$ may be compared with the corresponding slope, R_c/X_c, provided by the conventional approach for the falling rate period. These data for the same four cases (a), (b), (c) and (d), of figures 4.5 and 4.6 are summarized in Table

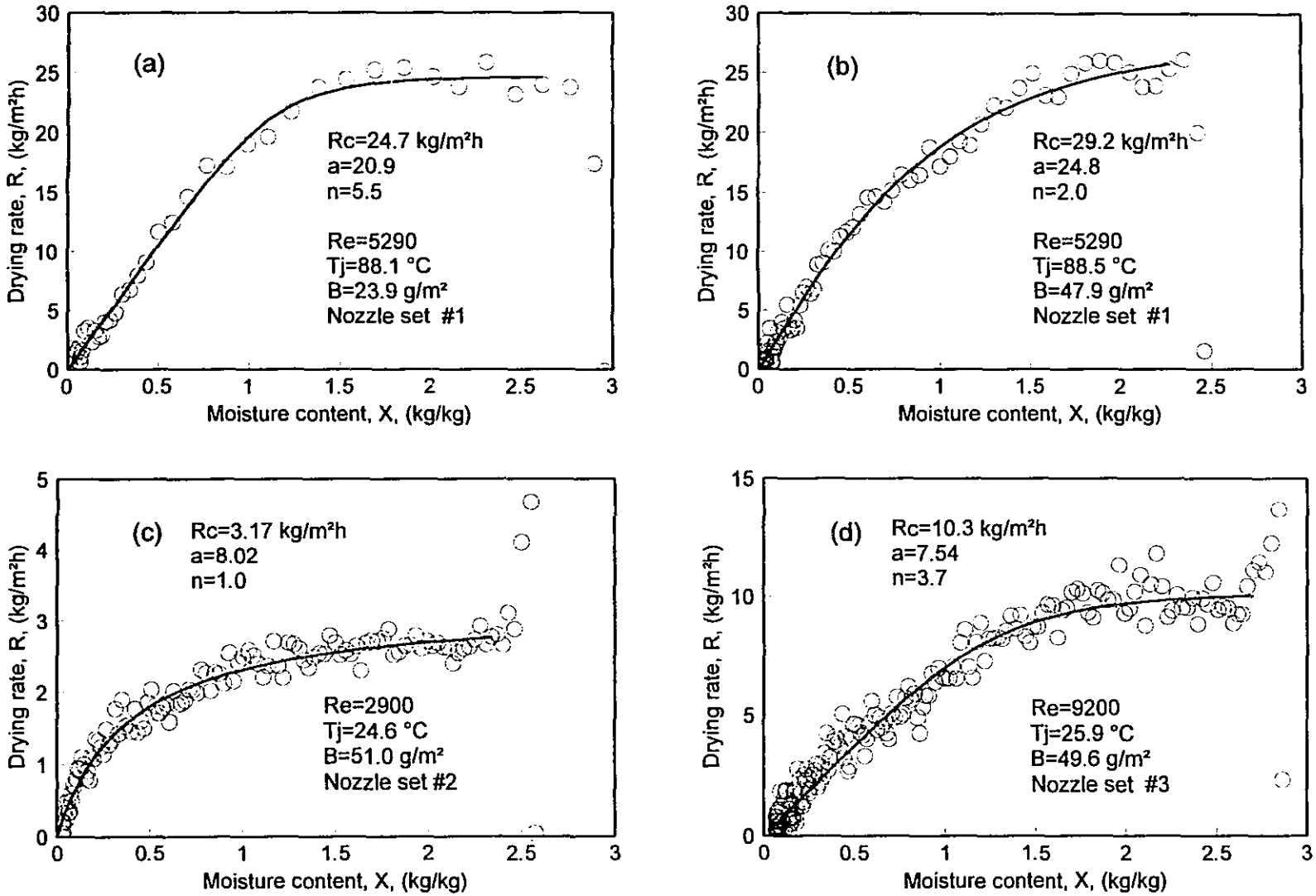

Figure 4.6 Quantitative representation of drying rate curves: CUE asymptotic approach

4.2. For cases (b), (c) and (d), it is evident from figure 4.5 that as $X \rightarrow 0$, the actual slope of the R-X curve is much greater than that given by the conventional treatment. For these cases the values of the CUE limiting asymptotic slope R/X=a, Table 4.2, are much larger than the corresponding values of R_c/X_c from the conventional treatment, with the latter clearly providing a poor representation of the actual R-X curve.

Table 4.2 Comparison of fitting results from conventional and CUE treatment

	Conventional treatment			CUE treatment	
Case	R_c	X_c	R_c/X_c	R_c	a
(a)	24.4	1.26	19.4	24.7	20.9
(b)	24.4	1.26	19.4	29.2	24.8
(c)	2.53	0.71	3.56	3.17	8.02
(d)	9.72	1.41	6.9	10.3	7.54

Although the conventional treatment is not acceptable for the falling rate period, it provides a good estimate of R_c. For case (a) on Table 4.2 and figures 4.5 and 4.6, the case with the longest, best defined period of constant rate drying, the value of R_c by the CUE method is only slightly higher than the best estimate of R_c from the conventional technique. When the constant rate period is short, the R_c value from the CUE method is substantially higher than the best estimate values of R_c by the conventional method. Thus for cases (b) and (c) the CUE method estimate of R_c is 20 -25% too high, as may be seen in Table 4.2 by comparison with the values of R_c determined conventionally. As short constant rate periods are the norm for the present study, the values of R_c determined by the CUE method are generally unrealistically high.

A basic feature of the CUE treatment is that it gives a continuous falling R-X relation from the beginning to the end of drying with no value of critical moisture content, X_c, i.e. no constant rate period. For cases of drying which exhibit only falling drying rate behavior, the CUE would give a good empirical fit and R_c becomes simply a fitting parameter, not to be interpreted as the value of constant drying rate. As the present case displays a constant rate period although typically quite a short one, the CUE method was therefore rejected for representing drying rate curves.

4.4.3 Power law treatment of the falling rate period

There is a practical alternative treatment which constitutes an intermediate position between the conventional and the CUE approaches. Thus one may retain the valid and useful concept of a constant rate and a falling rate period with the transition on the R-X curve at the critical moisture content X_c , and the constant drying rate R_c . Instead of forcing the falling rate period to be linear with X as does the conventional treatment for the entire period and the CUE model for an R→asymptote, it may be taken as nonlinear as a power law relation,

$$\frac{R}{R_c} = \left(\frac{X - X_e}{X_c - X_e}\right)^n$$

As $X_e \to 0$, hence $(X-X_e)/(X_c-X_e) \to X/X_c$, and the power law relation simply becomes:

$$\frac{R}{R_c} = \left(\frac{X}{X_c}\right)^n \tag{4.9}$$

with

$$\begin{cases} R = R_c & \text{at } X = X_c & \text{the critical point} \\ R = 0 & \text{at } X = 0 & \text{the final point} \end{cases}$$

For n=1 this approach reduces to the conventional treatment with R - X linear over the entire falling rate period. The power law approach has barely appeared in drying literature, having only been proposed by Keey (1972) and suggested by Strach for the drying of colloid materials in food industry (Gineburg, 1973). It has never been applied for drying paper.

For the same sets of typical drying rate data tested on figures 4.5 and 4.6, the results for the power law treatment are shown on figure 4.7. This model produces a clear intersection of the constant and falling rate periods. The disadvantage of a slightly exaggerated abruptness of the constant rate - falling rate period transition is more than compensated by obtaining a value of X_c which is not excessively sensitive to experimental variability around this transition region. The use of any model requiring the falling rate curve to be asymptotic to the constant rate line makes the value of X_c where

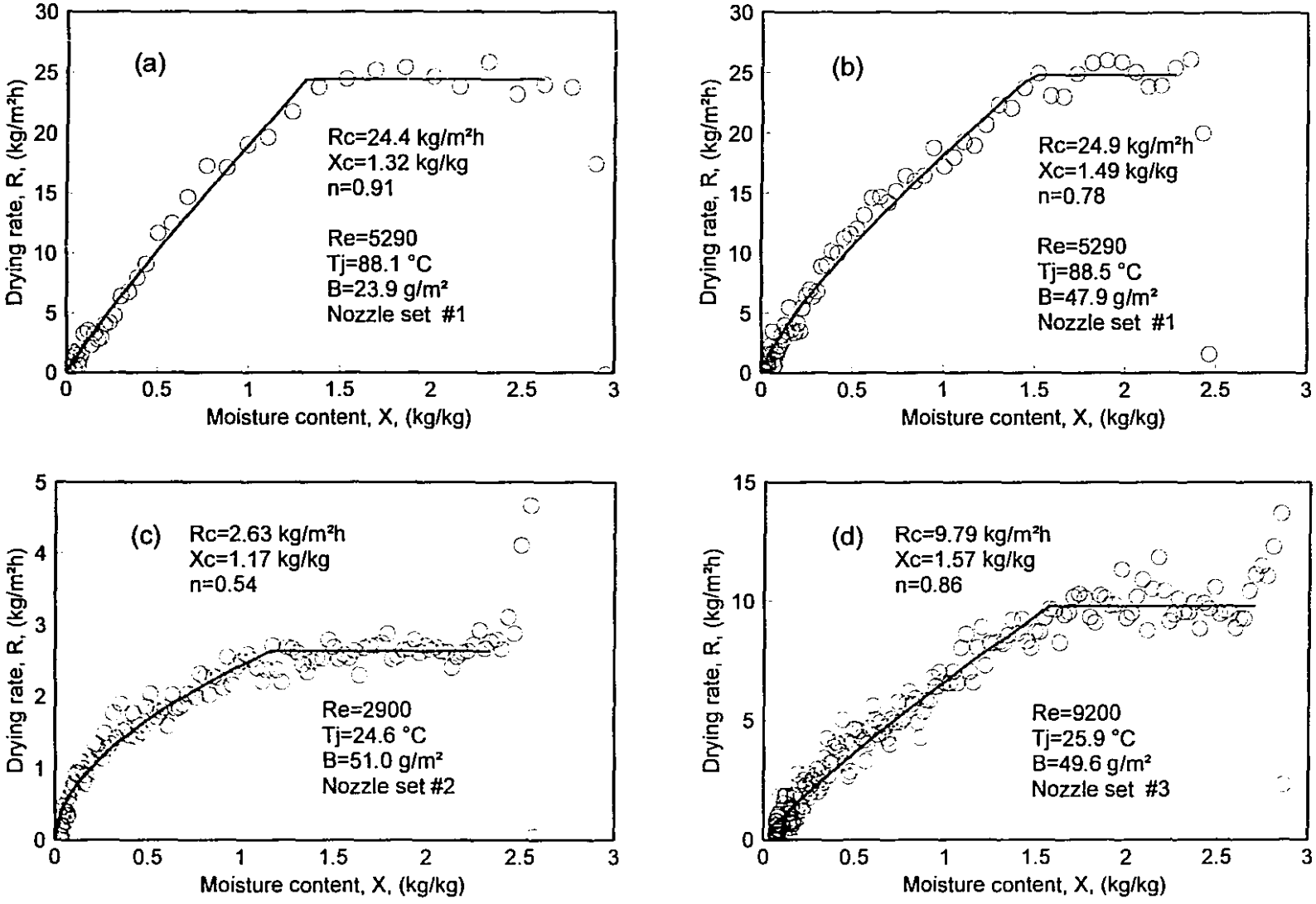

Figure 4.7 Quantitative representation of drying rate curves: power law approach

these two lines merge extraordinarily sensitive to normal small variability of measurements. Even for drying rate curves defined by a very large number of data points, as in the present case, such models by their nature will produce widely fluctuating and hence misleading values of critical moisture content.

For the same four test cases, the R_c values by the three approaches and the X_c values obtained are compared in Table 4.3. As noted earlier, the CUE method gives no critical moisture content and gives values of R_c which generally unrealistically high. With respect to R_c, there is little difference between the values produced by the conventional and the power law treatment. The major advantage of the latter over the former, in addition to the much better fit of the falling rate period data, concerns X_c. One consequence of the conventional treatment forcing a constant R - X slope for the entire falling rate period is that the predicted values of X_c are always unrealistically low. Only in the easy case (a) with its exceptionally long constant rate period is the X_c value determined conventionally not much below the X_c value from the power law treatment. In the more typical cases (b), (c) and (d), the values of X_c determined conventionally are seen in Table 4.3 to be, respectively, 15%, 40% and 10% below those obtained by the power law treatment. For all runs but three of very low initial moisture content where no constant drying rate occurred, the power law method provides a good quantitative representation of the entire drying rate behavior, and gives realistic values of the three quantitative parameters, R_c, X_c and n.

Table 4.3 Comparison of R_c and X_c from different treatments

	Conventional		CUE	Power law	
Case	R_c	X_c	R_c	R_c	X_c
(a)	24.4	1.26	24.7	24.4	1.32
(b)	24.4	1.26	29.2	24.9	1.49
(c)	2.53	0.71	3.17	2.63	1.17
(d)	9.72	1.41	10.3	9.79	1.57

The CUE approach forces the falling rate period to end with a linear R-X region while the power law treatment reverses this, with the $R \rightarrow 0$ region having a maximum nonlinearity and highest sensitivity to moisture content. Having the greatest nonlinearity

of R - X at the end of the falling rate period is consistent with the moisture diffusivity - moisture content measurements for paper. Thus the D -X relationship for paper as determined by Lee and Hinds (1981) and Navarri et al. (1992) shows moisture diffusivity D dropping very sharply at low moisture content, thus reducing the rate of transport of water to the impingement surface and thereby sharply reducing R. Thus for this additional reason the power law representation of the falling rate period was adopted for the impingement drying of paper. A detailed analysis of the 80 sets of values of R_c , X_c and n determined by the power law method is given subsequently.

4.5 Analysis of results

4.5.1 Constant Drying Rate, R_c

Figure 4.8 shows the effect on the constant drying rate, R_c , of (a) the temperature driving force, (b) air mass flow rate and (c) nozzle geometry and jet Reynolds number, with the values of R_c determined as described in section 4.4.3. As the analysis of section 4.3 confirmed that paper basis weight has no effect on constant drying rate, this parameter does not appear in the treatment of this section.

In impingement heat transfer the difference in temperature between the nozzle exit and the impingement surface, T_j - T_s , is the driving force for convective heat transfer. The present measurements confirmed that during the constant rate drying period the paper temperature measured at the support side of the sheet equals the wet bulb temperature. Since for the air-water system the wet bulb temperature which is determined by a dynamic balance of rate process is equal to the thermodynamically determined adiabatic saturation temperature of the inlet air, T_{as} , the ΔT for impingement heat transfer may be expressed as T_j - T_{as} . For all four levels of air mass flow rate used, a linear relationship was found between constant drying rate and temperature driving force, ΔT, figure 4.8(a). This linear relation is expected because the small variation of ΔT from 14.7 to 30 °C when T_j changes from 22 to 90 °C makes negligible the effect of evaporation flux on

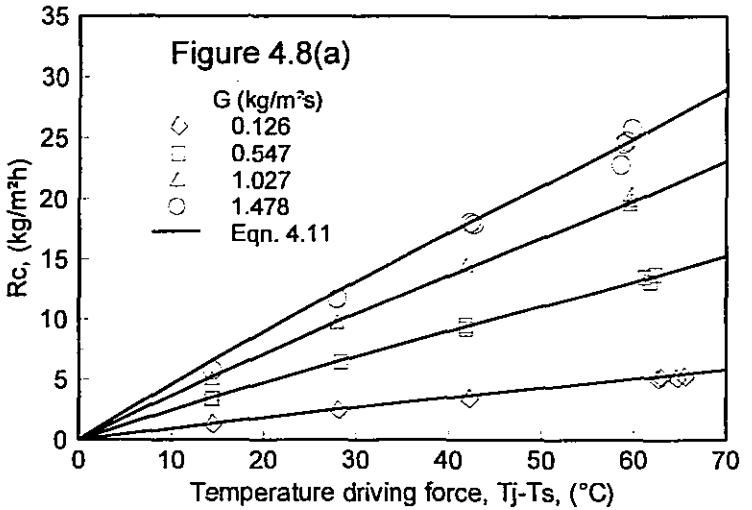

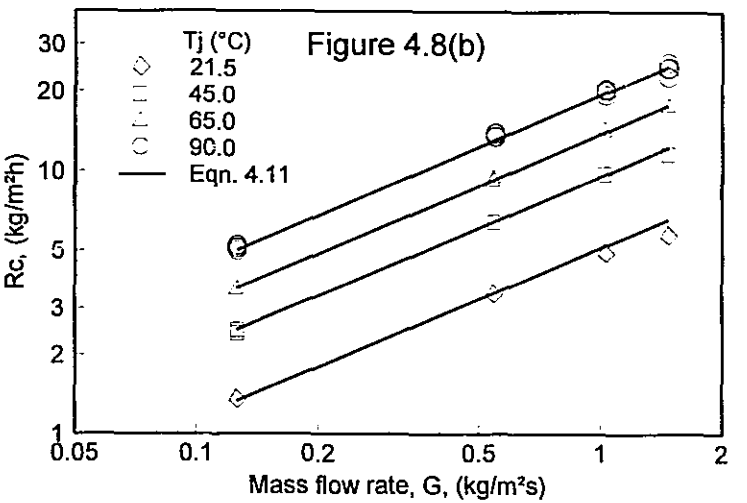

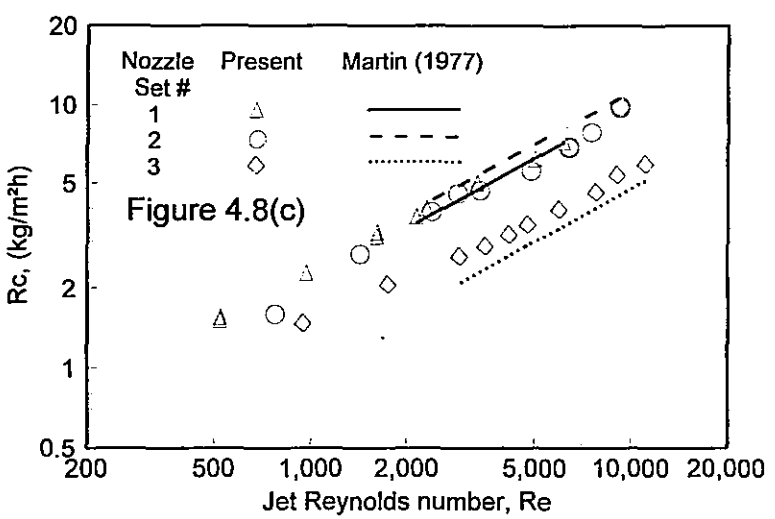

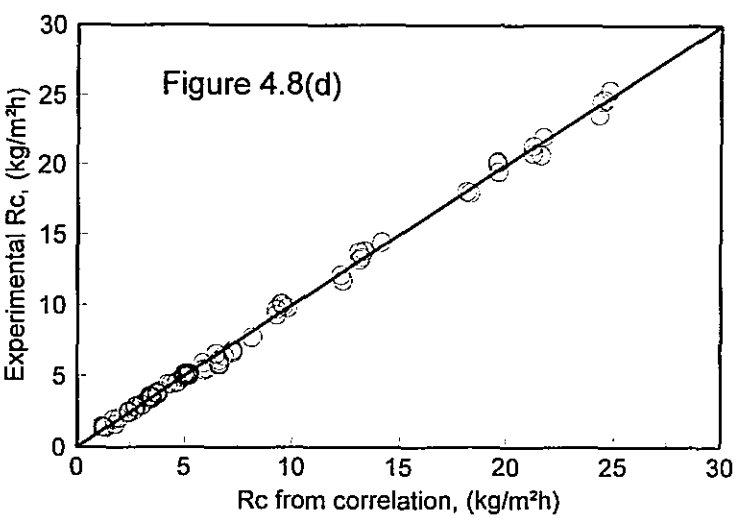

Figure 4.8 Constant drying rate relations (a) Rc - ΔT relation, (b) Rc - G relation, (c) Rc - Re relation; (d) Comparison of Rc by experiment and by correlation

impingement heat transfer coefficient, h, as Biot number is so small. Based on heat and mass balances, the constant drying rate becomes $R_c=h\,\Delta T/\lambda$. From the lowest to highest air temperature used the variation in T_{as} from 7.3 to 30 °C corresponds to less than a 2% decrease of λ, the latent heat. The convective heat transfer coefficient, h, also decreases to the same extent at each mass flow rate level for the same change of T_{as} . This decrease in h is not contradictory to the findings of Das et al. (1985) that h increases as temperature increases. The decrease in h here is due to the decrease of jet Reynolds number at a fixed G as a result of the viscosity increase with temperature.

The expected logarithmic relation between constant drying rate and air mass flow rate is demonstrated by the experimental data shown in figure 4.8(b) at the four levels of drying air temperature used. Thus the dependence of constant drying rate on jet Reynolds number will likewise be logarithmic.

The constant rate period is that part of the drying process during which the moisture content at the evaporating surface is sufficiently high that drying is heat transfer controlled. Therefore the constant rates of impingement drying should follow impingement heat transfer rates. The correlation of Martin (1977) for multiple jet impingement heat transfer, the most comprehensive available, incorporates both nozzle and flow variables in the following form:

$$\overline{Nu} = \left[1+\left(\frac{H/d}{0.6/\sqrt{f}}\right)^6\right]^{-0.05} \frac{\sqrt{f}\left(1-2.2\sqrt{f}\right)}{1+0.2\left(H/d-6\right)\sqrt{f}} Re^{2/3} Pr^{0.42} \qquad (4.10)$$

from which the constant drying rate can be calculated as:

$$R_{cM} = \left(\frac{3600\,\Delta T\,k}{\lambda\,d}\right)\overline{Nu} \qquad (4.11)$$

Table 4.4 shows the region of validity claimed for equation 4.11 and the experimental conditions for the present study.

With the confirmation of the absence of any effect on jet heat transfer coefficient of paper basis weight, section 4.3, or of the temperature driving force, figure 4.8(a), only one basis weight, B=50 g/m^2, and one temperature of drying air, T_j around 22 °C, were

therefore needed for determining R_c - Re data for examination of the effect of geometrical variables. Figure 4.8(c) shows the comparison between the present experimental measurements and the predictions from the correlation of Martin (1977). Not all the variables of nozzle geometry appear in Martin's correlation, for example, the geometry of the impingement exhaust ports relative to the nozzle array. Also, as only three nozzle sets were tested here, with the nozzle geometry variables, f and H/d, being interrelated, no analysis of individual geometric variables is possible.

Table 4.4 Comparison of validity region of equation 4.11 with present experimental conditions	
Validity region of eqn. 4.11	Present condition
2000 <Re< 100,000	449 <Re< 11,050
0.004 <f< 0.04	0.014 <f< 0.031
2 <H/d< 12	5.0 <H/d< 8.5

For all data of Re>2000 the mean value of the ratio of the present constant drying rate results to those calculated by the Martin correlation is recorded in Table 4.5 for each nozzle set as a nozzle geometry factor $C_g = R_c/R_{cM}$, with N indicating the number of experiments for each set. The values of the nozzle geometry factor for all three nozzle sets are within the ±15% validity range claimed for Martin's correlation. The lines in figures 4.8 (a) and (b) represent R_c calculated from equation 4.11 and the values of the nozzle geometry factor from Table 4.5, as is also the case for R_c calculated on figure 4.8(d). Even though equation 4.11 is valid only for Re>2000 it was found that for nozzle set #1 the whole Re range from 450 to 5300 is represented well with equation 4.11.

Table 4.5 Results for nozzle geometry factor C_g				
Nozzle Set #	C_g	N	σ for C_g	$2\sigma/C_g$ (%)
1	1.03	34	0.003	0.6
2	0.876	10	0.006	1.4
3	1.15	9	0.002	0.2

4.5.2 Critical moisture content, X_c

For all combinations of conditions used to determine critical moisture content, evaluated as described in section 4.4.3, these values of X_c ranged between 0.8 and 1.6 kg water/kg fibre. For this set of 80 values the following correlation was obtained:

$$X_c = a_c R_c^{b_c} B^{c_c}\left[1+\frac{d_c X_o}{f(H/d)}\right] \qquad (4.12)$$

The best fit values for the four parameters, designated in general as ε, are listed in Table 4.6, with R^2 being 0.55 .

Table 4.6	Correlation parameters for X_c		
Parameter	ε	σ for ε	2σ/ε (%)
a_c	0.46	0.059	26
b_c	0.11	0.011	20
c_c	0.12	0.031	52
d_c	0.02	0.004	40

Figure 4.9 compares experimental and calculated the values of X_c . The dashed lines shown, representing the 2σ limits of X_c from equation 4.12, indicate that this correlation predicts critical moisture content within about 0.17 kg water/kg fibre for the wide range of drying parameters Re, T_j, B and X_o recorded on Table 4.1 and nozzle geometry parameters f and H/d recorded on Table 3.1. Such a prediction provides general confirmation of the precision of the present measurements as well as the adequacy of the correlations.

The dependence of X_c on drying process conditions is now considered. From equation 4.3, the Sherwood approximate solution of the diffusion equation 4.1, the expression for X_c can be derived as $X_c = 4\,R_c L/(\rho\, D\, \pi^2)$. Similar results were obtained by Suzuki et al. (1977) who used drying intensity for surface drying, I_s , to represent their approximate solutions at two extremes, i.e. low intensity drying at I_s <2 and high intensity drying at I_s >2, with $I_s = R_c\, L/(\rho\, X_o\, D)$. They found

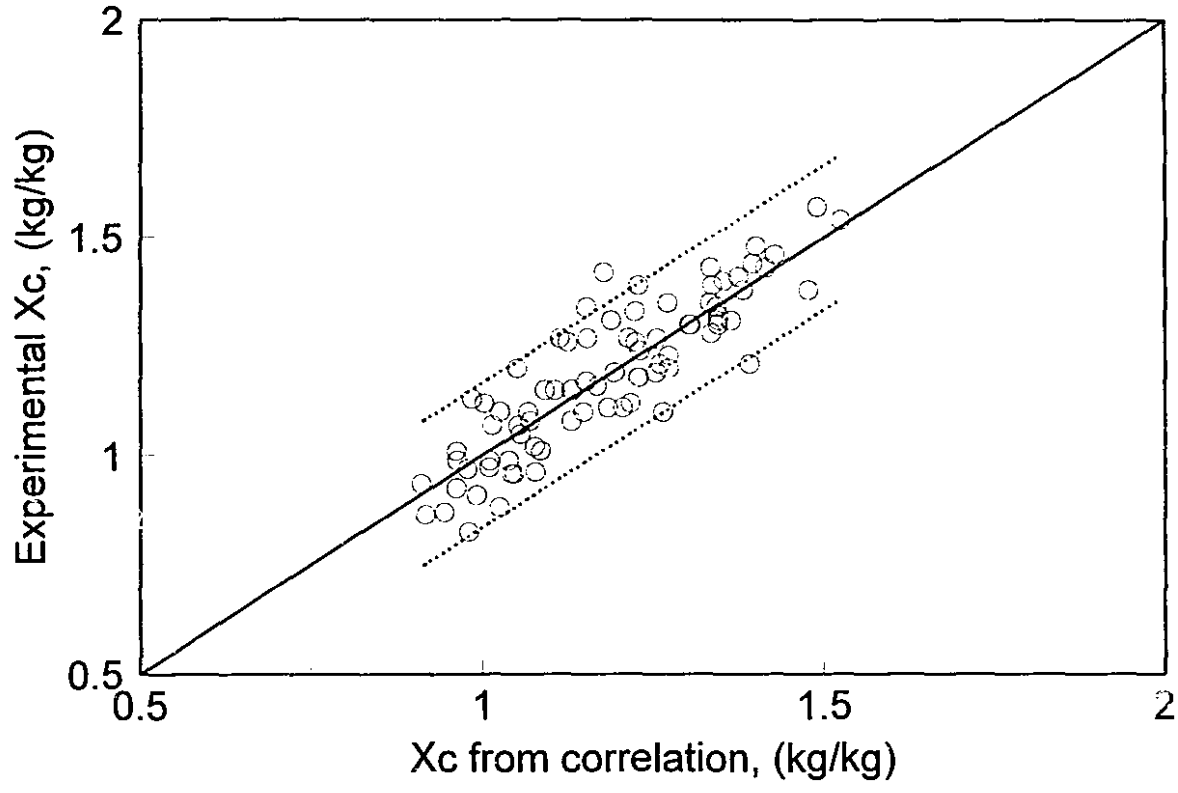

Figure 4.9 Comparison of Xc from correlation eqn. 4.12 with experimental Xc

$X_c/X_o = I_s/3$ for low intensity and $X_c/X_o = 1 - \pi/(4I_s)$ for high intensity drying. For the present study I_s ranges from 0 to 3.5, which covers the whole region of low intensity drying as well as part of high intensity drying, thus complicating the comparison. The trend of increase of critical moisture content with increasing values of constant drying rate R_c and paper thickness B for the present case is indicated by the positive values of the exponents b_c and c_c recorded in Table 4.6. It is not surprising that a dependence of X_c on D ($\propto T_s$) was not observed because the tested range of wet bulb temperature of the paper, only from 7.3 to 30 °C, was not sufficient to make this effect significant.

The dependence of critical moisture content on the thickness of drying material was reported long ago by Broughton (1945) for low intensity drying of clay and kaolin with a convective air flow parallel to the surface. For high intensity impingement drying of paper with both air and superheated steam Bond et al. (1992) likewise found X_c to increase with R_c but they did not observe a dependence of X_c on B. These differences probably derive from experimental techniques, with those of Bond et al. differing from the present investigation in two important ways. First, they used oscillating nozzles, which minimized the local flow nonuniformity effect associated with impingement drying. Moreover, because of the high temperature of the drying medium used they could not obtain the precisely defined R-X curves of the present study but had to base their analysis on moisture-time, X-t, relations from sets of batch drying experiments.

In contrast to conventional low intensity surface drying where initial moisture content is not a factor, the present study found X_c increases with X_o. This dependence of X_c on X_o may be due to nonuniform drying for the system of impinging jets. The local rate of heat transfer is highest directly under the nozzles, lowest at positions midway between the nozzle centerlines. Thus once drying starts, paper moisture content is no longer uniform in the plane of the sheet, but has minimum values directly under nozzles and higher values in the regions between nozzles. Therefore the value of X_c is reached locally at first directly under the nozzles, and subsequently in regions between nozzles. Once any significant fraction of a sheet is in the falling rate period, the entire sheet is considered to be in the falling rate period. The higher the value of X_o, the longer the

drying time before the falling rate starts and the bigger the differences of local moisture content will have become between the relatively dry and moist areas, hence the higher will be the sheet average moisture content, X_c.

The severity of local flow nonuniformity depends on nozzle geometry, the two major factors being the fraction of nozzle open area on the nozzle plate, commonly called the open area ratio f, and the nozzle to paper spacing H/d. The larger the value of either f or H/d, the smaller the local flow nonuniformity. For the three nozzle sets used here, each with a different f and H/d, the product of f and H/d provides a factor representing local nonuniformity of the flow. As the dependence of X_c on X_o in the present study derives also from the flow local nonuniformity, the variable X_o appears in equation 4.12 associated with the flow nonuniformity factor, 1/(f H/d) . In industrial practice of impingement drying of paper the rapid movement of the sheet under nozzles, which are always staggered in the direction perpendicular to sheet travel, averages out the nonuniform impinging jet flow thereby producing uniformly dried paper. In that case there is no local flow nonuniformity effect. In equation 4.12 the flow nonuniformity disappears as 1/(f H/d) goes to zero, in which case equation 4.12 becomes:

$$X_c = a_c R_c^{b_c} B^{c_c} \qquad (4.13)$$

Thus equation 4.13 is the correlation for X_c of general interest with the equipment specific flow nonuniformity, represented by 1/(f H/d) , having been eliminated. For industrial drying conditions where typical impingement hood operation would give R_c of about 200 kg/m^{2}h, equation 4.13 predicts the critical moisture content as 1.38 kg water/kg fibre for impingement drying of printing grades of paper and 1.21 kg/kg for drying tissue. For a paper moisture content after the wet press of a papermachine for printing papers of around 1.5 kg/kg, this indicates that if such grades of paper were dried in an impingement dryer, almost all of the water would be removed in the period of falling rate drying.

4.5.3 R-X relationship in the falling rate period, n

For the 80 combinations of drying conditions processed the R-X relation during the falling rate period, represented by the single parameter n in the power law equation 4.9, was found to vary from 0.54 to 1.2. From equation 4.9, $\left.\frac{dR}{dX}\right|_{x=x_c} = \frac{n R_c}{X_c}$. Thus for n < 1, $\left.dR/dX\right|_{x=x_c}$ is smaller than R_c/X_c, which corresponds to the falling drying rate R-X curve being concave downwards, as was found for most conditions used here. For n >1, $\left.dR/dX\right|_{x=x_c}$ is larger than R_c/X_c, and the falling drying rate curve is convex downwards. Values of n were found to correlate with drying parameters as follows:

$$n = a_n B^{b_n}\left[1+\frac{c_n}{f(H/d)}\right] \qquad (4.14)$$

with R^2 being 0.35 . The parameters are statistically significant and the best fit values are designated as ε listed in Table 4.7.

Table 4.7	Correlation parameters for n		
Parameter	ε	σ for ε	2σ/ε (%)
a_n	1.90	0.30	32
b_n	-0.26	0.04	31
c_n	0.042	0.015	71

In comparison of experimental and calculated values of n, figure 4.10, the 2σ limits shown by dashed lines indicate that values of the power law exponent for the falling rate curve are predicted by the correlation equation 4.14, with a substantial uncertainty of about 0.18 for values of n in the range 0.54 - 1.2.

The Sherwood approximation for the falling rate period of surface drying, equation 4.3, gives $dR/dX = \rho D\pi^2/(4L)$. From this approximation the power law parameter n would be expected to vary inversely with paper thickness, L , or paper basis weight, B, but not with the other variables of the present experiments, i.e. Re , T_j or X_0 .

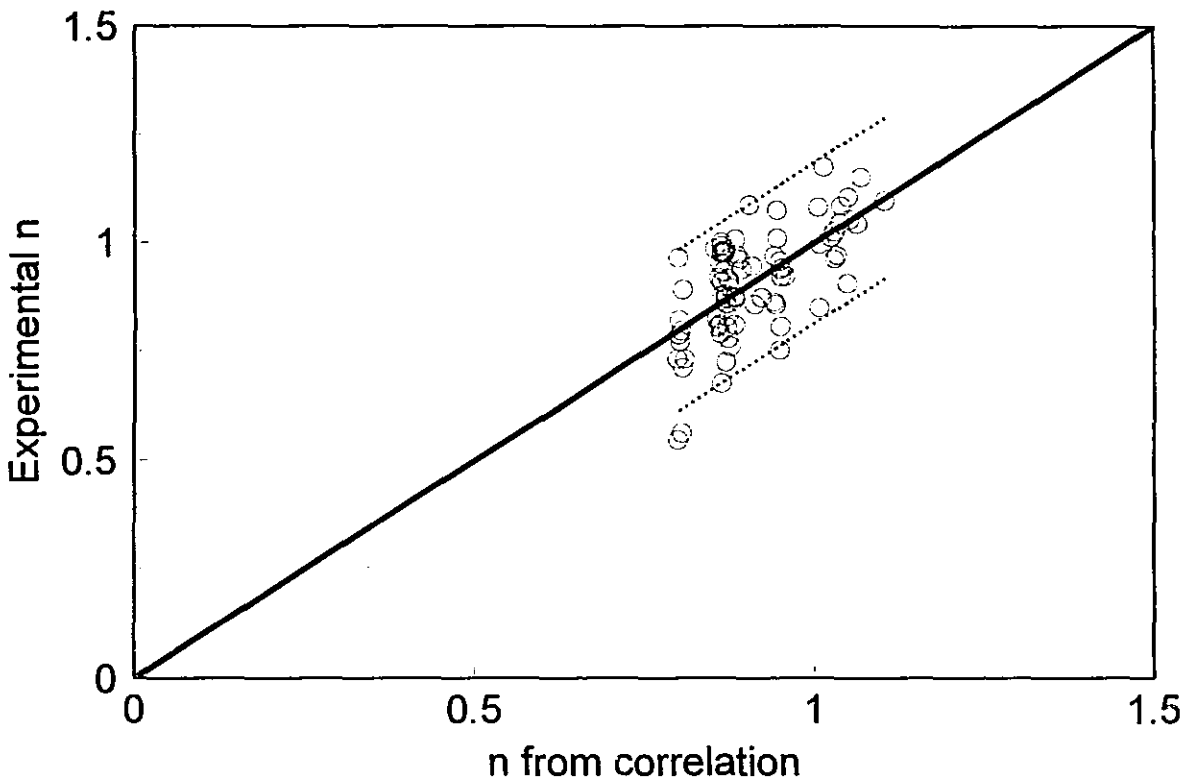

Figure 4.10 Comparison of n from correlation eqn 4.14 with experimental n

Thus the latter three variables are absent from equation 4.14 but paper basis weight B appears.

Equation 4.3 is for uniform surface drying while the present results are for drying under impinging jets where there is some moisture movement laterally from regions of locally higher to lower moisture content, in addition to the z-direction movement. Although in equation 4.14 the value of c_n for the local flow nonuniformity factor, 1/(fH/d), is significant, the value of R^2 and the statistical parameters listed in Table 4.7 suggest complex inter-relationships between nozzle geometry, drying conditions and behavior in the falling rate period. For industrial practice however, with the sheet moving at high speed under impinging jets so that there is no local flow nonuniformity effect, the 1/(f H/d) term disappears from equation 4.14 as described in the analysis concerning X_c. The general relation of the power law parameter n with B therefore becomes:

$$n = a_n B^{b_n} \qquad (4.15)$$

Although the power law representation of the falling rate curve has not previously been used for paper, Keey (1972) suggested that if the power law treatment were used the values of n would be in the range of 0.5 for fibrous material, 1 for other hygroscopic materials and 2 for non-hygroscopic materials. The values of n predicted by equation 4.15, 0.82 for paper with B of 25 g/m^2 and 0.69 for paper with B of 50 g/m^2, are then in the range proposed by Keey for hygroscopic fibrous materials.

4.6 Prediction of drying time and drying rate

With quantitative relationships now determined for constant drying rate, critical moisture content and the relationship between drying rate and moisture content in the falling rate period, the time for impingement drying of paper can be predicted with the correlations obtained. Specifically, drying time can be predicted through combination of equation 4.11 with the nozzle geometry factor C_g in Table 4.5, equations 4.12 and 4.14 for respectively, R_c , X_c and n, using $R=R_c$ over the constant rate period and the power law R-X relationship, equation 4.9, over the falling rate period. As the short transient period before the onset of the constant rate period was excluded in determining R_c , X_c and n, this very short period, in the order of 0.5 to 1 s for high temperature air and less than 5s for cases at ambient temperature, was likewise excluded from the drying time calculation, so the drying times determined apply from the start of the constant drying rate.

For nozzle set #1 (f=3.1%, H/d=5.0) the measured and predicted results for the experimental facility with representative conditions are shown in figures 4.11 and 12. For tissue grade paper, basis weight about 25 g/m^2, four levels of Re at the highest jet temperature tested are compared in figure 4.11. For printing paper, basis weight about 50 g/m^2, results at lowest Re, lowest T_j are shown on figure 4.12 (a); results for intermediate Re and T_j on figures 4.12(b) and (c); results for the highest Re and T_j tested are shown on figure 4.12 (d). Because equation 4.11 was found valid with nozzle set #1 for the entire Re range from 450 to 5300, conditions for drying time and drying rate could be chosen across this Re range. As the predictions are made for paper moisture content down to a value of 0.05 kg water/kg fibre, the values of experimental and predicted drying time indicated on these figures, $t_{0.05}$, are for that typical value of final moisture content.

For nozzle sets #2 (f=2.7%, H/d=8.5) and #3 (f=1.4%, H/d=7.6), since only one jet temperature and one basis weight were tested, results with Re around 2000 - 3000 and around the highest Re tested for each nozzle set, 9000 - 11000, were compared with the correlation predictions in figure 4.13.

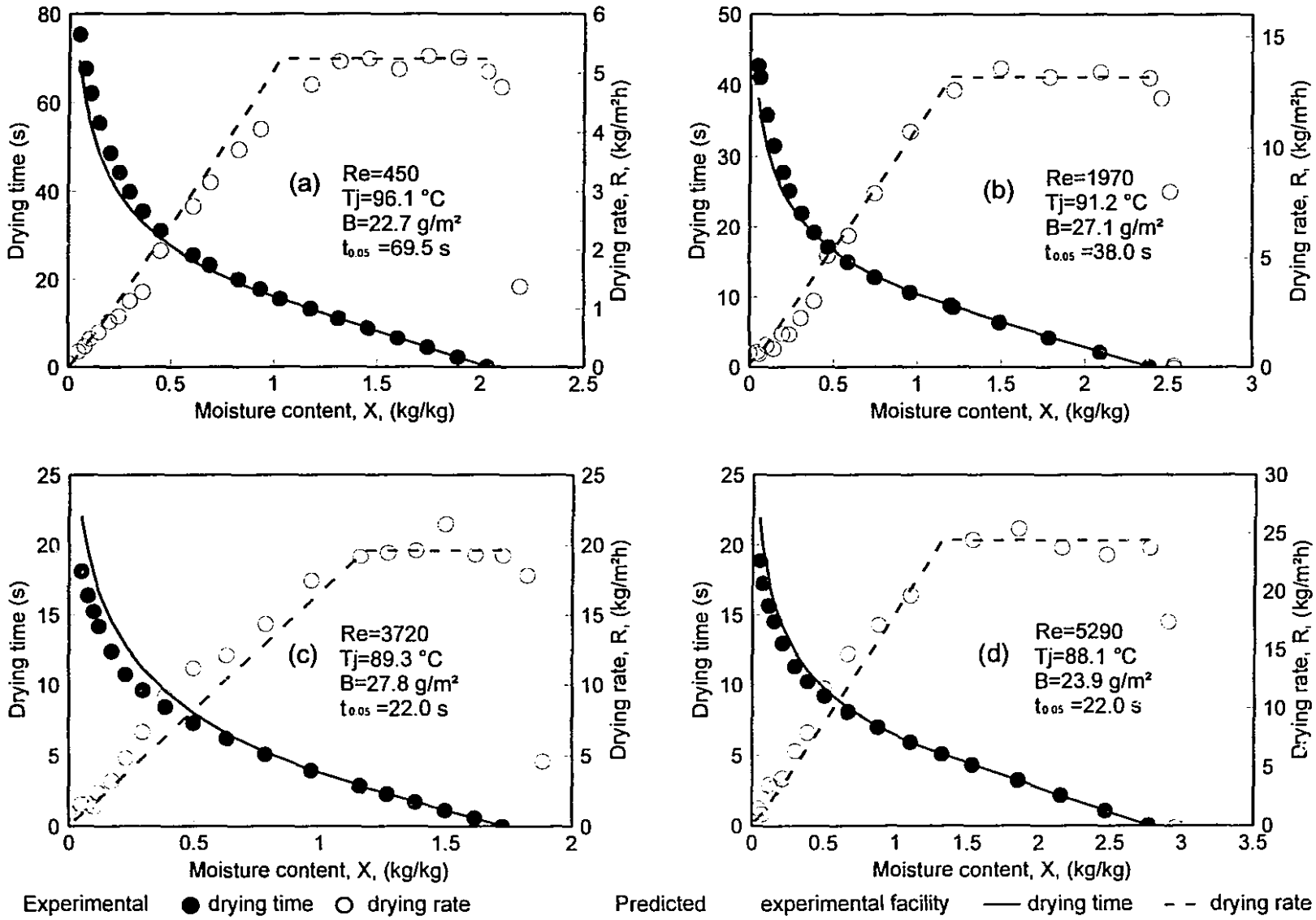

Figure 4.11 Comparison of measured and predicted results, nozzle set #1, B-25 g/m²;

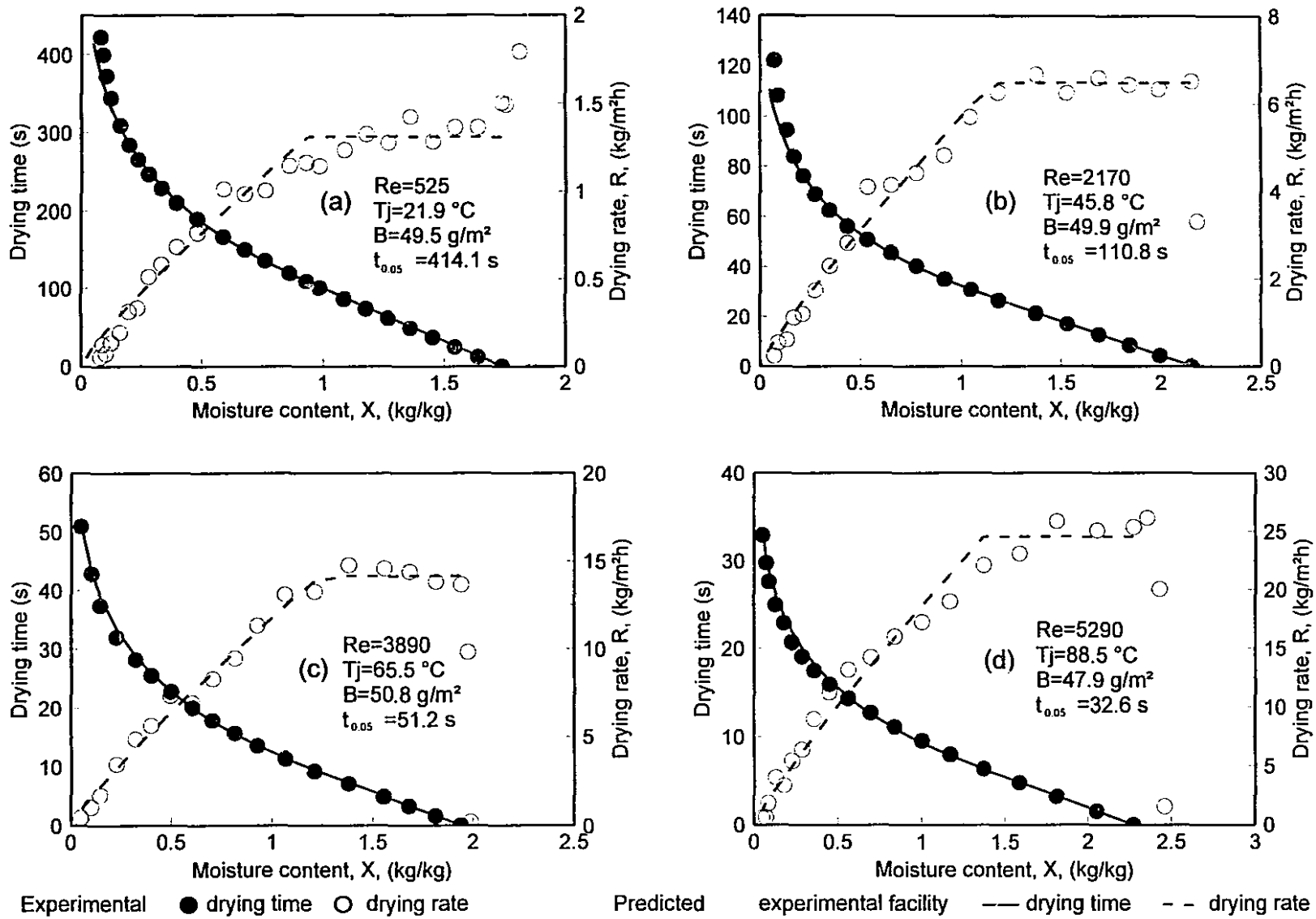

Figure 4.12 Comparison of measured and predicted results, nozzle set #1, B-50 g/m²;

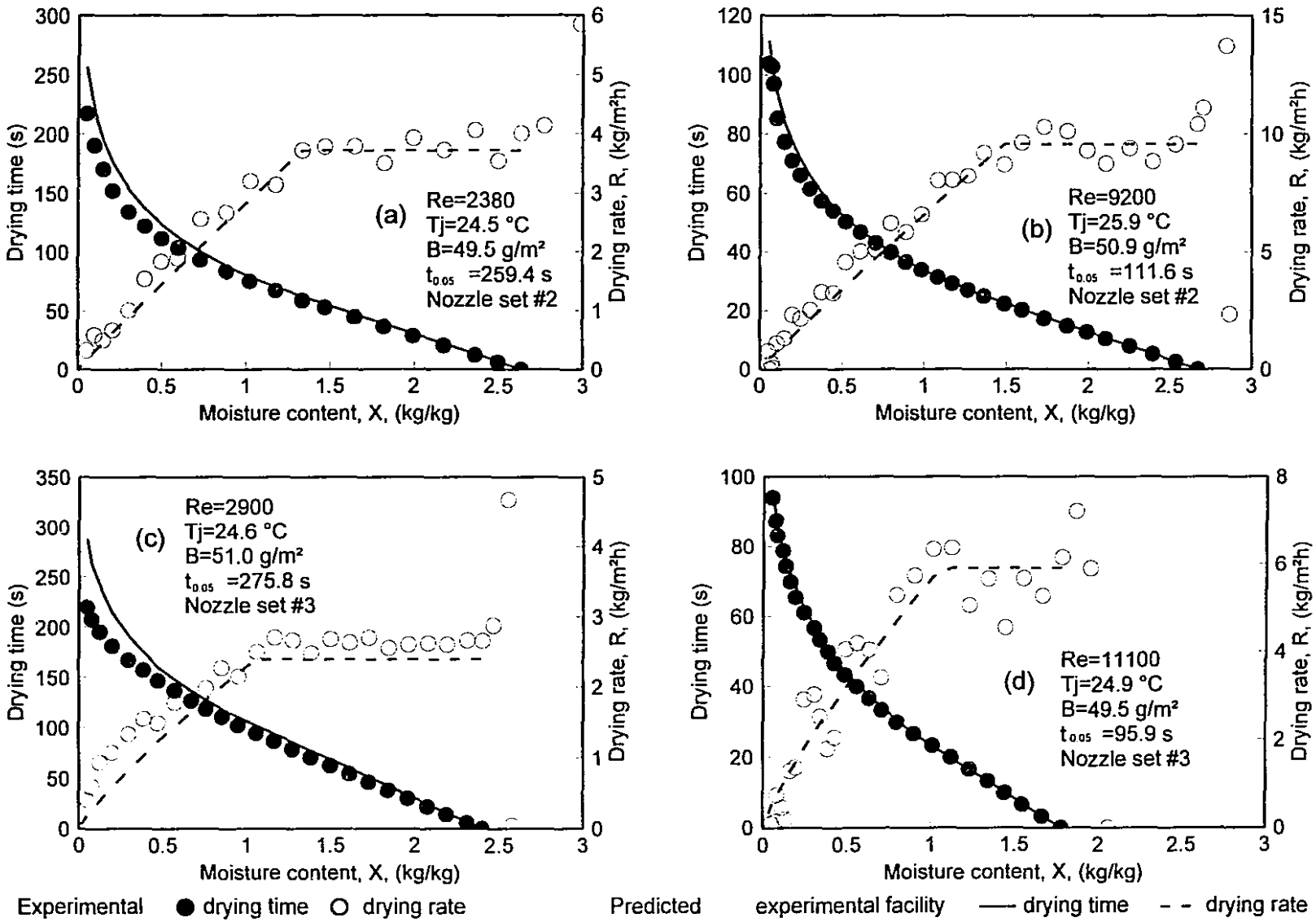

Figure 4.13 Comparison of measured and predicted results, nozzle sets #2 & #3, B-50 g/m²;

Drying time was very successfully predicted for all cases with nozzle set #1. For nozzle sets #2 and #3, the prediction was good for high Re but not for the two cases of Re in the range 2000 - 3000. These low values of Reynolds number were also for cases with the lowest temperature of drying air, i.e. the overall conditions of lowest drying rate, hence the most difficult conditions to measure and those subject to the greatest experimental uncertainty. Moreover these lowest intensity drying conditions are not of interest for industrial practice. In summary, the prediction of drying rates and drying times relative to those measured experimentally was good, particularly for drying conditions of greater practical relevance.

In industrial application of impingement drying of paper the local nonuniformity flow effect present in the laboratory study is absent due to the high speed movement of the wet sheet under staggered jets. Therefore drying time and drying rate are predicted with the correlations applicable without this effect, specifically, equations 4.11 and 4.13 for R_c and X_c and equations 4.9 and 4.15 for the R-X relationship in the falling rate period. For four representative conditions with the most studied nozzle geometry, nozzle set #1, figure 4.14 shows these predicted drying times and rates with no local flow nonuniformity effect as in industrial practice. The corresponding predicted drying times and rates for the present experimental facility shown for comparison are the curves from figures 4.11 (c) and (d) and figures 4.12 (c) and (d). The difference in values of R_c between the industrial case and the experimental facility is small, 3%, reflecting the value of the nozzle geometry factor C_g=1.03 from Table 4.5 for nozzle set #1. For the four cases shown the drying time, $t_{0.05}$, for the industrial case with no local flow nonuniformity effect averages about 30% less than in the experimental facility with this effect. This substantial reduction derives from two beneficial consequences of the absence of local nonuniformity, i.e. that for these four cases X_c averages 23 % lower and the falling rate exponent n is 21% lower. The advantage of the lower value of n is in giving a more advantageously curved falling rate period. The effect of the lower X_c and more curved falling rate period is readily seen on figure 4.14. For the four cases of figure 4.14 the average critical moisture content of 1 kg/kg indicates that with a typical moisture content after the wet press of a mill producing printing paper being about 1.5 kg/kg, 2/3

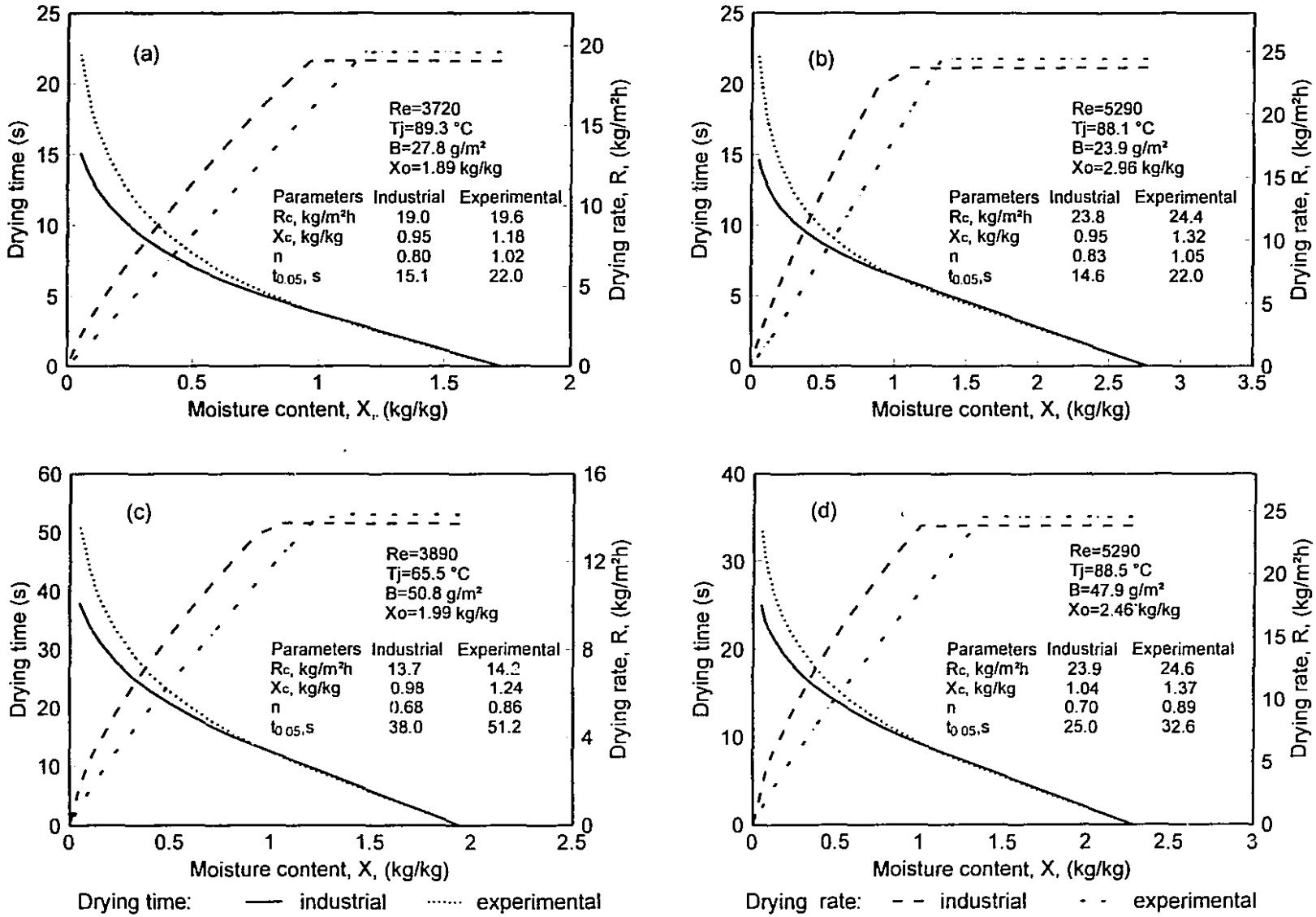

Figure 4.14 Comparison of predicted results for experimental facility and for industrial conditions, nozzle set #1

of the water would be removed in the falling rate drying period. As the laboratory conditions used correspond to much lower drying intensity than in industrial practice, X_c industrially would be about 1.4 kg/kg, as discussed in section 4.5.2, and drying would be controlled almost entirely by the falling rate period. The results of the present study underline the dominance of the falling rate period drying relationship in determining the industrial performance characteristics for air impingement drying of paper.

4.7 Summary

(1) Precisely defined drying rate curves were determined by high speed, on line measurements for the impingement drying of paper with three sets of nozzle arrays that cover a range of nozzle to paper spacing from 5 to 8.5 nozzle diameters, nozzle open area ratios from 1.4 to 3.1%, with nozzle exit air temperature from 20 to 90 °C, jet Reynolds number varying from 450 to 11100, and paper basis weight from 25 g/m^2 to 50 g/m^2. In all, 83 drying rate curves were determined for that number of sheets of paper.

(2) Three alternatives were tested for reducing the measured complete drying rate curves to quantitative parameters.

(a) Conventional treatment:

This procedure defines a constant drying rate R_c , a critical moisture content X_c , with a linear R-X relation during the falling rate period.

Although this procedure estimates R_c adequately, it provides a poor representation of the complete drying rate curve data, hence was rejected.

(b) Churchill asymptotic treatment:

The drying rate curve is defined by two asymptotes, $R=R_c$ for $X\rightarrow\infty$ and $R=aX$, a linear R-X relation for $X\rightarrow 0$, with a parameter n to define the drying rate in the region between the two asymptotes. The concept of a critical moisture content is absent from this approach, which gives a smooth R-X curve.

This procedure provides acceptable fits to the complete drying rate curve data but generally predicts values of R_c too high. As this approach provides only a continuous falling rate period from the start of drying, this otherwise attractive method, never before applied to drying, was therefore rejected for the present case of drying paper.

(c) Power law treatment of falling rate period:

This method provides a quantitative representation of drying rate curves in terms of R_c, X_c and a power law relation with a single parameter, n, for the falling rate period.

As the power law treatment provides acceptable fits to the complete drying rate curve data with realistic values of X_c and R_c from a statistical fitting of this model to the experimental data, this procedure and the values of the three parameters for each drying rate curve, X_c, R_c and n, were determined for 80 drying experiments, i.e. without the three experiments at low initial moisture content for which no constant rate drying period was obtained.

(3) For constant drying rate, the present results agree well with Martin's correlation of heat transfer from multiple round jets

$$R_{cM} = \left(\frac{3600\,\Delta T\,\kappa}{\lambda\, d}\right)\left[1+\left(\frac{H/d}{0.6/\sqrt{f}}\right)^6\right]^{-0.05} \frac{\sqrt{f}\left(1-2.2\sqrt{f}\right)}{1+0.2\left(H/d-6\right)\sqrt{f}}\,Re^{2/3}\,Pr^{0.42}$$

for which the region of validity claimed by Martin is $2000 < Re < 100{,}000$; $0.004 < f < 0.04$; $2 < H/d < 12$. A mean value of the ratio of measured R_c to the calculated R_{cM} at $Re > 2000$ for each nozzle set is recorded as a nozzle geometry factor $C_g = R_c/R_{cM}$, these values being 1.03 for nozzle set #1, 0.876 for nozzle set #2 1.15 for nozzle set #3, all of which are within ±15% of Martin's correlation, the claimed limits of accuracy of his equation.

(4) Values of critical moisture content were analyzed in relation with drying conditions, paper properties and nozzle geometry, and were correlated as:

$$X_c = 0.46\,R_c^{0.11}\,B^{0.12}\left[1+\frac{0.02\,X_o}{f(H/d)}\right]$$

The significant effect of X_o on X_c and the presence of the geometrical parameter, 1/(f H/d) , reflect the important effect of local flow nonuniformity for drying rate under stationary impinging jets. The above correlation predicts X_c with a 2σ uncertainty of 0.17 kg water/kg fibre, where the measured values of X_c were in the range 0.8 - 1.6 kg water/kg fibre.

(5) For the falling rate period, a statistical fitting of the data from all experiments according to the power law treatment $\frac{R}{R_c} = \left(\frac{X}{X_c}\right)^n$ gives values of the power law exponent, n, for which the general correlation was:

$$n = 1.90\ B^{-0.26}\left[1 + \frac{0.042}{f(H/d)}\right]$$

The values of n indicates the slope of the falling rate curve as it intersects the $R=R_c$ line when the drying rate and moisture content are expressed in normalized form, R/R_c and X/X_c. The experimentally determined values of n range from 0.54 to 1.2. The significant experimental variability in n suggests a complex relationship between nozzle geometry, drying conditions and behavior in the falling rate period. The R - X curvature towards the end of the falling rate period is consistent with the great sensitivity which has been reported for the effect of moisture content on the diffusivity of moisture in paper.

(6) Drying time was generally predicted well with a combination of the above correlations for R_c, X_c, and n for the range of drying process conditions listed in (1).

(7) Industrial practice of impingement drying of paper, where local flow nonuniformity does not exist because the sheet moves at high speed, corresponds to the limiting case of the present study with the local flow nonuniformity factor, 1/(f H/d) , going to zero. For this case the X_c relation given in (4) becomes:

$$X_c = 0.46\ R_c^{0.11}\ B^{0.12}$$

with X_c affected only by R_c and B. The above correlation predicts X_c of 1.21 kg water per kg fibre for tissue paper and 1.38 kg/kg for printing grades of paper dried with impinging jets at typical industrial conditions giving a constant drying rate R_c of 200 kg/m^{2}h. The

appearance of the variables R_c and B in this relation is consistent with the theoretical analyses of Sherwood and of Suzuki et al.

Similarly, in the absence of a local flow nonuniformity effect, the relation for the power law exponent for the falling rate period given in (5) becomes

$$n = 1.90\, B^{-0.26}$$

which predicts n as 0.82 and 0.69 for drying of paper of basis weight 25 g/m^2 and 50 g/m^2, respectively. This prediction supports the suggestion made by Keey as to the expected range of n for hygroscopic and fibrous materials.

With the two above general correlations for X_c and n, and that for R_{cM} given in item (3), drying history and drying time may be reliably predicted for the industrial impingement drying of paper within the range of variables for which these correlations were determined. Relative to the results for the experimental facility, drying times for the industrial case would be about 30% lower for nozzle set #1. This lower drying time derives from two consequences of the absence of a local flow nonuniformity effect, i.e. X_c about 23% and the falling rate exponent n 21% lower, giving a more advantageously curved falling rate period. With typical moisture content after the wet press of a mill being producing printing paper about 1.5 kg water/kg fibre, the results of the present study indicate the dominant importance of the falling rate period for air impingement drying of paper.

Chapter 5 Through drying of paper

5.1 Introduction

Tissue and other light grades of paper are often dried by the process of air through drying. The removal of water by flow of air through the wet sheet is used both for the high heat and mass transfer rates thereby obtained and for the high bulk that through drying promotes in the dried paper, a commercially valuable property for such grades. All previous research on through air drying of paper, reviewed in chapter 2, has been carried out with the same inlet air flow condition, i.e. a uniform flow with a flat velocity profile. In addition, no totally unsubjective quantitative representation of the complete through drying rate data is available. Although undertaken as one element leading to the study of combined impingement and through flow air drying of paper, the through drying part of this thesis research also provides unique measurements towards understanding the industrially important process of through drying of paper.

5.2 Experimental conditions

Three paper basis weights of handsheets freshly made from dry unbleached unbeaten laboratory kraft pulp from 100% black spruce were used, ranging from the levels corresponding to tissue, to toweling and to printing papers. Initial moisture contents typical for industrial practice of through drying, 1.5 - 3 kg water/kg fibre, were adopted. The four levels of air mass flow rate chosen were at the lower range of industrial practice, which is typically between 0.07 to 4 kg/m^{2}s. In their study of through drying with uniform inlet air flow, Polat O. et al. (1987) reported the dependence of transport coefficients on the temperature driving force $\Delta T = T_j - T_{as}$ in the constant rate period. Therefore four levels of air temperature were used, 22°, 45°, 65° and 90 °C. With the inlet dry air of dew point around -20 °C, these temperature values correspond to adiabatic

saturation temperatures, T_{as}, of 7.2°, 17°, 23.5° and 30 °C. This range of drying air temperatures is low relative to the industrial range of from 100 to 400 °C. However the purpose of the present study is not as a commercial pilot plant investigation but to study the fundamentals of through air drying preparatory to the examination in chapter 6 of the interaction between through drying and impingement drying. Nevertheless very rapid drying was achieved. At G=1.45 kg/m^{2}s and air temperature of 90 °C, tissue grade of paper, B=25 g/m^2, was dried in about 3.5 s from a moisture content of 2 down to 0.05 kg water/kg fibre.

The choice of which impingement nozzle array to use of the three sets tested in the impingement drying study was made by reference to the results analyzed in chapter 4. Nozzle set #1 (f=3.1%, H/d=5.0) has the advantage of providing constant drying rates which are logarithmic linear with jet Reynolds number from the lowest value (Re=450, G=0.125 kg/m^{2}s) to the upper flow limit tested (Re=5300, G=1.45 kg/m^{2}s). This nozzle set also has the highest open area ratio, f, which reduces the undesired effect of local nonuniformity of the impinging jet flow. Thus nozzle set #1 was selected for the study of through air drying of paper.

Table 5.1 lists the experimental conditions for the complete research program of 89 runs for through drying under impinging jets. Eight additional experiments were carried out with a uniform inlet air flow, i.e. without impinging jets, at low and high limits of drying intensities, to determine the effect on drying characteristics of changing this inlet air flow boundary condition.

Table 5.1	Experimental conditions for through drying
G, kg/m^{2}s	0.125, 0.55, 1.03, 1.45
T_j, °C	22, 45, 65, 90
B, g/m^2	25, 37, 50
X_o, kg/kg	1.5-3
Nozzle set	#1

5.3 Drying history curves

Figure 5.1 shows two sets of typical through drying data at, (a) low temperature and low through flow rate, and (b) high temperature and high through flow rate. To facilitate examination, data points are shown only for drying rate. While for pressure drop and temperature only the straight lines connecting the data points are displayed. Except when the data points are specifically required, subsequent figures show the straight lines which connect the data points. Variables monitored continuously were air temperature at the through flow exhaust, T_e, (the averaged value from measurements at three locations, as indicated in chapter 3 section 3.1); paper temperature at the exhaust side, T_p; pressure drop across the sheet, ΔP; and air humidity at the through flow exhaust, Y_e. By selecting a data acquisition frequency in the range 1 to 10Hz according to drying intensity ($G \cdot \Delta T$), an effectively continuous drying rate curve was documented. Drying rate R and paper moisture content X were determined from the Y_e measurements.

Air temperature at the through flow exhaust, T_e, follows the trend in drying rate according to the behavior of an adiabatic system, i.e. T_e is much below the inlet air temperature, T_j, during the early part of drying, then rises to approach T_j during the latter part of drying while the drying rate is dropping towards zero. Since dry air of dew point around -20 °C was used, a completely dry sheet was obtained at the end of drying. For the special case of drying with unheated air, the occurrence of the spike at the beginning of drying in figure 5.1(a) reflects the paper cooling to the adiabatic saturation temperature, as discussed in chapter 4 for impingement drying. As paper is not dried industrially in unheated air, this feature is of no practical interest. An exponential decay of pressure drop as paper moisture content decreases was observed, as reported by Polat O. et al. (1989). After the sheet moisture content has dropped to the fibre saturation point, about 0.80 kg water/kg fibre for the pulp used here, there is naturally little further decrease in pressure drop. Since momentum transport of air flow through moist and dry paper was extensively studied by Polat O. et al. (1989), Polat O. (1989) and Polat O. et al. (1993), these topics are therefore not dealt with further in the present study.

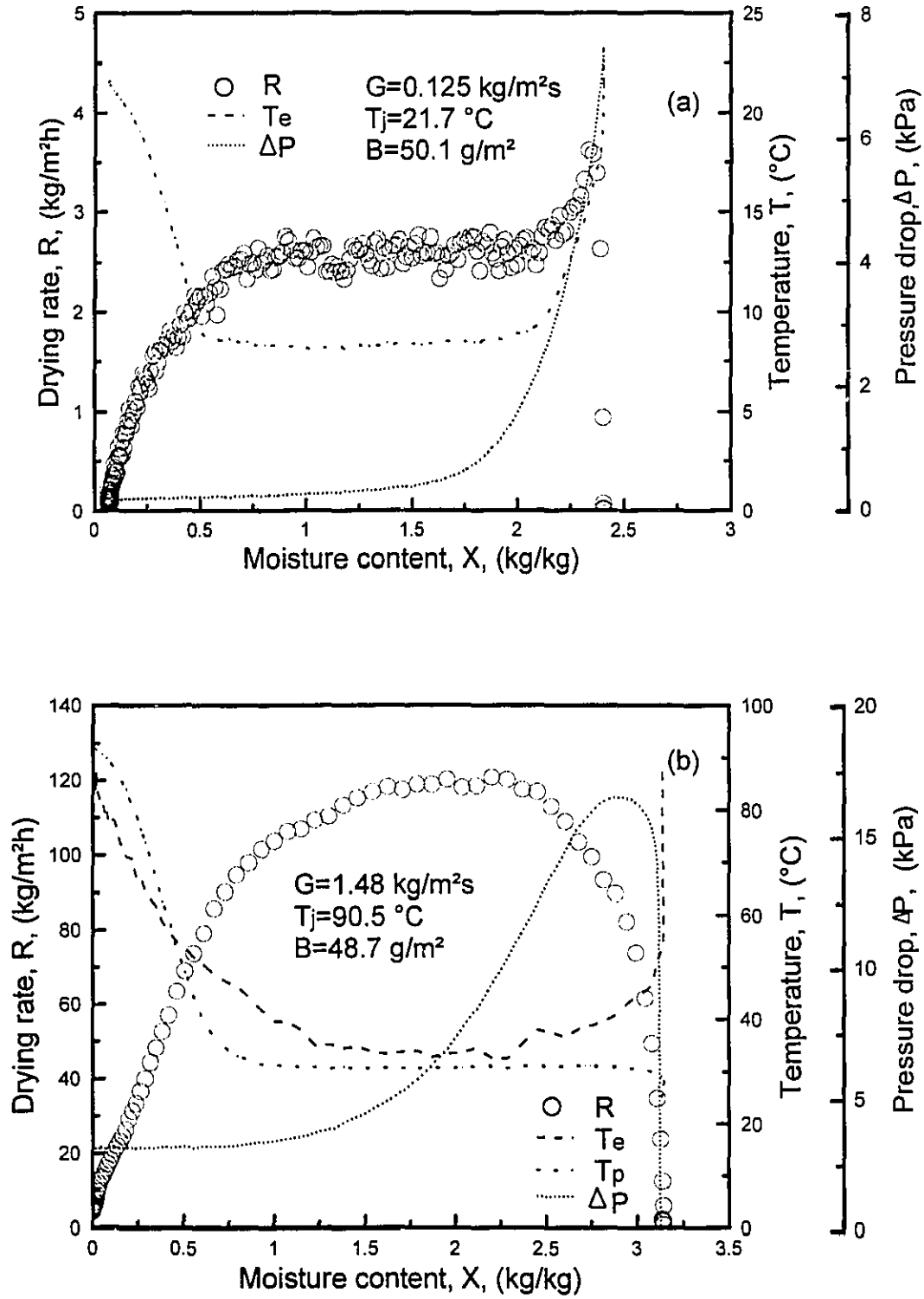

Figure 5.1 Typical through drying history curves
a) low intensity drying b) high intensity drying

For through drying with 90 °C air the increase of drying rate to the constant rate value occurs gradually while about 1 kg water/kg fibre is removed from the sheet, figure 5.1 (b). This behavior contrasts with impingement drying where this increase occurs over a very short transient period before the onset of the constant rate period, figure 4.1(b). For through drying with a uniform inlet air flow field, Polat O. et al. (1987) found that there are always two important drying periods, i.e. those of increasing drying rate and falling drying rate, while the existence of a constant rate period depends on drying process conditions. Before their work the great importance of the increasing rate period was not recognized. Conventionally this period had been incorrectly taken as a short transient period while the sheet temperature adjusts to the adiabatic saturation temperature, T_{as} , which is maintained during the constant rate period. In fact, figure 5.1 (b) shows that the paper temperature reaches T_{as} in a negligibly short period of time in contrast to the slow approach R to R_c . As about 1/3 of the water is removed in the increasing rate period for the condition of figure 5.1 (b), this drying period is evidently of central importance.

The observation that the transition from constant to falling rate drying is more gradual for through drying than for impingement drying reflects the fact that some local areas enter the falling rate period while the remainder of the sheet is still in the period of constant rate drying. This behavior results from the coupling between through flow rate and through drying rate which introduces a basic instability into the through drying process. Thus for any region where the local through flow rate is for any reason initially marginally higher than the mean flow rate, the local drying rate will from the start of drying be higher, which in turn increases the local sheet permeability, thereby increasing the local drying rate further yet. As measurements give only the sheet average drying rate, this sheet local nonuniformity effect can be inferred from the observed significantly more gradual transition from constant to falling rate drying here than observed in chapter 4 for impingement drying.

The value of the constant drying rate R_c for through drying is much higher than that for the impingement drying at comparable drying conditions due to the much larger transport area within the sheet for through drying. For example, for a 50 g/m^2 sheet dried

with 90°C air at G≈1.5 kg/m^{2}s, R_c is 25 kg/m^{2}h for impingement drying but is about five times as high, 120 kg/m^{2}h, for through air drying.

The inter-relationship among three aspects of the drying history curves, R, T_e and T_p , is recorded on figure 5.1(b). The falling rate drying period begins when the sheet moisture content is about 1.5 kg water/kg fibre, at which point there occurs the simultaneous onset of two effects - R begins to drop and T_e begins to rise, as is characteristic of the start of the falling rate period for any drying. Although T_e begins to rise, T_p , which is measured at the flow exit side of the sheet, remains at effectively the adiabatic saturation temperature, 30 °C, until sheet moisture content drops considerably further, to about 0.8 kg/kg. Thus it appears that for some time after the onset of the falling rate period the paper from the position of a drying front to the through flow exit side of the sheet remains at T_{as} . This T_e-T_p-X behavior constitutes evidence that through drying proceeds by a moving front. With these T_p - X profiles across the sheet combined with local nonuniformity of T_p - X in the plane of the sheet, it follows that complex three dimensional profiles of sheet temperature and moisture content develop during the falling rate period of through drying.

Figure 5.2 shows the effect of air temperature, T_j , on the drying rate curves at low and high values of mass flow rate, G, and paper basis weight, B. As T_j increases, R_c correspondingly increases. As the shape of the increasing drying rate curve remains about the same, this achievement of higher values of R_c corresponds to an expanded duration of the increasing rate period. The higher R_c for a higher T_j produces also a higher critical moisture content, X_c . Because the extent of both the increasing and falling rate periods expand as T_j increases, the extent of the constant rate period consequently decreases sharply. At T_j=90 °C, the highest for the present study, there remains no appreciable extent of constant rate period, only a maximum in drying rate. For this limiting case of the constant rate period just disappearing, figure 5.2 (b), 37% of the drying occurs during the increasing rate period and 63% during the falling rate period of drying.

The effect of air mass flow rate, G, on drying rate curves shown in figure 5.3 indicates that at low T_j, case (a), there is a long constant rate drying period at all levels of

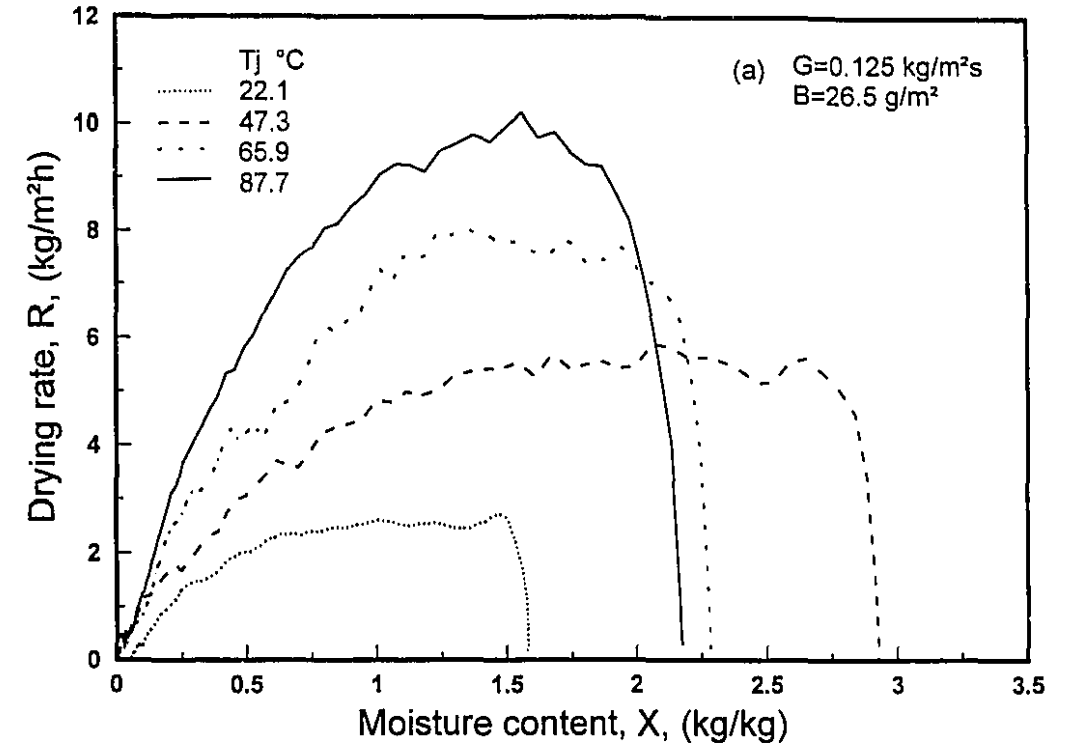

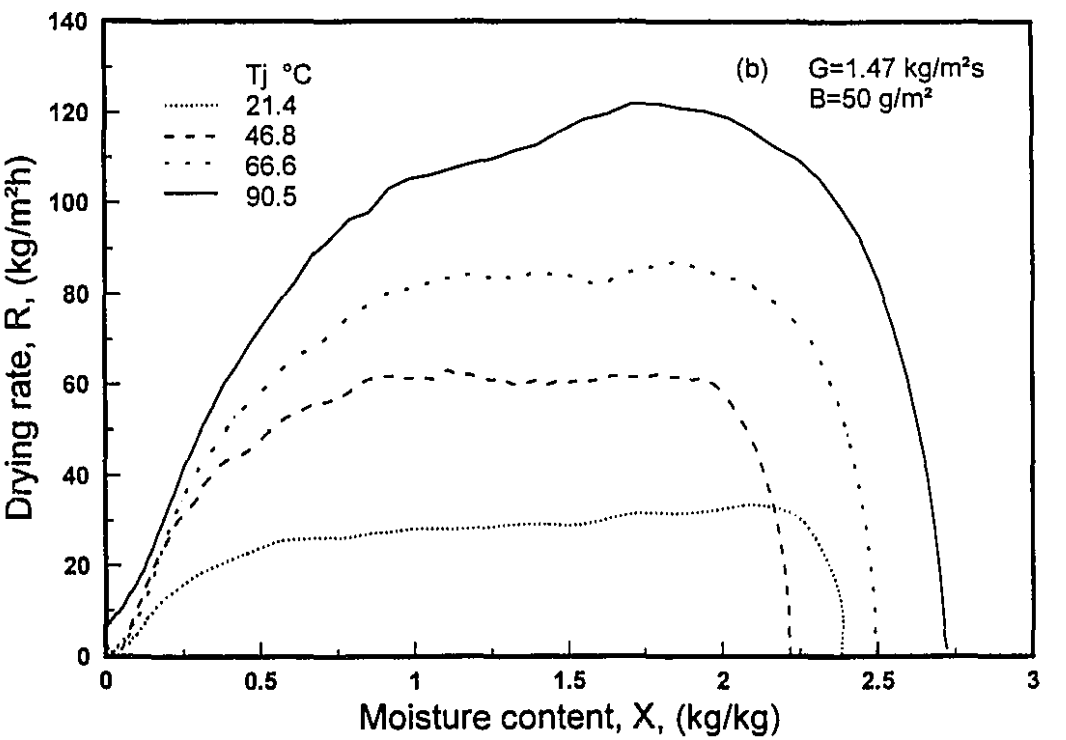

Figure 5.2 Effect of air temperature: a) low G, low B b) high G, high B

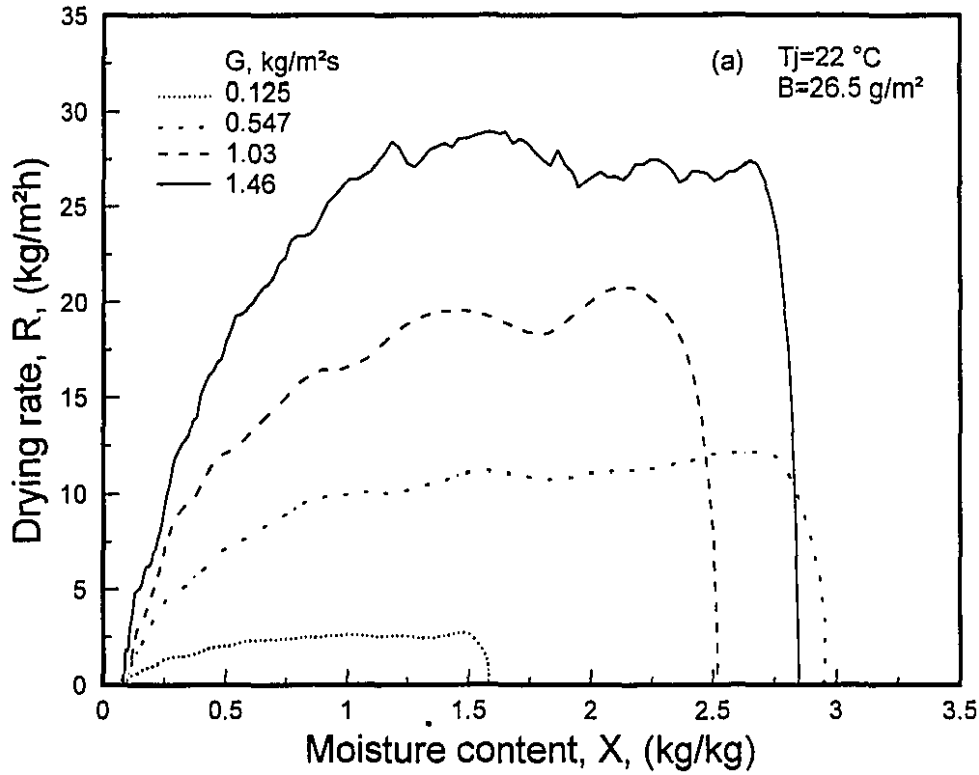

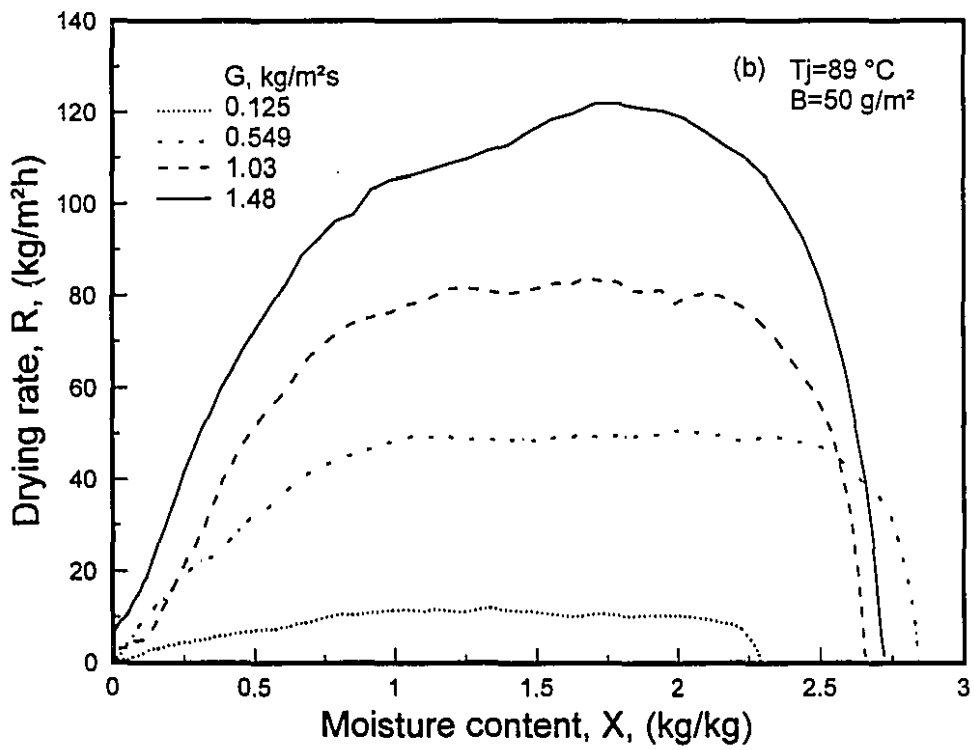

Figure 5.3 Effect of air through flow rate:
a) low Tj, low B; b) high Tj, high B

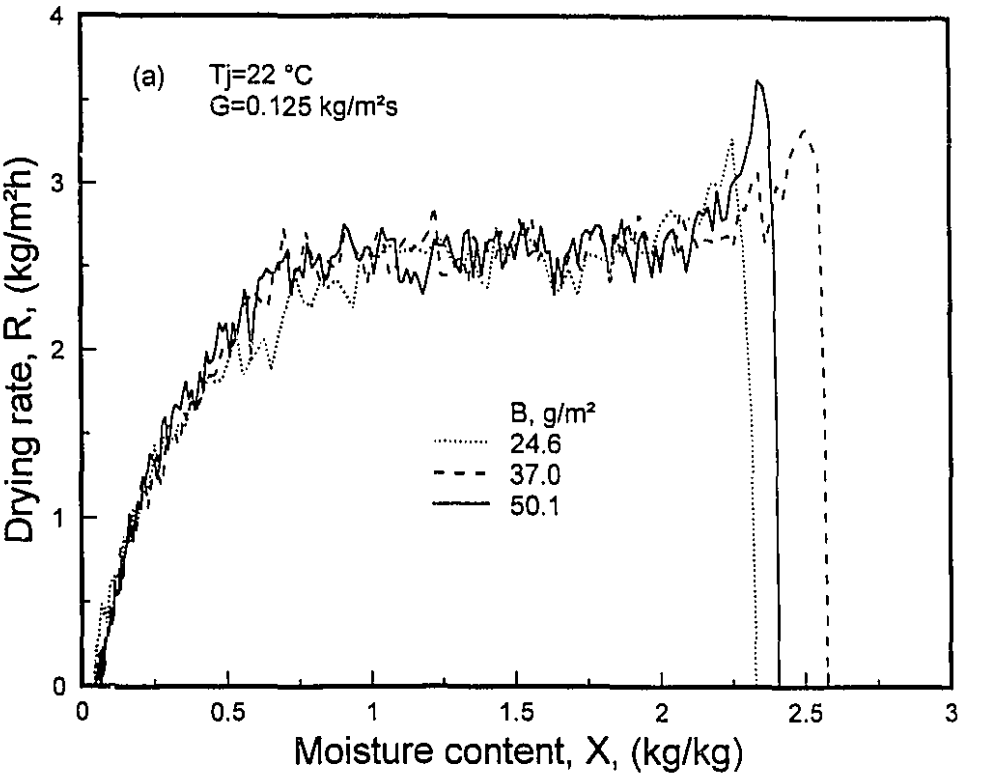

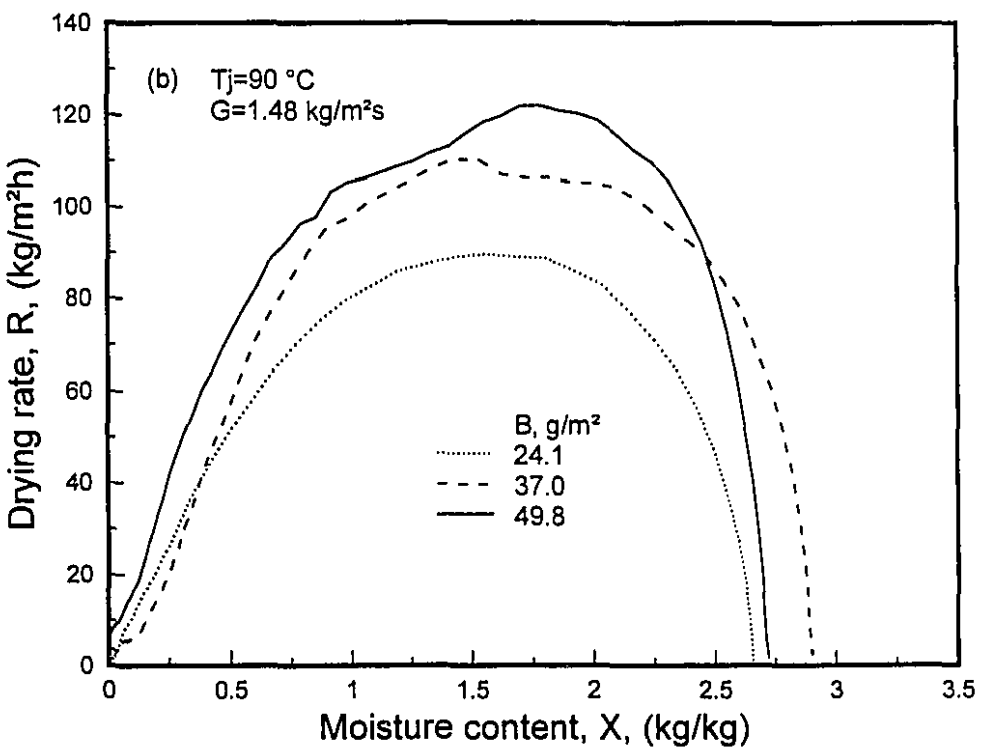

Figure 5.4 Effect of paper basis weight: a) low drying intensity; b) high drying intensity

G tested. At the highest jet temperature, case (b), the same trends occur as for the increase of T_j at constant G, figure 5.2. Thus on figure 5.3(b), increasing G causes increases in R_c and in the extent of both the increasing rate and falling rate periods, with a corresponding shrinkage of the constant rate period. As the limiting cases of maximum T_j, maximum G of figures 5.2(b) and 5.3(b) are the same, the distribution in drying between the periods is as noted above.

The effect of basis weight B on drying rate curves is shown in figure 5.4 at two levels of drying intensity, the lowest and highest used. At low drying intensity the effect of B on the R-X curve is insignificant as the sheet is sufficiently thick that the air exhausts essentially saturated at all basis weights. For the three values of sheet thickness tested, the high intensity drying conditions of figure 5.4(b) are such that for T_j=90 °C, G=1.48 kg/m^{2}s there is effectively no constant drying rate period. For these conditions the start of the falling drying rate period either terminates the increasing rate period or, at most, occurs just as the constant rate period is reached, this distinction being impossible to make when no period of constant rate drying occurs. For these drying conditions, when the sheet thickness is cut in half, i.e. B reduced from 50 to 24 g/m^2, the maximum drying rate drops by about 30%, indicating that the through flow exhausts are not saturated with water vapor.

Further analysis of the drying rate characteristics is given after a method has been developed for quantitative representation of the drying rate curves.

5.4 Quantitative representation of drying rate curves

5.4.1 R-X relationship in the increasing rate period

As through drying rate curves may consist of three drying rate periods, the increasing rate, constant rate and falling rate periods, quantitative representation of an entire drying rate curve requires five elements: the values of the constant drying rate R_c, the moisture content at the end of increasing rate period X_i, the critical moisture content

between the constant and falling rate periods X_c , and the R-X relationships in the increasing rate and falling rate periods. The number of elements required in quantifying drying rate curves increases from three for impingement drying to five for through drying because of the addition of the important increasing rate period R - X relation and X_i limiting moisture content.

Polat O. (1989) concluded that the increasing rate period of through air drying was defined and controlled not by the approach of the sheet to the adiabatic saturation temperature but by the increase in interfacial area between air and paper for heat and mass transfer, $a_p(X)$. Beginning with that concept, new analysis of the increasing rate period is now developed in order to indicate the form of the R - X relation, i.e. its dependence on the thermal and flow properties of the through flow air and the transport properties of the sheet. For a specific paper of basis weight B, when it is assumed that $h(X)a_p(X)$ is uniform in the z-direction and paper temperature is at T_{as}, the differential heat balance for a packed bed system, when integrated, gives:

$$T_j - T_e = \left(T_j - T_{as}\right)\left(1 - e^{-\frac{h(X)\, a_p(X)\, L}{G\, C_p}}\right) \qquad (5.1)$$

where $a_p(X)$ is the interfacial area, h(X) heat transfer coefficient based on the interfacial transport area within the wet sheet, L the paper thickness, C_p the heat capacity of air. That paper temperature T_p may reasonably be taken as constant at T_{as} throughout the increasing rate period was established by the many T_p - X profiles determined in the present study, for which the figure 5.1(b) profile is typical.

A heat balance over an adiabatic dryer gives the expression between the integrated drying rate R and drying conditions:

$$R = \frac{3600\, G\, C_p \left(T_j - T_e\right)}{\lambda} = \frac{3600\, G\, C_p \left(T_j - T_{as}\right)}{\lambda}\left(1 - e^{-\frac{h(X)\, a_p(X)\, L}{G\, C_p}}\right) \qquad (5.2)$$

Here the heat absorbed by the evaporating water is approximated as the latent heat term, neglecting the small sensible heat effect for the water vapor. The constant value of the integral drying rate for the entire sheet, R_c , becomes the limiting case at the end of the increasing rate period, when $h(X)a_p(X)$ has reached the value, ha_p at $X=X_i$, for which:

$$R_c = \frac{3600\, G\, C_p\, (T_j - T_{as})}{\lambda}\left(1 - e^{-\frac{h\, a_p\, L}{G\, C_p}}\right) \tag{5.3}$$

By dividing equations 5.2 and 5.3 the relationship for drying rate R in the increasing rate period relative to the constant drying rate R_c is obtained as

$$\frac{R}{R_c} = \frac{1 - e^{-\frac{h(X)\, a_p(X)\, L}{G\, C_p}}}{1 - e^{-\frac{h\, a_p\, L}{G\, C_p}}} \tag{5.4}$$

Approximating the relationship of $h(X)a_p(X)$ with X as linear during the increasing rate period, with $h(X)a_p(X) = ha_p$ at $X=X_i$, leads to:

$$h(X)a_p(X) = \frac{X_o - X}{X_o - X_i}\, ha_p \tag{5.5}$$

Finally, if n_i is defined as

$$n_i = \frac{h\, a_p\, L}{G\, C_p} \tag{5.6}$$

Equation 5.4 can be expressed as:

$$\frac{R}{R_c} = \frac{1 - e^{-n_i\left(\frac{X_o - X}{X_o - X_i}\right)}}{1 - e^{-n_i}} \tag{5.7}$$

Thus in addition to the coordinates (X_i , R_c) at the end of this period, n_i is the only parameter describing the R - X relation during the increasing rate period. Equation 5.7, a theoretically based form for R=f(X) during the increasing rate period, indicates that R increases exponentially as X decreases. Moreover the parameter n_i in this exponential relation is not simply an empirical constant but is related to flow and physical properties by equation 5.6. Before the fitting of this equation to the drying rate data can be made, R_c and X_i must be determined, as is treated in the following sections.

5.4.2 Complete drying rate curve: Churchill method for falling rate period

As the constant rate period for through air drying occurs between the increasing and falling rate periods, the value of R_c cannot be determined until both the increasing and the falling rate periods are defined quantitatively. Because the transitions from one drying rate period to the next are gradual, not sharp, the determination of X_i, X_c and R_c for through drying is a challenge. For the falling rate period in impingement drying, chapter 4, the conventional approach of a linear R-X relation was rejected for the evident curvature during this period. As the falling rate curves of through drying are generally even more curved than those of impingement drying, the conventional linear R-X treatment can therefore be rejected at the outset.

One approach is to consider the falling rate period as a region terminating at both ends as asymptotes. In this procedure, referred to as the Churchill-Usagi Equation (CUE) described fully in chapter 4, the two asymptotes would be $R=R_c$ for large X and a linear relationship, $R/X=a$, for $X\rightarrow 0$. The following method, termed procedure 1, uses equation 5.7 for moisture content above X_i and the CUE approach, adapted from equation 4.8, when $X \leq X_i$, i.e.

$$\frac{R}{R_c} = \frac{1 - e^{-n_i\left(\frac{X_o - X}{X_o - X_i}\right)}}{1 - e^{-n_i}} \qquad \text{for } X_o \geq X \geq X_i \qquad (5.7)$$

$$R = \left[(aX)^{-n_f} + R_c^{-n_f}\right]^{-1/n_f} \qquad \text{for } X_i \geq X \geq 0 \qquad (5.8)$$

with R_c, n_i, X_i, a and n_f statistically determined from the experimental measurements using the statistical regression package, SYSTAT.

Figure 5.5 shows the fitting of drying rate curves generated with procedure 1 to the experimental data from paper of B=25 g/m^2, dried by air at T_j of 90 °C, the highest for the present study, and at four levels of through flow rate. The best fit values of R_c, X_i, n_i, a and n_f are listed in each graph. The fitting in the increasing rate period is quite satisfactory, with a constant drying rate approached asymptotically, consistent with the

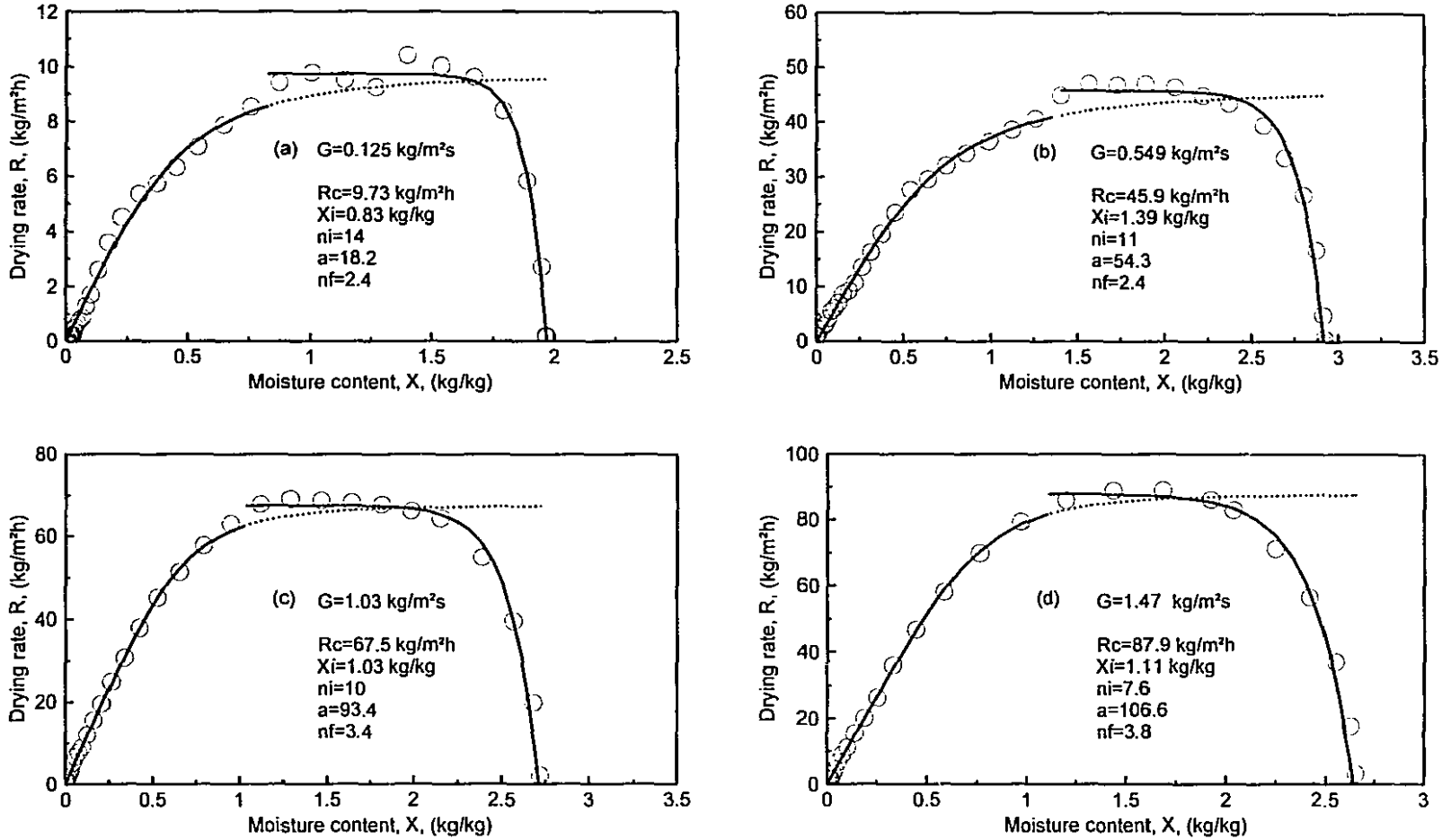

Figure 5.5 Fitting of through drying rate data at Tj=90 °C, B=25 g/m² with procedure 1

experimental data. This good fitting in the early part of drying confirms the general adequacy of equation 5.7 in representing the development of the increasing rate period, but with the deficiency of exaggerating the extent of the increasing rate period to cover what is clearly the constant rate period. Thus this procedure leads to R_c being approached at inconsistent values of moisture content for the two parts of the drying rate curves on figure 5.5. The absence from the CUE based model of a critical moisture content, X_c, makes it impossible to obtain by this method a continuous R - X curve for the entire drying process. Thus although equation 5.7 and the CUE based model fit the data well for the early and later part of drying, respectively, procedure 1 is not satisfactory for quantitatively representing the entire drying data from wet to dry.

5.4.3 Complete drying rate curve: Power law for falling rate period

The simple power law treatment of the falling rate period found appropriate for the case of impingement drying, chapter 4, would avoid the undesirable characteristics of CUE approach. Therefore procedure 2 was developed, using equation 5.7 for the increasing rate period and equation 5.9 adapted from equation 4.9, the power law R-X relationship, for the falling rate period.

$$\frac{R}{R_c} = \frac{1-e^{-n_i\left(\frac{X_o-X}{X_o-X_i}\right)}}{1-e^{-n_i}} \qquad \text{for} \quad X_o \geq X \geq X_i \qquad (5.7)$$

$$\frac{R}{R_c} = 1 \qquad \text{for} \quad X_i \geq X \geq X_c$$

and

$$\frac{R}{R_c} = \left(\frac{X}{X_c}\right)^{n_f} \qquad \text{for} \quad X_c \geq X \geq 0 \qquad (5.9)$$

with R_c, X_i, n_i, X_c, n_f to be determined statistically.

For drying rate curves generated with procedure 2, figure 5.6 shows the fitting to the same four sets of data seen for procedure 1 in figure 5.5. Now a continuous drying rate curve has been obtained for the rate data for complete drying from wet to dry. The value determined for constant drying rate R_c is observed on figure 5.6 to be consistent

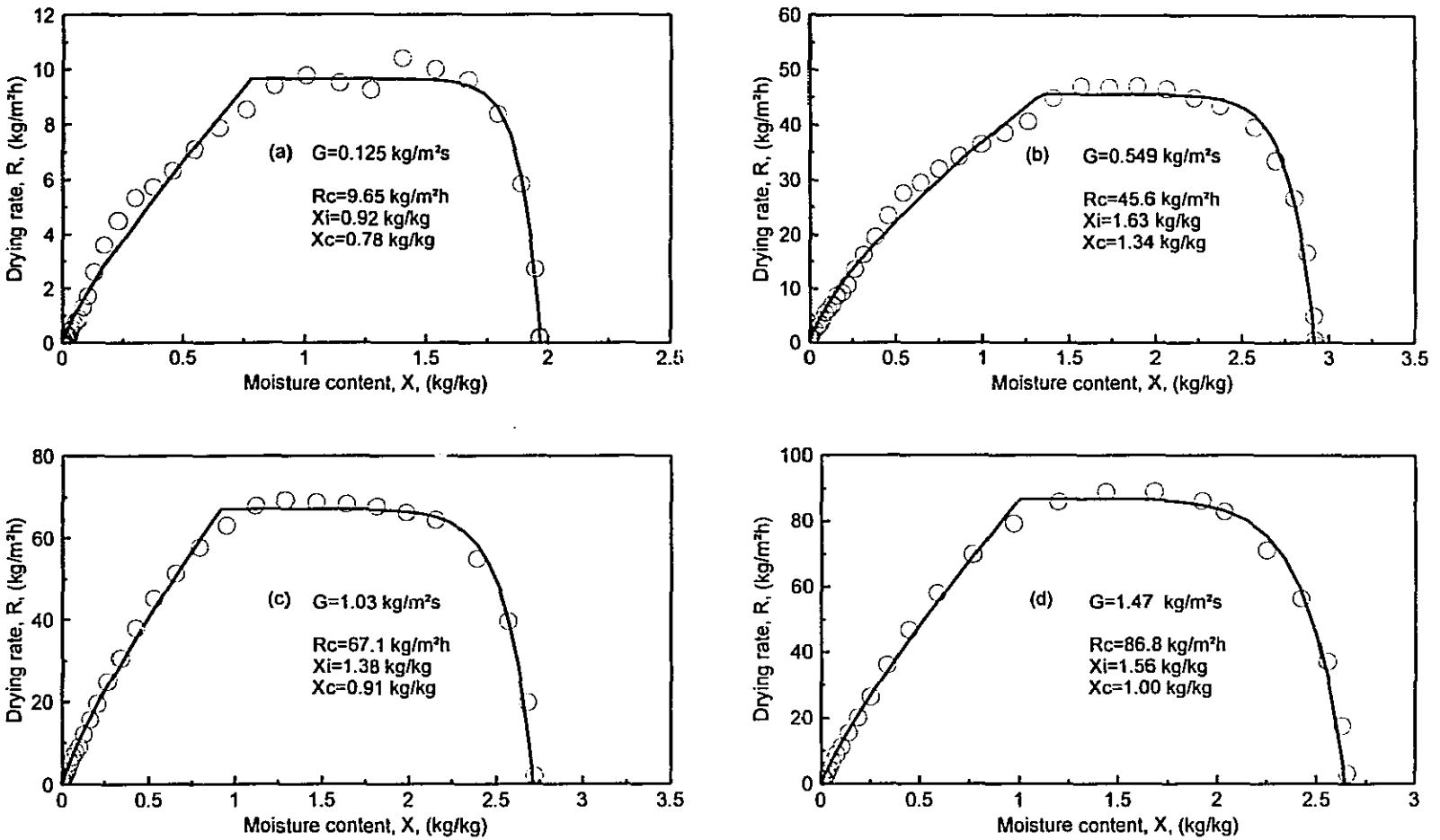

Figure 5.6 Fitting of through drying rate data at Tj=90 °C, B=25 g/m² with procedure 2

with the data over the central region of moisture content. However the transition from constant to falling rate period produced by this method is much more abrupt than is consistent with the experimental data. As noted in chapter 4, the simple power law R-X relationship has a near-linear section immediately below $X=X_c$ and has its maximum curvature as $X\rightarrow 0$. This characteristic was consistent with the experimental data for impingement drying but is clearly not so for through drying where a smooth transition occurs just below $X=X_c$ and a near-linear section as $X\rightarrow 0$. The determined values of X_c are therefore clearly too low, as is evident from figure 5.6. Thus procedure 2 is inconsistent with the measurements in two important ways. The R-X relationship, equation 2.7, for through drying of paper that Randall (1984) adopted from Gottsching and Rhodus (1977) for convective surface air drying of paper in the falling rate period, has the same unsatisfactory behavior for $X\rightarrow X_c$ as does the simple power law R-X relationship of procedure 2. Such relationships are therefore inappropriate to use.

For the power law R-X relationship to adequately represent the through drying falling rate data it is necessary to reverse the order of the curved and near-linear sections by replacing X/X_c and R/R_c with $1-X/X_c$ and $1-R/R_c$, obtaining

$$\frac{R}{R_c} = 1-\left(1-\frac{X}{X_c}\right)^{n_f} \tag{5.10}$$

Equation 5.10 has the property of $dR/dX = 0$ at $X=X_c$. Hence the falling rate period modeled by equation 5.10 approaches the constant rate period asymptotically. Procedure 2 can then be modified to procedure 3 by using the modified power law R-X relationship, equation 5.10, for the falling rate period.

With the same four sets of experimental measurements shown on figures 5.5 and 5.6, figure 5.7 shows the excellent fit of procedure 3 for the entire drying rate data. The values of constant drying rate R_c determined in this way are consistent with the measured R-X data. However, the result of having an asymptotic approach on either side of the constant rate period is that the length of this period becomes unrealistically short or vanishes. Within the precision of the numerical procedures there is effectively no difference between the values of X_i and X_c for the test cases of figure 5.7, with the

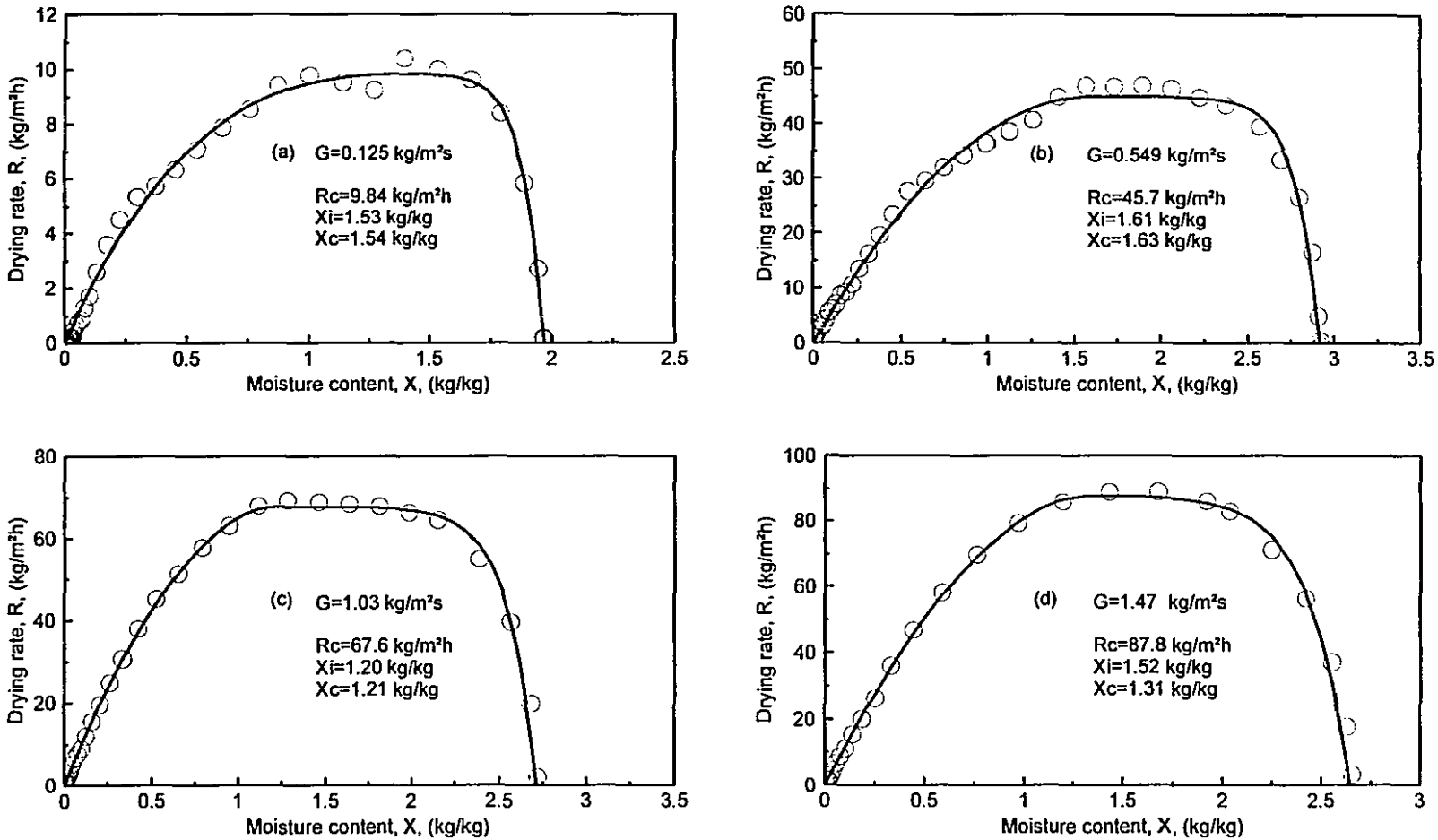

Figure 5.7 Fitting of through drying rate data at Tj=90 °C, B=25 g/m² with procedure 3

exception of case (d) where there is a constant rate period but one which, judged by the data, is unrealistically short.

When faced with the challenge in determining values of X_i and X_c for through drying paper without knowing the R-X relation in either the increasing or falling rate period, Polat O. (1989) developed the following practical method: when there was clearly a constant rate period and value of R_c but the transition was gradual from the increasing to the constant rate period or from the constant rate period to the falling rate period, he took as X_i or X_c the moisture content where the drying rate was $0.95R_c$. Where there was a constant rate period but with an irregular drying rate, he took as X_i and X_c the moisture contents at $R=0.95R_{max}$, then took as R_c the average rate over the period between X_i and X_c. Where there was no appreciable extent of constant rate period, Polat O. took as R_c the drying rate value 5% below the maximum drying rate, and defined X_i and X_c as the values of moisture content at the points of $R=0.95R_{max}$. Polat's choice of the 95% criterion was arbitrary.

As procedure 3 gives an excellent fit for complete drying rate curves, these curves provide a better basis for definition of X_i and X_c than the use by Polat O. of R_{max} values which are very sensitive to experimental noise. On the curves of normalized drying rate R/R_c for these same four drying conditions, figure 5.8, the two values of moisture content at Polat's criteria of $R=0.95R_c$ can be seen to give an over-estimated X_i and an under-estimated X_c , i.e. to exaggerate the length of the constant rate period. In order to select an appropriate criterion for defining the start and end of the constant rate period, and hence the values of X_i and X_c , Table 5.2 lists for the four figure 5.8 cases the values of X in the increasing and falling rate periods as a function of normalized drying rate, R/R_c , varying from 0.995 to 0.95 . Also included are the X_c and X_i values determined with procedure 3 as listed on figure 5.7. For one typical set of data, figure 5.8 (b), these values are shown on figure 5.9. There is no firm basis for adopting a particular value of normalized drying rate R/R_c as the standard for the definition of X_i and X_c and thereby the length of the constant rate period. However the value of $R/R_c=0.95$ used by Polat O. clearly appears to be too low, giving a constant rate period of exaggerated length, while the use of

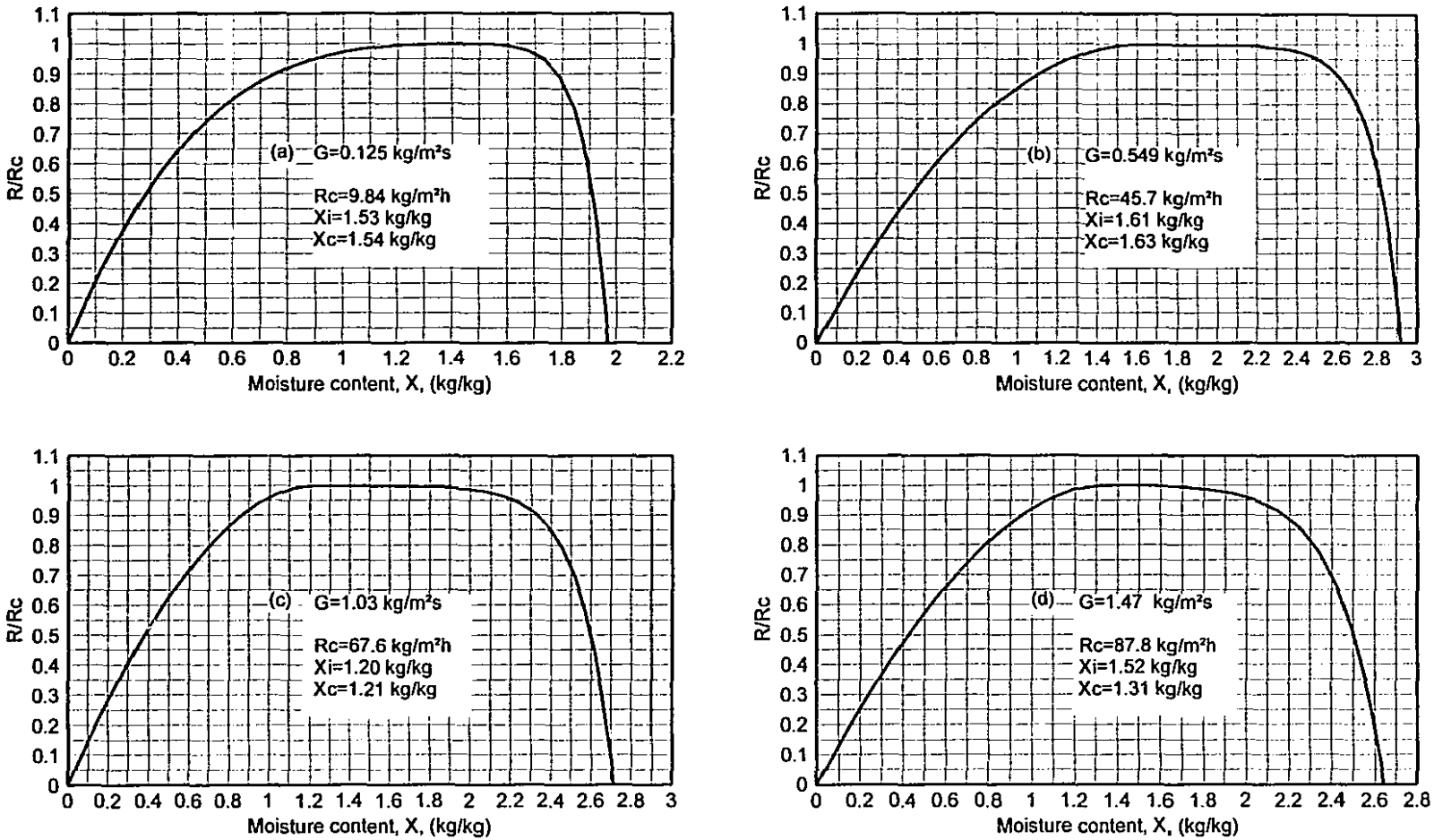

Figure 5.8 Normalized drying rate history at Tj=90 °C, B=25 g/m² with procedure 3

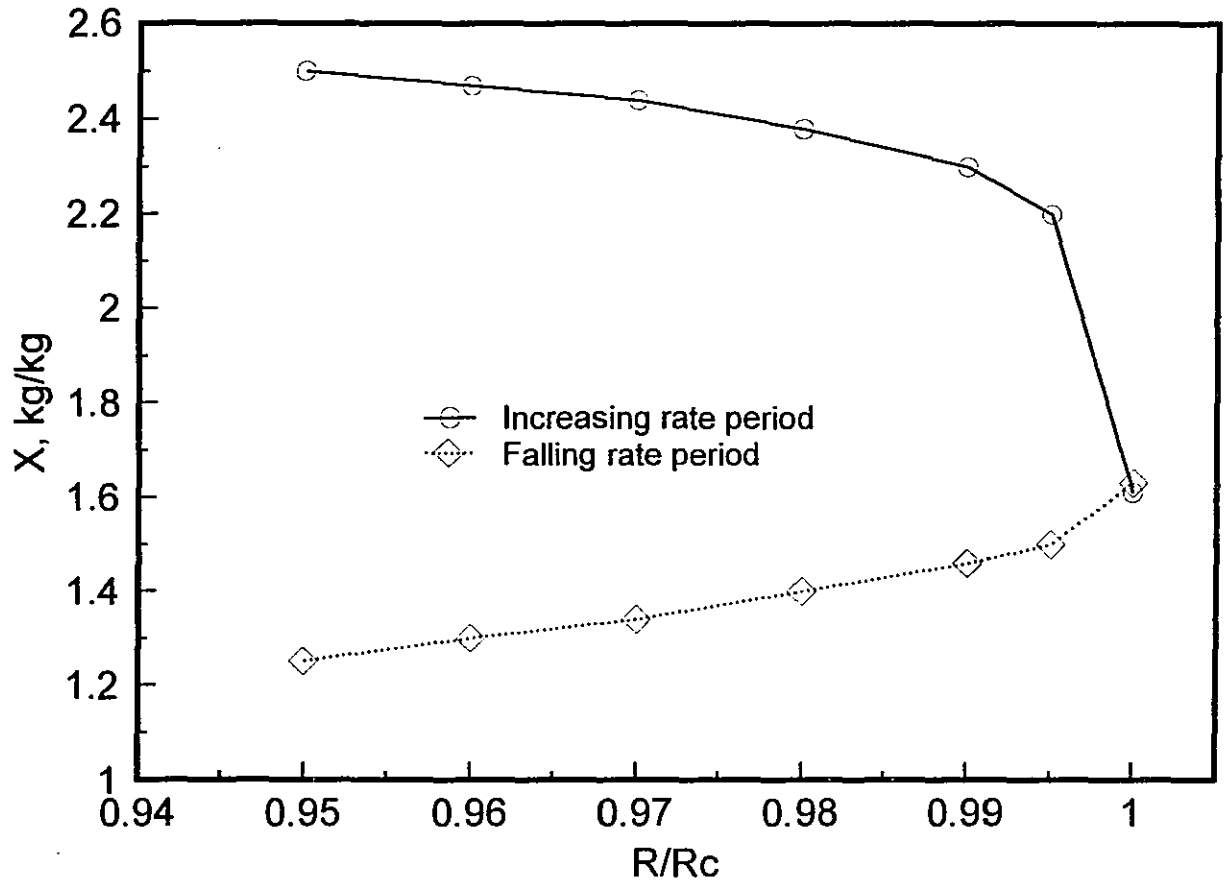

Figure 5.9 Moisture content during increasing and falling rate periods as a function of normalized drying rate for the complete drying rate curve by procedure 3

R/R_c=0.995 correspondingly appears on figure 5.9 to be clearly too high, giving an unrealistically short constant rate period.

Table 5.2 Values of moisture content in increasing and falling rate periods

Case / R/R_c	Increasing rate period				Falling rate period			
	(a)	(b)	(c)	(d)	(a)	(b)	(c)	(d)
Fig. 5.7	1.53	1.61	1.20	1.52	1.54	1.63	1.21	1.31
0.995	1.58	2.20	1.85	1.69	1.20	1.50	1.15	1.26
0.99	1.62	2.30	1.95	1.76	1.13	1.46	1.11	1.22
0.98	1.66	2.38	2.06	1.88	1.05	1.40	1.07	1.17
0.97	1.68	2.44	2.13	1.95	0.98	1.34	1.03	1.14
0.96	1.70	2.47	2.18	2.00	0.93	1.30	1.00	1.10
0.95	1.72	2.50	2.22	2.05	0.90	1.25	0.97	1.08

Figure 5.9 shows that the X - R/R_c relations change slowly for R/R_c from 0.95 to 0.98, while above 0.98 the values of X change rapidly. Thus R/R_c=0.98 was adopted as a rational value for determination of the extent of the constant rate period and hence of X_i and X_c. This method of determining X_i and X_c is denoted as procedure 4.

With the adoption of procedure 3 for determining R_c and procedure 4 for obtaining X_i and X_c, only a final step remains to obtain the complete quantitative expression for drying rate curves. This step, referred to as procedure 5, involves using the determined values of R_c, X_i and X_c in the equations

$$\frac{R}{R_c} = \frac{1 - e^{-n_i\left(\frac{X_o - X}{X_o - X_i}\right)}}{1 - e^{-n_i}} \qquad \text{for} \quad X_o \geq X \geq X_i \qquad (5.7)$$

and

$$\frac{R}{R_c} = 1 - \left(1 - \frac{X}{X_c}\right)^{n_f} \qquad \text{for} \quad X_c \geq X \geq 0 \qquad (5.10)$$

to obtain the power law exponents n_i and n_f from reapplying the statistical regression. This three step method, i.e. procedures 3, 4 and 5, is easily executed by computer.

For the same four test sets of experimental data, figure 5.10 shows the fitting of the complete drying rate data and the values of the set of quantitative parameters, R_c, X_i, X_c, n_i and n_f determined from the combined procedure 3, 4 and 5. The quality of fit to the

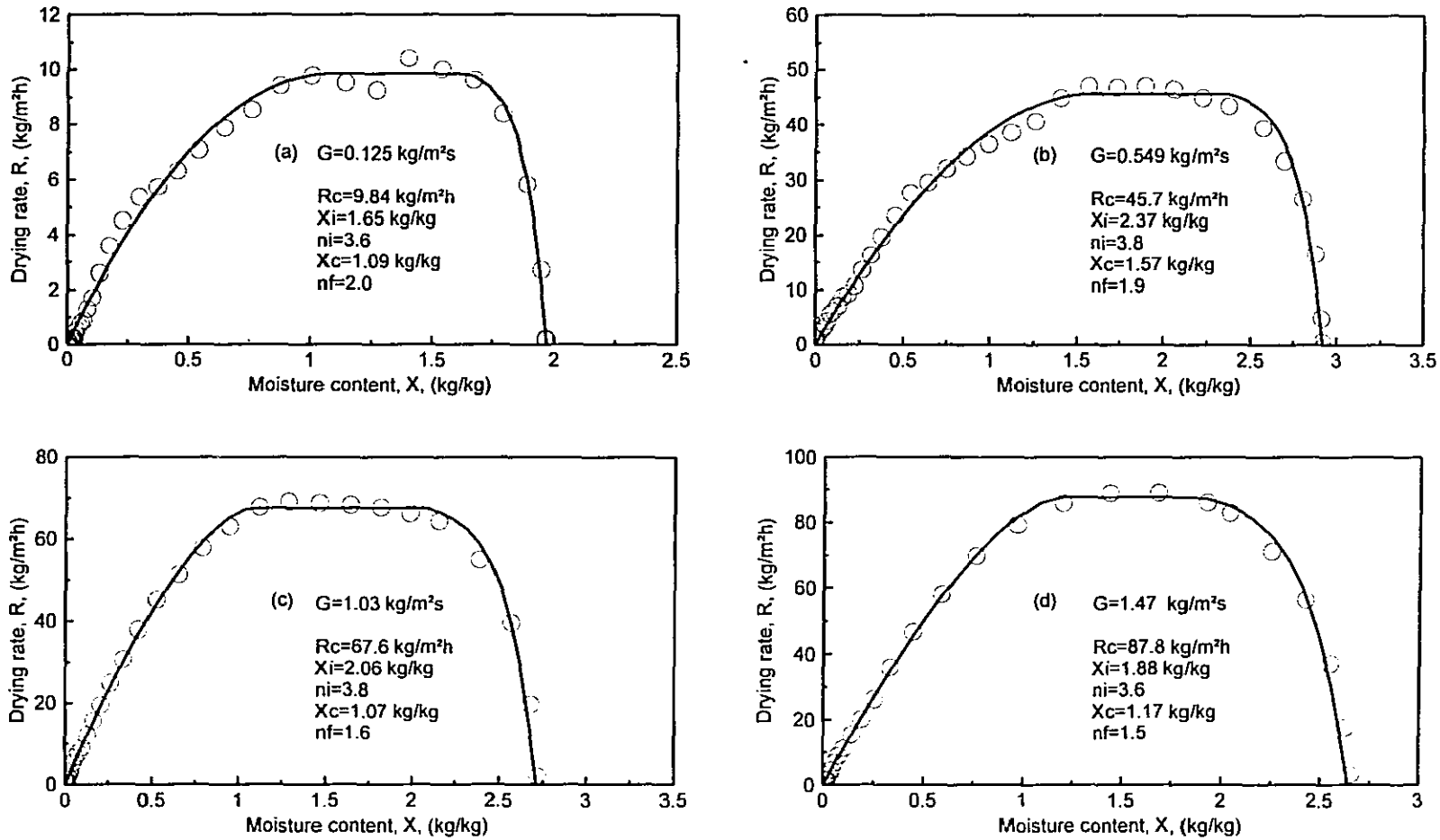

Figure 5.10 Fitting of through drying rate data at Tj=90 °C, B=25 g/m² with combined procedures 3, 4 & 5

drying rate data shown on figure 5.10 cannot be differentiated from that of figure 5.7. However the unreasonable sets of values of X_i and X_c of figure 5.7, where $X_i \approx X_c$, have been replaced now by values of X_i and X_c, which are realistic with respect to the measured R - X curves. Correspondingly, the extent of constant rate periods are also consistent with the R - X measurements. Thus the final composite method of procedures 3, 4 and 5 has the advantage of providing a complete drying rate curve giving an excellent fit to the data, with three well defined drying rate periods, and a quantitative representation of the drying rate curves in terms of five parameters, R_c, X_i, X_c, n_i and n_f which are obtained by one comprehensive procedure which is totally unsubjective and which is applied to the complete experimental data from the start to the end of drying, in the same way for all experiments.

Table 5.3 lists the values of R_c, X_i and X_c determined by the above procedure and by Polat's method for these four test cases. The values of R_c from these methods agree very well, but R_c is the easiest parameter to obtain. While the values of R_c by Polat's method are obtained from only the constant rate period, the present procedure has the advantage that the determined value of R_c is in harmony with the complete drying rate data. Relative to the present procedure, all the values of X_i and X_c from Polat's method are generally slightly higher for X_i and lower for X_c, as expected since he used $R/R_c=0.95$ while $R/R_c=0.98$ is used here.

Table 5.3 Comparison of values of R_c, X_i and X_c

	Combined procedure 3, 4 and 5			Polat O. method		
Case	R_c, kg/m^{2}h	X_i, kg/kg	X_c, kg/kg	R_c, kg/m^{2}h	X_i, kg/kg	X_c, kg/kg
(a)	9.84	1.65	1.09	9.78	1.73	0.86
(b)	45.7	2.38	1.40	46.6	2.28	1.39
(c)	67.6	2.06	1.07	67.8	2.15	0.99
(d)	87.8	1.88	1.17	87.9	2.00	1.13

Figure 5.11 provides a further demonstration of fitting, using procedures 3, 4 and 5, with results for four more conditions which cover the whole spectrum of drying intensity conditions from very low ($R_c \approx 5$) to very high ($R_c \approx 120$). It is interesting to note that seven out of the eight conditions tested in figures 5.10 and 5.11 give the value of

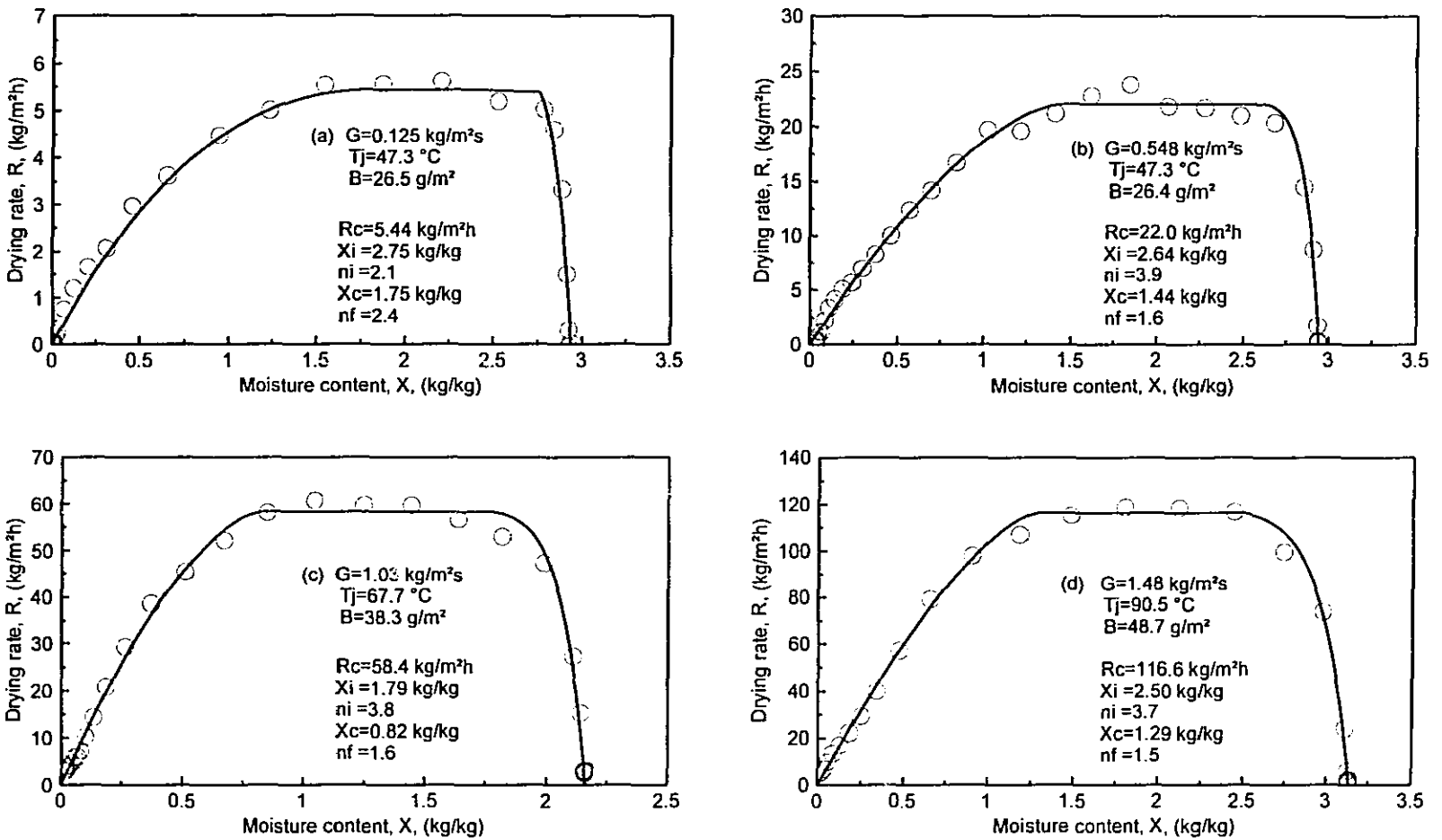

Figure 5.11 Fitting of through drying rate data from representative conditions with combined procedures 3, 4 & 5

n_i within narrow range 3.6-3.8, and that six out of eight values of n_f are in the limited range of 1.5-1.9 . This feature of stable values of n_i and n_f will be treated in section 5.5.4.

The combined procedures 3, 4 and 5 were then applied to all 89 experimental runs in order to obtain the quantitative representation of the drying rate data for each drying condition in terms of just five parameters, R_c , X_i , X_c , n_i and n_f . For those experiments carried out with unheated air, the initial short transient period while the paper was cooling was ignored as it has no relevance to the industrial practice. As such drying rate curves consist of only a constant and a falling rate period, there are no values of X_i and n_i .

5.5 Analysis of results

5.5.1. Moisture content at end of increasing rate period, X_i

For the 60 drying conditions which give an increasing rate period, i.e. all except those using unheated air, a significance test was carried out on the values of X_i with respect to the variables X_o , T_j , G and B. The extent of increasing rate period, X_o - X_i , was found to correlate with paper basis weight B and with the drying conditions G and $\Delta T = T_j - T_{as}$. A regression using equation 5.11 gave the best fit values listed in Table 5.4 with parameters designated as ε, with R^2 being 0.84.

$$X_o - X_i = a_i \, G^{b_i} \Delta T^{c_i} B^{d_i} \qquad (5.11)$$

Table 5.4 Correlation parameters for X_o-X_i

Parameter	ε	σ for ε	2σ/ε (%)	Polat O. (1989)
a_i	0.30	0.13	87	1
b_i	0.41	0.03	15	0.27
c_i	0.78	0.09	23	0.39
d_i	-0.73	0.07	19	-0.37

The extent of increasing rate period, X_o-X_i , calculated from equation 5.11, is seen on figure 5.12 to compare satisfactorily with the experimentally determined values in the

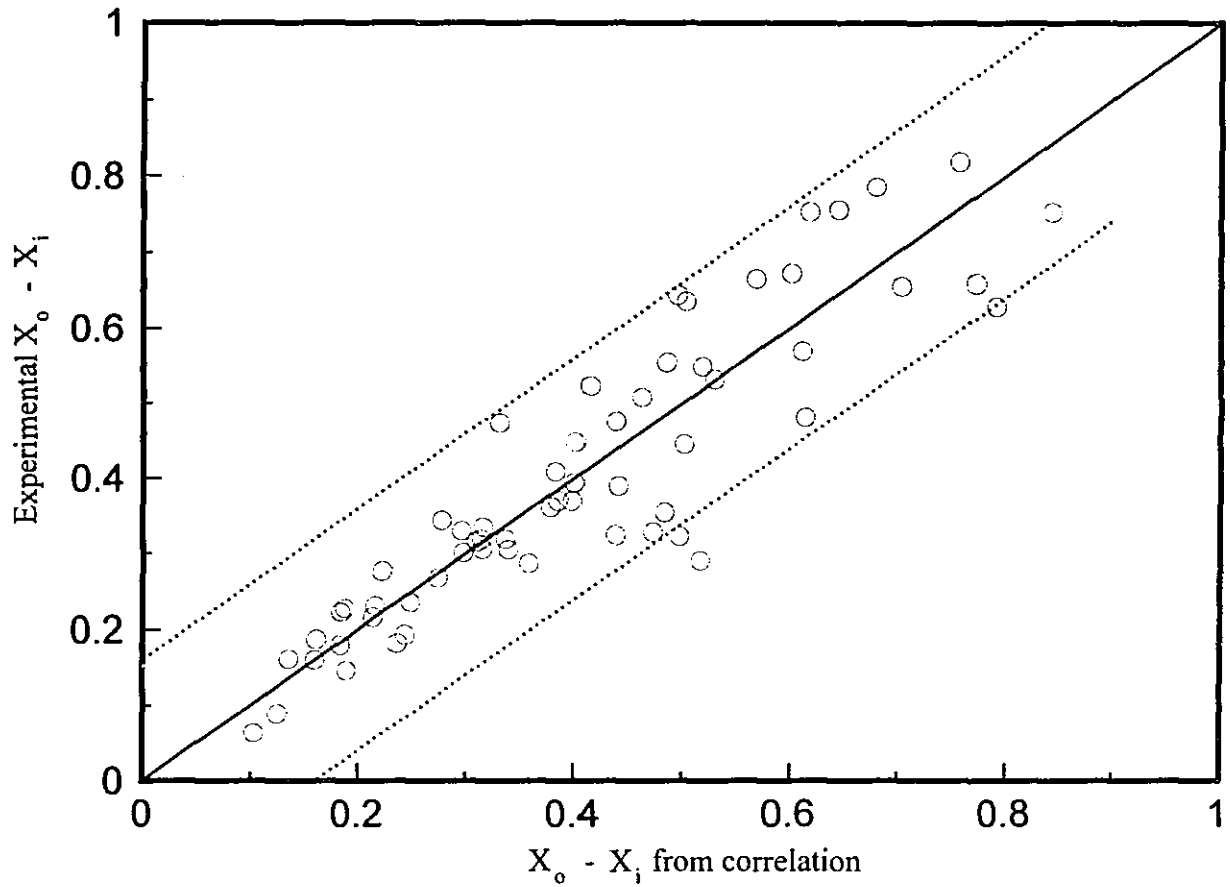

Figure 5.12 Extent of increasing rate period: comparison of experimental and calculated values from eqn. 5.11

range 0.10 to 0.84 kg/kg. The 2σ uncertainty of the calculated values of X_o-X_i is ± 0.16 kg/kg, represented by the dashed lines of figure 5.12. For drying from X_o of 2 kg water/kg fibre to a typical practical value of 5% final moisture content, the proportion of drying effected during the increasing rate period, $(X_o-X_i)/(X_o-0.05)$, predicted with equation 5.11 for the lowest basis weight - highest intensity drying conditions tested is 47%. For the higher intensity drying conditions of industrial practice, there would be no period of constant rate drying and the percentage of total drying occurring in the increasing rate period would probably remain at about that impressively high level.

As constant drying rate increases with G and ΔT it could be expected that the extent of the increasing rate period, X_o-X_i , would increase with G and ΔT, as is indeed shown by equation 5.11. The independence of X_o - X_i from paper initial moisture content X_o shows that the extent of the increasing rate period is not affected by paper permeability, which increases exponentially as paper moisture content decreases, Polat O. et al. (1989). This behavior can be explained by the fact that the development of transport area during the increasing rate period is achieved by opening pores, from larger to smaller ones. The negative dependence of X_o-X_i on B may be explained from the large increase of interfacial area, about 50% for dry paper (Polat O. 1989), for an increase in paper basis weight from 25 to 50 g/m^2. Hence the amount of water removed during the increasing rate period to develop the amount of interfacial area needed to get R up to R_c should be much less for 50 g/m^2 than for 25 g/m^2 paper, as is represented by $(X_o-X_i) \propto B^{-0.73}$.

The effect of temperature driving force ΔT on X_o-X_i for the present study is significantly higher than found by Polat O. (1989). There is a significant difference in data treatment between the two studies, with the present one using only the results with heated air while Polat O. included his measurements with unheated air. With ambient temperature drying air the initial transient due to paper cooling, which results in the peak value of R seen on figures 5.1(a) and 5.4(a) immediately after drying starts, has a distorting effect on the results. It is believed that the exclusion in the present study of such results provides a more soundly based correlation.

The difference in the effect of paper basis weight between this study and that of Polat O. derives from the difference in the range investigated, 25 to 50 g/m^2 with here, 25 to 250 g/m^2 by Polat O. The specific surface of paper becomes independent of basis weight for thicker papers. Thus considering the mechanism proposed above for the effect of basis weight on extent of the increasing rate period, this dependence should be much less when the high basis weight data are included, as is the case for Polat's study. Because the industrial interest in through drying focuses on for the 25-50 g/m^2 range of basis weight, the correlation obtained here, based on data only in this range, is of greater relevance.

5.5.2 Constant drying rate, R_c

During the constant rate period of through drying the sheet should be at the adiabatic saturation temperature of the inlet air, as was confirmed experimentally. During this period the drying rate driving force is that for heat transfer, $\Delta T=T_j-T_{as}$. From the R_c-ΔT results of figure 5.13 it is seen that at low levels of ΔT, R_c is independent of basis weight, indicating that the through flow exiting the sheet is saturated. For thicker paper, B of 50 g/m^2, a linear relationship between R_c and ΔT can be observed for all levels of air mass flow rate, G. However for higher levels of ΔT, the R_c-ΔT relation deviates from linearity with thin paper, B of 26.5 g/m^2. Stated otherwise, at higher levels of ΔT, R_c is not independent of B but decreases with the decrease of B, for which cases the through flow is evidently not saturated when it exits the sheet. This effect is illustrated again on figure 5.14 which, at four levels of drying temperature, shows directly the effect of G on R_c . The R_c-G relation was found to be independent of paper basis weight only at conditions of lower drying intensity. For the two lower values of G, figure 5.14 shows that R_c is independent of B for T_j of 22 °C. At T_j=89°C, figure 5.14 (d) shows that R_c is independent of B only at the lowest value of G, for which the through flow still exists saturated. At all other combinations of T_j and G, figures 5.13 (d) and 5.14 (d) show that the through flow does not become saturated even for the thicker paper, B=50 g/m^2, as the

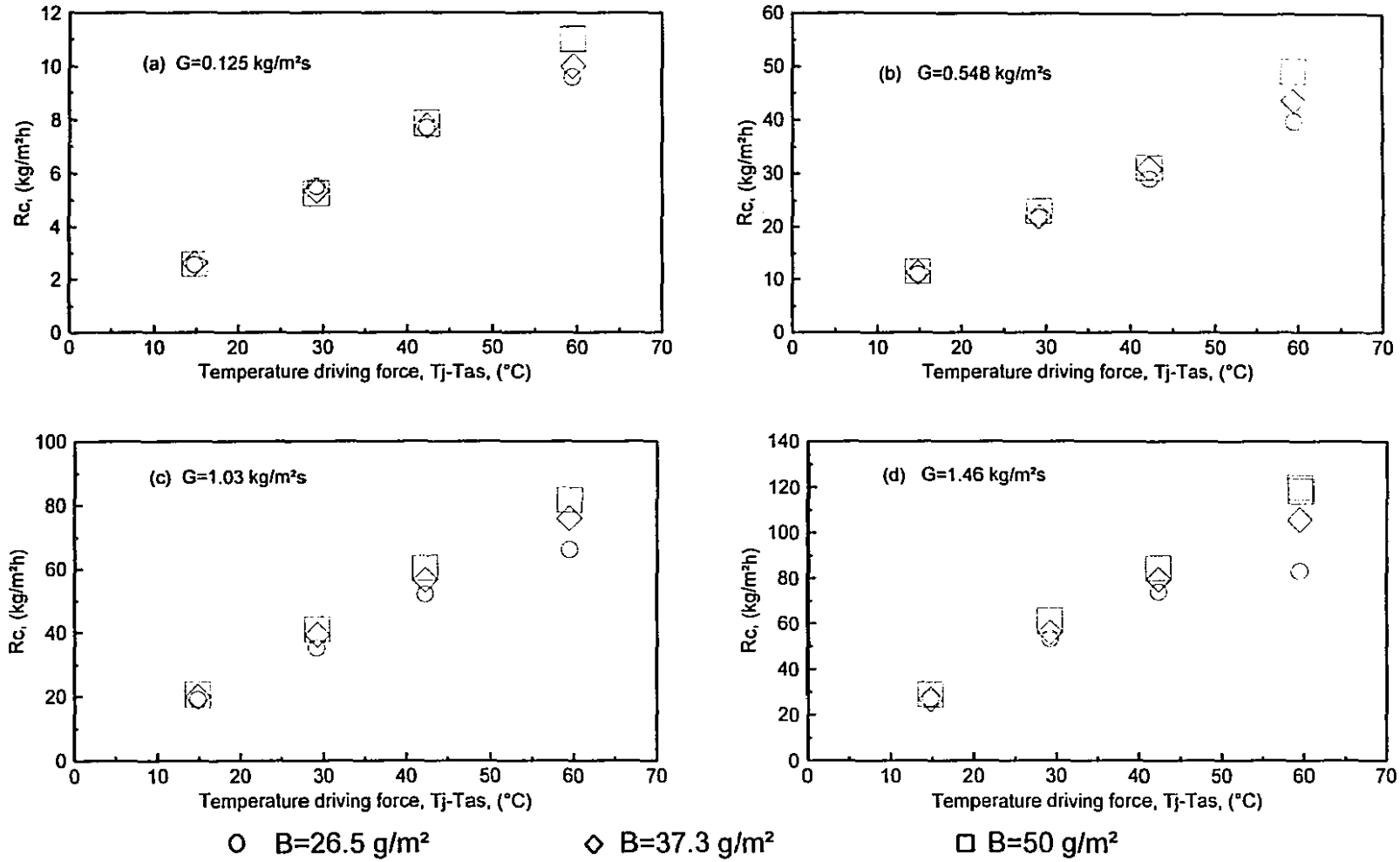

Figure 5.13 Effect of temperature driving force on constant drying rate

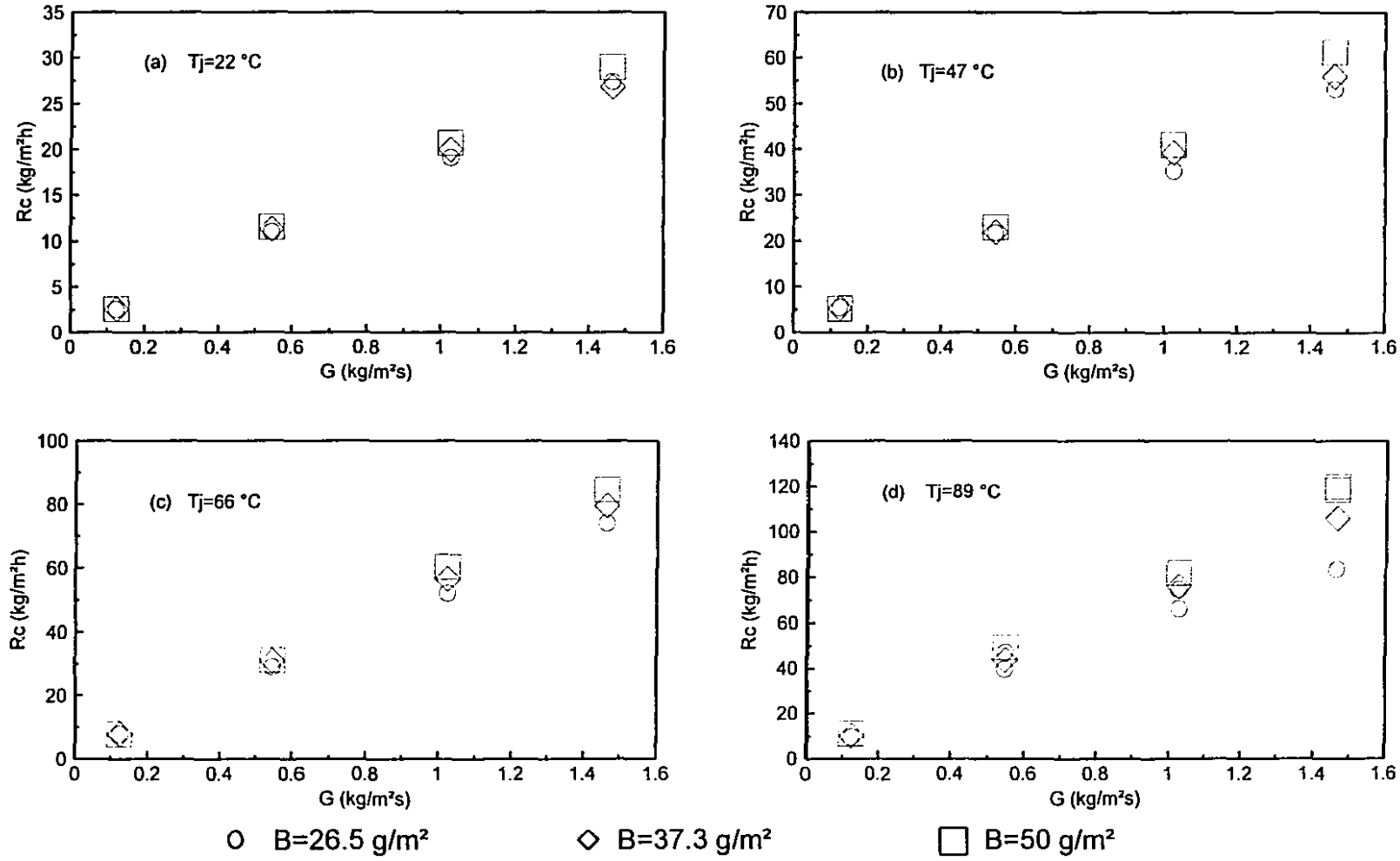

Figure 5.14 Effect of air mass flow rate on constant drying rate

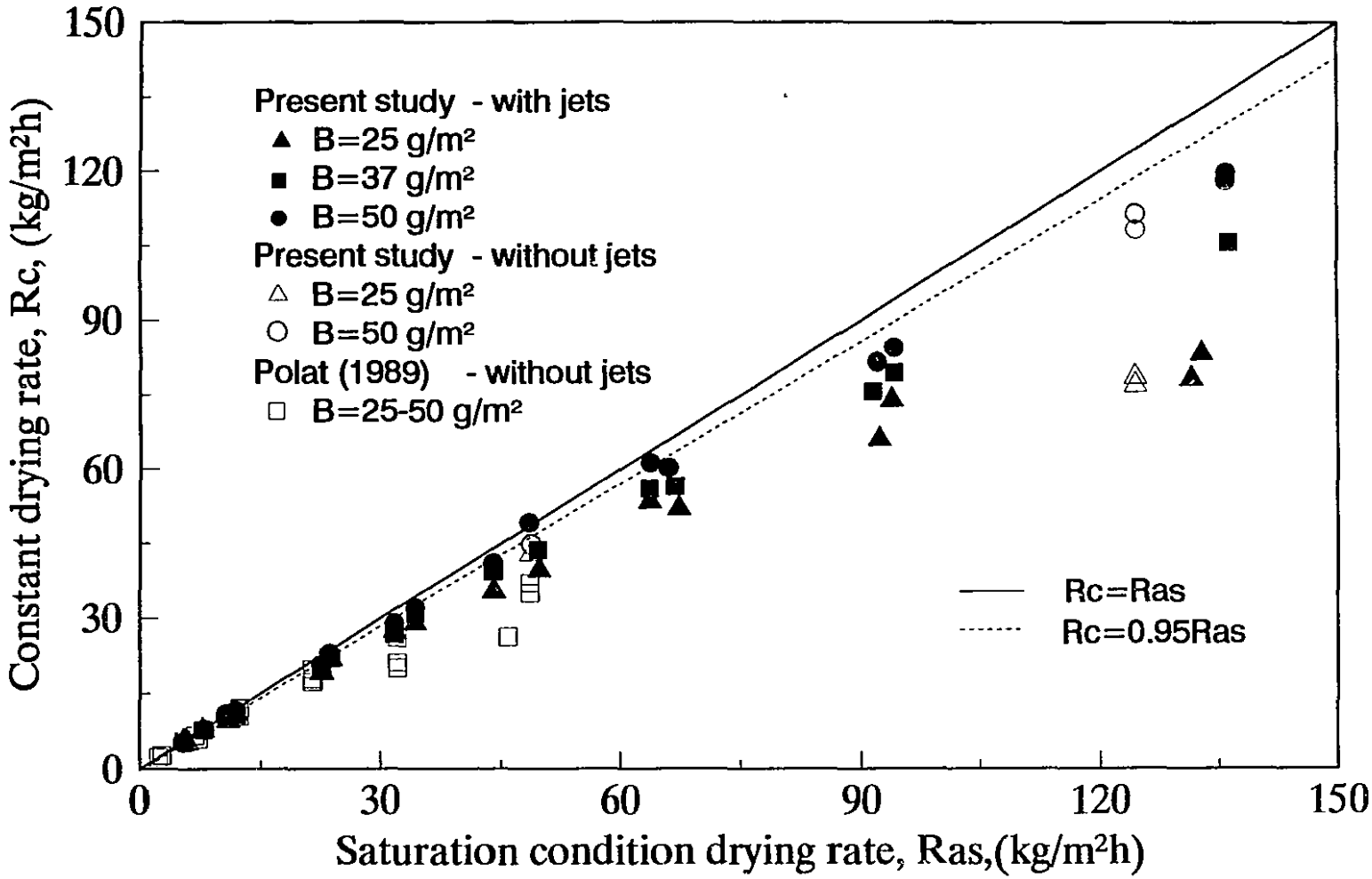

Figure 5.15 Relation of Constant Drying Rate to Saturation Drying Rate

paper does not provide sufficient interfacial area for the heat and mass transfer to produce saturated air out of the sheet.

The dependence of R_c on B can be further examined by comparing R_c with the maximum achievable through drying rate, R_{as}, when the through flow exits adiabatically saturated, figure 5.15. By definition, R_{as} is directly proportional to ΔT and G, independent of B. At low values of R_{as} the difference between R_c and R_{as} on figure 5.15 is insignificant. As the drying intensity increases, constant drying rate R_c becomes strongly dependent on B, indicating that the through flow exits the sheet at substantially below the saturation condition. At the highest drying intensity for the present investigation the through flow exited the sheet at 88% of saturation humidity for paper of basis weight B=50 g/m^2, but at only 62% of saturation for B=25 g/m^2. The present results for through drying with and without impinging jets follow the same trend. For through drying without impinging jets the results of Polat O. (1989) coincide with those of the present study at low levels of drying intensity but are below the present measurements in the range of drying intensities which are the highest ($R_{as} \approx 50$ kg/m^{2}h) of his study, but which correspond to intermediate levels of R_{as} here.

The treatment for the constant drying rate proceeds from the analysis of section 5.4.1, specifically equation 5.2,

$$R = \frac{3600GC_p\left(T_j - T_{as}\right)}{\lambda}\left(1 - e^{-\frac{h(X)\,a_p(X)\,L}{GC_p}}\right) \qquad (5.2)$$

For constant rate drying R is independent of X, and is denoted as R_c. During the constant rate period, R_c may be controlled solely by thermodynamics, i.e. $R_c=R_{as}$, which applies when $ha_pL \gg GC_p$, or $L \gg GC_p/(ha_p)$ for a sufficiently thick bed, the exponential part of equation 5.2 goes to zero. Alternatively if $R_c<R_{as}$, then R can be independent of X only when $h(X)a_p(X)$ remains at a constant value of ha_p. For the thermodynamic equilibrium case:

$$R_c = R_{as} = \frac{3600GC_p\left(T_j - T_{as}\right)}{\lambda} \qquad (5.12)$$

For the case of dynamic equilibrium with ha_p independent of X and $R_c<R_{as}$, equation 5.2 may be expressed in a Taylor's series as:

$$R_c = \frac{3600\, GC_p\Delta T}{\lambda}\left[\frac{h a_p L}{GC_p} - \frac{1}{2}\left(\frac{h a_p L}{GC_p}\right)^2 + \cdots + \frac{(-1)^{n+1}}{n!}\left(\frac{h a_p L}{GC_p}\right)^n + \cdots\right] \qquad (5.13)$$

While the existence of a constant rate period with $R_c=R_{as}$ is readily understandable, the observation of constant rate periods with R_c substantially below R_{as}, figure 5.15, requires examination. The development of interfacial area for heat and mass transfer, the predominant effect during the increasing rate period, does not stop at $X=X_i$ but continues during the constant rate period because, as will be seen subsequently, all the experimental values of X_i and most of those of X_c are higher than the fibre saturation point of X=0.8 kg/kg for the kraft pulp used. This continued opening of pores during the constant rate period has two effects, increasing $a_p(X)$ but decreasing the transfer coefficient h(X) because of the decreasing interstitial air velocity in the pores at constant G. During the constant rate period the thickness of the high moisture content region below the drying front would decrease, tending to decrease the drying rate. Thus the occurrence of a constant rate period with $R_c<R_{as}$ represents a dynamic equilibrium between an increasing $a_p(X)$ but a decreasing h(X) and decreasing thickness of the high moisture content region of the sheet.

As $h \propto Re^n$ with $Re = G\, d_p/\mu$, $a_p=f(X, B)$ and $L=f(B)$, but with a lack of relations among h(X), $a_p(X)$, G, X and B, equation 5.13 is expressed in a power law form as

$$R_c = a_r\, G^{b_r}\, \Delta T^{c_r}\, B^{d_r} \qquad (5.14)$$

Before continuing with the general case it may be noted that on figure 5.15 the R_c data falls into two categories, i.e. results that are at or close to the saturation limit of $R_c=R_{as}$, and those for which R_c is significantly below R_{as}. As $R_c=R_{as}$ is a thermodynamic limit which in practice is never quite reached, the region $0.95R_{as}<R_c<R_{as}$ may be taken as consisting of data for a close approach to saturation. Included in this region are essentially all the results at $R_{as}<15$ kg/m^{2}h. For all of the 89 combinations of conditions studied, 30 runs fall into the above definition of near-saturated exhaust, the other 59 tests

giving values of R_c substantially less than R_{as}. For conditions giving $R_c=R_{as}$, the values of the exponents in the power law correlation, equation 5.14, would be $b_r=c_r=1$ and $d_r=0$. For the 30 conditions giving near-saturated through flow exhausts, the best fit values of b_r, c_r, d_r in Table 5.5 indicate a very close approach to those limiting values. When b_r, c_r, d_r are taken as their 1, 1, 0 limit, the regression constant becomes $a_r=1.39$, a value which is very close to the theoretical value of $a_r=1.44$ from equation 5.12.

Table 5.5 Correlation parameters for R_c

	Near-Saturated conditions				Non-saturated		Polat O. (1989)
	ε	σ	ε	σ	ε	σ	ε
a_r	1.24	0.16	1.39	0.02	0.87	0.14	0.87
b_r	0.96	0.02	1		0.85	0.03	0.80
c_r	1.00	0.02	1		0.91	0.02	0.87
d_r	0.01	0.04	0		0.19	0.04	0.16
R^2	0.995		0.98		0.98		

For non-saturated conditions at the sheet exit, the effect of through flow rate on drying rate is indicated by the value of the exponent, $b_r=0.85$. It is not possible to draw quantitative inferences from this value because b_r is affected not only by the structure of the flow in the sheet but by the extent of displacement from saturation of the through flow exiting the paper. As noted earlier, $b_r=1$ for a saturated exhaust, while the data used for the non-saturated exhaust case corresponded to $0.95R_{as}>R_c>0.6R_{as}$. With this reservation, not recognized in the studies of others, it may however be noted that for through circulation drying of solids Marshall and Hougen (1942) obtained for this exponent a similar value, 0.8.

The exponent of ΔT, $c_r=0.91$, is within the range of 0.76 - 0.93 reported by Gummel (1977). As for the exponent for G, the ΔT exponent converges to $c_r=1$ for $R_c=R_{as}$, so all experimentally determined values for the non-saturated case are again affected by the degree of approach of R_c to R_{as}.

The sensitivity of R_c to B is the most complex of the equation 5.14 effects. The transport phenomena analysis of the constant rate period of through drying paper by Polat O. et al. (1992a) reported that the Sherwood number decreased sharply as basis weight

was increased from 25 to 50 g/m^2. For the same type of paper as used in the present study, Polat O. (1989) determined that because of paper structure changes, the specific surface a_p of dry paper increases by about 50% with increase of paper basis weight from 25 to 50 g/m^2, and that correspondingly the characteristic dimension d_p for air flow through the dry sheet decreases from about 17μm for B=25 g/m^2 to 4μm for B=50 g/m^2. Therefore in equation 5.13 not only does B directly affect L in the series terms, but a_p and h also depend on B. While d_r=0 represents the lack of dependence of R_c on B for the limit of a saturated through flow exhaust, the above factors cause the d_r exponent to increase from zero to about 0.2 for drying conditions with R_c lower than R_{as}.

Although the results of Polat O. remain the best available for comparison, it should be noted that the value of a_r=2.4 given by Polat O. (1989) and by Polat O. et al. (1992b) is not correct. On re-processing Polat's data the author found that the best fit value should be a_r=0.87, but the values of b_r, c_r and d_r found were those reported by Polat O. The through flow rate exponent, b_r=0.84, found here agrees with 0.80 obtained by Polat O. for through drying without impinging jets. The temperature driving force exponent, 0.86, is also in good agreement with 0.87 from Polat O. The paper basis weight exponent, 0.26, is higher than that obtained by Polat O. for two reasons. First, the present results exclude conditions giving near-saturated through flow exhausts while Polat O. did not separate his results which include considerable data for near-saturated exhausts for which it is shown here that the basis weight exponent approaches zero. Secondly, the range of B tested was 25 - 250 g/m^2 by Polat O., 25-50 g/m^2 here. Polat's results show that on all effects the sensitivity of results over the 25-50 g/m^2 range was much greater than above 50 g/m^2.

For the comparison between experimental and correlation values of R_c, figure 5.16, the Table 5.5 correlation parameters for near-saturated conditions, a_r=1.39, b_r=c_r=1 and d_r=0, were used for all results with $R_c \geq 0.95R_{as}$, and the values for non-saturated exhausts for all other cases. As the ±15% lines contain almost all of the experimental values of R_c, equation 5.14 represents the experimental results quite well in spite of all of the uncertainties noted above.

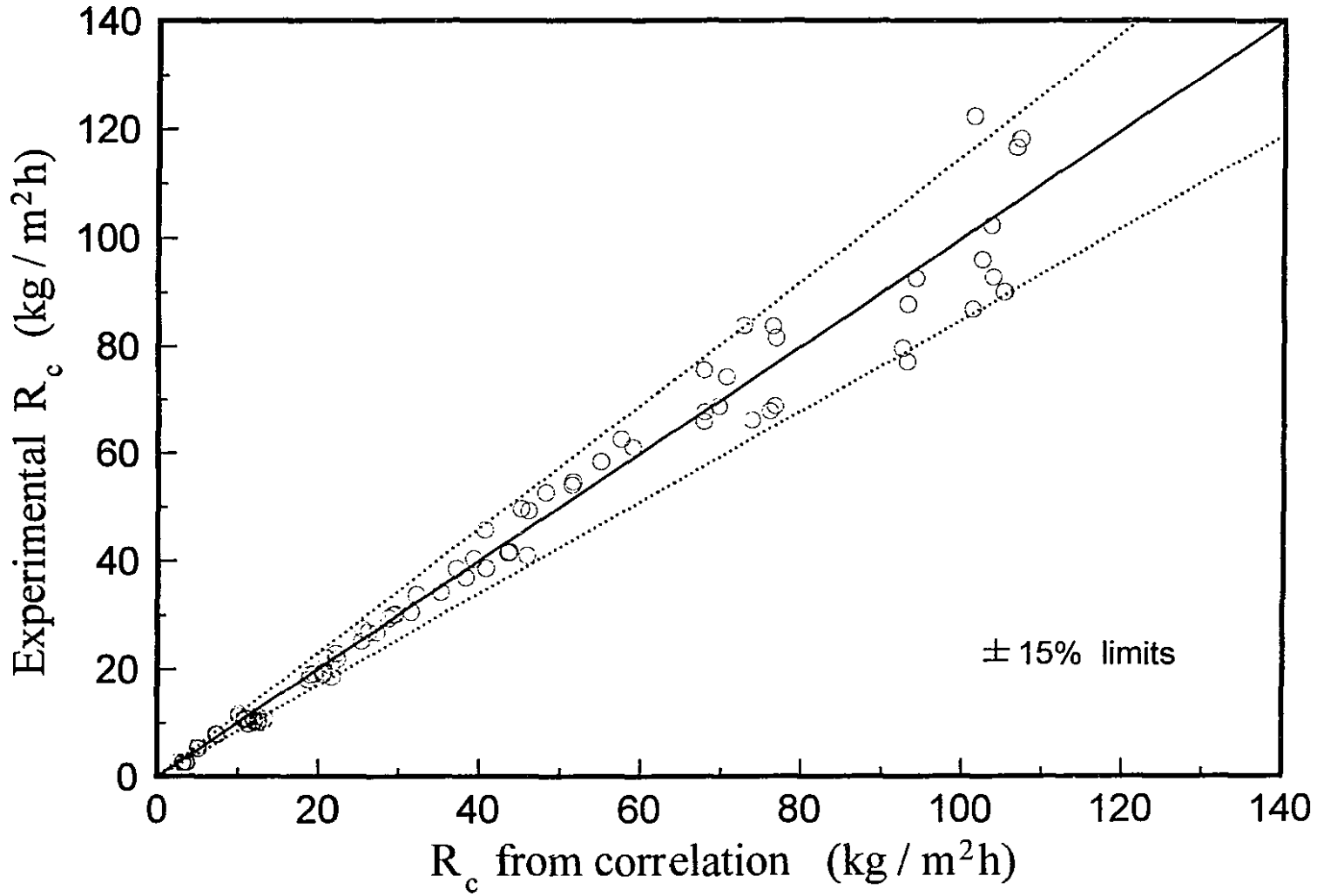

Figure 5.16 Comparison of Rc from correlation eqn. 5.14 with experimental Rc

5.5.3 Critical moisture content, X_c

The critical moisture content X_c is the that at which the drying rate can no longer be maintained at R_c . Analysis of the phenomena which bring this period to an end at $X=X_c$ requires analysis of the mechanisms which for some time maintain $R=R_c$. As detailed in section 5.5.2 concerning R_c , the principal effects which give rise to a period with R independent of X in the general case where $R_c<R_{as}$ are the simultaneous occurrence of an increasing $a_p(X)$, a decreasing h(X) and a decreasing thickness of the high moisture content region of the sheet below the drying front, which may be represented as B_w . As X decreases from X_i towards X_c , the progressively smaller size pores being opened to through flow would have less effect on interstitial air velocity and hence of decreasing h(X), than on increasing specific surface for heat and mass transfer, $a_p(X)$. However, the tendency for R to increase because of an increase in the product $h(X)a_p(X)$ is off-set by the decreasing thickness of wet region, B_w , thus maintaining $R=R_c$.

As the amount of water in the pores decreases, $a_p(X)$ eventually approaches an upper limit, as does the product $h(X)a_p(X)$. At that point the remaining effect, the decrease in B_w , would cause R to start dropping, i.e. for the falling rate period to start at $X=X_c$. Other phenomena associated with the falling rate period are decreasing vapor pressure and increasing heat of desorption of water for lower moisture content paper and increasing diffusional resistance for moisture removal from inside the fibers. With so many factors potentially contributing to controlling the falling rate period R-X curve it is not possible to know which of these was crucial to determining the critical moisture content point.

Another basic characteristic of through drying, described in section 5.3, is the basic instability of this process, i.e. that small differences in local sheet permeability initially at $X=X_o$ are amplified by the coupling between through flow rate and through drying rate, with the result that local moisture content becomes increasingly nonuniform in the plane of the sheet as drying proceeds. It follows that a sheet being through dried

will enter the falling rate period not when all parts of sheet simultaneously reach the critical moisture content, but when a significant part of the sheet can no longer locally maintain $R=R_c$. Therefore the average moisture content over the entire sheet, X_c, will be determined both by those drying variables which affect average conditions in the sheet and those which affect the degree of local nonuniformity in the sheet.

The sensitivity of X_c to the effect on sheet average conditions caused by the four variables studied, G, T_j, B and X_o as listed in Table 5.1, are considered first. The variables G and T_j affect constant rate period drying through the drying intensity, as represented by R_{as}, which varies directly with G and $\Delta T=T_j-T_{as}$. At constant B and X_o, an increase in R_{as} requires a greater thickness of the wet region of the sheet, i.e. greater B_w, to have sufficient transfer area to achieve R_c. Thus an increase in R_{as} would be expected to increase X_c.

For a specific X_o and R_{as}, the effect of basis weight would relate to the thickness of wet fibres, B_w, required to maintain drying rate at R_c. As this B_w value could be expected to be independent of the thickness of relatively dry fibres above the wet region, i.e. independent of $B-B_w$, it follows that a higher value of B should correspond to a lower value of X_c.

Considering now the effect of process conditions on the degree of local nonuniformity in the sheet during the constant rate period, a higher value of X_o, which allows a longer time for local nonuniformity of X to develop, would result in a higher sheet average value of X_c. This increase of X_c with X_o occurred also for pure impingement drying, chapter 4, for the same reason. However one drying process variable, through flow rate G, may act on development of local nonuniformity through a mechanism which is in addition to its effect via R_{as} ($\propto G\Delta T$) on sheet average conditions described earlier. At low G the low pressure drop across the sheet would be insufficient to open air flow channels through the smaller pores, with the result that such pores may remain for a longer time blocked to through flow. As local nonuniformity effects could thereby be enhanced by low G but reduced by high G, critical moisture content could be reduced with increasing G through this effect.

Thus X_c should be tested in the form

$$X_c = a_c X_o^{b_c} R_{as}^{c_c} B^{d_c} G^{e_c} \qquad (5.15)$$

Using values of X_c from the 89 experimental conditions, the results obtained are given as:

Table 5.6 Correlation parameters for X_c

Parameter	ε	σ for ε	2σ/ε (%)	Polat O. (1989)
a_c	0.67	0.23	69	0.28
b_c	0.58	0.16	55	1
c_c	0.15	0.04	53	0.13
d_c	-0.19	0.07	74	0
e_c	-0.17	0.04	47	-0.13

Thus a statistically significant correlation was obtained for the effect on X_c of the four drying process variables tested with, as expected from the above analysis, X_c increasing with X_o and R_{as} and decreasing with B and G. On the figure 5.17 comparison between experimental and equation 5.15 values of X_c the dotted lines show the 2σ uncertainty limits of 0.35 kg water/kg fibre. This uncertainty could be expected to be almost double that for X_i, 0.16 kg/kg on figure 5.16, as the uncertainty at the end of the constant rate period includes that at the start of this period. Hence a lower R^2 is expected for the X_c correlation than the R^2=0.84 for the X_i correlation. As the absolute values of c_c and e_c in equation 5.15 are effectively the same, the net effect of G and R_{as} ($\propto G\Delta T$) on X_c could be expressed in terms only of ΔT. However, as there are mechanistic reasons for separate effects by G and R_{as}, the correlation was retained in the equation 5.15 form. For the highest T_j - lowest B - highest X_o tested, equation 5.15 predicts X_c=1.3 kg/kg, which may be compared with the prediction of X_c=0.62 kg/kg for the lowest T_j - highest B - lowest X_o studied.

Polat O. (1989) did not detect the dependence of X_c on R_{as} and G that was found here, but reported a correlation of X_c with X_o and $\Delta T^{0.13}$. As $R_{as} \propto G\Delta T$, the values of c_c and e_c for Polat's case are given in Table 5.6 as 0.13 and -0.13 respectively. Three differences between the studies which may have contributed to this difference in X_c correlation are that the present study used a more standardized method of determining

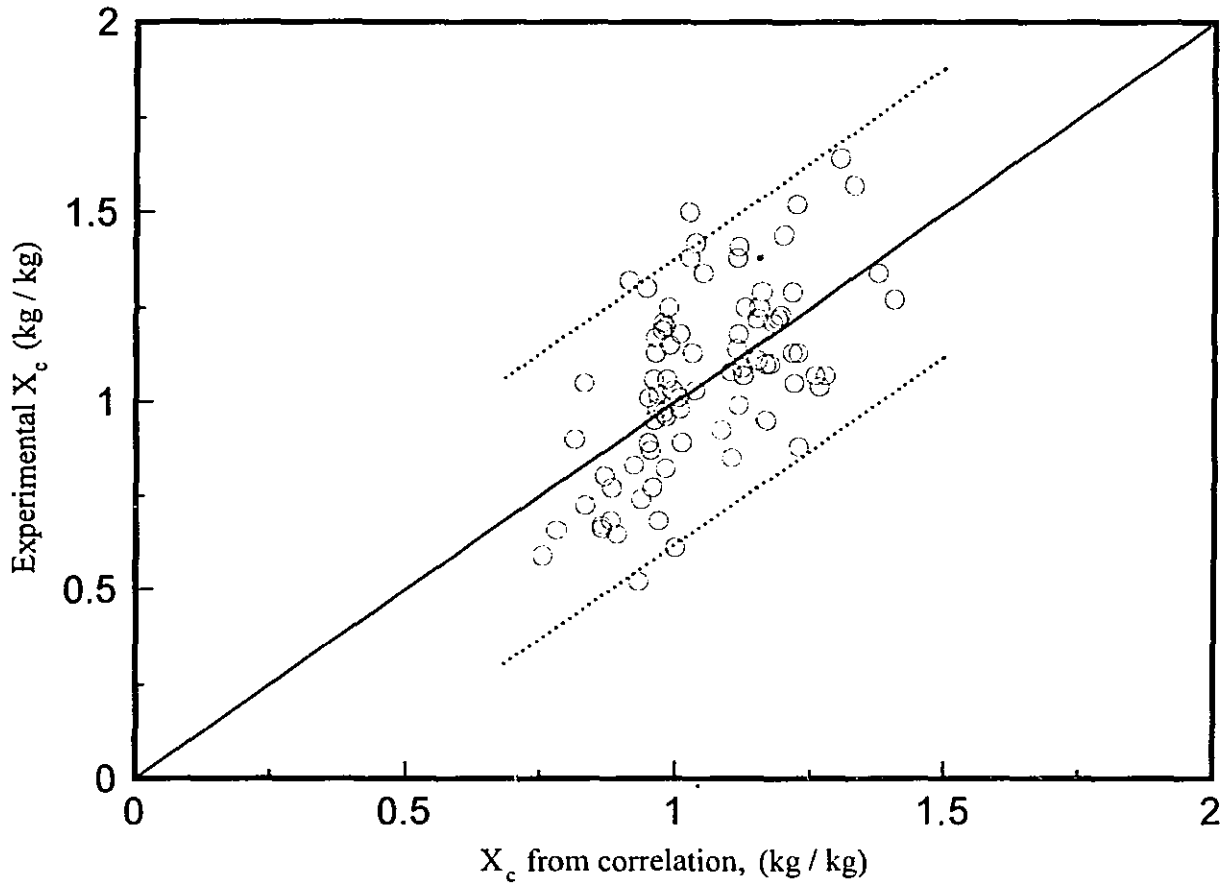

Figure 5.17 Comparison of Xc from correlation eqn. 5.15 with experimental Xc

X_c , that a much wider range of G was used (0.1-1.5 kg/m^{2}s compared to 0.1-0.5 kg/m^{2}s by Polat O.) and the use of a much narrower range of B (25-50 g/m^2 instead of 25-250 g/m^2). The higher values of G may have helped reduce the local nonuniformity effect for the present study, hence the smaller dependence of X_c on X_o obtained here than by Polat O. It may be for the same reason why Polat O. did not detect a paper basis weight effect although he used B up to 250 g/m^2.

With more than one third of the sheets dried in the present study being 25 g/m^2 paper, the well known difficulty of forming reproducible handsheets in the range of tissue paper no doubt is the source of a significant fraction of the experimental uncertainty in critical moisture content.

For each set of drying process conditions there exists a unique initial moisture content, denoted as X_o^{ic}, for which X_i=X_c and the constant drying rate is therefore reached only momentarily. From equations 5.11 and 5.15, X_o^{ic} can be expressed as:

$$X_o^{ic} = \frac{a_i G^{b_i} \Delta T^{c_i} B^{d_i}}{1 - a_c \left(X_o^{ic}\right)^{b_c - 1} R_{as}^{c_c} B^{d_c} G^{e_c}} \qquad (5.16)$$

X_o^{ic} increases as R_{as} increases and as B decreases. The present study provides measurements for through drying with a constant rate period, up to the limit of this period just vanishing, i.e. to the X_o=X_o^{ic} limit. For the higher drying intensity conditions of industrial air through drying of paper, X_o could be less than X_o^{ic} , with drying progressing directly from the increasing rate to the falling rate period.

5.5.4 Normalized drying rate curve, n_i and n_f

Having now analyzed X_i , R_c and X_c and obtained appropriate correlations, it remains only to treat the R-X curves in the increasing and falling rate periods, represented by the power law exponents n_i and n_f , in order to have all elements to describe quantitatively the complete drying rate curves. With respect to n_i it was noted in section 5.4.3 that for the eight test cases shown on figures 5.10 and 5.11, n_i values are within a narrow range despite the wide range of drying process conditions. For conditions giving

$R_c=R_{as}$, equation 5.2 may be rearranged by combining equations 5.5, 5.6 and 5.12 to give the R-R_c relation as:

$$R = R_c\left(1-e^{-n_i\frac{X_o-X}{X_o-X_i}}\right) \qquad (5.17)$$

With $R=0.98R_c$ at $X=X_i$, as used in the comprehensive procedure detailed in section 5.4.3, equation 5.17 gives a single value of $n_i=3.9$, independent of drying process conditions. For conditions that give R_c substantially below R_{as}, n_i would be expected to be somewhat lower than 3.9. The scatter in the determined n_i derives primarily from the curve fitting over an extent of increasing rate period, X_o - X_i, which varied greatly, from 0.1 to 0.84 kg/kg as seen in figures 5.10 and 5.11. Thus a universal value of $n_i=3.6$, the mean of the 60 values of n_i determined in the present study, may be used in equation 5.7 R-X relationship in the increasing rate period.

Similarly in the falling rate period, the power-law exponent n_f is almost normally distributed around a mean of 1.7, with a standard deviation of 0.4. A universal value of $n_f=1.7$ satisfactorily describes the R-X relationship in the falling rate period. Gummel and Schlünder (1980) found a similar behavior for air through drying of textiles and tissue paper. They reported that for each material tested a single normalized drying rate curve, R/R_c as a function of X/X_c, independent of drying process conditions, represented the results well. Randall (1984) also reported that for through drying of paper, equation 2.7 could be used to describe the R-X relationship in the falling rate period using a single value of his parameter a_f.

Air through drying may then be represented by a drying rate curve of universal form defined by the following equations, with $n_i=3.6$ and $n_f=1.7$.

$$\frac{R}{R_c}=\frac{1-e^{-n_i\left(\frac{X_o-X}{X_o-X_i}\right)}}{1-e^{-n_i}} \qquad \text{for} \quad X_o \geq X \geq X_i$$

$$\frac{R}{R_c}=1 \qquad \text{for} \quad X_i \geq X \geq X_c$$

and $$\frac{R}{R_c} = 1 - \left(1 - \frac{X}{X_c}\right)^{n_f} \qquad \text{for} \qquad X_c \geq X \geq 0$$

In the model of Polat O. et al. (1991) for through drying of paper, the R-X relationship in increasing rate period was in a similar form of equation 5.7 with $n_i \approx 3$, although it was not stated explicitly. Instead of treating the product of h(X) and $a_p(X)$ as a function of paper moisture content, equation 5.5, they applied over the increasing rate period the heat and mass transfer coefficient obtained from the constant drying rate results. For the interfacial transport area, Polat O. et al. obtained an exponential $a_p(X)$-X relationship, with $a_p(X) \propto \Delta P(X)^{-1/2}$, by assuming the pressure drop across the sheet, $\Delta P(X) \propto \exp(X)$, and $\Delta P(G) \propto G$ according to Darcy's law. The rapidly decreasing pressure drop was related to the increase in number of pores open for through flow, hence the interfacial area for heat and mass transfer.

During the falling rate period Polat O. et al. attributed the drop of drying rate to vapor pressure depression and increase of heat of desorption, the same as in the model of Crotogino and Allenger (1979) reviewed in chapter 2, section 2.4. Their model over predicts the drying rate.

Shown in figure 5.18 are comparisons of results when the universal values of n_i and n_f are used, relative to the results when the best fit values of n_i and n_f for each individual drying process condition, determined by procedures 3, 4 and 5. Cases (a) and (b) represent the highest and the lowest values of n_i found for the 60 experimental conditions that gave an increasing rate period, while cases (c) and (d) are the cases for the highest and the lowest values of n_f determined for the 89 conditions.

Although figure 5.18 shows the four worst cases out of all the experiments the differences in drying rate curves are relatively small between use of the universal n_i and n_f values relative to the best fit n_i and n_f values from the individual experiment. The agreement between X_i individually determined, and X_i determined using $n_i=3.6$ for the two worst cases, (a) and (b), are well within the 0.16 kg/kg uncertainty of equation 5.11 for X_i . The differences between X_c determined individually and that determined with $n_f=1.7$ are also within the uncertainty limits of equation 5.17 except for case (c). For this

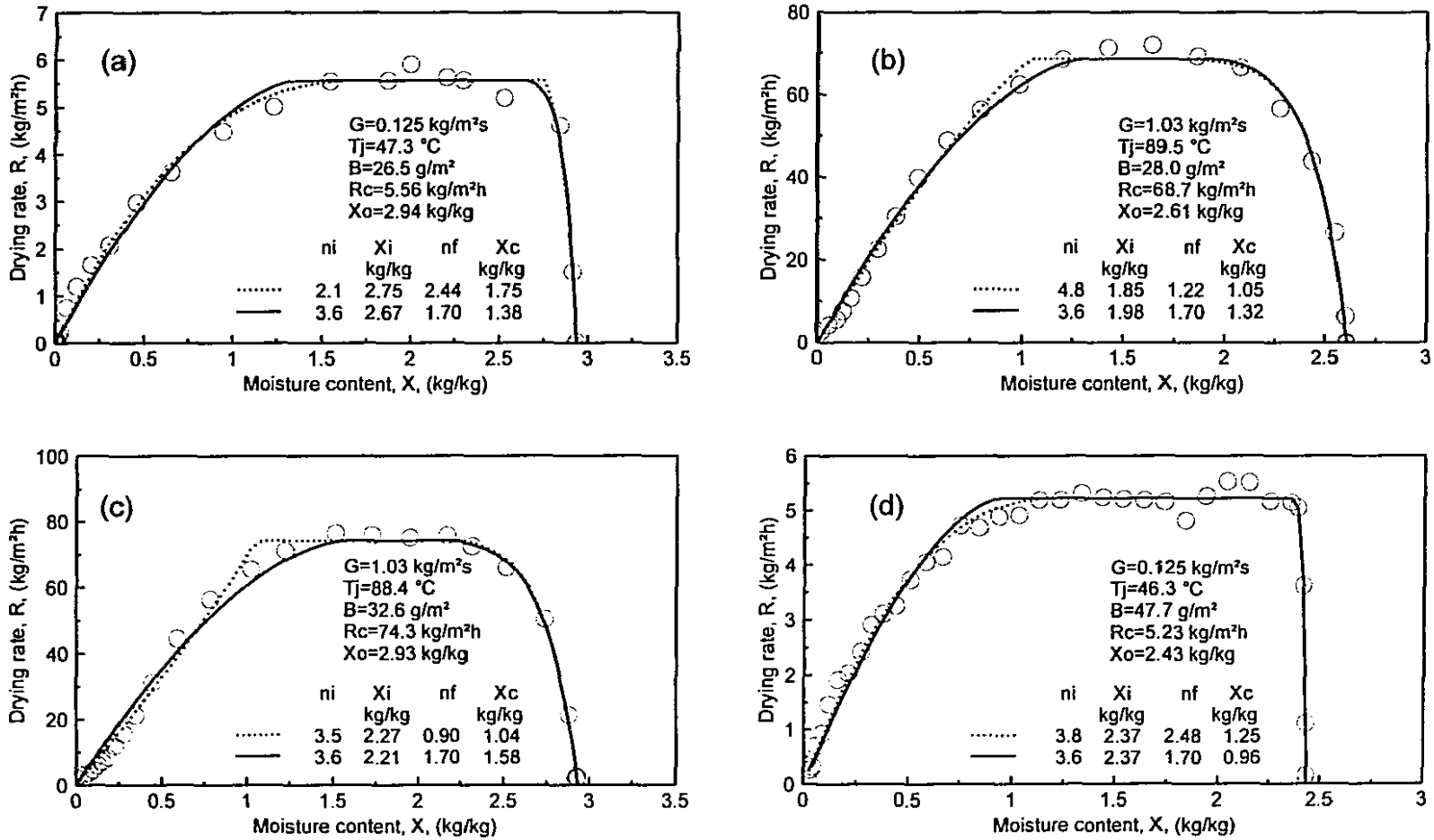

Figure 5.18 Comparison of fitting with normalized drying rate curve equations and with procedures 3, 4&5

extreme case however the normalized drying rate curve not only fits the data well but by visual inspection gives the more realistic value of X_c . Therefore, it is concluded that drying rate curves can be constructed using the universal values of the parameters n_i and n_f. This conclusion will be reinforced in section 5.6 where drying time, which is much more important than the individual parameters X_i , X_c , R_c , n_i and n_f , will be seen to be reliably calculated using the universal values of n_i and n_f.

5.5.5 Comparison with through drying without impinging jets

For through drying with and without impinging jets, the air flow and temperature fields are quite different above the moist sheet. With jets, the high heat and mass transfer coefficients under turbulent impinging flow leads to the air entering the sheet at a considerably lower temperature and higher humidity than for the air entering the drying chamber at the nozzle plate. For through drying without jets, the very low heat and mass transfer coefficients for a flat velocity profile - low turbulence flow approaching the paper surface leads to the air entering the sheet at a temperature and humidity little different from the flow entering the drying chamber. The potential advantage for the impingement case derives from the convective drying already accomplished before the flow enters the sheet. However, as the impingement flow enters the sheet at a lower temperature and higher humidity, it enters with a lower drying potential. As the boundary layer under turbulent impinging jets is so thin it is not feasible to determine how much drying is accomplished by the impingement heat and mass transfer process. However, of final importance is not the partitioning of the total drying between that of surface convection and that within the sheet, but whether the total drying rate is enhanced by impingement. This question can be answered by inspection of the drying rate curves for the two cases.

As noted in section 5.5.2, for through drying at low intensity or high paper basis weight, the exhaust air in the constant rate period is nearly saturated, therefore such conditions are inappropriate for testing for any difference in drying rate with or without impinging jets. From the 8 experiments made without jets, figure 5.19, shows the

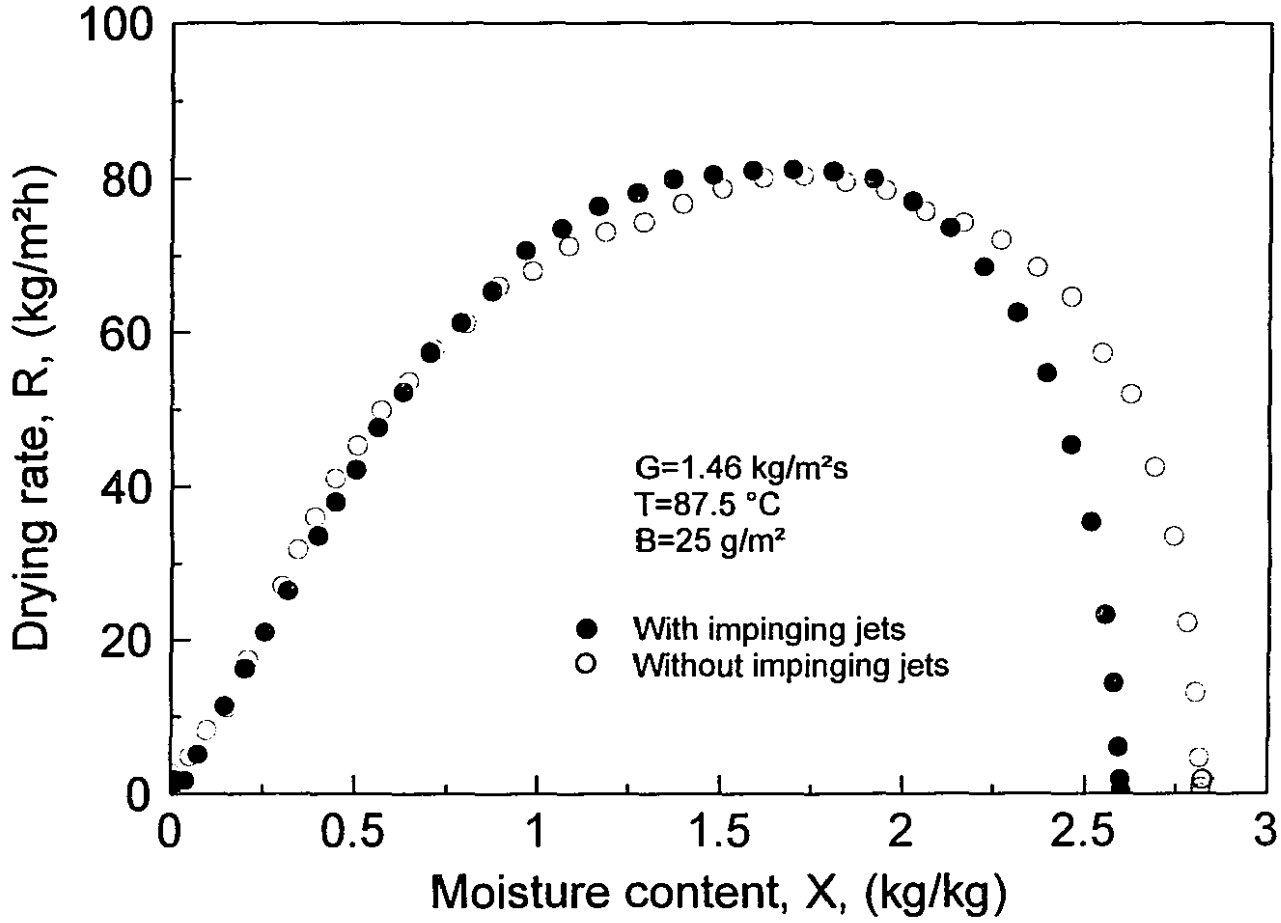

Figure 5.19 Comparison of through drying with and without impinging jets

comparison for the thinnest paper, B=25 g/m^2, through dried at the highest drying intensity. Table 5.7 lists values of the key quantitative parameters for these drying rate curves, determined using the equations of the universal drying rate curve.

Table 5.7 Comparison of through drying with and without impinging jets

	With impinging jets	Without impinging jets
X_o, kg/kg	2.60	2.83
R_c, kg/m^{2}h	80.0	78.5
X_i, kg/kg	1.95	2.12
X_c, kg/kg	1.42	1.33
X_o-X_i, kg/kg	0.65	0.71
$X_c/X_o^{0.58}$	0.82	0.73

With and without impinging jets the extent of the increasing rate period differs only by 0.05 kg/kg, much less than the 0.16 kg/kg uncertainty for the value of X_i predicted by equation 5.11. The increasing rate period would be expected to be independent of the use of impinging jets as this period reflects the development of area within the sheet for heat and mass transfer and is therefore governed by the paper structure, not by the conditions of the approach flow to the sheet. The values of R_c with and without jets agree within 2%, well within the accuracy of the measurement. This invariance of R_c indicates that the extra convective drying accomplished with jets before the flow enters the sheet is lost because of the corresponding drop in through drying potential due to the correspondingly higher humidity and lower temperature of air entering the sheet. The difference in X_c from the use of jets, 0.09 kg/kg, is likewise smaller than the experimental reproducibility of X_c . Thus the local nonuniformity associated with the impingement flow of the present study does not cause a significantly earlier onset of the falling rate period, as expected because falling rate periods of drying are controlled by conditions within the sheet and are unaffected by the nature of the approach flow of the air to the sheet.

One aspect of the present investigation to be considered in this comparison is the local nonuniformity under the impinging jets, a feature which does not exist in industrial practice where paper dried by impinging jets passes under the nozzles at speeds of up to

30 m/s. As the present data acquisition program has the ability to display the calculated drying history on screen, on-line as drying proceeds, the sheet can therefore be withdrawn from the drying chamber for a visual examination at any desired point in the drying. During the constant rate period no difference could be detected between drying with or without impinging jets, with the sheet appearing uniformly wet. After the falling rate starts, dry areas form randomly from the edge to the center of the sheet in a way which, with or without impinging jets, is indistinguishable. During the falling rate period with impinging jets, dry spots directly under the nozzles become visible in large scale wet regions. The finding that the use of impinging jets does not significantly change the value of X_c , Table 5.7, or change the R-X curve in the falling rate period, figure 5.19, establishes that the local nonuniformity generated by stationary impinging jets causes no significant changes to the drying in the falling rate period.

The conclusion is therefore that there is no measurable difference between the through drying of paper with or without impinging jets.

5.6 Prediction of drying time and drying rate

With quantitative relationships having been obtained for R_c , X_i and X_c relative to drying process conditions G, T_j , B and X_o , and the R-X relationships during the increasing and falling rate periods found in terms of n_i and n_f, drying time and drying rate may now be predicted for any condition for which R_c is reached even momentarily. For this purpose X_i , R_c and X_c are calculated using equations 5.11, 5.14 and 5.15. The R-X relationship over the increasing rate period, $X_o \geq X > X_i$, is described by equation 5.7 with the exponent n_i=3.6, while $R=R_c$ during the constant rate period, $X_i \geq X \geq X_c$. For the falling rate period, $X_c > X$, the R-X relation is given by equation 5.10 with the exponent n_f=1.7 . As equation 5.7 starts with R=0 at the initial moisture content X_o , it is evidently not possible to start the drying time calculation at $X=X_o$, R=0, the drying time calculation was therefore started at $X = X_o$ - 0.05 kg/kg.

For industrial operation where a constant pressure drop is maintained across the sheet during drying, the values of X_i , R_c , X_c and the R-X relationships in increasing rate and falling rate period would depend on the transient value of G which is a function of the rapidly changing paper moisture content X. The value of G can be calculated using ΔP-G-X correlations documented in Polat O. et al. (1989) for air flowing through wet paper made from the same kind of pulp as used here.

For the present study, figures 5.20 and 5.21 show the prediction of drying time and drying rate at eight representative drying conditions. The predicted total drying time to X=0.05 kg/kg, designated $t_{0.05}$, is listed in each graph. For the range of drying conditions from the lowest to the highest intensity of the present study and for the range of basis weights, with drying time varying from 5 to 68 s, the predictions are in very good agreement with the experimental measurements.

In connection with the R-X curves given in section 5.5.4, the differences between the structure of the drying rate model of Polat O. et al. (1991) and that of the present study were noted. With the Polat O. et al. model, their drying time curves during the increasing rate period were in some cases more optimistic than their measurements, but these differences were not substantial. During the falling rate period, however, their drying time curves were consistently overly optimistic by a substantial amount as a result of a consistent over-prediction of drying rate, as noted in section 5.5.4. Thus the good drying time predictions of figure 5.20 and 5.21 indicate that the difference in model structure for the falling rate period developed in the present study represents an advance over the earlier model of Polat O. et al.

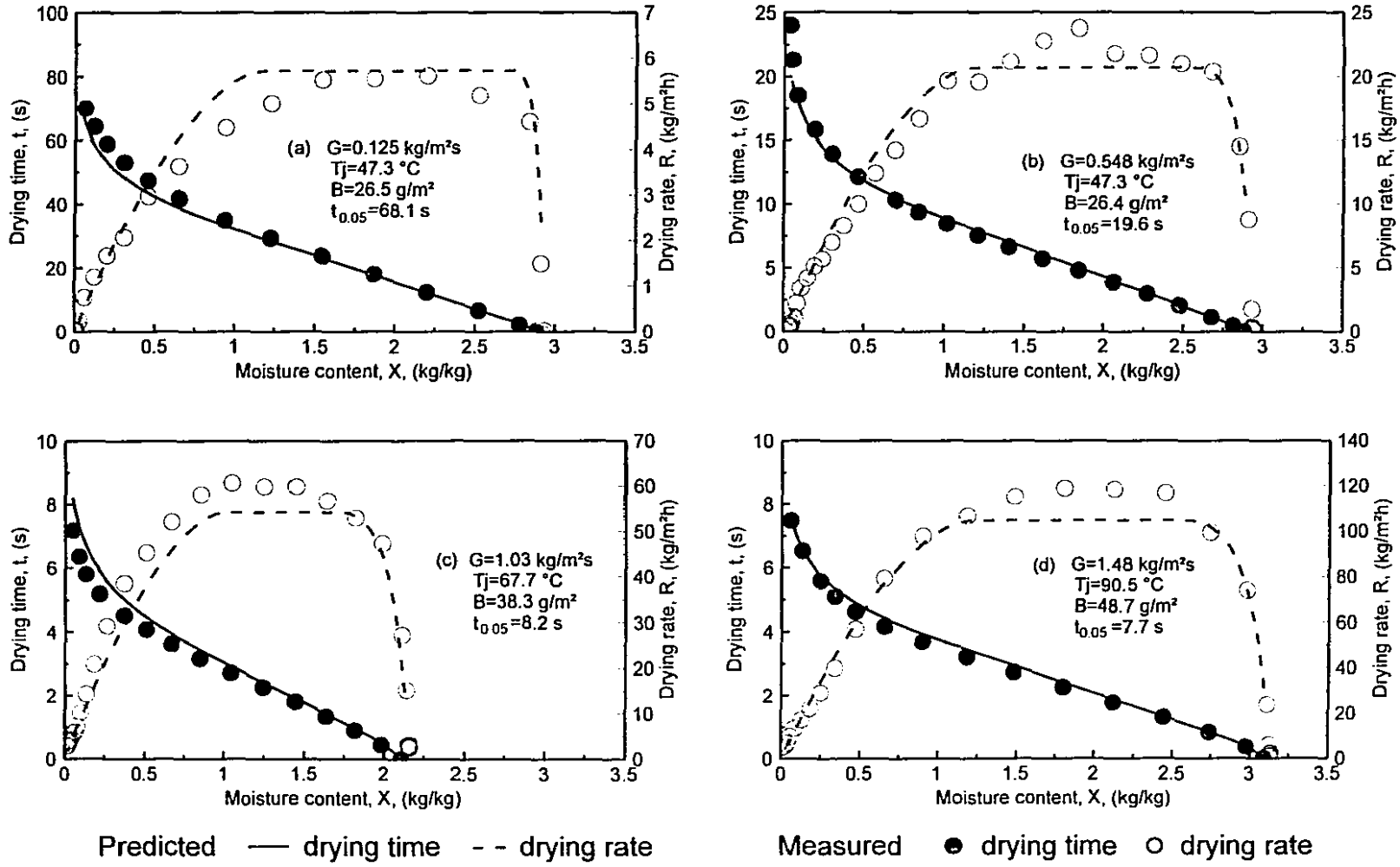

Figure 5.20 Comparison of predicted and measured results, part 1

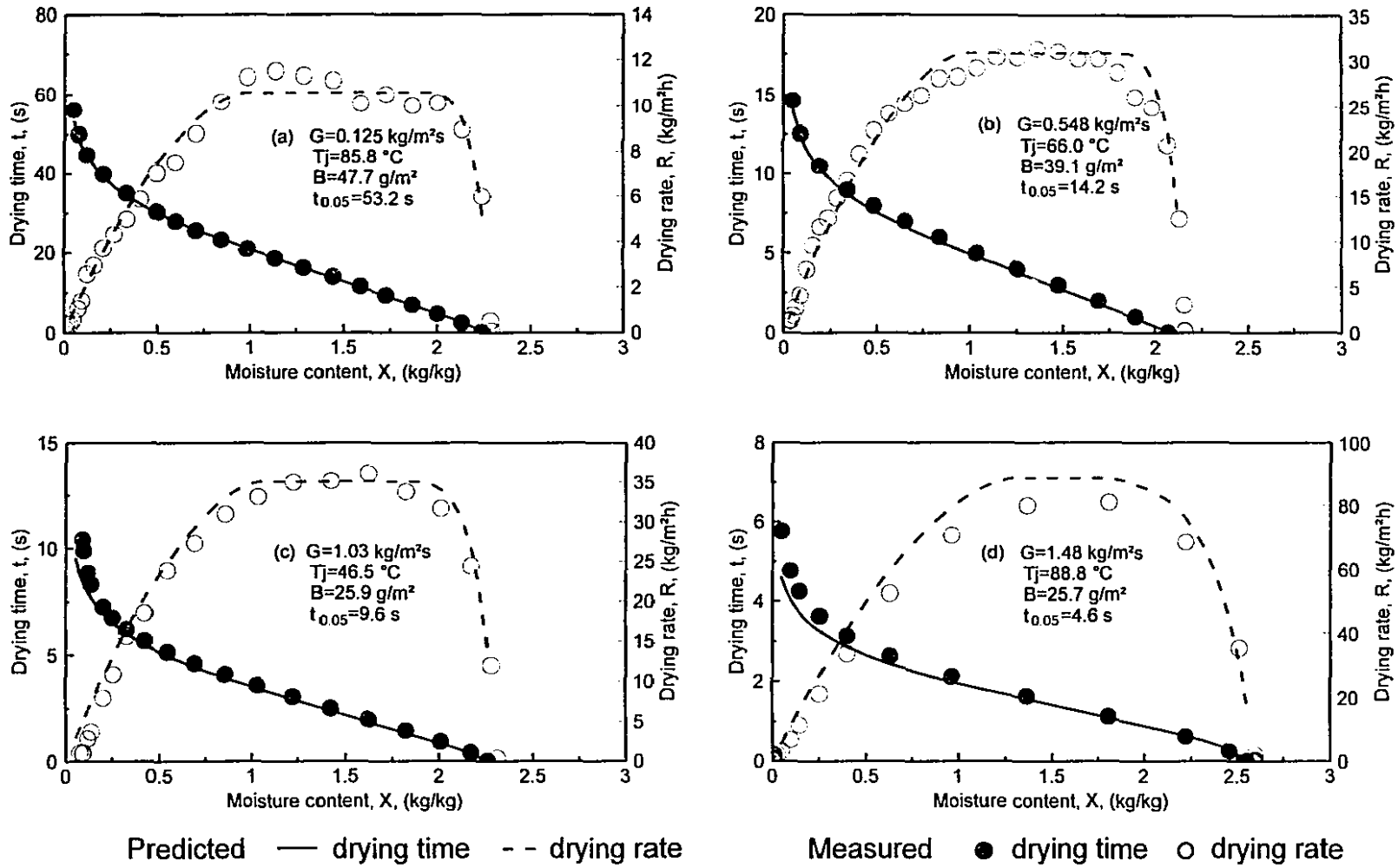

Figure 5.21 Comparison of predicted and measured results, part 2

5.7 Summary

(1) 89 experiments were carried out for through drying kraft handsheets of three basis weights, 25, 37 and 50 g/m^2, under impinging jets with mass flow rate ranging from 0.125 to 1.45 kg/m^{2}s and drying air temperatures from 22 to 90 ^{o}C. Eight more experiments carried out without impinging jets enabled comparison of through drying with this difference in the air inlet boundary condition.

Precisely defined drying rate curves were determined by fast response, on-line measurements of air humidity at the exhaust. Two drying rate periods, the increasing rate period and falling rate period, were observed for all experiments, with the generally present constant rate period just disappearing at the high intensity limit of drying process conditions tested.

(2) Based on a theoretical analysis, an exponential R-X relationship in the increasing rate period was obtained as

$$\frac{R}{R_c} = \frac{1-e^{-n_i\left(\frac{X_o-X}{X_o-X_i}\right)}}{1-e^{-n_i}}$$

with the exponent $n_i=ha_pL/(GC_p)$.

(3) Together with the above equation, five procedures were tested for quantitative representation of the entire through drying rate curve.

(a) Churchill asymptotic approach, procedure 1

When the above relation for the increasing rate period was combined with the Churchill approach for the subsequent part of drying, the data in the early and later part of drying were well fitted. However, as it is not possible to obtain with this method either a value of critical moisture content, X_c, or a continuous R-X relation for the entire drying rate curve, this approach was rejected.

(b) Power law approach for falling rate period, procedure 2

When a simple power law approach was tested for the falling rate period, the transition from the constant to falling rate period was inconsistent with the experimental

measurements. This treatment was therefore rejected.

(c) Modified power law approach for the falling rate period, procedure 3

With the power law relation applied with a change of variables from R/R_c and X/X_c , to $1-R/R_c$ and $1-X/X_c$, the location of the high and low curvature regions is reversed, with the low curvature section at the onset of the falling rate period, consistent with the experimental measurements. This modified power law relation,

$$\frac{R}{R_c} = 1 - \left(1 - \frac{X}{X_c}\right)^{n_f}$$

represents the falling rate data well. This approach combined with that for the increasing rate period generated a continuous drying rate curve that fits the experimental R-X data well, gives good values of the constant drying rate, R_c , but does not provide realistic values of X_i and X_c due to the constant rate period being approached asymptotically from both sides.

(d) Determination of X_i and X_c , procedure 4

Analysis of the results indicated that it is realistic to define the end of the increasing rate period X_i and the start of the falling rate period X_c as the moisture contents at $R=0.98R_c$ on the continuous R-X curve determined by procedure 3.

(e) Determination of n_i and n_f , procedure 5

The final step in quantitatively representing the entire drying rate data is determination of the values of n_i and n_f by reapplying the equations for the increasing rate and falling rate periods but now with the values of X_i , R_c and X_c determined in (c) and (d) above.

The composite procedure 3, 4 and 5 produces a drying rate curve consistent with experimental observations and with reasonable values of X_i , X_c and R_c . This procedure is totally unsubjective and is applied to all the experimental measurements to obtain the five parameters, R_c , X_i , X_c , n_i and n_f , to quantify the entire drying rate curve.

(4) The extent of the increasing rate period, X_o-X_i , was found to vary with the drying conditions and paper properties as

$$X_o - X_i = 0.30 G^{0.41} \Delta T^{0.78} B^{-0.73}$$

which predicts X_o-X_i with a 2σ uncertainty of 0.16 kg water/kg fibre. The dependence of X_o - X_i on G, ΔT and B is qualitatively consistent with those found by Polat O. (1989). As the above correlation excludes results for drying in ambient air, the exponent for ΔT is, as it should be, larger than 0.39 obtained by Polat O. The stronger dependence of X_i on B for the present study than -0.37 for Polat O. results from the difference in the range of B studied, 25-250 g/m^2 for Polat O. and 25-50 g/m^2 here. As the latter range is more likely to be used industrially for through drying the present correlation is more industrially relevant.

(5) For constant drying rate, the drying conditions produce two distinct groups, one for air exiting the sheet near-saturated and the other for non-saturated exhausts. For non-saturated exhausts, R_c correlated as

$$R_c = 0.87G^{0.85}\Delta T^{0.91}B^{0.19}$$

The exponents found here agree with those reported by Polat O. et al. (1992b). The dependence of R_c on ΔT also agrees with the exponent of 0.76 - 0.93 from the data of Gummel (1977). The dependence of R_c on B agrees with the value found by Polat O. The present work points out the limitation on the significance of these exponents depending on the degree of saturation in the exhaust.

In the limiting case of a saturated exhaust with drying rate controlled by thermo-dynamic equilibrium, R_c is independent of B and linearly proportional to the product $G\cdot\Delta T$ with a theoretically predictable proportionality constant that was confirmed experimentally to within 3%.

(6) The critical moisture content relates to drying process conditions as:

$$X_c = 0.67X_o^{0.58}R_{as}^{0.15}B^{-0.19}G^{-0.17}$$

The dependence of X_c on the drying conditions and paper properties is consistent with analysis. The difference from the dependence on conditions as found by Polat O. (1989) is the result from the focus here on conditions closer to industrial application.

(7) A unique paper initial moisture content, X_o^{ic}, exists for the constant drying rate only momentarily reached at given drying conditions for a given paper basis weight B. The value of X_o^{ic}, which can be predicted from the equations given in (4) and (6), increases with R_{as} and decreases with B.

(8) No measurable difference was found in through drying with and without impinging jets. The increasing rate period is governed mainly by the paper structure hence is unaffected by the nature of the approach flow to the sheet. During the constant rate period, the advantage of water removal by the turbulent impinging jets before the air enters the sheet is apparently lost because of the corresponding drop in heat and mass transfer potential. As the onset of the falling rate period and its development are governed by the paper structure, the effect of impinging jets flow is insignificant during the falling rate period.

(9) A normalized drying rate curve of universal form was obtained to represent quantitatively the complete through drying rate data as:

$$\frac{R}{R_c} = \frac{1 - e^{-3.6\left(\frac{X - X_i}{X_o - X_i}\right)}}{1 - e^{-3.6}} \qquad \text{for } X_o \geq X \geq X_i$$

$$\frac{R}{R_c} = 1 \qquad \text{for } X_i \geq X \geq X_c$$

$$\frac{R}{R_c} = 1 - \left(1 - \frac{X}{X_c}\right)^{1.7} \qquad \text{for } X_c > X > 0$$

The above form of universal falling drying rate curve differs from those reported by Gummel (1977) for through drying of tissue paper and textiles and by Randall (1984) of through drying of paper. However, the obtaining of a universal form of increasing rate curve for through air drying is specific to the present study.

(10) Drying time and drying rate were successfully predicted with the correlations for R_c, X_i, X_c and for the R-X relationships during the increasing and falling rate periods of the universal normalized drying rate curve.

Chapter 6 Combined Impingement and Through Air Drying of Paper

6.1 Introduction

The idea of a paper dryer making simultaneous use of two air drying mechanisms, impingement air drying and through air drying, was proposed and tested by Burgess et al. (1972a, b). This process, referred to in the present study as Combined Impingement and Through Air Drying, abbreviated as CITAD, is of interest for the potential advantages of higher drying rate than pure impingement drying and more uniform drying than pure through drying. The enhancement of impingement heat transfer by through flow, derived theoretically by Mickley et al. (1954) and Spalding (1960), was studied experimentally by Baines and Keffer (1979), Polat S. et al. (1990, 1991a, b) and Saad et al. (1992). In contrast, measurements of drying by CITAD have been limited to two reports of the development of a pilot plant and a subsequent short paper mill trial of this process by Burgess et al. The mill trial did not lead to industrial implementation of their process, referred to as a "Papridryer". As their pilot plant and mill trial scale work was not oriented to the study of drying kinetics, the nature of the interaction between impingement drying and through flow drying has never been determined. The overall results obtained by Burgess et al. were however impressive in that they reported obtaining drying rate of 186 kg/m^2h for an air temperature of 427 ^oC and jet velocity of 96.5m/s with 34% of the impingement nozzle exit flow was drawn through the sheet as through flow, as reviewed in chapter 2. Currently it is standard industrial practice to dry the lightest grades of paper, tissue and toweling, by air through drying, by air impingement drying or by the former followed by the latter technique. There is no current paper dryer incorporating simultaneous use of these two air drying techniques. Air drying of heavier grades of paper, which was the objective of the work by Burgess et al., is not industrial practice.

The objective of the present study of drying paper by the CITAD process is to provide the first measurements of the interaction of the impingement and through flow components in the combined process, and to do so over the complete limits from pure impingement to pure through flow drying.

6.2 Fundamental characteristics of the CITAD process

The research concerns the inter-relation of complex heat and mass transfer phenomena taking place above the surface, at the surface and within the paper as the sheet progresses rapidly from wet to dry under combined impingement and through air drying. For heat transfer under jets accompanied by flow through the impingement surface but without evaporation, the heat flux between air jets and the impingement surface has now been measured accurately (Polat S. 1988). For the comparable process but with evaporation at and beneath the impingement surface, it is not possible to determine the humidity of the air entering the impingement surface of the paper which means that it is not possible experimentally to separate the total drying into two unambiguous components, drying by impingement up to the surface of the wet sheet and drying by through flow beneath the wet sheet surface. For the CITAD process, air humidity at the impingement exhaust and through flow exhaust are the only feasible measurements.

A basic feature of combined impingement and through air drying is that all of the through flow air exhaust was initially part of the impingement flow to the wet surface of the sheet. Because part of the humidity measured in the through flow exhaust was therefore originally humidity in the impingement boundary layer above the paper surface and because it got there by impingement heat transfer, the water removal processes by air impingement and by through drying are individually nonadiabatic although the overall CITAD process is adiabatic. An alternate statement of this basic characteristic of the CITAD process is that the water vapor carried out in each exhaust stream does not represent the heat transfer from that air flow to the paper. It follows that the evaporation

rates from measurement of the humidity of the through flow exhaust cannot be interpreted as through drying rate, and likewise impingement exhaust measurements do not give an impingement drying rate. Thus with CITAD it is necessary to define two *water removal rates* to represent the moisture carried out in the impingement exhaust and in the through flow exhaust. The summation of the water removal rates of the two exhausts is the drying rate for CITAD.

6.3 Experimental conditions

The central aspects of the experimental procedure are that the three mass flow rates, impingement exhaust flow G_I, through flow exhaust G_T, and total flow of drying air $G=G_I+G_T$, were maintained constant from beginning to the end of drying, and that the ratio of through flow rate to the total drying air flow rate, $q_T=G_T/G$, could be varied over the entire range from 0 to 100%. Air mass flow rates are normalized as kg/m^2s to the area of the sheet being dried. The humidity of both exhaust streams was monitored continuously so that the water removal rates in the impingement and through flow exhausts, R_I and R_T, hence the total drying rate, $R=R_I+R_T$, were known as a function of sheet moisture content X throughout each drying test. Two levels of air temperature T_j were tested, i.e. unheated ambient air and the highest possible with the present equipment, around 90 °C, using paper of two basis weights B, 25 g/m^2 and 50 g/m^2, representative of tissue and printing papers, at initial moisture contents X_o from 2 - 4 kg water/kg fibre. Of the total of 144 experiments, about half were with each jet temperature and half with each basis weight. Nozzle set #1 was selected for all of the 144 experiments for reasons given in chapter 5. Complete experimental procedures are detailed in Appendix B and experimental results in Appendix E.

The experimental program was carried out in three stages. In part 1 (34 experiments) the impingement exhaust mass flow rate G_I was kept constant while total mass flow rate G varied in order to document the effect of through flow; in part 2 (40 experiments) the through flow mass flow rate G_T was kept constant and total mass flow

rate G was varied to investigate the effect of impingement; in part 3 (64 experiments) total mass flow rate G was kept constant and the mass flow rate ratio of through flow to total flow, $q_T=G_T/G$, was varied to complete the investigation of interaction of the two processes, water removal by impingement and by through flow, in the combined process of air drying paper. The paper basis weight effect was further studied at one drying condition, q_T=10%, G=1.0 kg/m^{2}s, T_j=90 °C with six levels of basis weight from 25 g/m^2 to 83 g/m^2. Table 6.1 lists the detailed experimental conditions.

Table 6.1 Experimental conditions for CITAD

	Part 1	Part 2	Part 3
G_I, kg/m^{2}s	0.5, 1.2		
G_T, kg/m^{2}s		0.1, 0.5	
q_T, %			0 -100
G, kg/m^{2}s	0.5 to 1.5	0.1 to 1.5	0.1 to 1.5
T_j, °C	20, 90	20, 90	20, 90
B, g/m^2	25, 50	25, 50	25, 50
X_0, kg/kg	2 - 4	2 - 4	2 - 4

6.4 Drying history curves for the CITAD process

Basic characteristics of this combined drying process are first identified. Figure 6.1 presents for the first time the key features of the water removal history for the CITAD process applied to paper. For clarity of representation, data points are shown only for the total drying rate R and its two components, R_I and R_T, while the temperatures are displayed by lines connecting the data points. Except when specifically needed, subsequent figures generally show straight lines between data points. Almost immediately after drying starts the rate of water removal by the impingement exhaust R_I reaches and remains at a constant value R_{Ic} until paper moisture content has decreased to the critical point X_c, around 1.7 kg water/ kg fibre for the figure 6.1 example, after which the impingement water removal rate starts to fall. One difference immediately evident for the impingement water removal rate curve is that the shape of the falling rate period of R_I

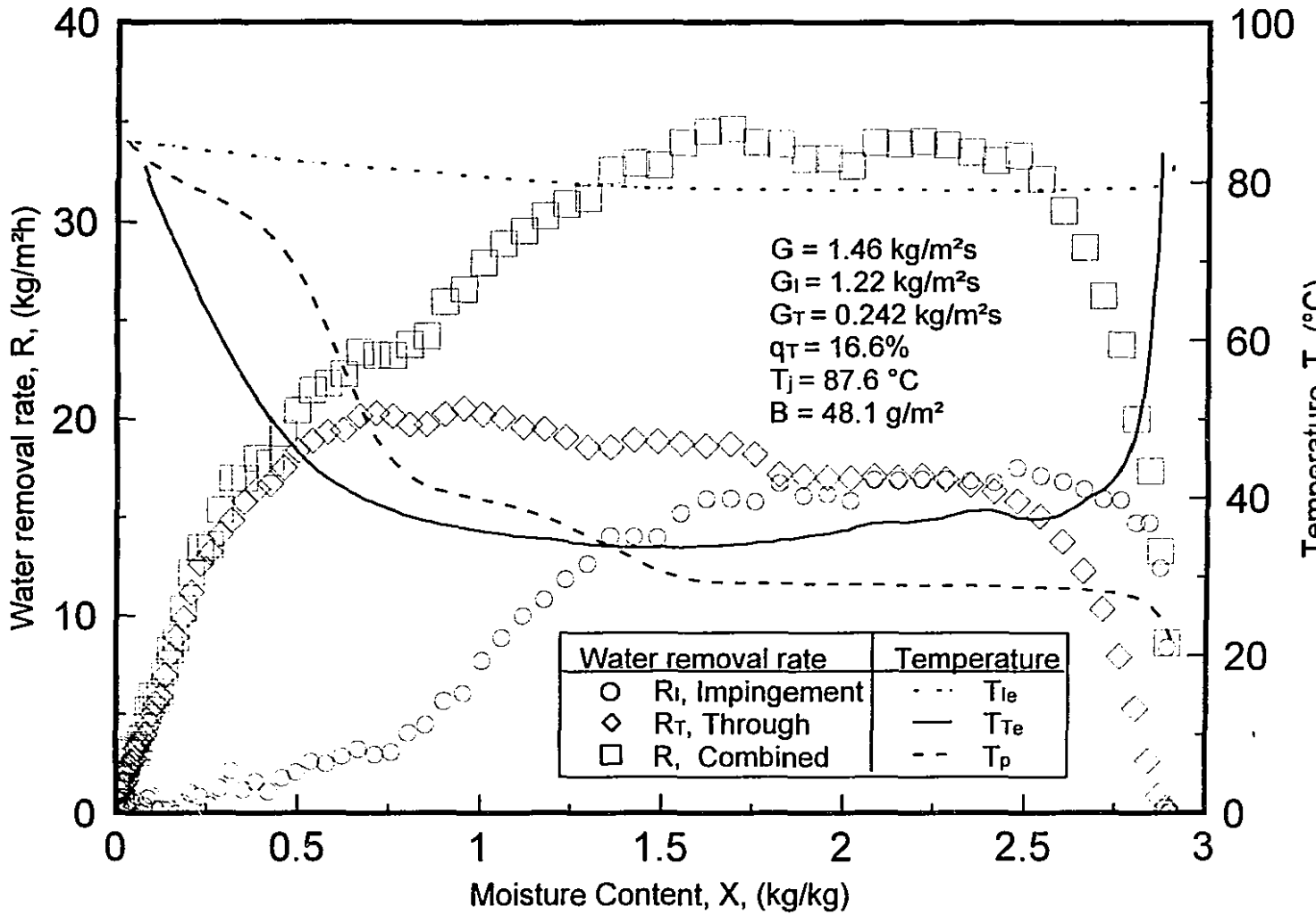

Figure 6.1 Drying history curves for drying by CITAD

is strongly convex downwards, just the opposite to typical concave downwards curves for the falling rate period of pure impingement drying of paper, chapter 4. Thus clearly the impingement water removal process in CITAD is basically different from pure impingement drying.

For the through flow exhaust water removal rate R_T, the process begins similarly to that of pure through drying with an important increasing rate period which extends until, for the figure 6.1 case, paper moisture content has dropped from 2.9 to about 2.3 kg/kg. A short constant rate period for through flow water removal ends at the moisture content which is the critical point for the impingement water removal rate, $X_c \approx 1.7$ kg/kg as noted above. Now a new and distinctive feature starts, one not seen in pure through drying, with R_T increasing again, reaching a maximum at $X \approx 0.7$ kg/kg for the case shown, at which point the falling rate period starts for the through flow water removal. The reasons for the occurrence in CITAD of this secondary increase of through flow water removal rate is analyzed subsequently.

The drying rate R for the combined process, i.e. $R_I + R_T$, shows characteristics of the two constituent drying processes with an increasing rate, a constant rate and a falling rate period, the latter starting at the critical point for the impingement water removal rate. The critical point for the combined drying rate curve coincides with that for the impingement water removal curve because for paper moisture contents below X_c the increase of through flow water removal rate R_T is less than the decrease in R_I. The critical moisture content can therefore be designated as X_c without further subscript. The falling rate period R - X curve is concave downwards because at this stage the total drying rate is dominated by through flow water removal.

The figure 6.1 CITAD drying history curves include various T - X curves as well as those for R-X. The air temperature at the impingement exhaust T_{Ie} almost immediately assumes a temperature of about 79 °C where it remains until the end of the constant water removal rate period, 8.6 °C below that at the nozzle exit, 87.6 °C. After the critical moisture content X_c is reached and R_I starts to fall, T_{Ie} naturally starts to increase. For through flow exhaust air, the initial decrease in temperature T_{Te} parallels the increasing

rate curve R_T over the moisture content range from 2.9 to 2.3 kg/kg. Thereafter T_{Te} remains at a relatively constant value slightly above the adiabatic saturation temperature of 29 °C for the figure 6.1 case, not only over the entire constant rate period but until X≈0.7 kg/kg which marks the start of the coupled effects of onset of the through flow exhaust falling rate period and increasing T_{Te}.

The paper temperature T_p measured at the through flow exhaust side of the sheet undergoes four distinct regions which reveal more yet about the CITAD process. First T_p undergoes a very fast increase from ambient temperature to the adiabatic saturation temperature of 29 °C, then remains at this temperature until the critical point X_c≈1.7 kg/kg. From that moisture content T_p increases slowly until the onset of the falling rate period of through flow water removal, X≈0.7 kg/kg. Thereafter one observes the typical behavior of R_T falling coupled with T_p increasing rapidly to approach T_j . Thus the measurements of the various temperatures and water removal rates provide a consistent and very informative record of the drying history for paper dried by the CITAD process.

6.5 Water removal rate curves

6.5.1 Effect of through flow on impingement water removal at fixed G_I

For two fixed levels of impingement exhaust mass flow rate, G_I of 0.5 and 1.2 kg/m^{2}s respectively, figures 6.2 and 6.3 show the impingement exhaust water removal rate curves for four levels of through flow mass flow rate G_T , starting with the limiting case of pure impingement drying, G_T=0=q_T . A common feature is that as through flow rate G_T increases, the level of constant rate of impingement exhaust water removal R_{Ic} decreases substantially, by 25-50% for the conditions of figures 6.2 and 6.3. In the falling rate period the change in R_I curves with the various levels of G_T becomes even stronger. In fact as moisture content decreases to X≈0.5 kg/kg, R_I becomes very low, in some cases approaching zero, whereas without through flow the corresponding impingement drying

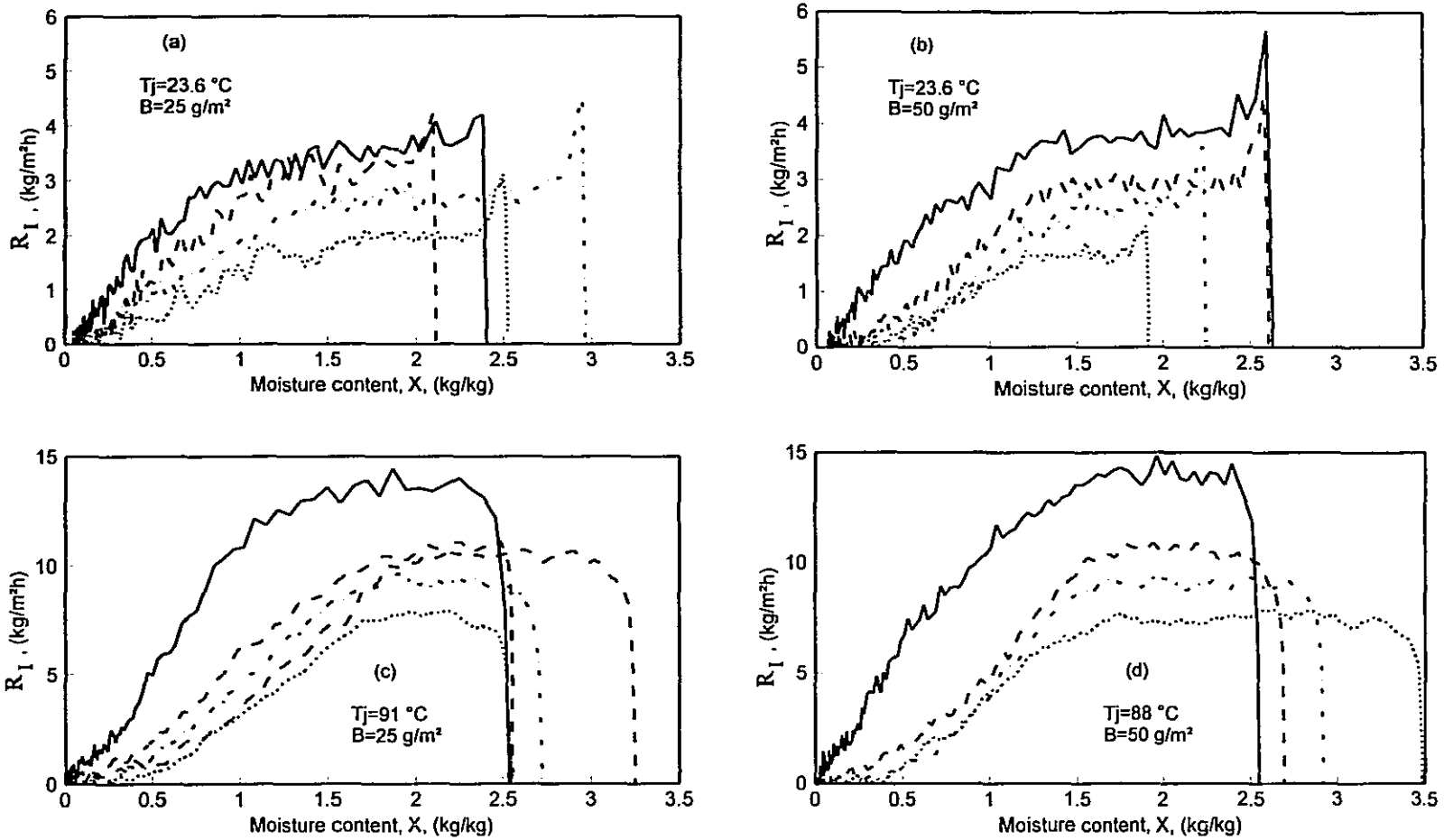

Figure 6.2 Effect of through flow rate on impingement water removal: G_I=0.50 kg/m²s

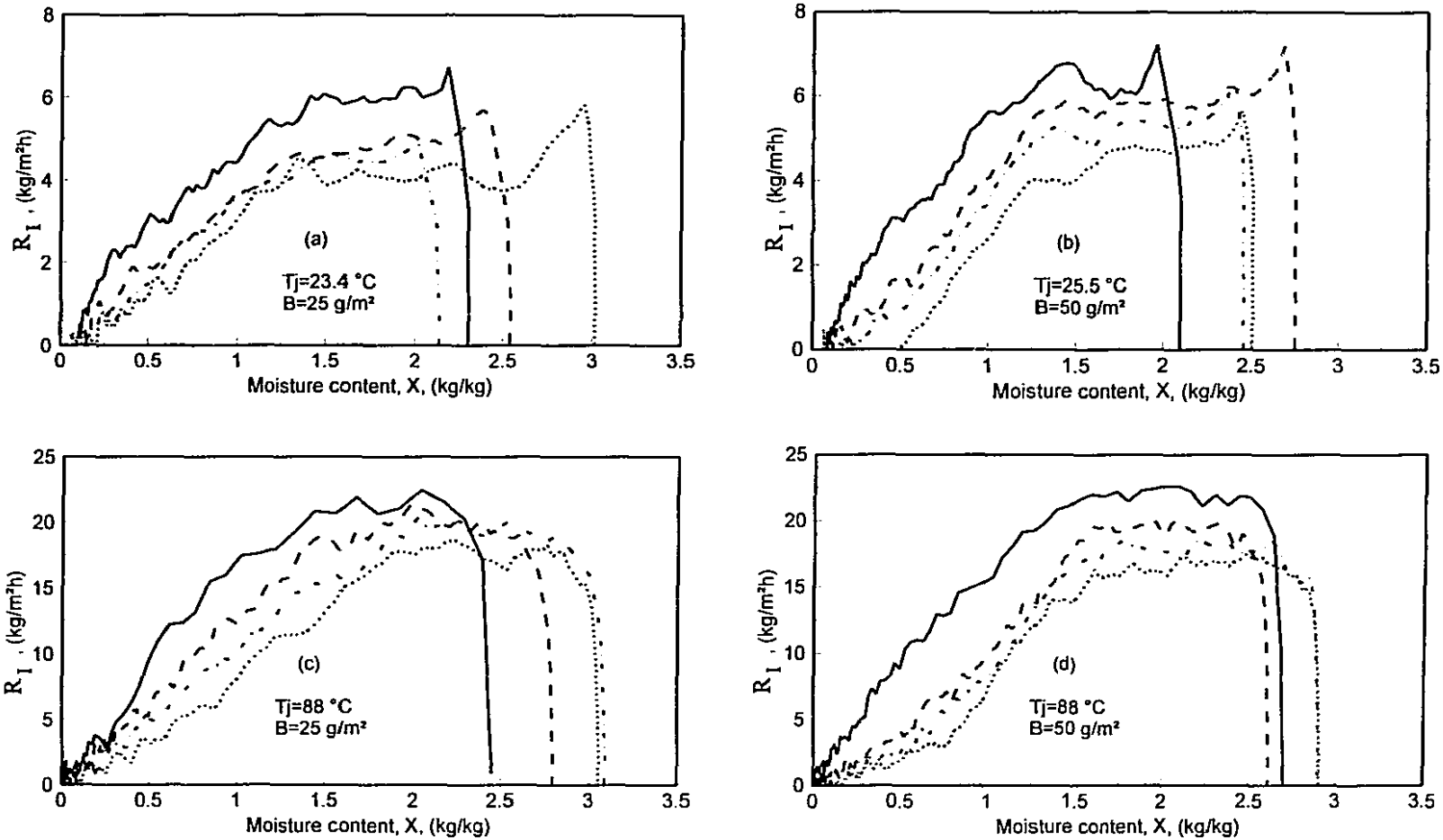

Figure 6.3 Effect of through flow rate on impingement water removal: G_I=1.2 kg/m²s

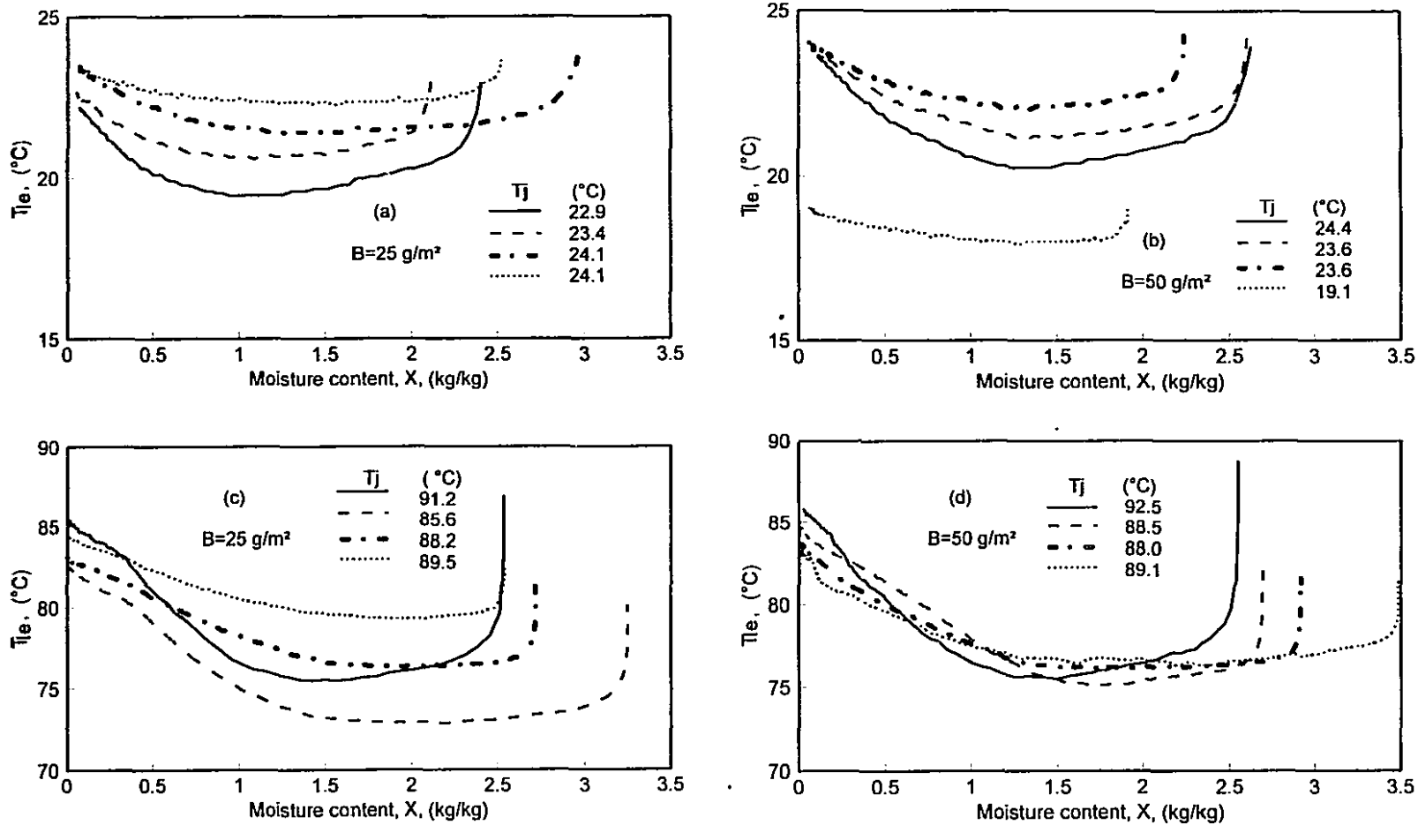

——— G_T=0 (q_T=0) - - - G_T=0.123 (q_T=19.7%) - - - G_T=0.24 (q_T=32.4%) ····· G_T=0.50 kg/m²s (q_T=50.0%)

Figure 6.4 Effect of through flow rate on impingement exhaust temperature: G_I=0.5 kg/m²s

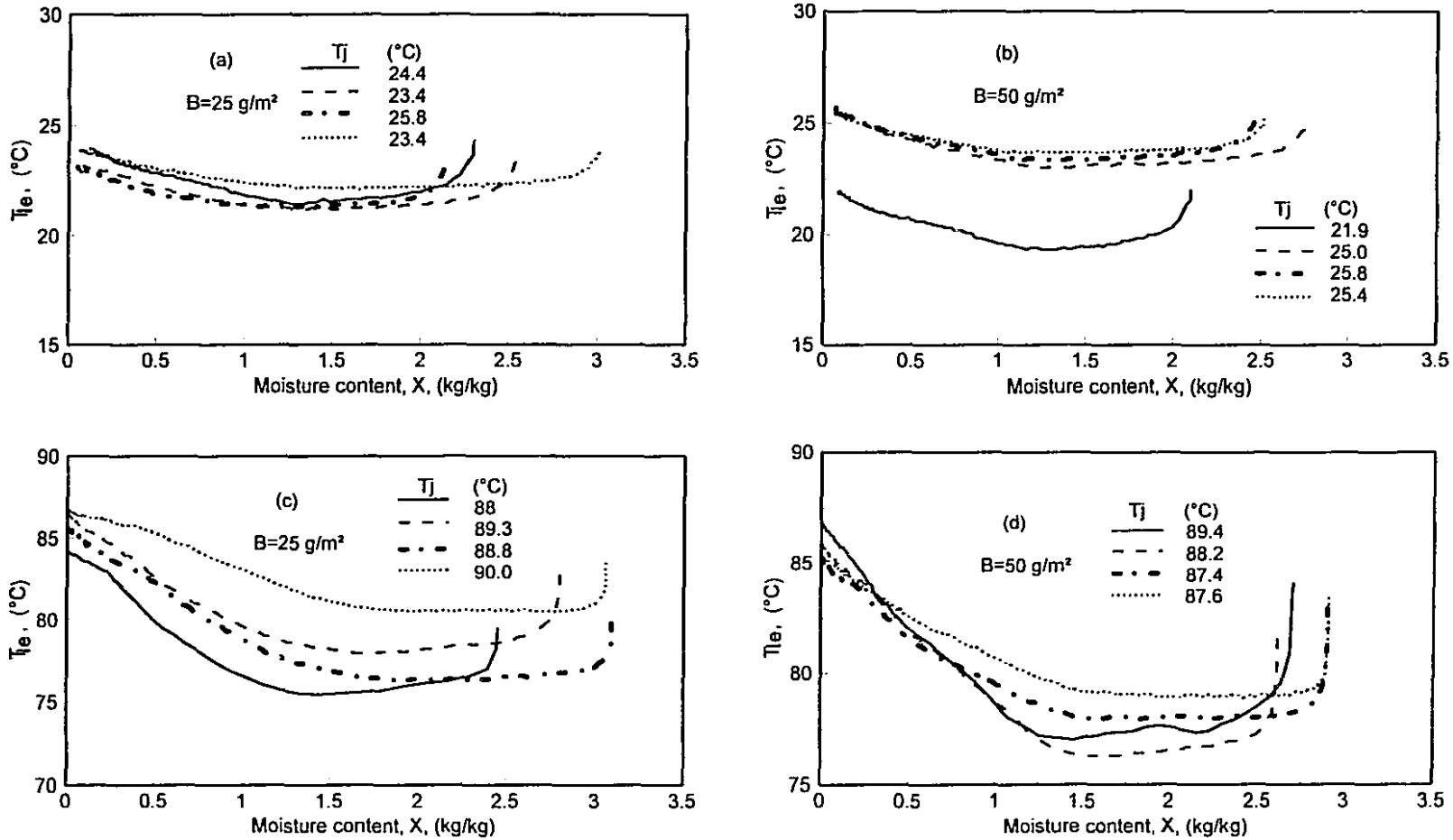

Figure 6.5 Effect of through flow rate on impingement exhaust temperature: G_I=1.2 kg/m²s

rate at X=0.5 kg/kg is typically about 1/3 to 1/2 of the corresponding R_c . These major differences in R_I are the result of humidity, originally present above the sheet due to evaporation by impingement, entering the sheet and leaving the dryer as part of the through flow exhaust water removal rate. Consequently the shape of the impingement exhaust falling rate curve changes from the concave downwards form characteristic of pure impingement drying, to convex downwards with the water removal rate approaching zero asymptotically when the through flow rate G_T is as much as 1/4 to 1/3 of the total drying air rate G. Another consequence of the sensitivity of R_I to G_T is that at constant G_I the critical moisture content X_c increases significantly as G_T increases.

For the conditions of figures 6.2 and 6.3 the effect on air temperature at impingement exhaust T_{Ie} caused by increasing G_T at constant G_I is shown on figures 6.4 and 6.5. In pure impingement drying (G_T=0) the T_{Ie} temperature is significantly less than T_j by the mixing into the impingement exhaust of the air coming from the impingement boundary layer, where the air has been cooled and humidified by the impingement heat and mass transfer processes. As G_T is increased from the G_T=0 limit, some cool humid air from the impingement boundary layer which formerly exited with G_I is drawn into the sheet with the through flow, which has the coupled effects of reducing R_I (figures 6.2 and 6.3) and increasing T_{Ie} (figures 6.4 and 6.5). Thus the water removal rates and temperatures of the impingement exhaust flows, figures 6.2 - 6.5, record a consistent pattern for the interaction of the impingement and through flows in the CITAD process.

6.5.2 Effect of impingement on through flow water removal at fixed G_T

For seven out of the eight cases shown, i.e. figures 6.6 and 6.7(a), (b), (c), there is little apparent effect of impingement exhaust flow rate on through flow water removal over the entire range from pure through drying to drying by CITAD for conditions dominated by the impingement exhaust flow rate. This stability of R_T relative to G_I is in sharp contrast to the opposite case, demonstrated by figures 6.2 and 6.3, of R_I being profoundly sensitive to and reduced by G_T for all levels of G_I or G_T and over the entire

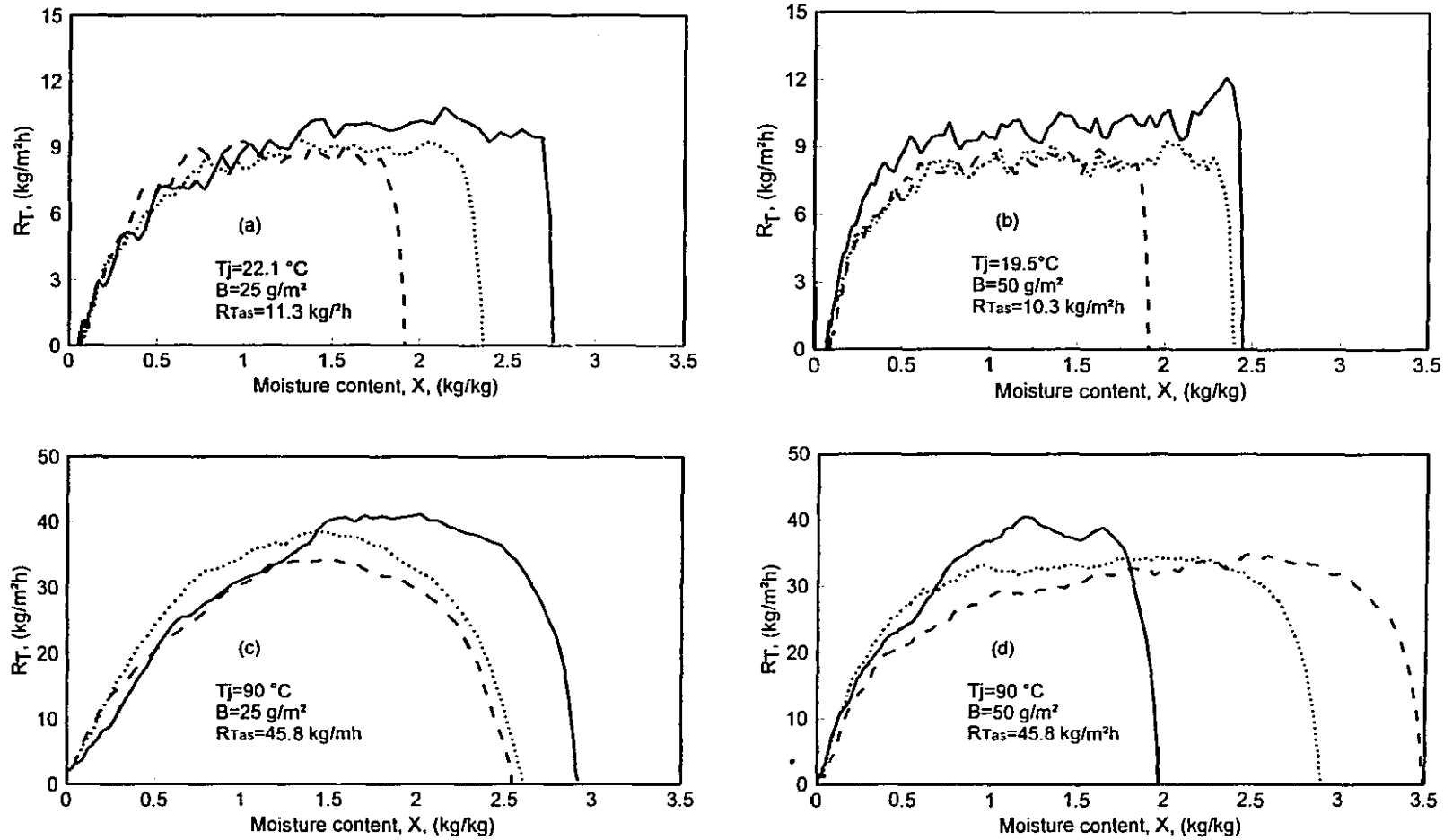

Figure 6.6 Effect of impingement exhaust rate on through flow water removal: G_T=0.508 kg/m²s

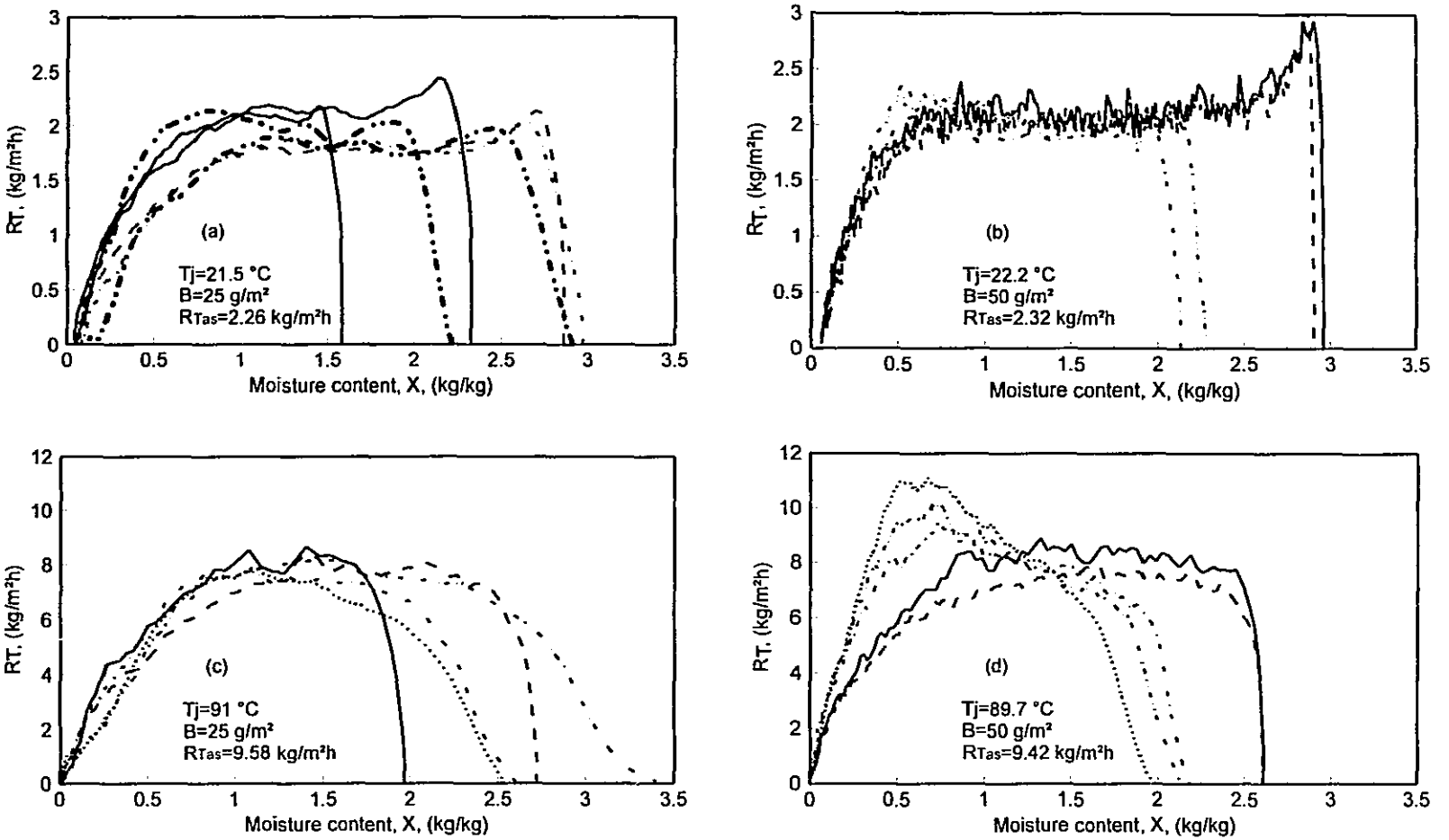

Figure 6.7 Effect of impingement exhaust rate on through flow water removal: G_T=0.104 kg/m²s

region from start to finish of drying. As R_T is generally little affected by G_I, also shown on figures 6.6 and 6.7 are the values of R_{Tas}, the value of R_T if the through flow exhaust were saturated at the adiabatic saturation temperature of the inlet drying air. Although it is not valid to apply R_{Tas} because the through flow water removal process is not adiabatic it nonetheless provides a useful reference. Examination of figures 6.6 and 6.7 shows that for all cases with R_{Tas}<15 kg/m^{2}h, the limit for pure through drying exhaust being near-saturated as analyzed in chapter 5, the values of water removal rate R_{Tc} reach 80-100% of R_{Tas} independent of paper basis weight. For cases with R_{Tas}>15 kg/m^{2}h the average of the peak values for the R_T-X curves is about $0.8R_{Tas}$, significantly below saturation. With the general insensitivity of R_{Tc} from G_I, it is not surprising that the R_{Tc}-R_{Tas} relation here is similar to the R_c-R_{as} relation analyzed in chapter 5.

The interesting exception to the general lack of significant effect of G_I on R_T is very evident for the combination of lowest G_T, highest T_j and highest B, the figure 6.7(d) case. Of this combination of conditions, lowest G_T and highest T_j maximize the relative importance of impingement heat transfer to the sheet, while high B extends the time for the drying to pass from the impingement side to the through flow exit side of the sheet. With the figure 6.7 (d) combination of G_T, T_j and B the through flow exhaust water removal rate is seen to increase and reach a maximum following its constant rate period. This effect can even be seen to a marginal extent for lower levels of q_T on figures 6.7 (a), (b) and (c). This maximum value of through flow water removal, R_{Tm}, increasing with higher impingement exhaust flow rate G_I, is 40% above the constant rate, figure 6.7(d), or 17% higher even than R_{Tas}.

As paper basis weight was observed to affect the through flow water removal rate, a set of experiments was carried out at six levels of B, from 25 to 83 g/m^2, with the importance of the impingement exhaust flow accentuated by fixing the ratio $G_T/G=q_T$ at the relatively low value of 10.1%, and the importance of the impingement heat transfer further maximized by using the highest available air temperature. The results of this set of experiments, figure 6.8, reinforce those of figure 6.7(d). The value of maximum R_{Tm} following the constant rate period increases with paper basis weight. No such increase after the constant rate period is ever observed in pure through drying. The values of

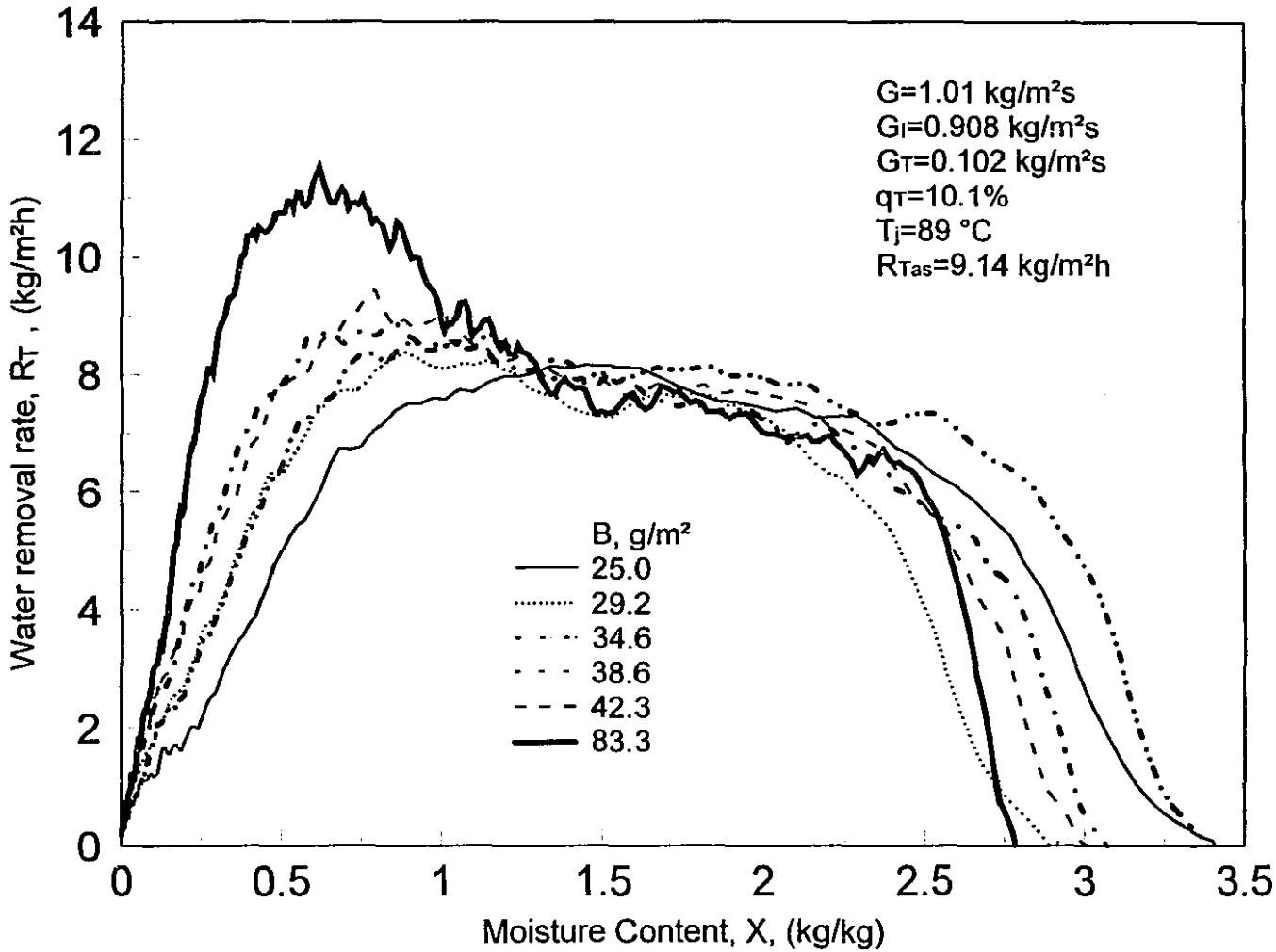

Figure 6.8 Effect of basis weight on through flow water removal rate at low through flow ratio

maximum R_T after the constant rate period may even exceed the rate R_{Tas}=9.14 kg/m^{2}h, for through flow exiting saturated at the adiabatic saturation temperature, 29.5 ^{0}C, which is the maximum possible value for pure through drying at $G=G_T$.

This remarkable feature of drying by the CITAD process, the occurrence sometimes of a maximum R_{Tm} in through flow water removal rate after the constant rate period requires analysis. For the figure 6.1 case this feature starts at a moisture content of about 1.7 kg/kg which marks the following four events: critical moisture content for both impingement exhaust water removal rate and total drying rate, X_c; start of an increase in paper temperature T_p after a steady value during the constant rate period; start of an increase in through flow water removal rate R_T after a steady value at R_{Tc}. This period, which may be termed as secondary increasing rate period, is a very important feature of the CITAD process for some drying conditions while being completely absent for others. The reasons why CITAD sometimes has such a period are now developed.

The two component processes, water removal by impingement and by through flow, would each normally have a "critical moisture content" associated with the particular process, after which paper temperature starts to rise and rate starts to fall. With the two water removal processes occurring simultaneously, the process which intrinsically has the higher value of critical moisture content and which is therefore reached earlier during the drying may behave qualitatively similarly in CITAD as when it is alone. By contrast the other water removal process, the one which if alone would have the lower critical moisture content, cannot behave similarly in CITAD as when alone. Specifically, by causing T_p to rise, as shown in figure 6.1 and for additional conditions in figure 6.9, the process of higher critical moisture content changes fundamentally the paper conditions for the process which, when alone, has the lower critical moisture content.

The research of chapters 4 and 5 shows that for the same drying process conditions, the critical moisture content for impingement drying is higher than for through drying. In drying by CITAD, because X_c for the R_I process occurs before that for R_T it is as expected in figures 6.1, 6.2, 6.3 and 6.9 that the impingement water removal rate curves are of two distinct periods, similar to the R-X curves for pure impingement

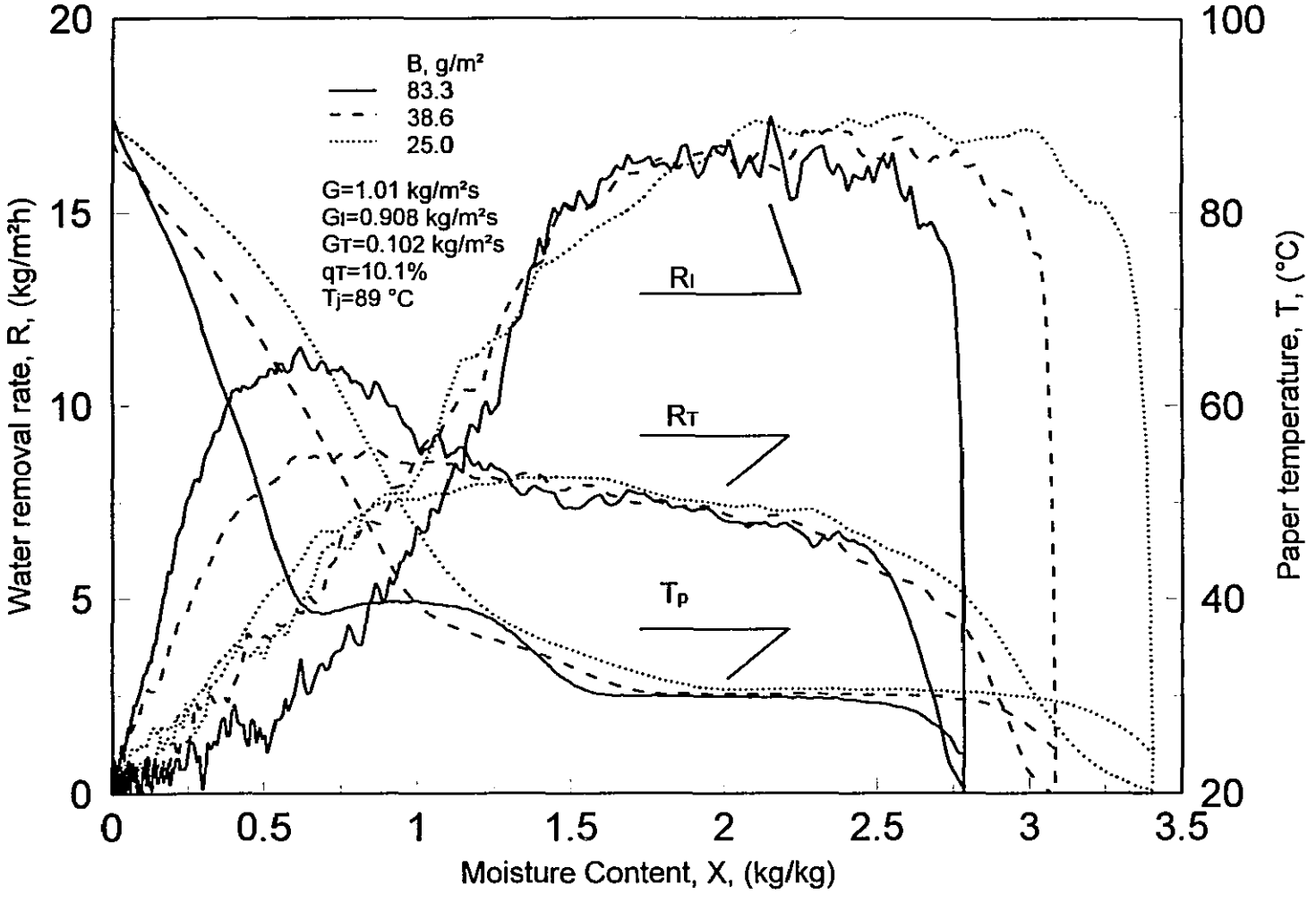

Figure 6.9 Drying history curves for CITAD at low q_T: Effect of basis weight

drying. However the behavior of the through flow water removal rate curves, figures 6.1, 6.7 and 6.9, is basically different from the R-X curves for pure through drying.

Although the secondary increasing rate period was observed for the conditions of figures 6.1, 6.7 and 6.8, the drying history curves of figure 6.9 permit a more detailed analysis. For B=83 g/m^2, figure 6.9 shows that as the constant rate periods for R_I-X and R_T-X come to an end at X≈1.6 kg/kg, the same coupling of events occurs as was seen less strongly on figure 6.1, i.e. as R_I starts to drop, T_p and R_T start to increase. T_p increases from about 30 °C to 39 °C. At X≈0.6 kg/kg again two coupled events occur, i.e. R_T enters the falling rate period, dropping rapidly towards R_T=0 at X=0, with T_p increasing rapidly towards T_j=89 °C at X=0, which is standard behavior for falling rate period drying. For 38.6 and 25 g/m^2 paper figure 6.9 shows that the values of X_c are correspondingly higher than for the thickest paper tested, so the beginning of the increasing of T_p and R_T at the start of the secondary increasing rate period occurs earlier. With these two thinner papers the sections of the T_p - X curves are not as distinct as with 83 g/m^2 paper but in both cases they show first a period of a relatively slow increase coincident with R_T increasing from the R_{Tc} value, and end with T_p increasing rapidly towards T_j as R_T falls.

At the moisture content X=X_c , paper temperature at the impingement surface starts to rise as R_I starts to fall. The increasing paper temperature for X<X_c during the falling rate period for R_I is convected into the interior of the sheet by the through flow, and very quickly the paper temperature at the through flow exit side, as seen by the T_p curves on figures 6.1 and 6.9, also starts to increase. Thus the paper temperature from one side of the sheet to the other is driven up by the increase in impingement surface paper temperature in the falling rate period for R_I . At X=X_c for the R_I process the sheet moisture content is still above what would be the "critical moisture content" for the R_T process which, therefore, is still governed by the driving force term P_v - P_T , where P_v and P_T represent the vapor pressure of water for the paper and for the through flow air. The maximum achievable value for R_T now would be the value saturated at the new level of paper temperature. This increasing temperature throughout the sheet while sheet moisture content is still relatively high for the R_T process thus gives rise to the observed secondary

increase in R_T . Eventually R_T must end in a falling rate period caused by some combination of the decrease in P_v at low X even at the ever increasing paper temperature, by the increase in diffusional resistance for water removal from inside the fibres and increase in heat of desorption of water with paper of decreasing moisture content. At the limiting moisture content, X_m , these effects exactly balance the tendency for R_T to increase, hence the R_T - X curve passes through the maximum point (X_m , R_{Tm}) after which through flow water removal is in its falling rate period.

The mechanism by which in the CITAD process R_T can be basically different from that in pure through drying thus derives from the R_I component of CITAD forcing T_p to increase at a moisture content for which R_T is still controlled by paper temperature. It follows that the extent of the maximum value of R_T would be increased (or be decreased or disappear) for conditions increasing (or decreasing) the role of R_I. For B=50 g/m^2, this behavior can be seen on figure 6.7 (d) where R_{Tm} does not occur for q_T of 84% and steadily increases in importance as q_T decreases over the range 23% - 10% - 7% as the role of R_I correspondingly increases. For q_T=10.1%, figures 6.8 and 6.9 likewise show that as basis weight increases, thereby extending the period during which the interior sheet temperature can be driven up by impingement heat transfer, the extent of the secondary increasing rate period increases. Quantitative analysis of R_{Tm} dependence on drying process conditions will be given in section 6.8.5.

6.5.3 Drying rate curves for CITAD at fixed G

Subsequent to the above analysis of the two components of the CITAD process, the water removal rates in the impingement and through flow exhausts, the summation of these two components, i.e. the total drying rate for CITAD, is now examined. Drying rate curves are shown for 25 g/m^2 and 50 g/m^2 paper, dried at two levels of air temperature, ambient and around 90 °C, with four levels of total inlet mass flow rate G of 0.125, 0.55, 1.03, 1.46 kg/m^2s respectively on figures 6.10, 6.11, 6.12 and 6.13. In all cases the through flow ratio $q_T=G_T/G$ was varied from 0 to 100%. Shown for reference are values

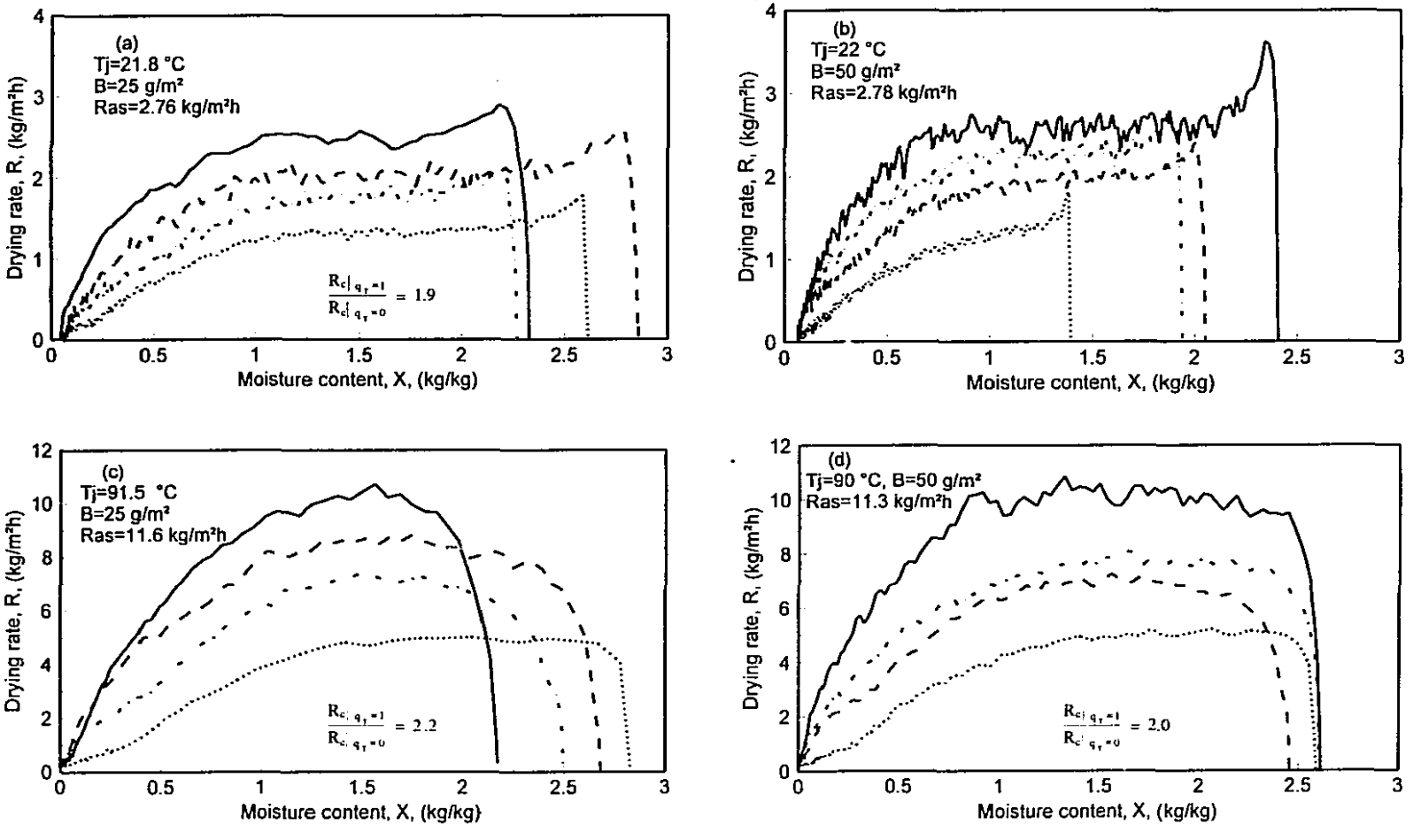

Figure 6.10 Effect of through flow ratio on CITAD drying rate: G=0.125 kg/m²s

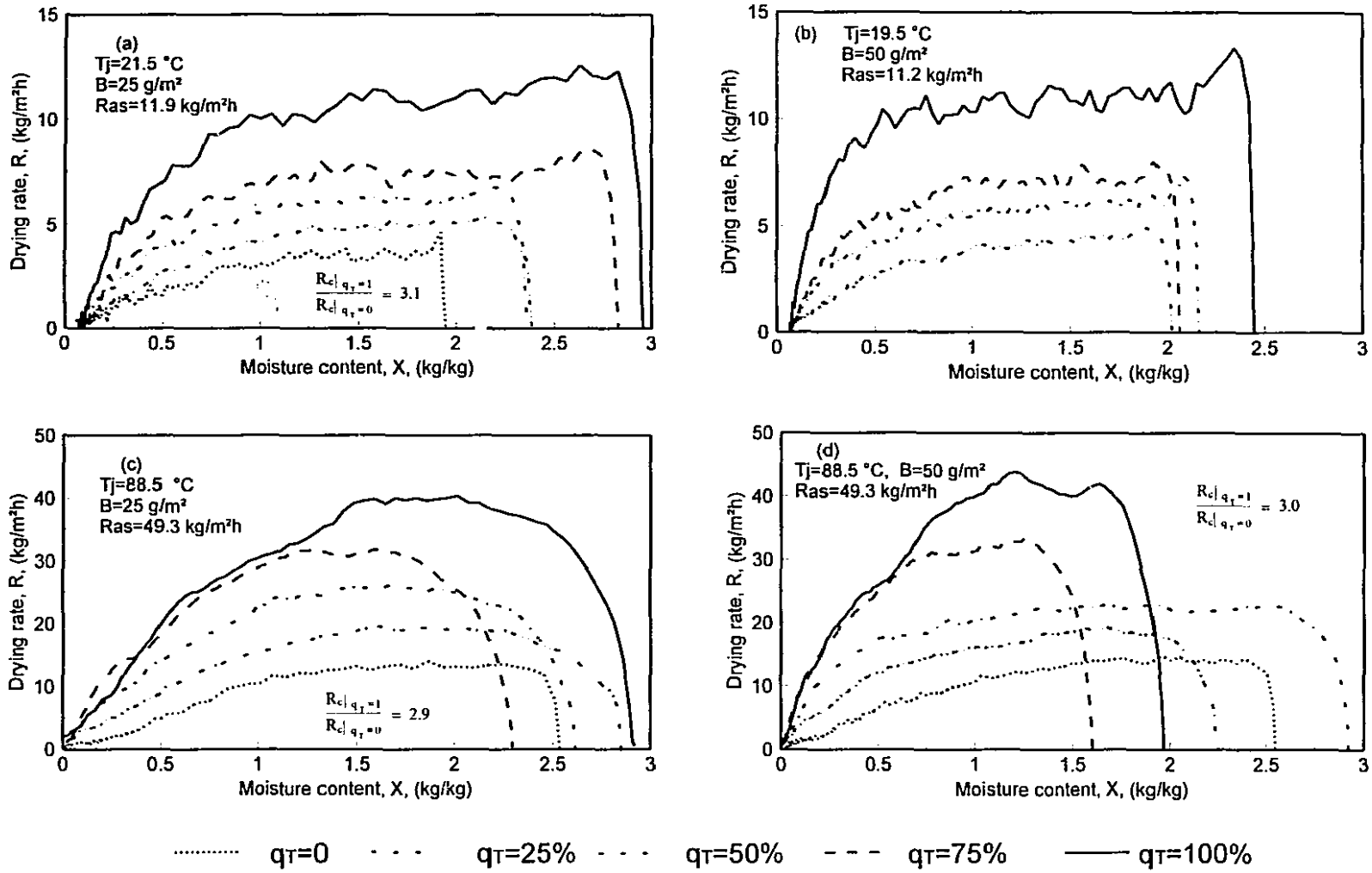

Figure 6.11 Effect of through flow ratio on CITAD drying rate: G=0.55 kg/m²s

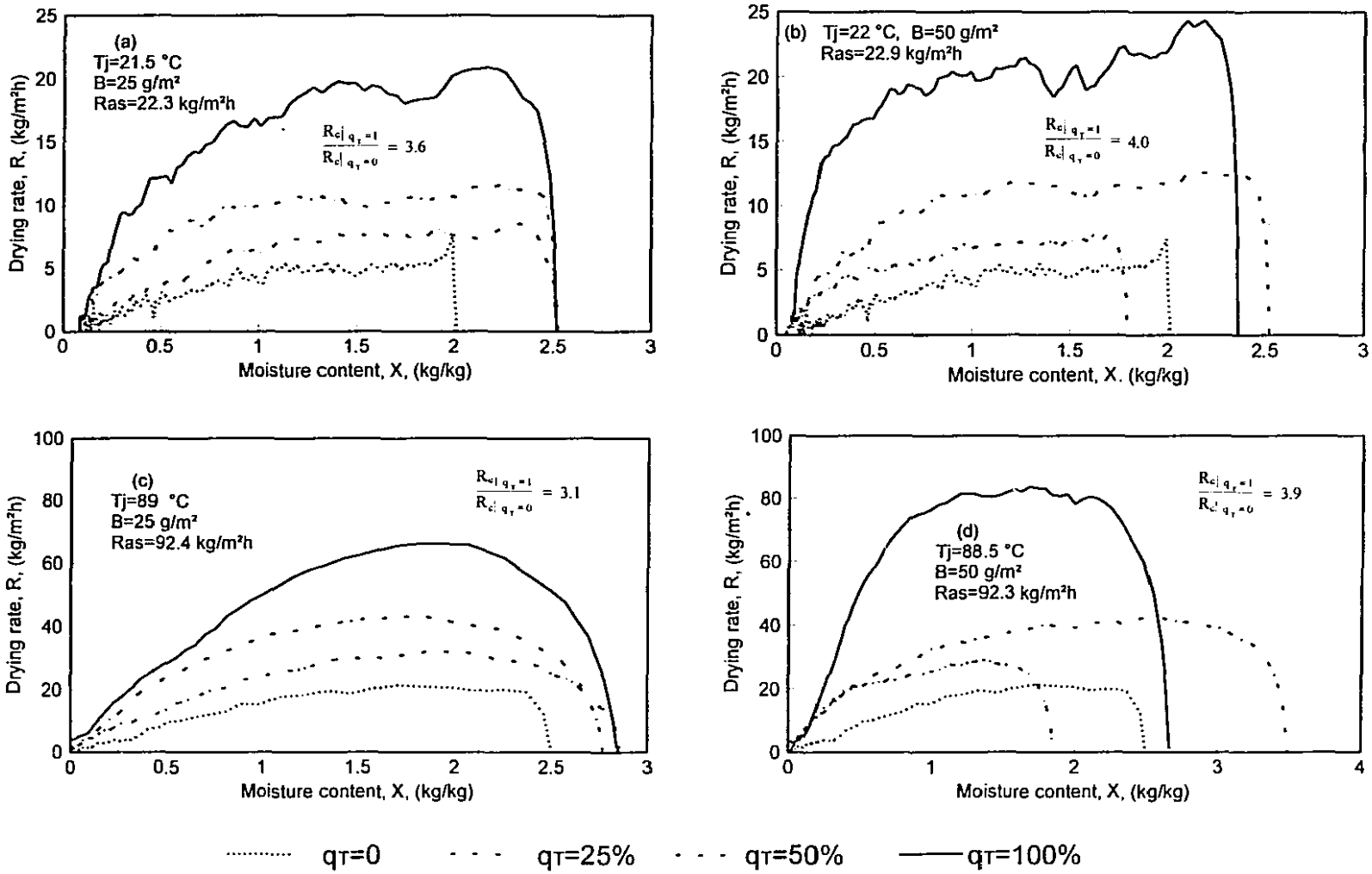

Figure 6.12 Effect of through flow ratio on CITAD drying rate: G=1.03 kg/m²s

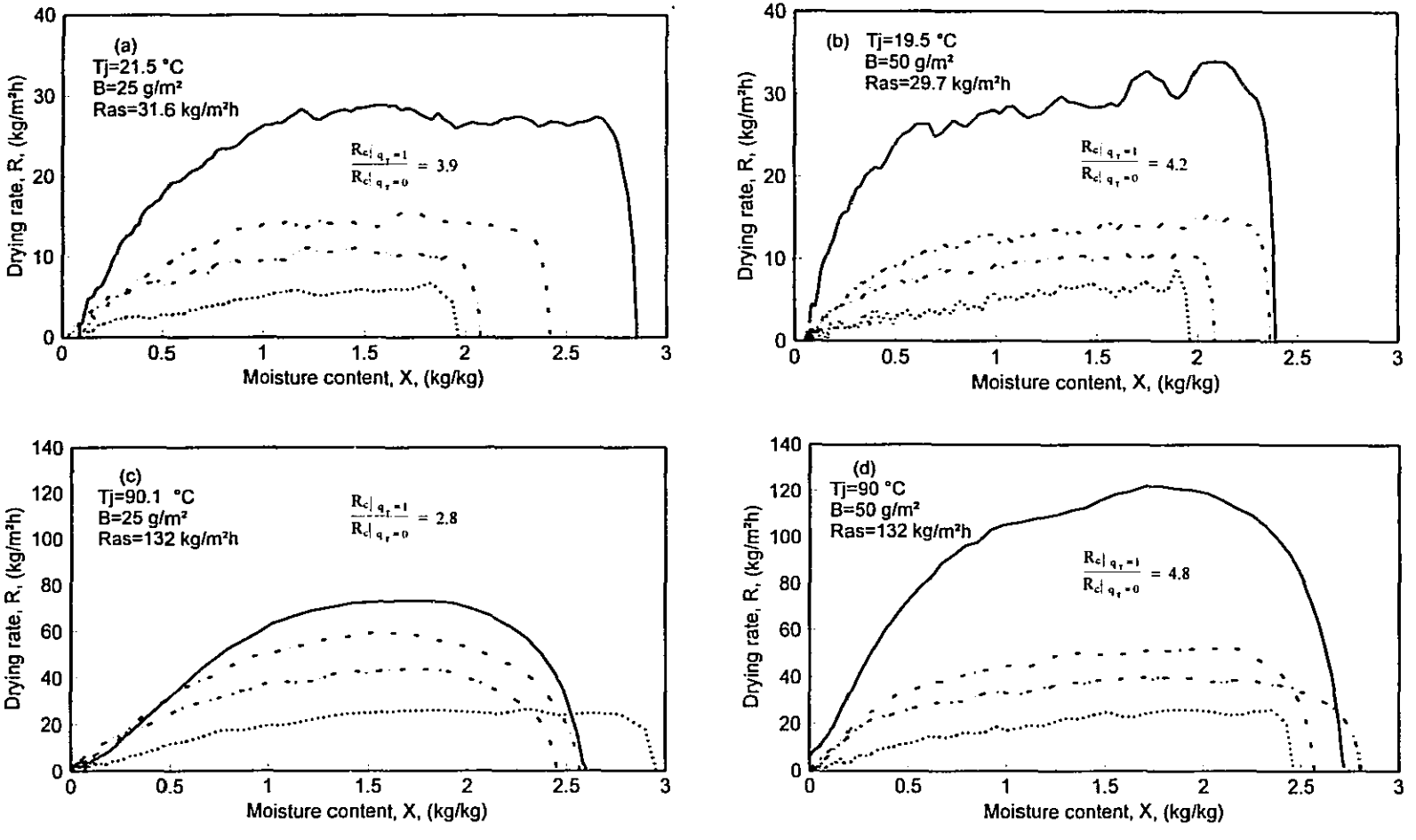

Figure 6.13 Effect of through flow ratio on CITAD drying rate: G=1.46 kg/m²s

of R_{as} , the maximum possible pure through drying rate with the exhaust saturated at the adiabatic saturation temperature of the inlet air.

The drying rate curves for air at ambient temperature are presented for reference only, as paper is never dried industrially in such low temperature air. At low G, figure 6.10, a short transient period of relatively high R at the start of drying occurs for all values of q_T from pure impingement and pure through drying. At high G this effect is seen only for q_T=0 because with higher G_T this transient effect becomes negligible. This transient period reflects the time for the paper temperature to drop from its initial ambient temperature to the wet bulb or adiabatic saturation temperature. As this limiting case of drying was discussed in chapters 4 and 5, the R-X curves for drying in ambient air by CITAD are not discussed further.

The most striking feature of the rate curves for drying by CITAD is the large increase in R as the contribution of through flow increases, i.e. as q_T goes from 0 to 100%. Because of the large contribution of R_T to R, drying rate curves for the CITAD process with as low as through flow ratio q_T=25% show the features of pure through drying rate curves, i.e. always with periods of increasing rate and falling rate, and a constant rate period if conditions so permit. With the change of q_T from 0 to 100% for 25 g/m^2 paper, the great sensitivity of CITAD rate to through flow ratio provides a doubling in the constant drying rate at the lowest air flow rate, G=0.125 kg/m^{2}s, increasing to a tripling of R_c at the highest air rate, G=1.46 kg/m^{2}s. These ratios in R_c are not significantly affected by drying air temperature over the limits from ambient air to $T_j \approx 90^\circ$C. It should be expected that this ratio of R_c between the q_T=0 and q_T=100% limits should vary over even a wider range for thicker paper. Thus for 50 g/m^2 paper at the lowest air rate, G=0.125 kg/m^{2}s, the constant drying rate for q_T=100% is again about double that for q_T=0, but as G increases so does this ratio so that by the highest air rate, G=1.46 kg/m^{2}s, this ratio of total drying rates is 4.5:1, again essentially independent of air temperature. The unique feature for through flow water removal rate after the constant rate period, i.e. the increase of R_T to a sometimes impressive maximum value, never appears on the total drying rate curves because over the region of X for the secondary

increase in R_T, the decrease in R_I is always greater yet, as can be seen on figures 6.1 and 6.9. Since the CITAD rate curves of figures 6.10 - 6.13 involve the complex interaction between impingement and through flow, the water removal rate by the impingement exhaust and by the through flow exhaust are now analyzed quantitatively.

6.6 Quantitative representation of water removal rate curves

6.6.1 Impingement water removal rate

Impingement water removal rate curves, figures 6.2 and 6.3, consist of a constant rate and a falling rate period just as for the pure impingement drying case of chapter 4. Analysis of pure impingement drying showed that the complete drying rate curve can be quantified with three parameters: constant drying rate R_c; critical moisture content X_c; the exponent for a power law R-X relationship over the falling rate period, n. Although there is a major difference over the falling rate period between the shapes of impingement water removal rate curves for CITAD (convex downwards) and pure impingement drying rate curves (typically concave downwards) as noted in sections 6.4 and 6.5.1, the power law R-X relation accommodates both cases with an exponent, n, greater or less than one.

It follows that in CITAD the impingement water removal rate curves may be quantified with three elements: $R_I=R_{Ic}$ for the constant rate period; X_c for juncture of the constant and falling rate periods; and the chapter 4 type power law relationship for R_I - X in the falling rate period:

$$\frac{R_I}{R_{Ic}} = \left(\frac{X}{X_c}\right)^{n_I} \tag{6.1}$$

As for the case of pure impingement drying, the parameters R_{Ic}, X_c and n_I are determined from the experimental data by statistical regression.

The fitting of sets of values of R_{Ic}, X_c and n_I and the resulting water removal rate curves for experimental data from four representative conditions is shown in figure 6.14. With through flow ratio q_T varied over a wide range, 5-50%, the fitting of the falling rate

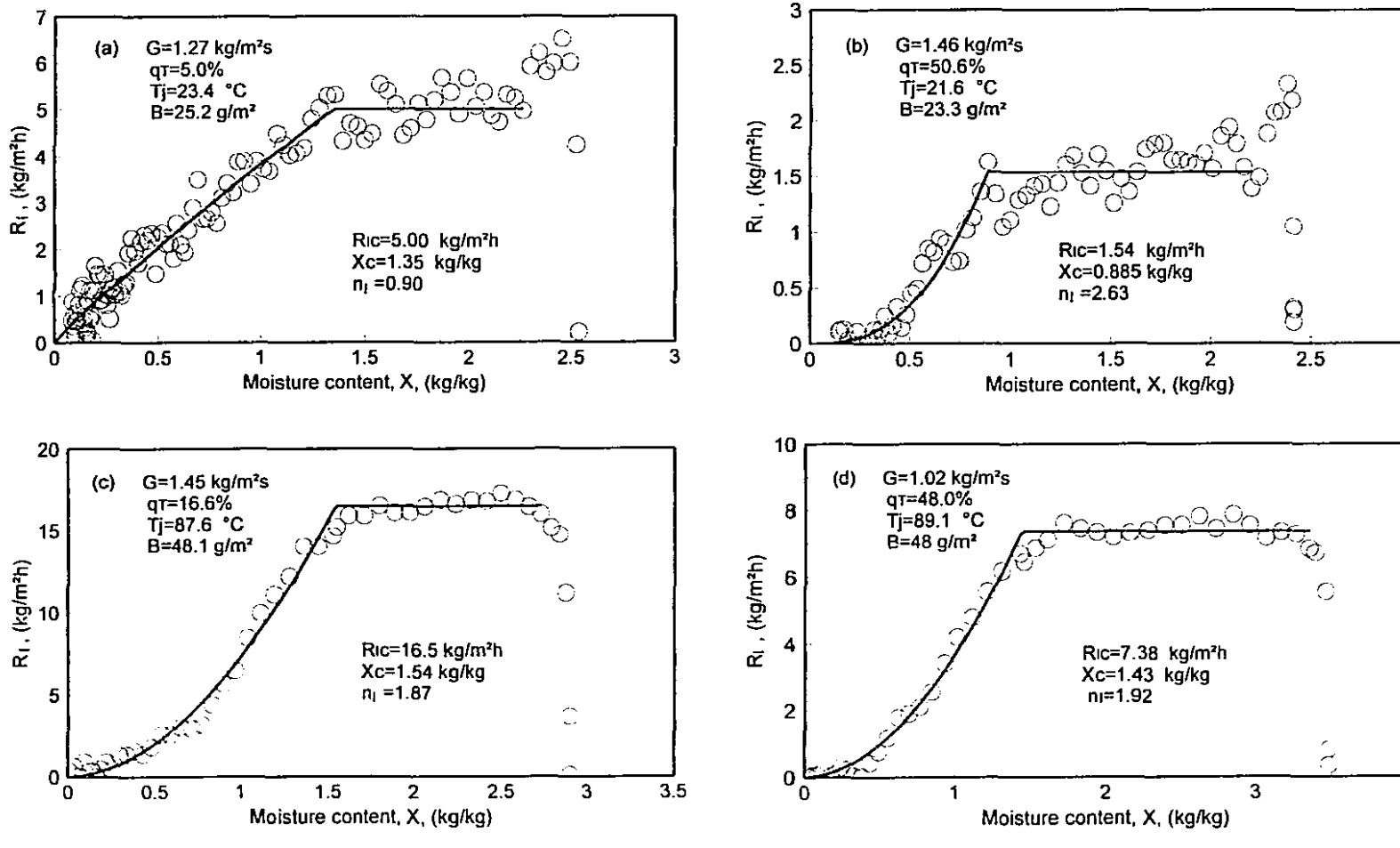

Figure 6.14 Quantitative representation of impingement exhaust water removal rate

period by the power law treatment is good, with the value of n_I seen to vary from less than one, typical of pure impingement drying, to considerably greater than one for drying by CITAD at substantial levels of q_T. Figure 6.14 (a) shows that as little through flow as q_T=5% is sufficient to remove almost all the concave downwards curvature, producing a near linear R - X relation with n_I=0.90 . By as low as a through flow ratio as q_T=16.6%, figure 6.14 (c) indicates the strongly convex downwards R - X curvature as R_I is greatly reduced by R_T . The sharp transition from the constant to falling rate period given by the power law method, although slightly exaggerating the actual transition which is however sometimes sharp, figure 6.14(a), but more often gradual, figures 6.14 (c) and (d), has the merit of giving a clearly defined X_c value. For high through flow ratio, figures 6.14 (b) and (d), the impingement water removal rate becomes effectively zero at a moisture content of about 0.4 kg/kg. A precise fitting of the R_I - X data in this region is of little practical significance because drying rate and drying time for CITAD are controlled not by R_I but by R_T which is very much higher than R_I.

Thus it is established that the above procedure of obtaining three parameters, R_{Ic}, X_c and the falling rate period exponent n_I provides an adequate and practical quantitative representation of the entire impingement water removal rate data. It was therefore applied to the experimental data for each of the 144 CITAD runs, using the same regression package, SYSTAT, as used in chapter 4 for pure impingement drying.

6.6.2 Through flow water removal rate: Increasing and constant rate period

In drying by CITAD the evolution of through flow water removal rate passes from the initial moisture content X_o successively through the values of moisture content X_{Ti} at the end of increasing rate period, critical moisture content X_c for total drying rate of CITAD, moisture content X_m when a maximum of R_T occurs, to dryness at X=0. This evolution shows both similarities to and differences from the drying history for pure through air drying, TAD. The analysis of section 6.5.2 showed that in drying by CITAD a

single value of X_c applies for impingement water removal, R_I, and for total drying rate, R. For the general case of through flow water removal no moisture content is referred to as the critical moisture content as that term in drying is always understood to represent the juncture of the constant and falling rate periods, while these two periods for the complete R_T - X curve may be separated by the secondary increasing rate period. Thus the constant rate period of R_T is terminated at the value of X_c for the R_I - X and R - X curves, and the falling rate period of R_T begins at the value of X_m.

For drying by TAD chapter 5 developed a method, referred to as combined procedures 3, 4 and 5, for treating an entire set of R - X data to extract the five quantitative parameters R_c, X_i, X_c, n_i and n_f. This comprehensive treatment cannot be applied to an entire R_T - X data set for CITAD because of the unique feature in the R_T - X curve of a maximum at (X_m, R_{Tm}) for some CITAD conditions. However, as the R_T - X curve for CITAD is analogous to the R-X curve for TAD over the moisture content range from X_o through X_{Ti} to X_c, and as X_c for R_I - X and R - X has been determined in section 6.6.1, a reduced version of the chapter 5 procedures 3, 4 and 5 can be applied to R_T-X data for $X_o \geq X \geq X_c$. Equation 5.7 for TAD rewritten for CITAD becomes:

$$\frac{R_T}{R_{Tc}} = \frac{1 - e^{-n_T \frac{X_o - X}{X_o - X_T}}}{1 - e^{-n_T}} \qquad \text{for } X_o \geq X \geq X_{Ti} \qquad (6.2)$$

$$\frac{R_T}{R_{Tc}} = 1 \qquad \text{for } X_{Ti} \geq X \geq X_c \qquad (6.3)$$

Because the asymptotic approach of R_T to R_{Tc} given by equation 6.2 results in under-estimated X_{Ti}, the above equations were fitted twice to the data. From the first fitting the value of R_{Tc} was retained and the value of X_{Ti} was determined as the moisture content at $R_T = 0.98R_{Tc}$, as in chapter 5, procedure 4. The exponent n_{Ti} was obtained by reapplying equation 6.2 to the experimental data but with the above values of R_{Tc} and X_{Ti}.

Figure 6.15 shows the above fitting procedures for four representative sets of experimental data. Because for intermediate values of q_T the R_T - X curves become very similar to the R - X curves for TAD, the data sets chosen for figure 6.15 are those for the more informative levels of lower q_T. The fitting of equation 6.2 to the increasing rate

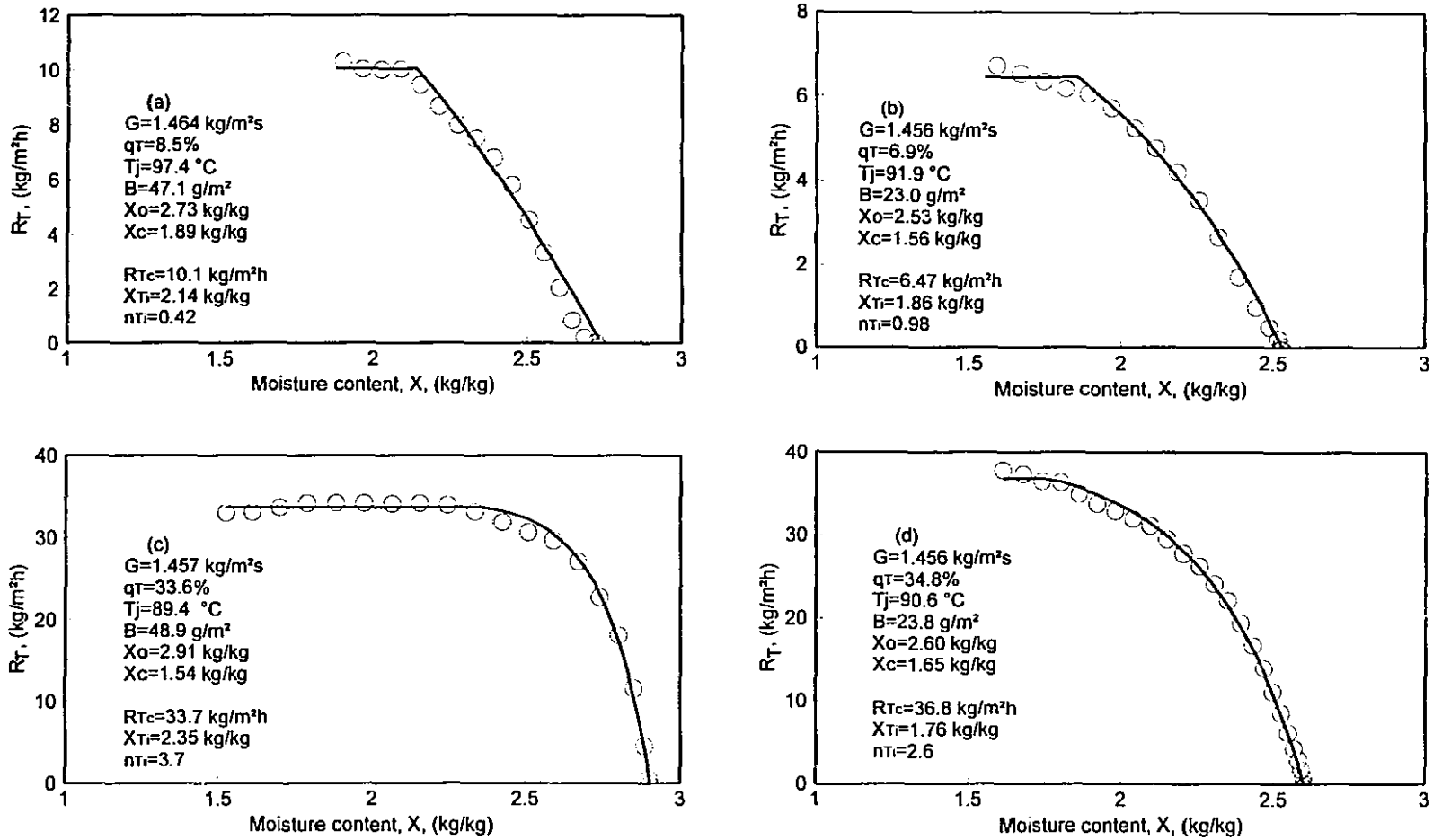

Figure 6.15 Fitting of through flow water removal data in increasing and constant rate periods

period data is very good and the constant through flow water removal rate R_{Tc} is estimated satisfactorily although the extent of constant rate period may be as short as only X_{Ti} - X_c=0.1 kg/kg, figure 6.15 (d). When the through flow ratio q_T is very low, in the range 7-8% for cases (a) and (b), the R_T - X relationship is nearly linear with n_{Ti} consequently low. At a through flow ratio still relatively low, q_T=33.6% in figure 6.15(c), the effect of impingement flow on the curvature of the R_T - X curve in the increasing rate period is not significant with the determined value of n_{Ti}=3.7, the same level for pure through drying. With the CITAD process conditions essentially the same for figure 6.15(c) and (d) except for paper thickness, it is impressive that the proportion of through flow water removal occurring in the increasing rate period changes by about a factor of two, from about 17% to 32%, when basis weight is halved from 49 to 24 g/m^2, with a much lower n_{Ti} for the thinner paper. As the increasing rate period reflects development of area for heat and mass transfer within the sheet, the larger extent of this period for the 24 g/m^2 sheet reflects the fact that such low basis weight sheets have a much lower specific surface than does 50 g/m^2 paper.

With confirmation of the good fitting from using equation 6.2 and the composite procedures for quantifying the data over the increasing rate and constant rate periods, this procedure was then applied to all 77 out of 88 experiments with T_j of 90 °C that the constant water removal rate period is reached at least momentarily. The entire data for each experiment yields a set of values of R_{Tc}, X_{Ti} and n_{Ti}.

6.6.3 Through flow water removal rate:
Secondary increasing rate and falling rate periods

The R_T-X relation over the entire period from the end of the constant rate period up to the maximum point (X_m, R_{Tm}), and down to dryness (0, 0), must incorporate the following properties:

First, the R_T-X curve must pass through the three points (X_c, R_{Tc}), (X_m, R_{Tm}) and (0,0).

Second, at $X=X_m$ there may be a maximum of $R_T=R_{Tm}$.

Third, for through flow ratio $q_T \rightarrow 100\%$, this equation should reduce to the R-X relationship, equation 5.10, for pure through drying.

Equation 6.4, an exponential power law relationship, meets all these requirements. The form of equation 6.4 makes it pass through (0,0) and (X_m, R_{Tm}) with the parabolic form ensuring a maximum of $R_T=R_{Tm}$ at $X=X_m$.

$$R_T = R_{Tm}\left\{1-\left[\left(\frac{e^{-C\frac{X}{X_c}}-e^{-C\frac{X_m}{X_c}}}{1-e^{-C\frac{X_m}{X_c}}}\right)^2\right]^{n_T}\right\} \tag{6.4}$$

When $X=X_c$, equation 6.4 becomes:

$$\frac{R_{Tc}}{R_{Tm}} = 1-\left[\left(\frac{e^{-C}-e^{-C\frac{X_m}{X_c}}}{1-e^{-C\frac{X_m}{X_c}}}\right)^2\right]^{n_T} \tag{6.5}$$

When the value chosen for C satisfies equation 6.5, then (X_c, R_{Tc}) would satisfy equation 6.4. Finally, when $q_T \rightarrow 100\%$, $C \rightarrow 0$ and equation 6.4 reduces to:

$$R_T = R_{Tc}\left[1-\left(1-\frac{X}{X_c}\right)^{2n_T}\right] \tag{6.6}$$

with $R_{Tm} \rightarrow R_{Tc}$ and $X_m \rightarrow X_c$ as $q_T \rightarrow 100\%$. This equation 6.6 is exactly the same as the power law R - X relation for pure through drying in the falling rate period, equation 5.10. Furthermore, $n_T=0.85$ can be obtained by comparing equation 6.6 with equation 5.10 because $n_I=1.7$ was found to be the universal power law exponent for all pure through drying experiments. Hence equation 6.4 becomes:

$$R_T = R_{Tm}\left\{1-\left[\left(\frac{e^{-C\frac{X}{X_c}}-e^{-C\frac{X_m}{X_c}}}{1-e^{-C\frac{X_m}{X_c}}}\right)^2\right]^{0.85}\right\} \tag{6.7}$$

Note that equation 6.7 is written as the square and then to the power of 0.85 because when $X>X_m$, $e^{-C\frac{X}{X_c}} < e^{-C\frac{X_m}{X_c}}$ and the group in small brackets is less than zero which cannot be taken to a real number exponent.

The fitting of equation 6.7 to four representative sets of through flow water removal data in the secondary increasing and falling rate periods is shown in figure 6.16, with the best fit values of X_m , R_{Tm} and C shown for each condition. For drying conditions which produce a secondary increasing rate period, the values of the maximum point (X_m , R_{Tm}) were predicted well, figures 6.16 (a) and (b). Where there is no such maximum, with the falling rate period following immediately the constant rate period, the R_T - X curve was also well represented, figures 6.16 (c) and (d). With this indication of the adequacy of equation 6.7 in quantitatively representing the complexity of the through flow water removal rate after the constant rate period, the R_T - X data for all 144 conditions tested for drying by CITAD were fitted to this equation, obtaining for each condition a set of best fit values of X_m , R_{Tm} and C.

The regression and experimental values of X_m and R_{Tm} are compared in figures 6.17 (a) and (b). As an accurate identification of the (X_m , R_{Tm}) point directly from the R_T-X curve requires a distinct R_{Tm} , only those cases with $R_{Tm} > 1.1R_{Tc}$ were considered. Figure 6.17 (a) shows that the equation 6.7 values of X_m are about 15% higher than the values taken directly from the drying rate curves. For those conditions where $R_{Tm}/R_{Tc}>1.2$ it is seen that $0.5<X_m<1$ kg/kg, hence a 15% error in X_m corresponds to only 0.075-0.15 kg/kg. For $R_{Tm}/R_{Tc}<1.2$, figure 6.16 shows that the R_T maximum region is flat and this small error in X_m has negligible effect on the general R_T - X fitting of the secondary increasing rate and falling rate periods provided R_{Tm} is determined accurately. Figure 6.17 (b) shows excellent agreement of experimental with best fitted values of R_{Tm} .

The parameter C can be calculated from equation 6.5 when X_m , X_c , R_{Tc} and R_{Tm} are known, but only by trial. Hence the regression was carried out with C retained as a parameter in equation 6.7, which was then not forced through the point (X_c , R_{Tc}). The prediction of R_{Tc} by equation 6.5 from the best fit values of X_m , R_{Tm} and C along with the known X_c therefore allows a performance check of equation 6.7. Figure 6.17 (c) shows the excellent comparison between all values of R_{Tc} determined using the procedure given in section 6.5.2 and R_{Tc} calculated from equation 6.5 using X_c , X_m , R_{Tm} and C. Such a comparison reinforced the adequacy of equation 6.7 in representing R_T - X data in the secondary increasing and falling rate periods.

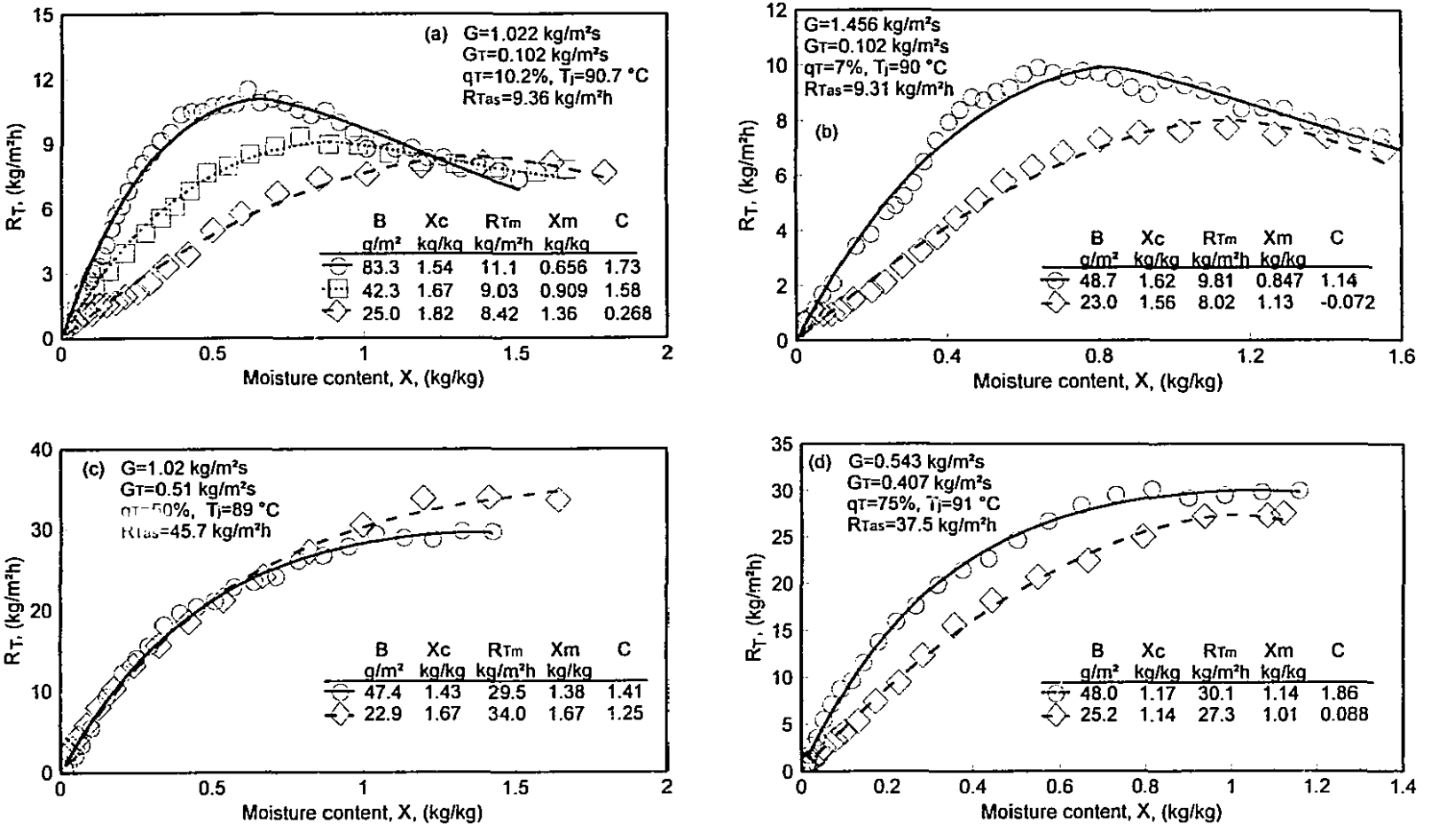

Figure 6.16 Fitting of equation 6.7 to through flow water removal rate data in post-constant rate periods

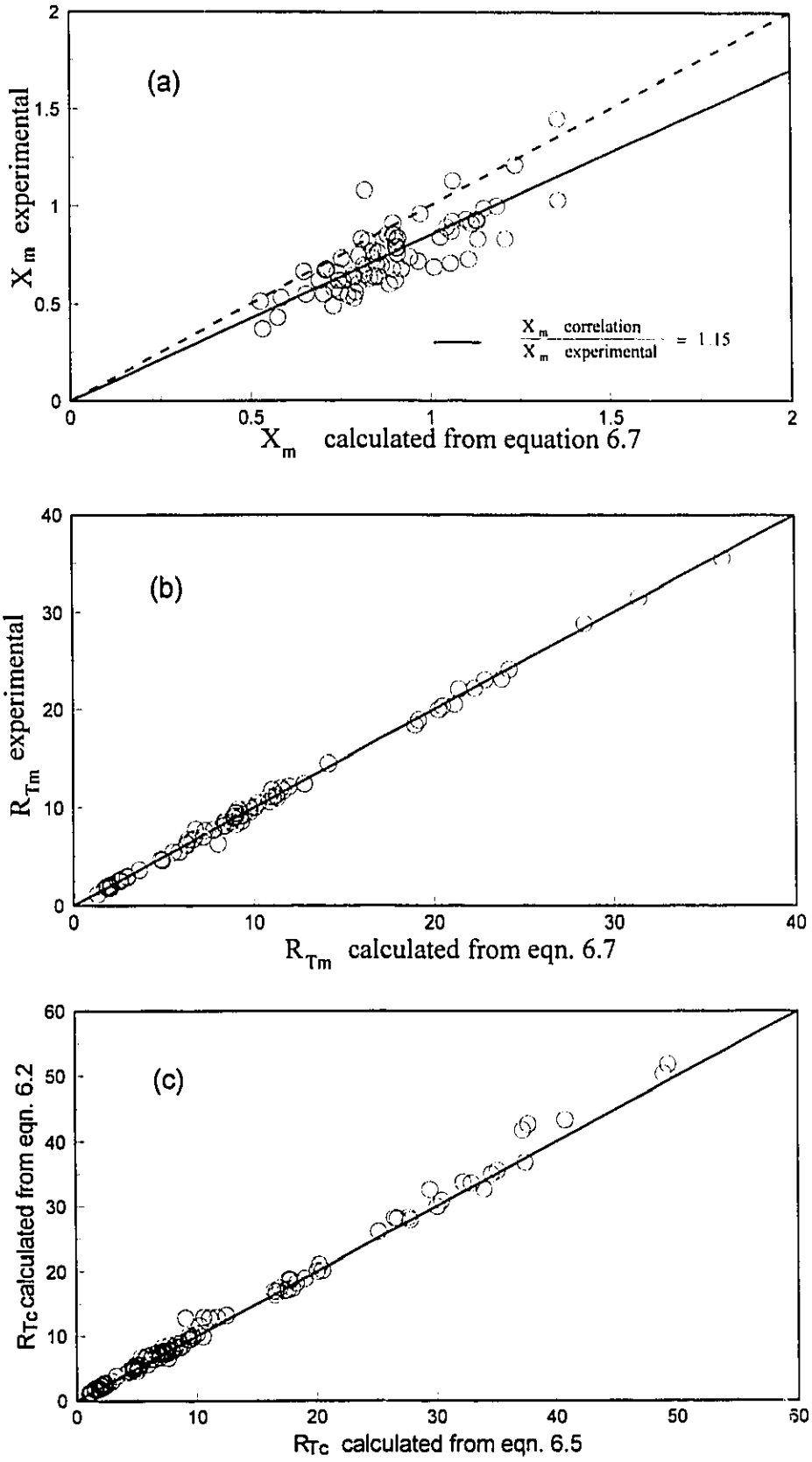

Figure 6.17 Performance check on through flow water removal correlations in the post-constant rate periods

Thus equation 6.7 is established as an adequate single representation of the R_T-X relationship over this region where it sometimes passes through a maximum, R_{Tm} , which separates the secondary increasing rate and falling rate periods, and sometimes is a monotonic function for the falling rate period when drying process conditions do not produce a secondary increasing rate period. The relationships of X_c , R_{Tc}, X_m and R_{Tm} with drying process conditions can now be determined.

6.7 Analysis of characteristics of impingement water removal

6.7.1 Constant impingement water removal rate, R_{Ic}

At a constant impingement exhaust rate G_I and variable through flow ratio q_T the through flow changes the flow field and temperature distribution above the sheet. Most importantly, at constant G_I and increasing q_T the impingement exhaust flow is increasingly deprived of the humidity in the impingement boundary layer above the sheet because air from the region close to the sheet is increasingly drawn into the sheet with the through flow. For drying by CITAD at constant G_I - variable q_T , figures 6.18 and 6.19 show for two levels of G_I the linear relationship between R_I in the constant rate period, R_{Ic} , and the through flow ratio q_T . The decrease in R_{Ic} may be expected by the loss, proportional to the through flow rate, of impingement boundary layer humidity from the impingement exhaust to the through flow. As these data concern R_{Ic} , paper thickness or basis weight should have no effect, as is confirmed by figures 6.18 and 6.19.

When the constant drying rate for pure impingement, R_{cI} , at total inlet mass flow rate of G_I is known, the constant impingement water removal rate, R_{Ic} , at this G_I and any q_T is therefore simply:

$$R_{Ic} = R_{cI}\left(1 - q_T\right) \qquad (6.8)$$

R_{cI} is affected by the nozzle exit values of Reynolds number and T_j as well as by various nozzle and impingement exhaust geometry variables as discussed in chapter 4, where R_{cI}

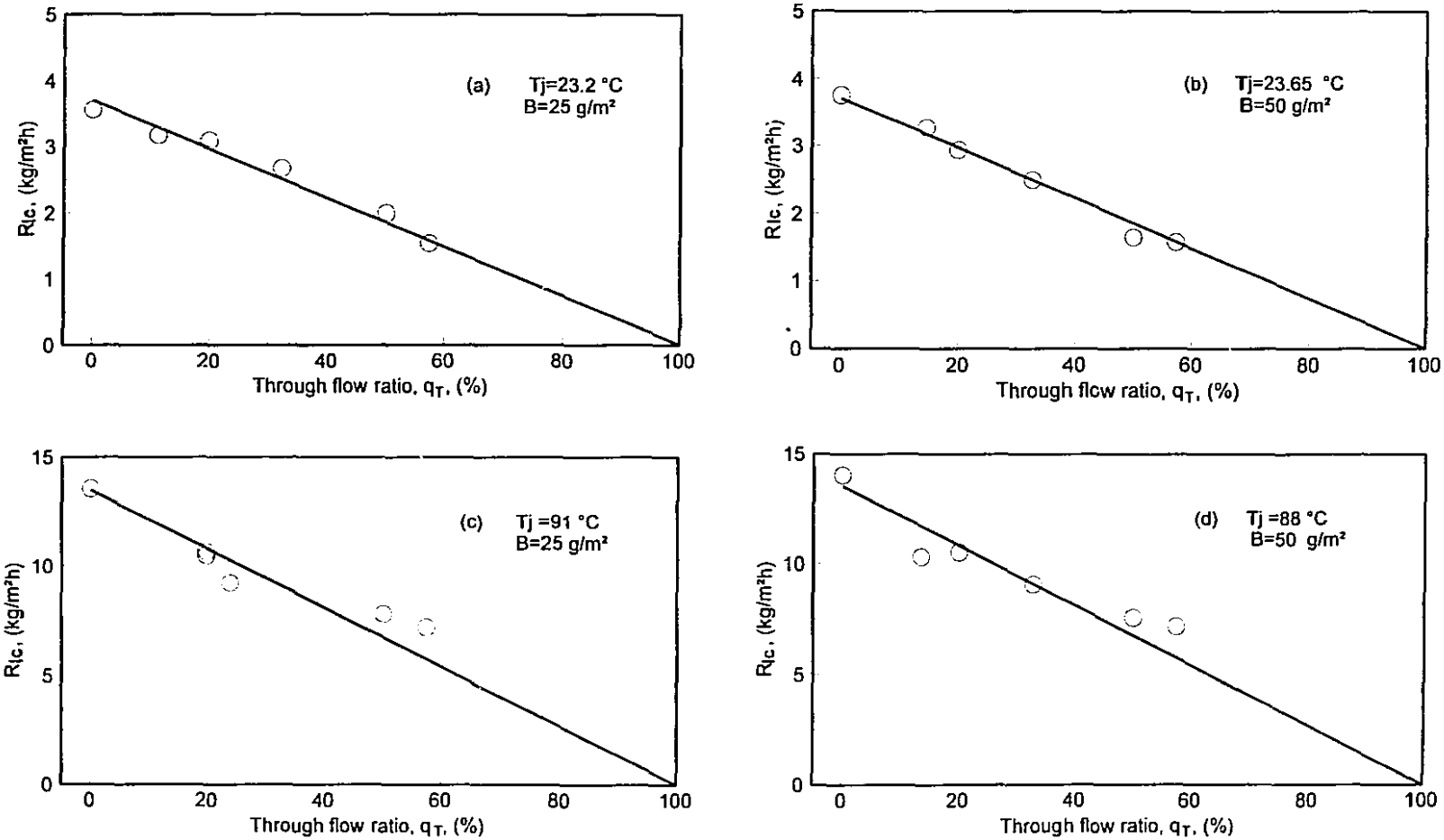

Figure 6.18 Effect of through flow ratio on impingement water removal rate in constant rate period: G_I=0.50 kg/m²s

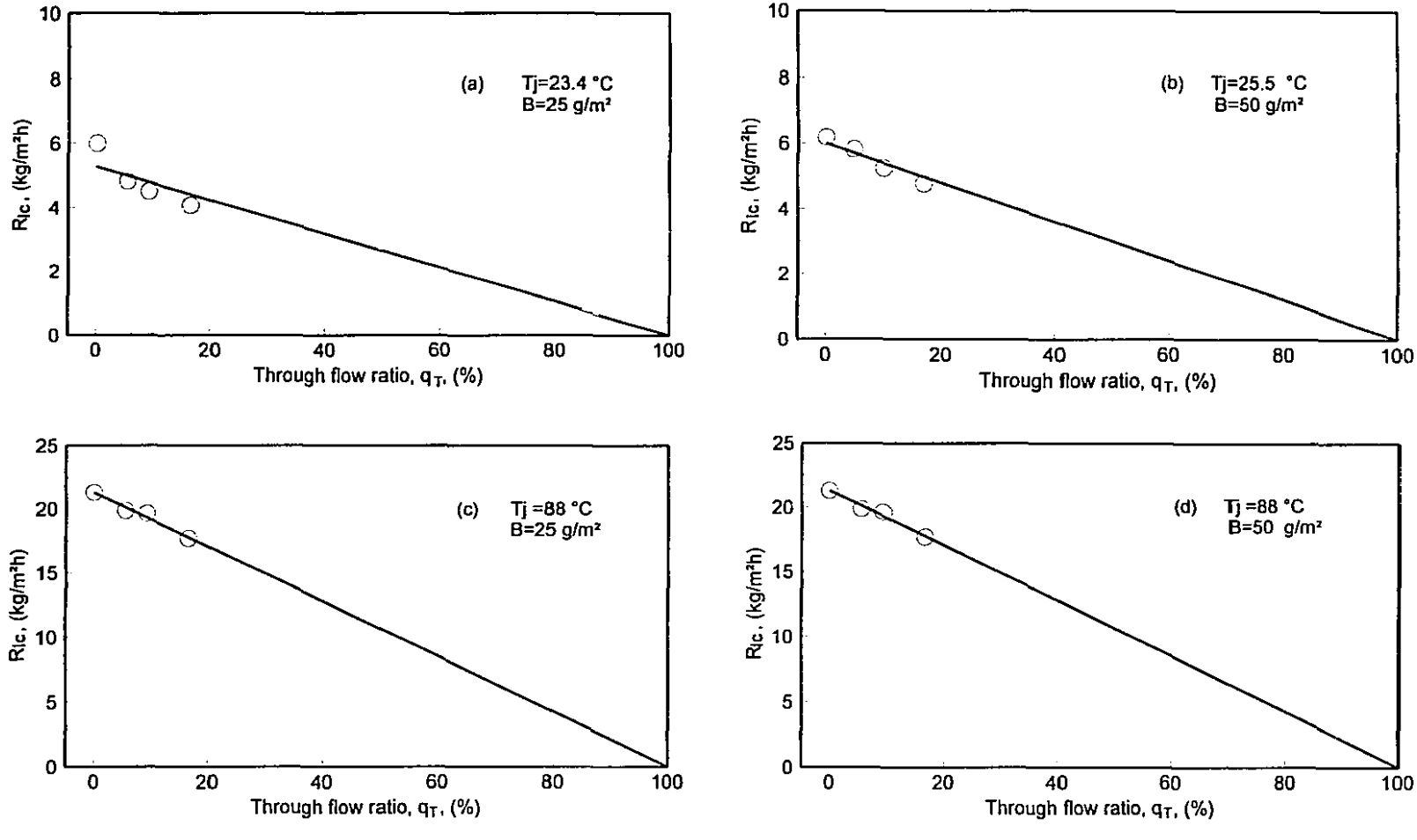

Figure 6.19 Effect of through flow ratio on impingement water removal rate in constant rate period: G_I=1.2 kg/m²s

is represented as equation 4.11. When instead, the total drying air mass flow rate G is held constant, at any through flow ratio q_T , the impingement exhaust flow rate would be $G_I=G(1-q_T)$. When the constant impingement drying rate for $G_I=G$ is known as R'_{cI} , the constant drying rate for pure impingement drying at $G_I = G(1-q_T)$ would be $(1-q_T)^{2/3}\ R'_{cI}$ as constant drying rate is proportional to jet mass flow rate to the power of 2/3, equation 4.14. Hence R_{Ic} becomes:

$$R_{Ic} = R'_{cI}\ (1-q_T)^{5/3} \qquad (6.9)$$

Figure 6.20 shows the comparison of the results from the present study, as summarized in equation 6.9, with the model predictions of Randall (1984) and Crotogino and Allenger (1979). Randall's model, assuming R_{Ic} independent of q_T at constant total G, is clearly quite unrealistic and should therefore be rejected. Although the trend of change in impingement water removal rate of the Crotogino and Allenger model is correct, the present measurements show that the decrease of R_{Ic} with q_T is not linear as they assumed, but decreases with $(1-q_T)^{5/3}$. Thus at q_T respectively of 25, 50 and 75%, the Crotogino and Allenger model would over estimate R_{Ic} substantially, by 21, 59 and 150%. These levels of q_T may be viewed from the perspective that for a specific case analyzed, Randall (1984) reported the economic optimum to be when through air is removing 33% of the total water load.

There is no contradiction between the present finding that in drying by CITAD at constant total drying air flow rate the constant impingement water removal rate decreases significantly with increasing through flow rate, and the finding of another recent study from this laboratory, Polat S. et al. (1990, 1991a,b), that with the same constraints, impingement heat transfer increases significantly with increasing through flow rate. Impingement heat transfer coefficients certainly increase as the boundary layer is thinned by increasing through flow rate into the impingement surface. However the present study focuses not on what happens at the impingement surface in drying by CITAD, but on what happens to the two exhaust streams, the impingement and through flow exhausts. With increasing through flow rate the significant increase in impingement heat transfer, hence the increase in evaporation rate at the impingement surface, is however not

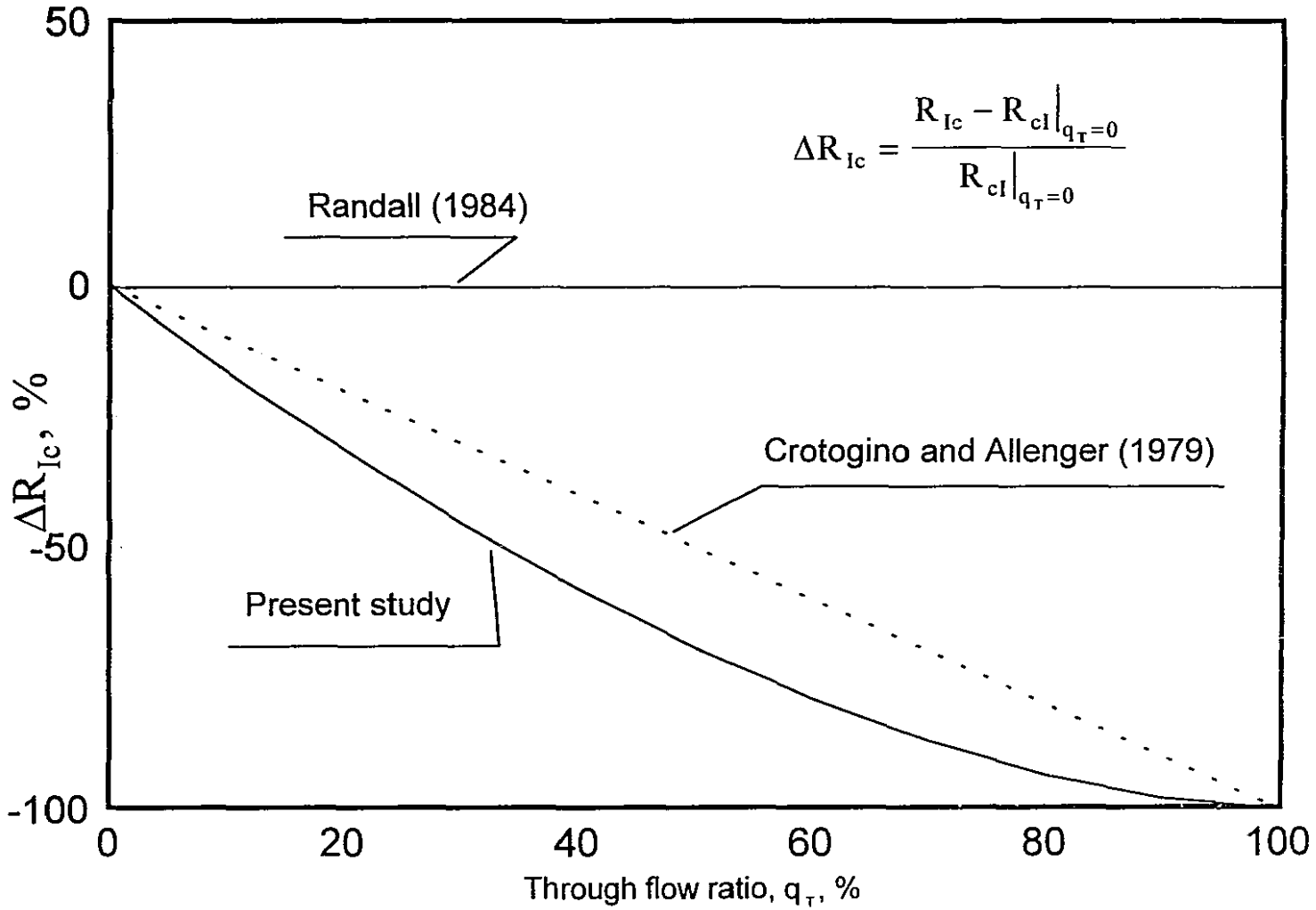

Figure 6.20 Effect of through flow ratio on constant water removal rate in the impingement exhaust at fixed total drying air mass flow rate

reflected by a correspondingly increased impingement exhaust water removal rate. This higher humidity boundary layer, which would be extremely difficult to measure, is to an increasing extent drawn into the sheet. As the impingement exhaust is progressively deprived of the humidity closer to the wet sheet this exhaust becomes of lower humidity and higher temperature. Thus at higher q_T , the benefits of higher impingement heat and mass transfer coefficients are reflected by higher humidity, lower temperature air in the through flow entering the sheet. Therefore concerning the effect of q_T on impingement water removal rate in drying by CITAD, there is no inconsistency between the experimental results of present study and those of Polat S. et al.

6.7.2 Critical moisture content, X_c

An understanding of the variation between 0.9 and 1.8 kg/kg for the 144 values of critical moisture content X_c determined in section 6.6.1 for the drying of paper by CITAD derives from two considerations, the behavior of X_{cI} , critical moisture content for pure impingement drying, and the variation of X_c in the presence of through flow in drying by CITAD. For pure impingement drying, X_{cI} increases with drying intensity and with paper basis weight, as is expected for surface drying. X_{cI} is also a function of nozzle geometry and paper initial moisture content for locally nonuniform flow conditions at the impingement surface, as given by equation 4.12. Because of the water removal from the sheet by through flow, the z-direction moisture content distribution will be different for CITAD from that in pure impingement drying. Specifically, after the paper surface is relatively dry and the impingement water removal rate is approaching its critical point, for sufficiently thick paper the wet portion of sheet towards the through flow exit side can still sustain a constant rate for through flow water removal. Because the determined X_c for CITAD is the volumetric average moisture content over the entire thickness of the sheet, such a removal of water by through flow would decrease the overall average value of moisture content, hence the determined X_c for the impingement water removal process. This effect of through flow is related to paper basis weight as follows:

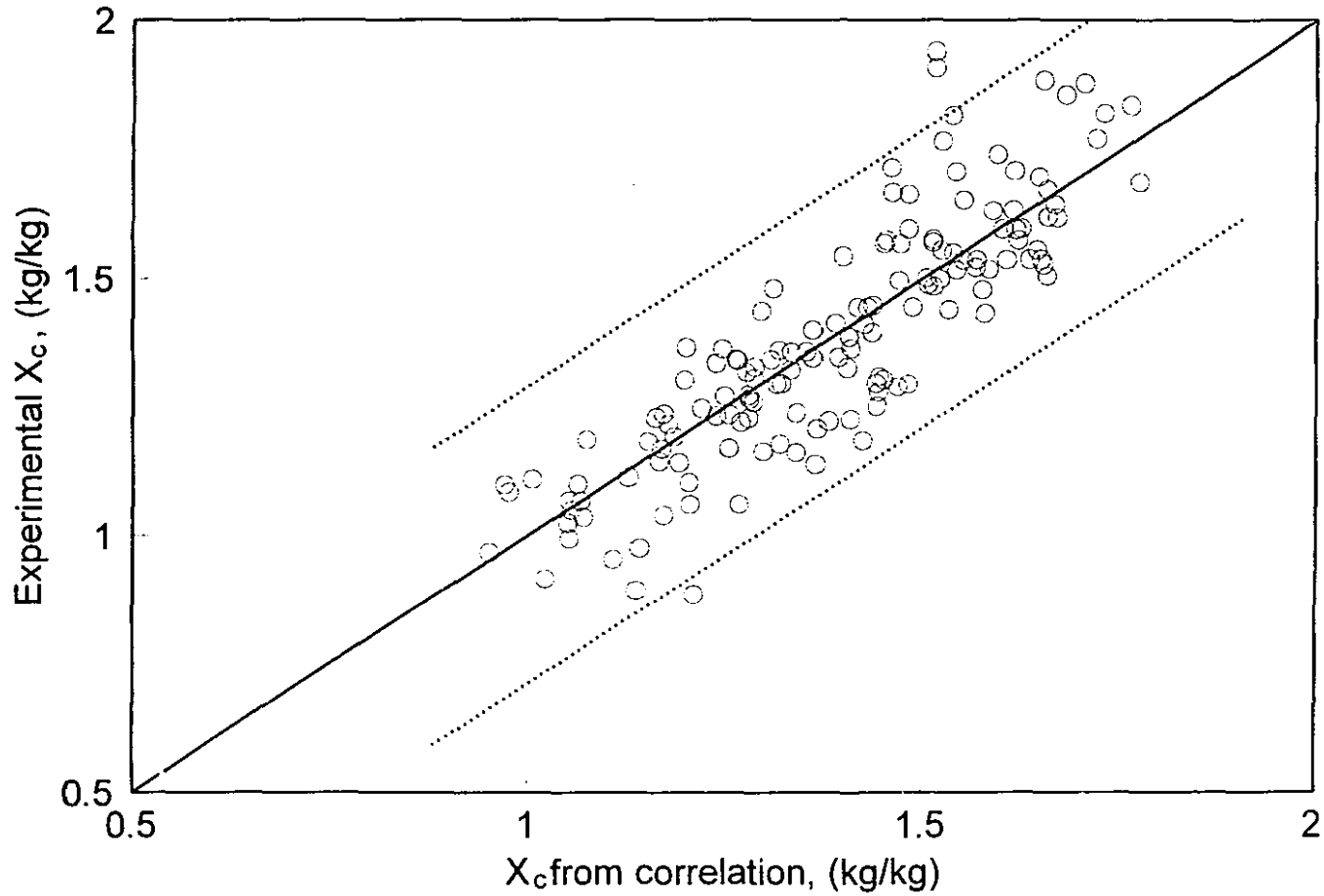

Figure 6.21 Comparison of X_c from correlation eqn. 6.10 with experimental X_c

$$\frac{X_c}{X_{cI}} = a_{xc}\, B^{b_{xc}} \qquad (6.10)$$

with R^2=0.74 and the best fit values of a_{xc} and b_{xc} listed in Table 6.2.

Table 6.2 Correlation parameters for X_c

Parameter	ε	σ	2σ/ε, %
a_{xc}	1.96	0.16	16
b_{xc}	-0.13	0.02	31

On the figure 6.21 comparison between experimental and calculated values of X_c the dashed lines represent the 2σ uncertainty limits of the prediction of equation 6.10, 0.28 kg/kg.

Equation 6.10 indicates that the values of X_c for drying by CITAD follow essentially the same relation with drying process conditions as X_{cI} for pure impingement drying, except for the paper thickness effect. As X_c for the CITAD process has not previously been determined, no comparison with the results of others is possible. The negative value of b_{xc} is expected, as the thicker paper would be of higher z-direction moisture gradient when there is no water removed from the bottom by through flow. X_c for CITAD is higher than X_{cI} , with the ratio of X_c/X_{cI} varying from 1 to 1.7, with an overall average value X_c/X_{cI}=1.2 for all the conditions tested. The increase in impingement heat transfer coefficient and hence in drying intensity at the paper surface because of through flow is believed to be a contributing cause to this earlier onset of the falling rate for impingement water removal than for pure impingement drying.

6.7.3 Impingement water removal in the falling rate period, n_I

The exponent, n_I , representing the R_I - X relation in the falling rate period of drying by CITAD was correlated, as was the critical moisture content, as a ratio to the value of the exponent n for the corresponding correlation for pure impingement drying, i.e. from equation 4.14 in chapter 4. The relationship obtained was:

$$\frac{n_l}{n} = \left(\frac{X_c}{X_{cl}}\right)\left(1 + a_{nl} B^{b_{nl}}\, q_T^{c_{nl}}\right) \qquad (6.11)$$

with R^2=0.66. Table 6.3 lists the best fit values of these parameters, designated as ε.

Table 6.3	Correlation parameters for n_l		
Parameter	ε	σ for ε	2σ/ε (%)
a_{nl}	0.069	0.004	12
b_{nl}	0.87	0.12	28
c_{nl}	0.26	0.04	31

In the figure 6.22 comparison between experimental n_l values determined as described in section 6.6.1 and those calculated by the above correlation, the dashed lines represent the 2σ=0.56 limits for n_l . The considerable complexity of the CITAD experiments leads to correspondingly greater uncertainty in the calculated parameters, noted for X_c in section 6.7.2 and seen here in the 2σ value for n_l being about three times that for pure impingement drying.

As noted first in section 6.4, the falling rate curves for impingement water removal in CITAD differ greatly from those for pure impingement drying in that the latter are general concave downwards, with most values of n in the range 0.5-1, while the former are convex downwards, with values of n_l in the range of 1-2.6. Although the presence of through flow reduces the R_l - X curves over the entire moisture content range, this difference is most dramatic in the falling rate period. In addition to the loss in CITAD of impinging boundary layer humidity into the through flow, discussed in section 6.6.1, CITAD brings also an important change in transport mechanism for moisture to reach the impingement surface. In the falling rate period of pure impingement drying, water reaches the surface by two mechanisms, i.e. humidity diffusion through the stagnant air in the pores and by moisture diffusion through the moist fibres, with the latter process probably slower than the former. In the falling rate period of CITAD, the humidity diffusion process is no longer effective because the through flow velocity of air in the pores exceeds the humidity diffusion in the opposite direction, leaving the relatively slower moisture diffusion through fibres as the only mechanism by which water reaches

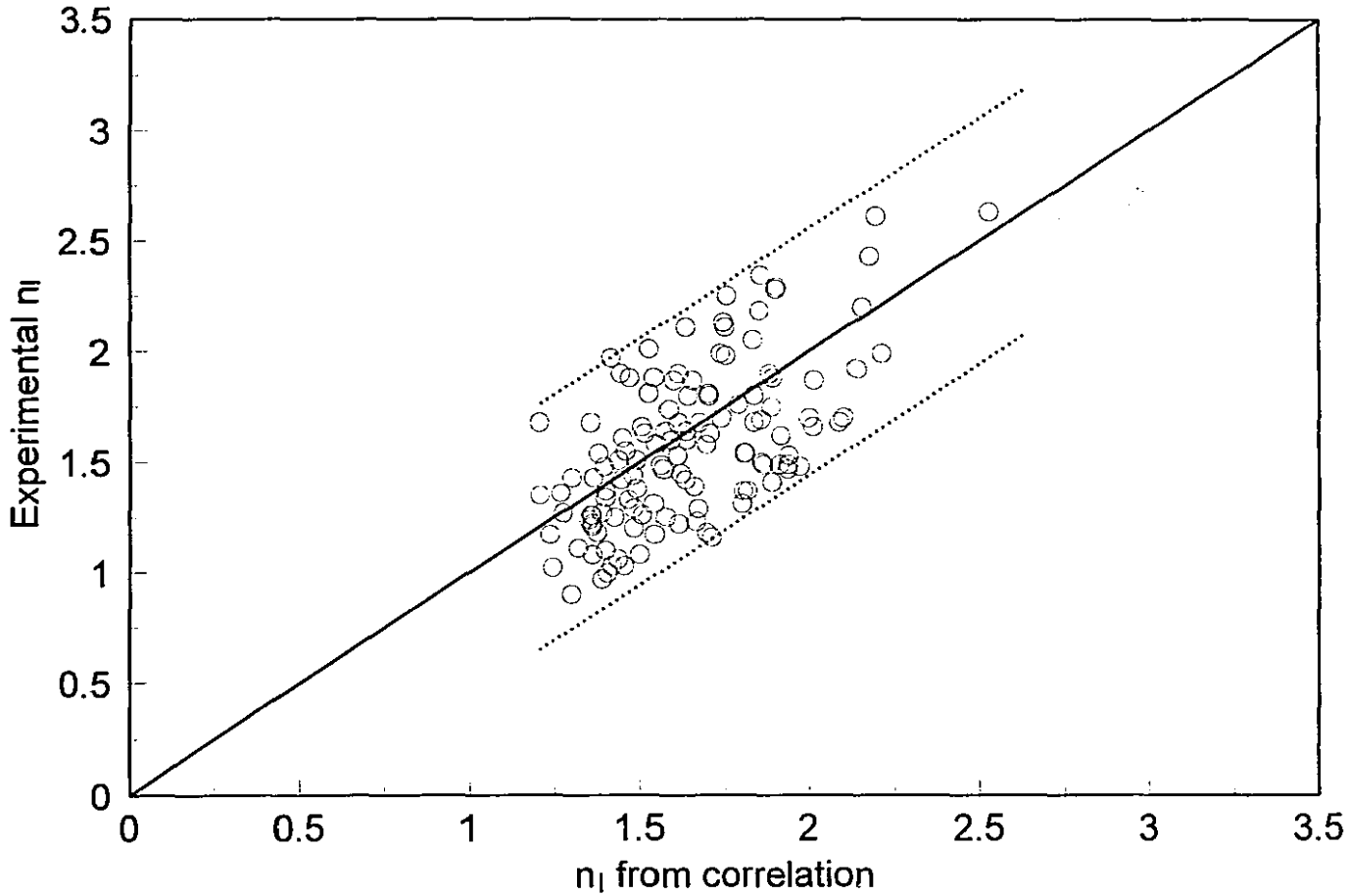

Figure 6.22 Comparison of n_l from correlation eqn. 6.11 with experimental n_l

the impingement surface. Moreover, published measurements by Lee and Hinds (1981) and Navarri et al. (1992) show that moisture diffusivity in moist paper decreases greatly in the range of 0<X<0.2 kg/kg, as was discussed in section 4.4.3 concerning the falling rate period of pure impingement drying. Thus CITAD brings a large reduction in rate of diffusion of moisture to be evaporated at the impingement surface, combined with loss of some of such evaporation by immediate convection back into the sheet by the entering through flow. These mechanisms explain the great change in curvature of the R_I - X curves from concave downwards for IAD to strongly convex downwards for CITAD.

6.8 Analysis of characteristics of through flow water removal

6.8.1 Moisture content at end of increasing rate period, X_{Ti}

The increasing rate period ends when the amount of water removed from the pores in the paper provides sufficient heat and mass transfer area for through flow air to reach the constant water removal rate. If, in the extreme case, water removal by impingement in CITAD drying made no contribution to the development of transport area within the sheet, then the extent of the increasing rate period for CITAD, X_o - X_{Ti}, would be simply the sum of moisture removed by through flow and by impingement, i.e. by R_T and R_I, until that removed by R_T reaches, X_o - X_i, the extent of increasing rate period for pure through drying at $G=G_T$. For this limiting case the value of X_{Ti} for CITAD would then be less than X_i by the entire amount of the moisture removed from impingement exhaust, $\Delta X_I = R_{Ic}\, t_{Ti}/B$, where t_{Ti} is the drying time for the increasing rate period. From equation 5.7, for pure through drying, $t_{Ti} = (X_o - X_i)B/\overline{R}_{Ti}$ with $\overline{R}_{Ti}$ expressed as:

$$\frac{R_{Tc}}{\overline{R}_{Ti}} = \frac{e^{n_i}-1}{e^{n_i}} \int_0^1 \frac{dW}{1-e^{n_i(W-1)}} \qquad \text{where } W = \frac{X - X_i}{X_o - X_i} \text{ and } n_i = 3.6$$

Defining $R_{Tc} / \overline{R}_{Ti} = C_{Ri}$, then C_{RI}=1.81 for W from 0 to 0.99. The moisture content X_{Ti} at the end of the increasing rate period of CITAD for the limiting case of water removal

by R_I making no contribution to the development of transport area within the sheet, becomes:

$$X_{Ti} = X_i - \Delta X_I = X_i - C_{Ri} \frac{R_{Ic}}{R_{Tc}}(X_o - X_i)$$

However, as moisture diffuses in the z-direction from within the sheet to evaporate at the impingement surface, water removal by impingement will make some contribution to the development of transport area within the sheet. Thus the amount of water removed during the increasing rate period for CITAD will be less than for the limiting case noted above. In the place of C_{Ri} in the above limiting case correlation, a parameter C_{Xi} may be determined from the experimental data. Hence the extent of the increasing rate period for through flow water removal of CITAD, $X_o - X_{Ti}$, may be correlated as:

$$X_o - X_{Ti} = (X_o - X_i)\left(1 + C_{Xi} \frac{R_{Ic}}{R_{Tc}}\right) \qquad (6.12)$$

Application of equation 6.12 for all experimental values of X_{Ti} from conditions giving at least a momentary constant rate period i.e. $X_{Ti} \geq X_c$, gives the best fit value of C_{Xi} as 1.07. This value of C_{Xi} is intermediate between 0 and 1.81, values that would apply, respectively, if the water removed by the impingement exhaust contributed fully or made no contribution to transport area development during the increasing rate period. One should expect that this contribution would depend on basis weight, and in fact C_{Xi} was found to be the case, giving $C_{Xi}=a_{xi}\ B^{bxi}$, hence providing the following general correlation of X_o-X_{Ti}:

$$X_o - X_{Ti} = (X_o - X_i)\left(1 + a_{xi} B^{b_{xi}} \frac{R_{Ic}}{R_{Tc}}\right) \qquad (6.13)$$

For pure through drying, $R_{Ic}=0$ and the value of X_o - X_{Ti} given by equation 6.13 converges to the value X_o - X_i, as should be the case. The correlation gave $R^2 = 0.43$, and the best fit values of the parameters, which are designated as ε, are listed in Table 6.4.

In the figure 6.23 comparison between experimental and correlation of X_o-X_{Ti}, which varied from 0.1 to 1.4 kg/kg, the 2σ uncertainty of 0.32 kg/kg, represented by the dotted lines, is twice that for simpler case of pure through drying. This larger scatter in

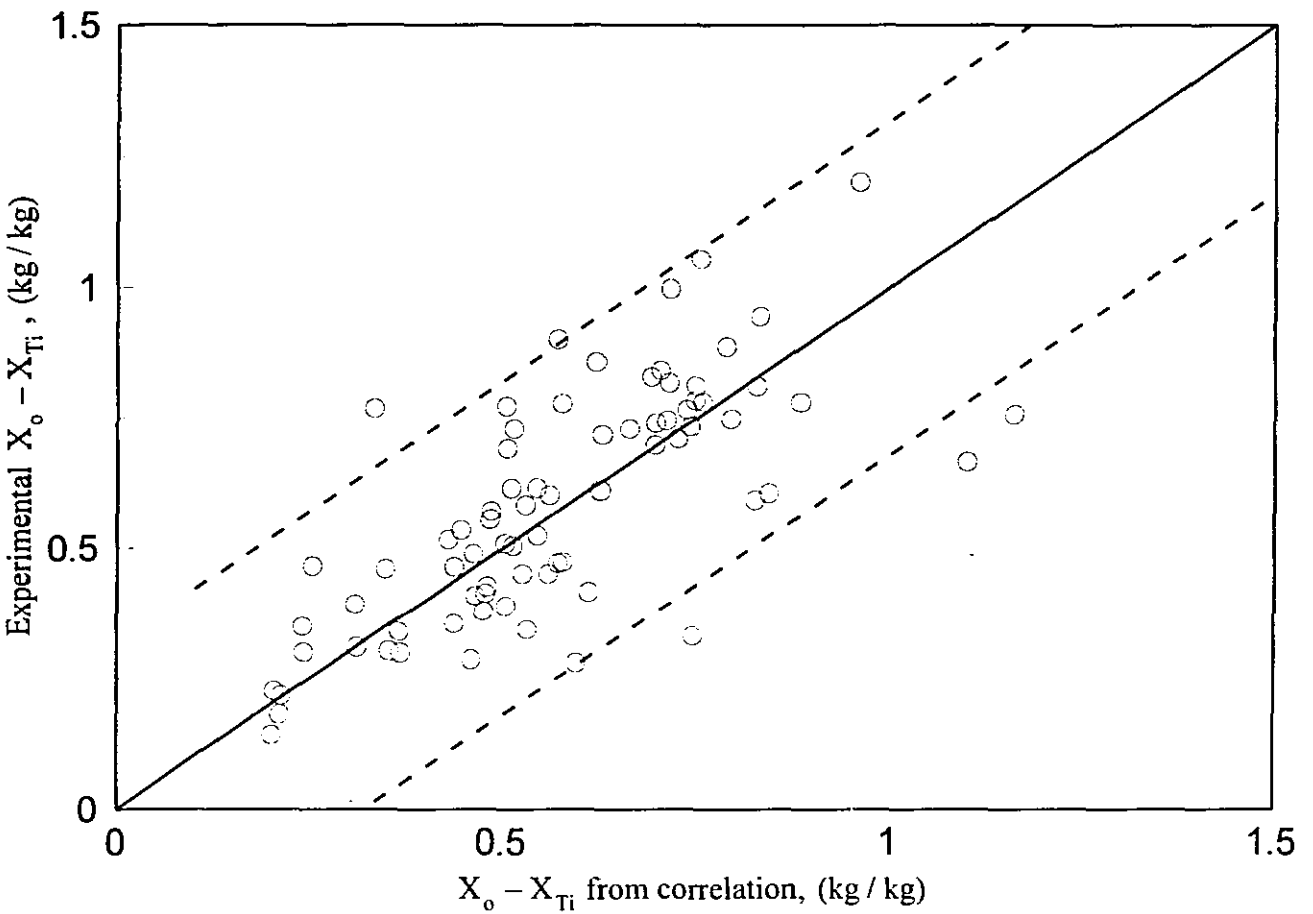

Figure 6.23 Comparison of experimental $X_o - X_{Ti}$ with those from correlation eqn. 6.13

the prediction by equation 6.13 of $X_o - X_{Ti}$ reflects the extra complication of the important interaction from impingement flow for drying by CITAD in addition to all the factors which affect $X_o - X_i$ in pure through drying, chapter 5.

Table 6.4 Correlation parameters for X_o-X_{Ti}			
Parameter	ε	σ for ε	2σ/ε (%)
a_{xi}	0.043	0.003	14
b_{xi}	0.92	0.18	39

As B increases the effectiveness of impingement water removal for development of transport area within the sheet should decrease and C_{Xi} should increase towards the limit of B=1.81 for no contribution to transport area. The finding that the exponent for B, b_x=0.92, is positive and not much below one reflects exactly this expectation, giving C_{Xi}=0.83 for B=25 g/m^2 and C_{Xi}=1.57 for B=50 g/m^2. As the limits of C_{Xi} are 0 and 1.81, the above values indicate that with 50 g/m^2 paper, water removed by impingement contributes little to the development of transport area within the sheet while for B=25 g/m^2 this contribution is substantial. Equation 6.13 predicts that for paper basis weight as high as 58 g/m^2, C_{Xi}=1.81 and hence the water removed by impingement flow would make negligible contribution to the development of transport area for heat and mass transfer within the sheet for through flow water removal during the increasing rate period. The consequence of this effect on the extent of the increasing rate period between CITAD and TAD operation is given in Table 6.5 for the conditions of figure 6.8.

Table 6.5 Extent of increasing rate period: Comparison for CITAD and for TAD		
	B=25 g/m^2	B=50 g/m^2
$X_o - X_i$, kg/kg	0.27	0.16
$X_o - X_{Ti}$, kg/kg	0.76	0.71
$(X_o - X_{Ti})/(X_o - X_i)$	2.8	4.4

The higher values of $X_o - X_{Ti}$ than $X_o - X_i$ reflect the fact that water removal by impingement contributes to only a limited extent to the development of area for heat and mass transfer within the sheet. The higher ratio of $(X_o - X_{Ti})/(X_o - X_i)$ for 50 g/m^2 paper

reflects even less contribution of impingement water removal to the development of transport area.

The constant drying rate values R_{Tc} and R_c apply over the extent of the constant rate period, X_{Ti} - X_c . For any drying process conditions there exists an initial moisture content for which the constant drying rate period is reached only momentarily at $X_{Ti}=X_c$. With an increase in q_T , X_c increases while X_{Ti} decreases, hence the extent of constant rate period decreases rapidly. From equations 6.10 and 4.12 for X_c and equations 6.13 and 5.11 for X_{Ti} , this initial moisture content X_o^{ic} can be calculated. For $X_o<X_o^{ic}$ there is no constant rate period. For the CITAD conditions used here, 77 out of the 88 experiments carried out at $T_j\approx90$ °C gave at least momentarily a constant rate period.

6.8.2 Through flow water removal in the increasing rate period, n_{Ti}

In equation 6.2 for the R_T - X curve in the increasing rate period the exponent n_{Ti} reflects the curvature of this relation, analogous to the exponent n_i for pure through drying, equation 5.7 of chapter 5. The exponential R_T - X relationship for CITAD is however complicated by the contribution from the impingement flow in CITAD. Thus the R_T - X curvature during the increasing rate period is reduced, figure 6.15, and n_{Ti} is correspondingly reduced from the universal value of $n_i=3.6$ for pure through drying. For CITAD operation at relatively low through flow, i.e. at q_T of 7-9%, figure 6.15 shows that although X_o - X_{Ti} is substantial, the R - X curve is almost linear, with $n_{Ti} < 1$. Based on above analysis, values of n_{Ti} for all CITAD experiments that give an increasing rate period, varying from -1.3 to 4.0, were correlated as:

$$n_{Ti} = 3.6\left[1 - a_{nT}\left(\frac{X_o - X_{Ti}}{X_o - X_i}\right)^{b_{nT}}\left(1 - q_T\right)^{c_{nT}}\right] \qquad (6.14)$$

with $R^2=0.66$ and the best fit parameters, designated as ε, listed in Table 6.6.

In the figure 6.24 comparison between experimental and calculated values of n_{Ti} the degree of scatter in n_{Ti} , $2\sigma=1.5$, reflects the measurement difficulties for drying by CITAD. The value of c_{nT} reflects the expected strong dependence of n_{Ti} on q_T . When

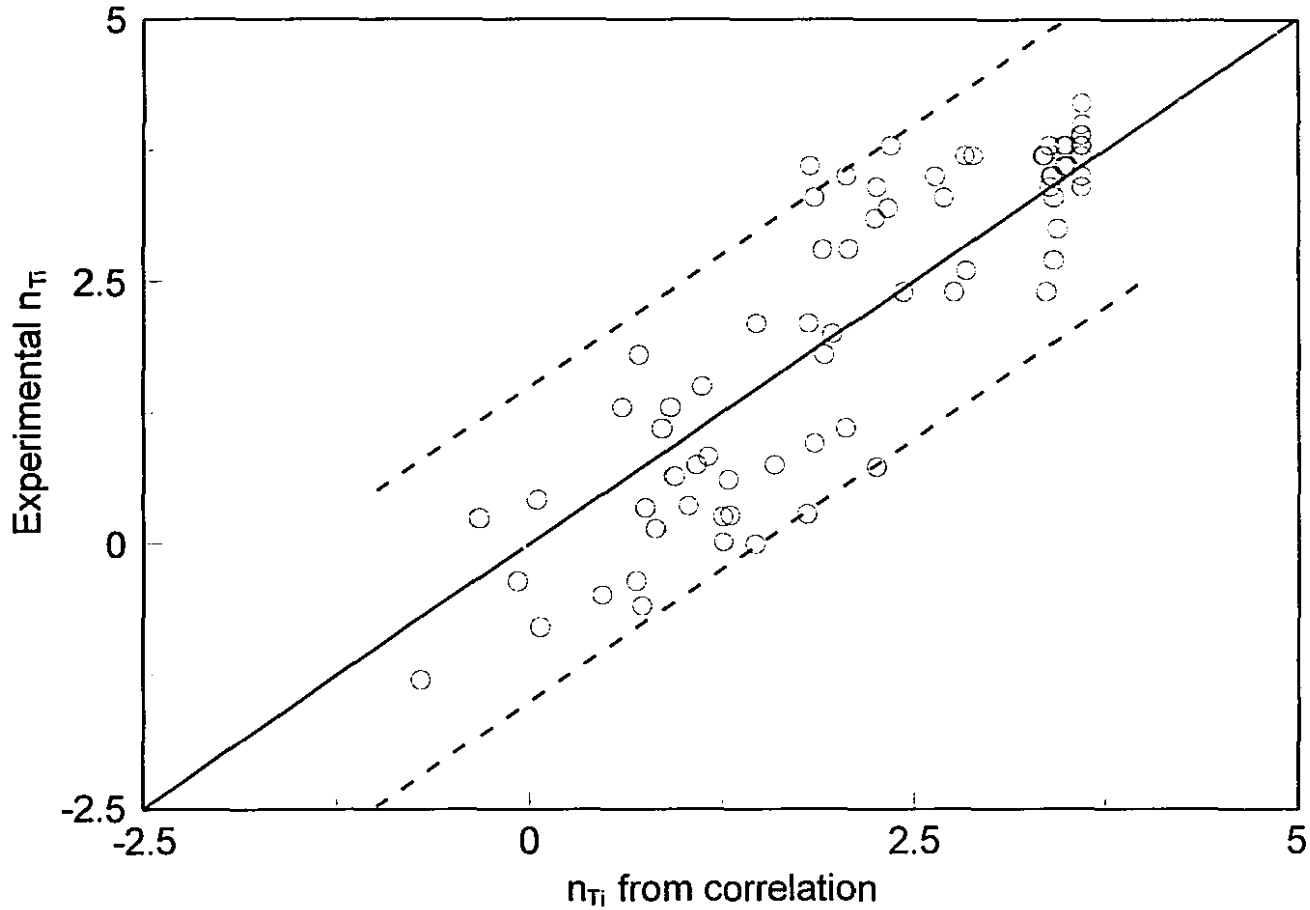

Figure 6.24 Comparison of n_{Ti} from correlation eqn. 6.14 with experimental n_{Ti}

q_T=1 equation 6.14 reduces, as it should, to the value for pure through drying, n_{Ti}=n_i=3.6 . The dependence of n_{Ti} on the ratio (X_o-X_{Ti}) / (X_o-X_i) indicates the paper basis weight effect because with an increase in B at a specific q_T , the analysis in the previous section shows that this ratio would increase, giving an increased n_{Ti} . Thus the R_T - X curvature of the increasing rate period is for thicker paper closer to that of pure through drying, which is consistent with the experimental results.

Table 6.6	Correlation parameters for n_{Ti}		
Parameter	ε	σ	2ε/σ (%)
a_{nT}	3.54	0.80	45
b_{nT}	-0.70	0.13	37
c_{nT}	5.93	0.85	29

6.8.3 Constant through flow water removal rate, R_{Tc}

In the figure 6.25 representation of data for through flow water removal in the constant rate period at four levels of through flow rate G_T , the values at q_T=100% are calculated from the chapter 5 correlation for pure TAD, equation 5.14. For low through flow water removal intensity, i.e. R_{Tas}<15 kg/m^{2}s, the parameters for near saturation in Table 5.5 were used. For all other cases the non-saturation condition parameters were applied.

At a fixed G_T , R_{Tc} was found to be independent of G_I , from the q_T=100% limit where G_I=0, down to the lowest experimental value of q_T , about 7%, where G_I is about 15 times the value of G_T . This independence of R_{Tc} with respect to G_I applies even for the thinnest sheets tested, B=25 g/m^2, for which some effect of G_I on R_{Tc} would not have been surprising. The relationship between the constant water removal rate R_{Tc} for CITAD and the corresponding R_{cT} for pure TAD at the same through flow rate G=G_T , is then simply:

$$R_{Tc}=R_{cT} \qquad (6.15)$$

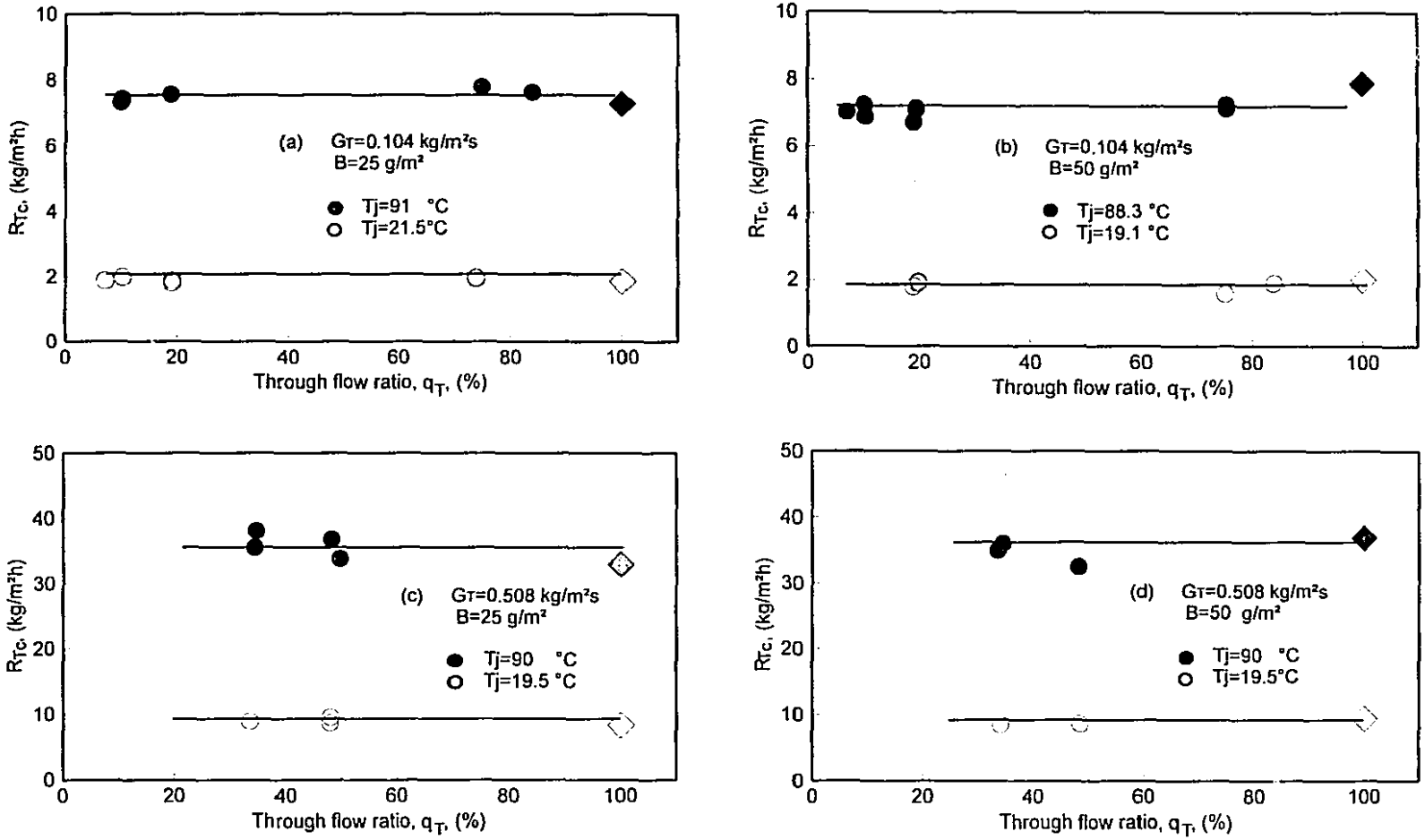

Figure 6.25 Through flow water removal rate in the constant rate period

The independence of R_{Tc} with respect to q_T or G_I derives from the paper temperature T_p being essentially independent of G_I during the constant rate period. In this period the impingement flow brings paper temperature to the wet bulb value T_{wb} , while through flow brings it to the adiabatic saturation temperature T_{as} . Thus paper temperature for drying by CITAD would be between T_{wb} and T_{as} depending on q_T . But for the air-water system T_{wb} and T_{as} are essentially identical. At constant G_T , as on figure 6.25, decreasing q_T means increasing G_I and increasing G, hence the temperature and humidity in the impingement flow boundary layer above the sheet change, thereby changing the temperature and humidity of the through flow entering the sheet. However figure 6.25 shows that such changes in through flow entering the sheet leave R_{Tc} quite unaffected. The conclusion is that such changes in heat and mass transfer potentials of the through flow entering the sheet cause no change in R_{Tc} because R_{Tc} is dominated by conditions within the sheet where paper temperature is invariant to q_T . The finding that R_{Tc} is independent of q_T is consistent with that in chapter 5, section 5.5.5, that impinging jets have no effect on drying rate for pure TAD.

The independence of constant through flow water removal rate from q_T provides experimental validation of one assumption made in the model of Crotogino and Allenger (1979). However, their further assumption that in CITAD the through flow exhaust is saturated at the adiabatic saturation temperature of the inlet air, i.e. $R_{Tc}=R_{Tas}$, is a poor approximation which leads to overpredicting R_{Tc} substantially, as discussed fully for the corresponding R_c - R_{as} relationship for TAD in chapter 5. For the CITAD conditions of figure 6.25(c), the Crotogino and Allenger model would over estimate the through flow constant water removal rate at T_j=90 °C by 30%. Even bigger differences between the Crotogino and Allenger model predictions and the actual drying rates would be expected at higher drying intensity, as analyzed subsequently in section 6.9.

6.8.4 Moisture content at maximum through flow water removal, X_m

After the constant rate period there are opposing effects on the through flow water removal rate, one tending to increase R_T by the paper temperature being driven up by the impingement heat transfer, and other effects tending to bring R_T into the falling rate period as discussed in section 6.5.2. The principal factors of the latter are the increase in resistance for water removal from inside the fibres, the depression of vapor pressure and the increase in heat of desorption of water with paper of low moisture content, and the decrease in heat transfer driving force, ΔT, as paper temperature is driven up by the falling rate period of R_I . Because CITAD performance is affected so strongly by through flow it is only at low values of q_T that the effect of impingement heat transfer is sufficiently strong to produce a secondary increasing rate period and hence a maximum at (X_m , R_{Tm}) in the R_T - X curve. X_m was found to vary from 0.5-1.5 kg/kg. At $X=X_m$ the opposing factors tending to increase and to decrease R_T are exactly in balance. For pure through drying at $G=G_T$, the equation 5.15 value of critical moisture content X_{cT} reflects the point where factors making R_T decrease become dominant. For CITAD, this balance of factors is in addition evidently a function of q_T. Therefore the CITAD parameters X_m , similar to the analysis of X_c and n_I , section 6.7.3, is also correlated relative to the corresponding TAD parameter X_{cT} , plus an additional CITAD factor, in this case q_T , as follows:

$$\frac{X_m}{X_{cT}} = \frac{1}{a_m + (1 - a_m) q_T} \tag{6.16}$$

with $\sigma=0.03$ for the best fit value of $a_m = 1.12$, indicating a good fit.

In the figure 6.26 comparison between X_m by experiment and by correlation, the dashed lines represent the 2σ uncertainty of 0.34 kg/kg of the X_m prediction, comparable with that of X_c for pure through drying. According to equation 6.16 the value of X_m always decreases with a decrease of q_T , which is consistent with the experimental result recorded in figure 6.7(d). Thus the smallest value of X_m/X_{cT} is 0.89 at $q_T=0$. As $q_T \rightarrow 100\%$, $X_m/X_{cT} \rightarrow 1$ as it should.

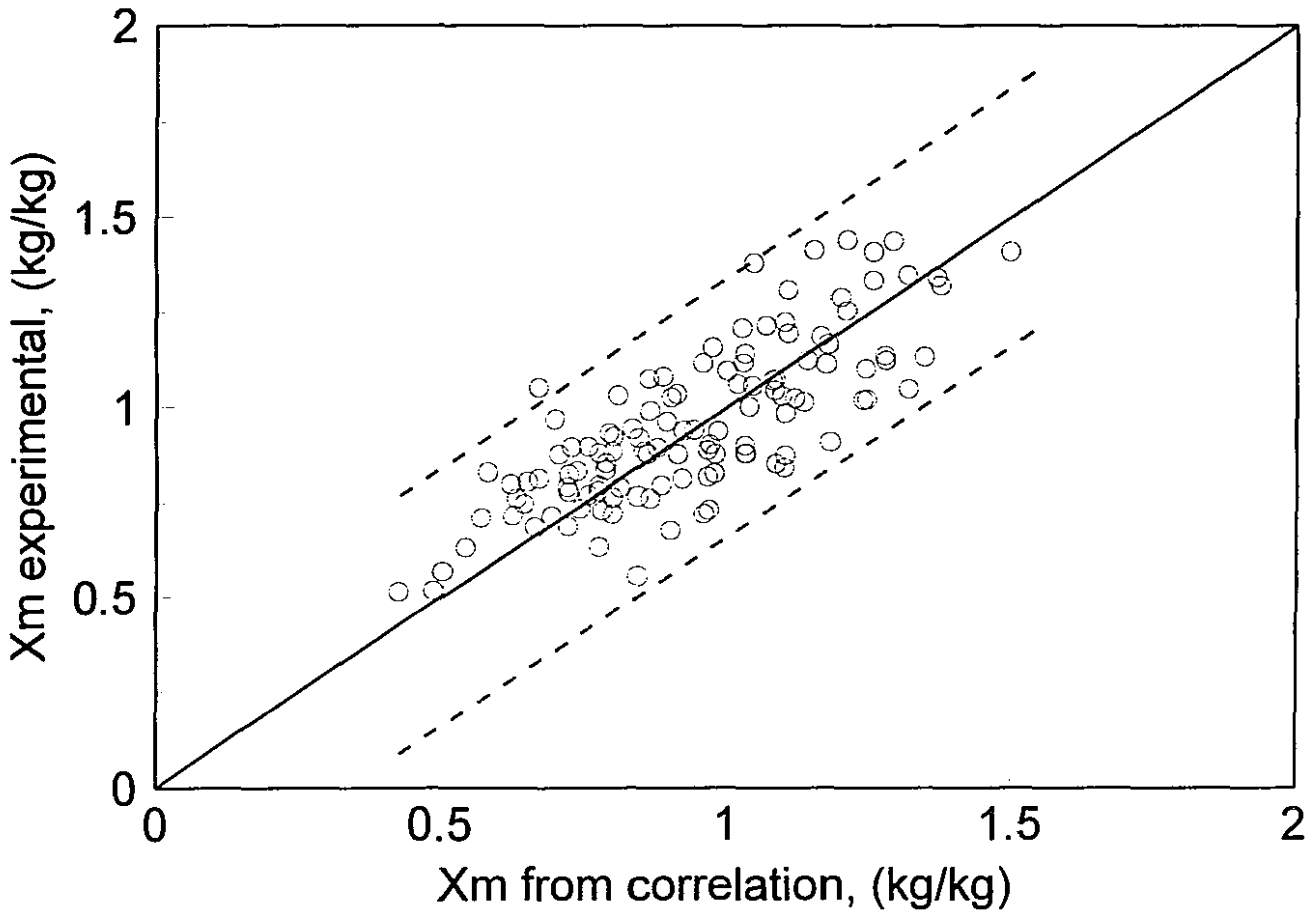

Figure 6.26 Comparison of Xm from correlation eqn. 6.16 with experimental Xm

6.8.5. Maximum through flow water removal rate, R_{Tm}

As analyzed in section 6.5.2 the secondary increase of R_T for some drying process conditions is due to the increase of paper temperature and hence the vapor pressure of water in a sheet having a moisture content sufficiently high that for pure through drying it would be still in the constant rate period.

According to the Clausius-Clapeyron equation:

$$\frac{dP_v}{P_v dT} = \frac{\lambda}{RT^2}$$

where P_v is the vapor pressure at temperature T, λ the latent heat, R the gas law constant. Driven by the increasing impingement surface paper temperature during the R_I falling rate period, paper temperature T_p increases from T_{as} (or from T_{wb}) the steady value during the constant rate period to some higher temperature, T_p' . The vapor pressure of free water in the sheet would change correspondingly:

$$P_v' = P_v^{as}\, e^{\frac{\lambda}{R}\left(\frac{1}{T_{as}} - \frac{1}{T_p'}\right)} \tag{6.17}$$

For a small change of T_p, $\frac{1}{T_{as}} - \frac{1}{T_p} = \frac{T_p - T_{as}}{T_{as} T_p} \approx \frac{T_p - T_{as}}{T_{as}^2}$. If the increase of paper temperature, T_p-T_{as}, is approximated as linear with the decrease of paper moisture content, X_c-X, then:

$$P_v' \approx P_v^{as}\, e^{-\alpha \frac{\lambda}{RT_{as}^2}(X - X_c)} \tag{6.18}$$

with α as a proportionality constant. The through flow exhaust water removal rate would then increase as:

$$R_T \approx R_{Tc} \cdot e^{-\alpha \frac{\lambda}{RT_{as}^2}(X - X_c)} \tag{6.19}$$

Equation 6.19 is valid when free water is present, which is evidently the case until the maximum in through flow water removal rate at the moisture content of $X=X_m$. Equation 6.19 then gives the expression for R_{Tm} as:

$$R_{Tm} = R_{Tc}\, e^{\alpha \frac{\lambda (X_c - X_m)}{RT_{as}^2}} \tag{6.20}$$

The relationship of the proportionality coefficient α, figures 6.1 and 6.9, with the relative importance of two factors, impingement heat transfer to the through flow water removal, R_{Ic}/R_{Tc}, and paper thickness represented by basis weight, may be expressed as:

$$\alpha = a_m \left(\frac{R_{Ic}}{R_{Tc}}\right)^{b_m} B^{c_m} \tag{6.21}$$

Eliminating α from equation 6.20 with equation 6.21, hence:

$$R_{Tm} = R_{Tc}\, e^{a_m \left(\frac{R_{Ic}}{R_{Tc}}\right)^{b_m} B^{c_m} \frac{\lambda (X_c - X_m)}{R T_{as}^2}} \tag{6.22}$$

The best values of a_m, b_m and c_m, designated as ε, are listed in Table 6.7.

Table 6.7 Correlation parameters for R_{Tm}

Parameter	ε	σ for ε	$2\sigma/\varepsilon$ (%)
a_m	0.62	0.28	90
b_m	0.42	0.09	43
c_m	0.51	0.19	75

For this correlation R^2 =0.61 . While R_{Tm} varies greatly, from 1 to 52 kg/m^{2}h, R_{Tm}/R_{Tc} varies only from 1 to 1.82. It is however impressive to have the maximum in the R_T - X curve be up to nearly twice the constant rate period value, R_{Tc} . The conditions giving the highest experimental value, R_{Tm}/R_{Tc} = 1.82, are q_T=4.6%, B=48.3 g/m^2, T_j=88.2 °C at G=1.28 kg/m^{2}s. Figure 6.27 shows the comparison of predicted and experimental R_{Tm} values. The positive values of b_m and c_m are consistent with the experimental observation that the more dominant the role of impingement heat transfer, the greater the increase of R_T with decrease of X, hence the higher the value of R_{Tm}.

With the relations of X_m and R_{Tm} to drying process conditions obtained, a quantitative analysis is now possible. For example, as paper basis weight increases, the increase in R_{Tm}/R_{Tc} can be analyzed as follows. From equations 6.10 and 4.12 for X_c , and 6.16 and 5.15 for X_m , the extent of the secondary increasing rate period would be:

$$X_c - X_m = 0.90 B^{-0.01} R_{Ic}^{0.11}\left[1 + \frac{0.02\, X_o}{f(H/d)}\right] - \frac{0.67 X_o^{0.58} R_{Tas}^{0.15} B^{-0.19} G_T^{-0.17}}{1.12 - 0.12\, q_T} \tag{6.23}$$

For the flow conditions of figure 6.8 and X_o=3 kg/kg, Table 6.8 lists the values of α and X_c - X_m corresponding to each R_{Tm}/R_{Tc} for three levels of basis weight. Table 6.8 clearly

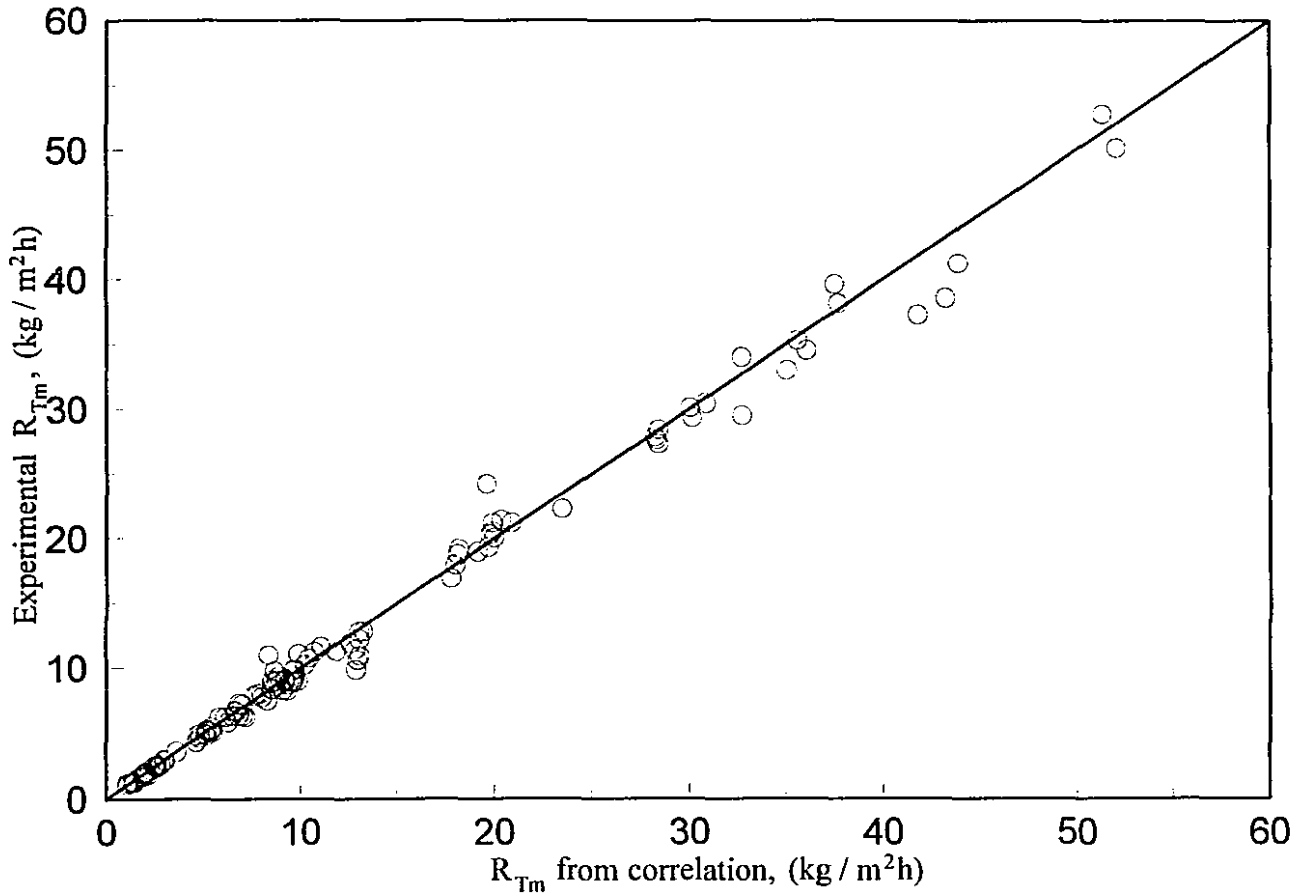

Figure 6.27 Comparison of R_{Tm} from correlation eqn. 6.22 with experimental R_{Tm}

shows that increasing paper thickness causes the extent of the secondary increasing rate period to increase, leading thereby to the increase in the peak value R_{Tm}/R_{Tc} of the secondary increasing rate period. For tissue grade paper, R_{Tm}/R_{Tc} is marginal while for printing grades of paper this effect is substantial. At lower through flow ratio, R_{Tm}/R_{Tc} could be higher yet, with 1.82 measured for B=48 g/m^2 paper at q_T of 4.6%.

Table 6.8 Effect of basis weight on R_{Tm}/R_{Tc}			
B, g/m^2	25	50	83
α	3.91	5.56	7.21
X_c-X_m, kg/kg	0.26	0.60	0.65
R_{Tm}/R_{Tc}	1.06	1.21	1.31

The effect of T_j on R_{Tm}/R_{Tc} can also be analyzed from equation 6.23. As R_{Ic} and R_{Tas} are both directly proportional to ΔT, X_c-X_m may be taken as proportional to $\Delta T^{0.13}$. For a change of air temperature from 22 ° to 90 °C, the corresponding increase in T_{as}, from 280 to 303 K, would be less than 8%. A change in $\Delta T=T_j-T_{as}$ from about 15 to 60 °C would result in a 20% increase in X_c-X_m. Hence a net increase in R_{Tm}/R_{Tc} with increase in T_j would be expected, as documented in figure 6.7 where R_{Tm} is seen strongly for $T_j \approx 90$ °C but not for $T_j \approx 22$ °C.

For industrial operation, where the local nonuniformity of the impingement flow is not a factor, the relation for X_c is equation 4.13 instead of equation 4.12, for which the extent of the secondary increasing rate period is obtained as:

$$X_c - X_m = 0.90B^{-0.01}R_{Ic}^{0.11} - \frac{0.67X_o^{0.58}R_{Tas}^{0.15}B^{-0.19}G_T^{-0.17}}{1.12 - 0.12\,q_T} \qquad (6.24)$$

which clearly indicates a dependence of X_c-X_m, and hence of R_{Tm}/R_{Tc}, on the paper initial moisture content X_o. Such a dependence could not easily be observed from the water removal rate curves. When X_o increases, X_c-X_m decreases due to an increase in X_m, and R_{Tm}/R_{Tc} then decreases.

There must exist a limiting value of paper initial moisture content, denoted as X_o^{mc}, where for any specific drying process conditions X_c-X_m=0 and $R_{Tm} = R_{Tc}$. There will be a secondary increasing rate period for $X_o<X_o^{mc}$ and no such period for $X_o>X_o^{mc}$.

For the present study this value of X_o can be calculated by trial and error from equation 6.23 or, for industrial operation, from equation 6.24,

$$\left(X_o^{mc}\right)^{0.58} = \frac{1.34 R_{Ic}^{0.11} B^{0.18} G_T^{0.17}}{R_{Tas}^{0.15}} \left(1.12 - 0.12\, q_T\right) \qquad (6.25)$$

Thus the value of X_o^{mc} for CITAD is predicted to increase with paper basis weight due to the combined result of the increase in X_c and decrease in X_m, while X_o^{mc} would decrease with an increase in q_T. Recalling that $R_{Tas} \propto G_T \Delta T$ and that $R_{Ic} \propto \Delta T$, the effects of ΔT and G_T on X_o^{mc} would be marginal.

6.8.6 Through flow water removal after the constant rate period

With the completion of analysis of X_c, R_{Tc}, X_m and R_{Tm}, through flow water removal rate R_T over the entire region after the constant rate period can now be predicted at any moisture content using equation 6.7. Before the present study the region after $X=X_c$ was naturally treated as an ordinary falling rate period as for through drying in the models of both Randall (1984) and Crotogino and Allenger (1979). For the falling rate period Randall (1984) used equation 2.7 to correlate the R_T - X relationship while Crotogino and Allenger considered factors leading to the decrease of R_T in this period, which they attributed to water vapor pressure depression and to increase of heat of desorption for water from paper of low moisture content. It is now seen that following the constant rate period the R_T - X curve may consist of two periods, the secondary increasing rate period to a maximum R_{Tm} at X_m, then the falling rate period, or else simply a conventional falling rate period if the impingement water removal process is not sufficiently important, as analyzed in section 6.5.2 and 6.8.5. Equation 6.7 has the merit of using only two points over the entire post-constant rate region, i.e. (X_c, R_{Tc}) and (X_m, R_{Tm}) to predict the complete R_T - X curve. At small values of q_T, where the CITAD process would more likely be employed in industry, the value of R_{Tm}/R_{Tc} could be impressive, especially for drying heavier paper. The reliability of equation 6.7 will be seen in the CITAD drying rate and drying time predictions of section 6.10.

6.9 Constant drying rate for CITAD, R_c

The constant drying rate for CITAD at a particular value of total inlet mass flow rate G is the sum of the constant rate values for impingement water removal and through flow water removal, $R_c=R_{Ic} + R_{Tc}$. With completion of the R_{Ic} and R_{Tc} analysis in sections 6.7.1 and 6.8.3, the complete picture for CITAD drying rate can now be examined. In the figure 6.28 comparison the values at $q_T=0$, pure impingement drying, and at $q_T=100\%$, pure through drying, were calculated from equations 4.11 and 5.14, respectively. As there is no industrial relevance for drying in ambient air the discussion is limited to the case of 90 °C air. Because of the higher rates for pure through drying, R_c increases with q_T as the through flow contribution increases, as seen in section 6.5.3. When the pure through drying and the pure impingement drying rates at a total mass flow rate of drying air G are represented as R'_{cT} and R'_{cI} , from equation 5.14, $R_{cT} \propto (G_T)^{0.85}$, hence $R_{cT}= R'_{cT}\, q_T^{0.85}$. Together with equations 6.9 and 6.15, one obtains:

$$R_c = R'_{cI}\left(1 - q_T\right)^{5/3} + R'_{cT}\, q_T^{0.85} \qquad (6.26)$$

Excellent agreement between the predictions of equation 6.26 and the experimental measurements is recorded in figure 6.28.

Shown in figure 6.28 also are the predictions of the Crotogino and Allenger (1979) model at the same drying conditions. As the trend of the model by Randall (1984) for the CITAD process is quite inconsistent with the present experimental measurements, as analyzed in section 6.7.1, it is not dealt with further here. Although the assumption of the Crotogino and Allenger model that the increase of R_c with q_T is effectively linear is seen on figure 6.28 to be not far from the experimental findings, their model however over estimates the R_c measured here for the CITAD process due to the over prediction of R_{Ic} and R_{Tc} , as analyzed in sections 6.7.1 and 6.8.3. For example, at G=1.46 kg/m^{2}s, T_j=90°C, and B=50 g/m^2, the Crotogino and Allenger model over predicts the constant drying rate of CITAD by 20, 31 and 32% at q_T respectively of 25, 50 and 75%. With 25 g/m^2 paper for the same conditions and same levels of q_T , the percentages by which their model over predicts are, respectively, 33, 46 and 49%.

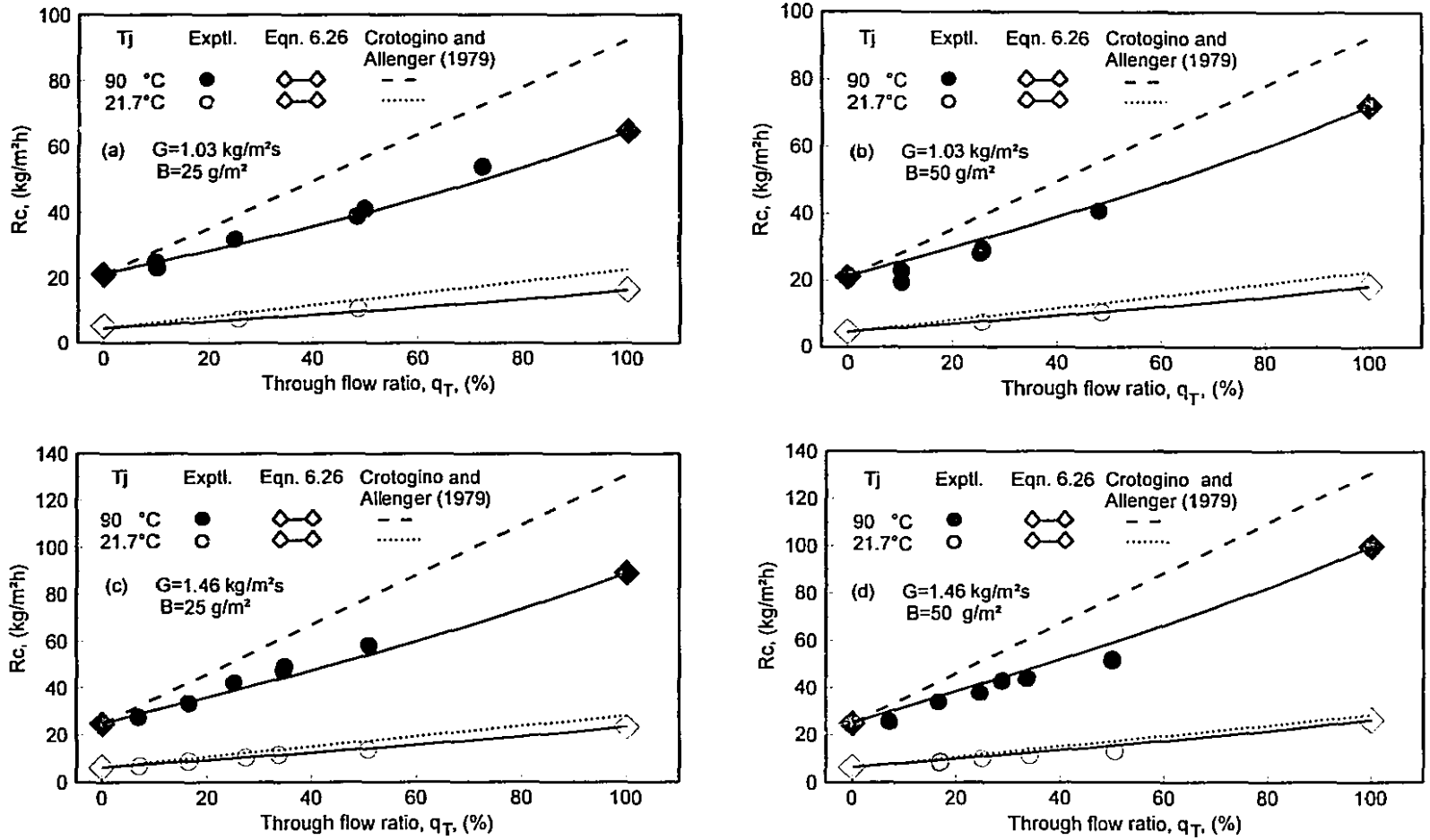

Figure 6.28 Effect of through flow ratio on constant drying rate of CITAD: Measurements and models

The only other measurements reported for a CITAD dryer are those of Burgess et al. (1972a). Although slot nozzles were used in their study, the findings with an array of round nozzles in the present study can still be applied as the through flow water removal is independent of the impinging jets. For impingement water removal, the correlation by Martin (1977) can be used to calculate R'_{cI} for slot nozzles. The change of impingement water removal rate with through flow ratio, q_T, should not be significantly different between arrays of round or slot nozzles. Martin's correlation for impingement heat transfer from slot nozzles, with $f_o = \frac{1}{\sqrt{60+2(H/w-4)^2}}$, is:

$$Nu_I = \frac{2}{3} f_o^{3/4} \left(\frac{2\,Re}{f/f_o + f_o/f} \right)^{2/3} Pr^{0.42} \qquad (6.27)$$

The geometric parameters for the Burgess et al. in pilot plant trial and the valid region for equation 6.27 are listed in Table 6.9.

Table 6.9 Geometric parameters for Martin's correlation and for Burgess et al.	
Burgess et al. (1972a)	Martin's correlation, eqn. 6.27
Nozzle opening, w=0.51 mm	
H/w= 16.1	1 <H/w< 80
35 <Re< 3860	1500 <Re< 40,000
Open area ratio, f=0.0134	0.008 <f< 2.5f_0(H/w)

The absolute humidity was assumed to be 0.03 kg water/kg air in the inlet air, as did Crotogino and Allenger, corresponding to a dew point of 32 °C. Effect of water vapor flux on the heat transfer coefficient was accounted as:

$$Nu_I = \frac{R'_{cI}\lambda w Bi}{1800\Delta T\, k \ln(1+Bi)} \text{ with Biot number } Bi = \frac{C_p \Delta T}{\lambda}.$$

Air physical properties were determined at the film temperature, i.e. $(T_j+T_{as})/2$, while latent heat was evaluated at T_{as}.

Burgess et al. (1972a) provide drying rates from their pilot plant only as average values over a considerable range of paper moisture content. Most of their data is for R averaged from X=1.9 down to X=0.04 kg/kg, which is not useful because such average values are dominated by the low value of R for nearly dry paper at the end of the falling

rate period of drying. The most useful data that they provided are four R-X curves obtained with 48.5 g/m^2 paper, and 96.5 m/s jet velocity. Based on equation 6.10, the critical moisture content for operation Burgess et al. is estimated to be around 1.2 kg/kg. Since the initial region would have the effect of increasing rate period, the mean values of drying rate from X=1.4 down to X=1.2 kg/kg can then be taken for comparison. Table 6.10 lists these four values of average drying rate $\bar{R}$ from Burgess et al. and R_c values predicted from the correlation of the present study. Their brief mill trial (Burgess et al. 1972b) reported the averaged drying rates for paper entering the dryer at 0.43 - 0.61 and exiting around 0.1 kg/kg, therefore cannot be used as the R-X relation is unknown.

Table 6.10 Comparison of R_c from Burgess et al. with R_c predicted from present study

Case	T_j (°C)	T_{as} (°C)	G (kg/m^{2}s)	G_T (kg/m^{2}s)	q_T (%)	$\bar{R}$ Burgess et al. (kg/m^{2}h)	R_c Predicted (kg/m^{2}h)
1	149	47.5	1.07	0.26	24	77	64
2	307	56	0.78	0.22	28	148	132
3	307	56	0.78	0.32	41	180	142
4	427	65	0.65	0.22	34	186	175

The values of Burgess et al. are only about 17% greater than the values of R_c obtained from the present model despite the great differences in experimental techniques between these studies. The biggest difference (27%) is for case 3, where their measured drying rate was also stated to have the highest uncertainty, 20 kg/m^{2}h, compared with 10 kg/m^{2}h accuracy claimed for case 1. The differences in nozzle geometry (round vs. slot) and in the geometry of the impingement exhaust ports have been noted. Also, equation 6.26 is derived from experiments with T_j of 22 - 90 °C with only the air convective heat transfer while the work of Burgess et al. was in the industrial range of T_j from 150° to over 400°C with the measured drying rate including contributions from surface conduction and radiation as reviewed in chapter 2 section 2.4. Thus it is interesting to have obtained the first drying rate data by the CITAD process that compares excellently with results of the pioneering investigation of Burgess et al.

6.10 Prediction of drying time and drying rate for CITAD

The various correlations for drying by pure impingement, by pure through flow and by CITAD, may now be integrated as follows into a comprehensive model for the prediction of drying time and drying rate for the CITAD process.

Specified variables:

total inlet air flow rate	G, kg/m^{2}s	
inlet air temperature	T_j, °C	
ratio, through flow : total flow	q_T, fraction	
paper basis weight	B, g/m^2	
initial moisture content	X_o, kg fibre/kg water	

Calculated variables:

impingement exhaust rate	G_I, kg/m^{2}s	($G(1-q_T)$)
through flow exhaust rate	G_T, kg/m^{2}s	(Gq_T)
impingement water removal constant rate	R_{Ic}, kg/m^{2}h	(eqn. 4.11 and 6.9)
through water removal constant rate	R_{Tc}, kg/m^{2}h	(eqn. 5.14 and 6.15)
critical moisture content	X_c, kg/kg	(eqn. 4.12 and 6.10)
exponent for R_I-X relationship in the falling rate period	n_I	(eqn. 4.14 and 6.11)
moisture content at the end of increasing rate period	X_{Ti}, kg/kg	(eqn. 5.11 and 6.13)
exponent for R_T-X relationship in increasing rate period	n_{Ti}	(eqn. 6.14)
maximum through flow water removal rate	R_{Tm}, kg/m^{2}h	(eqn. 6.21 and 6.22)
moisture content at R_{Tm}	X_m, kg/kg	(eqn. 5.15 and 6.16)
parameter for R_T-X relationship in region after constant rate period	C	(eqn. 6.5)

When $X_c<X_{Ti}$, i.e. when there is a period of constant rate drying, the complete drying rate and drying time curve can be predicted by using the knowledge obtained in this thesis as:

for	$X_o \geq X \geq X_{Ti}$	$R=R_{Ic} + R_T(X)$	(eqn. 6.2)
for	$X_{Ti} > X \geq X_c$	$R=R_{Ic} + R_{Tc}$	
for	$X_c > X$	$R=R_I(X) + R_T(X)$	(eqn. 6.1 and 6.7)

The good comparison obtained between experimental values of R and t and those predicted by the comprehensive model is shown on figure 6.29 and 6.30 for a range of values of drying air rate G, through flow ratio q_T , and paper basis weight B. The specified and calculated variables used in prediction of drying time and drying rate for

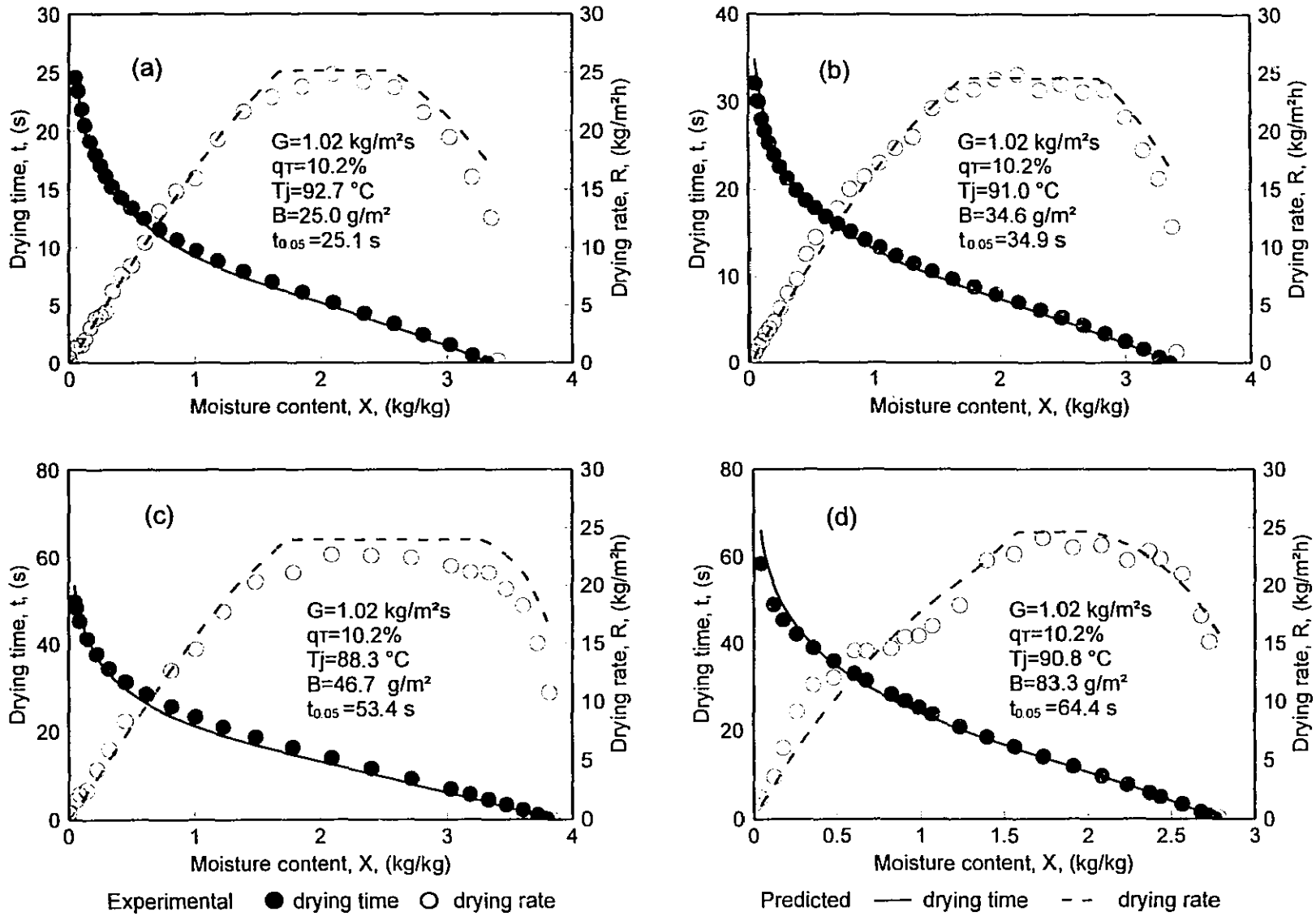

Figure 6.29 Comparison of experimental and predicted drying rate & drying time for CITAD: q_T=10.2% & G=1.02 kg/m²s

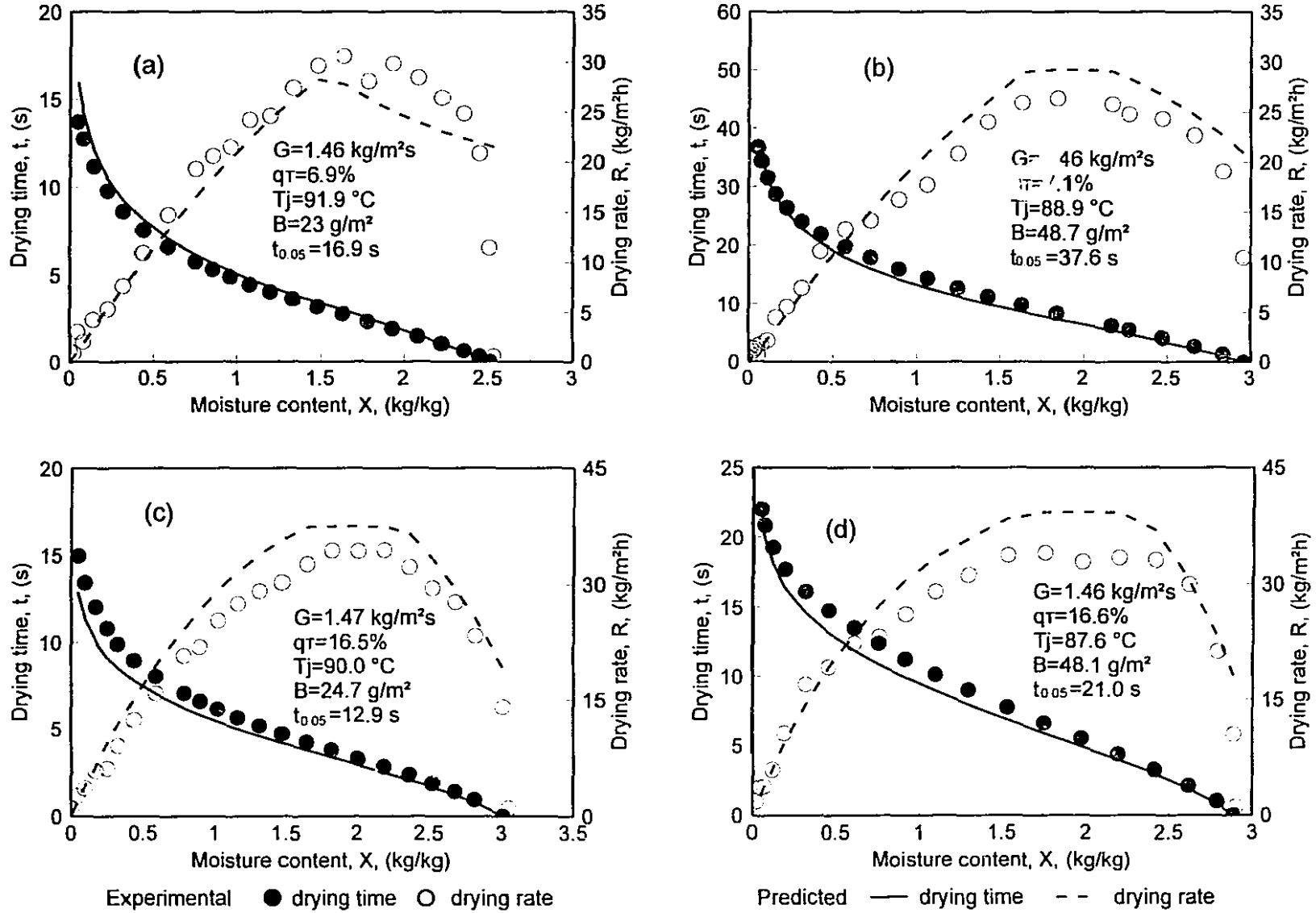

Figure 6.30 Comparison of experimental and predicted drying rate & drying time for CITAD: G=1.46 kg/m²s

conditions of figures 6.29 and 6.30 are listed in Appendix C. The predicted drying time at a final paper moisture content of 0.05 kg/kg is listed for each condition as $t_{0.05}$. The experimental drying time data is shown down to the same moisture content of 0.05 kg/kg. The above calculations and comparisons apply from the start of the constant rate period for impingement water removal. As the omitted transient period for impingement water removal rate is so short, figure 6.2 and 6.3, in the range of about 0.5 - 1 s drying time according to experimental measurements for conditions shown on figures 6.29 and 6.30, the effect on predicted drying times, about 13 - 65 s, is insignificant.

For industrial drying by CITAD the pressure drop across the sheet would be constant instead of the constant through flow rate G_T of the present investigation. For drying under constant pressure drop, through flow rate and hence through flow ratio q_T as well as the impingement exhaust flow rate G_I would vary with the rapidly changing paper moisture content and permeability. As discussed in chapter 5, section 5.6, the dynamic value of $G_T(X)$ can be calculated based on the ΔP-G-X relationship reported by Polat O. et al. (1989). Once G_T is obtained the correlations obtained in the present research may be applied for CITAD drying time and drying rate prediction.

The successful demonstration of the predictive model for drying rate and drying time in the CITAD process completes the objectives of this research. The detailed analysis of drying kinetics provides guidance concerning the interaction between impingement and through flow for future investigation of the CITAD process at higher intensity drying conditions. It is the author's hope that the addition of the present measurements to those of the pioneering study of this process in the 1960's may help the development of some type of commercial dryer based on the CITAD concept.

6.11 Summary

1) Two grades of paper, 25 and 50 g/m^2 basis weight, were dried by the CITAD process, with air of two levels of temperature, 22 °C and 90 °C. Experiments were made keeping the impingement exhaust mass flow rate G_I constant to test the effect of through flow; keeping the through flow exhaust mass flow rate G_T constant to study the impingement effect; finally keeping the total inlet air mass flow rate G constant and varying the ratio of through mass flow rate to the total inlet mass flow rate, $q_T=G_T/G$, from pure impingement to pure through drying, in order to complete the investigation of the interaction between the two components. Water removal rate curves for each exhaust flow were obtained. In total 144 experiments were conducted, including six tests of the basis weight effect.

2) The complete impingement water removal rate curve was represented quantitatively by three elements: constant impingement water removal rate R_{Ic}; critical moisture content X_c; and a power law R_I - X relationship over the falling rate period. Values of R_{Ic}, X_c and the power law exponent n_I were obtained statistically from the R_I-X data.

3) The impingement water removal rate over the entire R_I - X curve was found to be strongly reduced by through flow. Constant water removal rate R_{Ic} decreases with q_T as:

$$R_{Ic} = R_{ci} (1-q_T)$$

This decrease in R_{Ic} results from humidity present in the impingement boundary layer being incorporated into the through flow. This effect of through flow also changes the impingement exhaust air temperature. Thus although the entire CITAD process is adiabatic, each of the component processes, impingement water removal and through flow water removal, are individually nonadiabatic.

4) The same value of critical moisture content X_c applies for impingement water removal and for total drying rate, and correlates with drying process conditions as:

$$X_c = 1.96\, X_{cI}\, B^{-0.13}$$

In pure impingement drying $X_{cT} \propto B^{0.12}$. Finding an exponent with CITAD which cancels the 0.12 exponent for TAD reflects a decrease in the z-direction sheet moisture content gradient due to through flow water removal. X_c for CITAD is higher than for pure impingement drying because of through flow water removal and the increase in impingement heat transfer coefficient and drying intensity. For all conditions tested, X_c for CITAD averaged 20% higher than in pure impingment drying.

5) The exponent n_I for the power law R_I - X relationship over the falling rate period of impingement water removal was related as:

$$\frac{n_I}{n} = \left(\frac{X_c}{X_{cI}}\right)\left(1 + 0.069B^{0.87} q_T^{0.26}\right)$$

where n is the exponent for pure impingement drying.

In CITAD the shape of the impingement water removal rate curve is convex downwards instead of the typical concave downwards form for pure impingement drying. This difference is the consequence of the loss to the through flow air of impingement generated humidity, noted above, and the highly nonlinear diffusivity of moisture in relatively dry paper near the impingement surface. Hence n_I varies from 1 - 2.6 in CITAD compared with n<1 for most of the pure impingement drying.

6) For through flow water removal rate over the increasing rate period an exponential R_T - X relationship, adapted from pure through drying, represents the data well. The constant through flow water removal rate R_{Tc}, moisture content at the end of the increasing rate period X_{Ti}, and the exponent n_{Ti} were determined using procedures adapted form chapter 5.

7) The extent of the increasing rate period for through flow water removal is:

$$X_o - X_{Ti} = \left(X_o - X_i\right)\left(1 + 0.043B^{0.92}\frac{R_{Ic}}{R_{Tc}}\right)$$

The dependence on B is expected because the degree of effectiveness of water removed by impingement flow on development of transport area within the sheet depends on paper

thickness, being very effective for thin, 25 g/m^2 paper but only slightly so for 50 g/m^2 paper.

8) The n_{Ti} parameter in the R_T-X relationship during the increasing rate period is related to the through flow ratio q_T, and the increase in the extent of the increasing rate period relative to pure through drying as:

$$n_{Ti} = 3.6\left[1 - 3.54\left(\frac{X_o - X_{Ti}}{X_o - X_i}\right)^{-0.70}\left(1 - q_T\right)^{5.93}\right]$$

Water removal by the impingement exhaust reduces the curvature of the R_T - X relation in the increasing rate period, hence decreases n_{Ti} from its limiting value of 3.6 at q_T=1, pure through drying.

9) The constant water removal rate from through flow exhaust, R_{Tc}, is not significantly affected by the amount of impingement flow above the sheet, hence its value is the same as for pure through drying R_{cT}, i.e.

$$R_{Tc}=R_{cT}$$

This equality derives from the stability of paper temperature relative to q_T during the constant rate period, and is expected from the finding in chapter 5 of no difference in pure through drying with and without impinging jets.

10) A unique feature, a secondary increasing rate period, was found for through flow water removal rate after the critical moisture content X_c. For conditions making impingement a dominant effect R_T can increase and reach an impressive maximum value R_{Tm}, up to nearly double the R_{Tc} value. R_{Tm} increases with increasing B and decreasing q_T. For $X<X_c$ the falling rate period of impingement water removal drives up the paper temperature while there is still free water present within the sheet for the through flow water removal process, thus producing for CITAD this new drying rate period.

11) An empirical equation represents the R_T - X data for $X<X_c$ over both the secondary increasing rate period, the maximum at (X_m, R_{Tm}) and the falling rate period. As $q_T \rightarrow 1$, $X_m \rightarrow X_c$ and this relation reduces to the power law R-X relationship for pure through drying over the falling rate period:

$$R_T = R_{Tm}\left\{1-\left[\left(\frac{e^{-c\frac{X}{X_c}}-e^{-c\frac{X_m}{X_c}}}{1-e^{-c\frac{X_m}{X_c}}}\right)^2\right]^{0.85}\right\}$$

12) The moisture content X_m at R_{Tm} relates to the through flow ratio q_T as:

$$X_m = \frac{X_{cT}}{1.12-0.12\,q_T}$$

with X_{cT} the value for pure through drying. X_m is the moisture content where the factors making R_T increase just balance those causing the onset of the falling rate period.

13) Maximum through flow water removal rate R_{Tm} relates to process conditions as:

$$R_{Tm} = R_{Tc}\, e^{0.62\, B^{0.51}\left(\frac{R_{Ic}}{R_{Tc}}\right)^{0.42}\frac{\lambda\,(X_c-X_m)}{RT_{as}^2}}$$

As increase in R_{Ic}/R_{Tc} makes the impingement effect more important while an increase in basis weight extends the secondary increasing rate period, hence increases R_{Tm}.

14) Constant drying rate for CITAD, $R_c=R_{Ic}+R_{Tc}$, at a fixed value of G increases with q_T due to through drying rates being higher than for impingement drying, and relates with drying process conditions as:

$$R_c = R_{cI}'(1-q_T)^{5/3} + R_{Tc}'\, q_T^{0.85}$$

where R_{cI}' and R_{Tc}' are the constant drying rate at the same G for pure impingement and pure through drying. This relation satisfactorily predicts the pilot plant results of Burgess et al. (1972a), the only such data available. Of the two models which have been reported for drying paper by CITAD, that of Randall (1984) should be rejected as quite inconsistent with the measured effect of through flow on impingement water removal rates. The model of Crotogino and Allenger (1979) shows the correct trends but deviates quantitatively from the present measurements in over predicting drying rate.

15) Drying rate and drying time can be predicted with the experimentally based comprehensive model obtained for drying by the CITAD technique. Very good comparisons were obtained for eight widely different drying conditions tested for drying paper by the CITAD process.

Chapter 7 Conclusion

7.1 Contributions to knowledge

Impingement drying of paper

1) **Determination of complete drying rate curves:** Precisely defined drying rate curves were determined by high speed, on line measurements for the impingement drying of 83 kraft handsheets with three sets of nozzle arrays that cover a range of nozzle to paper spacing from 5 to 8.5 nozzle diameters, nozzle open area ratios 1.4 - 3.1%, jet Reynolds number 450 - 11100, with nozzle exit air temperature 20 - 90 °C, and paper basis weight 25 g/m^2 - 50 g/m^2.

2) **Quantitative representation of drying rate curves:** Complete curves were quantified satisfactorily with three parameters: constant drying rate R_c, critical moisture content X_c , and falling rate period power law exponent n . The Churchill and Usagi asymptotic treatment was shown to be inappropriate.

3) **Quantitative parameters:** The results for constant drying rate agree to ±15% with predictions from correlation by Martin (1977) of heat transfer rates for multiple round jets. The effect of drying process conditions on the other two parameters is

$$X_c = 0.46\, R_c^{0.11}\, B^{0.12}\left[1+\frac{0.02\, X_o}{f(H/d)}\right]$$

$$n = 1.90\, B^{-0.26}\left[1+\frac{0.042}{f(H/d)}\right]$$

4) **Prediction of drying time and drying rate:** Drying time was predicted by combination of the correlations for R_c , X_c and n. Industrial practice of impingement drying of paper, where local flow nonuniformity does not exist because of the sheet speed, corresponds to the limiting case of the present study with the local flow nonuniformity factor, 1/(f H/d), going to zero, for which

$$X_c = 0.46\, R_c^{0.11}\, B^{0.12}$$

$$n = 1.90\, B^{-0.26}$$

Drying rate and drying time were thereby predicted for industrial impingement drying of paper. With the typical moisture content after the wet press of a mill producing printing papers being about 1.5 kg/kg, the results indicate no constant rate drying period, with performance for air impingement drying of paper controlled by the falling rate period.

Through drying of paper

5) Determination of complete drying rate curves: Complete drying rate curves were determined for through drying 89 kraft handsheets with impinging jets at mass flow rates 0.125 - 1.45 kg/m^{2}s, air temperature 22 - 90 °C, with basis weights 25 g/m^2 (tissue); 37 g/m^2 (toweling) and 50 g/m^2 (printing paper). For determining the effect of the inlet flow condition, 8 experiments were carried out without impinging jets. Two drying rate periods, those of increasing rate and falling rate, occur for all cases with the existence of a constant drying rate period depending on drying conditions.

6) Quantitative representation of drying rate curves: The drying rate - moisture content relationship in the increasing rate period was derived from a packed bed heat balance analysis as:

$$\frac{R}{R_c} = \frac{1 - e^{-n_i\left(\frac{X - X_i}{X_o - X_i}\right)}}{1 - e^{-n_i}}$$ with the exponent $n_i = ha_pL/GC_p$.

This relation together with a power law, $R/R_c = 1 - (1 - X/X_c)^{nf}$ for the falling rate period provide the basis for statistical treatment of the entire data set. The end of the increasing rate period X_i, and the critical moisture content X_c were taken as the values at $R = 0.98R_c$. Five parameters, R_c, X_i, X_c, n_i and n_f provide a quantitative representation of the complete drying rate curves.

7) Quantitative parameters: The effect of drying process conditions on extent of increasing rate period was determined as:

$$X_o - X_i = 0.30G^{0.41}\Delta T^{0.78}B^{-0.73}$$

Constant drying rate data was segregated between conditions for which the air exited the sheet either near-saturated or distinctly unsaturated, as has not previously been done. For near-saturated exhausts, drying rate was confirmed to be directly proportional to flow rate and ΔT, independent of paper basis weight. When controlled by a dynamic balance between various rate phenomena, R_c relates to drying process conditions as:

$$R_c = 0.87G^{0.85}\Delta T^{0.91}B^{0.19}$$

Lumping of results for near-saturated and distinctly unsaturated exhausts, as done in all earlier work, does not provide a valid basis of analysis.

The effect of drying process conditions on critical moisture content is:

$$X_c = 0.67X_o^{0.58}R_{as}^{0.15}B^{-0.19}G^{-0.17}$$

The correlations for X_i, R_c and X_c were related to previous work and to the range of conditions used here.

8) **Effect of impinging jets as air inlet flow:** No difference was found in drying rate for through drying with and without impinging jets. As the increasing rate period and the onset and development of the falling rate period are all governed by factors related to the paper, the air approach flow structure has no effect. During the constant rate period, the advantage of increased water removal by the turbulent impinging jets before the air enters the sheet is lost because of the corresponding drop in heat and mass transfer potential of the air entering the sheet.

9) **Universal form of normalized drying rate curve:** As the increasing rate and falling rate periods were found to be represented satisfactorily for all conditions with a universal value of the respective exponents, n_i=3.6 and n_f=1.7, one normalized curve represents all paper through drying rates as:

$$\frac{R}{R_c} = \frac{1-e^{-3.6\left(\frac{X_o-X}{X_o-X_i}\right)}}{1-e^{-3.6}} \qquad \text{for } X_o \geq X \geq X_i$$

$$\frac{R}{R_c} = 1 \qquad \text{for } X_i \geq X \geq X_c$$

$$\frac{R}{R_c} = 1 - \left(1 - \frac{X}{X_c}\right)^{1.7} \qquad \text{for } X_c \geq X$$

Gummel (1977) and Randall (1984) reported similar behavior during falling rate periods of the through drying paper, but the universal form for the complete drying rate curve, including for the increasing drying rate period, is a contribution of the present study.

10) Prediction of drying time and drying rate: Drying time was predicted by a comprehensive model incorporating the correlations for R_c, X_i and X_c in connection with the universal drying rate curve.

Combined impingement and through air drying of paper

11) Determination of complete drying rate curves: Kraft handsheets of basis weight 25 and 50 g/m^2 were dried at air temperatures of 22 and 90 °C by the CITAD process. Water removal rate curves from the impingement and through flow exhausts were obtained with through flow ratio varying from 0 to 100%. In total 144 sheets were dried.

12) Fundamental characteristics: In the combined process part of the humidity in the through flow exhaust was originally humidity in the impingement boundary layer above the paper surface, having been evaporated by impingement heat transfer but not withdrawn in the impingement exhaust. Thus although the combined process is adiabatic, the two components are individually nonadiabatic, thus eliminating the simplifications appropriate for analysis of adiabatic processes. With this transfer of impingement generated humidity from the impingement exhaust to the through flow, and because the humidity of air entering the sheet cannot be determined, the total drying rate cannot be separated into an impingement and a through flow drying rate, but only into an impingement and through flow water removal rate.

A) Impingement water removal rate

13) Quantitative representation: Three parameters determined by statistical analysis, the constant impingement water removal rate R_{Ic} , critical moisture content X_c and power law exponent n_I for the falling rate period represent the complete impingement water removal rate curves.

14) Quantitative parameters: The effect of drying process conditions is:

$$R_{Ic} = R_{cI}\,(1-q_T)$$

$$X_c = 1.96\,X_{cI}\,B^{-0.13}$$

$$\frac{n_1}{n} = \left(\frac{X_c}{X_{cI}}\right)\left(1 + 0.069B^{0.87}q_T^{0.26}\right)$$

Impingement water removal rate is very sensitively reduced by through flow. This trend of R_I decrease is consistent with measured impingement exhaust air temperature increase and occurs because the through flow removes part of the impingement boundary layer humidity which, without through flow, would leave in the impingement exhaust.

The critical moisture content X_c for impingement water removal and for the overall drying rate curve is the same. While X_c for pure impingement drying increases with basis weight, that effect disappears in CITAD because through flow decreases the z-direction moisture content gradient.

The shape of the impingement water removal rate curve is convex downwards instead of the typical concave downwards form for pure impingement drying, again because the through flow air carries humidity in the impingement boundary layer into the through flow as well as the low diffusivity of moisture through low moisture content paper near the impingement surface of the sheet.

B) Through flow water removal rate

15) Unique feature in complete rate curves: For conditions where impingement heat transfer is a dominant effect the R_T - X curves display an effect not previously reported. This unique feature is that after the constant rate period R_T does not decrease

but increases and reaches a maximum value, R_{Tm} , which may be nearly double the constant rate value, R_{Tc} . The occurrence of this secondary increasing rate period derives from the fact that the impingement water removal process reaches its falling rate period earlier than that by through flow. Thus the failing rate R_I process drives up the paper temperature while the moisture content within the sheet is still sufficiently high that through flow water removal has not yet entered its falling rate period. Hence R_T increases with increasing paper temperature. The point X_m , R_{Tm} marks the end of this secondary increasing rate period and the start of the falling rate period for R_T . The complete R_T - X curve is quantified in terms of R_{Tc} , X_{Ti} , n_{Ti} and X_c for the increasing rate and constant rate periods, and during the secondary increasing rate and falling rate periods by the values of X_m and R_{Tm} .

$$R_T = R_{Tm}\left\{1-\left[\left(\frac{e^{-c\frac{X}{X_c}}-e^{-c\frac{X_m}{X_c}}}{1-e^{-c\frac{X_m}{X_c}}}\right)^2\right]^{0.85}\right\}$$

This comprehensive equation covers all drying below $X=X_c$, whether this consists of two water removal rate periods, the secondary increasing rate and falling rate periods or, for conditions giving no secondary increasing rate period, when the falling rate period starts at X_c .

16) Quantitative parameters: The effect of drying process conditions is:

$$X_o - X_{Ti} = (X_o - X_i)\left(1 + 0.043B^{0.92}\frac{R_{Ic}}{R_{Tc}}\right)$$

with the extent of the increasing rate period varying up to 1.4 kg/kg, in the order of half the total water removed by through flow. The contribution of R_I to the transport area development for through flow is small for 50 g/m^2 paper but substantial for thin paper of 25 g/m^2 basis weight.

$$n_{Ti} = 3.6\left[1 - 3.54\left(\frac{X_o - X_{Ti}}{X_o - X_i}\right)^{-0.70}(1-q_T)^{5.93}\right]$$

The water removal by impingement flow reduces the R_T - X curvature in the increasing rate period, hence decreases n_{Ti} from its limiting value of 3.6 for the highly curved R - X relation for q_T=1, to approach linearity for some conditions of the CITAD process.

The constant water removal rate in the through flow exhaust, R_{Tc} , is not significantly affected by the impingement flow, hence its value is the same as for pure through drying, $R_{Tc}=R_{cT}$.

$$X_m = \frac{X_{cT}}{1.12 - 0.12\, q_T}$$

where X_{cT} is the value for pure through drying. X_m is the point where factors making R_T increase just balance those causing the onset of falling rate period drying.

$$R_{Tm} = R_{Tc}\, e^{0.62\, B^{0.51} \left(\frac{R_{Ic}}{R_{Tc}}\right)^{0.42} \frac{\lambda (X_c - X_m)}{RT_{as}^2}}$$

R_{Tm} increases for conditions making impingement effect dominant such as increasing R_{Ic}/R_{Tc} . Increasing B extends the secondary increasing rate period, hence increases R_{Tm} .

17) **Constant CITAD drying rate, R_c :** For $R_c=R_{Ic}+R_{Tc}$, it was found that

$$R_c = R'_{cI}(1 - q_T)^{5/3} + R'_{Tc}\, q_T^{0.85}$$

where R_{cI}' is the constant drying rate for pure impingement at the same rate of total drying air G, and R_{Tc}' is likewise the rate for pure through drying for the same G. This correlation predicts well the pilot plant results of Burgess et al. (1972a), despite the great differences in experimental techniques from those used here.

18) **Models for prediction of drying time and drying rate:** The sensitive effect found of through flow on impingement water removal rate establishes that the model of Randall (1984), assuming no influence of through flow on impingement, is invalid. The Crotogino and Allenger (1979) model for combined impingement and through air drying follows the trends correctly but over predicts both components of water removal rates. The quantitative analysis of combined impingement and through air drying of paper was assembled into a comprehensive model validated by measured complete drying rate curves for 324 kraft handsheets, and with which the CITAD process drying time and drying rate can be predicted.

7.2 Recommendations for future studies

1) **Drying intensity:** With the principles determined from the present investigation at low air temperature, drying intensities should be increased with air temperatures of 300 - 500 °C to document CITAD characteristics at conditions of industrial drying intensity.

2) **Numerical study:** As it is a great experimental challenge to measure CITAD performance at high intensity conditions for which the drying could be completed in the order of a second, numerical studies should be carried out with the knowledge obtained in the present study as a guide.

3) **Pulp furnish and sheet formation:** As the results of the present investigation were for handsheets made from one furnish, i.e. unbleached, unbeaten kraft pulp, and as both the increasing rate period and the falling rate period are determined by phenomena within the sheet which can be a function of the pulp furnish and the sheet formation, the process of drying by CITAD should be investigated for other pulps and with papermachine formed sheets.

4) **Paper properties:** As the drying history of paper temperature and paper moisture content locally within the sheet would be quite different between printing grade paper dried by the CITAD process from that dried conventionally, the dependence of paper properties on drying conditions must be determined in addition to the drying rate results, in order to establish that good quality product could be obtained by drying with the CITAD process.

5) **Nozzle geometry:** A laboratory facility for the study of CITAD should be built in which the local nonuniformity of the impinging jet flow is eliminated by relative motion between the nozzle plate and the sheet.

References

Allander, C., 1961, " Air Impingement Drying, Evaporation from Thin Web on a Paper Machine Cylinder with Forced Convection ", TAPPI, 44, 5, pp332-337

Allerton, J., L.E. Brownell, and D.K. Katz, 1949, "Through-Drying of Porous Media", Chem. Eng. Prog., 45(10), pp619-635

Bagnoli, E., F.H. Fuller, and R.W. Norris, 1963, *Chemical Engineer's Handbook*, 4th Edition, J. H. Perry, C.H. Chilton and S.D. Kirkpatrick ed., McGraw-Hill Inc. Section 15, pp32-43

Baines, W.D. and J.F. Keffer, 1979, "Shear Stress Measurements for An Impinging Air Jet", Transactions of the Technical Section, Canadian Pulp and Paper Association, June; pp39-44

Bell, D.O., J. Seyed-Yagoobi and L.S. Fletch, 1991, " Recent Development in Paper Drying ", *Advances in Drying*, A.S. Mujumdar, Ed., New York, Marcel Dekker, pp203-261

Bond, J.F., 1991, " Drying Paper by Impinging Jets of Superheated Steam: Drying Rates and Thermodynamic Cycles", Ph. D. Thesis, Chem. Eng. Dept., McGill University, Montreal

Bond, J.F., R.H. Crotogino, W.J.M. Douglas, A.S. Mujumdar and A.R.P. van Heiningen, 1991, " Impingement Drying of Paper in Superheated Steam Impingement in the Constant Rate Period", Technology Today, 5, pp284-288

Bond, J.F., R.H. Crotogino, A.R.P. van Heiningen, and W.J.M. Douglas, 1992, " An Experimental Study of the Falling Rate Period of Superheated Steam Impingement Drying of Paper", Drying Technology, 10, 4, pp961-978

Bond, J.F., A.S. Mujumdar, A.R.P. van Heiningen, and W.J.M. Douglas, 1994a, " Drying Paper by Impinging Jets of Superheated Steam Part I: Constant Drying Rate in Superheated Steam", Can. J. Chem. Eng. 72, 3, pp446-451

Bond, J.F., A.S. Mujumdar, A.R.P. van Heiningen, and W.J.M. Douglas, 1994b, " Drying Paper by Impinging Jets of Superheated Steam Part II: Comparison of Steam and Air as Drying Fluids", Can. J. Chem. Eng. 72, 3, pp452-456

Broughton, D.B., 1945, " Prediction of Critical Moisture Content", Ind. Eng. Chem., 37, 12, pp1184-1185

Burgess, B.W., 1961, " The Drying of Web Materials", Pulp and Paper Magazine of Canada, 62, 6, ppT303-T309

Burgess, B.W., S.M. Chapman, 1968, "Turbulence Drying Process", United States Patent, #3,418,723

Burgess, B.W., 1971, " Future Trends in Drying", Paper Technology, 12, 6, ppT231-T244

Burgess, B.W., S.M. Chapman and W. Seto, 1972a, "The Papridryer Process, Part I, The Basic Concept and Laboratory Results", Pulp and Paper Magazine, Canada, 73, 11, pp314-322

Burgess, B.W., S.M. Chapman and W. Seto, 1972b, "The Papridryer Process, Part II, Mill Trials", Pulp and Paper Magazine of Canada, 73, 11, pp323-331

Butler, J.W.,1901, *The story of paper-making*, An account of paper-making from its earliest known record down to the present time, J.W. Butler Paper Company,

Chance, J.L., 1974, "Experimental Investigation of Air Impingement Heat Transfer under an Array of Impinging Jets", TAPPI, 57, 6, pp108-112

Chen, G., 1989, "Impingement Heat Transfer with A Re-entry Nozzle", M.Eng. thesis, Chem. Eng. Dept., McGill University, Montreal

Chen, G., V.G. Gomes, and W.J.M. Douglas, 1994, "Impingement Drying of Paper", *Drying '94*, Proceedings of 9th international drying symposium, Gold Coast, Australia, V. Rudolph and R.B. Keey Ed. pp1147-1154

Chu, C. C., S. Finelt, W. Hoerrner and M.S. Lin, 1959, "Drying with Superheated Steam-Air Mixtures", Industrial and Engineering Chemistry, 51, 3, pp275-280

Chu, J.C. and W.L. Kuo, 1967, "The Kinetics of Normal-Through Drying of Paper", TAPPI, 50, 8, pp405-415

Churchill, S. W. and R. Usagi, 1972, " A General Expression for the Correlation of Rates of Transfer and Other Phenomena", AIChE J. 18, pp1121-1128

Churchill, S. W. and H. Ozoe, 1973, " A Correlation for Laminar Free Convection from a Vertical Plate", J. Heat Transfer, Trans. ASME, 95c, pp540-541

Churchill, S. W. and R. Usagi, 1974, " A Standardized Procedure for Production of Correlations in the Form of a Common Empirical Equation", Ind. Eng. Chem. 13, pp39-44

Churchill, S. W., 1983, " The Development of Theoretically Based Correlations for Heat and Mass Transfer", Latin American Journal of Heat and Mass Transfer, 7, pp207-229

Churchill, S. W., 1992, " The Role of Analysis in the Rate Processes", Ind. Eng. Chem. Res., 31, 3, pp643-658

Cipra, B., 1993, " Fermat's Last Theorem Finally Yields ", Science, 261, pp32-33

Cirrito, A.J. 1963, " Paper Drying, Part III - Air Jet Impingement", The Paper Industry, 45, 8, pp433-435

Cirrito, A.J. 1964a, " Paper Drying, Part IIIA - (continued) Controlling Quality and Heat Rate in Impingement Drying", The Paper Industry, 45, 11, pp599-601

Cirrito, A.J. 1964b, " Paper Drying, Part IV - The Falling Rate Zones", The Paper Industry, 46, 2, pp115-118

Cirrito, A.J. 1964c, " Paper Drying, Part IV - (continued)", The Paper Industry, 46, 2, pp203-206

Clapperton R.H., 1967, *The paper-making machine, its invention, evolution and development*, Pergamon Press

Corboy, W.G. Jr., 1991, "Yankee Dryers", *Pulp an Paper Manufacture*, B.A. Thorp, Technical Ed., M.J. Kocureck, Ed., Joint Textbook Committee of the Paper Industry, TAPPI & CPPA, 7, pp 323-342

Crotogino, R.H., 1975, "The Growing Significance of Air Drying", Paper Technology 16, 4, T154-T164

Crotogino, R.H. and V. Allenger, 1979, "Mathematical Model of the Papridryer Process", Transactions of the Technical Section, CPPA, 5, 4, pp84-91

Cui, W.K., and A.S. Mujumdar, 1984, " A Novel Steam Jet and Double Effect Evaporation Dryer", *Drying '84*, A.S. Mujumdar, Ed., N.Y., Hemisphere, pp468-479

Cui, W.K., W.J.M. Douglas, and A.S. Mujumdar, 1985, " Impingement Steam Drying of Paper", Drying Technology, 3, 2, pp307-320

Daane, R.A. and S.T. Han, 1961, " An Analysis of Air Impingement Drying", TAPPI, 44, 1, pp

Darcy, H., 1856, *Les Fontaines Publiques de la Ville de Dijon*, V. Dalmont, Paris

Das, D. 1982, " Convective Heat Transfer under a Turbulent Impinging Slot Jet at Large Temperature Difference ", M. Eng. Thesis, Chem. Eng. Dept., McGill University, Montreal

Das, D. W. J. M. Douglas and R.H. Crotogino, 1985, " Convective Heat Transfer under a Turbulent Impinging Slot Jet at Large Temperature Difference ", *Drying '85*, A.S. Mujumdar, ed., Hemisphere, N.Y. pp354-359

Dean, J.A., 1985a, " Humidification and Drying ", *Lange's Handbook of Chemistry*, 13th Edition, McGraw-Hill Inc., Section 10, pp81

Dean, J.A., 1985b, " Solutions for Maintaining Constant Humidity ", *Lange's Handbook of Chemistry*, 13th Edition, McGraw-Hill Inc., Section 10, pp84.

De Acetis, J. and G. Thodos, 1960, "Mass and Heat Transfer in Flow of Gases Through Spherical Packings", Ind. Eng. Chem., 50, 12, pp1003-1006

Encyclopædia Britanica, 1974, "Macropædia, Knowledge in Depth ", 7, pp234-236

Forchheimer, P. 1901, "Wasserbewegung Durch Boden", Z. ver. Deutsch. Ing. 45, pp1782

Garden, R. and J.C. Akfirat, 1966, "Heat Transfer Characteristics of Impinging Two-dimensional Air Jets", J. Heat Transfer, 88, 1, pp101-108

Gauntner, J.W., J.N.B. Livingood and P. Hrycak, 1970, "Survey of Literature on Flow Characteristics of A Single Turbulent Jet Impinging on A Flat Plate", NASA, TN D-5652

Gomes, V.G., R.H. Crotogino and W.J.M. Douglas, 1992, " The Role of Local Nonuniformity in Through Drying of Paper", *Drying '92*, A.S. Mujumdar, Ed., Amsterdam, Elsevier, pp994-1006

Gottsching L., and Rhodius D. 1977, " Der Trocknungsverlauf Von Papier und Pappe in Abhangigkeit Von Trocknungstechnischer and Papier Technologischen Parametern", Das Papier, 10

Gummel, P., 1977, " Through Drying: An Experimental Study of Drying Rate and Pressure Losses in Through-Drying of Textiles and Paper", Ph.D. Thesis, University of Karlsrüke, Germany

Gummel, P. and E.U. Schlünder, 1980, "Through Air Drying of Textiles and Paper", *Drying '80,* A.S. Mujumdar, Ed., N.Y., Hemisphere, 1, pp357-366

Hougen, O.A., H.J. McCauley, and W.R. Marshall, Jr. " Limitations of Diffusion Equations in Drying", Trans. Amer. Inst. Chem. Eng. 34, pp183-209

Inoue, S., K. Eguchi and T. Imamoto, 1992, " Impinging Jet Dryer", Drying Technology, 10, 3, pp679-714

Journeaux, I., 1991, " Impinging Jet Heat Transfer and Thermal Deformation on Calender Rolls", Ph. D. thesis, Chem. Eng. Dept., McGill University, Montreal

Keey, R.B., 1972, *Drying, Principles and Practice*, Pengamon Press, UK, pp196-197

Kercher, D.M. and W.J. Tabakoff, 1970, " Heat Transfer by a Square Array of Round Air Jets Impinging Perpendicular to a Flat Surface Including the Effect of Spent Air ", J. of Eng. for Power, Trans ASME, 92, Ser. A, 1, pp73-82

Lebert A, and J-J, Bimbenet, 1991, " Drying Curves - A General Process for Their Representation", *Drying '91*, A.S. Mujumdar and I. Filková, ed., Elsevier, Amsterdam, pp181-190

Lee P. F. and J. A. Hinds, 1981, " Optimizing Dryer Performance: Modeling Heat and Mass Transfer within a Moist Sheet of Paper or Board ", TAPPI, 64, 12, pp39-44

Marshall, W.R. and O.A. Hougen, 1942, "Drying of Solids by Through Circulation", Trans. Am. Inst. Chem. Eng., 38, pp91-121

Martin, P.D., 1972, "Through Drying", Paper Tech., 13, 2, pp114-119

Martin, H., 1977, "Heat and Mass Transfer Between Impinging Gas Jets and Solid Surface", Advances in Heat Transfer, 13, Academic Press, pp1-60

McConnell, R.R., 1980, "A Literature Review of Drying Research in Pulp and Paper Industry" *Drying '80,* A.S. Mujumdar, Ed., N.Y., Hemisphere, 1, pp330-337

Mickley, H., R.C. Ross, A.L. Squyers and W.E. Stewart, 1954, "Heat, Mass and Momentum Transfer for Flow Over A Flat Plate with Blowing and Suction", NACA TN-3208

Moffat, R.J. and W.M. Kays, 1968, "The Turbulent Boundary Layer on A Porous Plate: Experimental Heat Transfer with Uniform Blowing and Suction", Int. J. Heat Mass Transfer, 11, pp1547-1566

Mujumdar, A.S. and W.J.M. Douglas, 1972, "Impingement Heat Transfer - Literature Review", Paper Presented at TAPPI Conf., New Orleans, USA

Mujumdar, A.S., 1982, " Recent Development in Paper Drying", IPPTA, 19, 1, pp72-76

Mujumdar, A.S., 1986, " Future Trends in Drying Technology, A Viewpoint " , *Drying '86*, A.S. Mujumdar, Ed., N.Y., Hemisphere, pp 213-216

Mujumdar, A.S., 1987, "Impingement Drying", *Handbook of Industrial Drying*, A.S. Mujumdar, Ed., New York, Marcel Dekker, pp461-474

Mujumdar, A.S., 1991, " Drying Technologies of the Future", Drying Technology, 9, 2, pp325-347

Mujumdar, A.S., 1992, *Class notes,* Drying, theory and industrial practice, Chem. Eng. Dept. McGill University, Montreal

Navarri, P., A. Genvaudan and J. Andrieu, 1992, "Preliminary Study of Drying of Coated Film Heated by Infrared Radiation ", *Drying'92*, A.S. Mujumdar, Ed., Amsterdam, Elsevier, pp722-728

Obot, N.T., A.S. Mujumdar, and W.J.M. Douglas, 1980, "Design Correlations for Heat and Mass Transfer Under Various Turbulent Impinging Jet Configurations", *Drying '80*, A.S. Mujumdar, Ed., N.Y., Hemisphere, 1, pp388-402

Obot, N.T., 1981, "Flow and Heat Transfer for Round Turbulent Jets Impinging on Permeable and Impermeable Surfaces", Ph.D. Thesis, Chem. Eng. Dept., McGill University, Montreal

Obot, N.T., 1982, " Effect of Suction on Impingement Heat Transfer ", *Heat Transfer 1982*, Proceedings of the 7th Int. Heat Transfer Conference, U. Grigull, E. Hahne, K. Stephen, Ed. pp389-394

Petrovic, L.J. and G. Thodos, 1968, "Mass Transfer in the Flow of Gases Through Packed Beds", Ind. Eng. Chem. Fundam., 7, 2, pp274-280

Pikulik, I.I., 1992, " Method for Manufacture of Smooth and Glossy Papers and Apparatus", United States Patent, #5,127,168

Pikulik, I.I., 1992, " High Intensity Drying of Paper", Pulp and Paper Reports, PPR 958, PAPRICAN, Canada

Polat, O., W.J.M. Douglas, and R.H. Crotogino, 1987, " Experimental Study of Through Drying of Paper", *Drying '87*, A.S. Mujumdar, Ed., N.Y., Hemisphere, pp290-295

Polat, O., R.H. Crotogino and W.J.M. Douglas, 1989, " Throughflow Across Moist and Dry Paper", *Fundamentals of Papermaking*, 2, pp731-742, C.F. Baker Ed., London, MEP ltd.

Polat, O., 1989, "Through Drying of Paper", Ph.D. Thesis, Chem. Eng. Dept., McGill University, Montreal

Polat, O., R.H. Crotogino, W.J.M. Douglas, 1991, "A Model of Through Drying Paper", Proceedings, Helsinki Symp. on Alternative Methods of Pulp and Paper Drying, Helsinki, pp 333 - 338

Polat, O., R.H. Crotogino, W.J.M. Douglas, 1992a, "Transport Phenomena Analysis of Through Drying Paper", Ind. Eng. Chem. Res., 31, pp736 - 743

Polat, O., R.H. Crotogino, W.J.M. Douglas, 1992b, "Through-Drying of Paper: A Review", *Advances in Drying*, A.S. Mujumdar, Ed., New York, Marcel Dekker

Polat, O., R.H. Crotogino, A.R.P. van Heiningen, W.J.M. Douglas, 1993, "Permeability and Specific Surface of Paper", J. Pulp Paper Sci., 19, 4, ppJ137-J141

Polat, S., B. Huang, A.S. Mujumdar and W.J.M. Douglas, 1988, "Numerical Flow and Heat Transfer under Impinging jets - A Review", Annual Review of Numerical Fluid Mechanics and Heat Transfer, 2, pp 152 - 197

Polat, S., 1988, "Transport phenomena under Jets Impinging on A Moving Surface with Throughflow", Ph.D. Thesis, Chem. Eng. Dept., McGill University, Montreal

Polat, S., and W.J.M. Douglas, 1990, " Heat Transfer under Multiple Slot Jets Impinging on a Permeable Moving Surface", A.I. Ch. E. Journal, 36, pp1370-1378

Polat, S., A.S. Mujumdar, and W.J.M. Douglas, 1991a, " Impingement Heat Transfer under a Confined Slot Jet, I. Effect of Surface Throughflow", Can. J. Chem. Eng., 69, pp266-273

Polat, S., A.S. Mujumdar, and W.J.M. Douglas, 1991b, " Impingement Heat Transfer under a Confined Slot Jet, II. Effect of Surface Motion and Throughflow", Can. J. Chem. Eng., 69, pp274-280

Polat S., 1993, "Heat and Mass Transfer in Impingement Drying", Drying Technology, 11, 6, pp1147 - 1176

Porter, H.F., P.Y. McCormick, R.L. Lucas and D.F. Wells, 1973, " Gas-solid systems", *Chemical Engineer's Handbook* , 5th edition, R.H. Perry and C.H. Chilton, ed. McGraw-Hill Inc. section 20, pp10-13

Porter, H.F., G.A. Shurr, D.F. Wells and K.T. Semrau, 1984, "Solids drying and gas-solid systems", *Chemical Engineer's Handbook* , 6th Edition, Perry, R.H., D.W. Green and J.O. Maloney ed., McGraw-Hill Inc. Section 20, pp10-12

Prahl, J.M., 1968, " Thermodynamics of Paper Fiber and Water Mixture ", Ph. D. Thesis, Harvard University, Cambridge, U.S.A.

Raj, P.P.K. and H.W. Emmons, 1975, "Transpiration Drying of Porous Hygroscopic Materials", Int. J. Heat Mass Transfer, 18, pp623-634

Randall, K.R., 1984, "Using High Velocity Impingement Air to Improve Through Drying Performance on Semi-permeable Webs", *Drying'84*, A.S. Mujumdar, Ed., Hemisphere, N.Y., pp254-263

Rohrer, J.W. and F.J. Gardiner, 1976, "Through-Drying: Heat Transfer Mechanism and Machine System Response", TAPPI, 59, 4, pp82-87

Saad, N.R., A.S. Mujumdar, and W.J.M. Douglas, 1980, " Heat Transfer under Multiple Turbulent Slot Jets Impinging on a Flat Plate ", *Drying '80*, A.S. Mujumdar, Ed., N.Y., Hemisphere, pp422-430

Saad, N.R., 1981, "Flow and Heat Transfer for Multiple Turbulent Impinging Slot Jets", Ph. D. Thesis, Chem. Eng. Dept., McGill University, Montreal

Saad, N.R. S. Polat and W.J.M. Douglas, 1992, " Confined Multiple Impinging Slot Jets without Crossflow Effects ", Int. J. Heat and Fluid Flow, 13, (1), pp2-14

Sayegh, N., I. Pikulik, and H.I. Simonsen, 1986, " A Survey of Dryer Sections of Canadian Newsprint Machines, Part II, Energy Consumption and Drying Rate", Pulp and Paper Research Institute of Canada

Schlünder, E.U., 1977, " On the mechanism of mass transfer in heterogeneous systems - in particular in fixed beds, fluidized beds and on bubble trays", Chem. Eng. Sci., 32, pp845-851

Schlünder, E.U., 1991, " Unusual Drying Rate Curves", *Drying '91*, A.S. Mujumdar and I. Filková, ed., Elsevier, Amsterdam, pp615-619

Sen Gupta, A. and G. Thodos, 1964, "Transitional Behaviour for the Simultaneous Mass and Heat Transfer of Gases Flowing Through Packed and Distended Beds of Spheres", Ind. Eng. Chem. Fundam., 3, 3, pp218-220

Sherwood, T.K., 1929, " The Drying of Solids - I", Ind. Eng. Chem., 21, 1, pp12-16

Sherwood, T.K., 1929, " The Drying of Solids - II", Ind. Eng. Chem., 21, 10, pp976-980

Sherwood, T.K., 1931, "Application of the Theoretical Diffusion Equations to the Drying of Solids", Ind. Eng. Chem., 29, pp190-202

Sherwood, T.K., 1941, " Drying ", *Chemical Engineer's Handbook* , 2nd edition, J.H. Perry, ed., McGraw-Hill Inc.

Sherwood, T.K. and Commings, 1933, " The Drying of Solids - V ", Ind. Eng. Chem. 25, 3, pp311-316

Shishido, I., M. Suzuki, and S. Ohtani, 1985, " A New Measurement Method of Liquid Transport Properties", *Drying '85*, R. Toei and A.S. Mujumdar, Ed., N.Y., Hemisphere, pp485-489

Smook, G.A., 1986, *Handbook for Pulp & Paper Technologists*, Joint Textbook Committee of the Paper Industry, M.J. Kocurek, Technical Ed., 2nd printing, TAPPI & CPPA

Sorrells, F.D., 1991, " Drying on Conventional Tissue Machines", 1991 Tissue Runnability Seminar, Seattle, U.S.A., TAPPI Press, pp125-130

Spalding, D.B., 1960, "A Standard Formulation of the Steady Convective Mass Transfer Problem", Int. J. Heat Mass Transfer, 1, pp192-207

Spraker, W.A., G.B. Wallis, and B.R. Yaros, 1969, " Analysis of Heat and Mass Transfer in the Yankee Dryer", Pulp and Paper Magazine of Canada, 70, 1, ppT1-T5

Strumillo, C. and Kudra, T., 1986, *Drying: Principles, Applications and Design,* New York, Gordon and Breach

Suzuki, M., R.B. Keey, and S. Maeda, 1977, "On the Characteristic Drying Curves", A.I.Ch.E. Symp. Ser., 73, 163, pp47-56

Gineburg, 1973, *Drying of Food, Principles and Technology*, Food Industry Press, USSR (Rus). Translated by Gao, K, 1986, and published by Light Industry Press, China, pp 300-301

Van Heiningen, A.R.P., 1982, "Heat Transfer under an Impinging Slot Jet", Ph. D. Thesis, Chem. Eng. Dept. McGill University, Montreal

Villalobos, J.A., 1975, "Engineering Considerations in Through Drying", BPBIF Inter. Water Removal Symp. (109 Conf.), London, March 20

Villalobos, J.A., 1986, "Thru-Drying, A Technology Review", Proc. PIRA Intl. Conf. on New Tech. in Web Consolidation and Drying, Brighton, Sussex, UK

Walser, R. and R.S. Swenson, 1968, "Air Through-Drying of Paper", TAPPI, 51, 4, pp184-190

Wedel, G.L. and J.L. Chance, 1977, "Analysis of Through-Drying", TAPPI, 60, 7, pp82-85

Wedel, G.L., 1980, " Air Impingement Heat Transfer ", TAPPI, 63, 8, pp89-92

Wenzel, L. and R. R. White (1951) "Drying Granular Solids in Superheated Steam", Industrial and Engineering Chemistry, 43, 8, pp1829-1837

Wilke, C.R. and O.A. Hougen, 1945, "Mass Transfer in the Flow of Gases Through Granulas Solids Extended to Low Modified Reynolds Numbers", Trans. Am. Inst. Chem. Eng., 41, pp445-451

Wilkinson, Leland. SYSTAT: *The System for Statistics,* Evanston, IL, SYSTAT, Inc., 1990

Appendix A Flow chart of data acquisition program

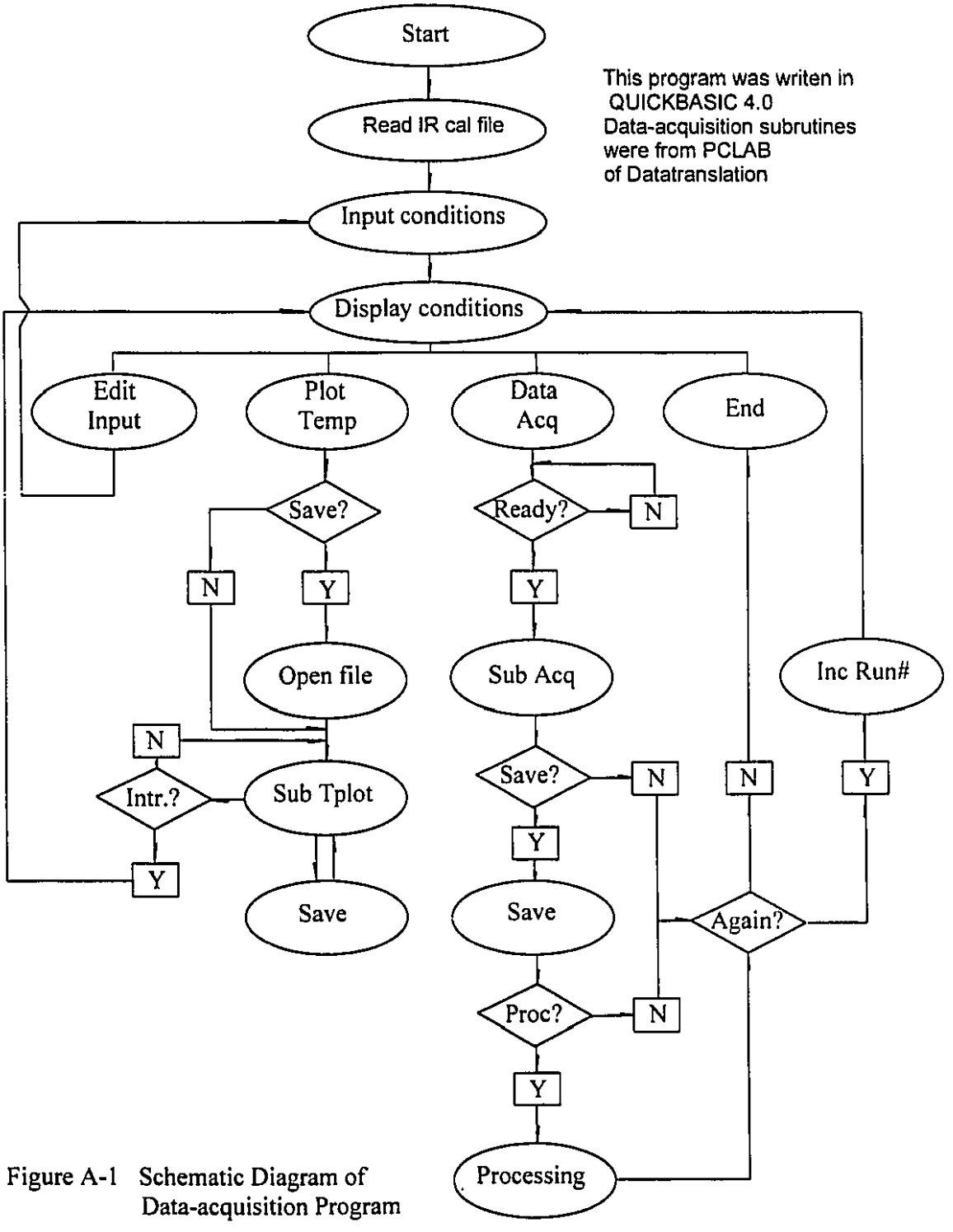

Figure A-1 Schematic Diagram of Data-acquisition Program

```
' $DYNAMIC
5  DECLARE FUNCTION rho! (x!, y!, T!)
   DECLARE FUNCTION vis# (ttt!)
   DECLARE SUB Tplot
   DECLARE SUB Acq
   DECLARE SUB Savedata
   DECLARE SUB TsHs
   CLEAR , , 1200
   ON ERROR GOTO ErrorProc
   DEFINT A-Z
   SCREEN 2
   '
10 KEY OFF
   CLS
   LINE (80, 20)-(560, 180), , BF
   LOCATE 5, 20, 1, 7, 7
   PRINT "                              "
   LOCATE 6, 20, 1, 7, 7
   PRINT " This  Program is Designed to  Perform "
   LOCATE 7, 20, 1, 7, 7
   PRINT " the  Data-acquisation for Experiments "
   LOCATE 8, 20, 1, 7, 7
   PRINT " of combined impingement  and  through "
   LOCATE 9, 20, 1, 7, 7
   PRINT "     flow  air  drying  of Paper      "
   LOCATE 11, 20, 1, 7, 7
   PRINT " Calibration  Coefficients of IRs  are "
   LOCATE 12, 20, 1, 7, 7
   PRINT " Pre-saved in a file named CCmmddr.PRN "
   LOCATE 14, 20, 1, 7, 7
   PRINT " Channel  5 -- Through Flow T at Back "
   LOCATE 15, 20, 1, 7, 7
   PRINT " Channel  6 -- Through Flow IR signal "
   LOCATE 16, 20, 1, 7, 7
   PRINT " Channel  7 -- Through Flow T at back "
   LOCATE 17, 20, 1, 7, 7
   PRINT " Channel  8 -- Pressure Transducer    "
   LOCATE 18, 20, 1, 7, 7
   PRINT " Channel  9 -- Through Flow T at Back "
   LOCATE 19, 20, 1, 7, 7
   PRINT " Channel 10 -- Jet & Paper Temp       "
   LOCATE 20, 20, 1, 7, 7
   PRINT " Channel 11 -- Impingement IR Signal  "
   LOCATE 21, 20, 1, 7, 7
   PRINT " Channel 12 -- IR cell Temperature    "
   LOCATE 22, 20, 1, 7, 7
   PRINT " Channel 13 -- Through Flow T at Back "
   LOCATE 25, 20, 1, 7, 7
   PRINT " press any key to continue ... ... "
15 IF INKEY$ = "" THEN 15
   '
   'The A/D converter is assumed to be set up for
   'SE, unipolar operation
   'DMA is not used for the data conversion
   'in this program
   '
   'The system  clock is used to control the sampling frequency
   'Time$ is set to zero at each loop
   'Timer is used to count the time elapsed
   'between scans
   '
   '
   'The sampling time is controlled by the operator
   '
   'Sampling frequency is changed according to the experimental
   'conditions     (see line 225)
   '
   'define constants
   '
   '
   DIM data.value(8, 2800) AS INTEGER
   DIM gain(0 TO 15) AS INTEGER
   DIM factor!(15)
   DIM begint!(2800)
   DIM sssr!(15), yy!(6)
   DIM xr!(15, 2)
```

```
DIM w!(6), y#(6), scaley!(6)
DIM mvo!(15)
DIM fai!(2, 2), mvis!(2), ymole!(2), mw!(2)
DIM h#(5)
'
'
'
tx0# = .1053451266#
tx1# = 16.87319253#
tx2# = -.1669079643#
nump = 0
ln% = 0
ccw = 0
nrun = 0
ccc = 48
adcschan = 6
adccchan = 13
mw!(1) = 18: mw!(2) = 28.97
fai!(1, 1) = 1: fai!(1, 2) = .775: fai!(2, 1) = 1.3583: fai!(2, 2) = 1
'
'Gain of the board
'
gain(4) = 1
gain(5) = 4
gain(6) = 8
gain(7) = 2
gain(8) = 8
gain(9) = 2
gain(10) = 2
gain(11) = 8
gain(12) = 4
gain(13) = 2
gain(14) = 2
gain(15) = 1
'
'Gain of the signal conditioner
'
'gainsc!(5) = 302.8
'gainsc!(6) = 1
'gainsc!(7) = 305.17
'gainsc!(8) = 304.13
'gainsc!(9) = 1
'gainsc!(10) = 305.75
'gainsc!(11) = 1
'gainsc!(12) = 1
'
factor!(5) = .0019665205#
factor!(6) = 1
factor!(7) = .003998016#
factor!(8) = .0022478171#
factor!(9) = .004006943#
factor!(10) = .0040038859#
factor!(11) = 1
factor!(12) = .0023216427#
factor!(13) = .0016364626#
factor!(14) = .0019222317#
'
'
mvo!(5) = -.2091859548#
mvo!(7) = -.033401853#
mvo!(8) = -.39186
mvo!(9) = -.001377932#
mvo!(10) = -.0397460027#
mvo!(12) = .035835663#
mvo!(13) = .3925755798#
mvo!(14) = -.33104
'
ra1! = .0862
ra2! = .4761
ra3! = -.1233
ra4! = .0668
ra5! = .2394
ra6! = .6315
ra7! = .1866
ra8! = .1951
'
'
```

```
cv1! = 1.7078
cv2! = -2.7307
cv3! = 1.312
cv4! = .0632
cv5! = .132
'
'TsHs data
h#(0) = .00356555707594#
h#(1) = .00041761607994#
h#(2) = -.0000048662175#
h#(3) = .0000005759864#
h#(4) = 0
'
'
'
DEF fnrho! (x!, y!, T!) = (x! + y!) * 1329.469 / (T! + 273.15) * .003484
'
' Rho air density in Kg/m**3
' x barabolic pressure in cm Hg
' y gage pressure in cm Hg
' T temperature in Deg. C
' air is considered as ideal gas with M=28.97

DEF fnvis# (tttt!) = (1.2147081# + 6.791181E-02 * (tttt! + 273.15) - .0000343# * (tttt! + 273.15) ^ 2) * .000001

'visicosity calculation valid 250 K to 400 K (-25 to 130 C)
'This correlation for the viscosity of air is valid over the
'range of 250 deg. K to 400 deg. K (-25 to 130 deg. C)
'The correlation was obtained by fitting a polynomial to
'the data given by Touloukian, Liley and Saxena
'in Thermophysical Properties of Matter, IFI/Plenum,
'N.Y. 1970
'Temperature is given in C and converted to K
'
'
17  CLS
    LOCATE 12, 20, 1, 7, 7
    INPUT " Input the IR calibration data filename "; cald$
    OPEN cald$ FOR INPUT AS #1
    INPUT #1, hh0#, a0#, a1#, a2#, rsq!, ai0#, ai1#, ai2#, rsqi!
    CLOSE #1
    '
    '
20  CLS
    '
    ' input the variables from the keyboard
    '
    '
    IF ln% <> 0 THEN 200
30  INPUT "   Input the date (mmdd)"; a$
    IF ln% <> 0 THEN 200
40  INPUT "   Input the run number of today (<100)"; B$
50  chk = LEN(B$)
    IF chk > 2 THEN
     INPUT "     Illegal run number, retry "; B$
     GOTO 50
    ELSE
     IF ln% <> 0 THEN
      GOTO 200
     ELSE
     END IF
    END IF
60  INPUT "   Input the ambient temperature (Deg C)"; tt!
    IF ln% <> 0 THEN 200
70  INPUT "   Input the temperature in the main rotameter (Deg. C)"; tr!
    IF ln% <> 0 THEN 200
80  INPUT "   Input the main rotameter reading   (CFM)   "; flowr!
    IF ln% <> 0 THEN
     LOCATE 21, 4, 1, 7, 7
    END IF
90  INPUT "   Input the pressure in the main rotameter (cmHg)"; pd!
    IF ln% <> 0 THEN
     LOCATE 22, 4, 1, 7, 7
    END IF
100 INPUT "   Input the pressure at the back of paper (cm M) "; p2!
    IF ln% <> 0 THEN 200
110 INPUT "   Input the barometric pressure (cmHg)"; p1!
```

```
    IF ln% <> 0 THEN 200
120 INPUT "   Input the through flow rotameter reading (SCFM) "; flowt!
    IF ln% <> 0 THEN 200
125 INPUT "   Input the vacuum at the rotameter (inHg) "; pt1!
    IF ln% <> 0 THEN 200
130 INPUT "   The level of Basis Weight (20,30,40,50) "; bb
    IF ln% <> 0 THEN 200
135 INPUT "   The pressure transducer is H  (h/H)   "; pans$
    IF pans$ = "h" OR pans$ = "H" THEN
     factor!(8) = .010426#
     mvo!(8) = -.5909
    ELSE
     'use low values as default
     factor!(8) = .0022478171#
     mvo!(8) = -.39186
    END IF

    '
140 'Another run returns to here with updated Tj!
    sum# = 0
     FOR i = 1 TO 40
      channel = 10
      CALL xav(channel, gain(channel), anolog.data)
      sum# = sum# + anolog.data / 40#
     NEXT i
      tj! = sum#
      tj! = tj! * factor!(channel) + mvo!(channel)
      tj! = tx0# + tx1# * tj! + tx2# * tj! ^ 2
      IF tj! < 10 THEN
       BEEP
       PRINT " Check the Power switch, make sure they are on "
       PRINT " Press any key to continue ... ... "
150      IF INKEY$ = "" THEN 150
       GOTO 140
      END IF
    PRINT "   The jet temperature is        ";
    PRINT USING "###.##"; tj!;
    PRINT " Deg. C"
160 '
    channel = 12
    sumt# = 0
    FOR i = 1 TO 30
     CALL xav(channel, gain(channel), analog.value)
     sumt# = sumt# + analog.value / 30!
    NEXT i
     sumt# = mvo!(channel) + factor!(channel) * sumt#
     trot! = tx0# + tx1# * sumt# + tx2# * sumt# * sumt#
    PRINT " The temperature is ";
    PRINT USING "###.#"; trot!
    IF ln% <> 0 THEN 200
    '
200 'Mass flux calculation
    '
    area1! = 3.1415926# * .1 ^ 2 / 4!          'flow area Square meter
    area2! = 3.1415926# * .103 ^ 2 / 4!        'paper area m2
    '
    rhoc! = fnrho!(76!, 0!, 25!)               'Kg/m3
    '
    'Main stream
    '
    denair! = fnrho!(p1!, pd!, tr!)
    ratio! = (ra1! + ra2! * EXP(ra3! * flowr!)) * (ra4! * flowr! ^ 2 + ra5! * flowr! + ra6!) / (ra7! * flowr! + ra8!)
    VSCfM! = flowr! * SQR(rhoc! / denair!) * ratio!     'CFM
    VSCfM! = VSCfM! * 4.719474E-04                      'cubic meter/sec
    g! = VSCfM! * denair! / area1!                      'Kg/m2s
    IF g! <= 0 THEN
     CLS
     LOCATE 5, 12, 1, 7, 7
     PRINT " You have to check if main flow rate is ZERO "
     LOCATE 7, 12, 1, 7, 7
     PRINT " Press any key to continue ... ... "
210  IF INKEY$ = "" THEN 210
    END IF
    '
    'Through Flow stream
    '
    IF flowt! = 0 THEN
```

```
    cvv! = 1
    ELSE
     cvv! = cv1! + cv2! * LOG(cv3! + cv4! / (cv5! - flowt!))
    END IF
    psv! = -2.54 * pt1!
    drotair! = fnrho!(p1!, psv!, trot!)
    vscfmt! = flowt! * SQR(rhoc! / drotair!) * cvv!      'CFM
    vscfmt! = vscfmt! * 4.719474E-04                     'cubic meter/sec
    gt! = vscfmt! * drotair! / area1!                    'Kg/m2s
   '
   '
220 'Reynolds number calculation
    visair# = fnvis#(tj!)
    'D! = .0028: F! = 61 * (2.8 / 103) ^ 2
    REJ! = g! * .0028 / (61! * (2.8 / 100) ^ 2) / visair#
    '
    'Calculate the space before character channels
    '
    '
    'Select the sampling frequency
    '
    'Avoid division by zero error
    '
    IF bb = 0 THEN bb = 50
    IF g! <= 0 THEN
     g! = .5
     ttt$ = " G was ZERO "
    END IF
    '
225 samft! = g! * (tj! + 5) / SQR(bb)
    IF samft! <= 1.5 THEN
     samf! = 1
    ELSE
     IF samft! < 3 THEN
      samf! = 2
     ELSE
      IF samft! <= 6.5 THEN
       samf! = 5
      ELSE
       samf! = 10
      END IF
     END IF
    END IF
    '
    'calculate the Ts and Rs
    '
    GOSUB TsHs
    '
230 '
    'Display the variables entered
    CLS
    PRINT "   1  The Date is (mm/dd) ....."; a$
    PRINT "   2  The Run Number is ....."; B$
    PRINT "   3  The Ambient Temperature is ....."; tt!; "  C"
    PRINT "   4  The jet temperature is .....";
    PRINT USING "###.##"; tj!;
    PRINT "  C"
    PRINT "   5  The Temperature in the main Rotameter is ....."; tr!; "  C"
    PRINT "   6  The Barometric pressure is ....."; p1!; " cmHg"
    PRINT "   7  The main Rotameter reading is ....."; flowr!; "CFM"
    PRINT "   8  The Pressure in the main Rotameter is ....."; pd!; " cmHg"
    PRINT "   9  The paper back pressure is ....."; p2!; " cmM"
    PRINT "   10 The throgh flow rotameter reading is ....."; flowt!; "CFM"
    PRINT "   11 The vacuum at the Rotameter is ....."; pt1!; " inHg"
    PRINT "   12 The Basis Weight level is ....."; bb; " g/m2"
    PRINT "   13 The sampling freqency is fixed as....."; samf!; " Hz"
    PRINT "   14 The air temperature at suction rotameter .....";
    PRINT USING "###.##"; trot!;
    PRINT " Deg. C"
    PRINT "   15 The pressure transducer range is .....";
    IF pans$ = "h" OR pans$ = "H" THEN
     PRINT " high"
    ELSE
     PRINT " low"
    END IF
    '
    '
```

```
    LOCATE 16, 4, 1, 7, 7
    PRINT " Massflow flux is ....."; g!; "Kg/m2s"
    LOCATE 17, 4, 1, 7, 7
    PRINT " Jet Reynolds number is ....."; REJ!; "      "
    LOCATE 18, 4, 1, 7, 7
    PRINT " Through flow mass flux is ....."; gt!; "Kg/m2s"
    LOCATE 19, 4, 1, 7, 7
    PRINT " The suction to overal flowrate ratio is.....";
    PRINT USING "##.###"; gt! / g!

    'Edit the variables here if necessary
    '
240 LOCATE 23, 15, 1, 7, 7
    INPUT "Type c/r to accept or the number to edit"; pe%
    IF p1! <= 0 THEN
     pe% = 8
     LOCATE 18, 4, 1, 7, 7
     PRINT " THe Barometric pressure can not be ZERO "
    ELSE
    END IF
    '
    LOCATE 20, 4, 1, 7, 7
    IF pe% = 0 THEN ln% = 100: GOTO 250
    IF pe% = 1 THEN ln% = 1: GOTO 30
    IF pe% = 2 THEN ln% = 2: GOTO 40
    IF pe% = 3 THEN ln% = 3: GOTO 60
    IF pe% = 4 THEN ln% = 4: GOTO 140
    IF pe% = 5 THEN ln% = 5: GOTO 70
    IF pe% = 6 THEN ln% = 6: GOTO 110
    IF pe% = 7 THEN ln% = 7: GOTO 80
    IF pe% = 8 THEN ln% = 8: GOTO 90
    IF pe% = 9 THEN ln% = 9: GOTO 100
    IF pe% = 10 THEN ln% = 10: GOTO 120
    IF pe% = 11 THEN ln% = 11: GOTO 125
    IF pe% = 12 THEN ln% = 12: GOTO 130
    IF pe% = 13 THEN ln% = 13: GOTO 240
    IF pe% = 14 THEN ln% = 14: GOTO 140
    IF pe% = 15 THEN ln% = 15: GOTO 135
    '
    LOCATE 22, 15, 1, 7, 7
    PRINT " Wrong line number. Redo it !!!!!!!": GOTO 240
250 CLS
    LINE (100, 70)-(540, 150), , BF
    LINE (94, 68)-(544, 152), , B
    LOCATE 10, 20, 1, 7, 7
    PRINT " 1  Edit the input parameters"
    LOCATE 12, 20, 1, 7, 7
    PRINT " 2  Plot Temperature History "
    LOCATE 14, 20, 1, 7, 7
    PRINT " 3  Start Data Acquisation   "
    LOCATE 16, 20, 1, 7, 7
    PRINT " 4  End of experiments       "
    LOCATE 18, 20, 1, 7, 7
    INPUT " Option to choose is "; opt
    IF opt = 1 THEN
     GOTO 230
    ELSE
     IF opt = 2 THEN
      GOSUB Tplot
     ELSE
      IF opt = 3 THEN
       GOSUB Acq
      ELSE
       IF opt = 4 THEN
        GOTO 280
       ELSE
        GOTO 250
       END IF
      END IF
     END IF
    END IF
260 CLS
    LINE (100, 70)-(540, 160), , BF
    LINE (96, 68)-(544, 162), , B
    LOCATE 12, 20, 1, 7, 7
    INPUT " Save the data "; sav$
    IF sav$ = "y" OR sav$ = "Y" THEN GOSUB Savedata
```

```
   IF sav$ = "n" OR sav$ = "N" THEN 270
   LOCATE 13, 30, 1, 7, 7
   PRINT " Only Y/N ": GOTO 260
   '
   '
270 'Check for another run
   '
   '
   '
   LOCATE 18, 20, 1, 7, 7
   INPUT " Another acquisition (y/n) "; g$
    IF (g$ = "y" OR g$ = "Y" OR g$ = "") THEN 'Automatically increase run number by 1
     nnn = LEN(B$)
     IF nnn = 2 THEN
      T$ = RIGHT$(B$, 1)
      c$ = LEFT$(B$, 1)
      B$ = T$
      ccc = ASC(c$)
      bbb = ASC(B$)
       IF bbb = 57 THEN
        ccc = ccc + 1
        bbb = bbb - 9
        B$ = CHR$(ccc) + CHR$(bbb)
       ELSE
        B$ = CHR$(ccc) + CHR$(bbb + 1)
       END IF
      ELSE
       bbb = ASC(B$)
        IF bbb = 57 THEN
         ccc = ccc + 1
         bbb = bbb - 9
         B$ = CHR$(ccc) + CHR$(bbb)
        ELSE
         B$ = CHR$(bbb + 1)
        END IF
      END IF
      GOTO 230
     ELSE
      IF (g$ = "n" OR g$ = "N") THEN
       GOTO 280
      ELSE
       LOCATE 20, 30, 1, 7, 7
       PRINT "Only Y/N"
       GOTO 270
      END IF
     END IF
280  CLS
    LOCATE 12, 25, 1, 7, 7
    PRINT " Byebye. Have a nice time! "
    END                          'This is the end of this program
    '
    'subroutines
Acq:
    ' measuring air temperature at the rotameter
    '
288  CLS
    LINE (100, 70)-(540, 160), , BF
    LINE (94, 68)-(544, 162), , B
    '
    lik = 0
    'Wait for the signal to start data-acquisation
    '
    '
    bs$ = ""
    LOCATE 12, 20, 1, 7, 7
    PRINT " Switch toggle switch 1 to the I R  position"
    LOCATE 14, 20, 1, 7, 7
    PRINT " Swicth toggle switch 2 to the Paper position"
    LOCATE 16, 20, 1, 7, 7
    PRINT " press ENTER to start data-acquisation "

290  bs$ = INKEY$
    IF bs$ <> CHR$(13) THEN 290
    '
    '
    'Draw the frame of the graph
    '
```

```
CLS
IF tj! < 0 THEN tj! = 1
scaley!(1) = (INT((tj! - 1) / 20!) + 1) * 20!
scaley!(2) = (INT((g! - .01) * bb) + 1)
scaley!(3) = INT(SQR((tj! + 5) / 15) + .5) * .015
scaley!(4) = scaley!(3)
scalex! = 10! / 5! / samf!
'
LOCATE 20, 13, 1, 7, 7
FOR i = 1 TO 4
 PRINT "          ";
 PRINT "|";
NEXT i
 PRINT
 LOCATE 21, 11, 1, 7, 7
 PRINT "0 ";
FOR i = 1 TO 5
 PRINT "       ";
 PRINT USING "##.#"; i * scalex!;
NEXT i
FOR i = 1 TO 5
 l = i * 4
 LOCATE l, 12, 1, 7, 7
 PRINT "-"
 LOCATE l, 8, 1, 7, 7
 PRINT scaley!(1) - (i - 1) * scaley!(1) / 4!
 LOCATE l, 72, 1, 7, 7
 PRINT "-"
 LOCATE l, 73, 1, 7, 7
 PRINT USING "##.#"; scaley!(2) - (i - 1) * scaley!(2) / 4!
 LOCATE l, 7, 1, 7, 7
 PRINT "-"
 LOCATE l, 1, 1, 7, 7
 PRINT USING "#.###"; scaley!(3) - (i - 1) * scaley!(3) / 4!
NEXT i
LINE (46, 155)-(46, 27)
LINE (570, 155)-(90, 27), , B
LOCATE 23, 33, 1, 7, 7
PRINT " Time Elapsed (min) "
LOCATE 2, 7, 1, 7, 7
PRINT " .... T  (Deg C) "
LOCATE 23, 3, 1, 7, 7
PRINT "____ H Kg/Kg"
LOCATE 2, 69, 1, 7, 7
PRINT "_ _ _ P Kpa"
'
v = 90
FOR k = 1 TO 4
 w!(k) = 155
 y#(k) = 0
NEXT k
'
LOCATE 2, 23, 1, 7, 7
PRINT "Press ESC key to stop "; : PRINT ttt$
ttt$ = ""
'
'
CALL xinit
CALL xsecw(ecw)
lloop = 0
ans$ = ""
TIME$ = "00:00:00"
delayt! = TIMER
compt0! = -.005
compt1! = 1! / samf!
'
DO WHILE ans$ <> CHR$(27) AND lloop < 2799
'
lloop = lloop + 1
begint!(lloop) = TIMER
'
'
nloop% = 20! / samf!
 FOR channel = adcschan TO adcechan
  sum# = 0
  '
  FOR i = 1 TO nloop%
```

```
    CALL xav(channel, gain(channel), anolog.data)
    sum# = sum# + anolog.data
   NEXT i
  '
  data.value(channel, lloop) = sum# / nloop%
  '
 NEXT channel
 '
 'Draw the P, H , T curves vs real time
 '
 x! = TIMER / scalex! / 60! / 5! * 480! + 90
 '
 '
 'Temperature  Deg C
 '
 y#(1) = data.value(7, lloop) * factor!(7) + mvo!(7)
 y#(1) = tx0# + tx1# * y#(1) + tx2# * y#(1) ^ 2
 '
 '
 'Pressure Drop Kpa
 '
 y#(2) = data.value(8, lloop) * factor!(8) + mvo!(8)
 '
 'Humidity Kg/Kg Through Flow
 '
 y#(3) = a0# + a1# * data.value(6, lloop) + a2# * data.value(6, lloop) * data.value(6, lloop)
 y#(3) = y#(3) * (tr! + 273!) / 298! / p1! / rhoc! * 76! / 1000!   'kg/Kg
 '
 'Humidity Kg/Kg  Impingement Flow
 '
 '
 y#(4) = ai0# + ai1# * data.value(11, lloop) + ai2# * data.value(11, lloop) * data.value(11, lloop)
 y#(4) = y#(4) * (tj! + 273!) / 298! / p1! / rhoc! * 76! / 1000!   'kg/Kg
 '
 FOR i = 1 TO 4
  y#(i) = 156! - y#(i) * 128! / scaley!(i)
 NEXT i
 '
300  'Draw lines
 '
 LINE (v, w!(1))-(x!, y#(1)), , , &HAAAA
 LINE (v, w!(2))-(x!, y#(2)), , , &H3333
 LINE (v, w!(3))-(x!, y#(3)), , , &HFFFF
 LINE (v, w!(4))-(x!, y#(4)), , , &HFFFF
 '
 '
 v = x!
 FOR i = 1 TO 4
  w!(i) = y#(i)
 NEXT i
 '
 'Loop to delay
 '
 '
  compt! = begint!(lloop) + compt0! + compt1!
   DO UNTIL delayt! > compt!
   delayt! = TIMER
   LOOP
 '
 ans$ = INKEY$
 '
 LOOP
 samt! = TIMER
 '
 '
 CALL xgec(error.code)
 CALL xterm
 '
 '
 '
 CLS
 LINE (100, 70)-(540, 160), , BF
 LINE (96, 68)-(544, 162), , B
 LOCATE 12, 20, 1, 7, 7
 PRINT " Error-code  is "; error.code
 LOCATE 14, 20, 1, 7, 7
 PRINT " Acquisition completed "
```

```
'
   LOCATE 16, 20, 1, 7, 7
   PRINT " press any key to continue "
310  IF INKEY$ = "" THEN 310
   '
   '
   RETURN


Savedata:
   '
   llk = 1
   '


   LOCATE 14, 16, 1, 7, 7
   INPUT " The initial weight of paper sample (g) "; WI!
   LOCATE 15, 16, 1, 7, 7
   INPUT " The final weight of paper sample   (g) "; WF!
   '
330  LOCATE 16, 16, 1, 7, 7
   nump = nump + 1
   IF nump = 1 THEN
    INPUT " The file path (without slash) is  "; newp$
    transs$ = newp$
   ELSE
    PRINT " The file path (without slash) is  "; transs$;
    INPUT newp$
    IF LEFT$(newp$, 1) = "Y" OR LEFT$(newp$, 1) = "y" OR newp$ = "" THEN
     newp$ = transs$
    ELSE
    END IF
   END IF
   LOCATE 17, 16, 1, 7, 7
   IF nump = 1 THEN
    INPUT " The drive of the data file (A-C) is "; drv$
    transs1$ = drv$
   ELSE
    PRINT " The drive of the data file (A-C) is "; drv$;
    INPUT drv$
    IF drv$ = "" OR LEFT$(drv$, 1) = "y" OR LEFT$(drv$, 1) = "Y" THEN
     drv$ = transs1$
    ELSE
    END IF
   END IF
   drv$ = LEFT$(drv$, 1)
   '
   '
340  path1$ = drv$ + newp$
   '
   '
   '
   dd1$ = path1$ + "\r" + a$ + B$ + ".prn"
   dd2$ = path1$ + "\p" + a$ + B$ + ".prn"
   '
   '
   '
350  CLS
   LINE (100, 70)-(540, 160), , BF
   LINE (96, 68)-(544, 162), , B
   LOCATE 12, 20, 1, 7, 7
   PRINT " Are you sure to save the raw data to file "
   LOCATE 14, 15, 1, 7, 7
   PRINT " "; dd1$;
   INPUT "  Y/N"; fl$
    IF (fl$ = "y" OR fl$ = "Y" OR fl$ = "") THEN 370
360   LOCATE 16, 15, 1, 7, 7
    INPUT " Input the new filename (must without .ext) "; main1$
    LOCATE 17, 15, 1, 7, 7
    INPUT " Input the drive for the abve filename "; drv1$
    drv1$ = LEFT$(drv1$, 1) + ":"
    dd1$ = drv1$ + main1$ + ".prn"
    GOTO 350
    '
370  CLS
   LINE (100, 70)-(540, 160), , BF
   LINE (96, 68)-(544, 162), , B
   '
```

```
'open file #1
'
'
380 OPEN dd1$ FOR OUTPUT AS #1
'
'
LOCATE 10, 20, 1, 7, 7
PRINT " Saving the raw experimental data "
'
'saving the experimental conditions
'
WRITE #1, " The experimental conditions are:"
WRITE #1, "1  The Date is (mm/dd) .....", "", "", "", "", "", "", "", a$
WRITE #1, "2  The Run Number is .....", "", "", "", "", "", "", "", B$
WRITE #1, "3  The IR Calibration Coefficient A0 is .....", "", "", "", "", "", "", "", a0#
WRITE #1, "4  The IR Calibration Coefficient A1 is .....", "", "", "", "", "", "", "", a1#
WRITE #1, "5  The IR Calibration Coefficient A2 is .....", "", "", "", "", "", "", "", a2#
WRITE #1, "5r The R square of IR calibration    is .....", "", "", "", "", "", "", "", rsq!
WRITE #1, "3i The Ir Calibration Coefficient Ai0 is .....", "", "", "", "", "", "", "", ai0#
WRITE #1, "4i The Ir Calibration Coefficient Ai1 is .....", "", "", "", "", "", "", "", ai1#
WRITE #1, "5i The Ir Calibration Coefficient Ai2 is .....", "", "", "", "", "", "", "", ai2#
WRITE #1, "5r The R square of IR calibration    is .....", "", "", "", "", "", "", "", rsqi!
WRITE #1, "6  The Ambient Temperature is .....", "", "", "", "", "", "", "", tt!, "  C"
WRITE #1, "7  The jet temperature is .....", "", "", "", "", "", "", "", tj!, "  mv"
WRITE #1, "8  The Temperature in the main Rotameter is .....", "", "", "", "", "", "", "", tr!, "  C"
WRITE #1, "9  The main rotameter reading is .....", "", "", "", "", "", "", "", flowr!, "CFM"
WRITE #1, "9t The through flow rotameter reading is .....", "", "", "", "", "", "", "", flowt!, "CFM"
WRITE #1, "9v The vacuum at the rotameter is .....", "", "", "", "", "", "", "", pt1!, "in Hg"
WRITE #1, "10 The Barometric pressure is .....", "", "", "", "", "", "", "", p1!, " cmHg"
WRITE #1, "11 The Pressure in the Rotameter is .....", "", "", "", "", "", "", "", pd!, " cmHg"
WRITE #1, "12 The paper back pressure is .....", "", "", "", "", "", "", "", p2!, " cmM"
WRITE #1, "13 The start channel number is .....", "", "", "", "", "", "", "", adcschan
WRITE #1, "14 The End Channel Number is .....", "", "", "", "", "", "", "", adcechan
WRITE #1, "15 The sampling freqency is .....", "", "", "", "", "", "", "", samfl, " Hz"
WRITE #1, "16 The temperature at suction rotameter is .....", "", "", "", "", "", "", "", trot!, " Deg. C"
WRITE #1,
WRITE #1, " The Massflow flux is .....", "", "", "", "", "", "", "", g!, "Kg/m2s"
WRITE #1, " The Through Flow Mass flux is .....", "", "", "", "", "", "", "", gt!, "Kg/m2s"
WRITE #1, " The jet Reynolds number is .....", "", "", "", "", "", "", "", REJ!
PRINT #1,
WRITE #1, "Wini=", WI!, " g"
WRITE #1, "Wfin=", WF!, " g"
WRITE #1, "Tacq=", samt!, " S"
WRITE #1, "Ts=", ts!, " Deg C"
WRITE #1, "Rs=", Rs!, "Kg/m2h"
PRINT #1,
PRINT #1,
WRITE #1, "....."
WRITE #1, " Raw Data of file ", "", "", "", dd1$
WRITE #1, " ", " ", " ", " ", " ", " ", " Channels"
WRITE #1, " Time (s)  "
PRINT #1, "time",
 FOR i = adcschan TO adcechan
  PRINT #1, i,
 NEXT i
PRINT #1,
WRITE #1, "....."
'
'
'
FOR i = 1 TO lloop
PRINT #1, USING "###.##"; begint!(i);
 FOR channel = adcschan TO adcechan
 PRINT #1, USING "#####.#"; data.value(channel, i);
 NEXT channel
 PRINT #1,
NEXT i
'
'
LOCATE 12, 20, 1, 7, 7
PRINT " Data successfully saved! "
'
 CLOSE #1
'
385 'check for data processing
'
LOCATE 14, 20, 1, 7, 7
```

```
   INPUT " Processing the raw data "; sms$
   IF sms$ = "y" OR sms$ = "Y" OR sms$ = "" THEN 390
   IF sms$ = "n" OR sms$ = "N" THEN 430
   LOCATE 15, 30, 1, 7, 7
   PRINT " Only Y/N ": GOTO 385
   '
   '
390 CLS
   LINE (100, 70)-(540, 160), , BF
   LINE (96, 68)-(544, 162), , B
   LOCATE 12, 16, 1, 7, 7
   PRINT " Are you sure to save the processed data to file "
   LOCATE 14, 15, 1, 7, 7
   PRINT " "; dd2$;
   INPUT "  Y/N"; FLI$
   IF (FLI$ = "y" OR FLI$ = "Y" OR FLI$ = "") THEN 410
400  LOCATE 16, 15, 1, 7, 7
   INPUT " Input the new filename (must without .ext) "; main1$
   LOCATE 18, 15, 1, 7, 7
   INPUT " Input the drive for the above filename "; drv1$
   drv1$ = LEFT$(drv1$, 1) + ":"
   dd2$ = drv1$ + main1$ + ".prn"
   GOTO 390
   '
   '
   '
410 CLS
   LINE (100, 70)-(540, 160), , BF
   LINE (96, 68)-(544, 162), , B
   '
   'Processing the data
   llk = 2
   '
420 OPEN dd2$ FOR OUTPUT AS #2
   WRITE #2, " This is the processed data from "
   WRITE #2, dd1$
   WRITE #2, "Rej=", REJ!
   WRITE #2, " Tj= ", tj!
   WRITE #2, " G= ", g!
   WRITE #2, " Ts= ", ts!
   WRITE #2, " Rs= ", Rs!
   WRITE #2, " Gt= ", gt!
   WRITE #2, " Gi= ", g! - gt!

   '
   LOCATE 16, 20, 1, 7, 7
   PRINT " Processing the data while saving "
   PRINT #2,
   WRITE #2, " Time (s)", "T5", "T7", "T9", "T10", "T12", "T13", "P8", "Dair!", "Viss!", "His", "Hts", "H(im)", "R(im)", "H(T)", "R(T)"
   PRINT #2,
   '
   FOR channel = adcschan TO adcechan
    sssr!(channel) = 0
   NEXT channel
   '
   te! = y#(1)
   FOR i = 1 TO lloop
    PRINT #2, USING "###.##"; begint!(i);
    FOR channel = adcschan TO adcechan
     sssr!(channel) = data.value(channel, i)
     IF sssr!(channel) < 0 THEN sssr!(channel) = 0
     IF channel = 11 THEN            ' Impingement flow
      hhei# = ai0# + ai1# * sssr!(channel) + ai2# * sssr!(channel) * sssr!(channel)
     ELSE
      IF channel = 8 THEN
       ppp# = sssr!(channel) * factor!(channel) + mvo!(channel)
       pdair! = -ppp# / 101.33 * 76! / 2! + p2! * 2.95 / 13.6
      ELSE
       IF channel = 6 THEN         ' Through flow
        hhc# = a0# + a1# * sssr!(channel) + a2# * sssr!(channel) * sssr!(channel)
       ELSE
        sssr! = sssr!(channel) * factor!(channel) + mvo!(channel)
        sssr! = tx0# + tx1# * sssr! + tx2# * sssr! ^ 2
        IF channel = 7 THEN
         te! = sssr!
         tdair! = (tj! + te!) / 2!
        ELSE
```

```
          IF channel = 5 THEN
           tej! = sssr!
          ELSE
           IF channel = 12 THEN
            tet! = sssr!
           ELSE
           END IF
          END IF
         END IF
        PRINT #2, USING "####.##"; sssr!;
       END IF
      END IF
     END IF
    NEXT channel
'
hhci# = hhci# * (tej! + 273!) / 298! / p1! / rhoc! * 76! / 1000! 'kg/Kg
rri! = hhci# * (g! - gt!) * 3600! * area1! / area2!
hhc# = hhc# * (tet! + 273!) / 298! / (p1! + p2! * 2.95 / 13.6 / 4! - ppp# / 101.33 * 76) / rhoc! * 76! / 1000! 'kg/Kg
rr! = hhc# * g! * 3600! * area1! / area2!
'
'calculate air density
'
dairr! = fnrho!(p1!, pdair!, tdair!)
'
'calculate viscosity of air and water vapor mixture
'
mvis!(2) = fnvis#(tdair!) * 1000000!
mvis!(1) = .355 * mvis!(2)
ymole!(1) = hhc# / mw!(1)
ymole!(1) = ymole!(1) / (1! / mw!(2) + ymole!(1))
ymole!(2) = 1! - ymole!(1)
Viss! = 0
FOR I = 1 TO 2
 sigma! = 0
 FOR j = 1 TO 2
  sigma! = sigma! + ymole!(j) * fai!(I, j)
 NEXT j
 Viss! = Viss! + ymole!(I) * mvis!(I) / sigma!
NEXT I
'
'calculate through exhaust absolute humidity
'
hhts# = h#(0)
FOR ki = 1 TO 3
 hhts# = hhts# + h#(ki) * te! ^ ki
NEXT ki
'
'calculate impingement absolute humidity
'
'
hhis# = h#(0)
FOR ik = 1 TO 3
 hhis# = hhis# + h#(ik) * tex! ^ ik
NEXT ik
PRINT #2, USING "####.##"; ppp#;
PRINT #2, USING "###.####"; dairr!;
PRINT #2, USING "####.###"; Viss!;
PRINT #2, USING "###.#####"; hhis#;
PRINT #2, USING "###.#####"; hhts#;
PRINT #2, USING "###.#####"; hhci#;
PRINT #2, USING "###.##"; rri!;
PRINT #2, USING "###.#####"; hhc#;
PRINT #2, USING "###.##"; rr!;
PRINT #2,
NEXT i
'
CLOSE #2
'
'
430  RETURN 270
'
TsHs:
'This is the subroutin for calculating Ts and Rs
'
'
lm0! = 1075.18
lm1! = -1.01816
```

```
    cc0! = .24 * 1.8
    cc1! = .44 * 1.8
    '
    hhn0# = hh0# * (tt! + 273!) / 298! / p1! / rhoc! * 76! / 1000!    'kg/Kg'
    '
    calp1! = cc1! + lm1!
    calp2! = lm0! - cc1! * tj!
    '
    IF tj! < 18 THEN
     ts! = 5.5
     GOTO 460
    END IF
    '
    ts! = tj! * .5
    dift! = -.005
450  ts! = ts! + dift!
     comlh# = hhn0# * lm0! + cc0! * tj! - h#(0) * calp2!
     comrh# = ts! * (cc0! - hhn0# * lm1!)
     FOR i = 1 TO 4
      comrh# = comrh# + ts! ^ i * (h#(i - 1) * calp1! + h#(i) * calp2!)
     NEXT i
     comrl# = comlh# - comrh#
     IF tj! < 19.2 THEN
      dift! = -.005
     ELSE
      dc! = ABS(comrl# / comlh#)
      dift! = -5 * dc!
     END IF
     IF ABS(comrl#) > .0005 * ABS(comlh#) THEN 450
460  hhs# = h#(0)
     FOR i = 1 TO 3
      hhs# = hhs# + h#(i) * ts! ^ i
     NEXT i
     hhs# = hhs# + (cc0! + cc1! * hhs#) * (tj! - ts!) / (lm0! + lm1! * ts!) + hhn0#
     hhs# = hhs# / 2!
     Rs! = 3600! * g! * hhs# * area1! / area2!
     RETURN
     '
ErrorProc:
     '
     'Error recovery subroutine
     '
     CLS
     LINE (120, 30)-(440, 90), , BF
     LOCATE 5, 30, 1, 7, 7
     BEEP
     PRINT "  ERROR  "
     LOCATE 7, 20, 1, 7, 7
     PRINT " Press any key to continue ... ..."
500  IF INKEY$ = "" THEN 500
     CLS
     LOCATE 12, 20, 1, 7, 7
     '
     SELECT CASE ERR
      CASE 76:
       PRINT " Path not found , retry "
       IF sst = 999 THEN RESUME 530
       RESUME 330
      CASE 53
       PRINT " File not found , retry "
       RESUME 17
      CASE 61:
       PRINT " Disk Full, change another disk "
       LOCATE 13, 20, 1, 7, 7
       PRINT " Press any key to continue ... ..."
510    IF INKEY$ = "" THEN 510
       IF llk = 1 THEN RESUME 380
       IF llk = 2 THEN RESUME 420
      CASE 71:
       PRINT " Disk drive not ready "
       LOCATE 13, 20, 1, 7, 7
       PRINT " Press any key to continue ... ..."
520    IF INKEY$ = "" THEN 520
       RESUME
      CASE ELSE:
       'disable error trapping and
       'print standard system message
```

```
    ON ERROR GOTO 0
   END SELECT
   '
Tplot:
   '
   'Temperature history ploting subroutine
   '
   CLS
   sst = 0
   LOCATE 12, 20, 1, 7, 7
   INPUT " Do you want to save the Temperature History "; tan$
   IF tan$ = "y" OR tan$ = "Y" THEN
    CLS
    sst = 999
530  LOCATE 12, 20, 1, 7, 7
    INPUT " The filename is "; tfile$
    OPEN tfile$ FOR OUTPUT AS #1
   ELSE
   END IF
   CLS
   LOCATE 20, 13, 1, 7, 7
   FOR i = 1 TO 4
    PRINT "          ";
    PRINT "|";
   NEXT i
   PRINT
   LOCATE 21, 11, 1, 7, 7
   PRINT "0   ";
   FOR i = 1 TO 5
    PRINT "       ";
    PRINT i * 5;
   NEXT i
   FOR i = 1 TO 4
   l = i * 4
    LOCATE l, 12, 1, 7, 7
    PRINT "-"
    LOCATE l, 8, 1, 7, 7
    PRINT 120 - (i - 1) * 30
   NEXT i
   LINE (570, 156)-(90, 27), , B
   LOCATE 23, 33, 1, 7, 7
   PRINT " Time Elapsed  (min) "
   LOCATE 2, 3, 1, 7, 7
   PRINT "Temperature   ";
   PRINT "Deg C"
   v = 90
   FOR i = 1 TO 6
    w!(i) = 156
   NEXT i
   TIME$ = "00:00:00"
   c$ = ""
   DO WHILE c$ = ""
    c$ = INKEY$
    dd! = TIMER + 3.11
    delay! = 0

     DO UNTIL delay! > 0 OR c$ <> ""
     delay! = TIMER - dd!
     LOOP

    x! = TIMER / 25! / 60! * 480!
    x! = x! + 90
   IF sst = 999 THEN
    PRINT #1, timer$;
   END IF
    FOR tchannel = 1 TO 6
    IF tchannel = 1 THEN channel = 5
    IF tchannel = 2 THEN channel = 7
    IF tchannel = 3 THEN channel = 9
    IF tchannel = 4 THEN channel = 10
    IF tchannel = 5 THEN channel = 12
    IF tchannel = 6 THEN channel = 13
    sum# = 0
     FOR li = 1 TO 20
      CALL xav(channel, gain(channel), anolog.data)
      sum# = sum# + anolog.data / 20#
     NEXT li
```

```
 tj2! = sum#
 tj2! = tj2! * factor!(channel) + mvo!(channel)
 tj2! = tx0# + tx1# * tj2! + tx2# * tj2! ^ 2
 yy!(tchannel) = tj2!
 IF sst = 999 THEN PRINT #1, USING "###.#"; tj2!;
 NEXT tchannel
IF sst = 999 THEN PRINT #1,
FOR i = 1 TO 6
l = 15 + i * 9
LOCATE 3, l, 1, 7, 7
PRINT USING "###.#"; yy!(i)
NEXT i
FOR i = 1 TO 6
 yy!(i) = 156 - yy!(i) * 128! / 120!
 LINE (v, w!(i))-(x!, yy!(i))
 v = x!
 w!(i) = yy!(i)
NEXT i
LOOP
CALL xterm
IF sst = 999 THEN CLOSE #1
RETURN 140
```

Appendix B Experimental procedure

Preparation of test sheets

Handsheets of all basis weight were prepared from dry, unbleached, unbeaten laboratory kraft pulp, 100% black spruce, according to CPPA Standard C.4. Freshly made handsheets were stacked in turn with thin plastic sheets and sealed in a plastic bag. Then they were stored in a refrigerator for later drying experiments.

Calibration of the IR-Analyzer as a moisture meter

During IR calibration, air is circulated continuously until equilibrium is attained in a closed system which consists of the measuring chamber of the IR analyzer, the saturated salt solution container, the dew point meter and a circulation fan. The signals from IR absorbance and from the dew point meter were acquired by computer. Dew point reading was converted to humidity according to the humidification table given by Dean (1985a). A secondary polynomial correlation of humidity with absorbance was then obtained as a calibration curve using Lotus123.

The salt solutions and their relative humidities used in the calibration runs are listed in Table B.1. Equilibrium relative humidity is a strong function of ambient temperature for some salt solutions. The humidity of the dry compressed air and ambient air were also measured by the dew point meter and used for calibration purposes.

Table B.1 Salt solutions and their relative humidities at 20 °C used for IR calibration (Dean 1985a)

Solid phase	Relative humidity, %
$LiCl \cdot H_2O$	12.0
$CH_3COOK \cdot 1.5H_2O$	23.0
$MgCl_2 \cdot 6H_2O$	33.0
$Mg(NO_3)_2 \cdot 6H_2O$	55.0
NaCl	75.7
KBr	84.0
KNO_3	93.0
K_2SO_4	97.0

Drying experiments

1) Open the main compressed air line and adjust the air flow rate to the desired value, meanwhile monitor the humidity of the dry air both by the IR analyzer and, for calibration purposes, by the dew point meter.

2) Connect the measuring chamber of the IR analyzer(s) to the calibration system, and follow the calibration procedure described above.

3) Upon the completion of the calibration runs, reconnect the measuring chamber of the IR analyzer to the drying apparatus with two T-valves.

4) Turn on the vacuum pump for warm up if CITAD experiments are to be conducted.

5) Run data acquisition program and adjust the air heater controls to the desired inlet air temperature, monitor the air temperature with the on-line screen display of temperature reading and fine tune the heater controls as required.

6) For CITAD experiments, set the vacuum value upstream of the critical flow valve to achieve a stable through flow rate by adjusting the load share of the two vacuum regulators. Adjust the vacuum gage reading and that from the rotameter to obtain a desired through flow rate. Once it's done, shut the ball valve on the inlet line of vacuum pump to protect the pump from oil flooding.

7) Cut the 103mm diameter test sheet for the sample holder from a 160mm diameter handsheet using a specifically designed stainless steel punch. Place the test sheet into the sample holder described in chapter 3, and secure it in place with the six screws of the sample holder to prevent any air by-passing. Add water to the wet sheet if higher moisture content is desired using a spray can.

8) Open the through flow line for CITAD experiments. Start the data acquisition to monitor the drying conditions prior to the experiment.

9) After 10-30 seconds, weigh the sample holder - sheet assembly on a top-loading electronic balance then insert it immediately into the drying chamber.

10) Upon the completion of the experiment judged from the on-line screen drying history display, stop the data-acquisition, pull out the sample and weigh the

sample holder - sheet assembly again. Immediately shut the vacuum line for CITAD experiments.

11) Save the acquired digital data.

12) Convert the digital data into temperature, pressure and humidity readings and calculate the drying rate, moisture content of paper sheet.

13) Remove the paper from the sample holder and placed it into a 104°C oven for at least 8 hours prior to obtaining the bone dry weight for basis weight, initial and final moisture content determination.

14) Check mass balance from the IR humidity measurement against that of the electronic balance. Any experiment with error of mass balance higher than 5% was rejected for further data processing.

15) Further process the data from the successful experiments using Lotus 123 for windows as well as SYSTAT for windows if necessary. The graphical output was prepared by Freelance Presentation for Windows and printed out from HP Laser Jet IV.

Appendix C Variables used in drying time and drying rate prediction for CITAD process

Case / Variable	Figure 6.29				Figure 6.30			
	(a)	(b)	(c)	(d)	(a)	(b)	(c)	(d)
G, kg/m^{2}s	1.02	1.02	1.02	1.02	1.46	1.46	1.47	1.46
T_j, °C	92.7	91.0	88.3	90.8	91.9	88.9	90.0	87.6
q_T, %	10.2	10.2	10.2	10.2	6.9	7.1	16.5	16.6
B, g/m^2	25.0	34.6	46.7	83.3	23.0	48.7	24.7	48.1
X_o, kg/kg	3.40	3.41	3.84	2.78	2.53	2.97	3.05	2.90
G_I, kg/m^{2}s	0.916	0.916	0.916	0.916	1.36	1.36	1.23	1.22
G_T, kg/m^{2}s	0.104	0.104	0.104	0.104	0.101	0.104	0.243	0.242
R_{Ic}, kg/m^{2}h	16.2	15.8	15.4	15.8	21.5	20.7	17.6	17.1
X_c, kg/kg	1.69	1.71	1.74	1.58	1.62	1.66	1.65	1.60
n_I	1.35	1.44	1.58	1.96	1.28	1.50	1.42	1.73
R_{Tc}, kg/m^{2}h	8.94	8.75	8.57	8.81	8.68	8.55	19.9	22.1
X_{Ti}, kg/kg	2.57	2.79	3.28	2.03	1.43	2.14	2.31	2.32
n_{Ti}	0.69	0.82	2.06	1.83	-1.11	0.86	0.76	0.92
X_m, kg/kg	1.37	1.29	1.30	0.97	1.17	1.10	1.29	1.10
R_{Tm}, kg/m^{2}h	9.53	9.75	9.80	11.3	9.68	10.3	21.1	24.6
C	0.36	0.43	0.27	0.84	0.74	0.72	0.79	1.08
$R_{0.05}$, kg/m^{2}h	0.82	0.84	0.76	1.24	1.10	1.08	1.95	2.61
$t_{0.05}$, s	25.1	34.9	53.4	64.4	16.0	37.6	12.9	21.0

Appendix D Error analysis

Total rms error is expressed as $\delta f = \left[\sum_{i=1}^{n}\left(\frac{\partial f}{\partial x_i}\delta x_i\right)^2\right]^{\frac{1}{2}}$

1) Basis weight:

$$B = \frac{4W}{\pi D^2}$$

with W the bone dry weight
D the sheet diameter.

$$\frac{\delta B}{B} = \left[\left(\frac{\partial B}{\partial W}\frac{\delta W}{B}\right)^2 + \left(\frac{\partial B}{\partial D}\frac{\delta D}{B}\right)^2\right]^{\frac{1}{2}} = \left[\left(\frac{\delta W}{W}\right)^2 + \left(-\frac{2\delta D}{D}\right)^2\right]^{\frac{1}{2}}$$

As $\delta W = 0.0005$g, $W > 0.21$ g
$\delta D = 0.0005$m, $D = 0.103$ m

Hence $\frac{\delta B}{B} < 1\%$

2) Inlet air mass flow rate:

$G = \rho V / A$

and $\rho = \frac{P M}{R T}$, $V = V_s\sqrt{\frac{\rho_s}{\rho}}$

so $G = \frac{V_s\sqrt{\rho_s}}{A}\sqrt{\frac{PM}{RT}}$

with
- ρ air density
- ρ_s air density at standard conditions, constant
- V volumetric flow rate from rotameter
- V_s volumetric flow rate from rotameter at standard conditions
- A cross section area of drying chamber, constant
- P absolute pressure at rotameter
- M air molecule weight, constant
- T air temperature at rotameter

$$\frac{\delta G}{G} = \left[\left(\frac{\partial G}{\partial P}\frac{\delta P}{G}\right)^2 + \left(\frac{\partial G}{\partial V_s}\frac{\delta V_s}{G}\right)^2 + \left(\frac{\partial G}{\partial T}\frac{\delta T}{G}\right)^2\right]^{\frac{1}{2}}$$

$$\frac{\delta G}{G} = \left[\left(\frac{\delta P}{2P} \right)^2 + \left(\frac{\delta V_s}{V_s} \right)^2 + \left(- \frac{\delta T}{2T} \right)^2 \right]^{\frac{1}{2}}$$

as $\delta P = 0.13$ kPa, $P > 101$ kPa
$\delta T = 0.5$ K, $T > 290$ K
$\delta V_s / V_s < 0.7\%$ from calibration

Hence $\frac{\delta G}{G} < 0.8\%$

3) Through flow rate of CITAD:

Similarly for through flow mass flow rate of CITAD, G_T:

$$G_T = \frac{V_{Ts} \sqrt{\rho_s}}{A} \sqrt{\frac{P_T M}{R T_T}}$$

with
- V_{Ts} volumetric flow rate from rotameter at standard conditions
- ρ_s air density at standard conditions, constant
- A cross section area of drying chamber, constant
- P_T absolute pressure at rotameter on through flow exhaust line
- M air molecule weight, constant
- T_T air temperature at rotameter on through flow exhaust line

$$\frac{\delta G_T}{G_T} = \left[\left(\frac{\partial G_T}{\partial P_T} \frac{\delta P_T}{G_T} \right)^2 + \left(\frac{\partial G_T}{\partial V_{Ts}} \frac{\delta V_{Ts}}{G_T} \right)^2 + \left(\frac{\partial G_T}{\partial T_T} \frac{\delta T_T}{G_T} \right)^2 \right]^{\frac{1}{2}}$$

$$= \left[\left(\frac{\delta P_T}{2P_T} \right)^2 + \left(\frac{\delta V_{Ts}}{V_{Ts}} \right)^2 + \left(- \frac{\delta T_T}{2T_T} \right)^2 \right]^{\frac{1}{2}}$$

as $\delta P_T < 0.5$ kPa, $P_T > 35$ kPa
$\delta T_T < 2$ K
$T_T > 280$ K
$\delta V_{Ts} / V_{Ts} < 0.8\%$ from calibration

Hence $\frac{\delta G_T}{G_T} < 1.2\%$

4) Impingement flow rate:

$$G_I = G - G_T$$

$$\frac{\delta G_I}{G_I} = \left[\left(\frac{\partial G_I}{\partial G} \frac{\delta G}{G_I} \right)^2 + \left(\frac{\partial G_I}{\partial G_T} \frac{\delta G_T}{G_I} \right)^2 \right]^{\frac{1}{2}}$$

$$\frac{\delta G_I}{G_I} = \left[\left(\frac{\delta G}{G} \right)^2 \frac{1}{(1-q_T)^2} + \left(- \frac{\delta G_T}{G_T} \right)^2 \left(\frac{q_T}{1-q_T} \right)^2 \right]^{\frac{1}{2}}$$

with q_T the through flow ratio, G_T/G

as $\frac{\delta G}{G} < 0.8\%$

$\frac{\delta G_T}{G_T} < 1.2\%$

<u>For the 3 runs with q_T=0.83</u>

$\frac{\delta G_I}{G_I} < 7.5\%$

For all other CITAD experiments q_T<0.75

Hence $\frac{\delta G_I}{G_I} < 4.9\%$

5) Constant drying rate:

$R_c = 3600\ G\ (Y_e - Y_i) = 3600\ G\ \Delta Y$

with G as the flow rate
Y_e exhaust air humidity
Y_i inlet air humidity

$$\frac{\delta R_c}{R_c} = \left[\left(\frac{\partial R_c}{\partial G} \frac{\delta G}{R_c} \right)^2 + \left(\frac{\partial R_c}{\partial \Delta Y} \frac{\delta \Delta Y}{R_c} \right)^2 \right]^{\frac{1}{2}} = \left[\left(\frac{\delta G}{G} \right)^2 + \left(\frac{\delta \Delta Y}{\Delta Y} \right)^2 \right]^{\frac{1}{2}}$$

as $\frac{\delta G}{G} < 0.8\%$ and

<u>For pure impingement drying,</u>

$\delta\Delta Y$<0.0001 kg/kg air and ΔY>0.002 kg/kg air

Hence $\frac{\delta R_c}{R_c} < 5.1\%$

<u>For pure through drying,</u>

$\delta\Delta Y$<0.0001 kg/kg air and ΔY>0.006 kg/kg air

Hence $\frac{\delta R_c}{R_c} < 1.8\%$

6) Constant water removal rate from impingement exhaust:

$R_{Ic}=3600G_I(Y_{Ie}-Y_i)=3600G_I\Delta Y_I$

$$\frac{\delta R_{Tc}}{R_{Tc}}=\left[\left(\frac{\partial R_{Tc}}{\partial G_T}\frac{\delta G_T}{R_{Tc}}\right)^2+\left(\frac{\partial R_{Tc}}{\partial \Delta Y_T}\frac{\delta \Delta Y_T}{R_{Tc}}\right)^2\right]^{\frac{1}{2}}=\left[\left(\frac{\delta G_T}{G_T}\right)^2+\left(\frac{\delta \Delta Y_T}{\Delta Y_T}\right)^2\right]^{\frac{1}{2}}$$

as $\frac{\delta G_I}{G_I} < 4.8\%$

$\delta\Delta Y_I<0.0001$ kg/kg air and

For ambient air at q_T=75%,

$\Delta Y_I\approx0.0005$ kg/kg air

$\frac{\delta R_{Ic}}{R_{Ic}}$ can be up to 21%.

For conditions with T_j of 90 °C

$\Delta Y_I>0.002$ kg/kg air

Hence $\frac{\delta R_{Ic}}{R_{Ic}} < 7\%$

7) Constant water removal rate from through flow exhaust:

$R_{Tc}=3600G_T(Y_{Te}-Y_i)=3600G_T\Delta Y_T$

$$\frac{\delta R_{Tc}}{R_{Tc}}=\left[\left(\frac{\partial R_{Tc}}{\partial G_T}\frac{\delta G_T}{R_{Tc}}\right)^2+\left(\frac{\partial R_{Tc}}{\partial \Delta Y_T}\frac{\delta \Delta Y_T}{R_{Tc}}\right)^2\right]^{\frac{1}{2}}=\left[\left(\frac{\delta G_T}{G_T}\right)^2+\left(\frac{\delta \Delta Y_T}{\Delta Y_T}\right)^2\right]^{\frac{1}{2}}$$

as $\frac{\delta G_T}{G_T} < 1.2\%$

$\delta\Delta Y_T<0.0001$ kg/kg air and $\Delta Y_T>0.006$ kg/kg air

Hence $\frac{\delta R_{Tc}}{R_{Tc}} < 2.1\%$

E1: Experimental conditions and important data for pure impingement drying

Nozzle set	d	f	H/d	G	B	Tj	Twb	Re	Xo	Xc	Rc	n
1	2.38	0.031	5	0.125	25.6	23.6	8.10	525	2.62	0.99	1.42	1.03
1	2.38	0.031	5	0.125	48.7	22.0	7.29	525	1.85	1.01	1.36	0.87
1	2.38	0.031	5	0.125	49.5	21.9	7.35	525	1.86	0.93	1.31	0.93
1	2.38	0.031	5	0.125	50.1	21.9	7.27	525	1.39	0.86	1.33	0.98
1	2.38	0.031	5	0.125	51.0	21.9	7.35	525	0.268	.	.	.
1	2.38	0.031	5	0.232	50.4	21.9	7.28	975	1.87	0.99	2.02	0.95
1	2.38	0.031	5	0.386	48.6	21.9	7.28	1620	2.08	1.10	2.85	0.73
1	2.38	0.031	5	0.386	49.3	21.9	7.28	1620	2.11	1.08	2.78	0.98
1	2.38	0.031	5	0.502	25.2	22.8	7.72	2110	2.90	1.15	3.57	0.97
1	2.38	0.031	5	0.502	25.6	22.9	7.79	2110	2.40	0.99	3.43	0.96
1	2.38	0.031	5	0.507	46.0	24.4	7.80	2130	2.63	1.27	3.77	0.88
1	2.38	0.031	5	0.507	47.1	24.4	7.80	2130	2.93	1.31	3.71	0.90
1	2.38	0.031	5	0.546	49.0	21.8	7.28	2300	1.95	1.02	3.46	0.98
1	2.38	0.031	5	0.547	45.9	21.9	7.27	2300	1.78	0.96	3.36	0.87
1	2.38	0.031	5	0.786	49.9	21.8	7.24	3300	2.08	1.26	4.47	0.68
1	2.38	0.031	5	1.03	49.9	21.7	7.23	4320	2.01	1.08	5.00	1.00
1	2.38	0.031	5	1.19	47.2	24.4	7.80	5010	2.30	1.42	5.94	0.76
1	2.38	0.031	5	1.19	48.1	24.4	7.80	5010	2.68	1.39	6.05	0.81
1	2.38	0.031	5	1.19	49.9	22.1	7.30	5010	1.37	.	.	.
1	2.38	0.031	5	1.19	50.9	21.9	7.29	5010	2.10	1.17	5.35	0.92
1	2.38	0.031	5	1.46	48.4	22.5	7.50	6150	1.96	1.34	6.44	0.86
1	2.38	0.031	5	1.47	46.0	21.7	7.23	6170	1.96	1.15	5.78	0.81
1	2.38	0.031	5	0.126	45.3	45.6	17.4	498	1.82	0.97	2.40	0.97
1	2.38	0.031	5	0.126	49.9	45.4	17.2	498	1.51	0.91	2.42	0.99
1	2.38	0.031	5	0.547	49.9	45.8	17.4	2170	2.19	1.11	6.49	0.98
1	2.38	0.031	5	1.03	48.7	45.4	17.3	4070	2.36	1.27	9.73	0.88
1	2.38	0.031	5	1.47	51.7	45.2	17.2	5820	1.84	1.33	11.7	0.83
1	2.38	0.031	5	0.125	52.2	66.2	24.0	474	1.94	1.01	3.50	0.99
1	2.38	0.031	5	0.543	48.0	65.7	23.7	2060	2.06	1.27	9.56	0.92
1	2.38	0.031	5	0.543	50.1	65.7	23.7	2060	2.52	1.23	9.25	0.91
1	2.38	0.031	5	1.03	50.8	65.5	23.6	3890	1.99	1.35	14.6	0.81
1	2.38	0.031	5	1.47	50.5	66.6	23.9	5540	2.03	1.30	18.0	0.79
1	2.38	0.031	5	1.47	51.5	66.2	23.8	5540	2.22	1.43	18.1	0.81
1	2.38	0.031	5	0.126	19.7	95.0	30.3	449	1.94	1.12	5.15	1.10
1	2.38	0.031	5	0.126	22.7	96.1	30.8	449	2.20	1.20	5.24	1.04
1	2.38	0.031	5	0.125	23.6	91.5	30.0	449	2.83	1.27	4.86	1.05
1	2.38	0.031	5	0.125	24.7	92.3	29.7	449	2.74	1.15	4.72	1.09
1	2.38	0.031	5	0.126	28.0	93.3	30.4	449	1.97	1.07	5.18	1.08
1	2.38	0.031	5	0.126	41.9	92.8	30.2	449	2.54	1.16	5.09	1.09
1	2.38	0.031	5	0.125	44.5	94.0	30.2	449	2.98	1.26	4.99	0.96
1	2.38	0.031	5	0.126	48.7	92.9	30.3	449	2.59	1.19	4.97	0.98
1	2.38	0.031	5	0.508	47.7	89.5	29.2	1820	2.79	1.39	12.1	0.91
1	2.38	0.031	5	0.549	22.2	91.7	30.0	1970	2.11	1.10	13.2	1.15
1	2.38	0.031	5	0.549	27.1	91.2	30.0	1970	2.54	1.18	13.4	1.18
1	2.38	0.031	5	0.549	41.2	90.8	29.8	1970	2.01	1.24	13.6	0.95
1	2.38	0.031	5	0.549	49.8	92.5	30.3	1970	2.55	1.35	13.8	0.88
1	2.38	0.031	5	1.03	23.8	89.0	29.5	3720	2.50	1.21	20.0	1.11
1	2.38	0.031	5	1.03	27.8	89.3	29.6	3720	1.89	1.11	19.7	0.85
1	2.38	0.031	5	1.03	40.6	89.2	29.5	3720	2.45	1.34	20.3	0.86
1	2.38	0.031	5	1.03	43.9	89.1	29.5	3720	2.37	1.31	20.3	0.94
1	2.38	0.031	5	1.19	24.8	88.0	29.2	4290	2.76	1.30	20.8	1.04
1	2.38	0.031	5	1.19	28.0	88.0	29.2	4290	2.45	1.20	20.7	1.01
1	2.38	0.031	5	1.19	45.7	89.0	29.1	4280	2.69	1.44	20.6	1.01
1	2.38	0.031	5	1.19	48.0	89.4	29.3	4280	2.70	1.43	21.9	0.83
1	2.38	0.031	5	1.46	42	96.4	30.9	5240	1.59	.	.	.
1	2.38	0.031	5	1.48	23.9	88.1	25.2	5290	2.96	1.32	24.5	0.91
1	2.38	0.031	5	1.48	27.7	87.7	29.1	5290	2.16	1.10	23.7	1.00
1	2.38	0.031	5	1.48	38.9	89.3	29.5	5290	2.19	1.28	25.8	0.87
1	2.38	0.031	5	1.48	47.9	88.5	29.3	5290	2.46	1.48	24.7	0.78
2	1.59	0.014	7.6	0.125	49.6	24.4	8.38	772	2.86	1.12	1.59	0.96
2	1.59	0.014	7.6	0.125	49.6	24.8	8.68	772	1.79	.	.	.
2	1.59	0.014	7.6	0.232	50.4	24.3	8.33	1430	2.66	1.19	2.59	1.08
2	1.59	0.014	7.6	0.386	49.5	24.5	8.57	2380	3.02	1.31	3.80	0.81
2	1.59	0.014	7.6	0.466	50.3	24.5	8.58	2880	2.75	1.30	4.42	1.01
2	1.59	0.014	7.6	0.546	51.4	24.5	8.58	3370	2.75	1.40	4.54	0.86
2	1.59	0.014	7.6	0.789	49.6	24.6	8.55	4870	2.79	1.38	5.51	0.75
2	1.59	0.014	7.6	1.04	49.3	24.7	8.62	6390	2.58	1.41	6.69	0.94
2	1.59	0.014	7.6	1.04	51.3	24.9	8.75	6390	2.63	1.21	6.79	0.97
2	1.59	0.014	7.6	1.21	48.0	25.1	8.79	7460	2.79	1.46	7.73	0.92
2	1.59	0.014	7.6	1.50	48.5	25.7	9.14	9200	3.10	1.54	9.84	0.94
2	1.59	0.014	7.6	1.50	49.2	25.4	8.91	9200	2.82	1.38	9.92	0.92
2	1.59	0.014	7.6	1.50	50.9	25.9	9.21	9200	2.87	1.57	9.79	0.86
3	3.75	0.027	8.5	0.125	50.8	24.5	8.46	943	1.85	0.93	1.41	0.79
3	3.75	0.027	8.5	0.232	50.4	24.5	8.46	1750	1.88	0.87	1.95	0.77
3	3.75	0.027	8.5	0.385	51.0	24.6	8.58	2900	2.58	1.10	2.60	0.55
3	3.75	0.027	8.5	0.466	50.8	24.6	8.60	3515	1.87	0.82	2.75	0.82
3	3.75	0.027	8.5	0.545	48.7	24.6	8.59	4110	1.73	0.97	3.12	0.73
3	3.75	0.027	8.5	0.545	49.7	24.6	8.55	4110	1.78	1.13	3.14	0.56
3	3.75	0.027	8.5	0.628	51.4	24.6	8.57	4720	2.01	1.07	3.39	0.73
3	3.75	0.027	8.5	0.785	50.1	24.7	8.63	5920	2.21	0.96	3.93	0.80
3	3.75	0.027	8.5	1.03	51.0	24.8	8.63	7730	1.78	0.88	4.36	0.97
3	3.75	0.027	8.5	1.19	49.5	24.9	8.71	8980	1.95	1.05	5.31	0.71
3	3.75	0.027	8.5	1.47	49.5	24.9	8.71	11100	2.06	0.96	5.97	0.89

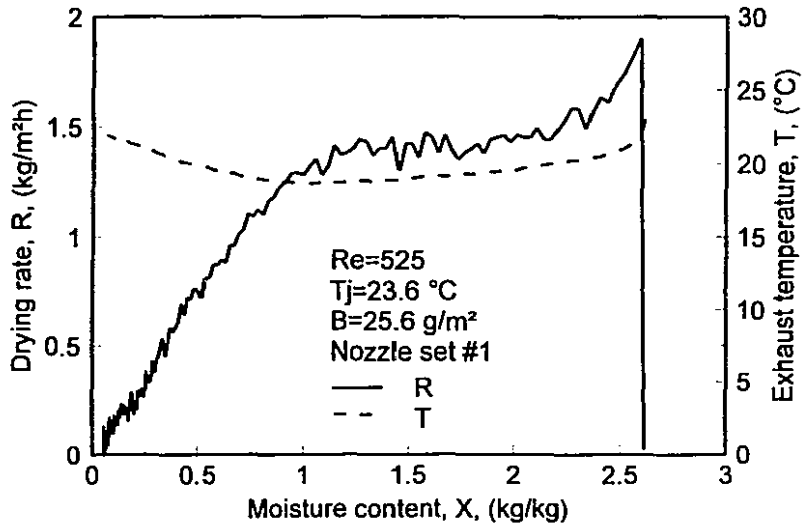
Drying rate, R, (kg/m²h)
Exhaust temperature, T, (°C)
Moisture content, X, (kg/kg)
Re=525
Tj=23.6 °C
B=25.6 g/m²
Nozzle set #1
R
T

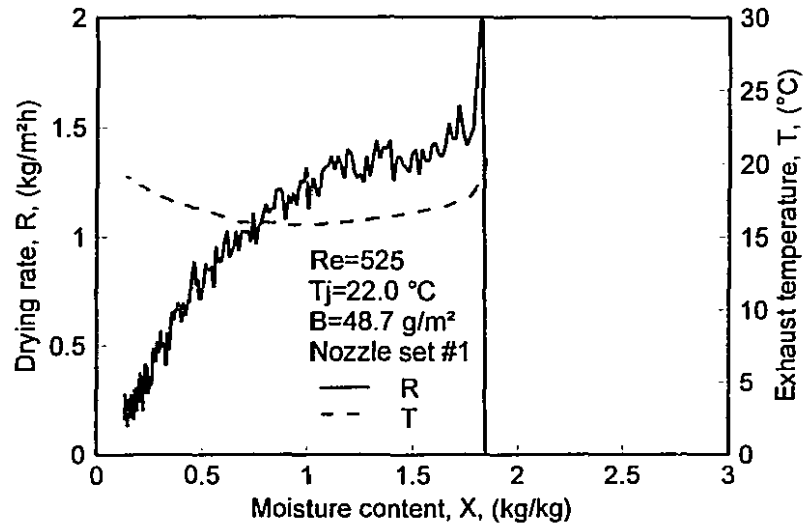
Drying rate, R, (kg/m²h)
Exhaust temperature, T, (°C)
Moisture content, X, (kg/kg)
Re=525
Tj=22.0 °C
B=48.7 g/m²
Nozzle set #1
R
T

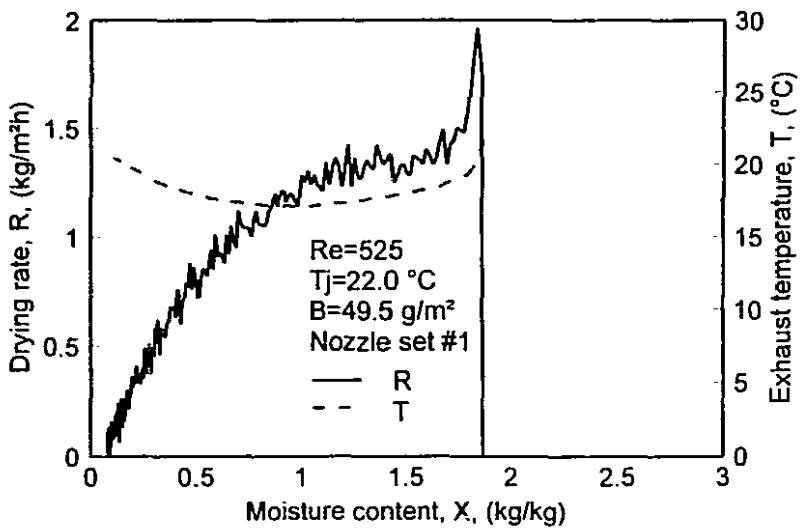
Drying rate, R, (kg/m²h)
Exhaust temperature, T, (°C)
Moisture content, X, (kg/kg)
Re=525
Tj=22.0 °C
B=49.5 g/m²
Nozzle set #1
R
T

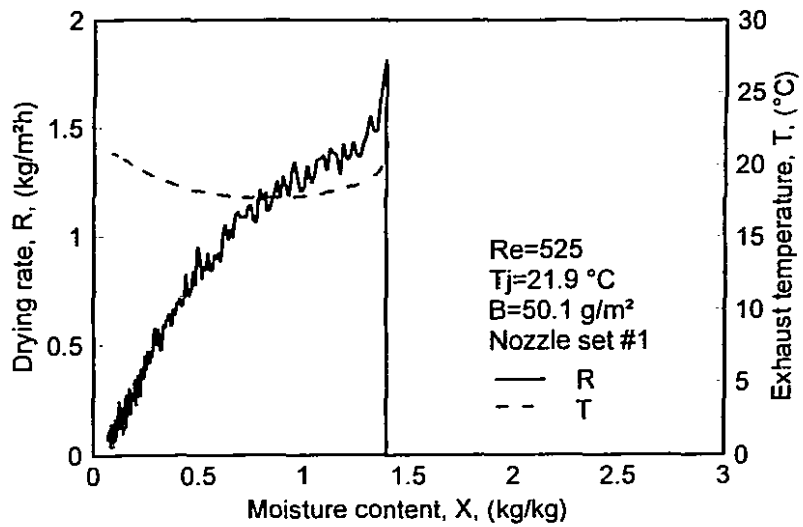
Drying rate, R, (kg/m²h)
Exhaust temperature, T, (°C)
Moisture content, X, (kg/kg)
Re=525
Tj=21.9 °C
B=50.1 g/m²
Nozzle set #1
R
T

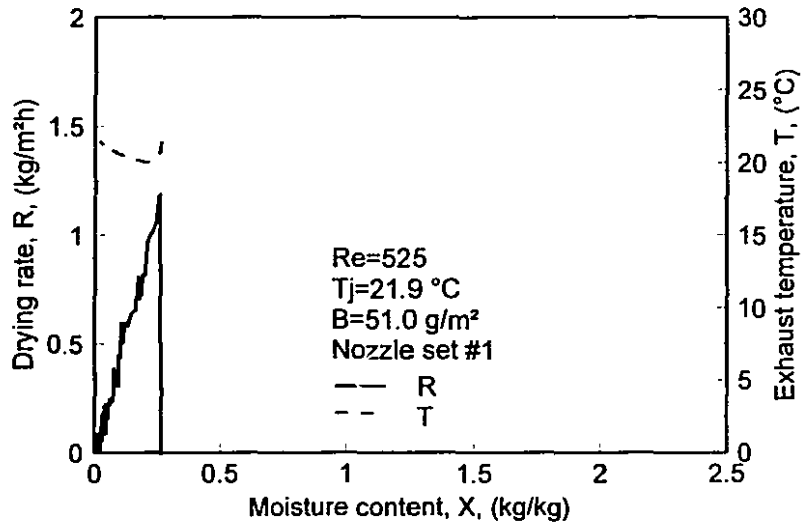
Drying rate, R, (kg/m²h)
Exhaust temperature, T, (°C)
Moisture content, X, (kg/kg)
Re=525
Tj=21.9 °C
B=51.0 g/m²
Nozzle set #1
R
T

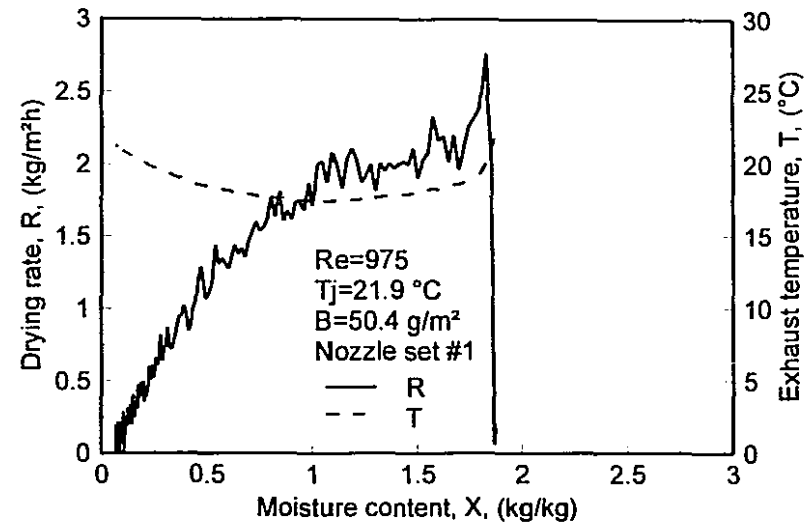
Drying rate, R, (kg/m²h)
Exhaust temperature, T, (°C)
Moisture content, X, (kg/kg)
Re=975
Tj=21.9 °C
B=50.4 g/m²
Nozzle set #1
R
T

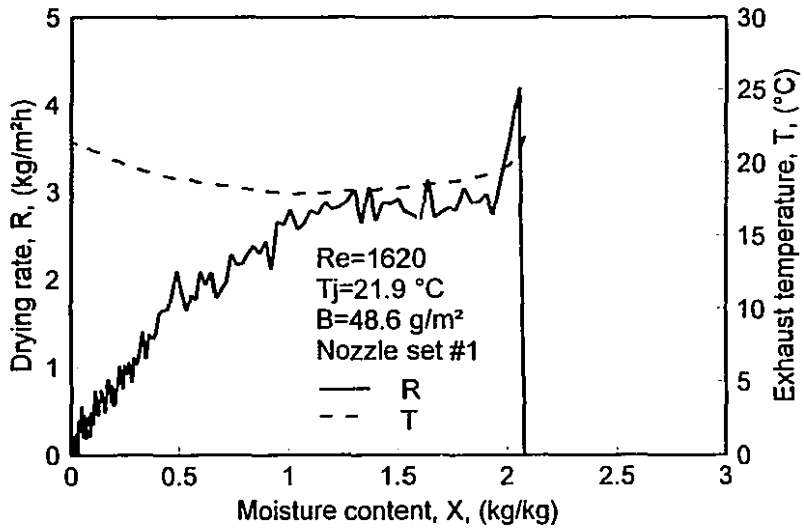
Drying rate, R, (kg/m²h)
Exhaust temperature, T, (°C)
Moisture content, X, (kg/kg)
Re=1620
Tj=21.9 °C
B=48.6 g/m²
Nozzle set #1
R
T

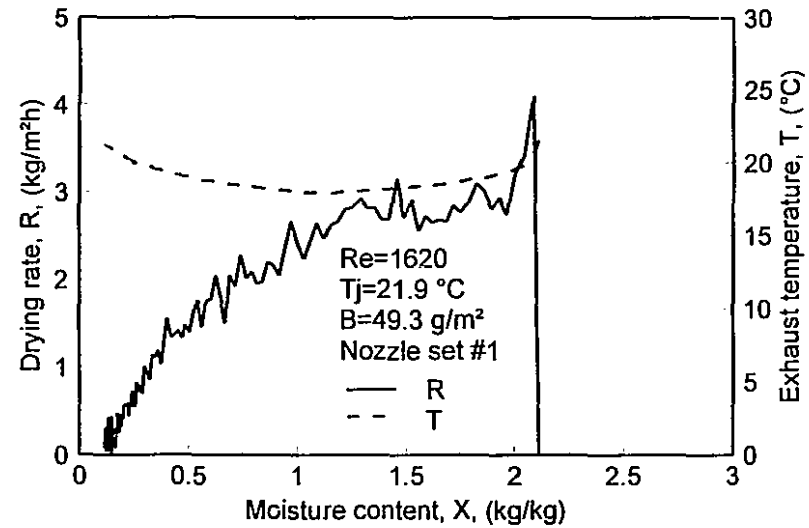
Drying rate, R, (kg/m²h)
Exhaust temperature, T, (°C)
Moisture content, X, (kg/kg)
Re=1620
Tj=21.9 °C
B=49.3 g/m²
Nozzle set #1
R
T

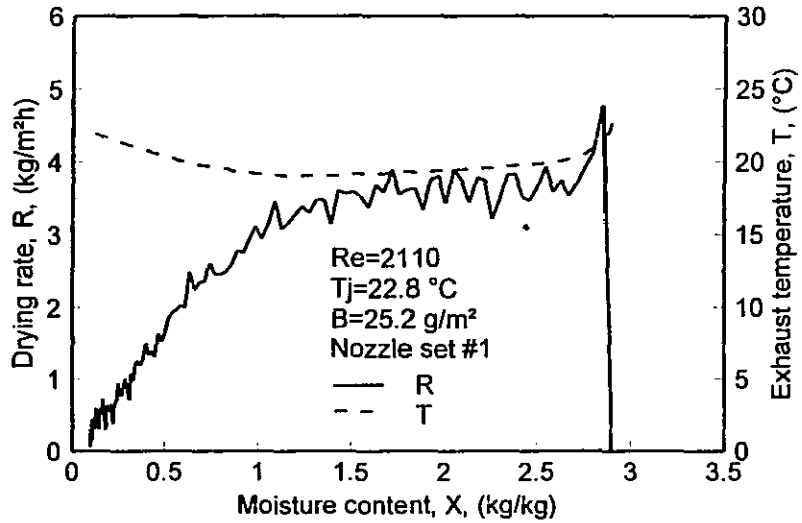
Drying rate, R, (kg/m²h)
Exhaust temperature, T, (°C)
Moisture content, X, (kg/kg)
Re=2110
Tj=22.8 °C
B=25.2 g/m²
Nozzle set #1
R
T

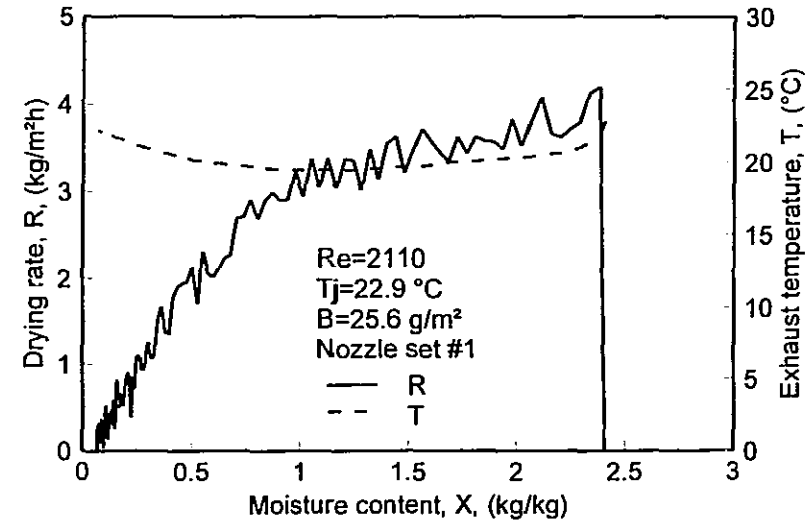
Drying rate, R, (kg/m²h)
Exhaust temperature, T, (°C)
Moisture content, X, (kg/kg)
Re=2110
Tj=22.9 °C
B=25.6 g/m²
Nozzle set #1
R
T

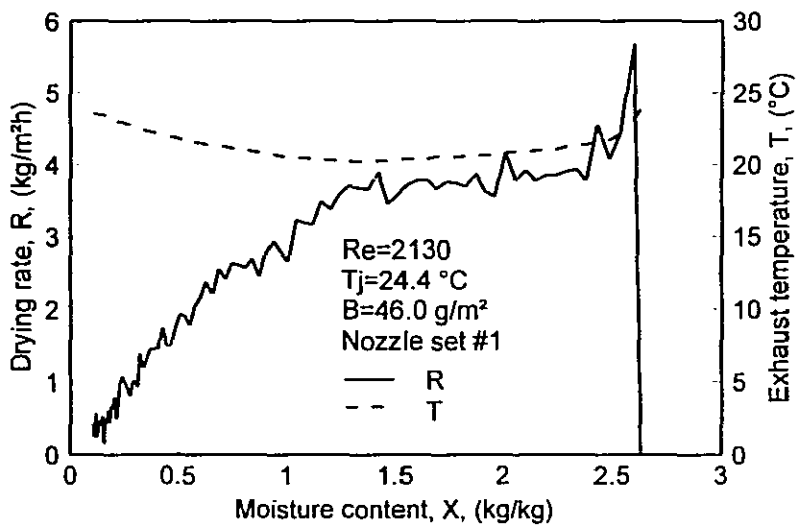
Drying rate, R, (kg/m²h)
Exhaust temperature, T, (°C)
Moisture content, X, (kg/kg)
Re=2130
Tj=24.4 °C
B=46.0 g/m²
Nozzle set #1
R
T

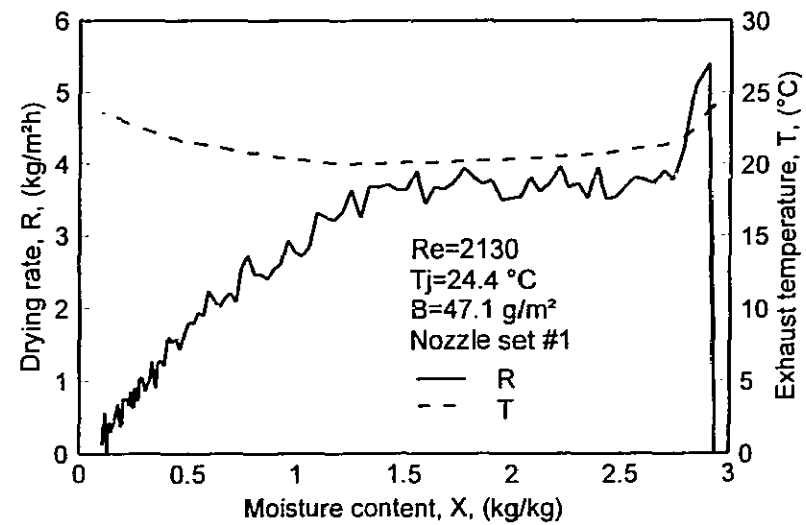
Drying rate, R, (kg/m²h)
Exhaust temperature, T, (°C)
Moisture content, X, (kg/kg)
Re=2130
Tj=24.4 °C
B=47.1 g/m²
Nozzle set #1
R
T

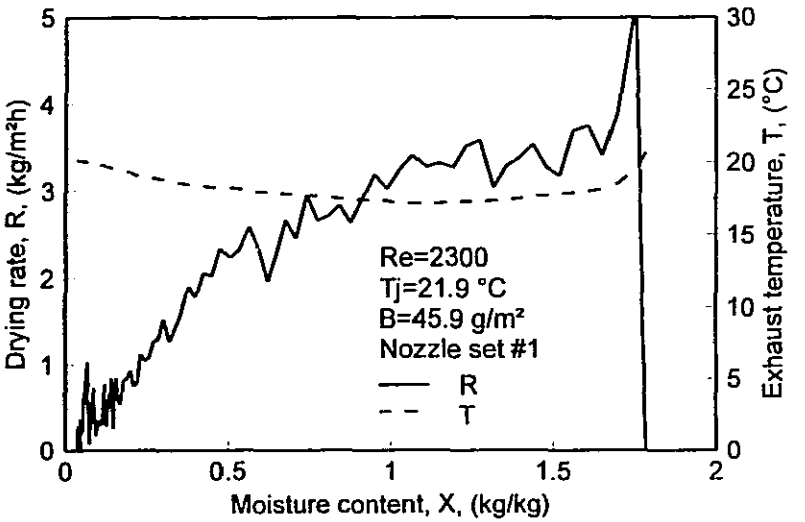
Drying rate, R, (kg/m²h)
Exhaust temperature, T, (°C)
Moisture content, X, (kg/kg)
Re=2300
Tj=21.9 °C
B=45.9 g/m²
Nozzle set #1
R
T

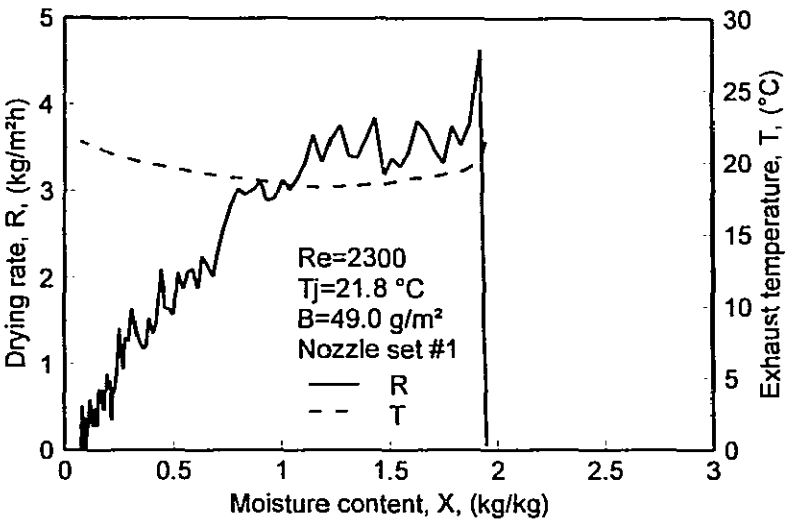
Drying rate, R, (kg/m²h)
Exhaust temperature, T, (°C)
Moisture content, X, (kg/kg)
Re=2300
Tj=21.8 °C
B=49.0 g/m²
Nozzle set #1
R
T

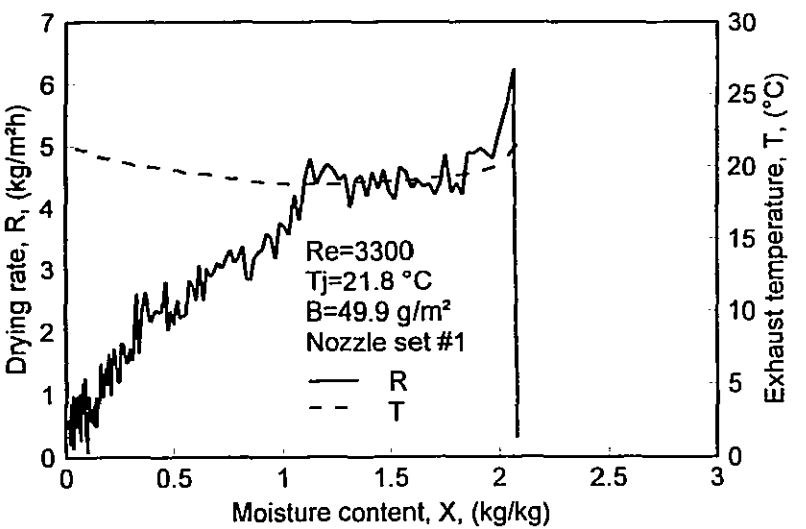
Drying rate, R, (kg/m²h)
Exhaust temperature, T, (°C)
Moisture content, X, (kg/kg)
Re=3300
Tj=21.8 °C
B=49.9 g/m²
Nozzle set #1
R
T

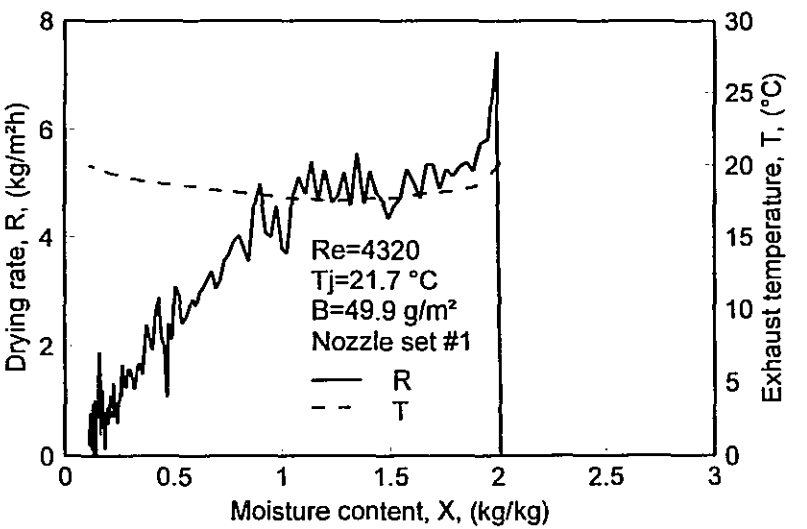
Drying rate, R, (kg/m²h)
Exhaust temperature, T, (°C)
Moisture content, X, (kg/kg)
Re=4320
Tj=21.7 °C
B=49.9 g/m²
Nozzle set #1
R
T

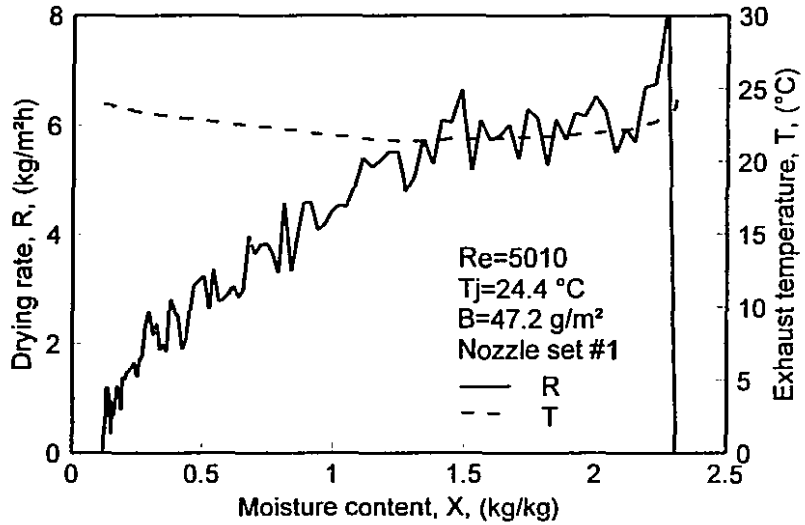
Drying rate, R, (kg/m²h)
Exhaust temperature, T, (°C)
Moisture content, X, (kg/kg)
Re=5010
Tj=24.4 °C
B=47.2 g/m²
Nozzle set #1
R
T

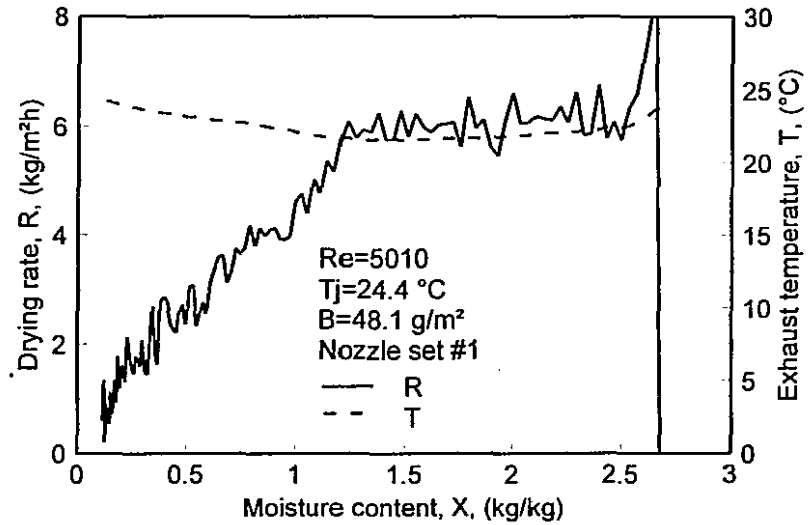
Drying rate, R, (kg/m²h)
Exhaust temperature, T, (°C)
Moisture content, X, (kg/kg)
Re=5010
Tj=24.4 °C
B=48.1 g/m²
Nozzle set #1
R
T

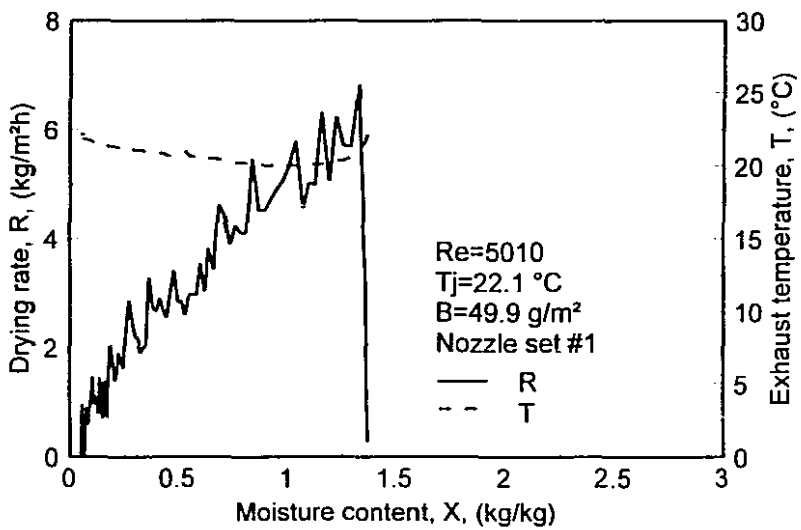
Drying rate, R, (kg/m²h)
Exhaust temperature, T, (°C)
Moisture content, X, (kg/kg)
Re=5010
Tj=22.1 °C
B=49.9 g/m²
Nozzle set #1
R
T

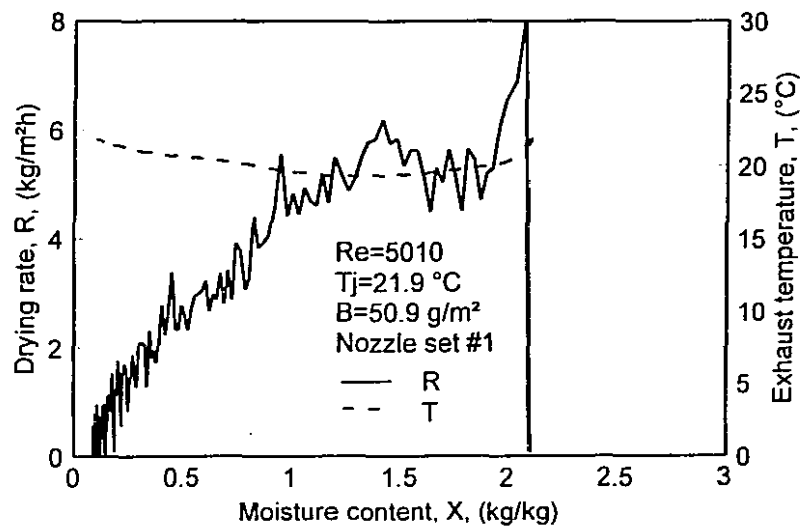
Drying rate, R, (kg/m²h)
Exhaust temperature, T, (°C)
Moisture content, X, (kg/kg)
Re=5010
Tj=21.9 °C
B=50.9 g/m²
Nozzle set #1
R
T

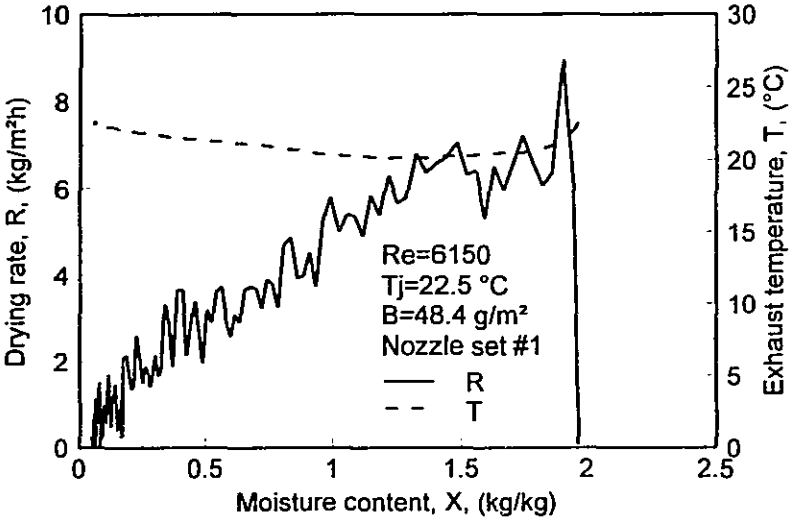
Drying rate, R, (kg/m²h)
Exhaust temperature, T, (°C)
Moisture content, X, (kg/kg)
Re=6150
Tj=22.5 °C
B=48.4 g/m²
Nozzle set #1
R
T

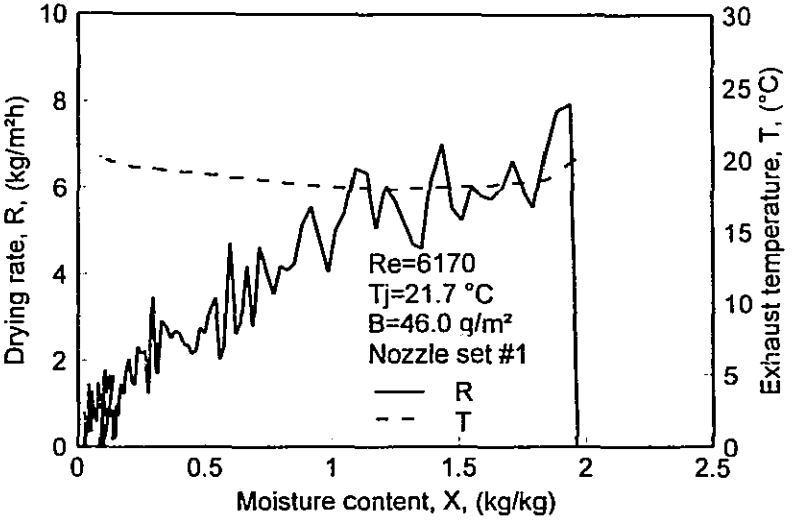
Drying rate, R, (kg/m²h)
Exhaust temperature, T, (°C)
Moisture content, X, (kg/kg)
Re=6170
Tj=21.7 °C
B=46.0 g/m²
Nozzle set #1
R
T

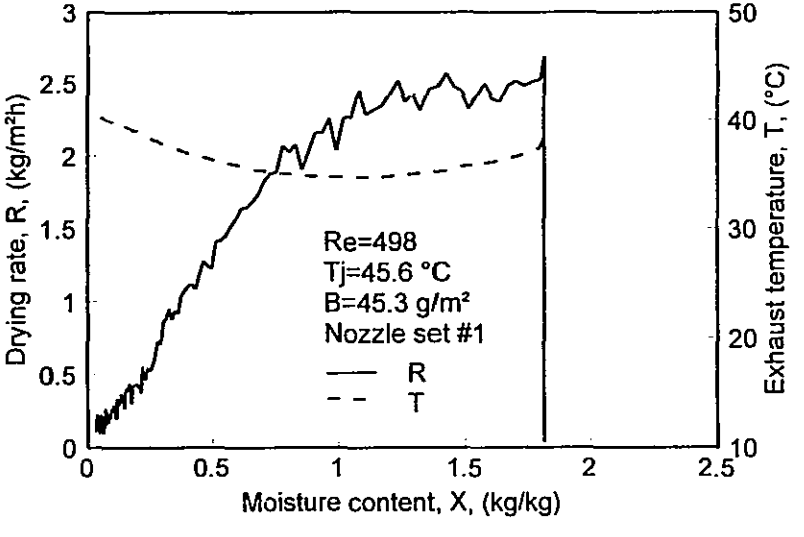
Drying rate, R, (kg/m²h)
Exhaust temperature, T, (°C)
Moisture content, X, (kg/kg)
Re=498
Tj=45.6 °C
B=45.3 g/m²
Nozzle set #1
R
T

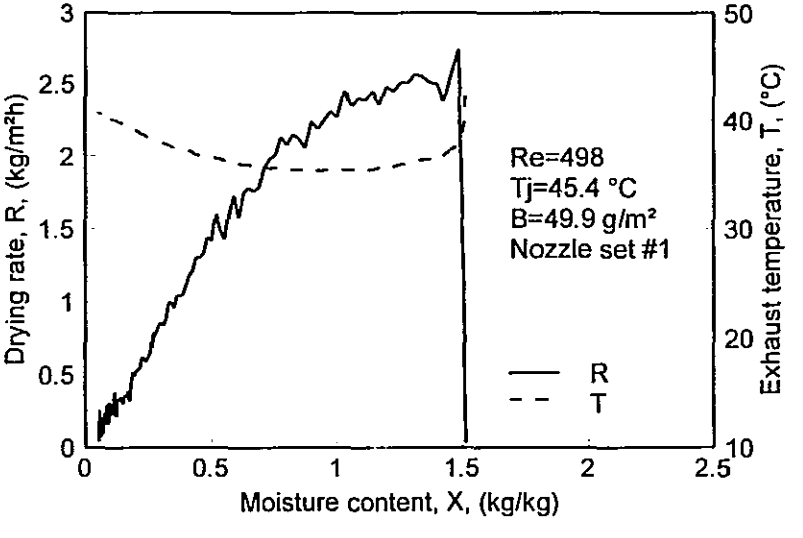
Drying rate, R, (kg/m²h)
Exhaust temperature, T, (°C)
Moisture content, X, (kg/kg)
Re=498
Tj=45.4 °C
B=49.9 g/m²
Nozzle set #1
R
T

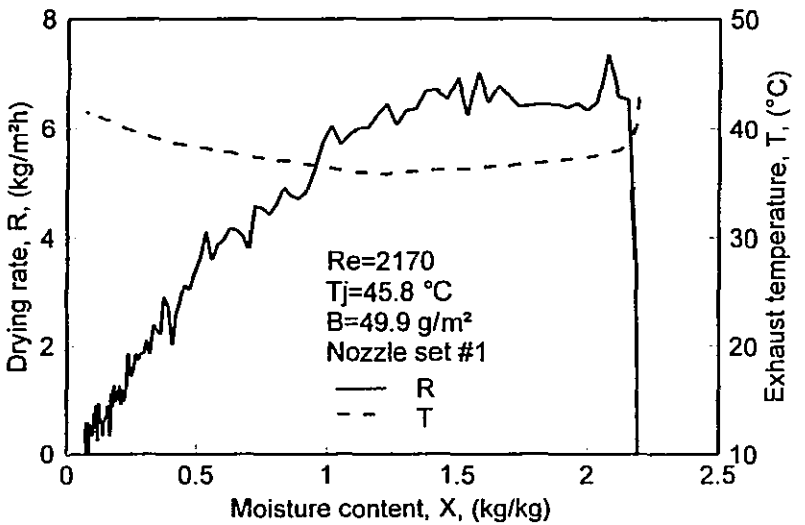
Drying rate, R, (kg/m²h)
Exhaust temperature, T, (°C)
Moisture content, X, (kg/kg)
Re=2170
Tj=45.8 °C
B=49.9 g/m²
Nozzle set #1
R
T

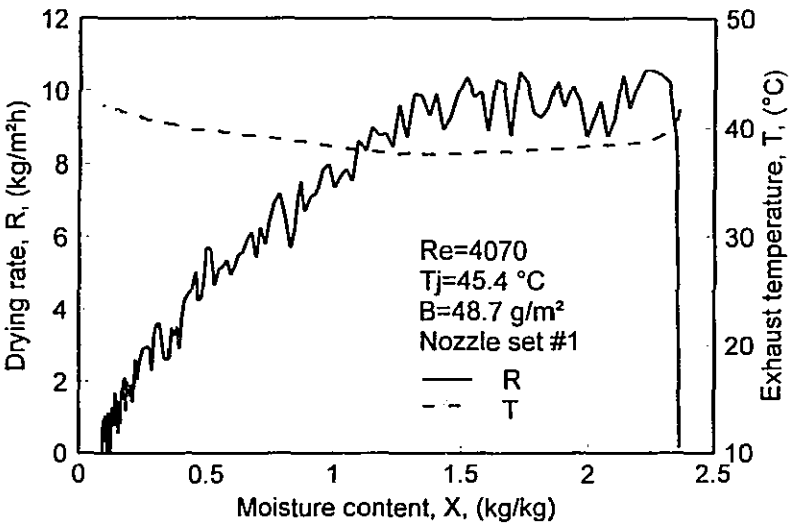
Drying rate, R, (kg/m²h)
Exhaust temperature, T, (°C)
Moisture content, X, (kg/kg)
Re=4070
Tj=45.4 °C
B=48.7 g/m²
Nozzle set #1
R
T

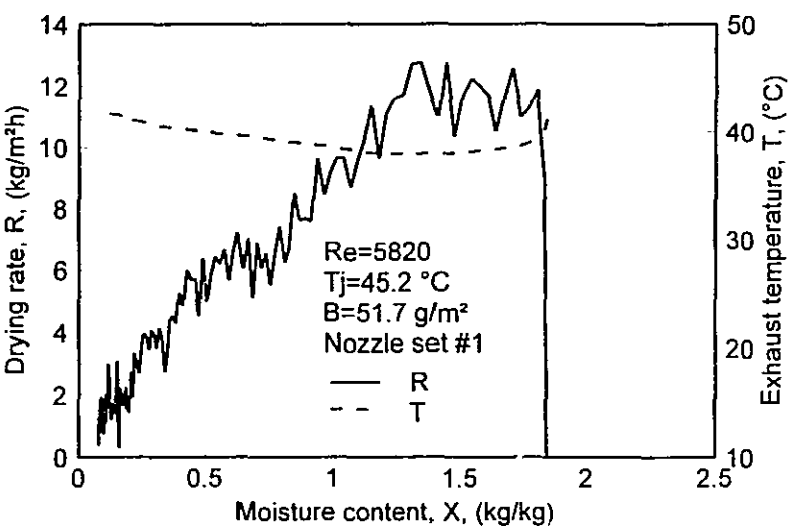
Drying rate, R, (kg/m²h)
Exhaust temperature, T, (°C)
Moisture content, X, (kg/kg)
Re=5820
Tj=45.2 °C
B=51.7 g/m²
Nozzle set #1
R
T

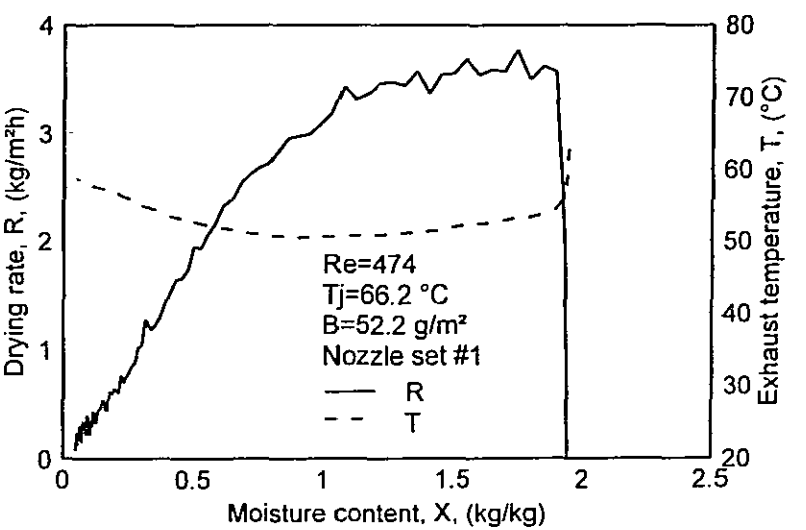
Drying rate, R, (kg/m²h)
Exhaust temperature, T, (°C)
Moisture content, X, (kg/kg)
Re=474
Tj=66.2 °C
B=52.2 g/m²
Nozzle set #1
R
T

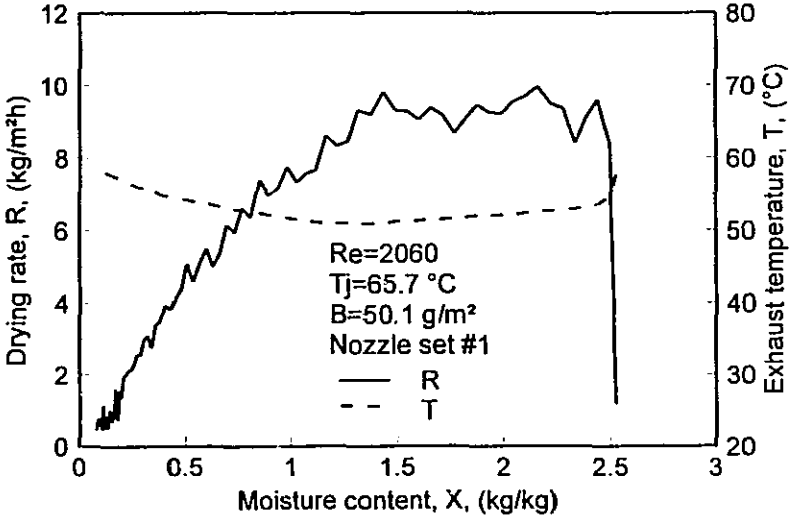
Drying rate, R, (kg/m²h)
Exhaust temperature, T, (°C)
Moisture content, X, (kg/kg)
Re=2060
Tj=65.7 °C
B=50.1 g/m²
Nozzle set #1
R
T

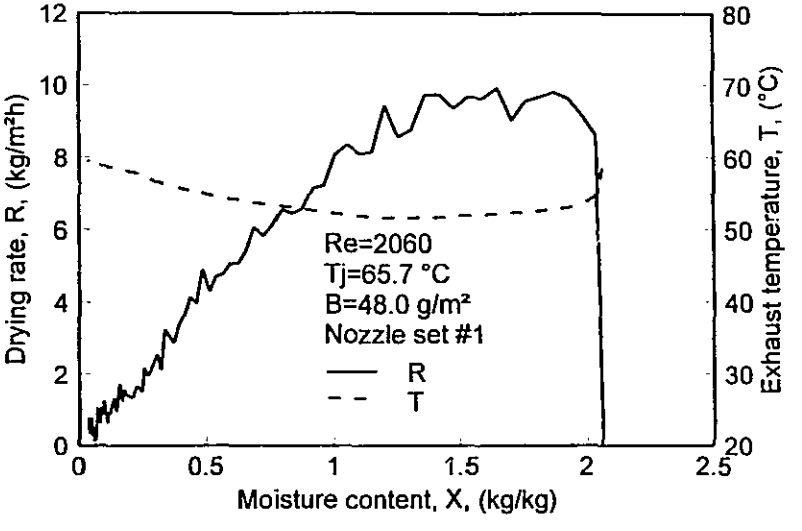
Drying rate, R, (kg/m²h)
Exhaust temperature, T, (°C)
Moisture content, X, (kg/kg)
Re=2060
Tj=65.7 °C
B=48.0 g/m²
Nozzle set #1
R
T

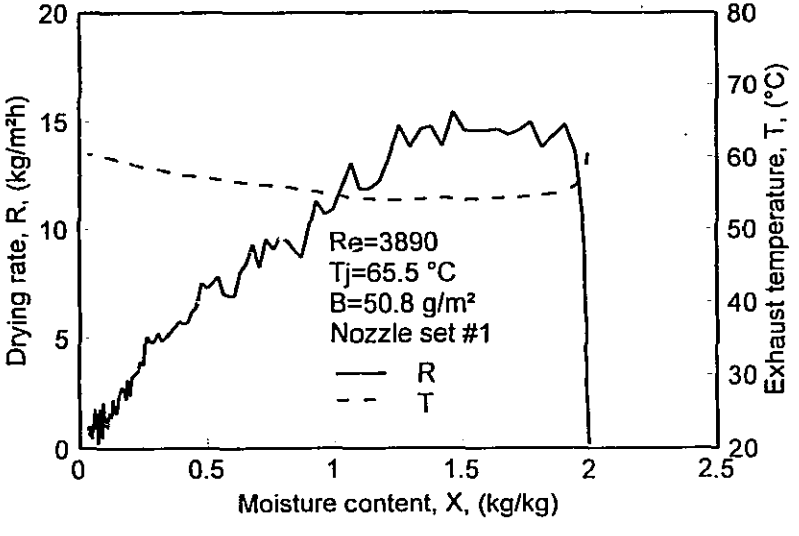
Drying rate, R, (kg/m²h)
Exhaust temperature, T, (°C)
Moisture content, X, (kg/kg)
Re=3890
Tj=65.5 °C
B=50.8 g/m²
Nozzle set #1
R
T

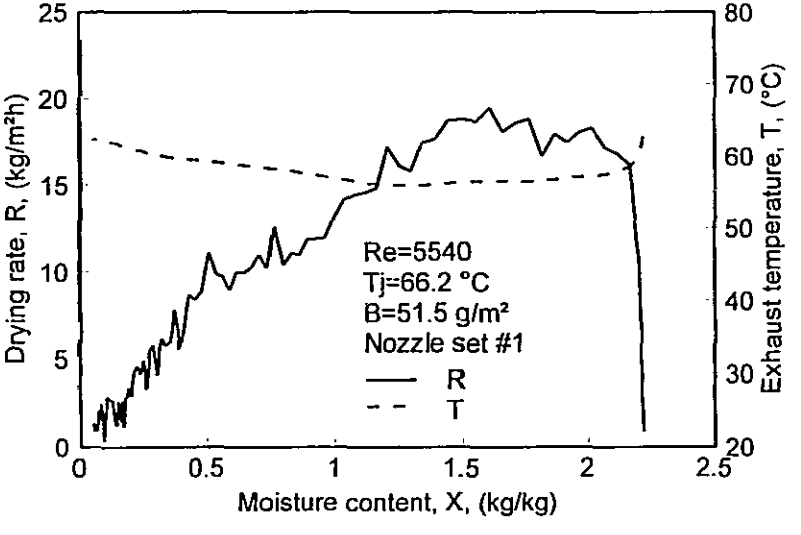
Drying rate, R, (kg/m²h)
Exhaust temperature, T, (°C)
Moisture content, X, (kg/kg)
Re=5540
Tj=66.2 °C
B=51.5 g/m²
Nozzle set #1
R
T

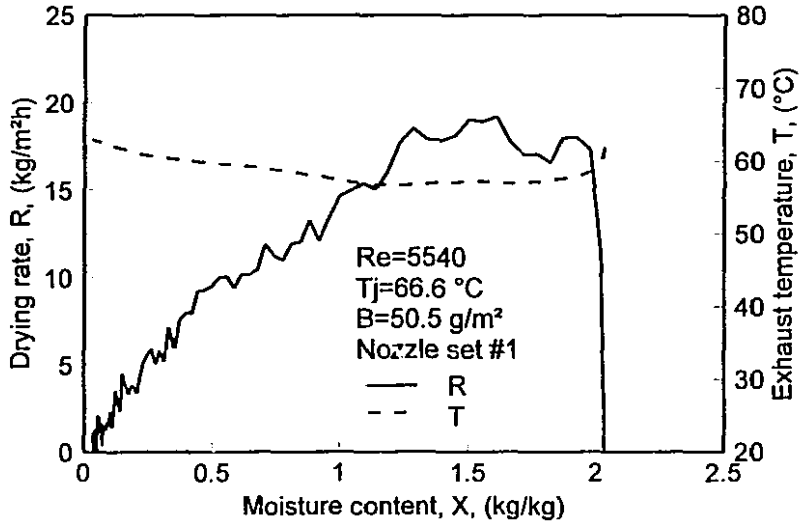
Drying rate, R, (kg/m²h)
Exhaust temperature, T, (°C)
Moisture content, X, (kg/kg)
Re=5540
Tj=66.6 °C
B=50.5 g/m²
Nozzle set #1
R
T

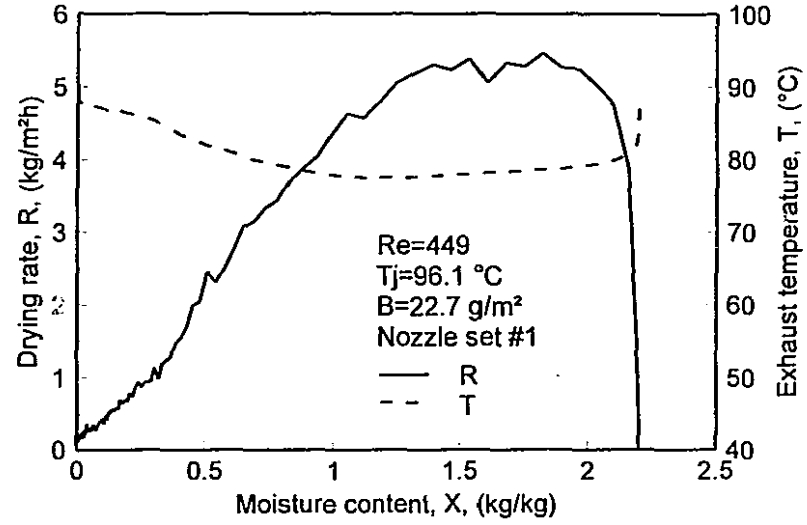
Drying rate, R, (kg/m²h)
Exhaust temperature, T, (°C)
Moisture content, X, (kg/kg)
Re=449
Tj=96.1 °C
B=22.7 g/m²
Nozzle set #1
R
T

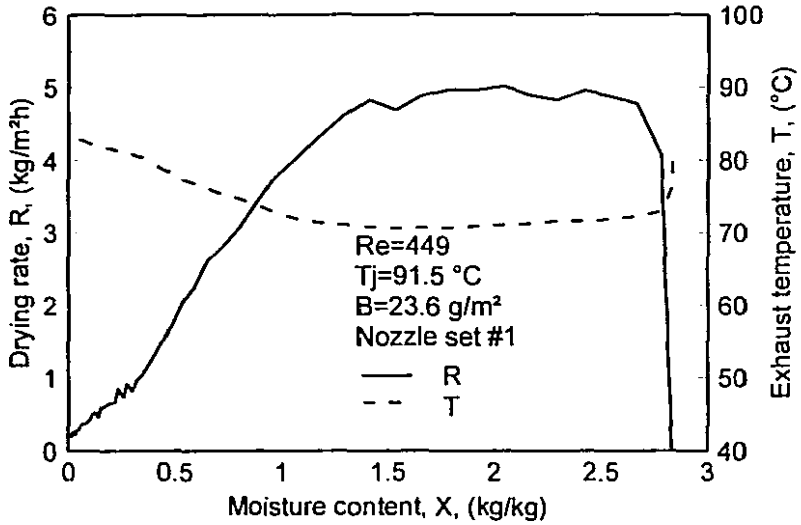
Drying rate, R, (kg/m²h)
Exhaust temperature, T, (°C)
Moisture content, X, (kg/kg)
Re=449
Tj=91.5 °C
B=23.6 g/m²
Nozzle set #1
R
T

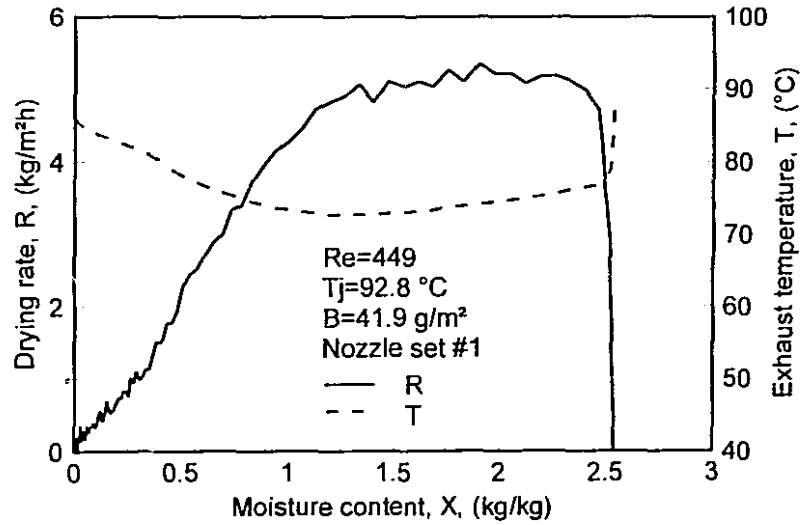
Drying rate, R, (kg/m²h)
Exhaust temperature, T, (°C)
Moisture content, X, (kg/kg)
Re=449
Tj=92.8 °C
B=41.9 g/m²
Nozzle set #1
R
T

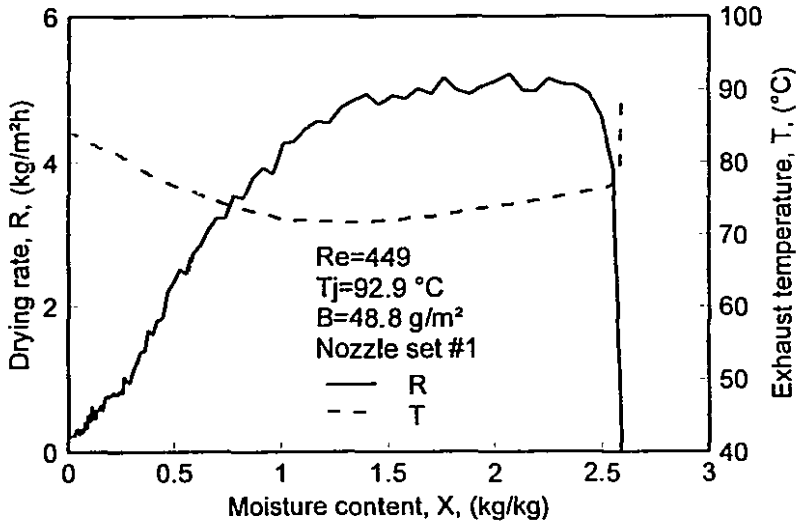
Drying rate, R, (kg/m²h)
Exhaust temperature, T, (°C)
Moisture content, X, (kg/kg)
Re=449
Tj=92.9 °C
B=48.8 g/m²
Nozzle set #1
R
T

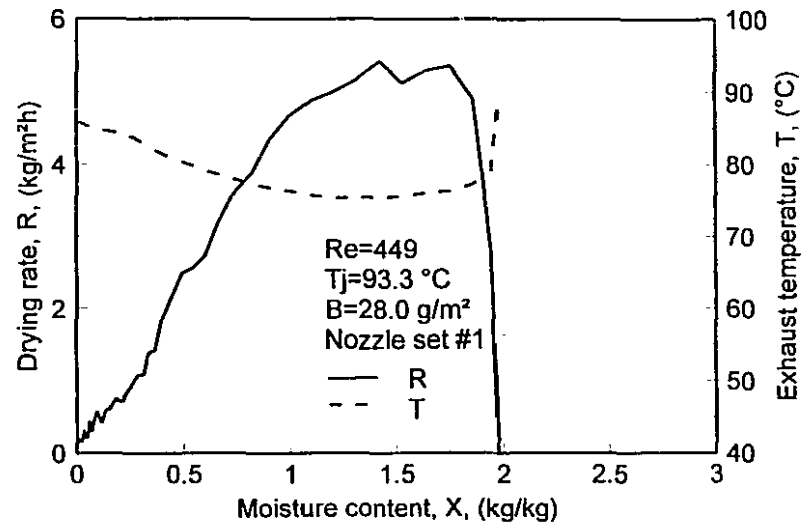
Drying rate, R, (kg/m²h)
Exhaust temperature, T, (°C)
Moisture content, X, (kg/kg)
Re=449
Tj=93.3 °C
B=28.0 g/m²
Nozzle set #1
R
T

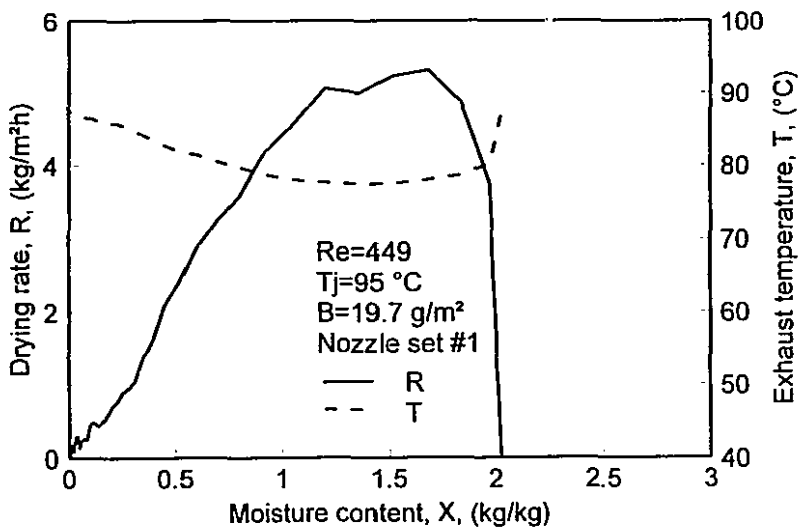
Drying rate, R, (kg/m²h)
Exhaust temperature, T, (°C)
Moisture content, X, (kg/kg)
Re=449
Tj=95 °C
B=19.7 g/m²
Nozzle set #1
R
T

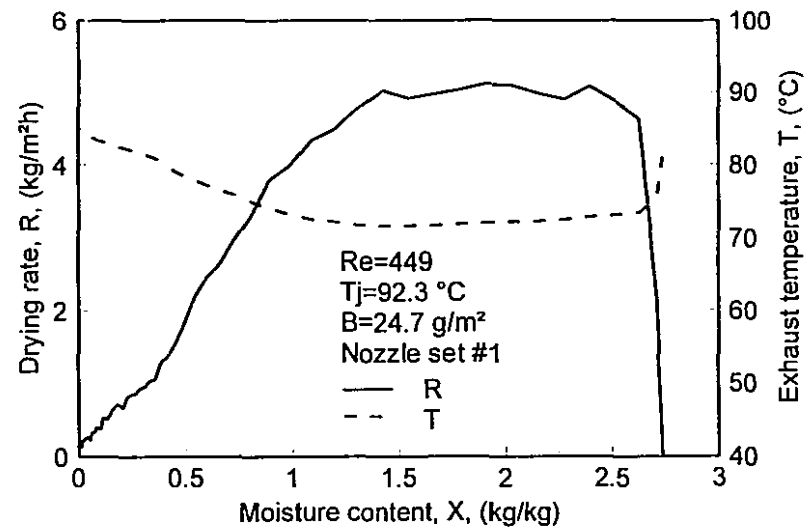
Drying rate, R, (kg/m²h)
Exhaust temperature, T, (°C)
Moisture content, X, (kg/kg)
Re=449
Tj=92.3 °C
B=24.7 g/m²
Nozzle set #1
R
T

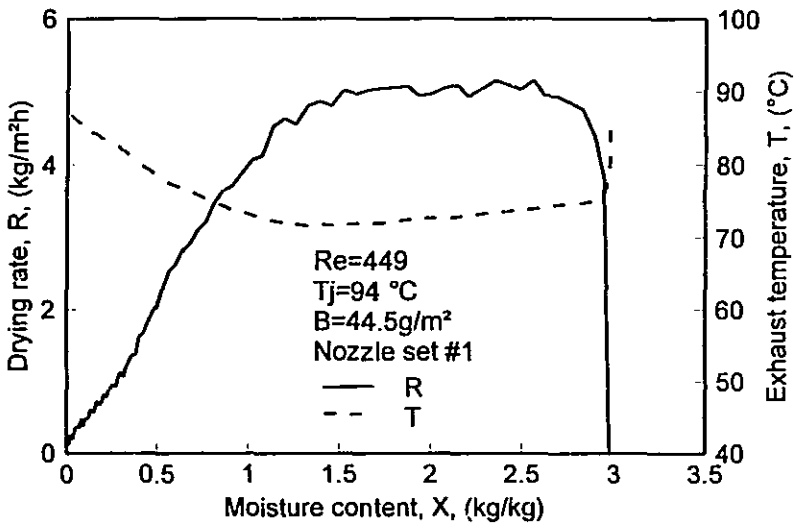
Drying rate, R, (kg/m²h)
Exhaust temperature, T, (°C)
Moisture content, X, (kg/kg)
Re=449
Tj=94 °C
B=44.5g/m²
Nozzle set #1
R
T

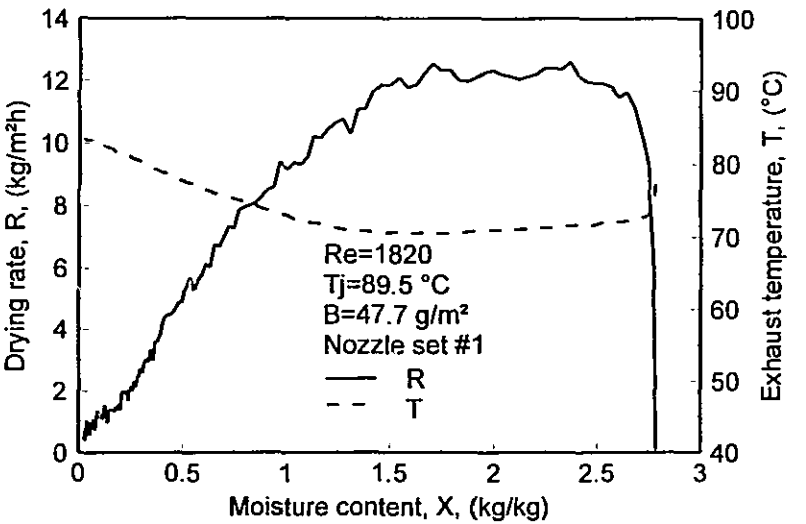
Drying rate, R, (kg/m²h)
Exhaust temperature, T, (°C)
Moisture content, X, (kg/kg)
Re=1820
Tj=89.5 °C
B=47.7 g/m²
Nozzle set #1
R
T

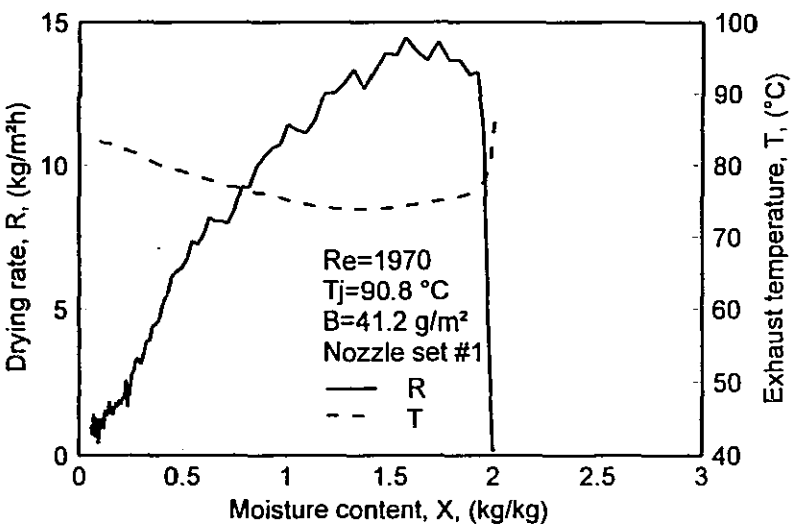
Drying rate, R, (kg/m²h)
Exhaust temperature, T, (°C)
Moisture content, X, (kg/kg)
Re=1970
Tj=90.8 °C
B=41.2 g/m²
Nozzle set #1
R
T

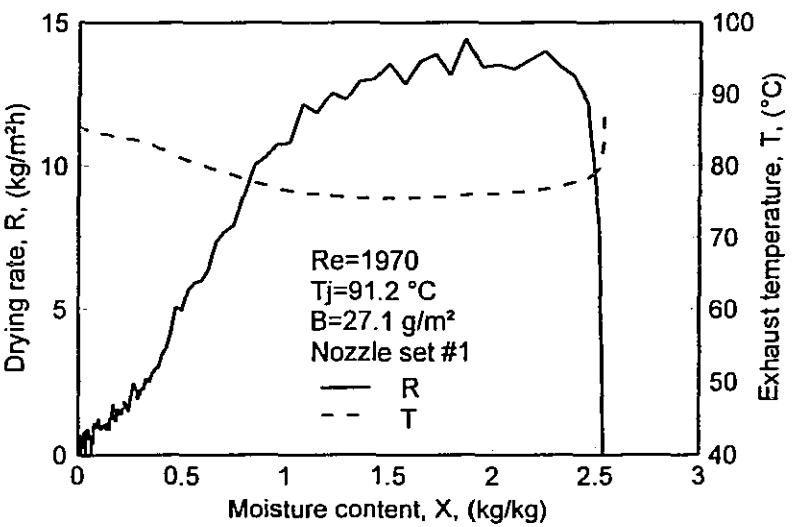
Drying rate, R, (kg/m²h)
Exhaust temperature, T, (°C)
Moisture content, X, (kg/kg)
Re=1970
Tj=91.2 °C
B=27.1 g/m²
Nozzle set #1
R
T

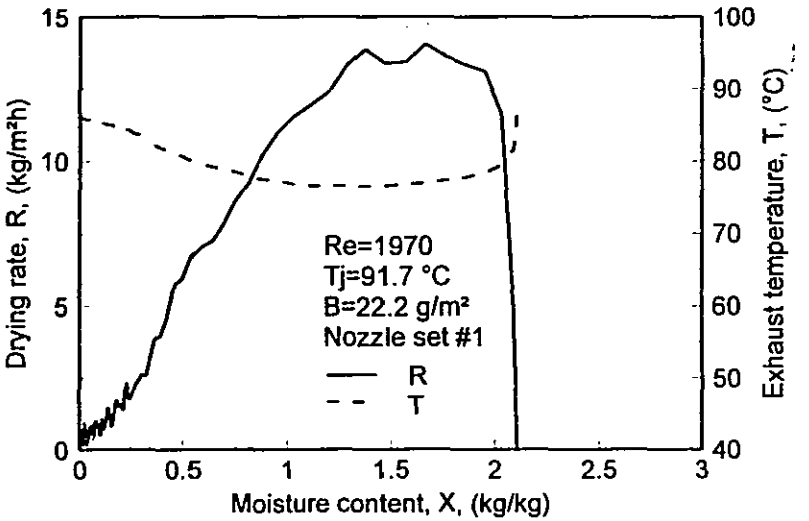
Drying rate, R, (kg/m²h)
Exhaust temperature, T, (°C)
Moisture content, X, (kg/kg)
Re=1970
Tj=91.7 °C
B=22.2 g/m²
Nozzle set #1
R
T

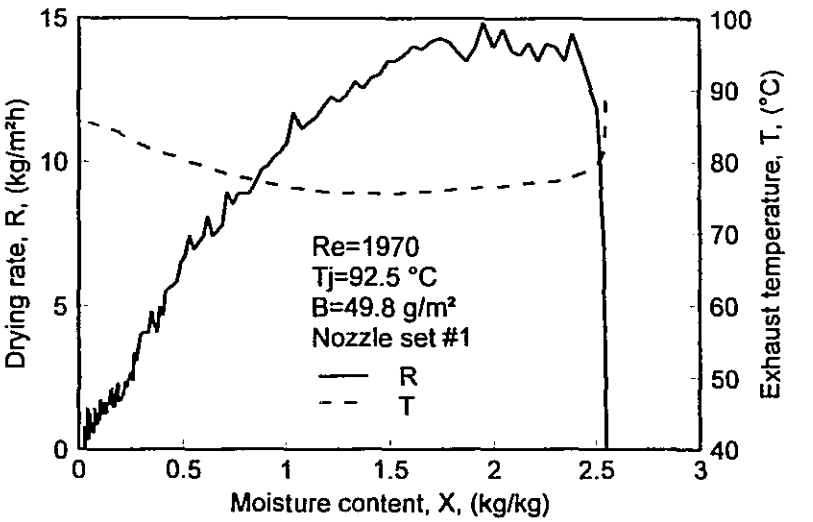
Drying rate, R, (kg/m²h)
Exhaust temperature, T, (°C)
Moisture content, X, (kg/kg)
Re=1970
Tj=92.5 °C
B=49.8 g/m²
Nozzle set #1
R
T

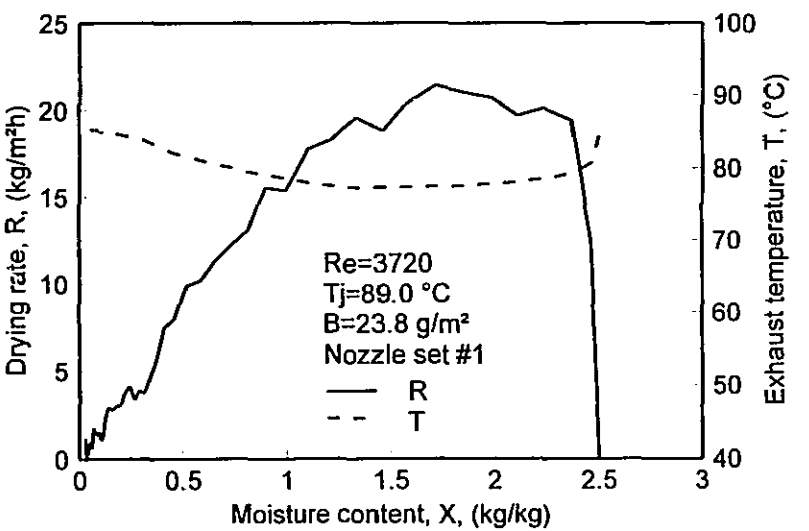
Drying rate, R, (kg/m²h)
Exhaust temperature, T, (°C)
Moisture content, X, (kg/kg)
Re=3720
Tj=89.0 °C
B=23.8 g/m²
Nozzle set #1
R
T

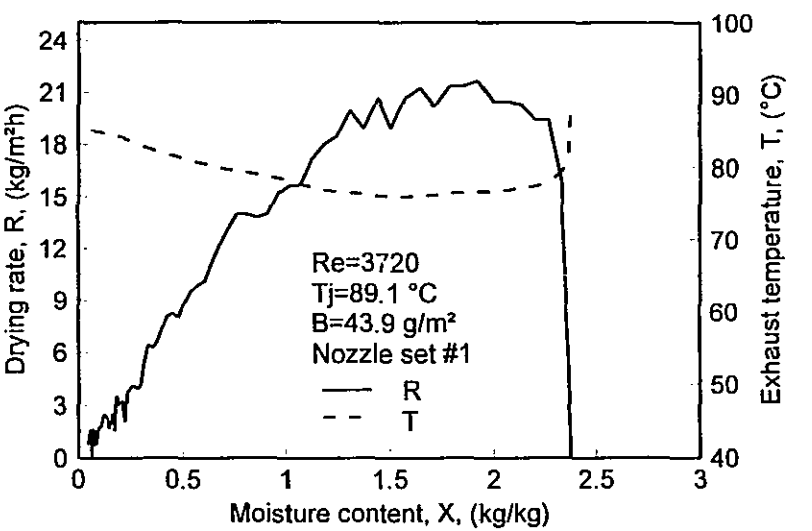
Drying rate, R, (kg/m²h)
Exhaust temperature, T, (°C)
Moisture content, X, (kg/kg)
Re=3720
Tj=89.1 °C
B=43.9 g/m²
Nozzle set #1
R
T

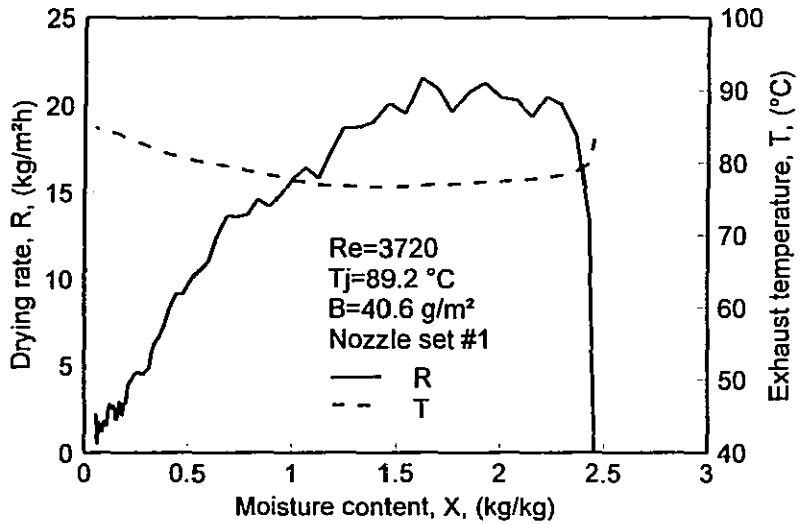
Drying rate, R, (kg/m²h)
Exhaust temperature, T, (°C)
Moisture content, X, (kg/kg)
Re=3720
Tj=89.2 °C
B=40.6 g/m²
Nozzle set #1
R
T

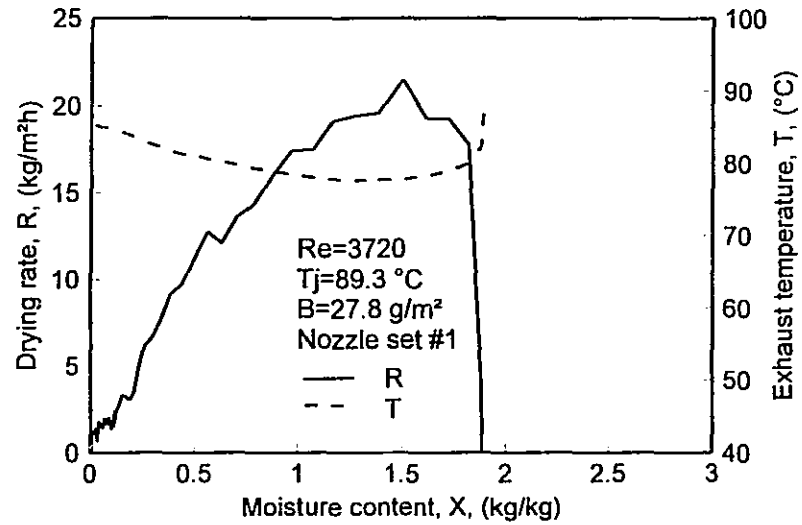
Drying rate, R, (kg/m²h)
Exhaust temperature, T, (°C)
Moisture content, X, (kg/kg)
Re=3720
Tj=89.3 °C
B=27.8 g/m²
Nozzle set #1
R
T

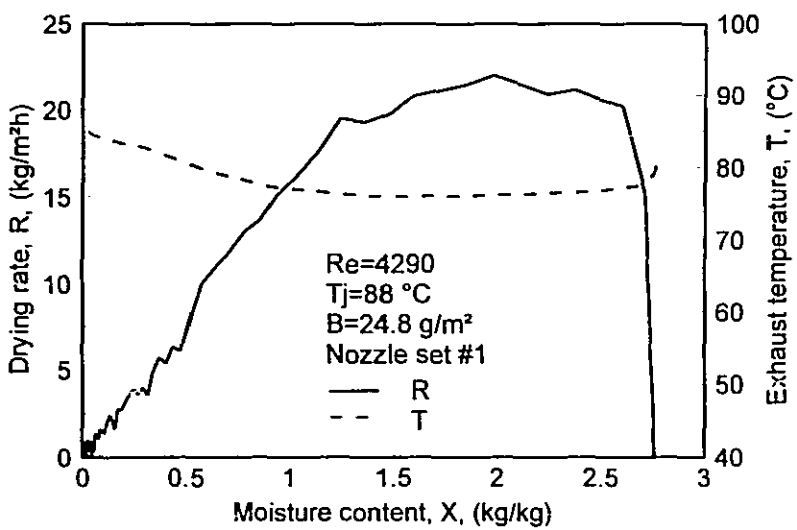
Drying rate, R, (kg/m²h)
Exhaust temperature, T, (°C)
Moisture content, X, (kg/kg)
Re=4290
Tj=88 °C
B=24.8 g/m²
Nozzle set #1
R
T

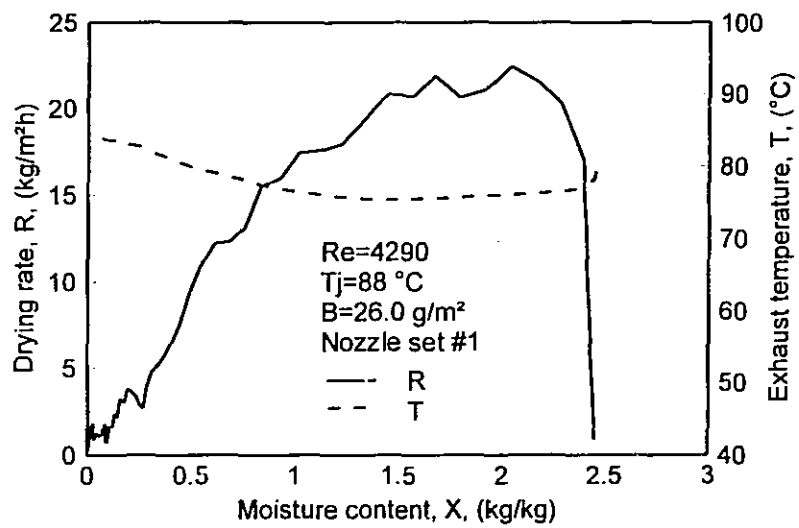
Drying rate, R, (kg/m²h)
Exhaust temperature, T, (°C)
Moisture content, X, (kg/kg)
Re=4290
Tj=88 °C
B=26.0 g/m²
Nozzle set #1
R
T

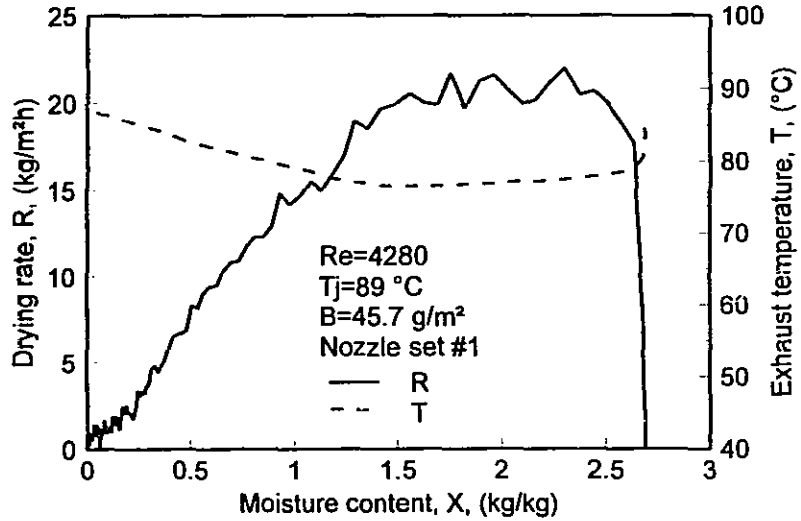
Drying rate, R, (kg/m²h)
Exhaust temperature, T, (°C)
Moisture content, X, (kg/kg)
Re=4280
Tj=89 °C
B=45.7 g/m²
Nozzle set #1
R
T

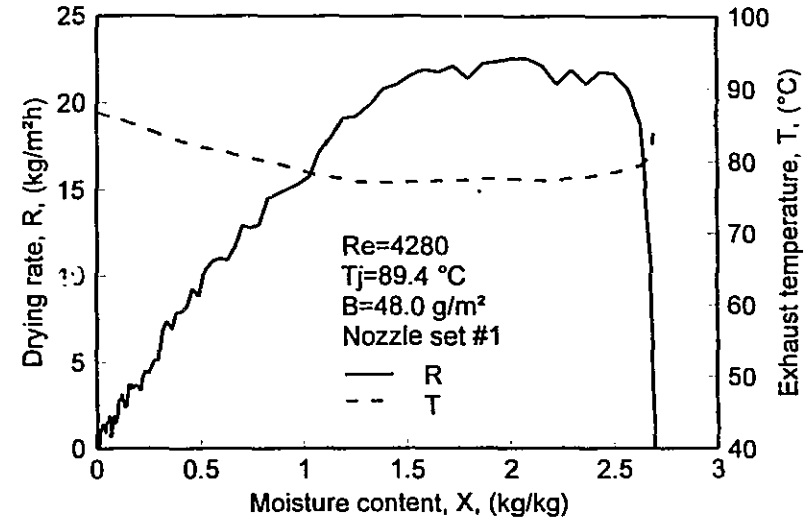
Drying rate, R, (kg/m²h)
Exhaust temperature, T, (°C)
Moisture content, X, (kg/kg)
Re=4280
Tj=89.4 °C
B=48.0 g/m²
Nozzle set #1
R
T

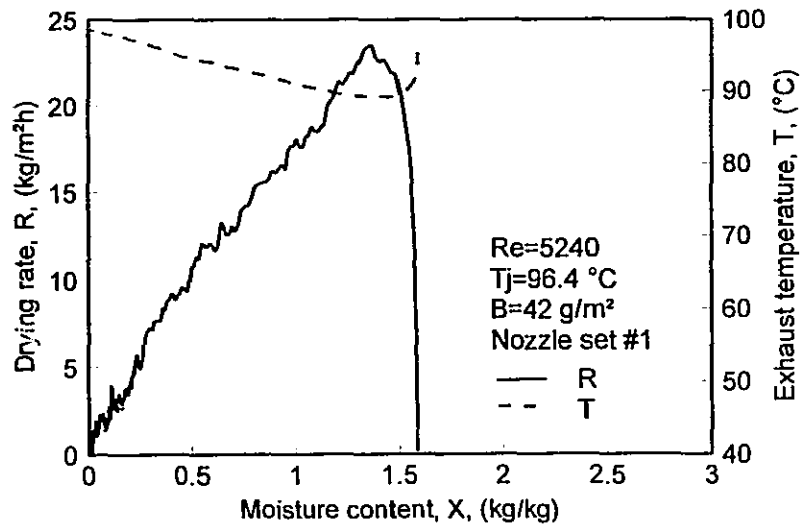
Drying rate, R, (kg/m²h)
Exhaust temperature, T, (°C)
Moisture content, X, (kg/kg)
Re=5240
Tj=96.4 °C
B=42 g/m²
Nozzle set #1
R
T

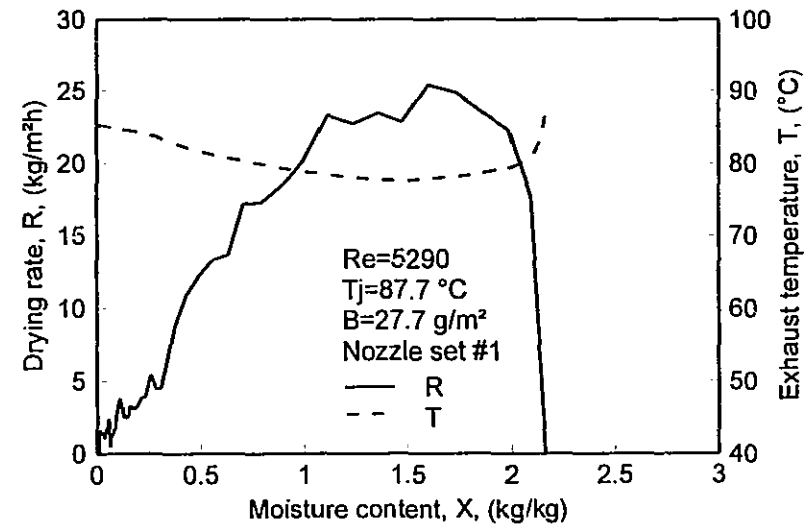
Drying rate, R, (kg/m²h)
Exhaust temperature, T, (°C)
Moisture content, X, (kg/kg)
Re=5290
Tj=87.7 °C
B=27.7 g/m²
Nozzle set #1
R
T

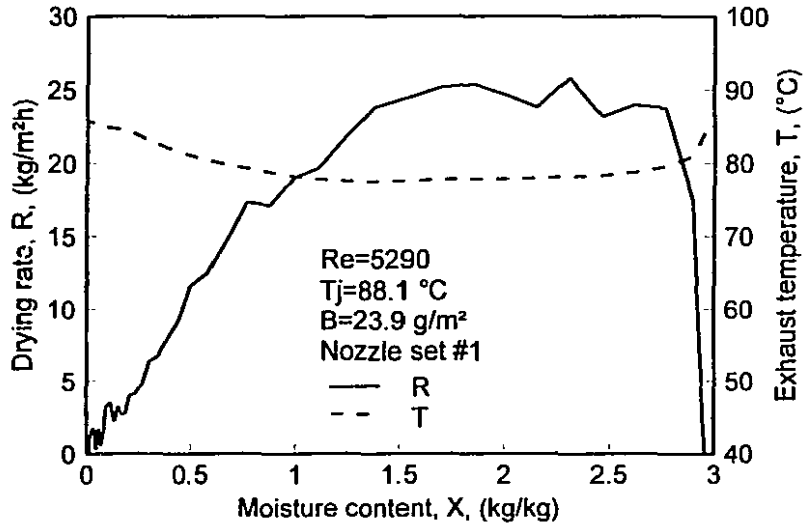
Drying rate, R, (kg/m²h)
Exhaust temperature, T, (°C)
Moisture content, X, (kg/kg)
Re=5290
Tj=88.1 °C
B=23.9 g/m²
Nozzle set #1
R
T

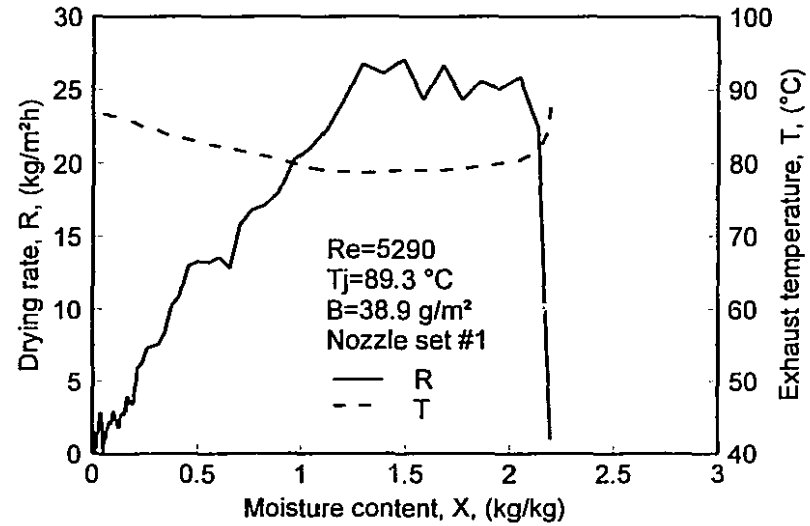
Drying rate, R, (kg/m²h)
Exhaust temperature, T, (°C)
Moisture content, X, (kg/kg)
Re=5290
Tj=89.3 °C
B=38.9 g/m²
Nozzle set #1
R
T

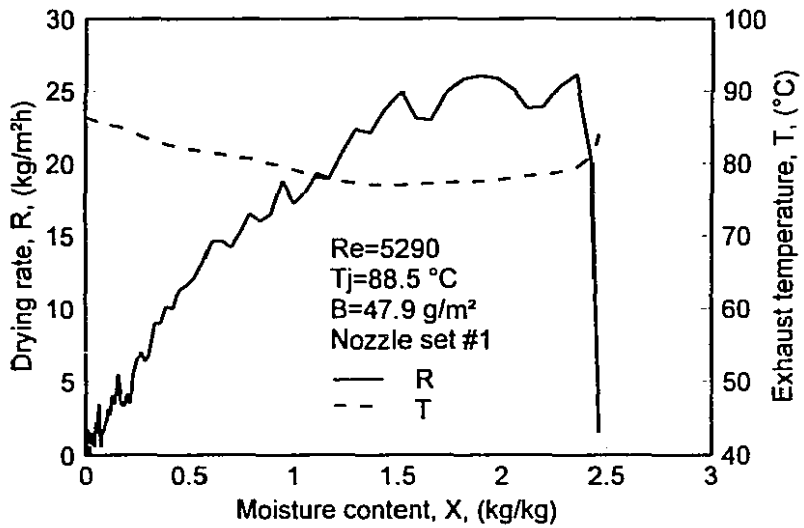
Drying rate, R, (kg/m²h)
Exhaust temperature, T, (°C)
Moisture content, X, (kg/kg)
Re=5290
Tj=88.5 °C
B=47.9 g/m²
Nozzle set #1
R
T

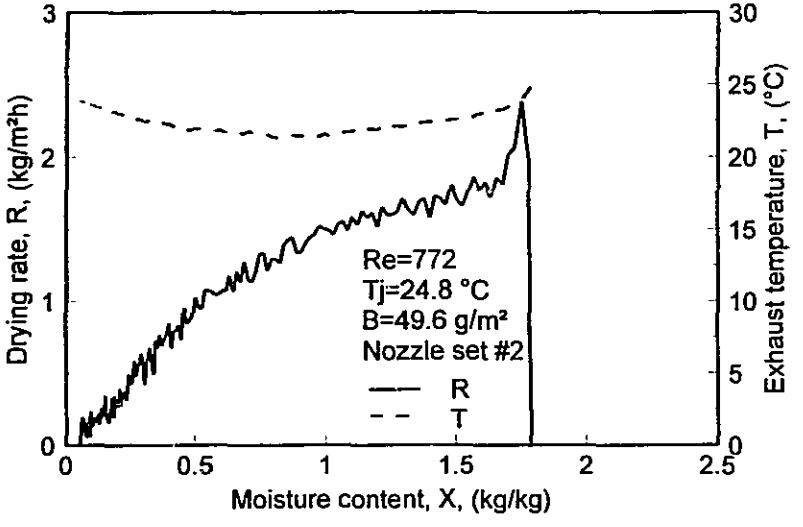
Drying rate, R, (kg/m²h)
Exhaust temperature, T, (°C)
Moisture content, X, (kg/kg)
Re=772
Tj=24.8 °C
B=49.6 g/m²
Nozzle set #2
R
T

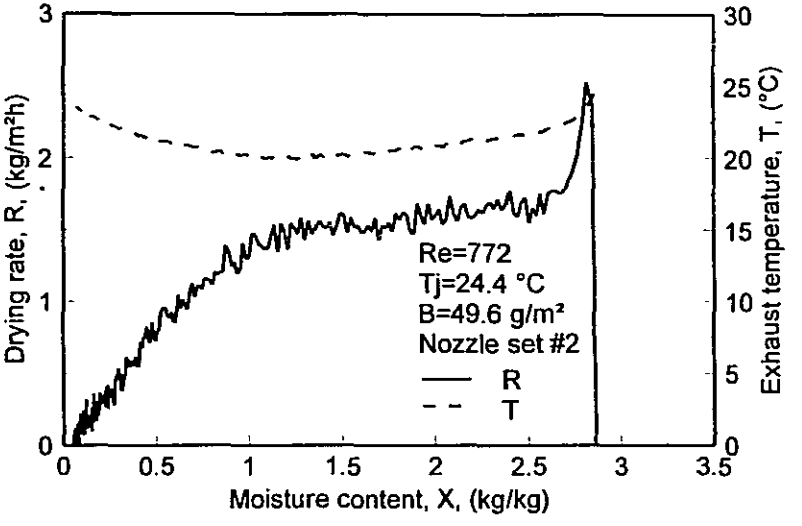
Drying rate, R, (kg/m²h)
Exhaust temperature, T, (°C)
Moisture content, X, (kg/kg)
Re=772
Tj=24.4 °C
B=49.6 g/m²
Nozzle set #2
R
T

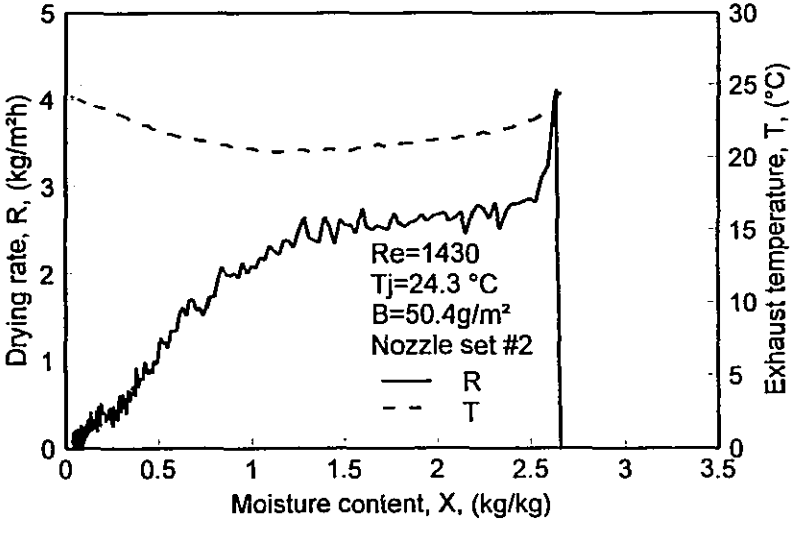
Drying rate, R, (kg/m²h)
Exhaust temperature, T, (°C)
Moisture content, X, (kg/kg)
Re=1430
Tj=24.3 °C
B=50.4g/m²
Nozzle set #2
R
T

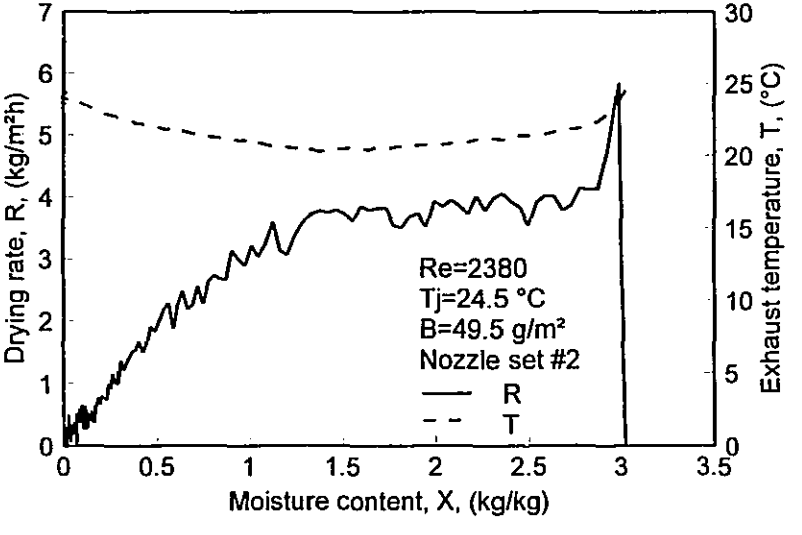
Drying rate, R, (kg/m²h)
Exhaust temperature, T, (°C)
Moisture content, X, (kg/kg)
Re=2380
Tj=24.5 °C
B=49.5 g/m²
Nozzle set #2
R
T

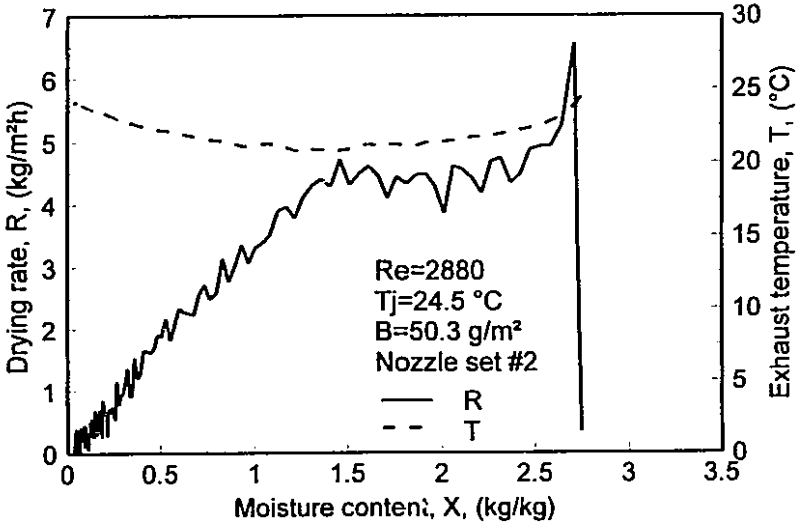
Drying rate, R, (kg/m²h)
Exhaust temperature, T, (°C)
Moisture content, X, (kg/kg)
Re=2880
Tj=24.5 °C
B=50.3 g/m²
Nozzle set #2
R
T

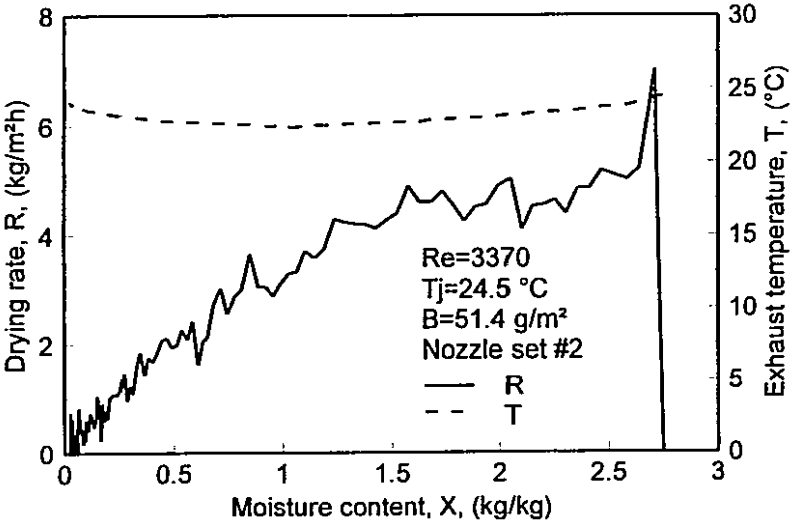
Drying rate, R, (kg/m²h)
Exhaust temperature, T, (°C)
Moisture content, X, (kg/kg)
Re=3370
Tj=24.5 °C
B=51.4 g/m²
Nozzle set #2
R
T

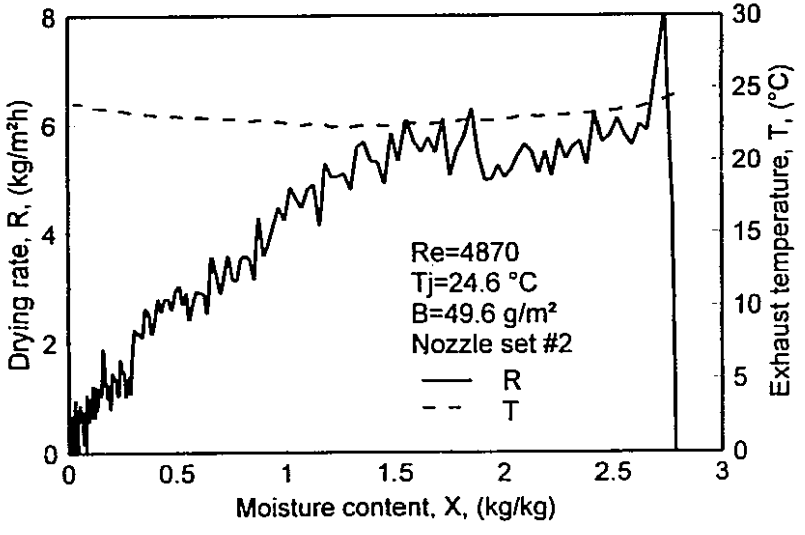
Drying rate, R, (kg/m²h)
Exhaust temperature, T, (°C)
Moisture content, X, (kg/kg)
Re=4870
Tj=24.6 °C
B=49.6 g/m²
Nozzle set #2
R
T

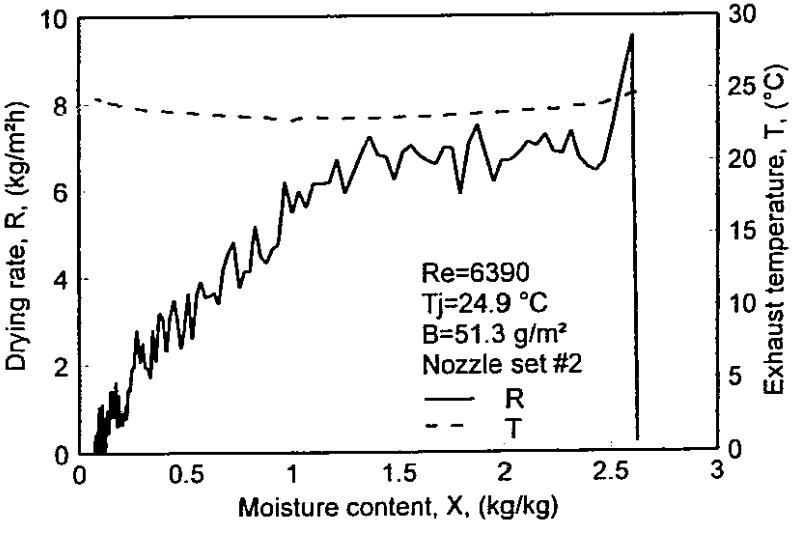
Drying rate, R, (kg/m²h)
Exhaust temperature, T, (°C)
Moisture content, X, (kg/kg)
Re=6390
Tj=24.9 °C
B=51.3 g/m²
Nozzle set #2
R
T

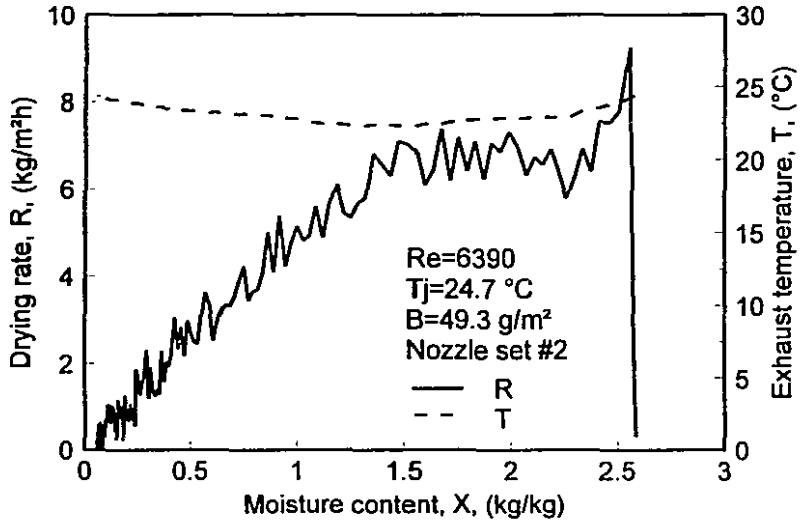
Drying rate, R, (kg/m²h)
Exhaust temperature, T, (°C)
Moisture content, X, (kg/kg)
Re=6390
Tj=24.7 °C
B=49.3 g/m²
Nozzle set #2
R
T

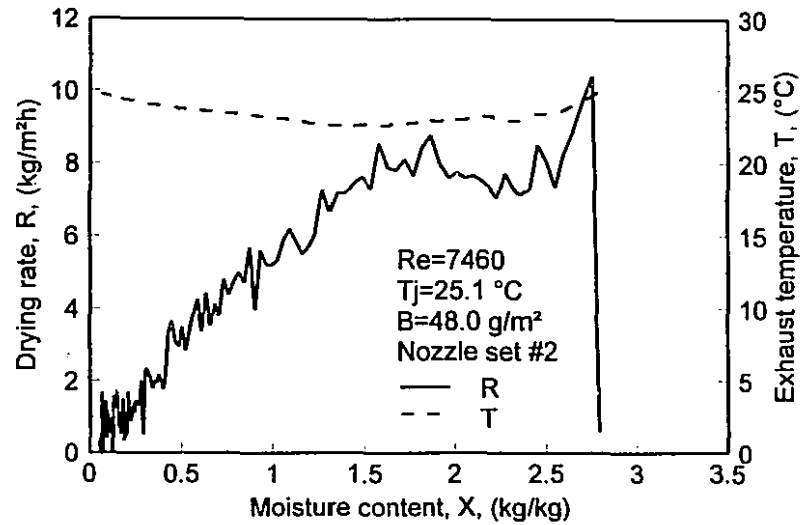
Drying rate, R, (kg/m²h)
Exhaust temperature, T, (°C)
Moisture content, X, (kg/kg)
Re=7460
Tj=25.1 °C
B=48.0 g/m²
Nozzle set #2
R
T

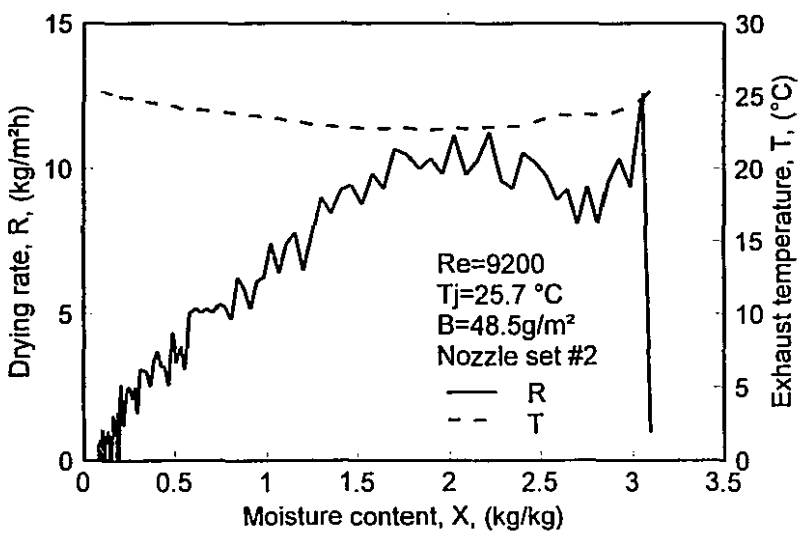
Drying rate, R, (kg/m²h)
Exhaust temperature, T, (°C)
Moisture content, X, (kg/kg)
Re=9200
Tj=25.7 °C
B=48.5g/m²
Nozzle set #2
R
T

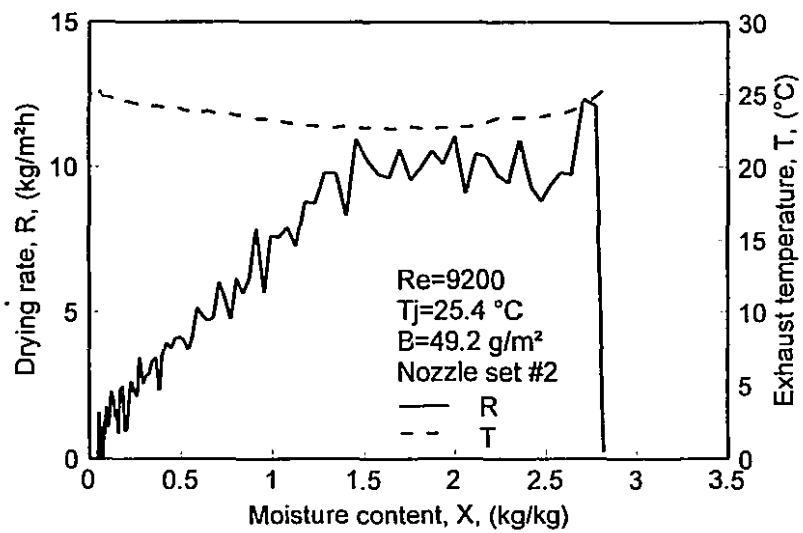
Drying rate, R, (kg/m²h)
Exhaust temperature, T, (°C)
Moisture content, X, (kg/kg)
Re=9200
Tj=25.4 °C
B=49.2 g/m²
Nozzle set #2
R
T

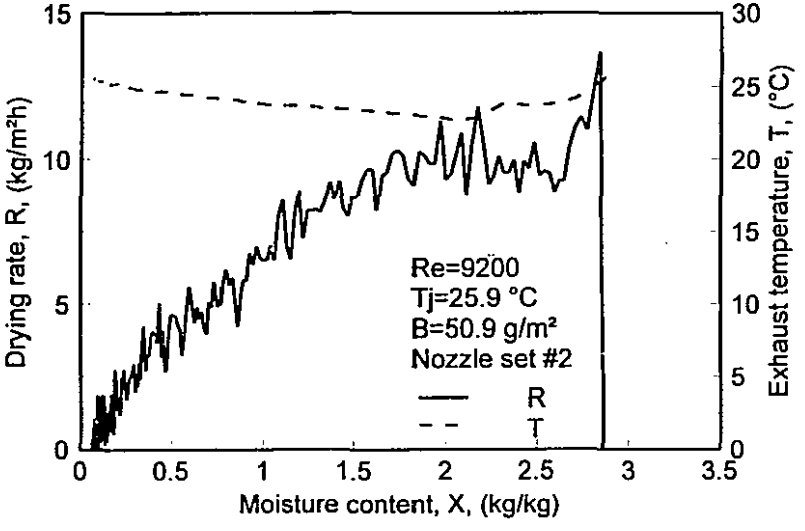
Drying rate, R, (kg/m²h)
Exhaust temperature, T, (°C)
Moisture content, X, (kg/kg)
Re=9200
Tj=25.9 °C
B=50.9 g/m²
Nozzle set #2
R
T
0
5
10
15
20
25
30
0.5
1
1.5
2
2.5
3
3.5

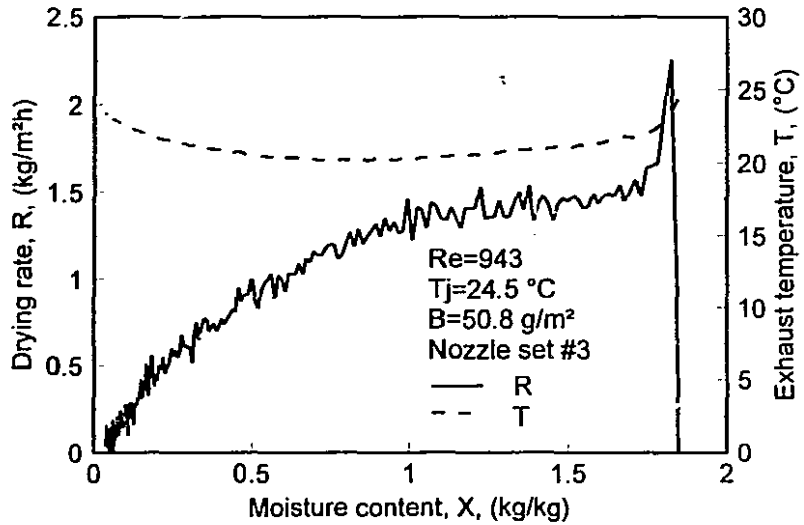
Drying rate, R, (kg/m²h)
Exhaust temperature, T, (°C)
Moisture content, X, (kg/kg)
Re=943
Tj=24.5 °C
B=50.8 g/m²
Nozzle set #3
R
T

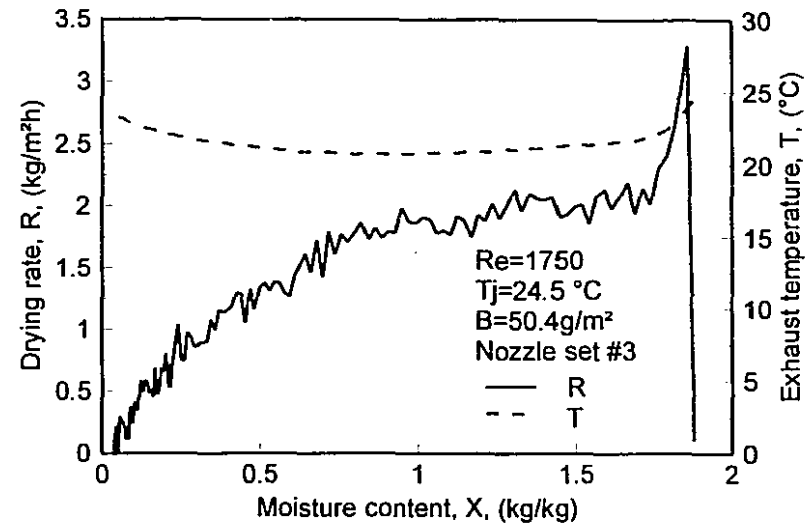
Drying rate, R, (kg/m²h)
Exhaust temperature, T, (°C)
Moisture content, X, (kg/kg)
Re=1750
Tj=24.5 °C
B=50.4g/m²
Nozzle set #3
R
T

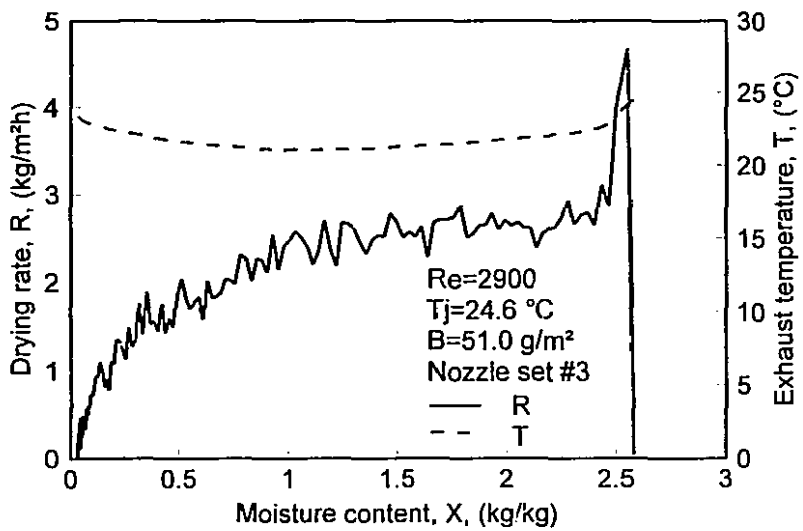
Drying rate, R, (kg/m²h)
Exhaust temperature, T, (°C)
Moisture content, X, (kg/kg)
Re=2900
Tj=24.6 °C
B=51.0 g/m²
Nozzle set #3
R
T

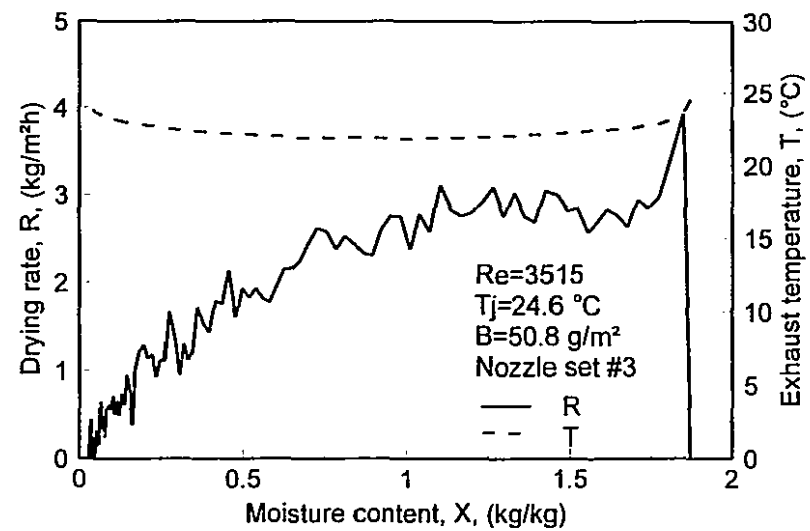
Drying rate, R, (kg/m²h)
Exhaust temperature, T, (°C)
Moisture content, X, (kg/kg)
Re=3515
Tj=24.6 °C
B=50.8 g/m²
Nozzle set #3
R
T

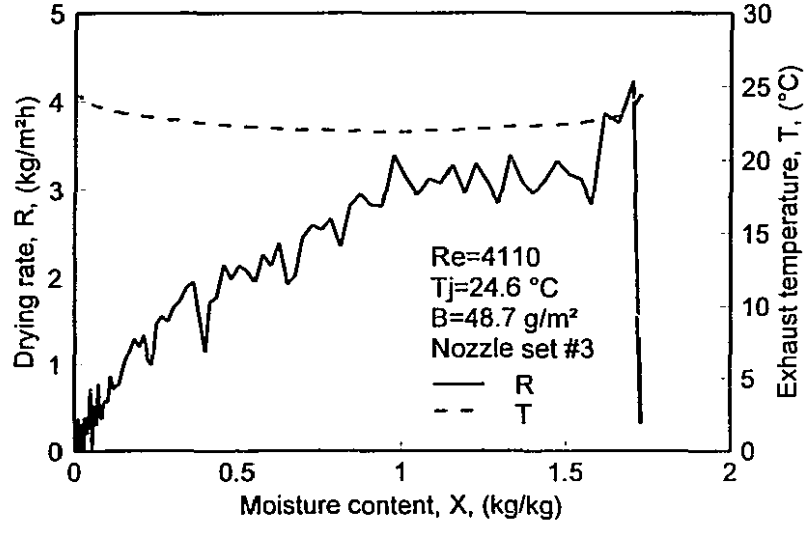
Drying rate, R, (kg/m²h)
Exhaust temperature, T, (°C)
Moisture content, X, (kg/kg)
Re=4110
Tj=24.6 °C
B=48.7 g/m²
Nozzle set #3
R
T

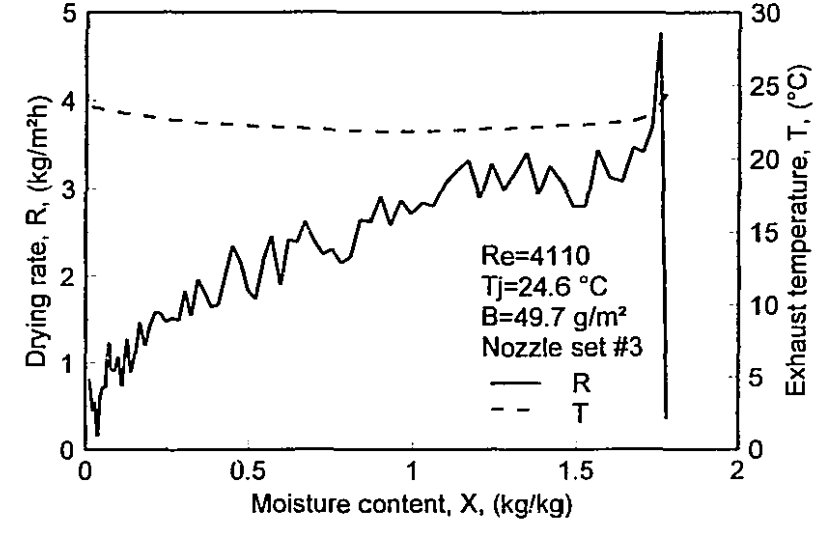
Drying rate, R, (kg/m²h)
Exhaust temperature, T, (°C)
Moisture content, X, (kg/kg)
Re=4110
Tj=24.6 °C
B=49.7 g/m²
Nozzle set #3
R
T

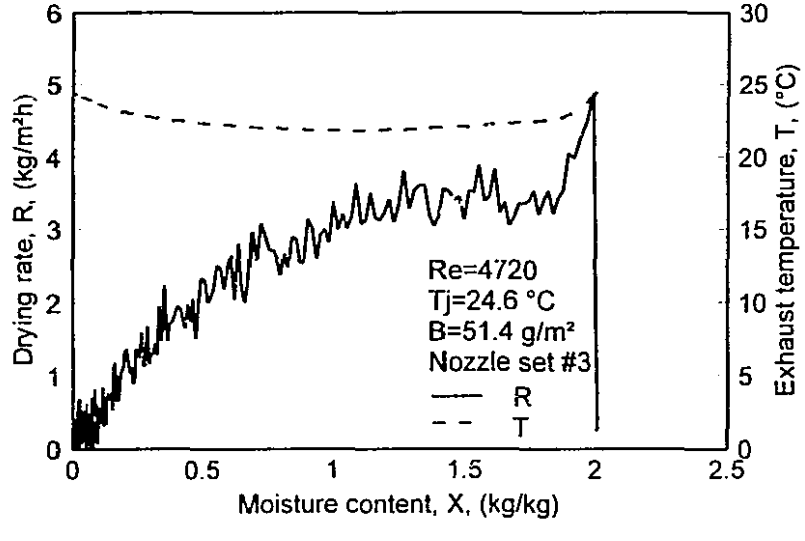
Drying rate, R, (kg/m²h)
Exhaust temperature, T, (°C)
Moisture content, X, (kg/kg)
Re=4720
Tj=24.6 °C
B=51.4 g/m²
Nozzle set #3
R
T

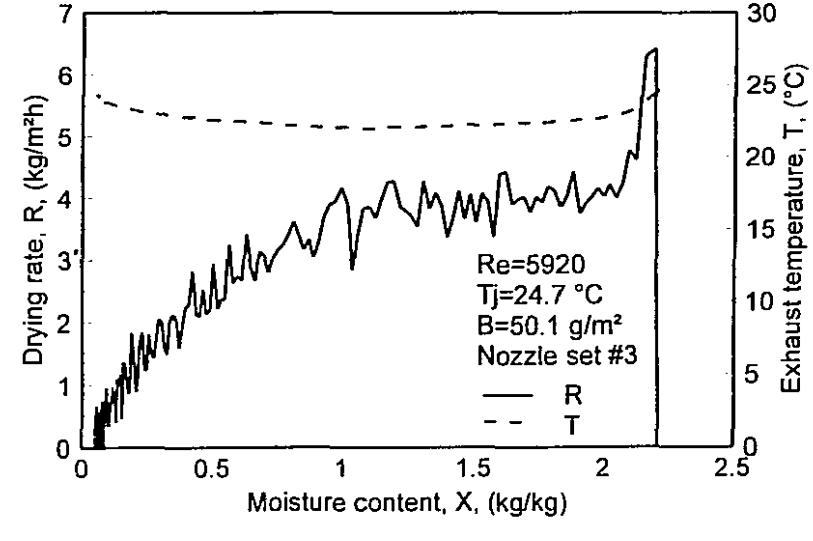
Drying rate, R, (kg/m²h)
Exhaust temperature, T, (°C)
Moisture content, X, (kg/kg)
Re=5920
Tj=24.7 °C
B=50.1 g/m²
Nozzle set #3
R
T

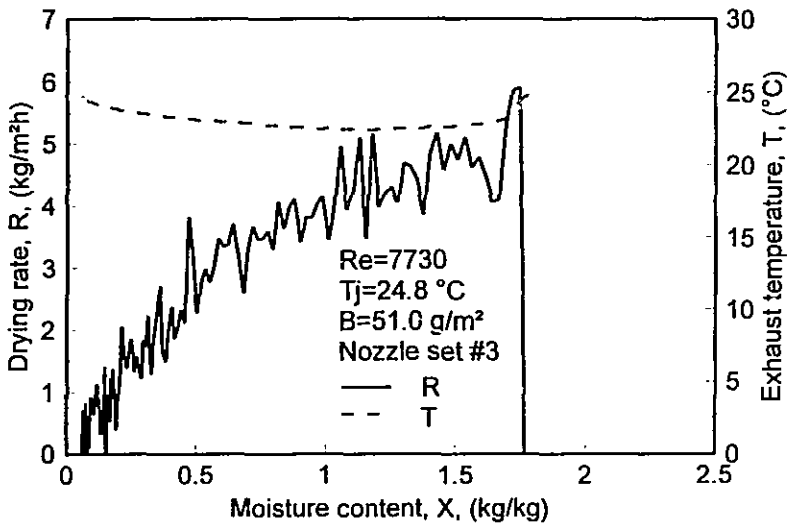
Drying rate, R, (kg/m²h)
Exhaust temperature, T, (°C)
Moisture content, X, (kg/kg)
Re=7730
Tj=24.8 °C
B=51.0 g/m²
Nozzle set #3
R
T

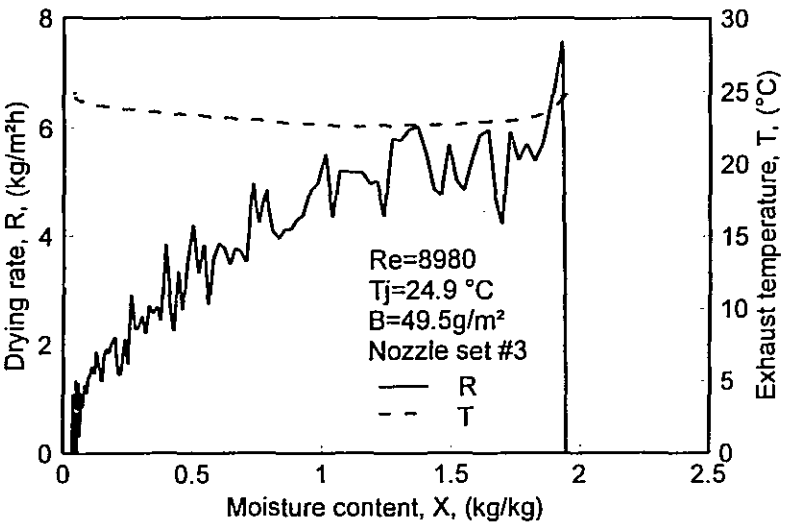
Drying rate, R, (kg/m²h)
Exhaust temperature, T, (°C)
Moisture content, X, (kg/kg)
Re=8980
Tj=24.9 °C
B=49.5g/m²
Nozzle set #3
R
T

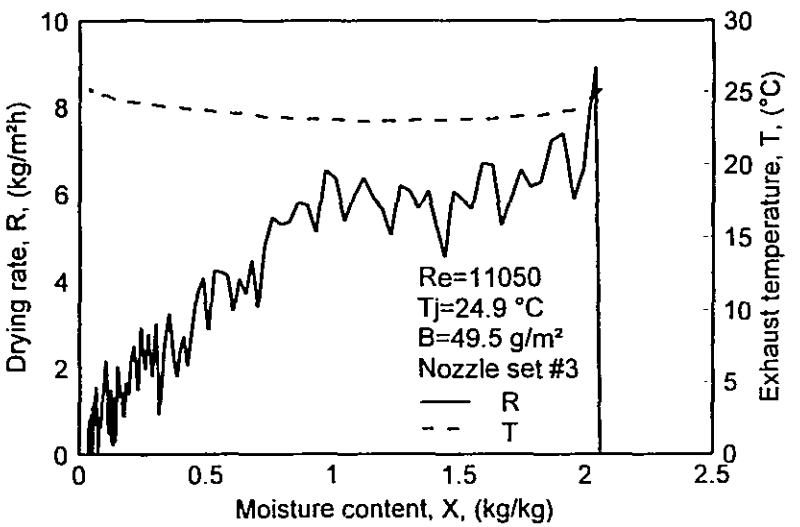
Drying rate, R, (kg/m²h)
Exhaust temperature, T, (°C)
Moisture content, X, (kg/kg)
Re=11050
Tj=24.9 °C
B=49.5 g/m²
Nozzle set #3
R
T

E2: Experimental conditions and important data for pure through drying

G	B	Tj	Tas	Xo	Xi	Xc	Ras	Rc	n	ni
0.125	21.6	22.2	7.30	2.21	.	1.06	2.80	2.58	1.98	.
0.125	22.0	22.2	7.30	2.09	.	1.01	2.80	2.56	1.80	.
0.125	24.6	22.2	7.30	2.33	.	1.15	2.80	2.59	2.43	.
0.125	26.3	22.1	7.25	1.58	.	0.66	2.79	2.54	1.22	.
0.125	37.0	21.6	7.03	2.58	.	0.68	2.75	2.62	1.19	.
0.125	39.7	22.2	7.30	2.54	.	0.89	2.80	2.53	2.11	.
0.125	46.7	22.2	7.30	2.96	.	0.61	2.80	2.56	1.52	.
0.125	50.1	21.7	7.08	2.41	.	0.68	2.76	2.60	1.32	.
0.546	21.5	22.1	7.27	2.43	.	0.98	12.2	10.5	1.25	.
0.546	22.2	22.1	7.27	2.24	.	1.06	12.2	10.8	1.78	.
0.546	27.6	22.1	7.27	2.76	.	1.42	12.2	10.7	2.10	.
0.546	38.6	22.1	7.27	2.59	.	0.74	12.2	10.5	1.32	.
0.546	47.9	22.1	7.27	2.65	.	1.32	12.2	10.3	2.37	.
0.547	26.4	21.6	7.03	2.96	.	0.93	12.0	10.7	1.19	.
0.547	38.5	21.6	7.03	2.58		0.52	12.0	11.1	0.93	.
0.547	49.6	21.6	7.03	2.44	.	0.66	12.0	11.1	1.50	.
1.03	23.6	22.1	7.27	2.32	.	0.87	22.9	18.1	1.13	.
1.03	26.5	21.8	7.11	2.54	.	1.20	22.6	19.0	1.64	.
1.03	28.7	22.1	7.27	2.81	.	1.38	22.9	19.2	1.38	.
1.03	39.0	22.1	7.27	2.47	.	1.80	22.9	19.5	1.90	.
1.03	40.0	21.8	7.11	2.48	.	0.65	22.6	19.1	1.31	.
1.03	49.0	22.1	7.27	2.95	.	1.82	22.9	18.6	2.00	.
1.03	50.2	21.8	7.11	2.36	.	0.72	22.6	20.6	1.88	.
1.46	27.0	21.4	6.90	2.84	.	1.03	31.8	27.4	1.41	.
1.46	37.8	21.4	6.90	2.09	.	0.90	31.8	26.8	1.53	.
1.46	50.4	21.4	6.90	2.38	.	1.05	31.8	29.4	2.48	.
1.47	22.6	22.1	7.27	2.37		0.98	32.7	25.1	1.33	.
1.47	27.1	22.1	7.27	2.56	.	1.21	32.7	26.8	1.46	.
1.47	49.1	22.1	7.27	2.80	.	2.05	32.7	30.0	1.86	.
0.125	26.5	47.3	17.9	2.94	2.75	1.89	5.44	5.56	2.44	2.13
0.125	37.9	47.6	18.0	2.20	2.11	1.19	5.49	5.36	2.13	3.06
0.125	47.7	48.3	17.6	2.43	2.37	1.25	5.33	5.23	2.48	3.77
0.548	28.4	47.3	17.9	2.94	2.64	1.44	23.8	22.0	1.59	3.86
0.548	38.1	47.3	17.9	2.42	2.24	1.18	23.8	21.8	1.79	3.80
0.548	48.5	47.0	17.8	2.39	2.24	1.30	23.6	22.8	2.09	3.78
1.03	25.9	46.5	17.6	2.31	1.94	1.13	44.1	34.1	1.50	3.77
1.03	34.8	46.4	17.6	2.28	1.96	1.02	44.0	38.6	2.04	3.83
1.03	47.1	46.4	17.6	2.07	1.83	0.67	44.0	40.3	1.34	3.83
1.46	26.6	46.8	17.7	2.74	2.26	1.07	63.8	52.6	1.34	3.87
1.46	38.3	46.8	17.7	2.16	1.86	0.83	63.8	54.6	1.50	3.89
1.46	50.7	46.8	17.7	2.22	1.95	0.77	63.8	61.0	1.54	3.87
0.125	26.4	65.9	23.7	2.29	2.07	1.25	7.85	7.96	1.82	3.87
0.125	39.5	66.0	23.8	2.31	2.15	1.34	7.86	7.97	2.21	3.81
0.125	50.8	67.4	24.1	2.20	2.04	0.97	8.05	7.87	1.54	3.67
0.548	28.0	66.0	23.8	2.41	2.05	1.18	34.4	30.1	1.87	3.84
0.548	39.1	66.0	23.8	2.16	1.83	0.96	34.4	30.5	1.72	3.84
0.548	51.3	66.0	23.8	2.40	2.21	1.03	34.4	33.7	1.51	3.75
1.03	26.0	68.1	24.4	2.33	1.80	0.85	67.3	54.0	1.40	3.79
1.03	38.3	67.7	24.2	2.16	1.79	0.82	66.8	58.4	1.63	3.84
1.03	51.6	66.9	24.0	2.30	1.96	0.77	65.9	62.5	1.32	3.84
1.46	26.0	66.5	23.9	2.80	2.13	1.13	93.9	75.5	0.98	3.61
1.46	37.4	66.6	23.9	2.73	2.22	0.99	94.1	83.8	1.37	3.73
1.46	48.4	66.6	23.9	2.50	2.09	0.89	94.1	83.7	1.30	3.63
0.125	23.2	90.9	29.9	1.97	1.65	1.09	11.5	9.84	2.03	3.62
0.125	23.2	91.1	30.0	2.90	2.59	1.27	11.6	9.74	2.17	2.76
0.125	26.3	87.7	29.1	2.17	1.83	1.25	11.0	11.2	2.06	3.59
0.125	35.5	87.7	29.1	2.26	1.98	1.14	11.0	11.7	1.80	3.84
0.125	38.6	91.1	30.0	2.48	2.25	1.10	11.6	9.90	2.33	3.82
0.125	43.6	86.2	28.8	1.89	1.66	0.95	10.8	10.2	1.63	3.81
0.125	48.4	91.1	30.0	2.61	2.43	1.11	11.6	10.0	2.47	3.88
0.125	49.5	92.9	30.4	2.07	1.85	1.01	11.8	10.7	2.25	4.08
0.547	20.9	89.3	29.6	2.86	2.38	1.34	49.2	36.9	1.53	2.64
0.547	28.9	89.4	29.6	2.37	2.01	1.29	49.3	38.6	1.62	3.27
0.547	38.0	90.4	29.8	2.63	2.24	1.10	50.0	41.4	2.27	3.63
0.547	48.0	91.0	30.0	1.69	1.38	0.80	50.5	40.9	2.18	3.72
0.549	26.6	90.2	29.7	2.92	2.37	1.57	49.6	45.7	1.88	3.77
0.549	37.7	89.9	29.6	2.83	2.38	1.52	49.6	49.2	1.91	3.84
0.549	43.1	88.3	29.3	1.97	1.68	1.17	48.7	41.6	2.01	3.18
0.549	48.0	88.3	29.3	2.84	2.37	0.95	48.5	49.6	1.57	3.99
1.03	25.7	88.7	29.4	2.86	2.07	1.64	92.3	65.6	1.58	3.42
1.03	32.6	88.4	29.3	2.93	2.27	1.04	91.5	74.3	0.90	3.46
1.03	50.3	88.5	29.3	2.66	2.14	1.08	92.0	81.5	1.30	3.76
1.03	24.7	89.2	29.5	2.71	2.06	1.07	92.6	67.6	1.56	3.80
1.03	26.0	89.5	29.6	2.61	1.85	1.05	92.9	68.7	1.22	4.77
1.03	37.8	89.5	29.6	2.72	2.43	1.21	92.9	68.1	1.89	3.98
1.03	46.6	88.8	29.5	2.06	1.67	1.13	92.1	67.8	2.05	3.51
1.03	47.2	89.2	29.5	3.30	2.97	1.80	92.6	68.8	2.24	2.73
1.47	24.1	90.6	29.9	2.64	1.89	1.07	135	87.8	1.52	3.60
1.47	27.5	89.7	29.6	2.53	1.71	1.23	133	92.4	1.65	3.40
1.47	37.4	90.8	29.9	2.62	2.05	1.22	135	86.8	2.22	3.63
1.47	47.7	88.9	29.5	2.65	2.20	1.69	132	102	1.84	3.17
1.47	48.3	88.9	29.5	1.38	1.06	0.59	132	92.7	1.07	3.09
1.47	51.7	88.9	29.5	2.40	2.07	1.50	132	90.0	1.96	3.01
1.48	48.9	87.2	29.1	2.75	2.20	1.41	129	96.0	1.62	3.75
1.48	25.7	88.8	29.4	2.60	1.97	1.13	133	79.6	1.22	3.63
1.48	26.5	88.8	29.4	2.50	1.84	1.22	132	77.1	1.04	3.05
1.48	37.0	90.7	29.8	2.91	2.16	0.88	136	122	1.04	3.72
1.48	48.7	90.5	29.8	3.14	2.50	1.29	136	117	1.48	3.73
1.48	49.8	90.5	29.8	2.72	2.08	1.38	136	118	2.05	3.48
(Through drying without jets)										
0.544	24.8	21.5	7.03	2.56	.	.	11.9	10.3	1.83	.
0.544	24.1	21.5	7.03	2.39	.	.	11.9	10.4	1.88	.
0.544	49.5	21.5	7.03	2.42	.	.	11.9	10.4	1.27	.
0.544	50.3	21.5	7.03	2.33	.	.	11.9	10.6	1.6	.
1.45	24.1	86.2	28.8	2.06	1.33	1.16	125	77.7	2.01	3.35
1.45	25.1	86.2	28.8	2.63	2.11	1.23	125	77.5	1.52	3.68
1.45	49.7	86.2	28.8	2.56	2.04	1.08	125	116	1.88	3.75
1.45	49.3	86.2	28.8	2.42	1.95	0.98	125	119	1.74	3.76

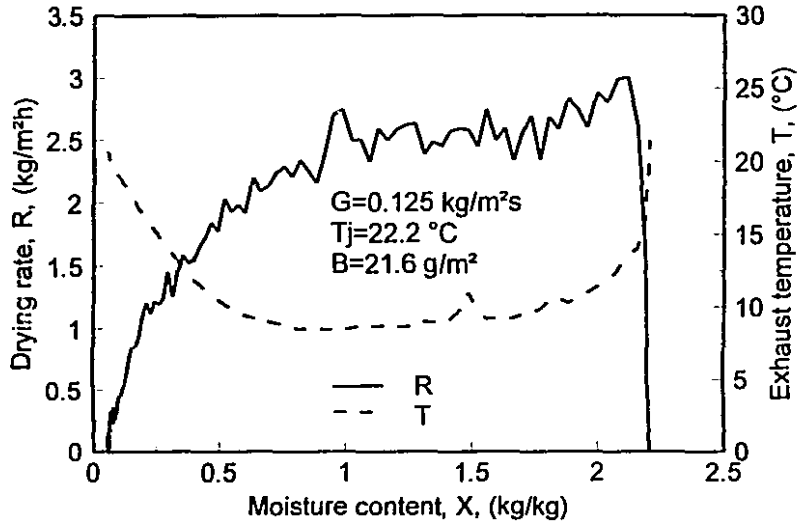
Drying rate, R, (kg/m²h)
Exhaust temperature, T, (°C)
Moisture content, X, (kg/kg)
G=0.125 kg/m²s
Tj=22.2 °C
B=21.6 g/m²
R
T

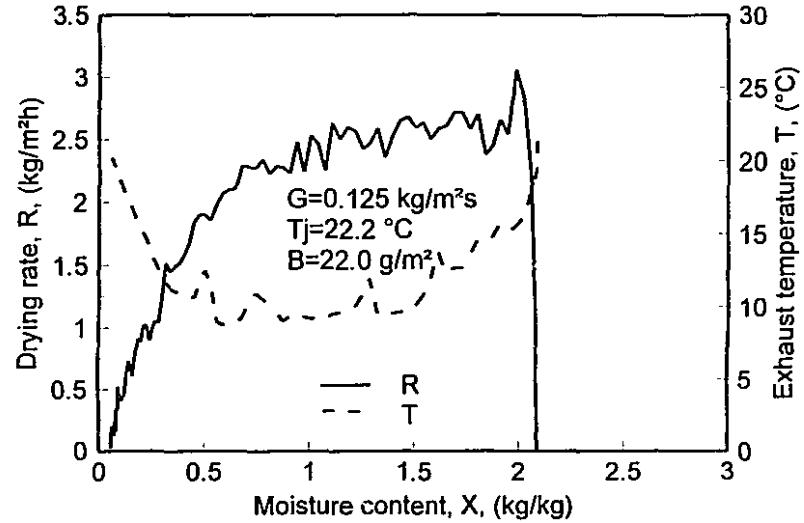
Drying rate, R, (kg/m²h)
Exhaust temperature, T, (°C)
Moisture content, X, (kg/kg)
G=0.125 kg/m²s
Tj=22.2 °C
B=22.0 g/m²
R
T

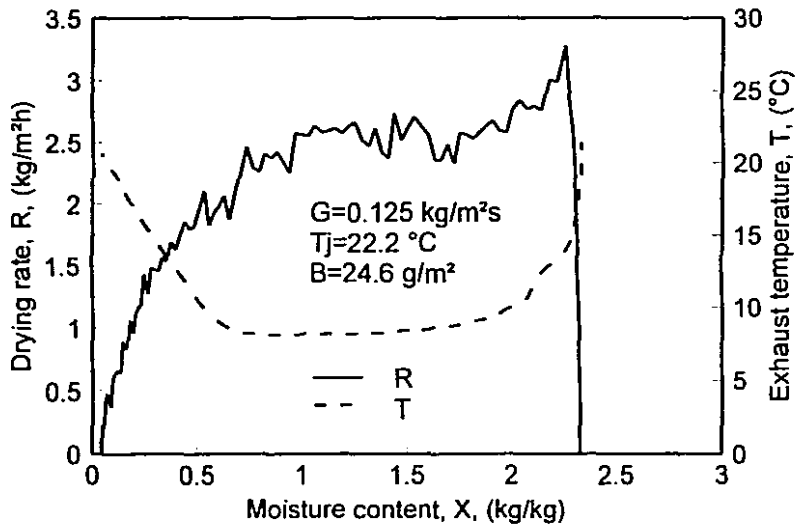
Drying rate, R, (kg/m²h)
Exhaust temperature, T, (°C)
Moisture content, X, (kg/kg)
G=0.125 kg/m²s
Tj=22.2 °C
B=24.6 g/m²
R
T

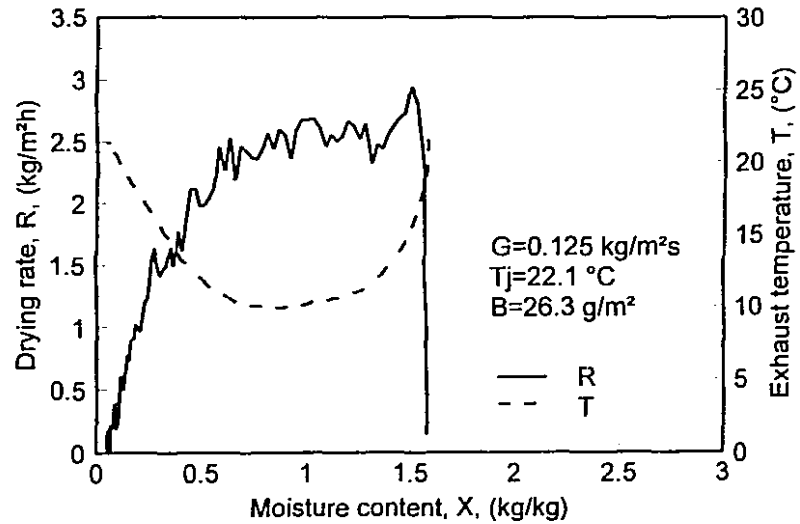
Drying rate, R, (kg/m²h)
Exhaust temperature, T, (°C)
Moisture content, X, (kg/kg)
G=0.125 kg/m²s
Tj=22.1 °C
B=26.3 g/m²
R
T

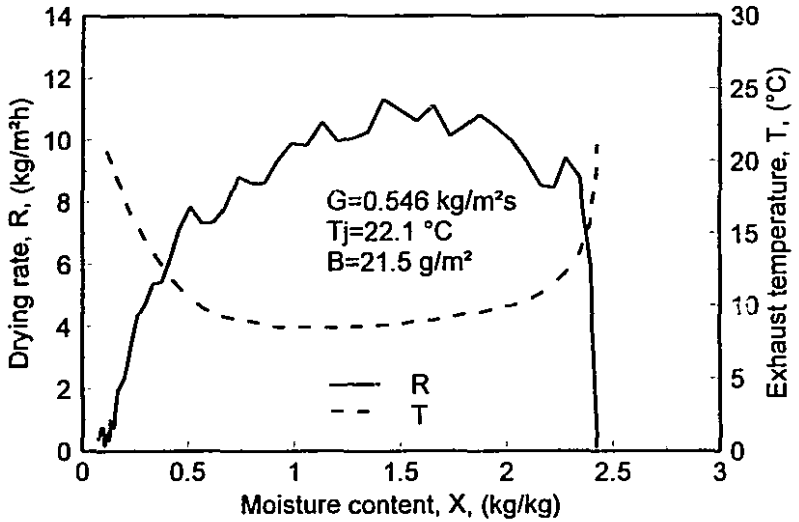
G=0.546 kg/m²s
Tj=22.1 °C
B=21.5 g/m²
R
T
Drying rate, R, (kg/m²h)
Exhaust temperature, T, (°C)
Moisture content, X, (kg/kg)

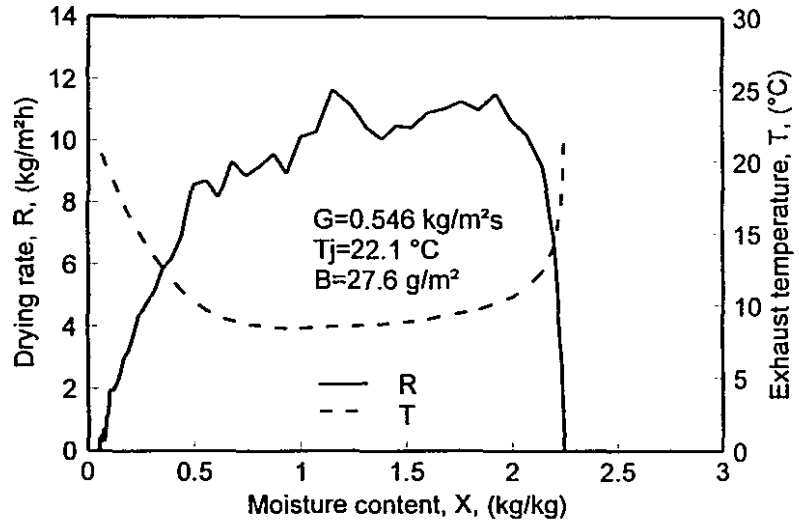
G=0.546 kg/m²s
Tj=22.1 °C
B=27.6 g/m²
R
T
Drying rate, R, (kg/m²h)
Exhaust temperature, T, (°C)
Moisture content, X, (kg/kg)

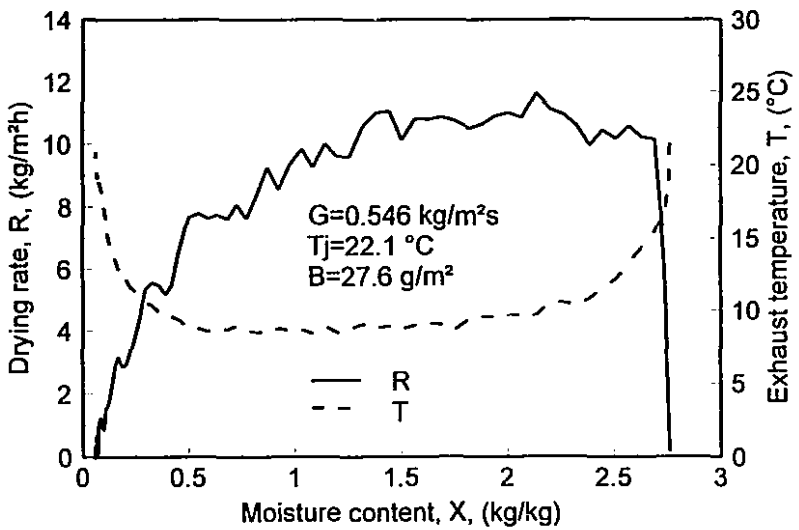
G=0.546 kg/m²s
Tj=22.1 °C
B=27.6 g/m²
R
T
Drying rate, R, (kg/m²h)
Exhaust temperature, T, (°C)
Moisture content, X, (kg/kg)

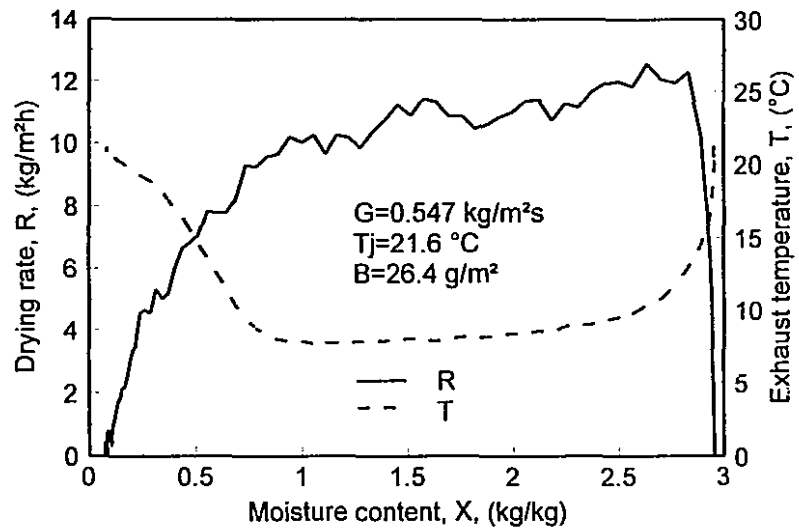
G=0.547 kg/m²s
Tj=21.6 °C
B=26.4 g/m²
R
T
Drying rate, R, (kg/m²h)
Exhaust temperature, T, (°C)
Moisture content, X, (kg/kg)

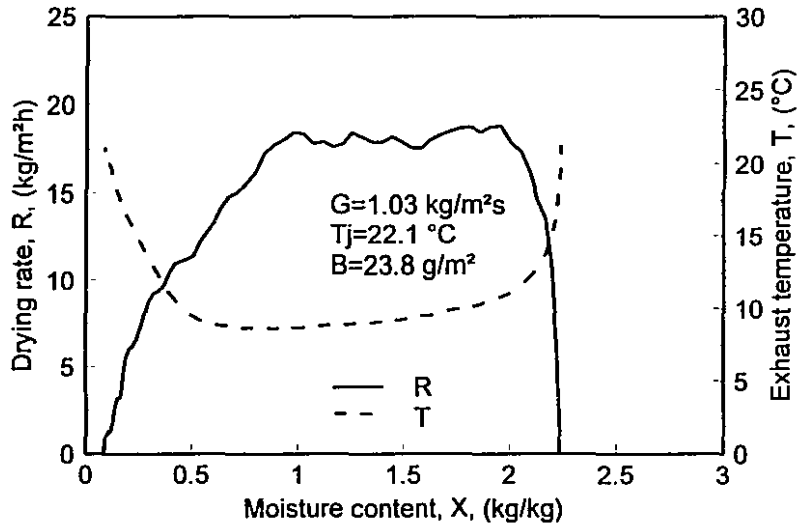
Drying rate, R, (kg/m²h)
Exhaust temperature, T, (°C)
Moisture content, X, (kg/kg)
G=1.03 kg/m²s
Tj=22.1 °C
B=23.8 g/m²
R
T

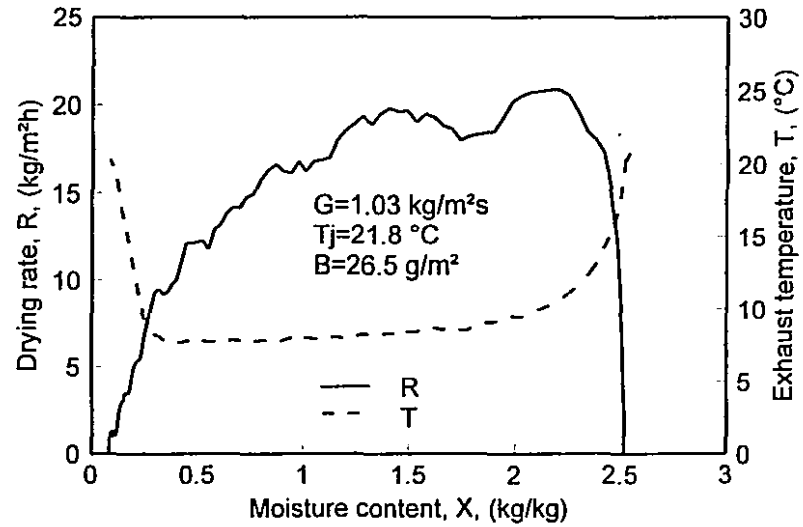
Drying rate, R, (kg/m²h)
Exhaust temperature, T, (°C)
Moisture content, X, (kg/kg)
G=1.03 kg/m²s
Tj=21.8 °C
B=26.5 g/m²
R
T

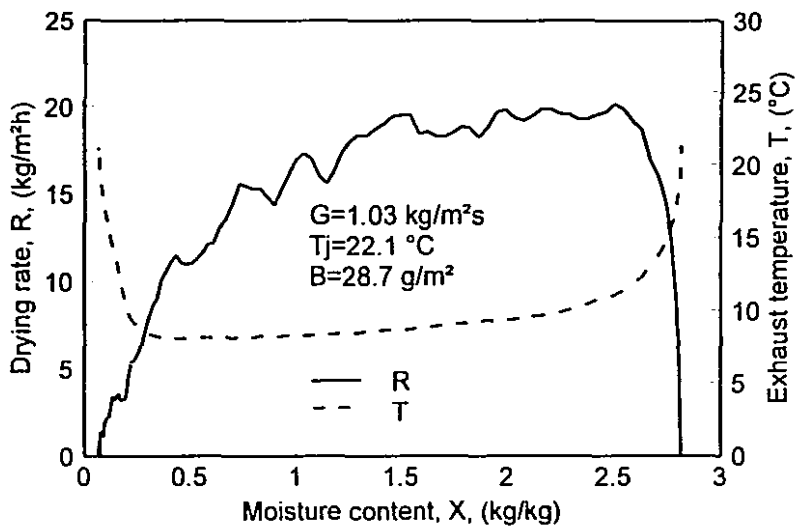
Drying rate, R, (kg/m²h)
Exhaust temperature, T, (°C)
Moisture content, X, (kg/kg)
G=1.03 kg/m²s
Tj=22.1 °C
B=28.7 g/m²
R
T

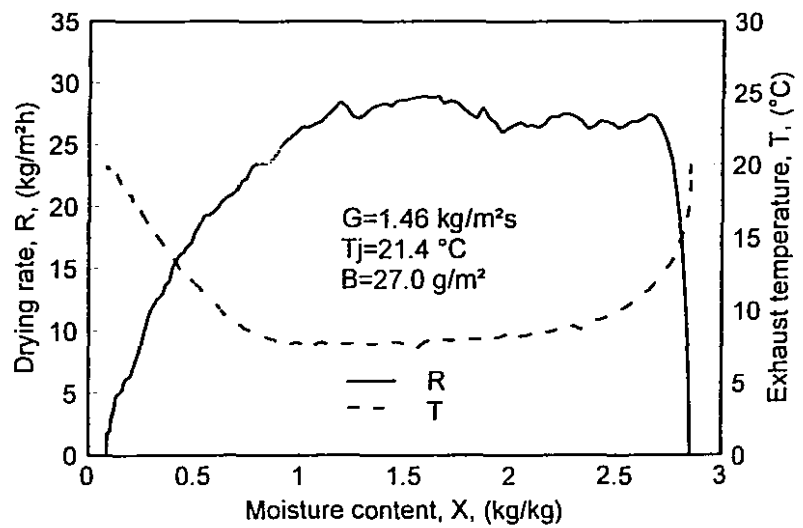
Drying rate, R, (kg/m²h)
Exhaust temperature, T, (°C)
Moisture content, X, (kg/kg)
G=1.46 kg/m²s
Tj=21.4 °C
B=27.0 g/m²
R
T

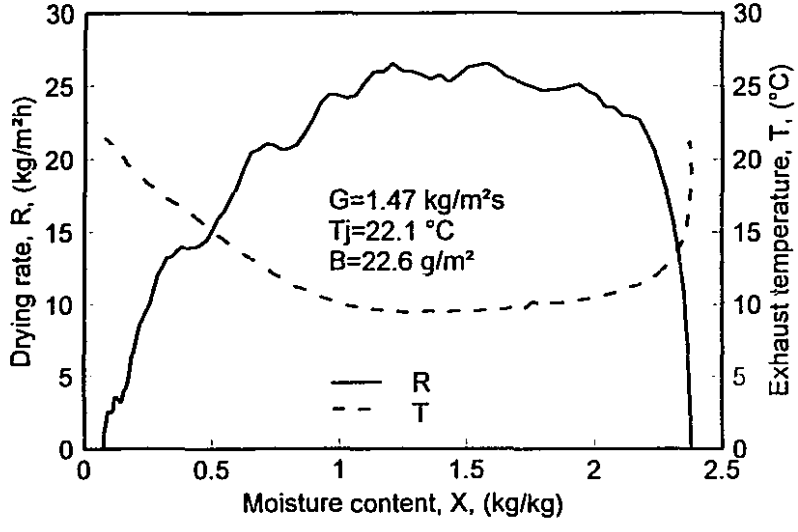
G=1.47 kg/m²s
Tj=22.1 °C
B=22.6 g/m²
R
T
Drying rate, R, (kg/m²h)
Exhaust temperature, T, (°C)
Moisture content, X, (kg/kg)

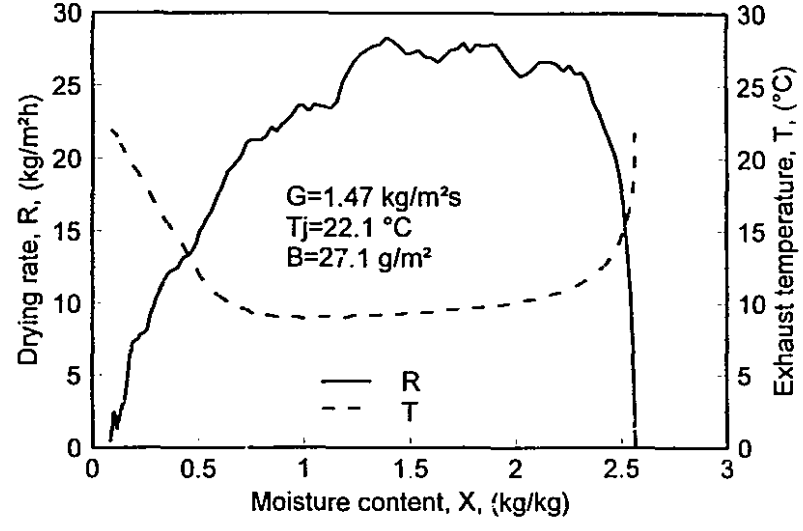
G=1.47 kg/m²s
Tj=22.1 °C
B=27.1 g/m²
R
T
Drying rate, R, (kg/m²h)
Exhaust temperature, T, (°C)
Moisture content, X, (kg/kg)

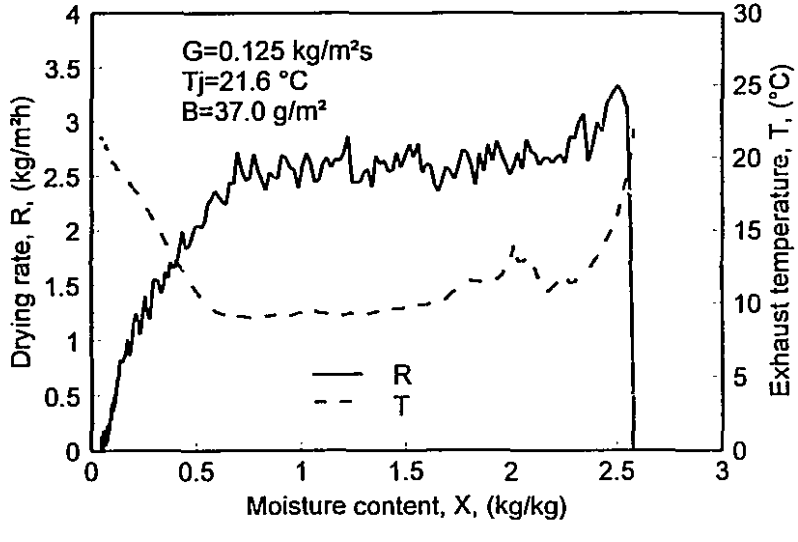
G=0.125 kg/m²s
Tj=21.6 °C
B=37.0 g/m²
R
T
Drying rate, R, (kg/m²h)
Exhaust temperature, T, (°C)
Moisture content, X, (kg/kg)

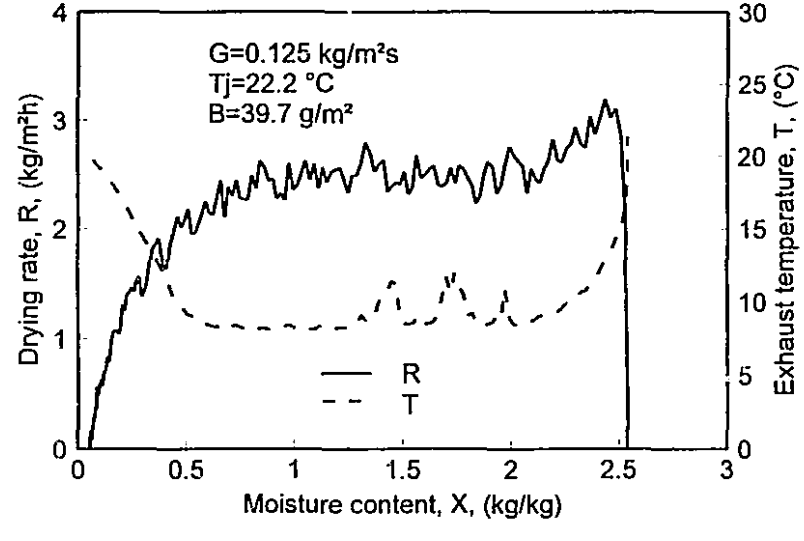
G=0.125 kg/m²s
Tj=22.2 °C
B=39.7 g/m²
R
T
Drying rate, R, (kg/m²h)
Exhaust temperature, T, (°C)
Moisture content, X, (kg/kg)

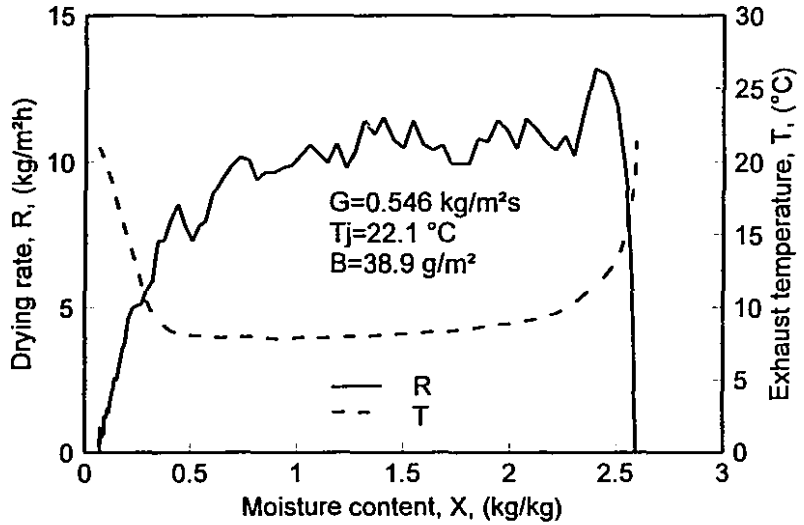
G=0.546 kg/m²s
Tj=22.1 °C
B=38.9 g/m²
R
T
Drying rate, R, (kg/m²h)
Exhaust temperature, T, (°C)
Moisture content, X, (kg/kg)

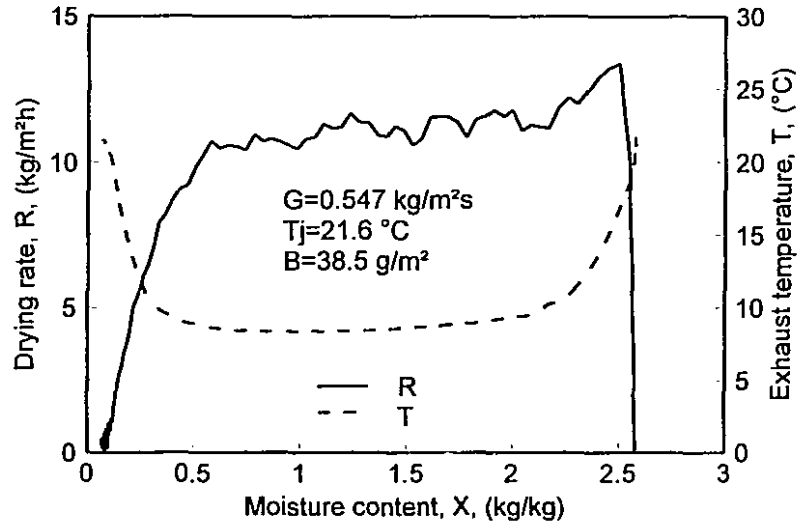
G=0.547 kg/m²s
Tj=21.6 °C
B=38.5 g/m²
R
T
Drying rate, R, (kg/m²h)
Exhaust temperature, T, (°C)
Moisture content, X, (kg/kg)

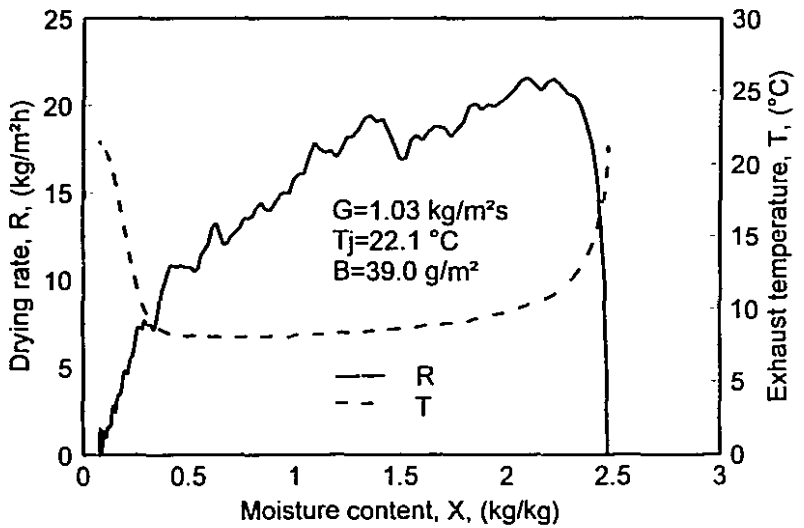
G=1.03 kg/m²s
Tj=22.1 °C
B=39.0 g/m²
R
T
Drying rate, R, (kg/m²h)
Exhaust temperature, T, (°C)
Moisture content, X, (kg/kg)

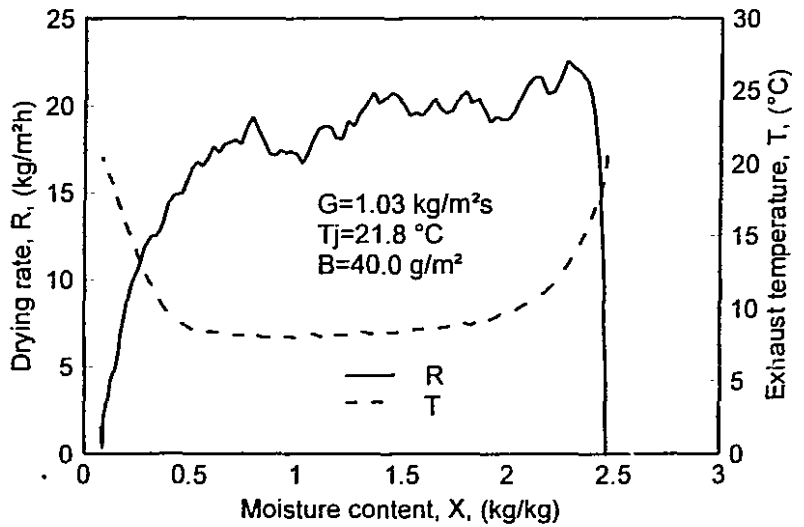
G=1.03 kg/m²s
Tj=21.8 °C
B=40.0 g/m²
R
T
Drying rate, R, (kg/m²h)
Exhaust temperature, T, (°C)
Moisture content, X, (kg/kg)

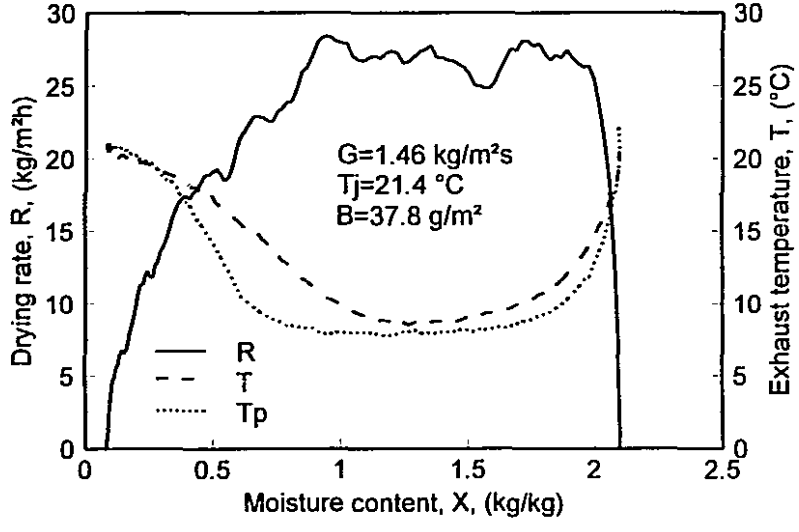
G=1.46 kg/m²s
Tj=21.4 °C
B=37.8 g/m²
R
T
Tp
Drying rate, R, (kg/m²h)
Exhaust temperature, T, (°C)
Moisture content, X, (kg/kg)

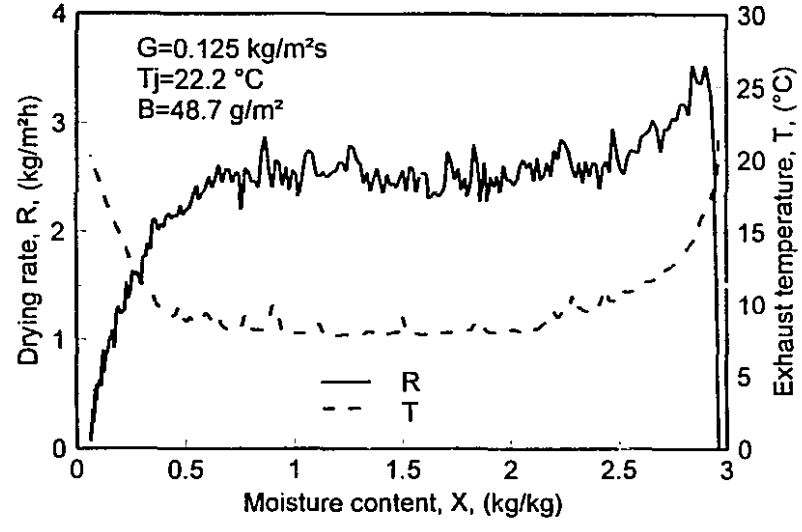
G=0.125 kg/m²s
Tj=22.2 °C
B=48.7 g/m²
R
T
Drying rate, R, (kg/m²h)
Exhaust temperature, T, (°C)
Moisture content, X, (kg/kg)

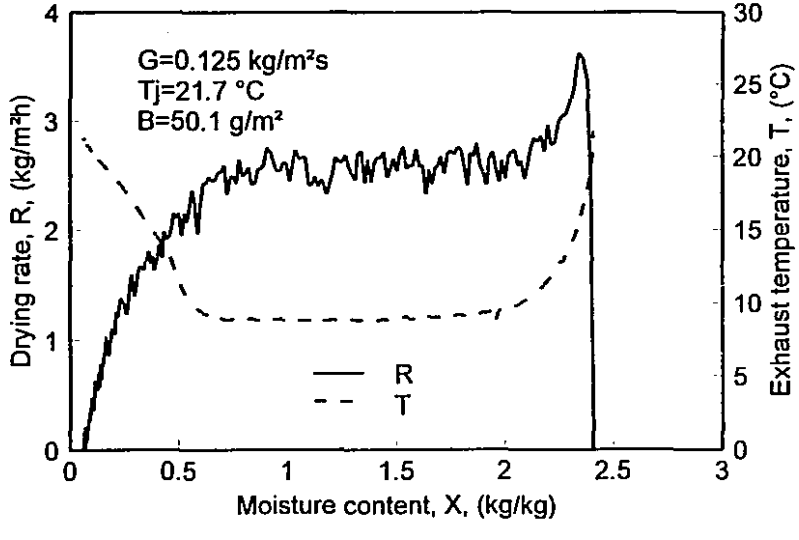
G=0.125 kg/m²s
Tj=21.7 °C
B=50.1 g/m²
R
T
Drying rate, R, (kg/m²h)
Exhaust temperature, T, (°C)
Moisture content, X, (kg/kg)

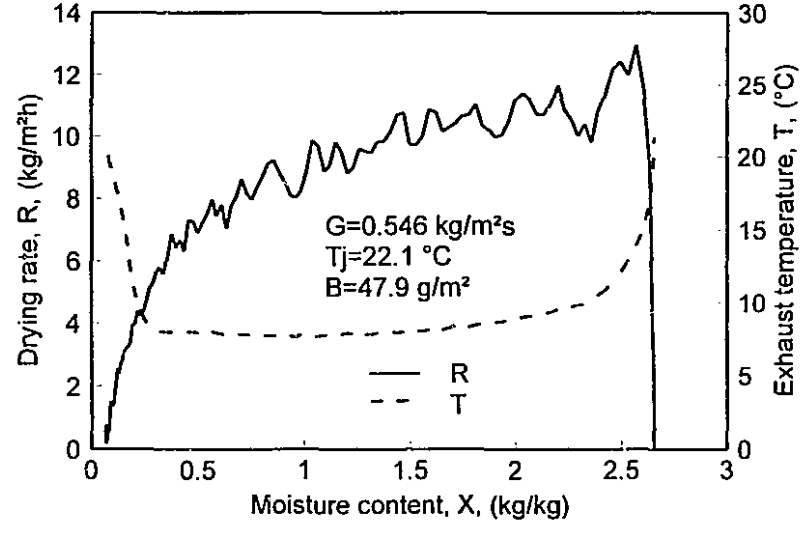
G=0.546 kg/m²s
Tj=22.1 °C
B=47.9 g/m²
R
T
Drying rate, R, (kg/m²h)
Exhaust temperature, T, (°C)
Moisture content, X, (kg/kg)

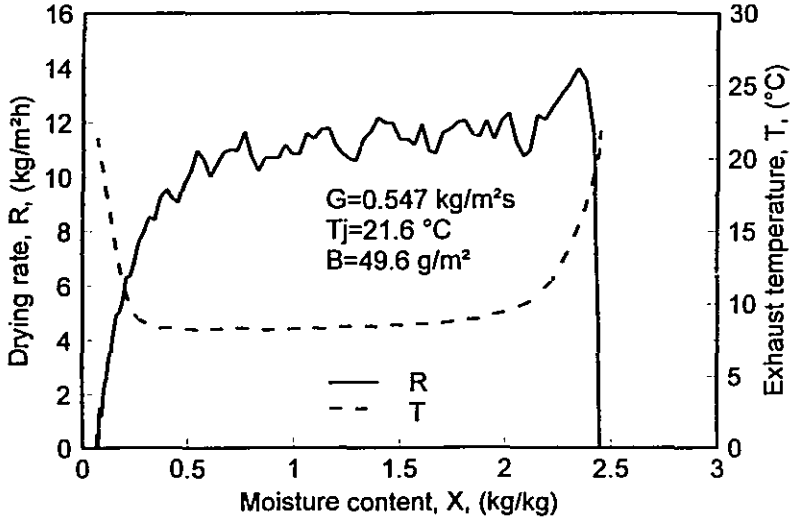
G=0.547 kg/m²s
Tj=21.6 °C
B=49.6 g/m²
R
T
Drying rate, R, (kg/m²h)
Exhaust temperature, T, (°C)
Moisture content, X, (kg/kg)

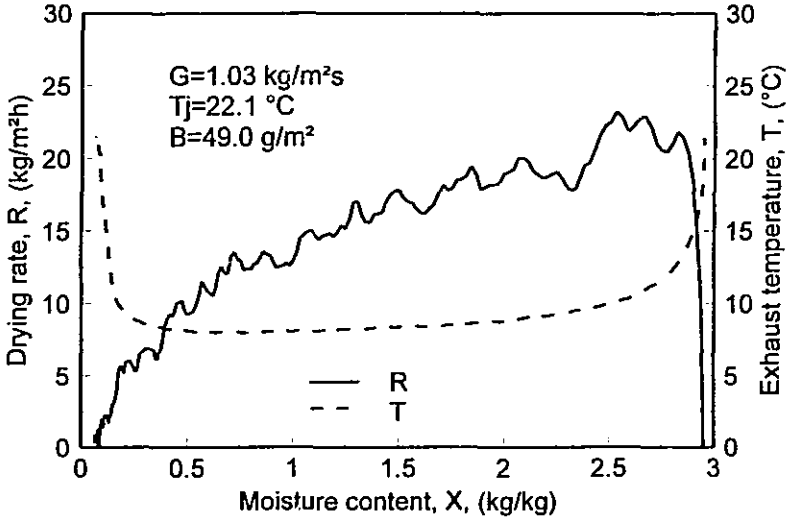
G=1.03 kg/m²s
Tj=22.1 °C
B=49.0 g/m²
R
T
Drying rate, R, (kg/m²h)
Exhaust temperature, T, (°C)
Moisture content, X, (kg/kg)

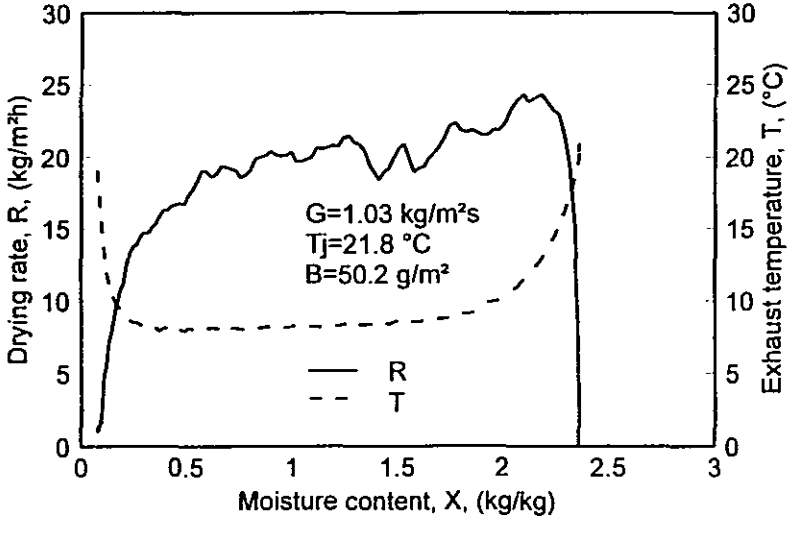
G=1.03 kg/m²s
Tj=21.8 °C
B=50.2 g/m²
R
T
Drying rate, R, (kg/m²h)
Exhaust temperature, T, (°C)
Moisture content, X, (kg/kg)

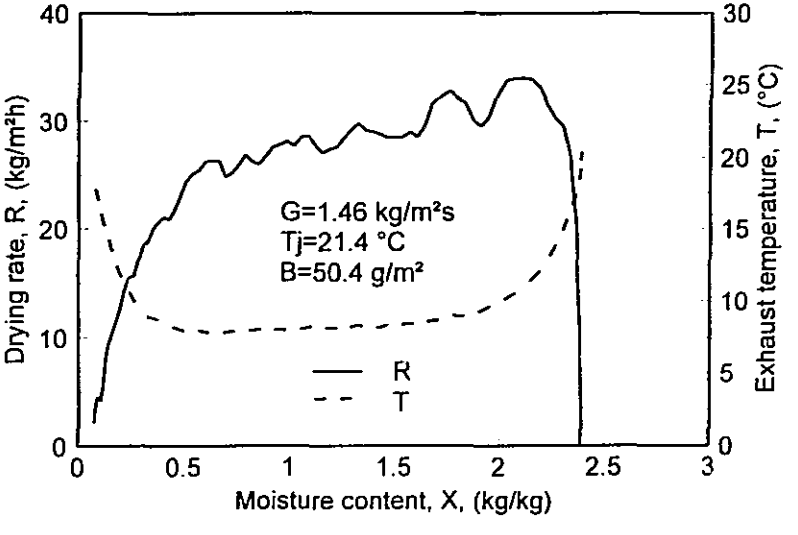
G=1.46 kg/m²s
Tj=21.4 °C
B=50.4 g/m²
R
T
Drying rate, R, (kg/m²h)
Exhaust temperature, T, (°C)
Moisture content, X, (kg/kg)

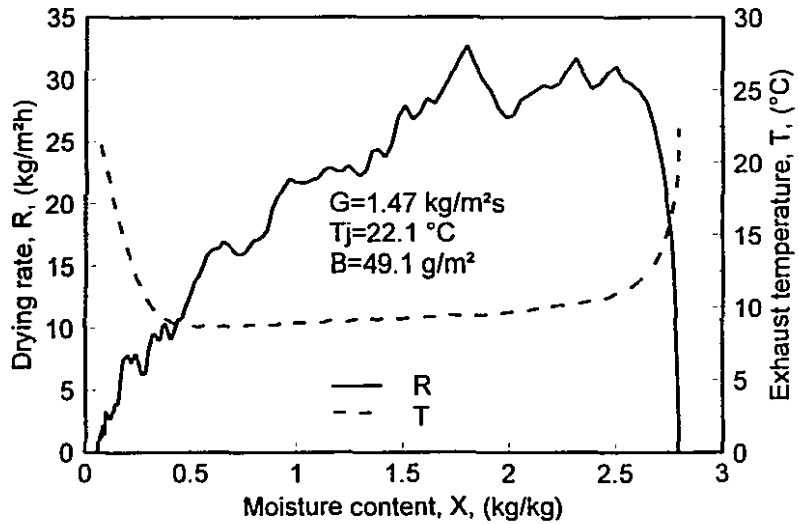
G=1.47 kg/m²s
Tj=22.1 °C
B=49.1 g/m²
R
T
Drying rate, R, (kg/m²h)
Exhaust temperature, T, (°C)
Moisture content, X, (kg/kg)

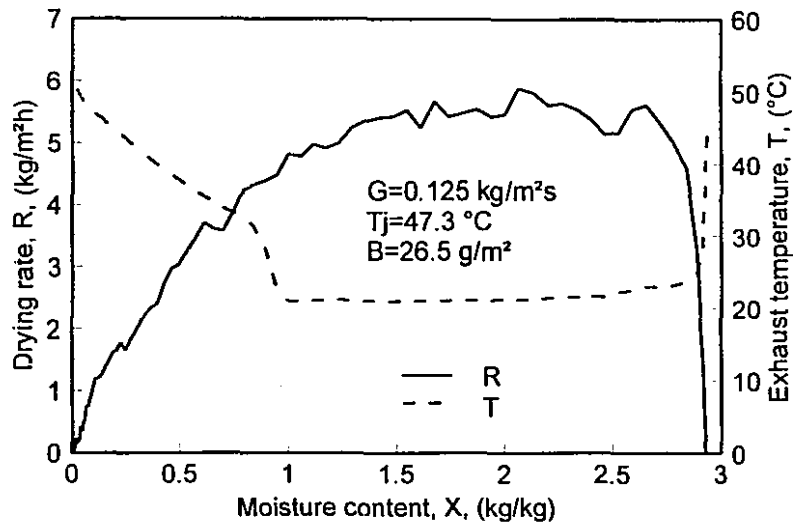
G=0.125 kg/m²s
Tj=47.3 °C
B=26.5 g/m²
R
T
Drying rate, R, (kg/m²h)
Exhaust temperature, T, (°C)
Moisture content, X, (kg/kg)

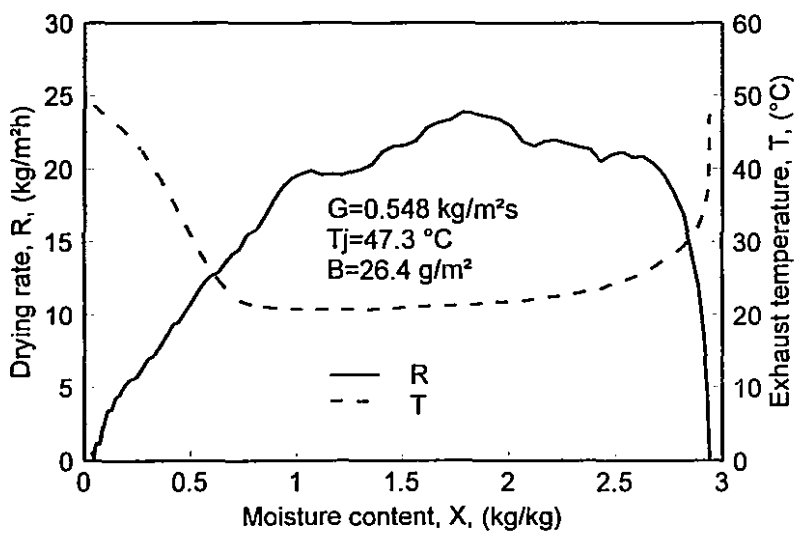
G=0.548 kg/m²s
Tj=47.3 °C
B=26.4 g/m²
R
T
Drying rate, R, (kg/m²h)
Exhaust temperature, T, (°C)
Moisture content, X, (kg/kg)

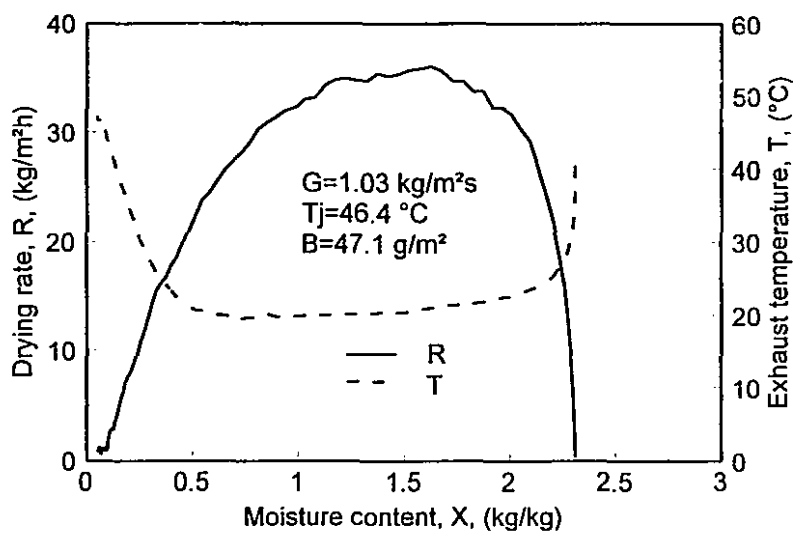
G=1.03 kg/m²s
Tj=46.4 °C
B=47.1 g/m²
R
T
Drying rate, R, (kg/m²h)
Exhaust temperature, T, (°C)
Moisture content, X, (kg/kg)

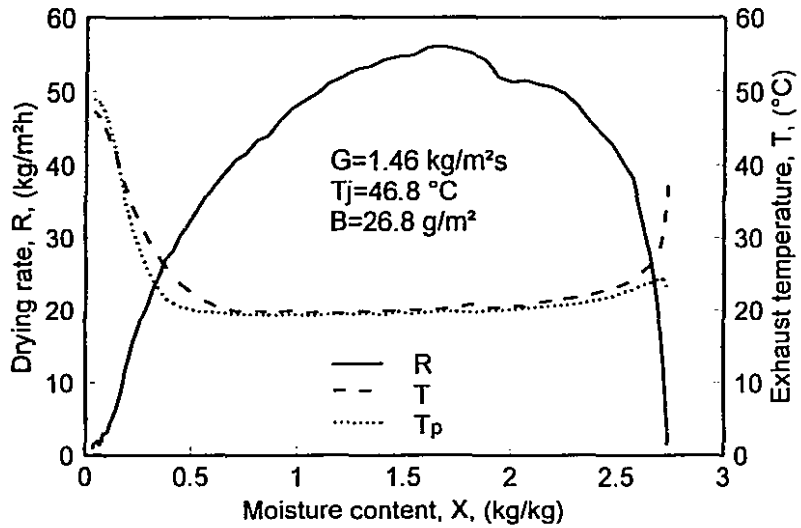
G=1.46 kg/m²s
Tj=46.8 °C
B=26.8 g/m²
R
T
Tp
Drying rate, R, (kg/m²h)
Exhaust temperature, T, (°C)
Moisture content, X, (kg/kg)

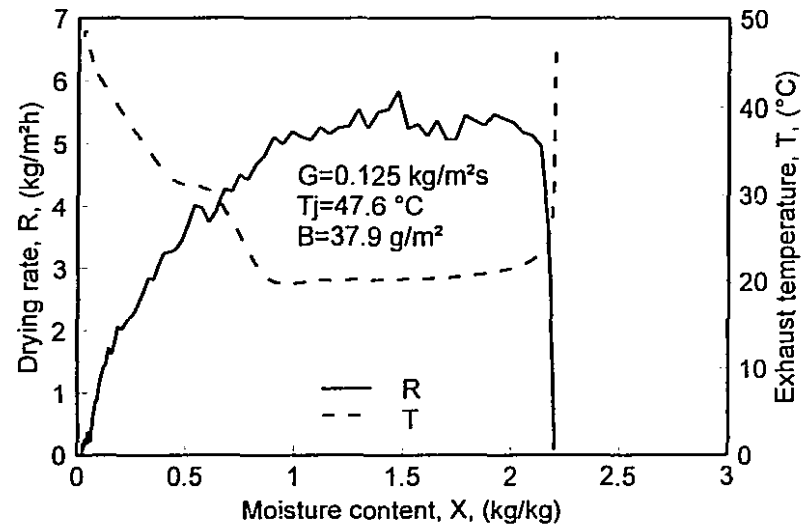
G=0.125 kg/m²s
Tj=47.6 °C
B=37.9 g/m²
R
T
Drying rate, R, (kg/m²h)
Exhaust temperature, T, (°C)
Moisture content, X, (kg/kg)

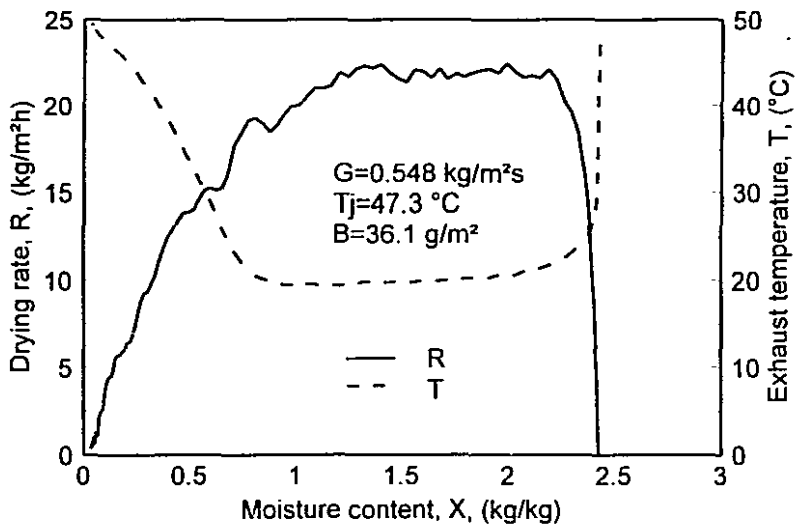
G=0.548 kg/m²s
Tj=47.3 °C
B=36.1 g/m²
R
T
Drying rate, R, (kg/m²h)
Exhaust temperature, T, (°C)
Moisture content, X, (kg/kg)

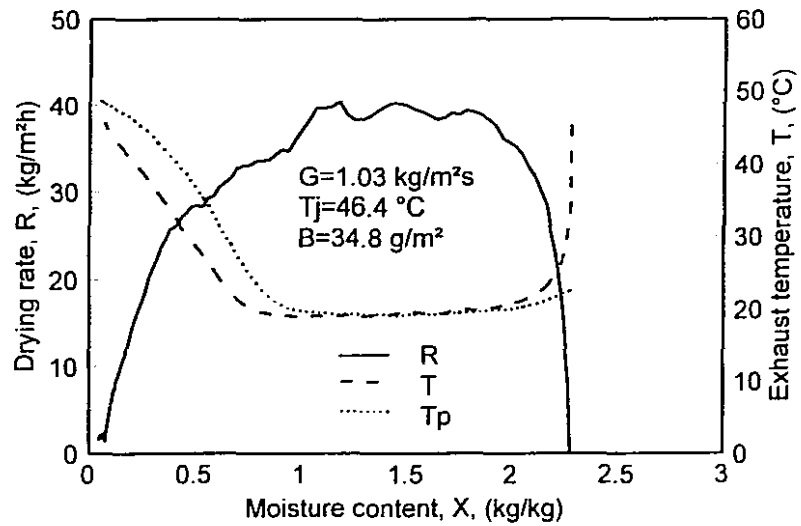
G=1.03 kg/m²s
Tj=46.4 °C
B=34.8 g/m²
R
T
Tp
Drying rate, R, (kg/m²h)
Exhaust temperature, T, (°C)
Moisture content, X, (kg/kg)

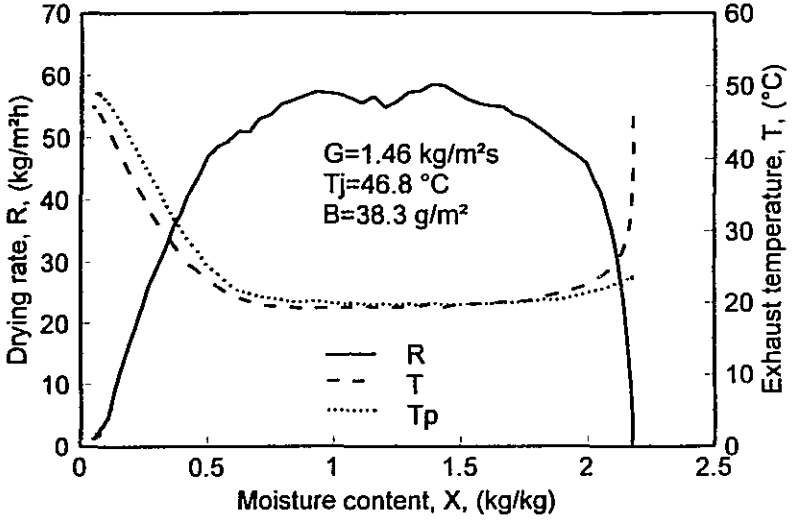
G=1.46 kg/m²s
Tj=46.8 °C
B=38.3 g/m²
R
T
Tp
Drying rate, R, (kg/m²h)
Exhaust temperature, T, (°C)
Moisture content, X, (kg/kg)

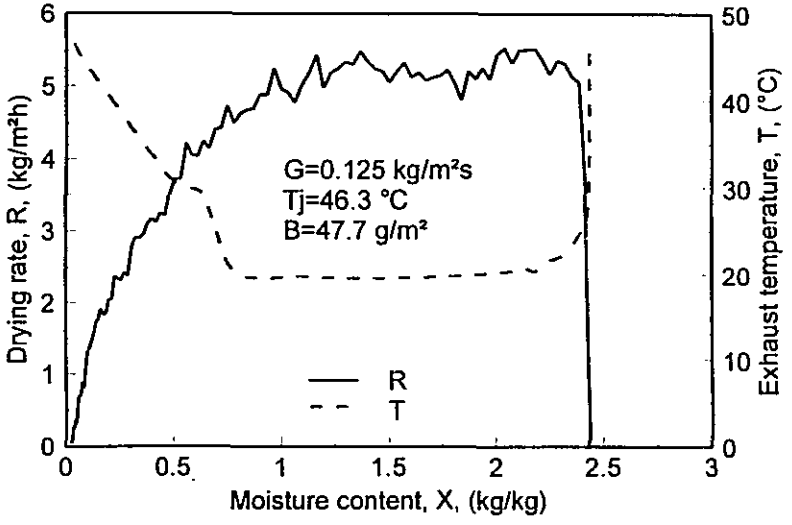
G=0.125 kg/m²s
Tj=46.3 °C
B=47.7 g/m²
R
T
Drying rate, R, (kg/m²h)
Exhaust temperature, T, (°C)
Moisture content, X, (kg/kg)

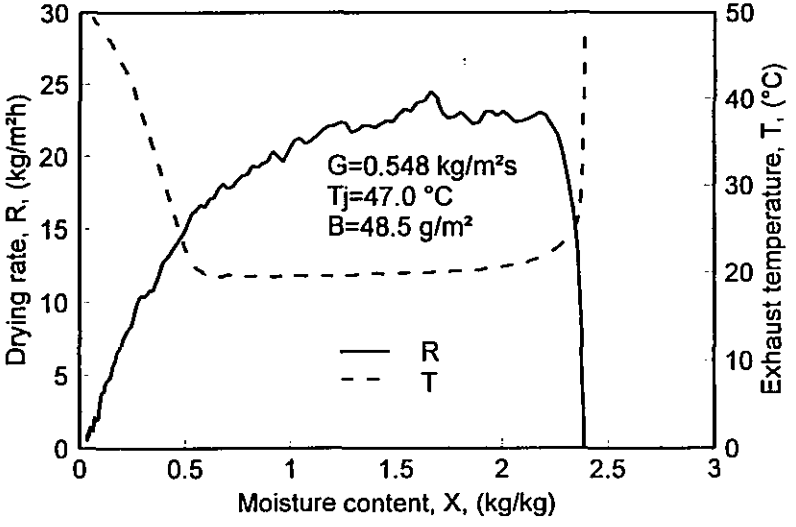
G=0.548 kg/m²s
Tj=47.0 °C
B=48.5 g/m²
R
T
Drying rate, R, (kg/m²h)
Exhaust temperature, T, (°C)
Moisture content, X, (kg/kg)

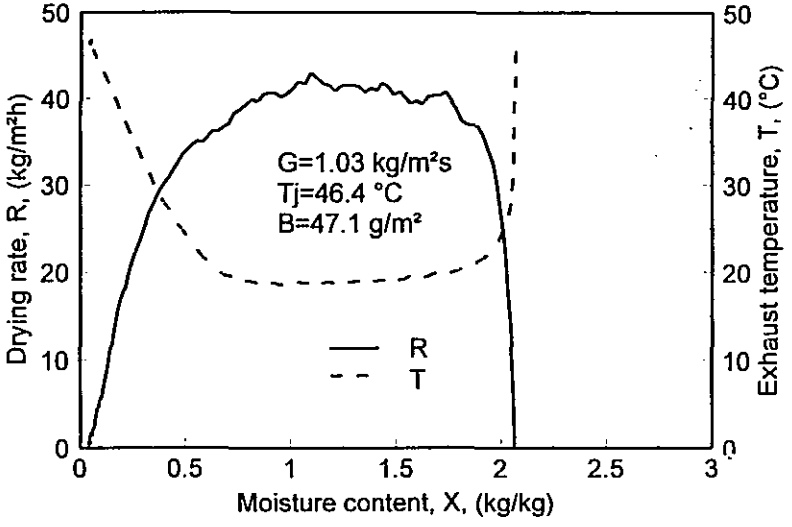
G=1.03 kg/m²s
Tj=46.4 °C
B=47.1 g/m²
R
T
Drying rate, R, (kg/m²h)
Exhaust temperature, T, (°C)
Moisture content, X, (kg/kg)

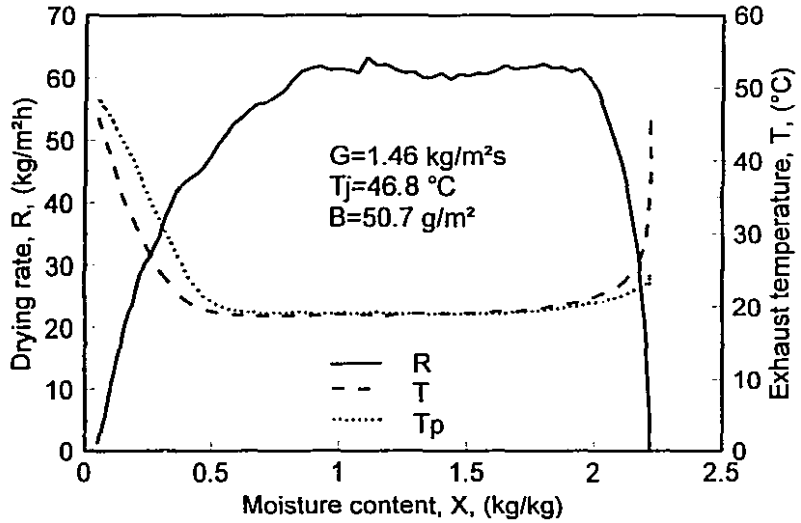
G=1.46 kg/m²s
Tj=46.8 °C
B=50.7 g/m²
R
T
Tp
Drying rate, R, (kg/m²h)
Exhaust temperature, T, (°C)
Moisture content, X, (kg/kg)

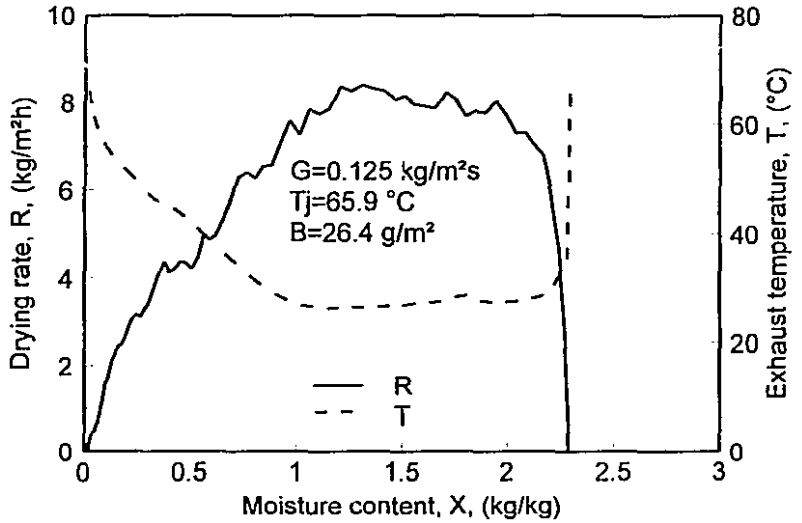
G=0.125 kg/m²s
Tj=65.9 °C
B=26.4 g/m²
R
T
Drying rate, R, (kg/m²h)
Exhaust temperature, T, (°C)
Moisture content, X, (kg/kg)

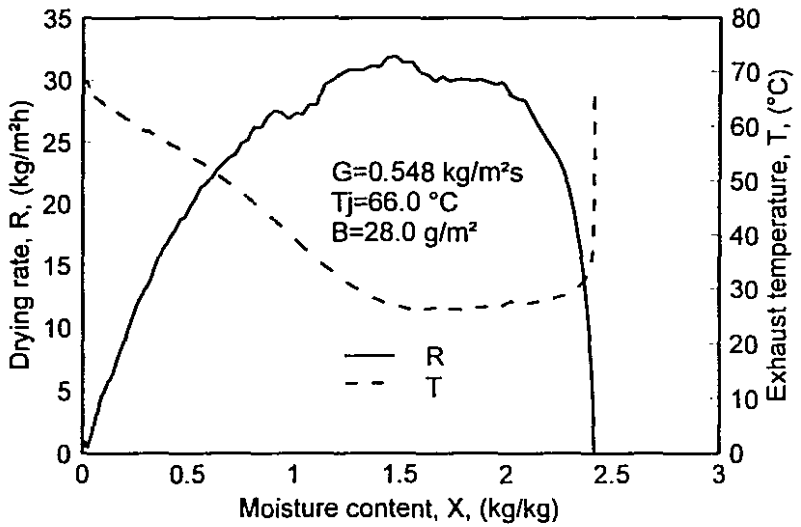
G=0.548 kg/m²s
Tj=66.0 °C
B=28.0 g/m²
R
T
Drying rate, R, (kg/m²h)
Exhaust temperature, T, (°C)
Moisture content, X, (kg/kg)

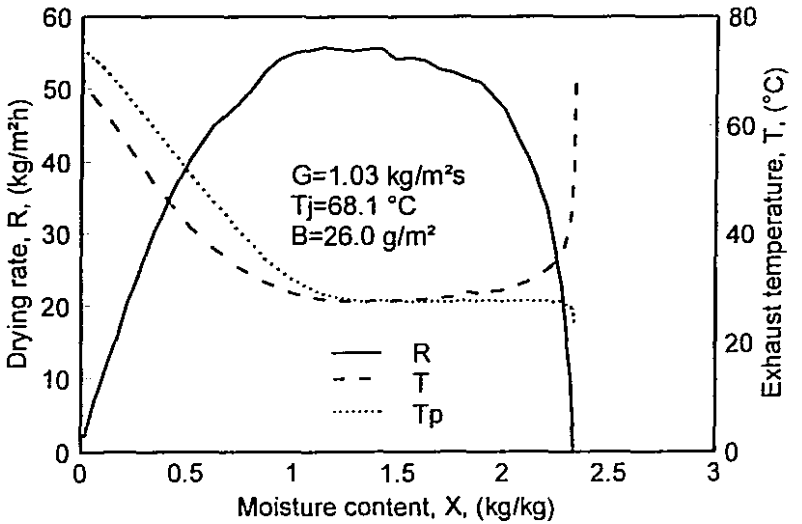
G=1.03 kg/m²s
Tj=68.1 °C
B=26.0 g/m²
R
T
Tp
Drying rate, R, (kg/m²h)
Exhaust temperature, T, (°C)
Moisture content, X, (kg/kg)

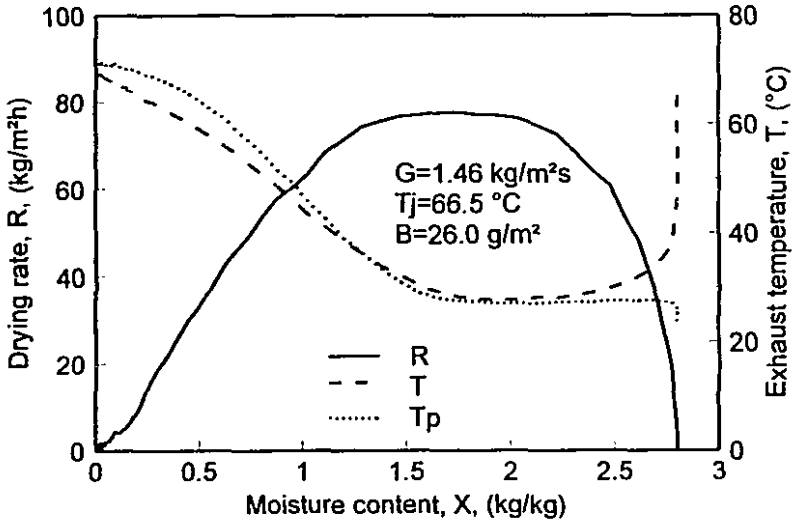
G=1.46 kg/m²s
Tj=66.5 °C
B=26.0 g/m²
R
T
Tp
Drying rate, R, (kg/m²h)
Exhaust temperature, T, (°C)
Moisture content, X, (kg/kg)

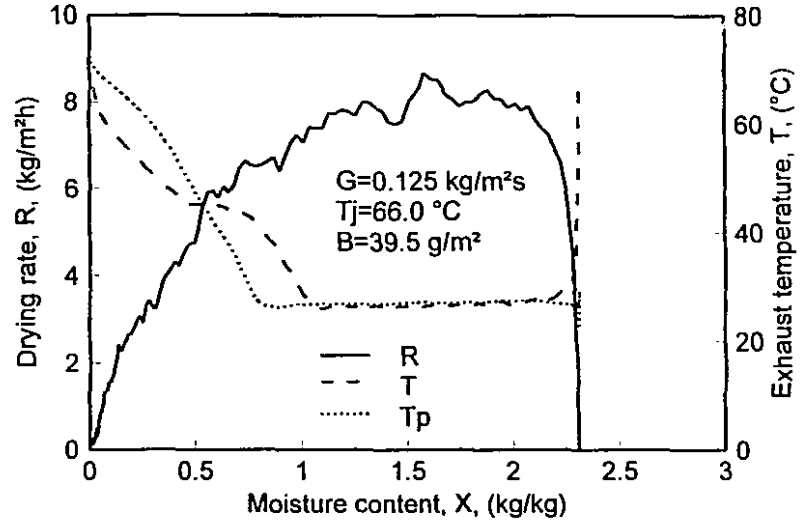
G=0.125 kg/m²s
Tj=66.0 °C
B=39.5 g/m²
R
T
Tp
Drying rate, R, (kg/m²h)
Exhaust temperature, T, (°C)
Moisture content, X, (kg/kg)

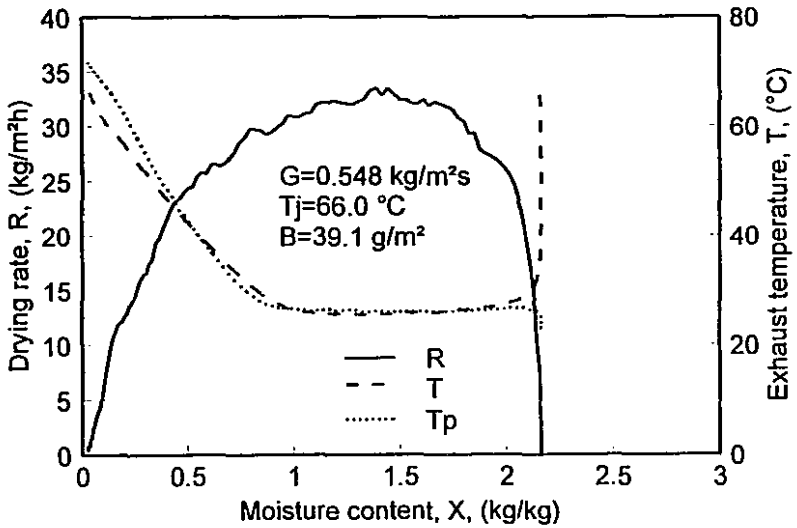
G=0.548 kg/m²s
Tj=66.0 °C
B=39.1 g/m²
R
T
Tp
Drying rate, R, (kg/m²h)
Exhaust temperature, T, (°C)
Moisture content, X, (kg/kg)

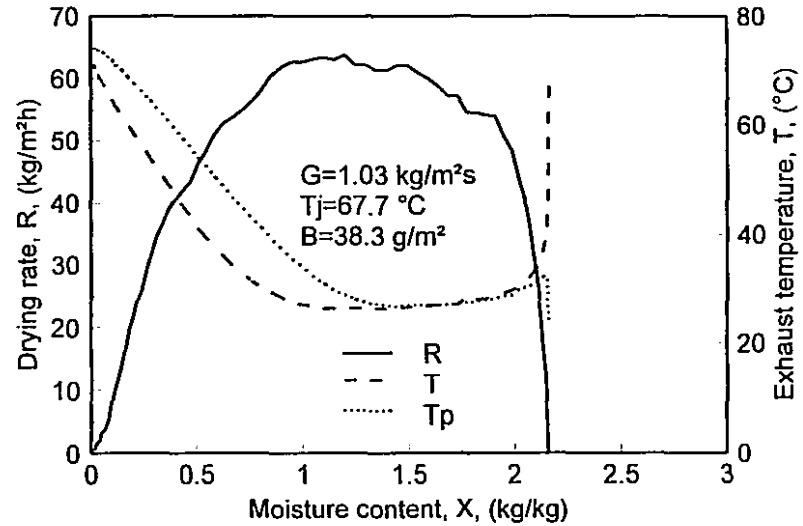
G=1.03 kg/m²s
Tj=67.7 °C
B=38.3 g/m²
R
T
Tp
Drying rate, R, (kg/m²h)
Exhaust temperature, T, (°C)
Moisture content, X, (kg/kg)

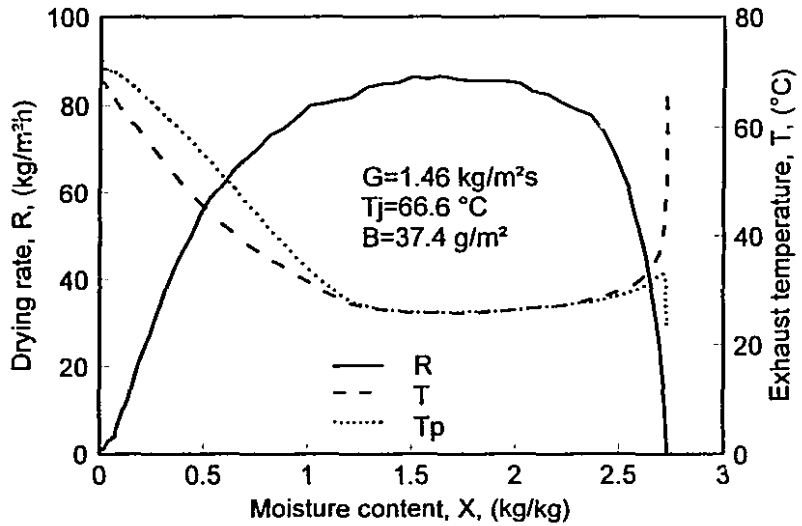
G=1.46 kg/m²s
Tj=66.6 °C
B=37.4 g/m²
R
T
Tp
Drying rate, R, (kg/m²h)
Exhaust temperature, T, (°C)
Moisture content, X, (kg/kg)

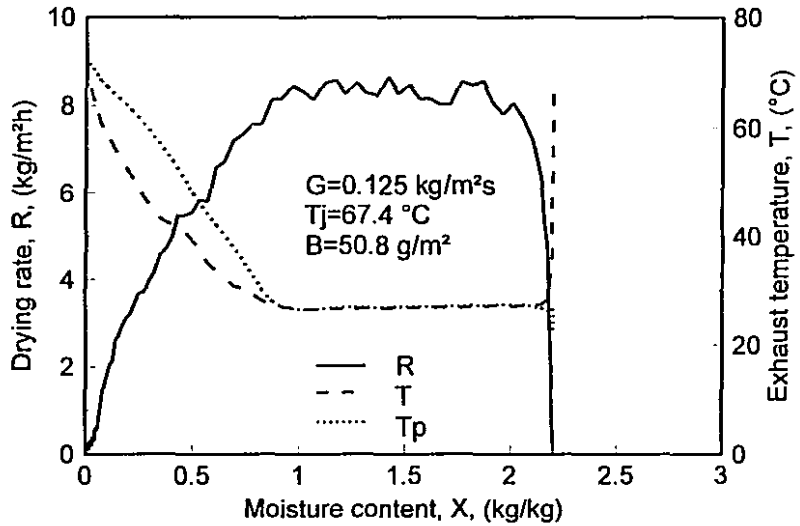
G=0.125 kg/m²s
Tj=67.4 °C
B=50.8 g/m²
R
T
Tp
Drying rate, R, (kg/m²h)
Exhaust temperature, T, (°C)
Moisture content, X, (kg/kg)

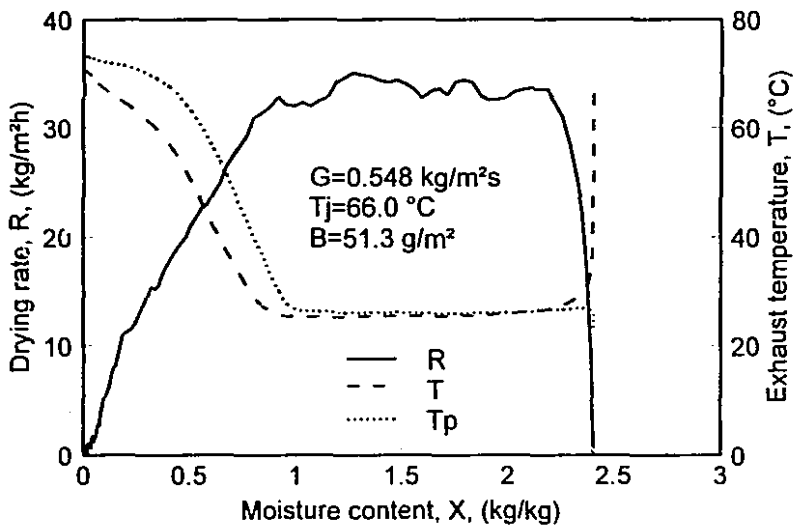
G=0.548 kg/m²s
Tj=66.0 °C
B=51.3 g/m²
R
T
Tp
Drying rate, R, (kg/m²h)
Exhaust temperature, T, (°C)
Moisture content, X, (kg/kg)

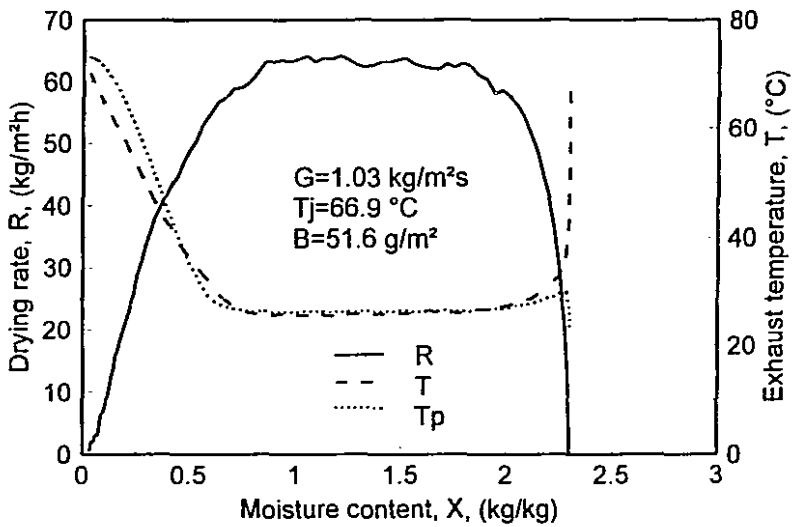
G=1.03 kg/m²s
Tj=66.9 °C
B=51.6 g/m²
R
T
Tp
Drying rate, R, (kg/m²h)
Exhaust temperature, T, (°C)
Moisture content, X, (kg/kg)

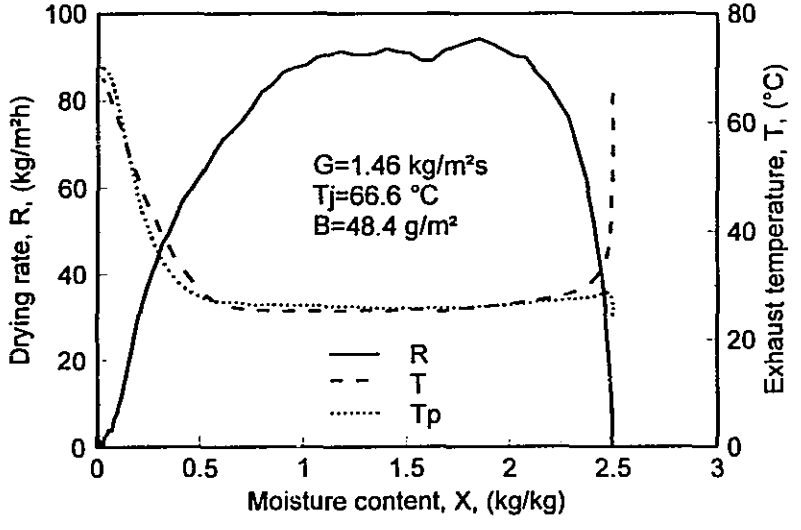
G=1.46 kg/m²s
Tj=66.6 °C
B=48.4 g/m²
R
T
Tp
Drying rate, R, (kg/m²h)
Exhaust temperature, T, (°C)
Moisture content, X, (kg/kg)

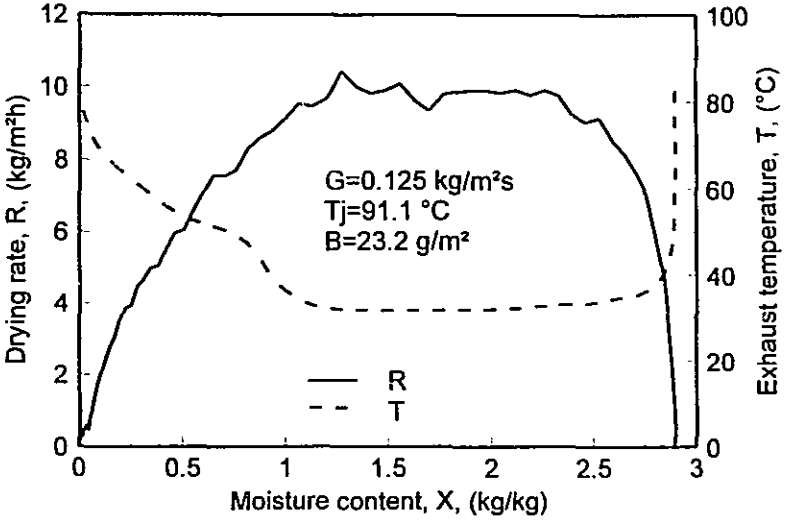
G=0.125 kg/m²s
Tj=91.1 °C
B=23.2 g/m²
R
T
Drying rate, R, (kg/m²h)
Exhaust temperature, T, (°C)
Moisture content, X, (kg/kg)

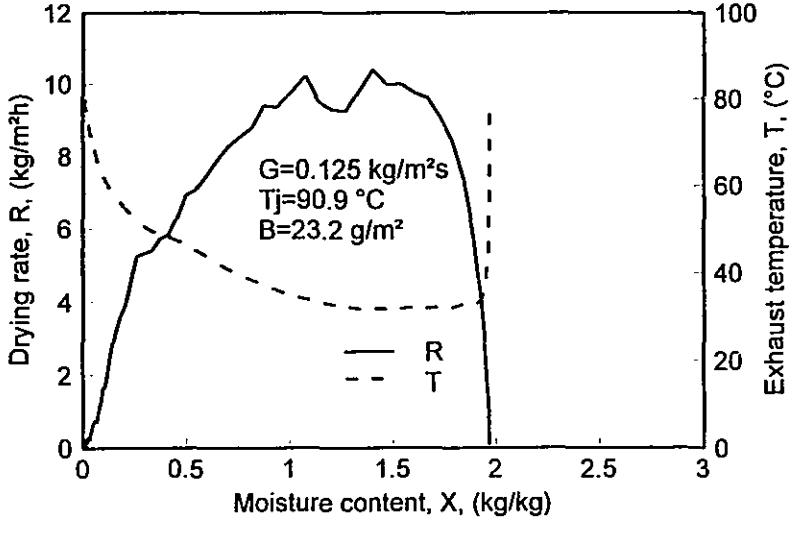
G=0.125 kg/m²s
Tj=90.9 °C
B=23.2 g/m²
R
T
Drying rate, R, (kg/m²h)
Exhaust temperature, T, (°C)
Moisture content, X, (kg/kg)

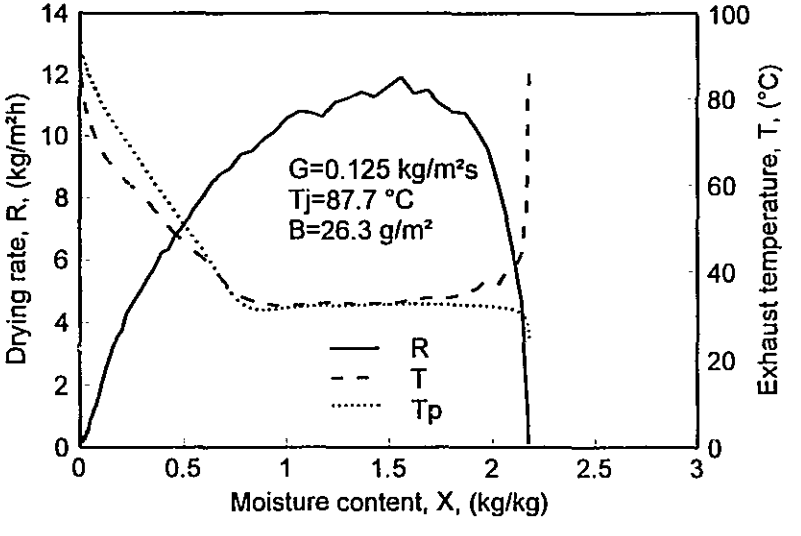
G=0.125 kg/m²s
Tj=87.7 °C
B=26.3 g/m²
R
T
Tp
Drying rate, R, (kg/m²h)
Exhaust temperature, T, (°C)
Moisture content, X, (kg/kg)

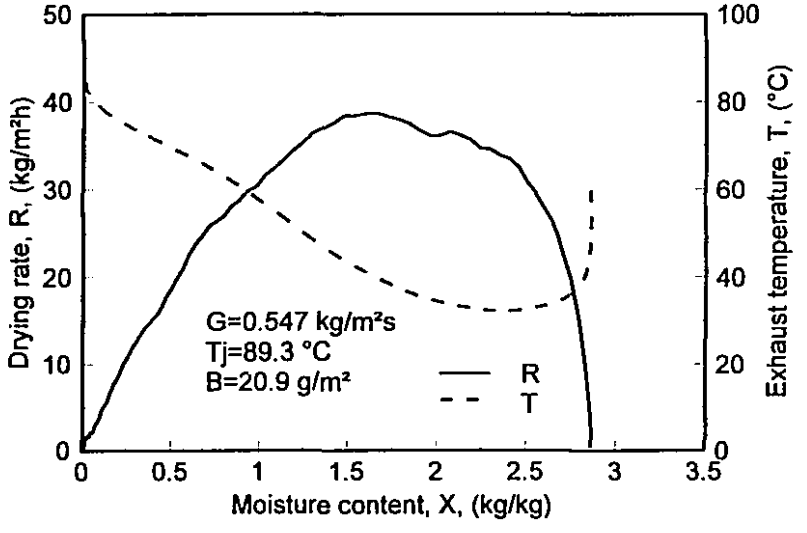
G=0.547 kg/m²s
Tj=89.3 °C
B=20.9 g/m²
R
T
Drying rate, R, (kg/m²h)
Exhaust temperature, T, (°C)
Moisture content, X, (kg/kg)

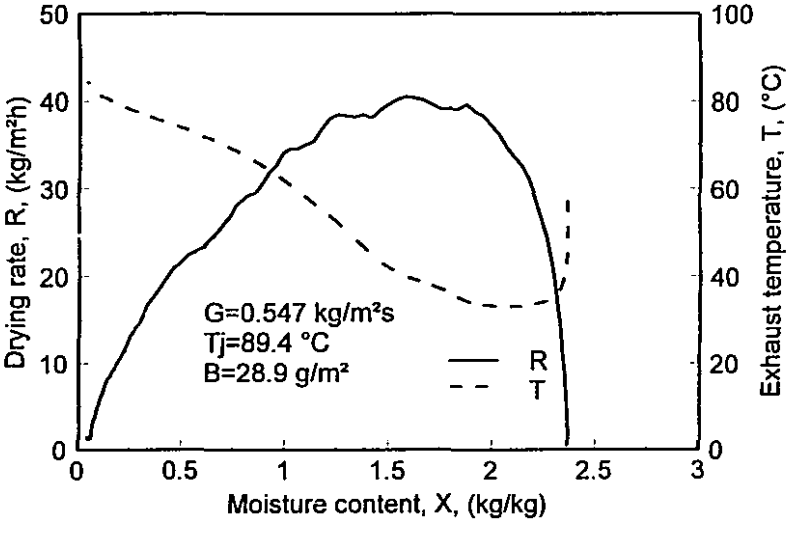
G=0.547 kg/m²s
Tj=89.4 °C
B=28.9 g/m²
R
T
Drying rate, R, (kg/m²h)
Exhaust temperature, T, (°C)
Moisture content, X, (kg/kg)

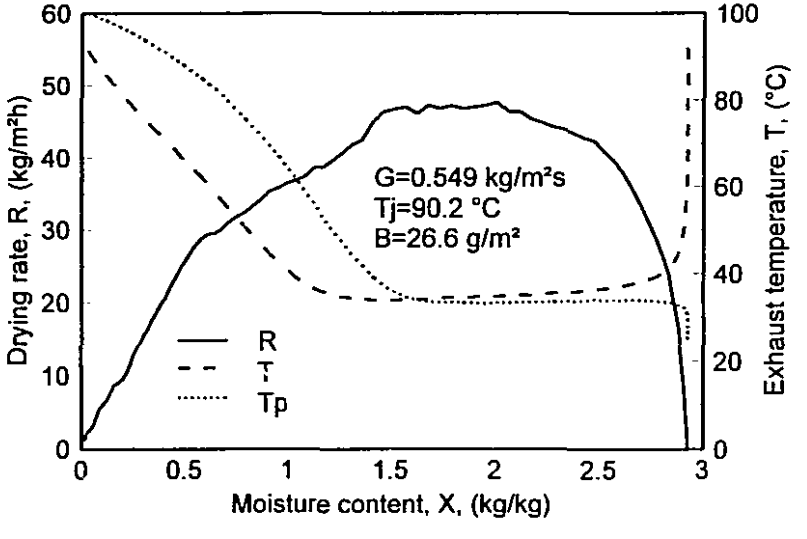
G=0.549 kg/m²s
Tj=90.2 °C
B=26.6 g/m²
R
T
Tp
Drying rate, R, (kg/m²h)
Exhaust temperature, T, (°C)
Moisture content, X, (kg/kg)

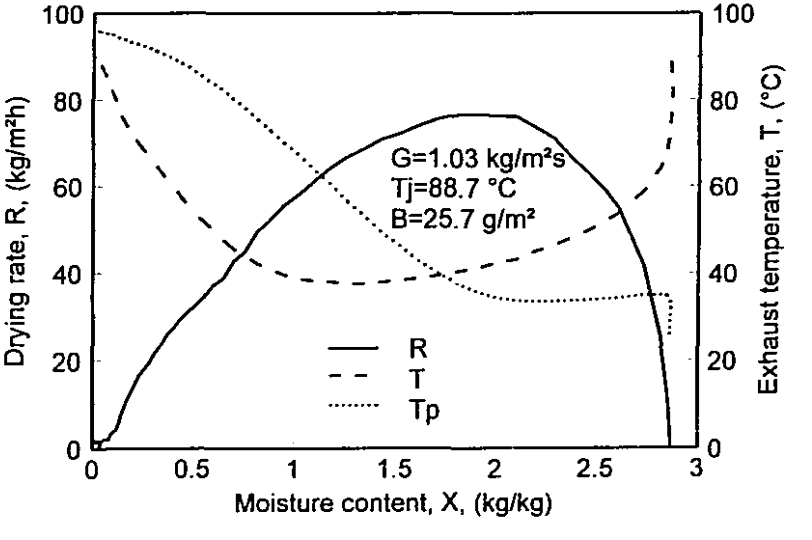
G=1.03 kg/m²s
Tj=88.7 °C
B=25.7 g/m²
R
T
Tp
Drying rate, R, (kg/m²h)
Exhaust temperature, T, (°C)
Moisture content, X, (kg/kg)

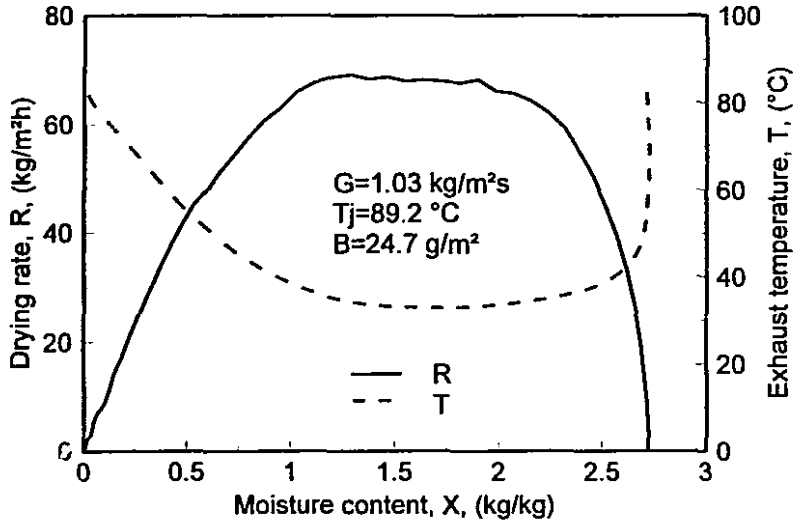
G=1.03 kg/m²s
Tj=89.2 °C
B=24.7 g/m²
R
T
Drying rate, R, (kg/m²h)
Exhaust temperature, T, (°C)
Moisture content, X, (kg/kg)

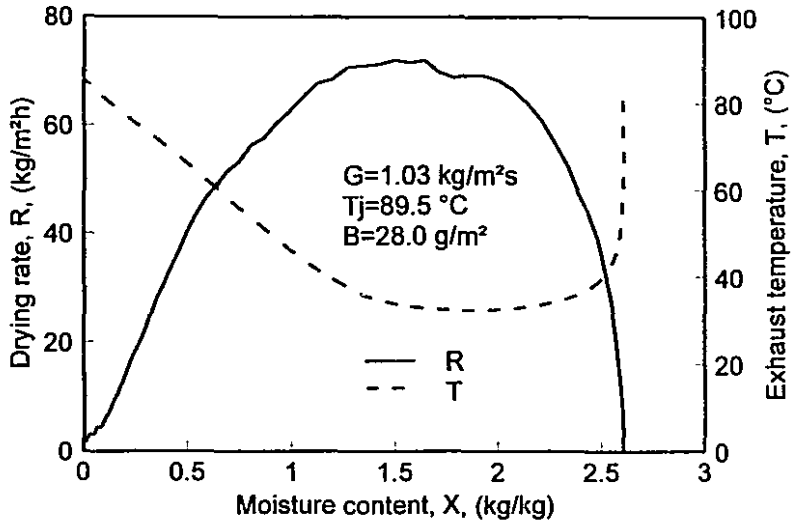
G=1.03 kg/m²s
Tj=89.5 °C
B=28.0 g/m²
R
T
Drying rate, R, (kg/m²h)
Exhaust temperature, T, (°C)
Moisture content, X, (kg/kg)

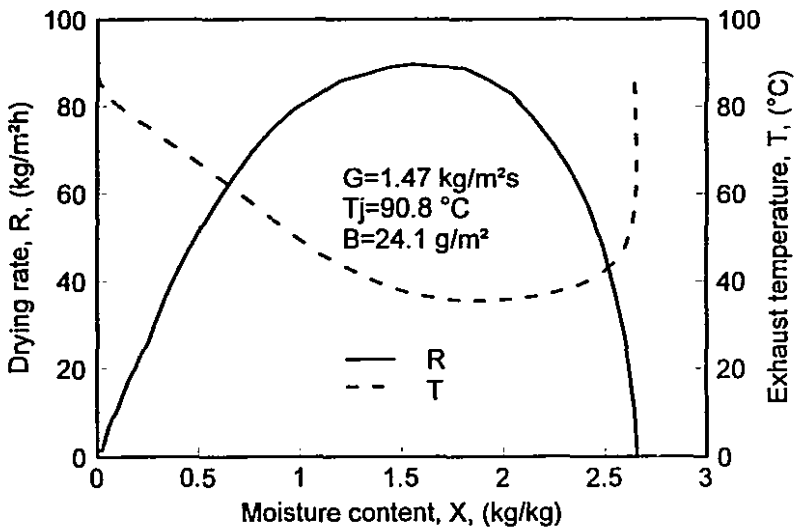
G=1.47 kg/m²s
Tj=90.8 °C
B=24.1 g/m²
R
T
Drying rate, R, (kg/m²h)
Exhaust temperature, T, (°C)
Moisture content, X, (kg/kg)

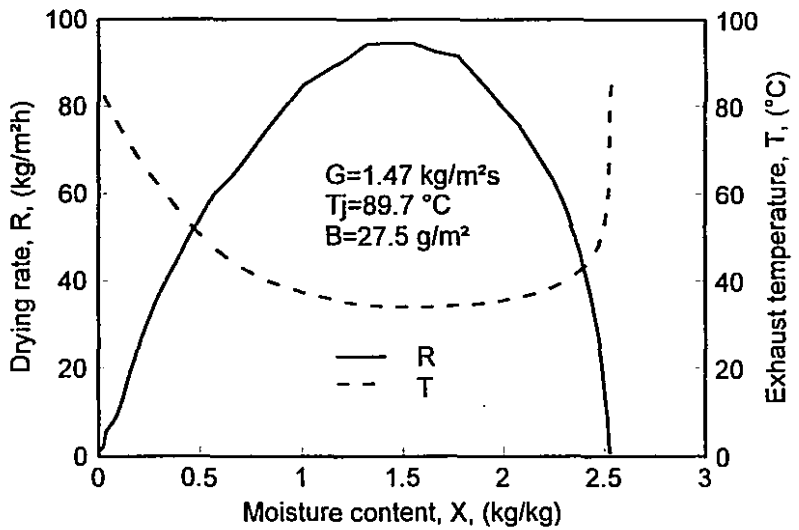
G=1.47 kg/m²s
Tj=89.7 °C
B=27.5 g/m²
R
T
Drying rate, R, (kg/m²h)
Exhaust temperature, T, (°C)
Moisture content, X, (kg/kg)

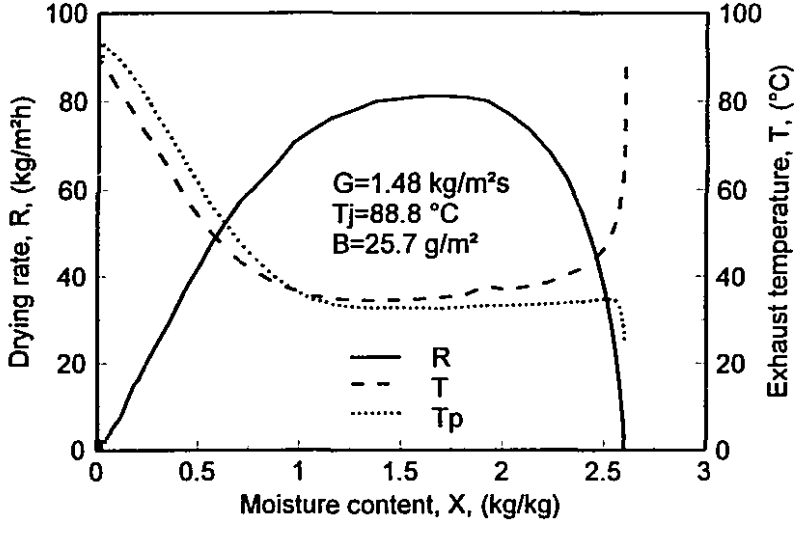
G=1.48 kg/m²s
Tj=88.8 °C
B=25.7 g/m²
R
T
Tp
Drying rate, R, (kg/m²h)
Exhaust temperature, T, (°C)
Moisture content, X, (kg/kg)

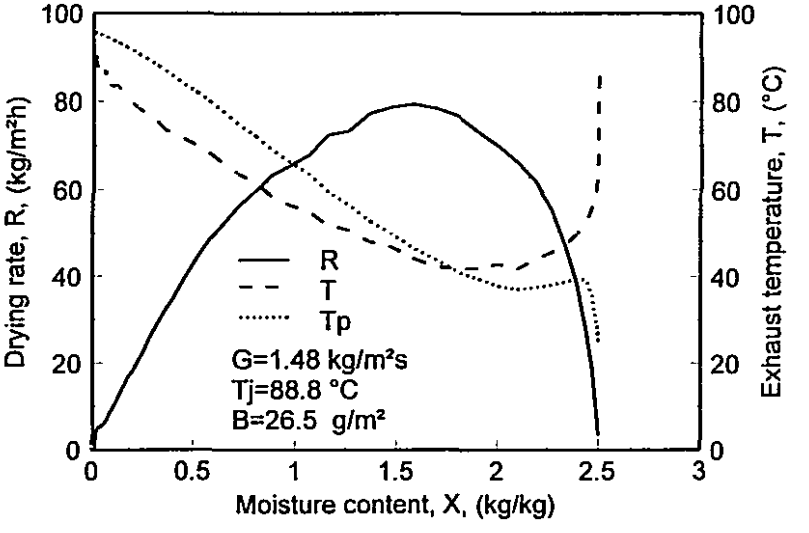
R
T
Tp
G=1.48 kg/m²s
Tj=88.8 °C
B=26.5 g/m²
Drying rate, R, (kg/m²h)
Exhaust temperature, T, (°C)
Moisture content, X, (kg/kg)

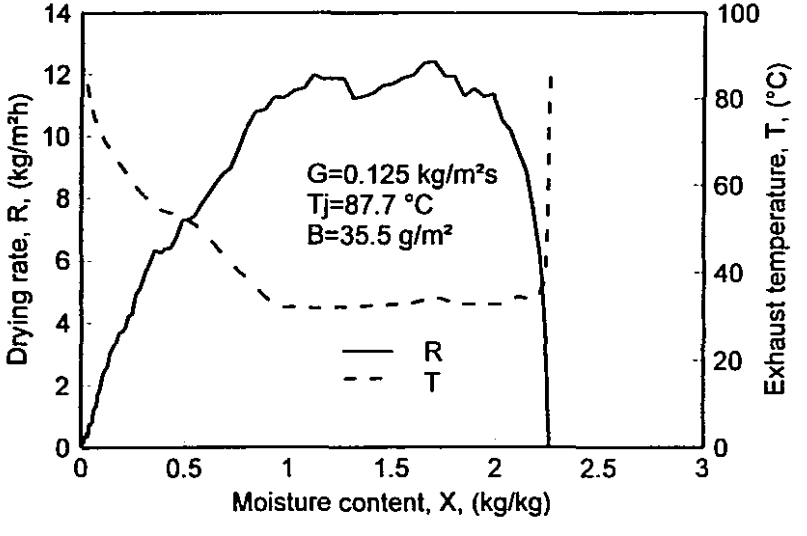
G=0.125 kg/m²s
Tj=87.7 °C
B=35.5 g/m²
R
T
Drying rate, R, (kg/m²h)
Exhaust temperature, T, (°C)
Moisture content, X, (kg/kg)

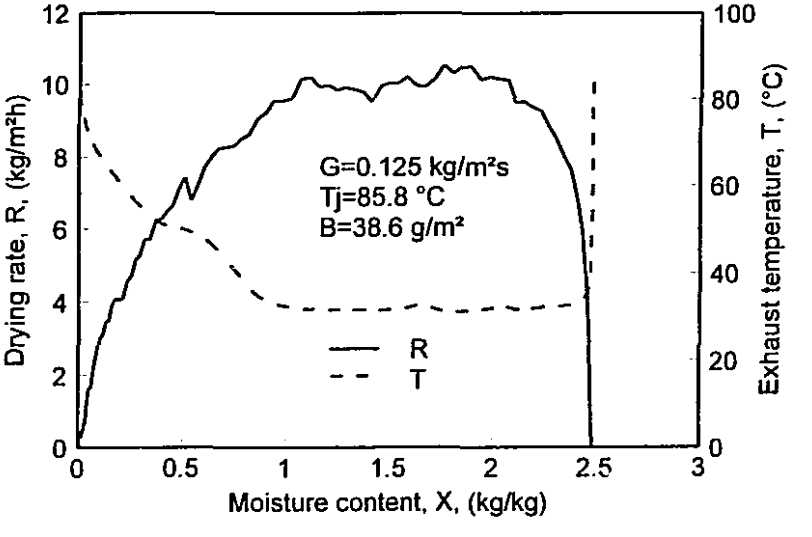
G=0.125 kg/m²s
Tj=85.8 °C
B=38.6 g/m²
R
T
Drying rate, R, (kg/m²h)
Exhaust temperature, T, (°C)
Moisture content, X, (kg/kg)

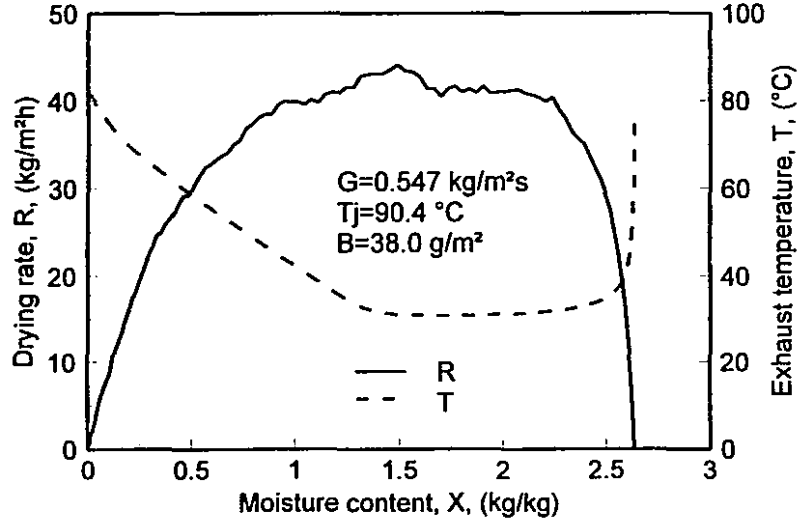
G=0.547 kg/m²s
Tj=90.4 °C
B=38.0 g/m²
R
T
Drying rate, R, (kg/m²h)
Exhaust temperature, T, (°C)
Moisture content, X, (kg/kg)

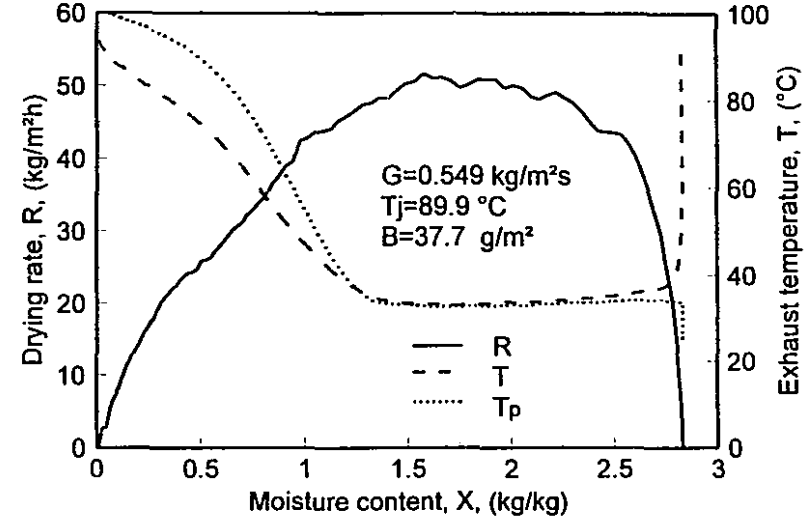
G=0.549 kg/m²s
Tj=89.9 °C
B=37.7 g/m²
R
T
Tp
Drying rate, R, (kg/m²h)
Exhaust temperature, T, (°C)
Moisture content, X, (kg/kg)

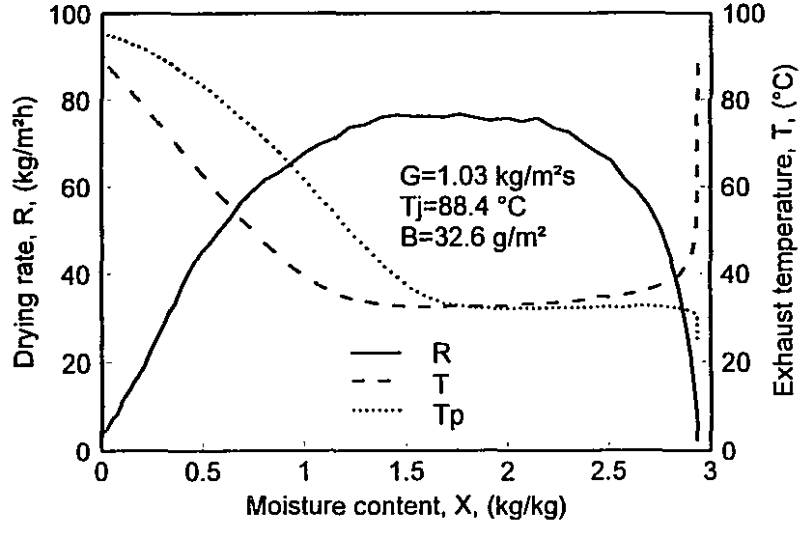
G=1.03 kg/m²s
Tj=88.4 °C
B=32.6 g/m²
R
T
Tp
Drying rate, R, (kg/m²h)
Exhaust temperature, T, (°C)
Moisture content, X, (kg/kg)

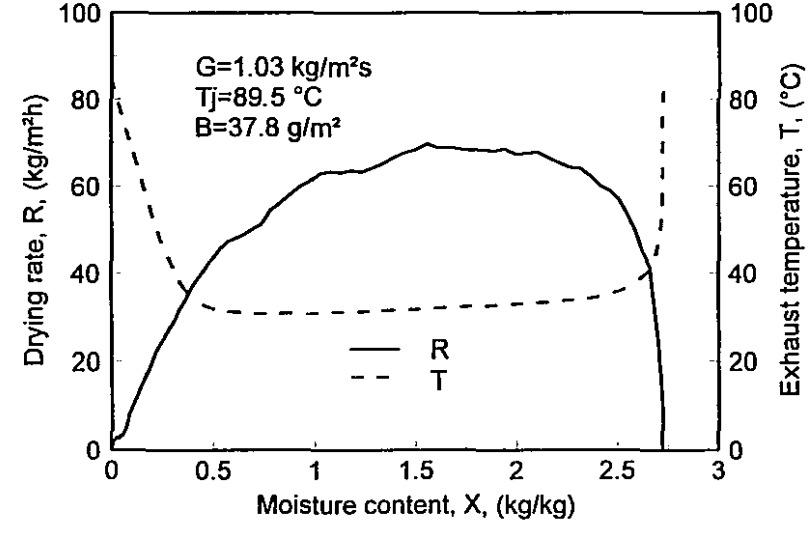
G=1.03 kg/m²s
Tj=89.5 °C
B=37.8 g/m²
R
T
Drying rate, R, (kg/m²h)
Exhaust temperature, T, (°C)
Moisture content, X, (kg/kg)

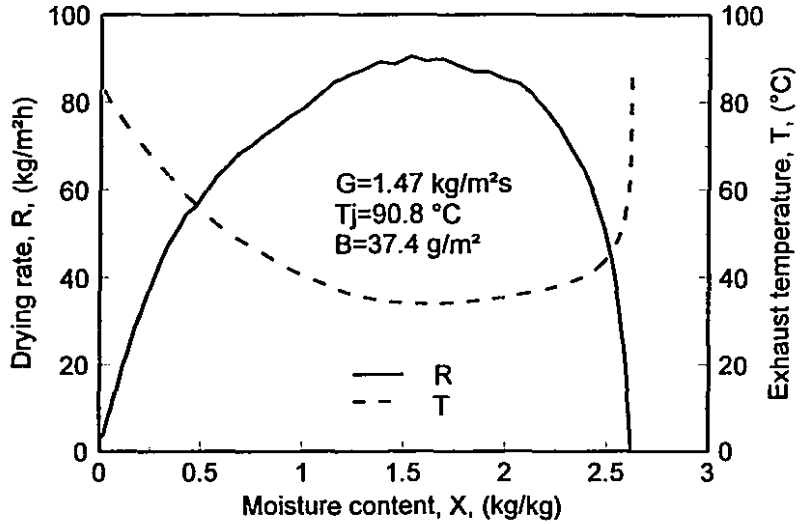
G=1.47 kg/m²s
Tj=90.8 °C
B=37.4 g/m²
R
T
Drying rate, R, (kg/m²h)
Exhaust temperature, T, (°C)
Moisture content, X, (kg/kg)

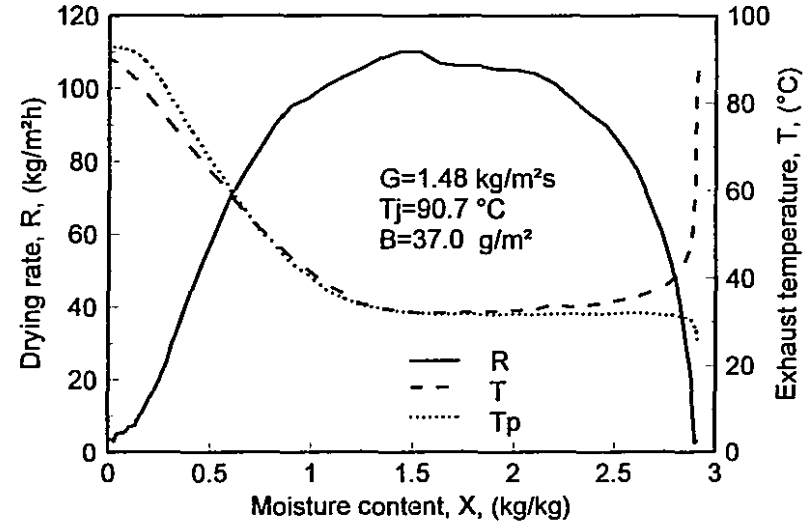
G=1.48 kg/m²s
Tj=90.7 °C
B=37.0 g/m²
R
T
Tp
Drying rate, R, (kg/m²h)
Exhaust temperature, T, (°C)
Moisture content, X, (kg/kg)

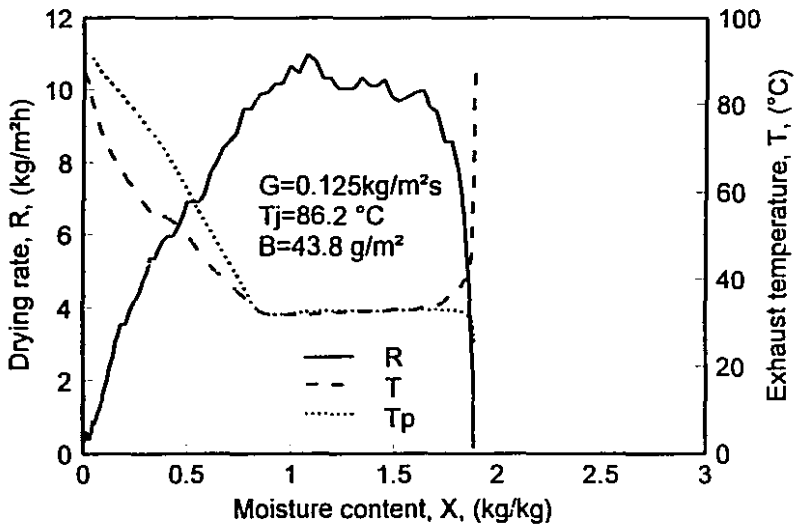
G=0.125kg/m²s
Tj=86.2 °C
B=43.8 g/m²
R
T
Tp
Drying rate, R, (kg/m²h)
Exhaust temperature, T, (°C)
Moisture content, X, (kg/kg)

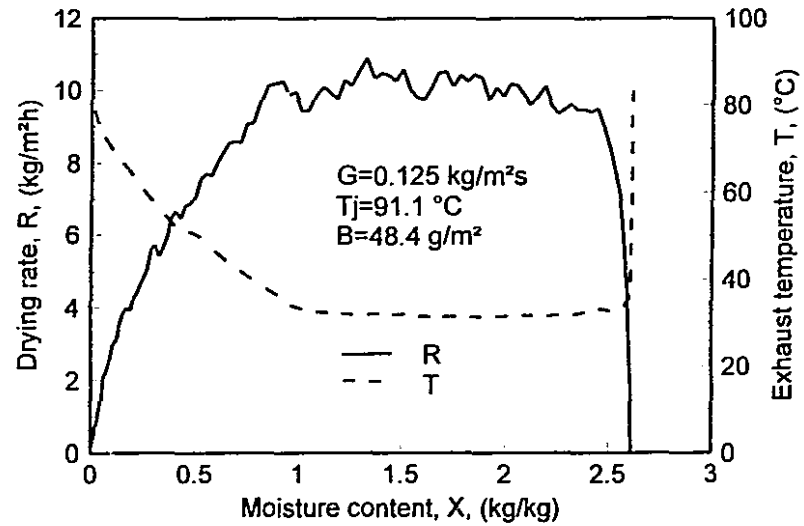
G=0.125 kg/m²s
Tj=91.1 °C
B=48.4 g/m²
R
T
Drying rate, R, (kg/m²h)
Exhaust temperature, T, (°C)
Moisture content, X, (kg/kg)

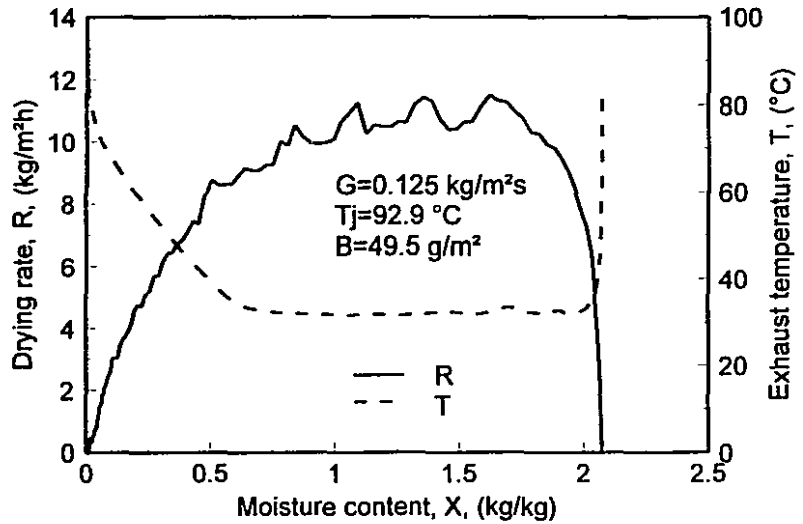
G=0.125 kg/m²s
Tj=92.9 °C
B=49.5 g/m²
R
T
Drying rate, R, (kg/m²h)
Exhaust temperature, T, (°C)
Moisture content, X, (kg/kg)

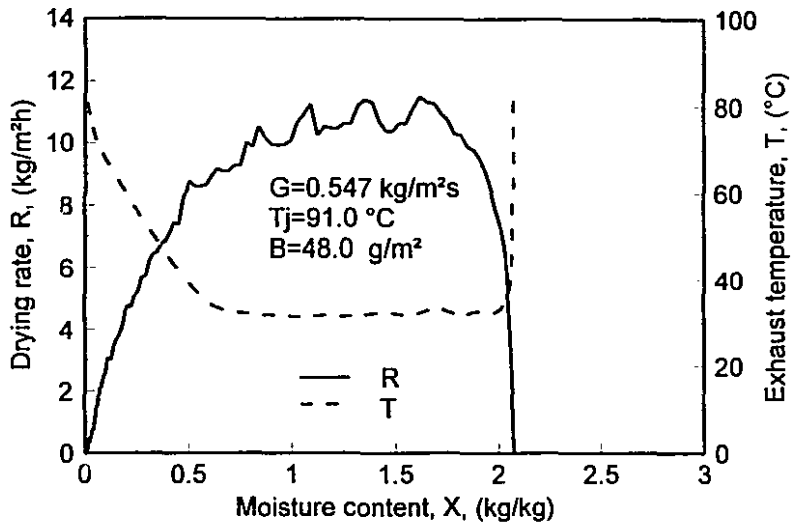
G=0.547 kg/m²s
Tj=91.0 °C
B=48.0 g/m²
R
T
Drying rate, R, (kg/m²h)
Exhaust temperature, T, (°C)
Moisture content, X, (kg/kg)

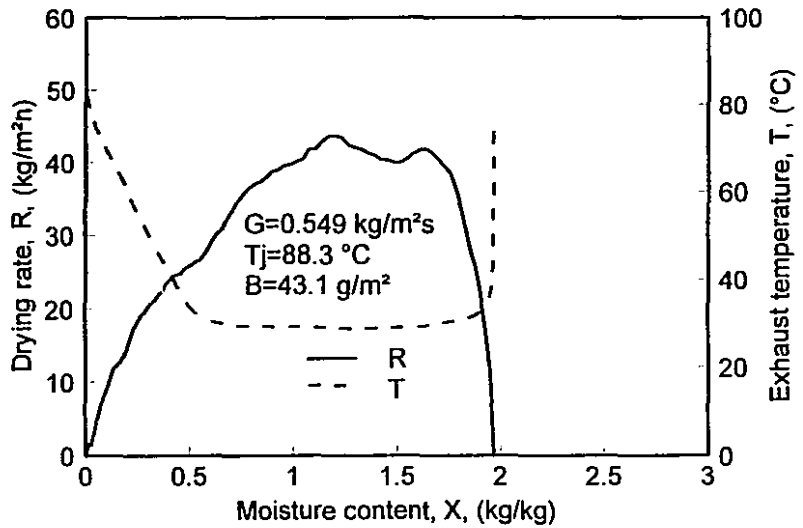
G=0.549 kg/m²s
Tj=88.3 °C
B=43.1 g/m²
R
T
Drying rate, R, (kg/m²h)
Exhaust temperature, T, (°C)
Moisture content, X, (kg/kg)

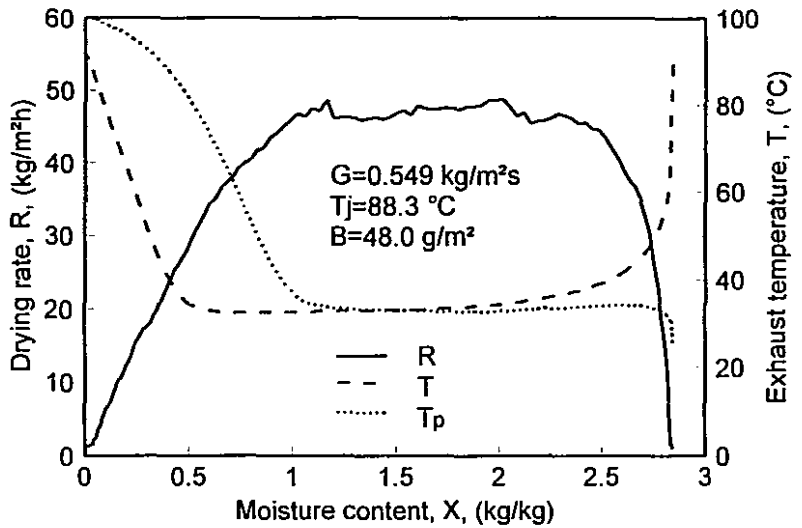
G=0.549 kg/m²s
Tj=88.3 °C
B=48.0 g/m²
R
T
Tp
Drying rate, R, (kg/m²h)
Exhaust temperature, T, (°C)
Moisture content, X, (kg/kg)

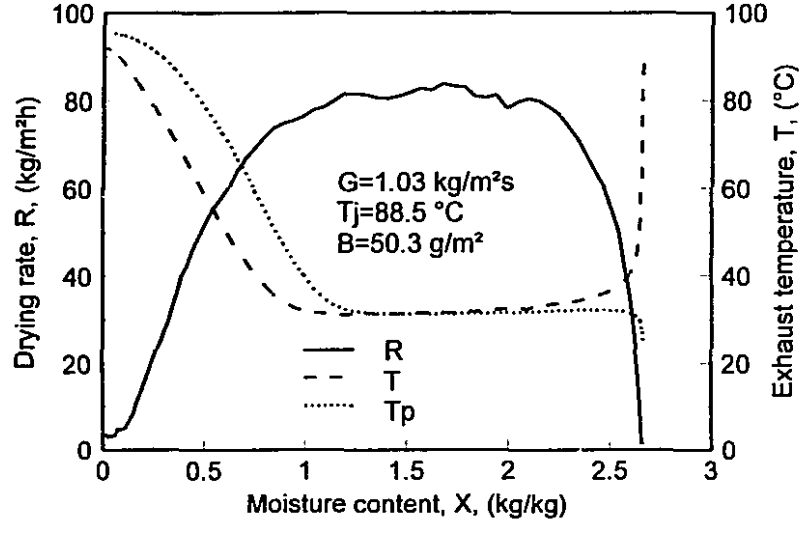
G=1.03 kg/m²s
Tj=88.5 °C
B=50.3 g/m²
R
T
Tp
Drying rate, R, (kg/m²h)
Exhaust temperature, T, (°C)
Moisture content, X, (kg/kg)

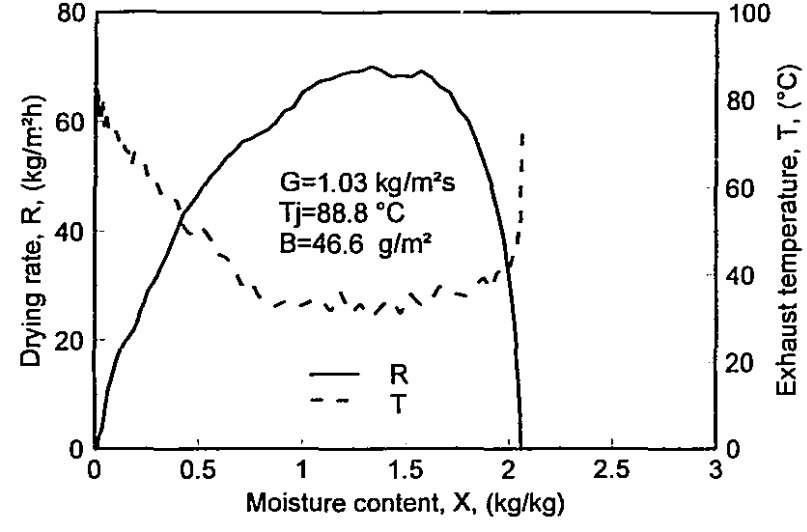
G=1.03 kg/m²s
Tj=88.8 °C
B=46.6 g/m²
R
T
Drying rate, R, (kg/m²h)
Exhaust temperature, T, (°C)
Moisture content, X, (kg/kg)

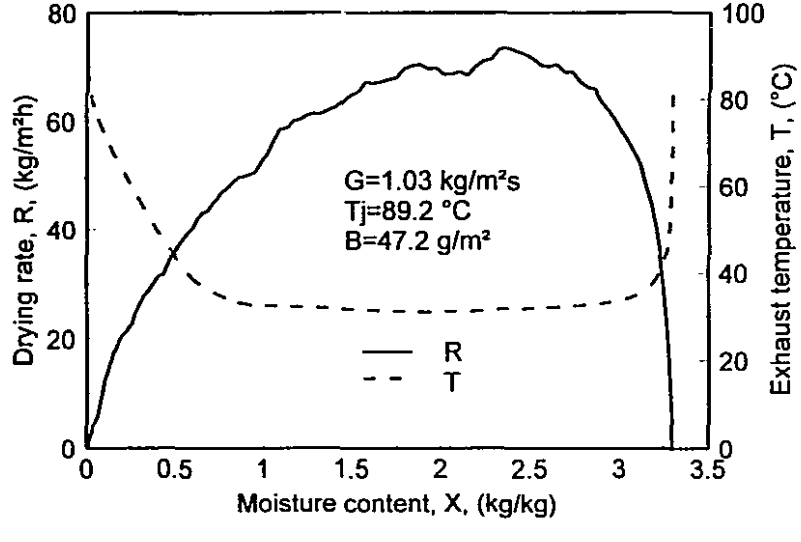
G=1.03 kg/m²s
Tj=89.2 °C
B=47.2 g/m²
R
T
Drying rate, R, (kg/m²h)
Exhaust temperature, T, (°C)
Moisture content, X, (kg/kg)

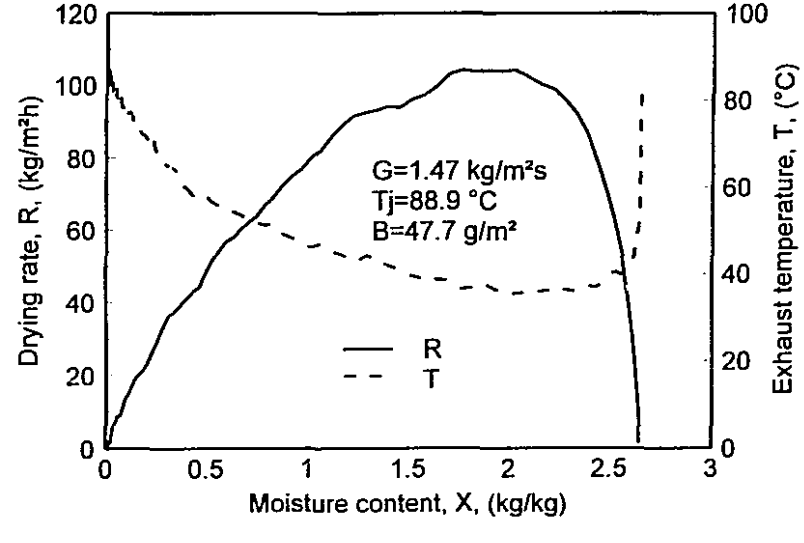
G=1.47 kg/m²s
Tj=88.9 °C
B=47.7 g/m²
R
T
Drying rate, R, (kg/m²h)
Exhaust temperature, T, (°C)
Moisture content, X, (kg/kg)

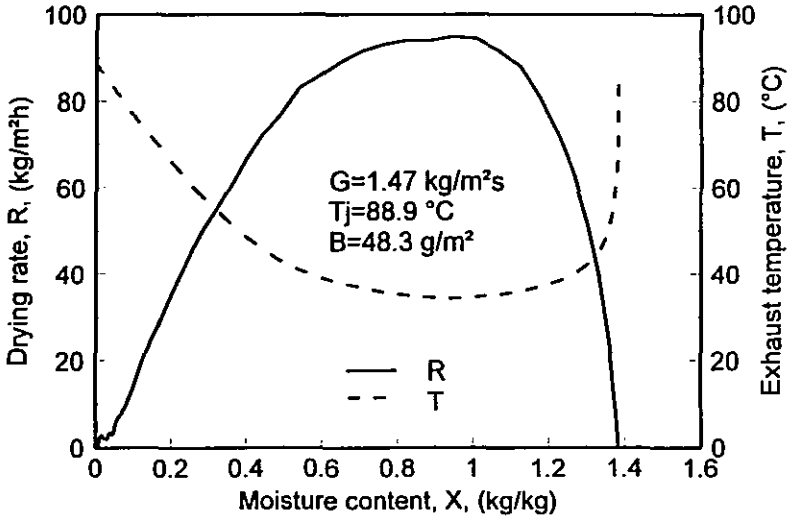
G=1.47 kg/m²s
Tj=88.9 °C
B=48.3 g/m²
R
T
Drying rate, R, (kg/m²h)
Exhaust temperature, T, (°C)
Moisture content, X, (kg/kg)

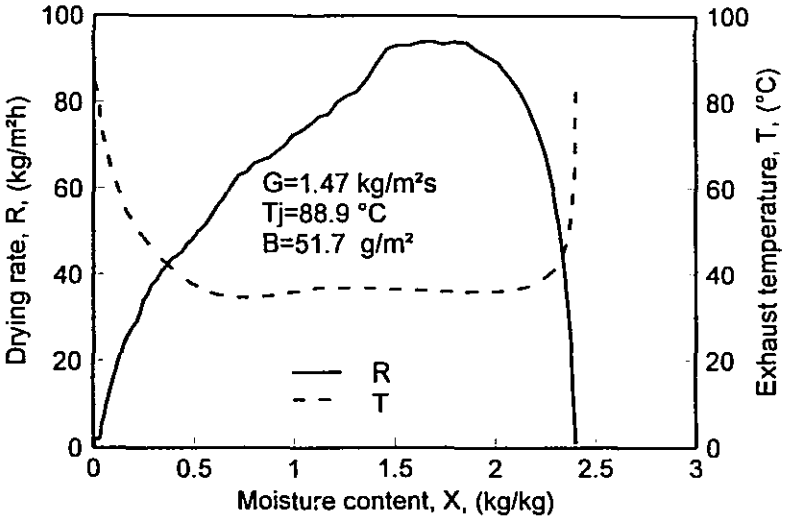
G=1.47 kg/m²s
Tj=88.9 °C
B=51.7 g/m²
R
T
Drying rate, R, (kg/m²h)
Exhaust temperature, T, (°C)
Moisture content, X, (kg/kg)

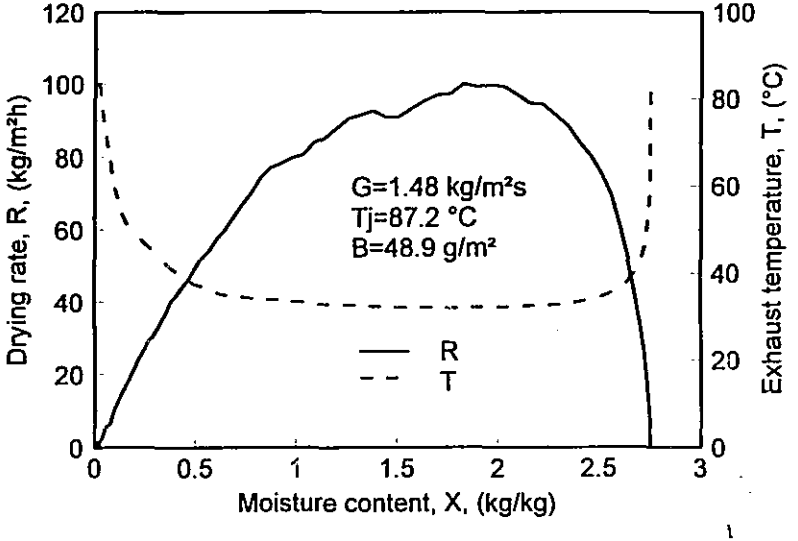
G=1.48 kg/m²s
Tj=87.2 °C
B=48.9 g/m²
R
T
Drying rate, R, (kg/m²h)
Exhaust temperature, T, (°C)
Moisture content, X, (kg/kg)

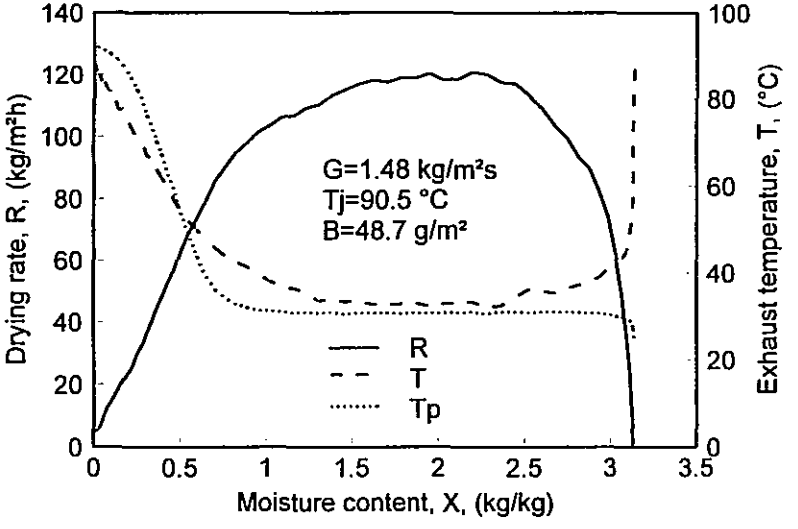
G=1.48 kg/m²s
Tj=90.5 °C
B=48.7 g/m²
R
T
Tp
Drying rate, R, (kg/m²h)
Exhaust temperature, T, (°C)
Moisture content, X, (kg/kg)

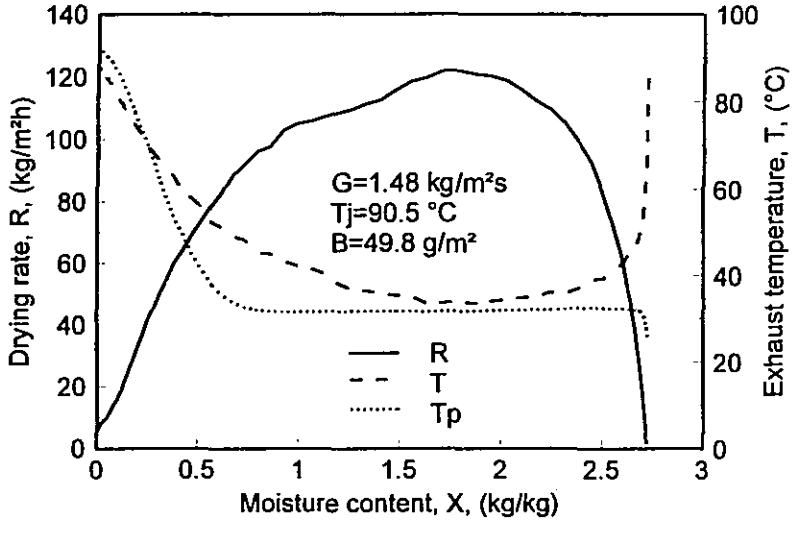
Drying rate, R, (kg/m²h)
Exhaust temperature, T, (°C)
Moisture content, X, (kg/kg)
G=1.48 kg/m²s
Tj=90.5 °C
B=49.8 g/m²
R
T
Tp
0
20
40
60
80
100
120
140
0
0.5
1
1.5
2
2.5
3

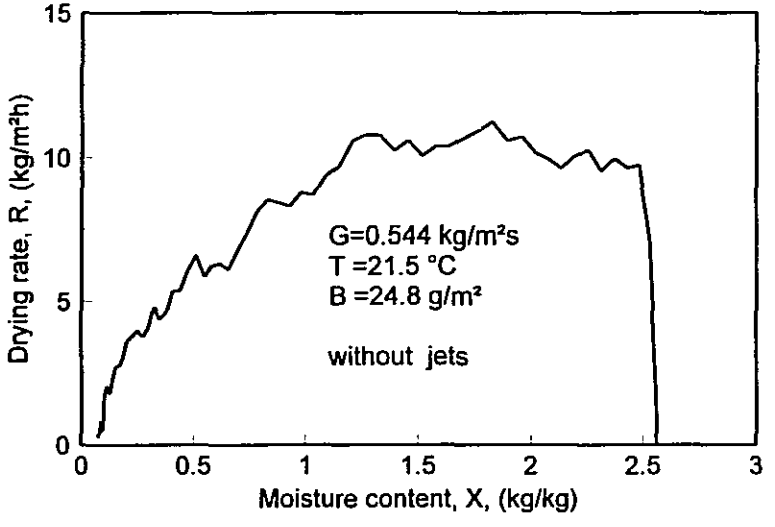
Drying rate, R, (kg/m²h)
Moisture content, X, (kg/kg)
G=0.544 kg/m²s
T =21.5 °C
B =24.8 g/m²
without jets

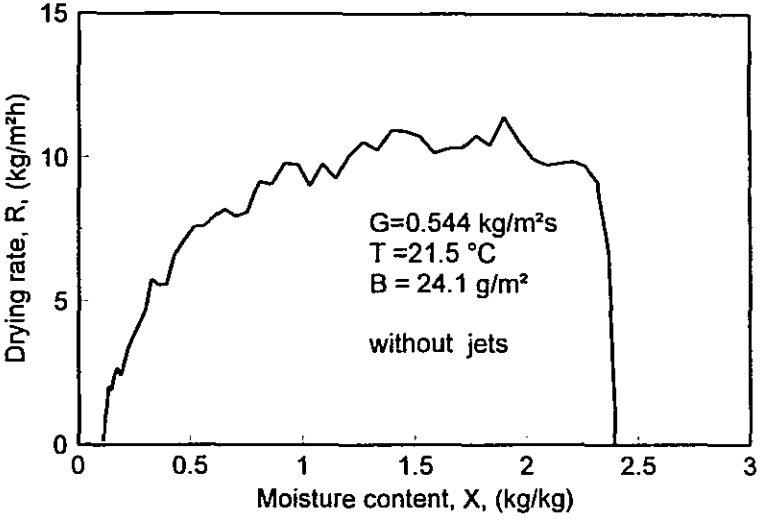
Drying rate, R, (kg/m²h)
Moisture content, X, (kg/kg)
G=0.544 kg/m²s
T =21.5 °C
B = 24.1 g/m²
without jets

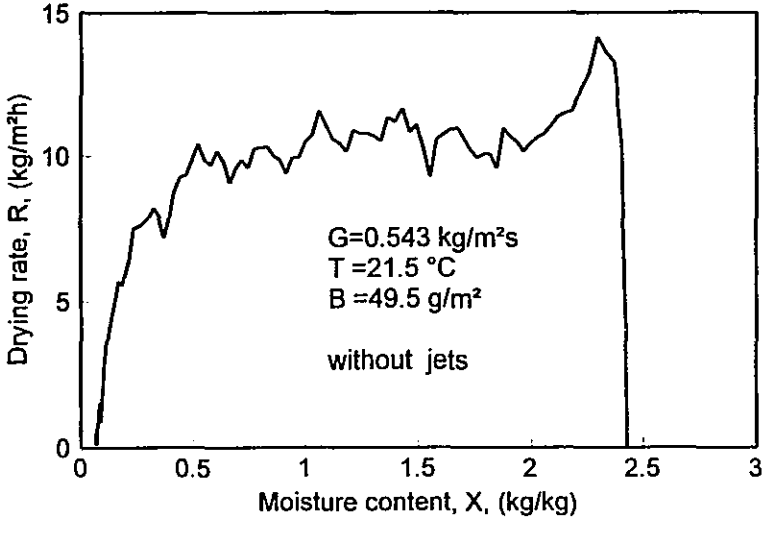
Drying rate, R, (kg/m²h)
Moisture content, X, (kg/kg)
G=0.543 kg/m²s
T =21.5 °C
B =49.5 g/m²
without jets

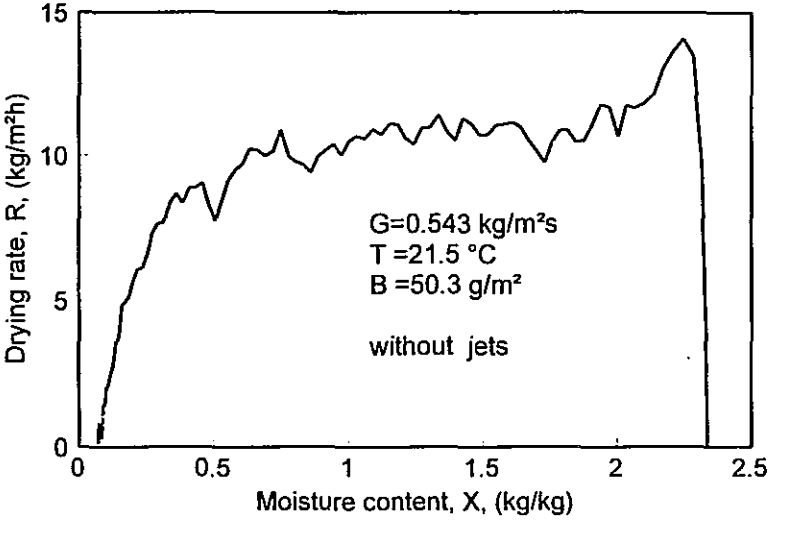
Drying rate, R, (kg/m²h)
Moisture content, X, (kg/kg)
G=0.543 kg/m²s
T =21.5 °C
B =50.3 g/m²
without jets

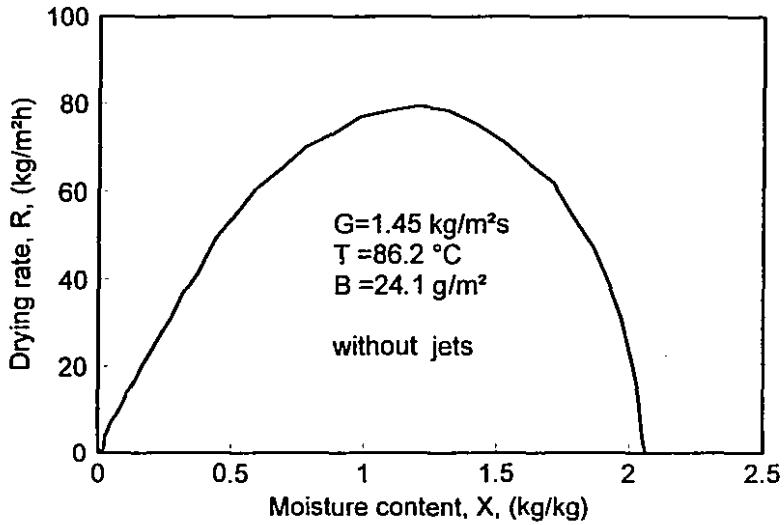
Drying rate, R, (kg/m²h)
Moisture content, X, (kg/kg)
G=1.45 kg/m²s
T =86.2 °C
B =24.1 g/m²
without jets

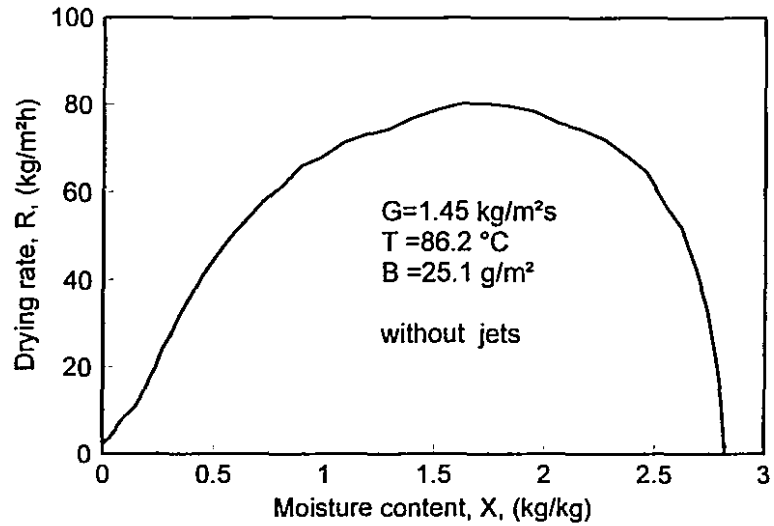
Drying rate, R, (kg/m²h)
Moisture content, X, (kg/kg)
G=1.45 kg/m²s
T =86.2 °C
B =25.1 g/m²
without jets

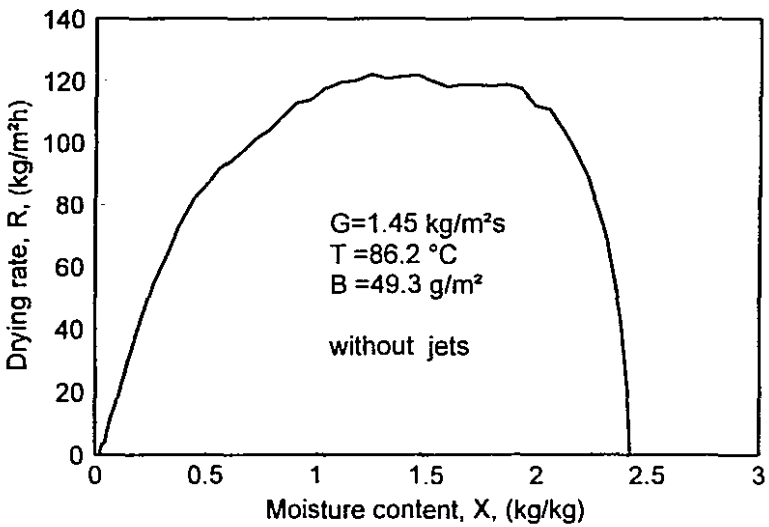
Drying rate, R, (kg/m²h)
Moisture content, X, (kg/kg)
G=1.45 kg/m²s
T =86.2 °C
B =49.3 g/m²
without jets

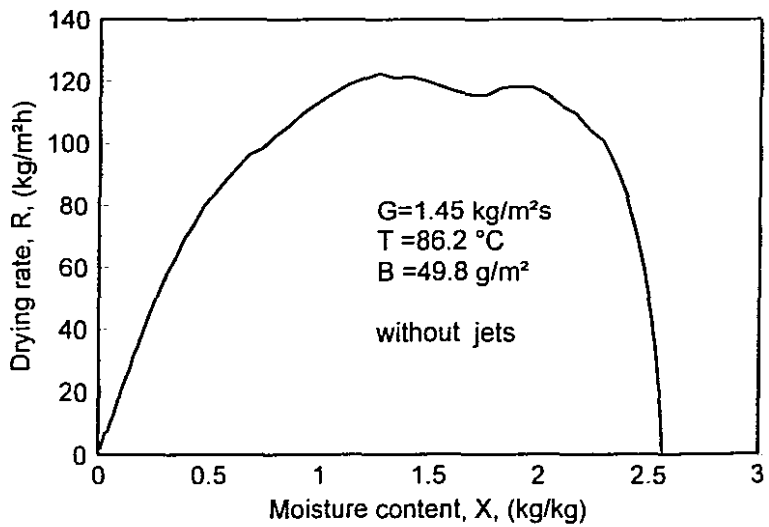
Drying rate, R, (kg/m²h)
Moisture content, X, (kg/kg)
G=1.45 kg/m²s
T =86.2 °C
B =49.8 g/m²
without jets

E3: Experimental conditions and important data for CITAD drying

G	B	qT	GT	GI	Tj	Ts	Xo	Ric	Xc	n	RTc	XTi	nTi	RTm	Xm	C
0.125	22.8	50.9	0.063	0.062	21.9	7.27	2.30	0.565	1.04	1.49	1.21			1.19	1.08	0.182
0.125	24.6	50.9	0.063	0.062	21.8	7.24	2.27	0.564	1.07	1.69	1.24			1.25	1.78	1.064
0.125	24.4	73.8	0.092	0.032	21.8	7.24	2.86	0.291	1.03	1.13	1.76			1.69	1.01	0.304
0.125	24.0	73.8	0.092	0.032	21.8	7.24	1.89	0.280	0.97	1.48	1.72					
0.542	24.1	19.2	0.104	0.436	21.7	7.17	2.97	2.42	1.24	1.29	1.82			1.89	1.03	-0.549
0.542	25.4	19.2	0.104	0.438	21.5	7.06	2.77	2.52	1.30	1.25	1.88			1.93	1.14	0.353
0.542	24.4	26.2	0.142	0.400	21.2	6.94	2.36	2.22	1.24	1.39	2.74			2.67	1.06	0.237
0.542	24.7	48.0	0.260	0.282	21.5	7.06	2.36	1.42	1.14	1.82	4.81			4.67	1.08	0.500
0.542	24.5	73.3	0.397	0.145	21.4	7.02	2.83	0.637	0.98	1.43	6.75			6.36	0.82	-1.264
0.561	25.8	10.8	0.063	0.518	23.4	8.03	3.30	2.89	1.23	1.22	1.26			1.25	1.07	0.375
0.561	26.0	10.8	0.063	0.518	23.4	8.03	2.02	3.11	1.17	1.26	1.33			1.26	0.93	0.582
0.621	26.0	19.8	0.123	0.498	23.1	7.90	2.11	3.12	1.06	1.50	2.46			2.48	0.78	1.384
0.740	25.4	32.3	0.239	0.501	24.1	8.38	2.96	2.67	1.36	1.18	4.83			4.97	1.14	0.403
1.01	25.9	10.2	0.103	0.910	26.8	9.66	1.91	4.12	1.27	1.10	2.33			2.45	0.91	0.369
1.01	30.2	10.2	0.103	0.910	26.9	9.75	2.74	4.17	1.41	1.18	2.25			2.56	1.11	-0.166
1.02	23.6	10.2	0.104	0.916	21.3	6.96	2.56	3.96	1.35	1.00	1.93			1.82	1.07	-0.395
1.02	24.8	25.5	0.260	0.760	21.3	7.00	2.52	2.92	1.48	1.06	4.62			4.93	1.21	-0.415
1.02	25.1	47.9	0.489	0.531	22.1	7.36	1.92	1.69	1.23	1.99	8.62			9.33	0.90	0.018
1.02	26.6	48.0	0.488	0.529	24.1	8.34	2.52	1.89	1.27	1.37	9.49			9.94	1.03	0.344
1.02	23.8	72.3	0.737	0.283	22.1	7.36	2.39	0.715	0.95	1.48	12.8			9.86	0.80	-0.416
1.02	24.5	72.3	0.737	0.283	22.1	7.36	1.94	0.690	1.05	1.66	13.2			12.9	0.94	-0.039
1.18	25.8	56.9	0.674	0.510	24.1	8.38	2.87	1.58	1.34	1.37	12.9			12.2	1.14	0.229
1.27	25.2	4.97	0.063	1.21	23.4	8.03	2.54	5.00	1.35	0.90	1.26			1.34	1.10	-1.237
1.31	26.0	9.37	0.123	1.19	23.1	7.90	2.14	4.40	1.18	1.31	2.45			2.62	0.93	0.198
1.46	24.0	7.14	0.104	1.35	21.2	6.94	2.92	4.99	1.31	1.03	1.85			2.04	1.12	-1.024
1.45	25.0	16.5	0.239	1.21	23.4	8.03	3.01	4.05	1.19	1.54	5.00			4.86	1.02	-0.133
1.46	24.5	27.3	0.397	1.06	22.1	7.38	2.07	3.29	1.22	1.16	7.35			7.25		2.402
1.46	24.8	33.6	0.489	0.967	22.2	7.42	2.36	3.04	1.44	1.17	8.92			9.00	1.20	0.630
1.46	23.2	50.6	0.737	0.719	21.6	7.15	2.42	1.54	0.89	2.63	12.8			11.5	0.81	-0.794
1.01	35.6	10.2	0.103	0.910	26.7	9.66	2.22	4.16	1.36	1.08	2.28			2.60	0.90	0.361
1.01	41.8	10.2	0.103	0.910	26.9	9.75	2.33	4.25	1.36	1.27	2.33			2.69	0.79	0.948
0.124	47.8	49.5	0.061	0.063	22.1	8.60	2.05	0.701	1.10	1.41	1.30			1.28	0.90	1.208
0.126	49.2	50.2	0.063	0.063	19.1	5.20	2.27	0.519	1.07	1.47	1.05			1.07	0.90	0.763
0.124	48.4	75.0	0.093	0.031	22.0	8.60	1.94	0.338	1.10	1.29	1.95			1.95	1.04	1.050
0.125	47.9	75.1	0.094	0.031	19.1	5.20	2.32	0.250	1.09	1.49	1.59			1.59	0.92	0.685
0.124	48.4	63.9	0.104	0.020	23.8	7.52	2.91	0.196	1.11	1.14	2.24			2.28	0.86	0.576
0.124	48.3	63.9	0.104	0.020	23.8	7.52	2.65	0.202			2.24					
0.550	48.6	19.4	0.107	0.443	18.5	4.96	2.13	2.27	1.25	1.47	1.80			1.93	0.80	0.495
0.550	46.9	25.2	0.139	0.411	19.1	5.20	2.02	2.17	1.37	1.29	2.30			2.55	0.90	0.436
0.541	46.3	48.3	0.261	0.280	22.4	6.90	2.16	1.53	1.04	2.61	5.24			5.21	0.80	0.640
0.541	46.5	73.9	0.400	0.141	22.0	6.60	1.98	0.822	1.19	1.53	7.83			8.09	0.94	0.631
0.550	47.8	74.1	0.408	0.142	19.1	5.20	2.06	0.632	0.99	1.57	8.45			8.35	0.87	0.094
0.582	47.5	14.5	0.084	0.498	23.8	7.50	2.25	3.05	1.32	1.33	1.77			2.02	0.79	0.937
0.582	47.1	14.5	0.084	0.498	23.8	7.50	2.34	3.03	1.31	1.38	1.82			2.10	0.86	0.350
0.621	46.7	19.8	0.124	0.497	23.6	7.40	2.61	2.93	1.30	1.60	2.71			2.97	0.82	0.672
0.621	47.2	19.8	0.124	0.497	23.8	7.50	1.96	3.05	1.34	1.51	2.65			2.98	0.83	0.823
0.740	46.7	32.8	0.243	0.497	23.6	7.40	2.24	2.50	1.36	2.11	5.16			5.51	0.94	0.780
1.03	47.6	25.6	0.267	0.766	19.4	5.26	1.79	2.74	1.10	2.18	4.40			4.84	0.73	1.046
1.03	48.5	48.5	0.500	0.530	19.1	5.20	1.91	1.65	1.16	1.88	8.30			9.02	0.89	-0.351
1.27	46.5	4.90	0.061	1.20	25.0	8.10	2.75	5.90	1.30	1.34	1.39			1.71	0.70	1.107
1.27	47.3	58.1	0.737	0.531	21.8	7.23	2.26	1.55	1.19	1.87	12.9			10.6	1.11	1.045
1.36	45.7	10.0	0.135	1.22	25.8	8.50	2.46	5.21	1.22	1.87	3.09			3.65	0.69	1.296
1.45	48.4	16.8	0.244	1.21	25.4	8.30	2.51	4.54	1.21	2.68	5.63			6.27	0.79	0.557
1.45	47.8	16.8	0.244	1.21	24.8	8.00	2.32	4.49	1.16	2.71	5.36			6.27	0.75	0.355
1.47	47.9	25.0	0.367	1.10	20.4	5.70	2.08	3.68	1.27	1.63	6.53			7.21	0.84	0.395
1.47	46.9	34.0	0.498	0.968	19.9	5.50	2.40	2.89	1.33	1.70	8.35			8.59	1.00	1.105
1.47	48.4	50.4	0.739	0.727	20.5	5.80	2.38	2.12	1.23	1.40	11.6			11.3	0.97	0.131
0.124	24.1	50.0	0.062	0.062	31.7	30.0	2.50	2.49	1.26	1.75	4.69	1.73	3.6	4.37	1.26	1.319
0.124	24.2	75.0	0.093	0.031	31.0	29.9	2.68	1.17	1.06	1.40	7.15	2.29	3.8	6.27	1.06	1.212
0.125	24.0	84.0	0.105	0.020	31.7	30.0	2.72	0.675	0.89	1.02	7.57	2.41	3.8	7.16		1.266
0.541	24.4	19.0	0.103	0.418	31.0	29.9	2.60	10.6	1.50	1.49	7.15	1.99	-0.01	7.79	1.06	0.885
0.541	25.0	26.1	0.141	0.400	89.7	29.6	2.85	9.44	1.55	1.45	9.93	2.25	0.73	10.8	1.28	1.355
0.541	25.1	51.0	0.276	0.265	88.4	29.3	2.61	5.81	1.41	1.90	20.0	1.84	3.6	20.0	1.41	1.094
0.541	24.2	74.7	0.404	0.137	89.0	29.4	2.29	2.88	1.23	1.70	28.3	1.71	3.7	27.7	1.23	0.710
0.541	25.2	74.9	0.405	0.136	88.3	29.3	3.02	2.72	1.14	1.20	28.2	2.41	3.8	27.3	1.01	0.088
0.624	23.3	19.6	0.122	0.502	85.6	28.7	3.25	10.4	1.63	1.81	8.63	2.47	0.28	9.05	1.36	1.053
0.624	23.5	19.6	0.122	0.502	88.2	29.3	2.55	10.7	1.94	1.68	8.27	2.13	3	8.74	1.63	1.082
0.742	25.7	32.1	0.238	0.504	88.2	29.2	2.72	9.13	1.57	1.64	17.2	2.10	3.3	18.7	1.20	0.932
1.02	24.2	10.0	0.102	0.917	87.2	29.0	2.91	17.2	1.53	1.08	7.35	2.02	1.3	7.55	1.18	0.916
1.02	25.0	10.2	0.103	0.919	92.7	30.2	3.40	17.0	1.82	1.11	7.31	2.46	-0.36	8.42	1.36	0.268
1.02	29.2	10.2	0.103	0.919	91.3	29.9	2.92	16.7	1.70	1.24	7.32	2.17	-0.5	8.35	1.05	1.080
1.02	24.5	25.0	0.255	0.764	89.0	29.4	2.85	13.1	1.74	1.44	18.9	2.13	1.1	19.3	1.49	1.341
1.02	23.6	48.2	0.494	0.530	87.8	29.2	2.77	7.18	1.67	1.42	35.0	1.91	3.3	35.3	1.45	0.797
1.02	22.9	49.8	0.507	0.512	89.5	29.6	2.54	7.66	1.67	1.90	32.7	1.81	2.7	34.0	1.67	1.251
1.02	22.4	72.4	0.738	0.281	91.0	29.7	2.88	3.83	1.55	1.31	51.8	1.88	3.4	50.1	1.41	0.164
1.28	24.8	6.03	0.077	1.20	89.3	29.5	2.79	19.4	1.51	1.03	5.48	1.59	1.8	5.85	1.19	-0.260
1.32	23.9	9.37	0.124	1.20	88.8	29.4	3.09	19.4	1.88	1.02	8.09	2.31	-0.36	9.42	1.36	0.380
1.46	23.0	6.94	0.101	1.36	91.9	30.1	2.53	22.8	1.56	0.97	6.47	1.86	0.98	8.02	1.13	-0.072
1.47	24.7	16.5	0.241	1.22	90.0	29.6	3.05	17.6	1.86	1.26	16.4	2.32	0.34	17.9	1.43	0.601
1.46	24.0	25.1	0.366	1.09	90.4	29.8	2.45	15.8	1.52	1.23	27.9	1.71	2.8	27.9	1.44	1.964
1.46	24.0	34.5	0.502	0.954	91.1	29.9	2.50	13.1	1.71	1.58	35.6	1.75	2.4	39.6	1.24	0.611
1.46	23.8	34.8	0.506	0.950	90.6	29.8	2.60	12.6	1.65	1.68	36.8	1.76	2.8	38.2	1.43	0.922
1.46	24.4	50.8	0.741	0.717	90.1	29.7	2.57	8.06	1.57	2.47	50.4	1.75	3	52.8	1.30	-0.053
1.02	31.3	10.2	0.103	0.919	92.5	30.2	2.58	16.3	1.63	1.22	6.62	1.97	-0.8	8.40	0.91	2.274
1.02	34.6	10.2	0.103	0.919	91.0	29.9	3.41	16.6	1.77	1.21	7.62	2.63	0.14	8.76	1.13	0.985
1.02	38.6	10.2	0.103	0.919	90.7	29.8	3.08	16.5	1.65	1.25	7.47	2.03	2.1	8.91	0.88	1.607
0.125	47.4	49.0	0.062	0.063	92.6	30.0	2.46	2.33	1.34	1.80	4.59	1.99	3.8	5.15		2.083
0.124	48.4	50.7	0.063	0.061	94.3	30.3	2.00	2.17	1.30	1.54	4.96	1.70	3.8	5.18	0.92	1.175
0.124	47.8	50.7	0.063	0.061	94.5	30.3	1.80	2.14	1.24	1.49	5.03	1.45	3.6	5.27	0.95	1.683
0.125	49.8	74.1	0.093	0.032	89.7	29.3	2.60	1.09	1.22	1.68	6.44	2.46	4.2	6.36		2.102
0.124	48.3	75.4	0.093	0.031	98.0	31.1	2.51	1.07	1.15	1.55	8.06	2.29	4			
0.124	47.5	75.4	0.093	0.031	97.0	30.8	1.35	0.959	0.92	1.02	7.60	1.17	3.9	7.88	0.92	1.877
0.125	46.6	83.2	0.104	0.021	92.0	29.9	2.55	0.760	1.11	1.55	7.87	2.32	3.9	8.54		1.542
0.544	47.7	14.2	0.077	0.467	85.4	28.4	2.66	9.69	1.82	1.27	5.63	2.41	0.26	6.58	1.13	1.601
0.544	47.7	14.2	0.077	0.467	85.2	28.3	2.72	10.2	1.77	1.43	5.44	2.27	0.01	6.69	1.06	0.968
0.544	48.4	14.2	0.077	0.467	88.9	29.1	2.21	10.2	1.57	1.48	5.58	1.74	0.61	7.30	0.86	0.942
0.545	45.7	19.1	0.104	0.441	89.8	29.3	2.32	9.36	1.58	1.88	6.82	1.98	0.27	11.0	0.75	1.094
0.543	47.4	19.5	0.106	0.437	91.5	29.8	1.25	9.33	1.16	1.76				9.78	0.53	0.966
0.543	48.3	19.5	0.106	0.437	90.8	29.6	2.71	9.13	1.50	1.53	7.36	2.32	0.75	8.89	0.84	1.698
0.543	48.4	19.5	0.106	0.437	92.6	29.9	2.19	9.46	1.45	1.60	7.87	1.68	1.8	9.15	0.75	2.177
0.545	46.6	24.8	0.135	0.410	90.2	29.4	3.16	8.20	1.54	1.58	9.54	2.62	2.4	11.3	0.90	1.420
0.543	48.3	25.2	0.137	0.406	91.7	29.8	2.24	8.71	1.45	1.68	9.83	1.95	0.96	11.7	0.80	1.617
0.543	46.7	25.3	0.137	0.406	91.5	29.7	1.55	8.78	1.32	1.80				11.5	0.65	1.771
0.544	48.3	26.4	0.144	0.400	87.4	28.8	2.48	8.47	1.72	1.61				11.9	1.10	1.682
0.544	48.4	44.2	0.240	0.304	85.9	28.5	2.13	6.17	1.40	2.34	16.7	1.67	3.7	20.3	0.87	1.404
0.545	47.9	48.1	0.262	0.283	89.9	29.4	2.92	5.21	1.28	1.58	17.0	2.62	2.4	16.9	0.85	2.656
0.543	48.9	48.8	0.265	0.278	93.2	30.1	1.86	5.52	1.34	2.29	20.2	1.52	3.5	21.2	0.98	1.868
0.543	48.0	74.4	0.404	0.139	94.1	30.3	1.60	2.54	1.17	2.20	30.0	1.30	3.5	30.1	1.14	1.862

E3: Experimental conditions and important data for CITAD drying (continued)

G	B	qT	GT	GI	Tj	Te	Xo	Rlc	Xc	n	RTc	XTi	nTi	RTm	Xm	C
0.624	48.5	19.7	0.123	0.501	88.5	29.1	2.69	10.4	1.56	1.64	8.85	2.00	3.1	10.2	0.91	1.287
0.742	49.0	32.6	0.242	0.500	88.0	29.0	2.92	9.02	1.44	2.28	16.9	2.40	3.7	19.2	0.92	1.193
1.02	42.3	10.2	0.104	0.918	90.8	29.8	3.01	16.8	1.67	1.37	7.70	2.20	0.83	9.03	0.91	1.582
1.02	42.6	10.2	0.104	0.920	88.3	29.0	2.27	14.1	1.58	1.68	6.94	1.57	0.64	9.02	0.82	1.072
1.02	42.7	10.2	0.103	0.919	90.5	29.8	3.03	16.6	1.62	1.42	7.71	2.26	0.75	9.27	0.91	1.311
1.02	46.7	10.2	0.104	0.920	88.3	29.0	3.84	15.0	1.84	1.26	7.54	2.41	3.5	8.28	1.15	1.222
1.02	83.3	10.2	0.104	0.918	90.8	29.8	2.78	16.2	1.54	2.01	7.46	2.00	3.6	11.1	0.66	1.73
1.02	44.9	10.2	0.104	0.899	88.8	29.1	2.85	15.8	1.58	1.55	7.38	2.14	0.36	8.98	0.75	2.284
1.02	46.0	10.3	0.105	0.918	87.9	28.9	2.16	15.0	1.49	1.51	6.70	1.83	-1.3	9.76	0.71	1.616
1.02	49.5	10.3	0.105	0.918	86.4	28.6	1.54	14.3	1.33	1.66				10.1	0.59	1.242
1.02	47.8	25.5	0.261	0.763	89.1	29.2	3.17	10.9	1.60	1.61	17.5	2.60	3.8	19.0	1.01	1.48
1.02	47.2	25.9	0.265	0.758	87.3	28.3	2.06	10.7	1.40	2.13	18.7	1.57	3.4	21.4	0.81	1.413
1.02	47.4	25.9	0.265	0.758	88.1	29.0	1.84	11.0	1.36	2.25	18.2	1.43	2.8	21.2	0.77	1.784
1.02	47.4	48.0	0.491	0.533	89.1	29.2	3.48	7.38	1.43	1.92	32.6	3.02	3.8	29.5	1.30	1.411
1.02	47.7	48.2	0.494	0.530	87.9	29.2	2.68	7.49	1.29	1.99	30.9	2.32	3.7	30.5	1.23	2.127
1.19	48.8	55.8	0.665	0.526	89.7	29.6	2.88	6.81	1.30	1.65	41.8	2.47	0.28	37.2	1.30	1.243
1.28	48.3	4.6	0.059	1.22	88.2	29.0	2.81	19.3	1.60	1.36	3.84	1.85	-0.6	8.77	0.58	2.019
1.37	45.9	9.9	0.136	[illegible]	87.3	28.8	3.53	20.4	1.69	1.20	10.4	2.17	3.3	11.0	0.94	2.415
1.37	46.0	9.9	0.136	[illegible]	87.4	28.8	2.90	17.8	1.54	1.63	10.1	2.07	1.5	12.0	0.76	1.844
1.46	48.7	7.1	0.103	[illegible]	88.9	29.2	2.97	18.8	1.62	1.54	7.34	2.16	1.1	9.81	0.65	1.141
1.46	44.2	7.2	0.105	[illegible]	90.9	29.6	1.45	19.6	1.25	1.88				10.9	0.53	0.963
1.46	48.1	7.2	0.105	1.	90.2	29.4	2.03	21.0	1.52	1.43				10.8	0.71	1.322
1.46	46.8	8.5	0.124	1.34	95.0	30.5	1.72	20.1	1.45	1.97				14.2	0.73	0.543
1.46	47.1	8.5	0.124	1.34	97.4	31.0	2.73	20.9	1.69	1.35	10.1	2.14	0.42	12.8	1.06	1.143
1.46	48.1	16.6	0.242	1.22	87.6	28.9	2.90	16.4	1.54	1.67	17.4	2.43	1.3	20.5	0.85	2.002
1.46	46.6	16.8	0.246	1.22	94.1	30.3	1.91	16.3	1.60	1.90				22.9	0.83	1.721
1.46	47.2	16.8	0.246	1.22	92.7	30.0	2.04	17.6	1.91	1.17				23.8	0.74	1.972
1.46	47.7	16.8	0.246	1.22	94.2	30.3	2.79	17.1	1.60	1.74	21.0	1.89	2.1	22.3	0.97	1.693
1.46	49.0	16.8	0.246	1.22	92.0	29.8	1.88	15.6	1.50	2.29	17.1	1.60	0.24	24.2	0.79	1.277
1.46	46.6	24.6	0.359	1.10	89.6	29.3	2.80	13.4	1.52	2.11	26.1	2.30	2	26.4	0.90	1.764
1.46	48.3	27.7	0.403	1.05	91.4	29.7	2.64	14.6	1.48	1.68	28.1	2.12	3.2	20.3	0.97	1.536
1.46	46.7	27.8	0.405	1.05	89.8	29.3	1.87	12.9	1.39	1.98				31.5	0.64	1.456
1.46	46.7	28.9	0.423	1.04	94.5	30.3	3.05	13.0	1.71	1.80	33.6	2.32	3.5	34.5	1.09	2.397
1.46	47.9	28.9	0.423	1.04	95.7	30.7	1.76	12.5	1.45	2.61				36.0	0.82	1.719
1.46	48.9	33.6	0.489	0.968	89.4	29.3	2.91	11.3	1.54	2.05	33.7	2.35	3.7	33.0	1.16	2.033
1.46	47.9	50.0	0.728	0.729	88.6	29.1	2.57	7.35	1.31	2.43	43.4	2.19	3.4	41.2	1.14	1.471
1.46	48.4	50.0	0.728	0.729	87.9	28.9	2.93	7.98	1.49	1.70	42.7	2.50	3.5	38.5	1.31	0.519

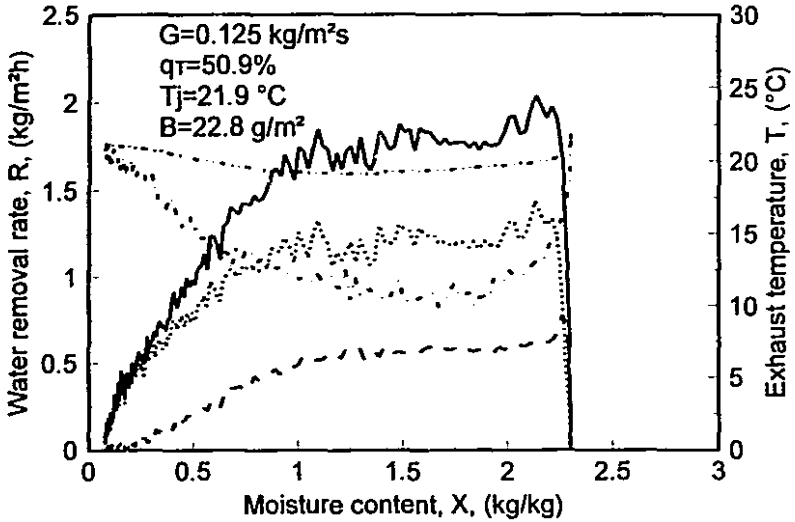
G=0.125 kg/m²s
qT=50.9%
Tj=21.9 °C
B=22.8 g/m²
Water removal rate, R, (kg/m²h)
Exhaust temperature, T, (°C)
Moisture content, X, (kg/kg)

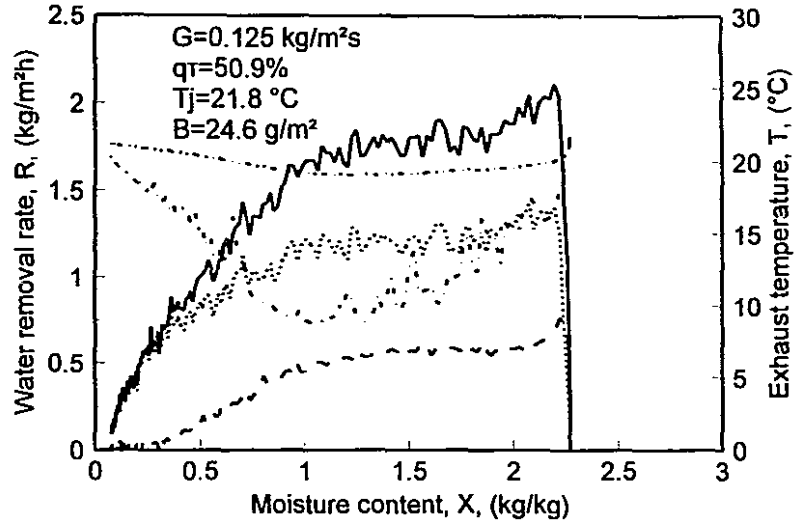
G=0.125 kg/m²s
qT=50.9%
Tj=21.8 °C
B=24.6 g/m²
Water removal rate, R, (kg/m²h)
Exhaust temperature, T, (°C)
Moisture content, X, (kg/kg)

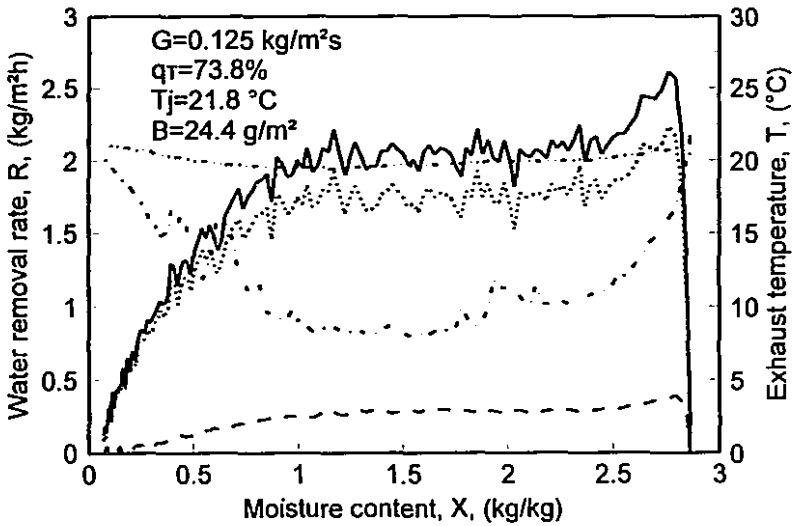
G=0.125 kg/m²s
qT=73.8%
Tj=21.8 °C
B=24.4 g/m²
Water removal rate, R, (kg/m²h)
Exhaust temperature, T, (°C)
Moisture content, X, (kg/kg)
R
RI
RT

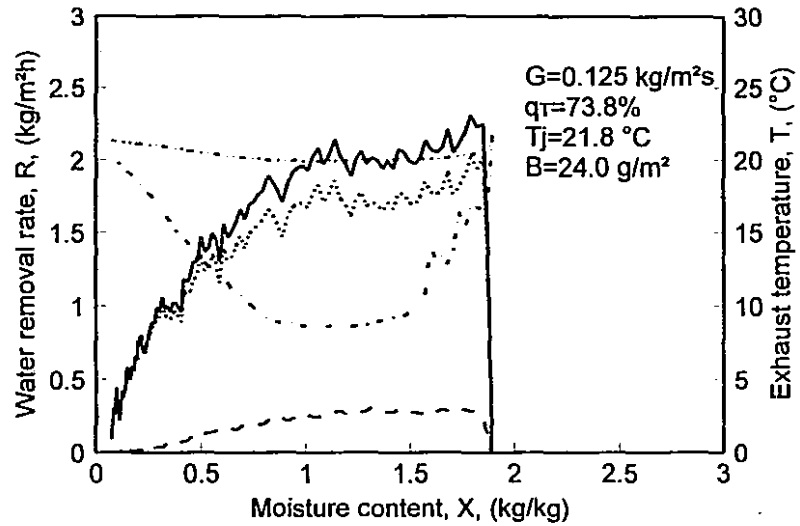
G=0.125 kg/m²s
qT=73.8%
Tj=21.8 °C
B=24.0 g/m²
Water removal rate, R, (kg/m²h)
Exhaust temperature, T, (°C)
Moisture content, X, (kg/kg)
TIe
TTe

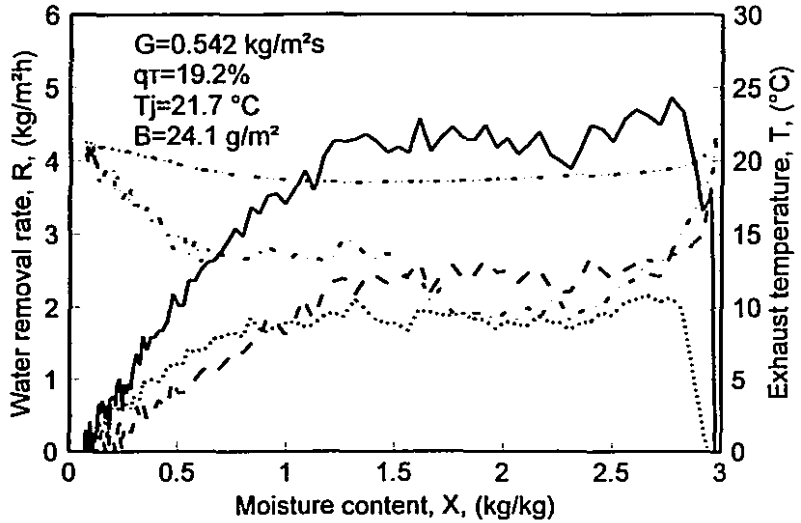
G=0.542 kg/m²s
qT=19.2%
Tj=21.7 °C
B=24.1 g/m²
Water removal rate, R, (kg/m²h)
Exhaust temperature, T, (°C)
Moisture content, X, (kg/kg)

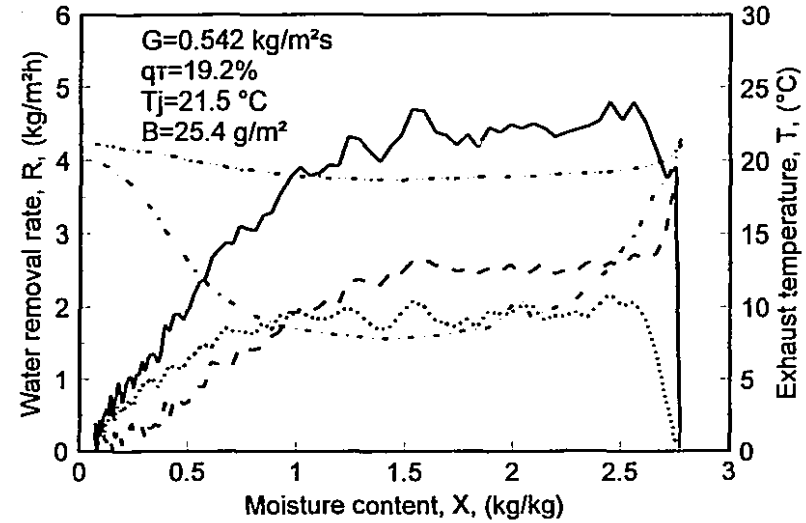
G=0.542 kg/m²s
qT=19.2%
Tj=21.5 °C
B=25.4 g/m²
Water removal rate, R, (kg/m²h)
Exhaust temperature, T, (°C)
Moisture content, X, (kg/kg)

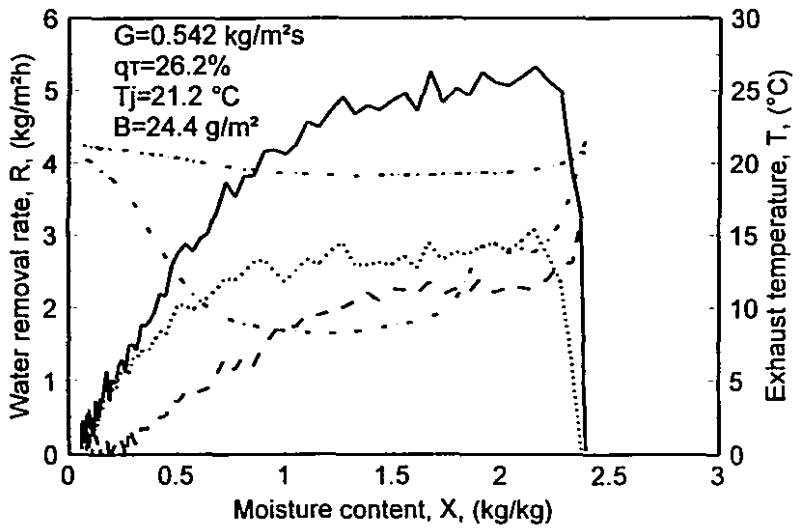
G=0.542 kg/m²s
qT=26.2%
Tj=21.2 °C
B=24.4 g/m²
Water removal rate, R, (kg/m²h)
Exhaust temperature, T, (°C)
Moisture content, X, (kg/kg)
R
RI
RT

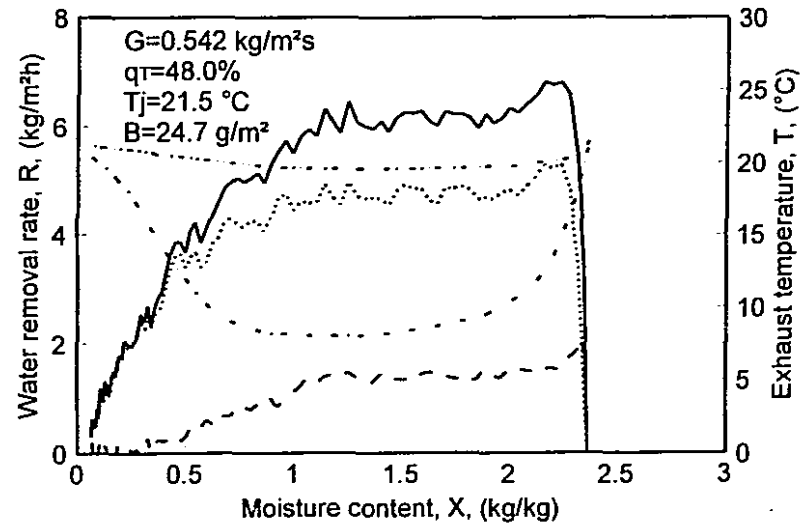
G=0.542 kg/m²s
qT=48.0%
Tj=21.5 °C
B=24.7 g/m²
Water removal rate, R, (kg/m²h)
Exhaust temperature, T, (°C)
Moisture content, X, (kg/kg)
TIe
TTe

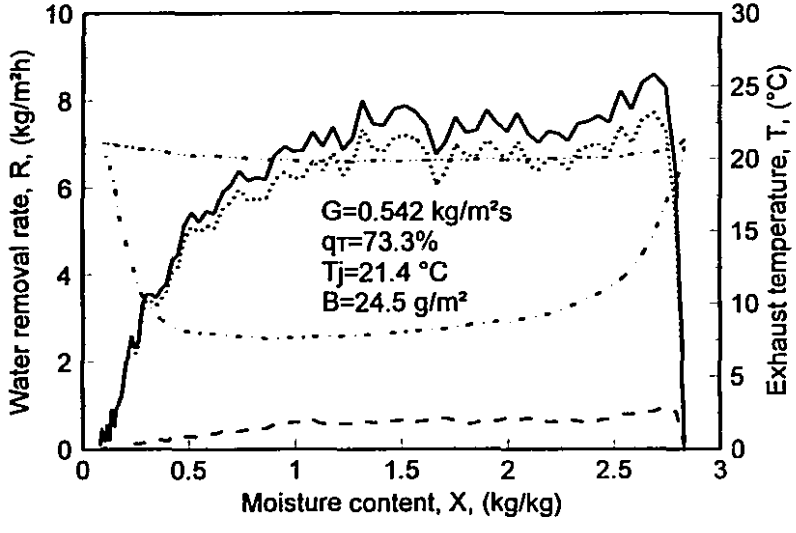
G=0.542 kg/m²s
qT=73.3%
Tj=21.4 °C
B=24.5 g/m²
Water removal rate, R, (kg/m²h)
Exhaust temperature, T, (°C)
Moisture content, X, (kg/kg)

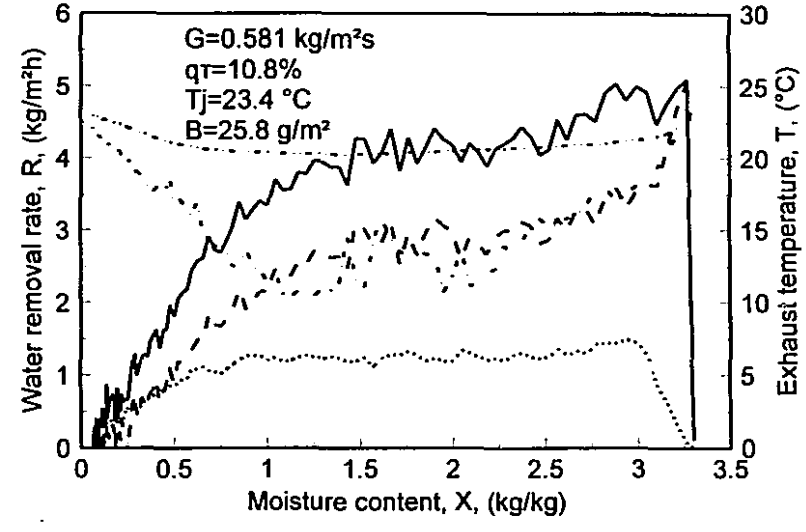
G=0.581 kg/m²s
qT=10.8%
Tj=23.4 °C
B=25.8 g/m²
Water removal rate, R, (kg/m²h)
Exhaust temperature, T, (°C)
Moisture content, X, (kg/kg)

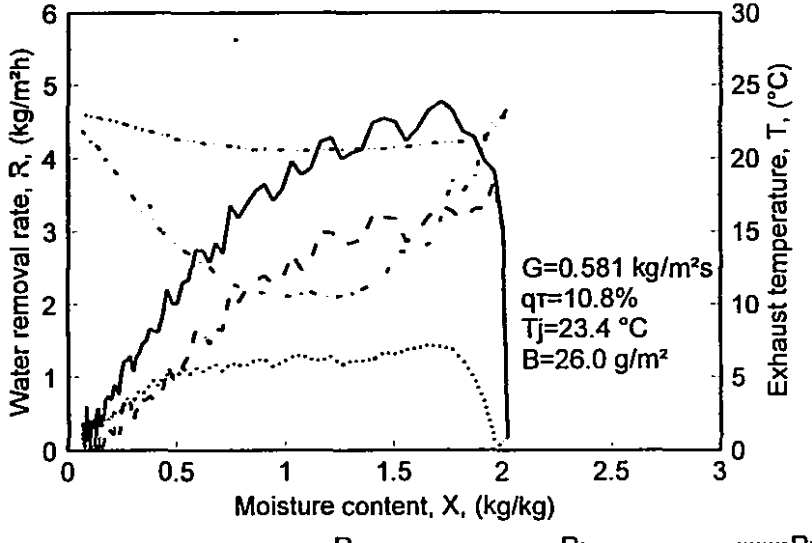
G=0.581 kg/m²s
qT=10.8%
Tj=23.4 °C
B=26.0 g/m²
Water removal rate, R, (kg/m²h)
Exhaust temperature, T, (°C)
Moisture content, X, (kg/kg)
R
RI
RT

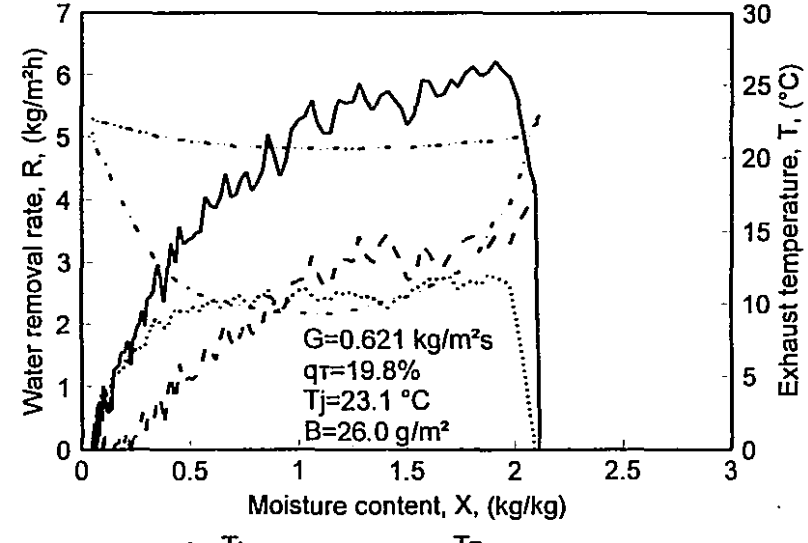
G=0.621 kg/m²s
qT=19.8%
Tj=23.1 °C
B=26.0 g/m²
Water removal rate, R, (kg/m²h)
Exhaust temperature, T, (°C)
Moisture content, X, (kg/kg)
TIe
TTe

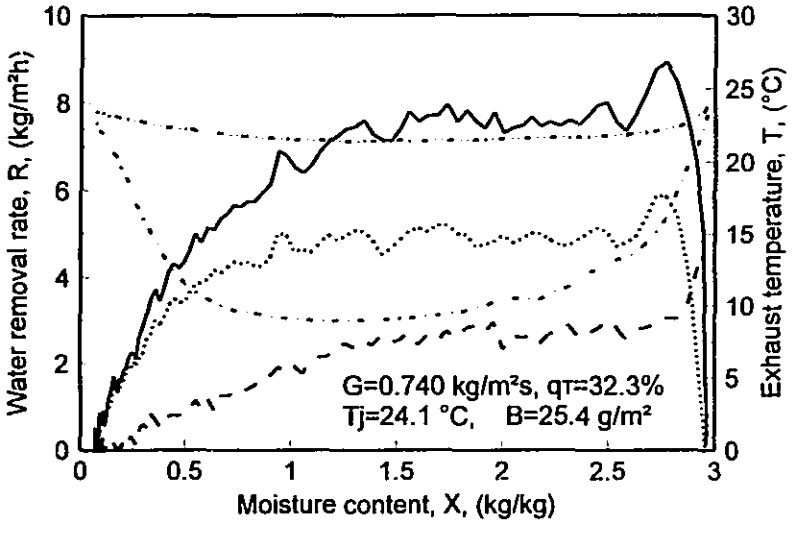
Water removal rate, R, (kg/m²h)
Exhaust temperature, T, (°C)
Moisture content, X, (kg/kg)
G=0.740 kg/m²s, qT=32.3%
Tj=24.1 °C, B=25.4 g/m²

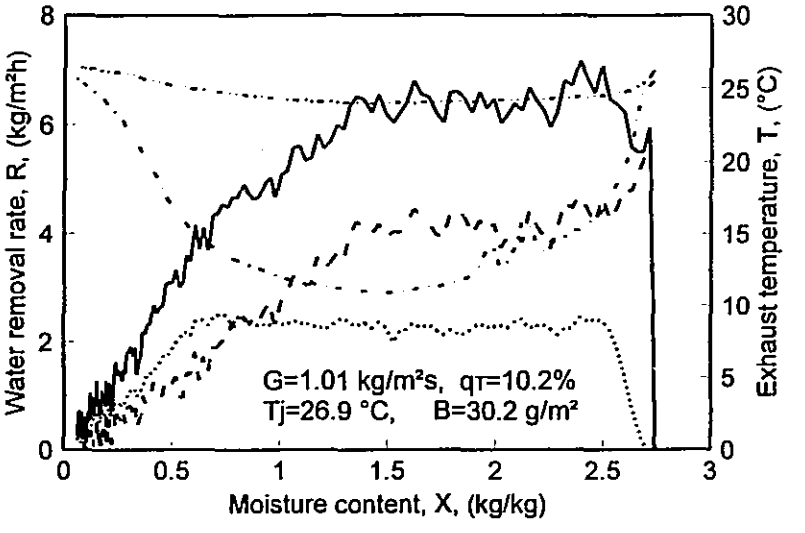
Water removal rate, R, (kg/m²h)
Exhaust temperature, T, (°C)
Moisture content, X, (kg/kg)
G=1.01 kg/m²s, qT=10.2%
Tj=26.9 °C, B=30.2 g/m²

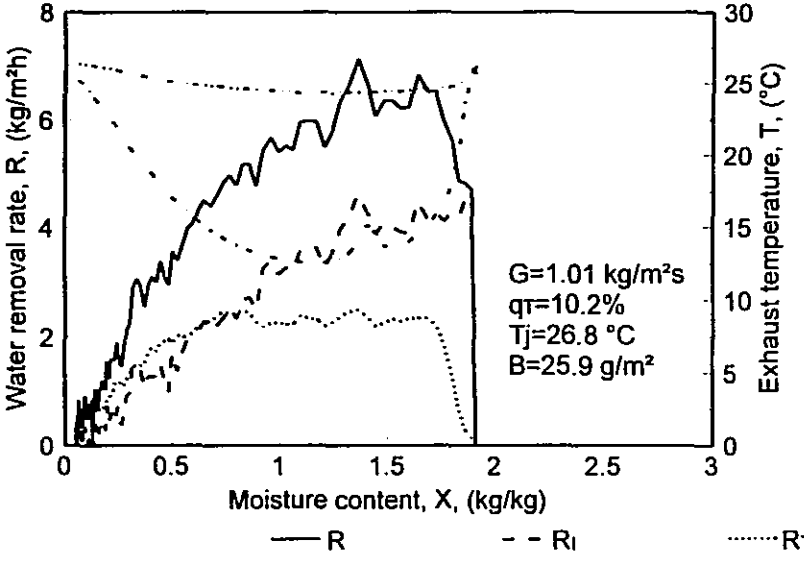
Water removal rate, R, (kg/m²h)
Exhaust temperature, T, (°C)
Moisture content, X, (kg/kg)
G=1.01 kg/m²s
qT=10.2%
Tj=26.8 °C
B=25.9 g/m²
R
RI
RT

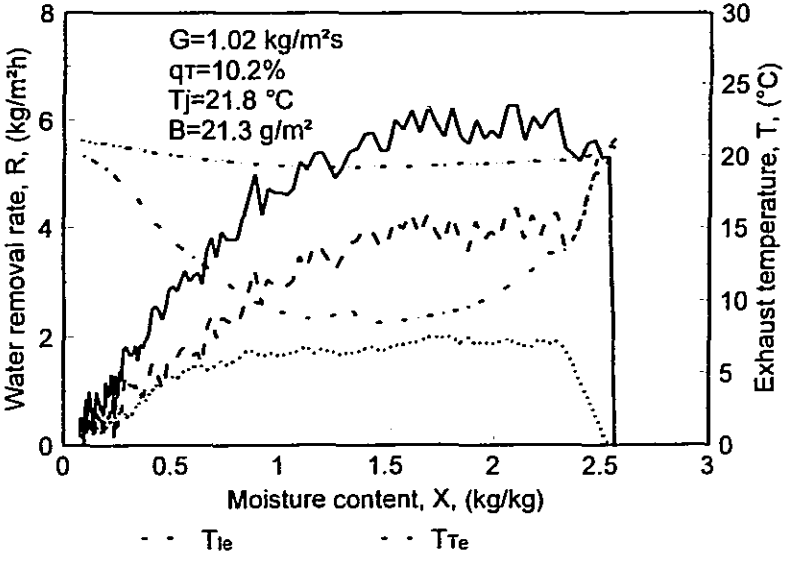
Water removal rate, R, (kg/m²h)
Exhaust temperature, T, (°C)
Moisture content, X, (kg/kg)
G=1.02 kg/m²s
qT=10.2%
Tj=21.8 °C
B=21.3 g/m²
TIe
TTe

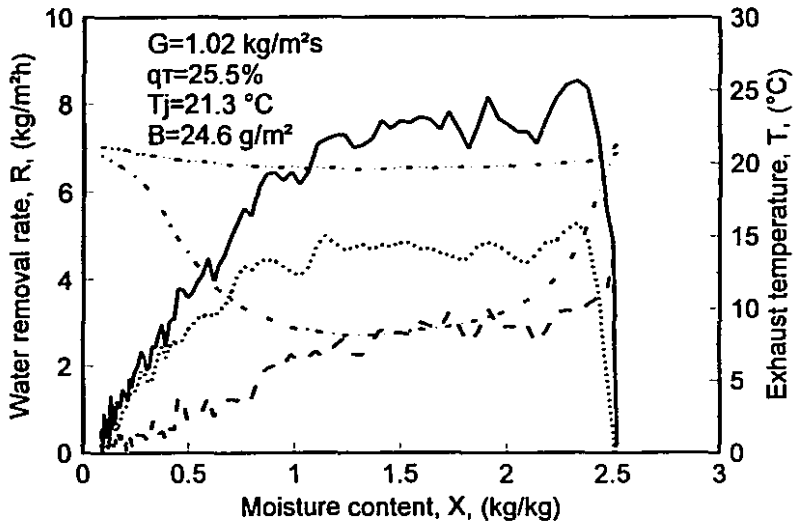
G=1.02 kg/m²s
qT=25.5%
Tj=21.3 °C
B=24.6 g/m²
Water removal rate, R, (kg/m²h)
Exhaust temperature, T, (°C)
Moisture content, X, (kg/kg)

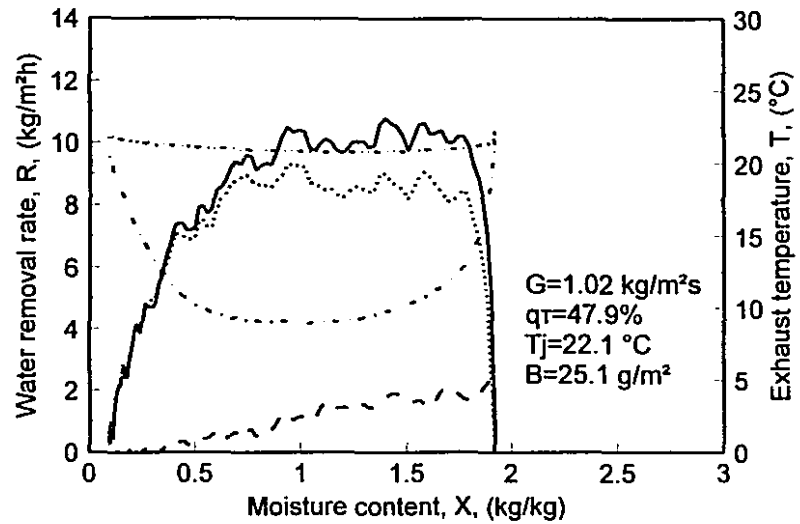
G=1.02 kg/m²s
qT=47.9%
Tj=22.1 °C
B=25.1 g/m²
Water removal rate, R, (kg/m²h)
Exhaust temperature, T, (°C)
Moisture content, X, (kg/kg)

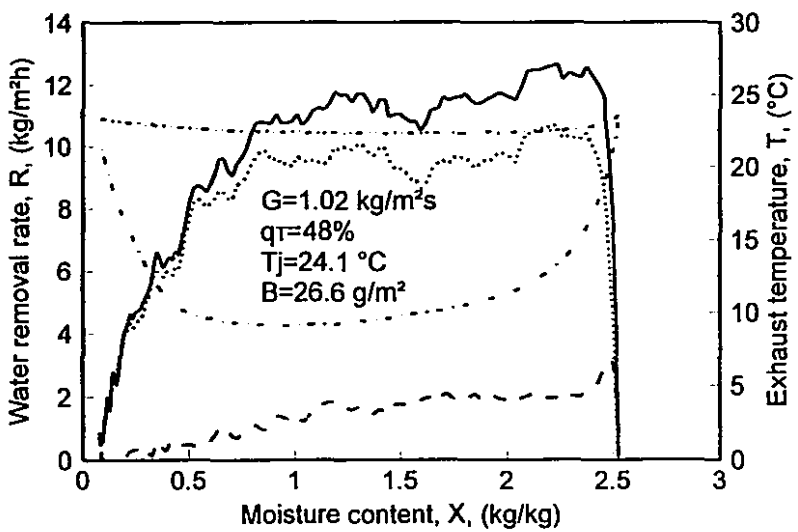
G=1.02 kg/m²s
qT=48%
Tj=24.1 °C
B=26.6 g/m²
Water removal rate, R, (kg/m²h)
Exhaust temperature, T, (°C)
Moisture content, X, (kg/kg)
R
RI
RT

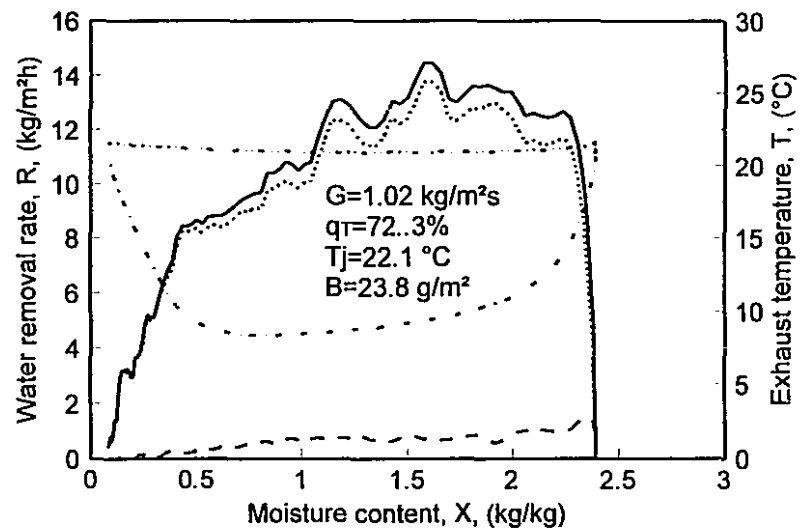
G=1.02 kg/m²s
qT=72..3%
Tj=22.1 °C
B=23.8 g/m²
Water removal rate, R, (kg/m²h)
Exhaust temperature, T, (°C)
Moisture content, X, (kg/kg)
TIe
TTe

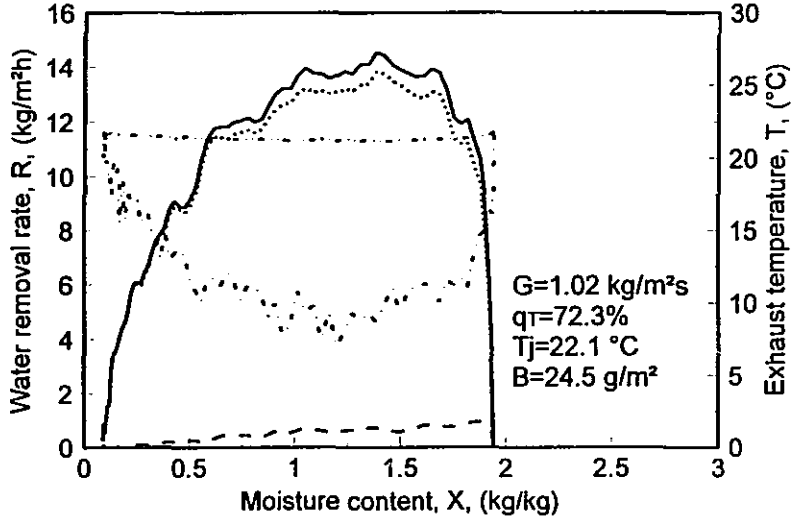
Water removal rate, R, (kg/m²h)
Exhaust temperature, T, (°C)
Moisture content, X, (kg/kg)
G=1.02 kg/m²s
qT=72.3%
Tj=22.1 °C
B=24.5 g/m²

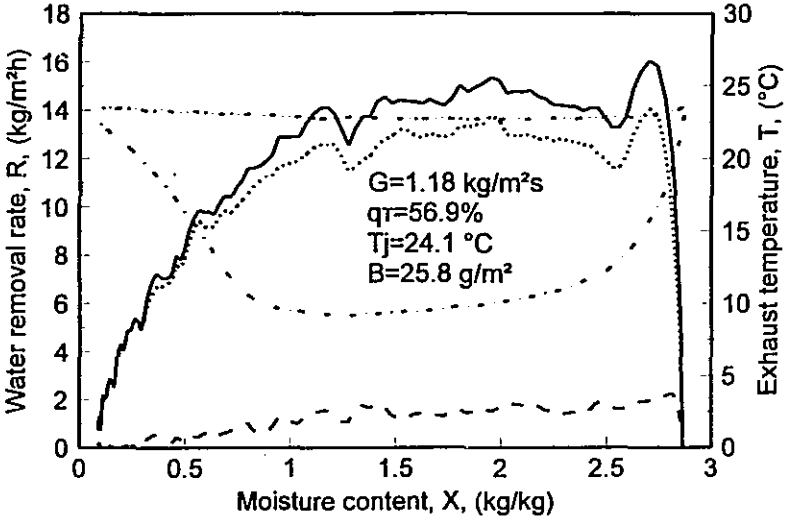
Water removal rate, R, (kg/m²h)
Exhaust temperature, T, (°C)
Moisture content, X, (kg/kg)
G=1.18 kg/m²s
qT=56.9%
Tj=24.1 °C
B=25.8 g/m²

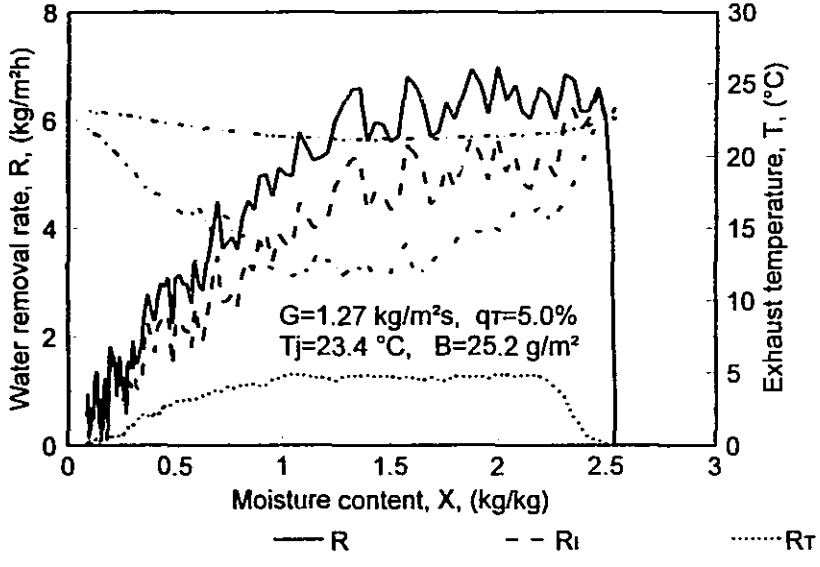
Water removal rate, R, (kg/m²h)
Exhaust temperature, T, (°C)
Moisture content, X, (kg/kg)
G=1.27 kg/m²s, qT=5.0%
Tj=23.4 °C, B=25.2 g/m²
R
RI
RT

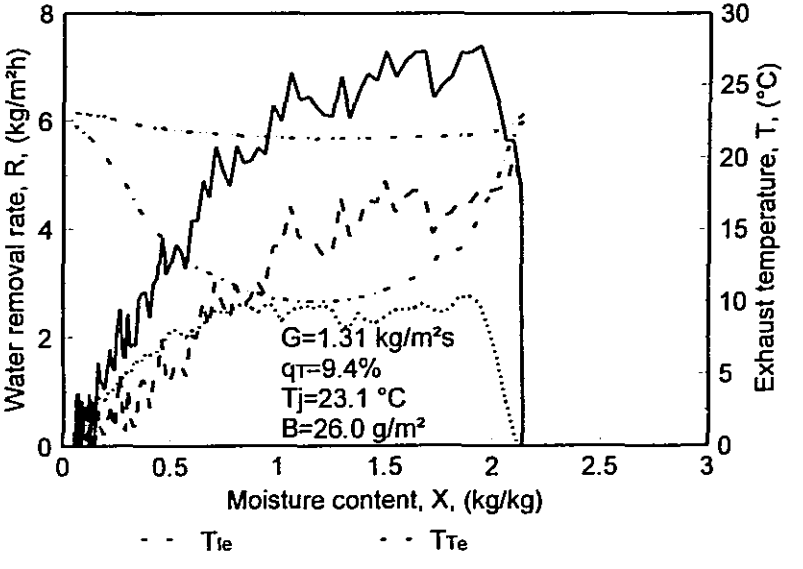
Water removal rate, R, (kg/m²h)
Exhaust temperature, T, (°C)
Moisture content, X, (kg/kg)
G=1.31 kg/m²s
qT=9.4%
Tj=23.1 °C
B=26.0 g/m²
TIe
TTe

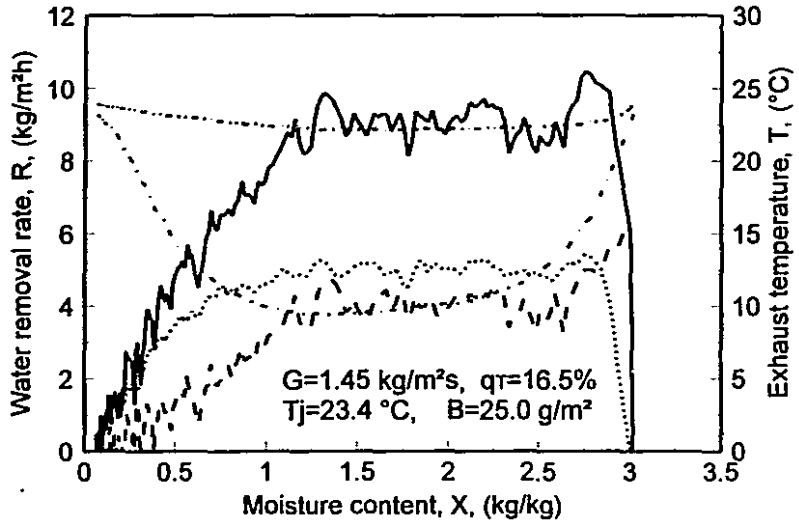
Water removal rate, R, (kg/m²h)
Exhaust temperature, T, (°C)
Moisture content, X, (kg/kg)
G=1.45 kg/m²s, qT=16.5%
Tj=23.4 °C, B=25.0 g/m²

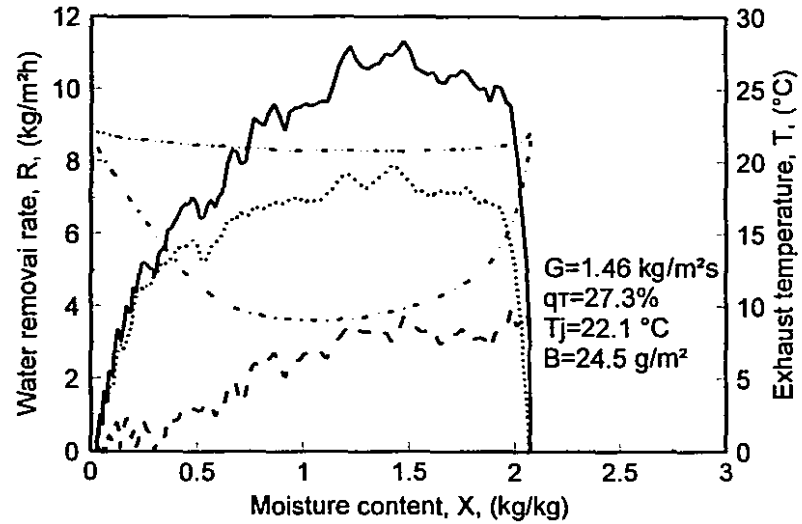
Water removal rate, R, (kg/m²h)
Exhaust temperature, T, (°C)
Moisture content, X, (kg/kg)
G=1.46 kg/m²s
qT=27.3%
Tj=22.1 °C
B=24.5 g/m²

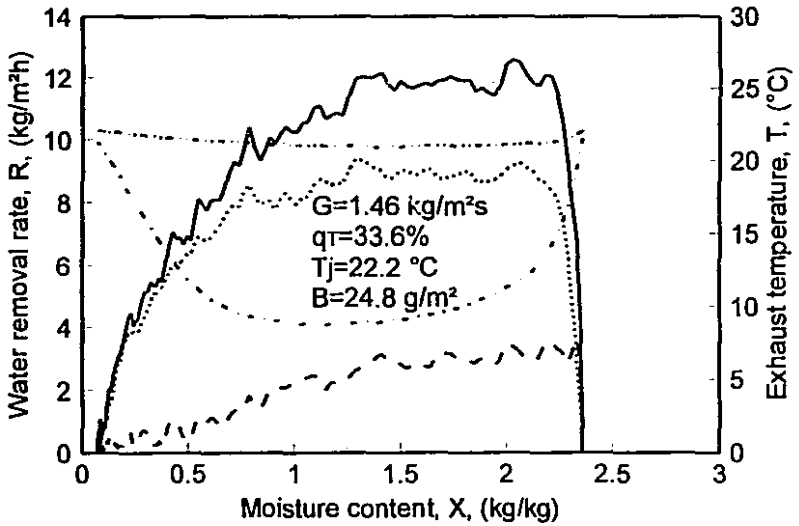
Water removal rate, R, (kg/m²h)
Exhaust temperature, T, (°C)
Moisture content, X, (kg/kg)
G=1.46 kg/m²s
qT=33.6%
Tj=22.2 °C
B=24.8 g/m²
R
RI
RT

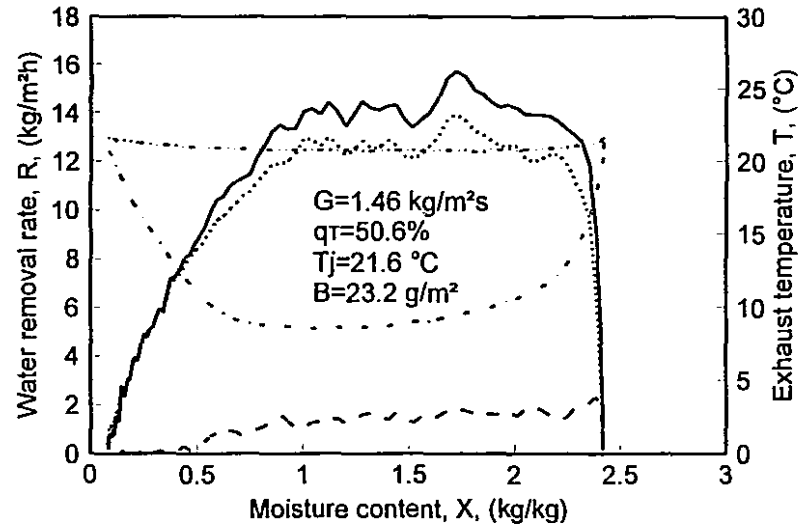
Water removal rate, R, (kg/m²h)
Exhaust temperature, T, (°C)
Moisture content, X, (kg/kg)
G=1.46 kg/m²s
qT=50.6%
Tj=21.6 °C
B=23.2 g/m²
TIe
TTe

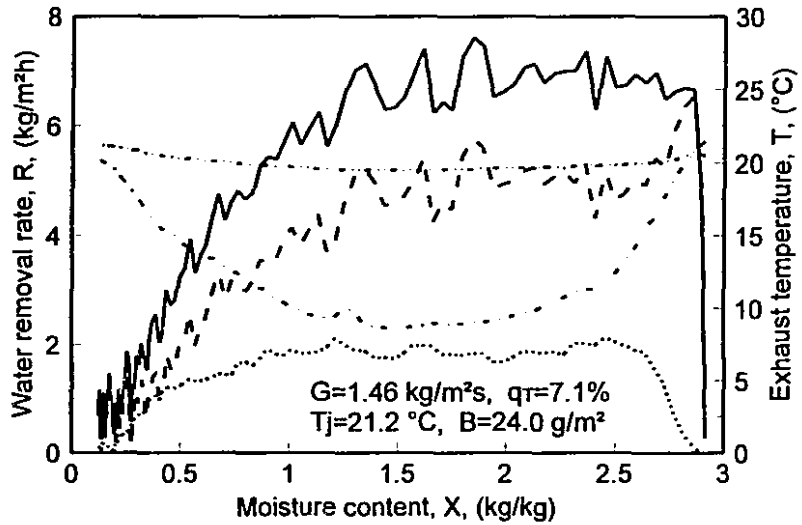
Water removal rate, R, (kg/m²h)
Exhaust temperature, T, (°C)
Moisture content, X, (kg/kg)
G=1.46 kg/m²s, qT=7.1%
Tj=21.2 °C, B=24.0 g/m²

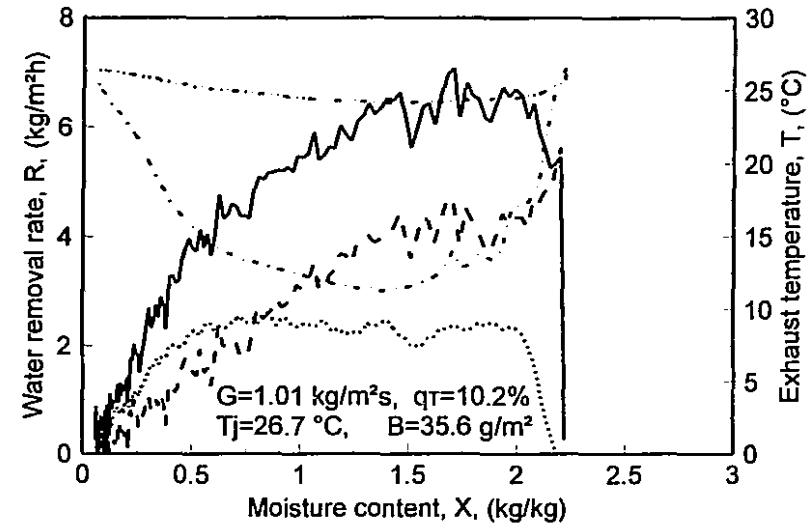
Water removal rate, R, (kg/m²h)
Exhaust temperature, T, (°C)
Moisture content, X, (kg/kg)
G=1.01 kg/m²s, qT=10.2%
Tj=26.7 °C, B=35.6 g/m²

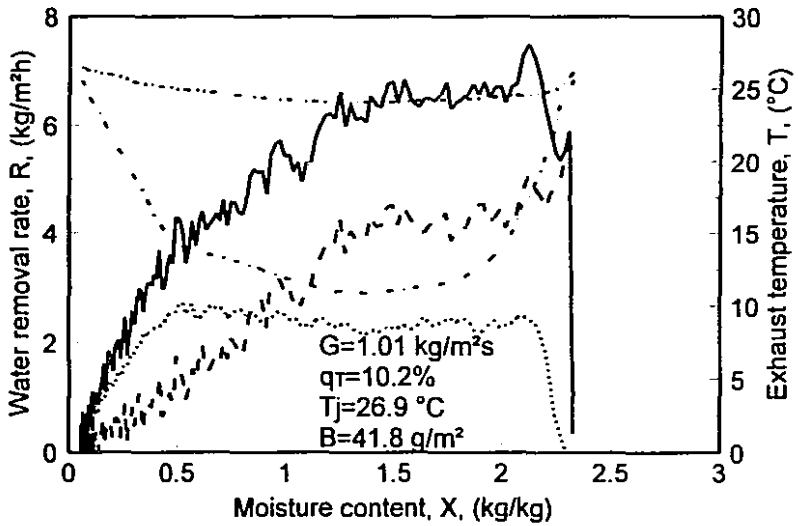
Water removal rate, R, (kg/m²h)
Exhaust temperature, T, (°C)
Moisture content, X, (kg/kg)
G=1.01 kg/m²s
qT=10.2%
Tj=26.9 °C
B=41.8 g/m²
R
RI
RT

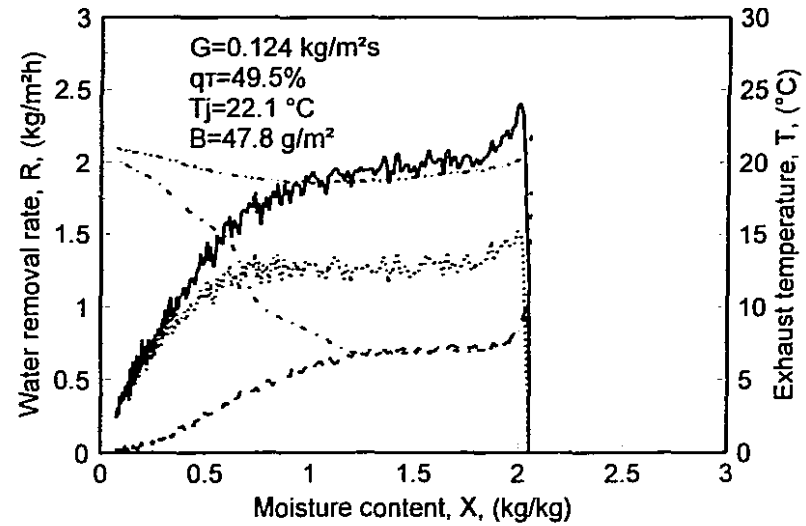
Water removal rate, R, (kg/m²h)
Exhaust temperature, T, (°C)
Moisture content, X, (kg/kg)
G=0.124 kg/m²s
qT=49.5%
Tj=22.1 °C
B=47.8 g/m²
TIe
TTe

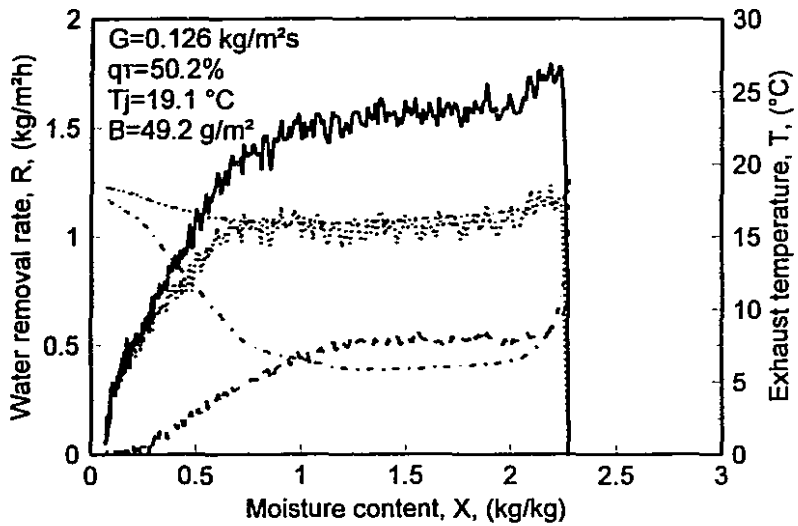
G=0.126 kg/m²s
qT=50.2%
Tj=19.1 °C
B=49.2 g/m²
Water removal rate, R, (kg/m²h)
Exhaust temperature, T, (°C)
Moisture content, X, (kg/kg)

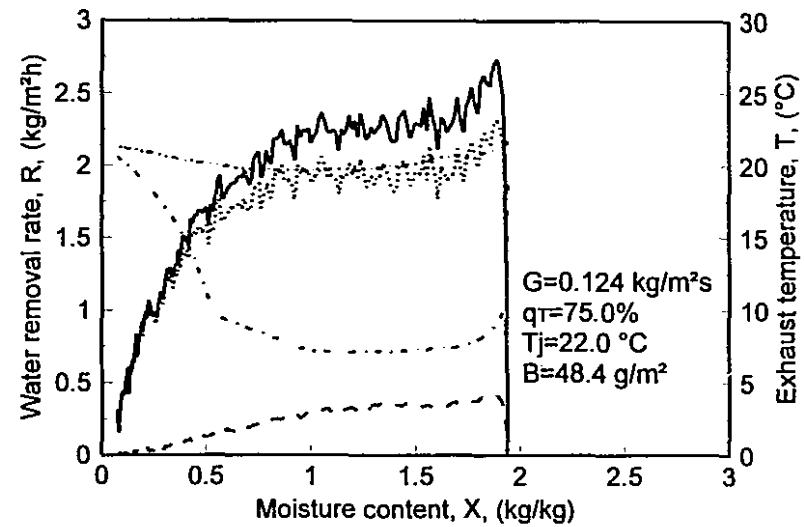
G=0.124 kg/m²s
qT=75.0%
Tj=22.0 °C
B=48.4 g/m²
Water removal rate, R, (kg/m²h)
Exhaust temperature, T, (°C)
Moisture content, X, (kg/kg)

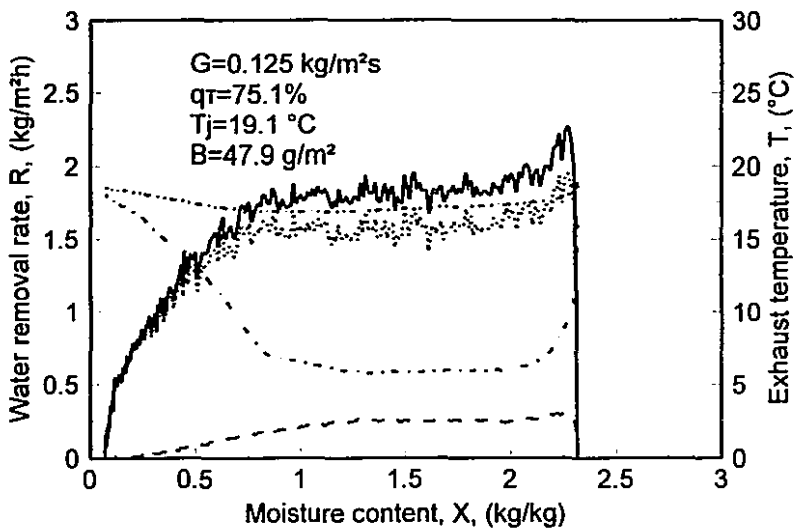
G=0.125 kg/m²s
qT=75.1%
Tj=19.1 °C
B=47.9 g/m²
Water removal rate, R, (kg/m²h)
Exhaust temperature, T, (°C)
Moisture content, X, (kg/kg)
R
RI
RT

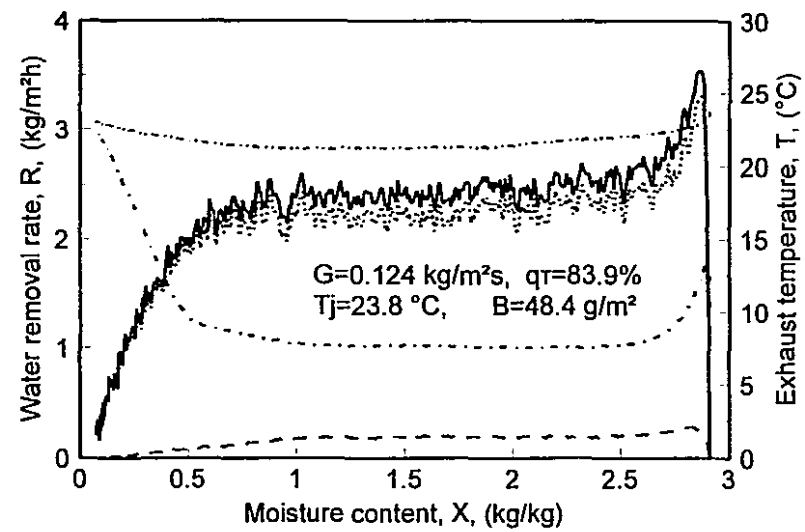
G=0.124 kg/m²s, qT=83.9%
Tj=23.8 °C, B=48.4 g/m²
Water removal rate, R, (kg/m²h)
Exhaust temperature, T, (°C)
Moisture content, X, (kg/kg)
TIe
TTe

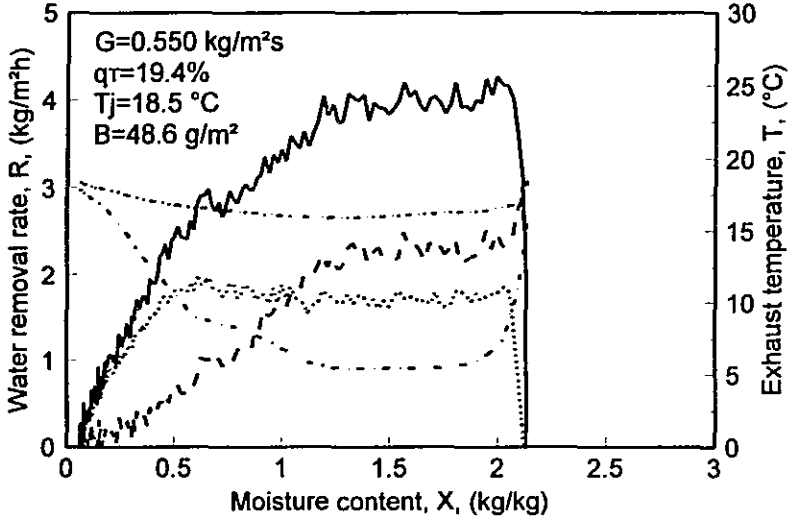
G=0.550 kg/m²s
qT=19.4%
Tj=18.5 °C
B=48.6 g/m²
Water removal rate, R, (kg/m²h)
Exhaust temperature, T, (°C)
Moisture content, X, (kg/kg)

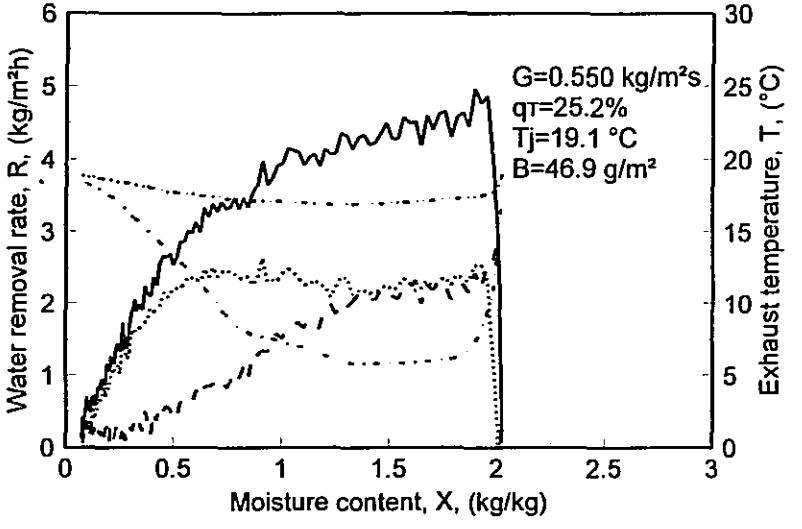
G=0.550 kg/m²s
qT=25.2%
Tj=19.1 °C
B=46.9 g/m²
Water removal rate, R, (kg/m²h)
Exhaust temperature, T, (°C)
Moisture content, X, (kg/kg)

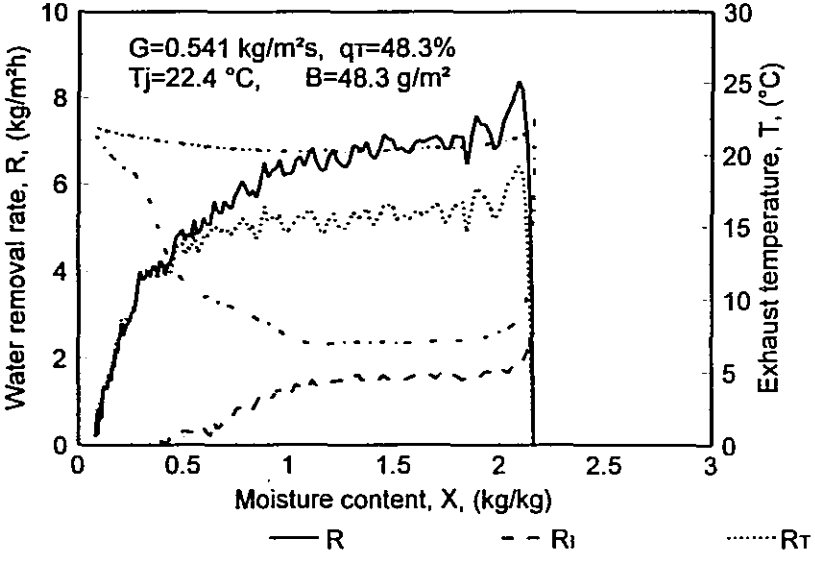
G=0.541 kg/m²s, qT=48.3%
Tj=22.4 °C, B=48.3 g/m²
Water removal rate, R, (kg/m²h)
Exhaust temperature, T, (°C)
Moisture content, X, (kg/kg)
R
RI
RT

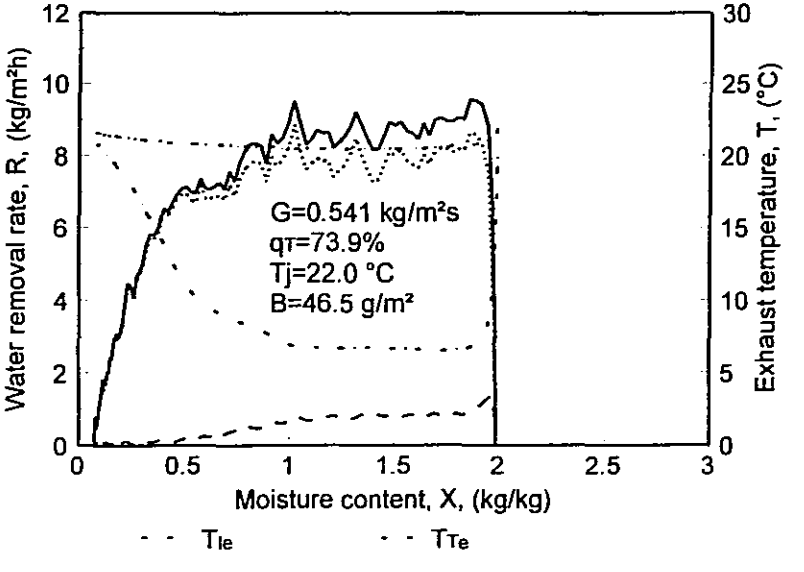
G=0.541 kg/m²s
qT=73.9%
Tj=22.0 °C
B=46.5 g/m²
Water removal rate, R, (kg/m²h)
Exhaust temperature, T, (°C)
Moisture content, X, (kg/kg)
TIe
TTe

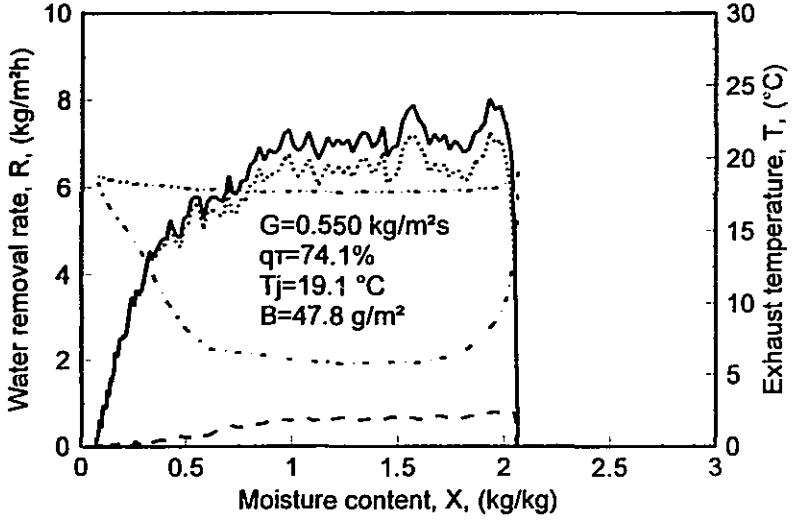
G=0.550 kg/m²s
qT=74.1%
Tj=19.1 °C
B=47.8 g/m²
Water removal rate, R, (kg/m²h)
Exhaust temperature, T, (°C)
Moisture content, X, (kg/kg)

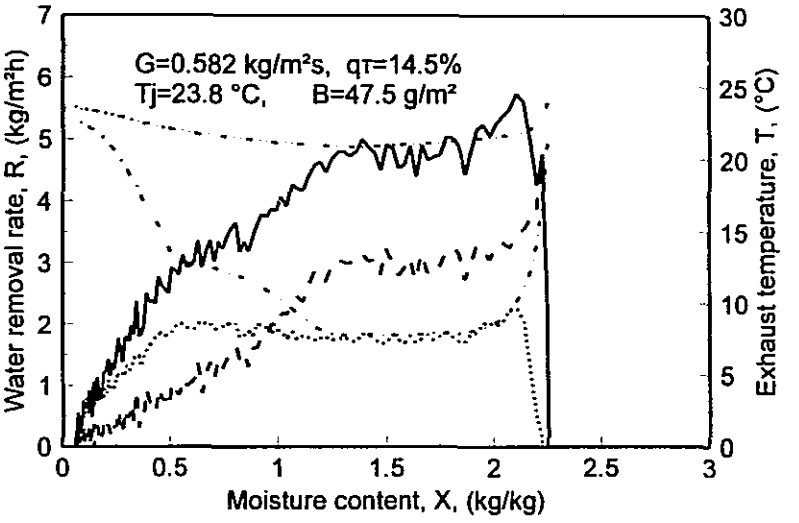
G=0.582 kg/m²s, qT=14.5%
Tj=23.8 °C, B=47.5 g/m²
Water removal rate, R, (kg/m²h)
Exhaust temperature, T, (°C)
Moisture content, X, (kg/kg)

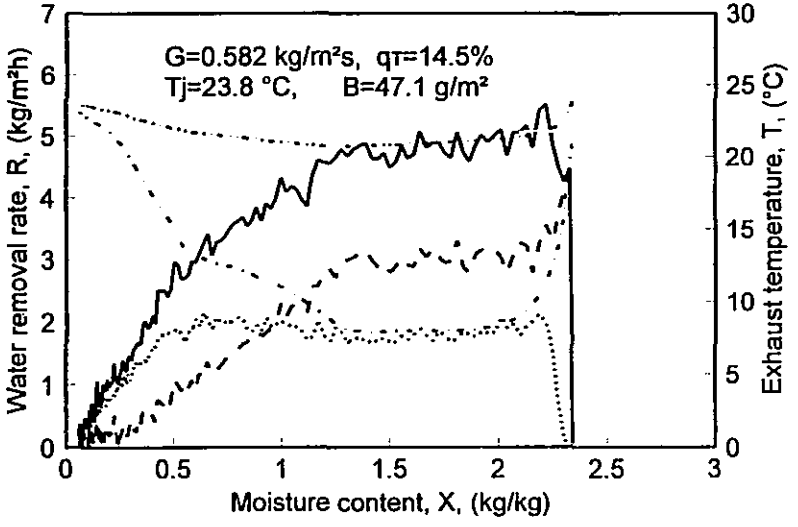
G=0.582 kg/m²s, qT=14.5%
Tj=23.8 °C, B=47.1 g/m²
Water removal rate, R, (kg/m²h)
Exhaust temperature, T, (°C)
Moisture content, X, (kg/kg)
R
RI
RT

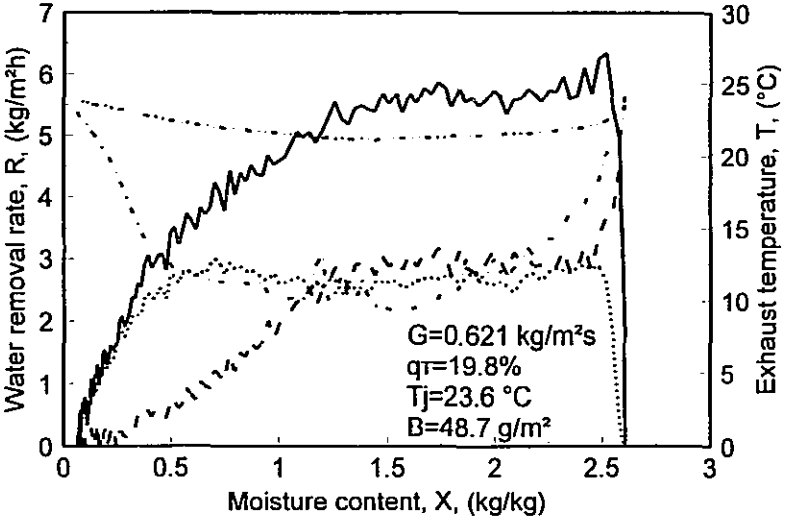
G=0.621 kg/m²s
qT=19.8%
Tj=23.6 °C
B=48.7 g/m²
Water removal rate, R, (kg/m²h)
Exhaust temperature, T, (°C)
Moisture content, X, (kg/kg)
TIe
TTe

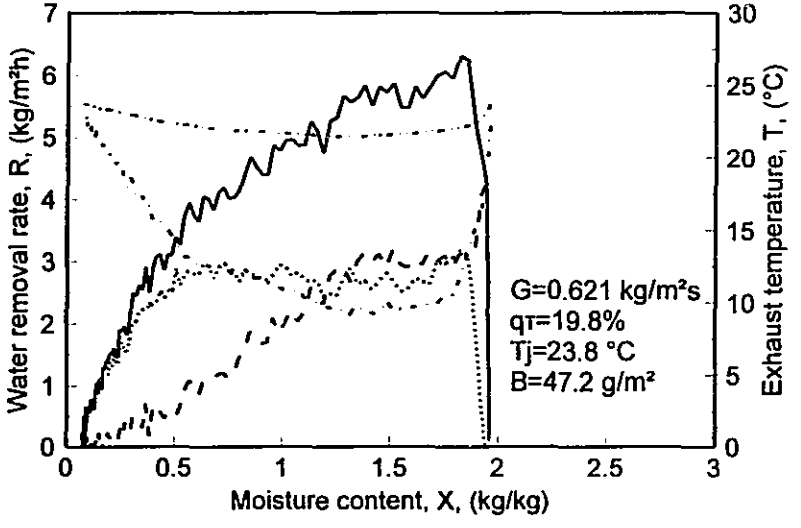
Water removal rate, R, (kg/m²h)
Exhaust temperature, T, (°C)
Moisture content, X, (kg/kg)
G=0.621 kg/m²s
qT=19.8%
Tj=23.8 °C
B=47.2 g/m²

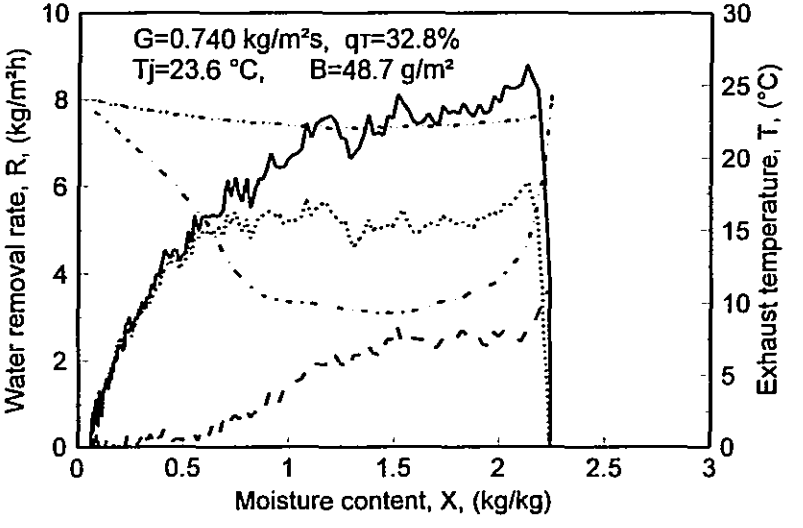
Water removal rate, R, (kg/m²h)
Exhaust temperature, T, (°C)
Moisture content, X, (kg/kg)
G=0.740 kg/m²s, qT=32.8%
Tj=23.6 °C, B=48.7 g/m²

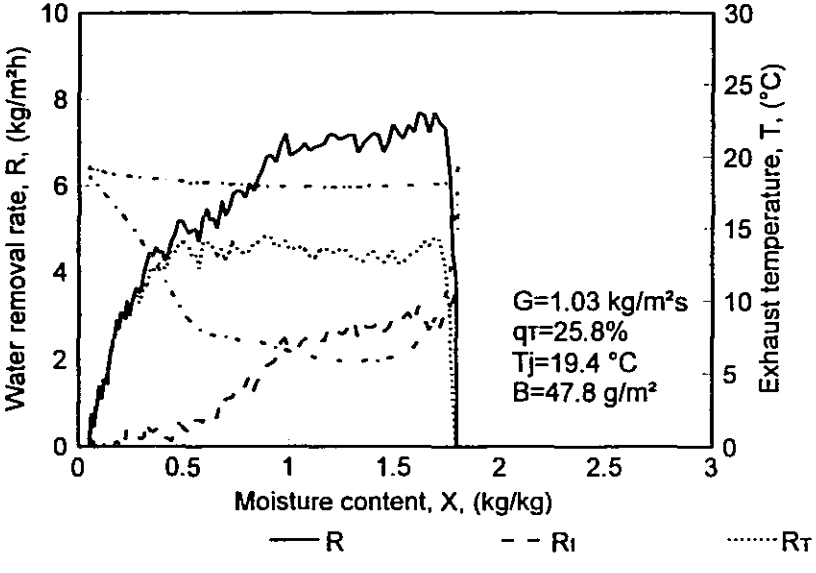
Water removal rate, R, (kg/m²h)
Exhaust temperature, T, (°C)
Moisture content, X, (kg/kg)
G=1.03 kg/m²s
qT=25.8%
Tj=19.4 °C
B=47.8 g/m²
R
RI
RT

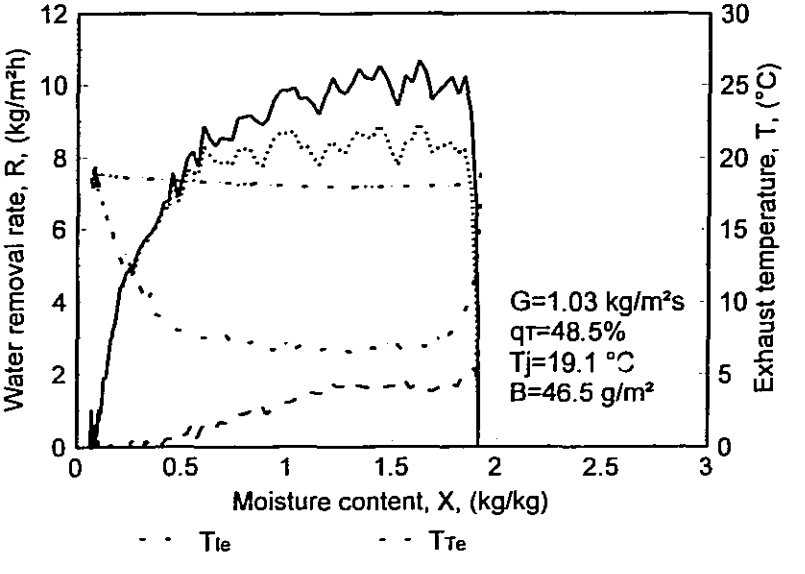
Water removal rate, R, (kg/m²h)
Exhaust temperature, T, (°C)
Moisture content, X, (kg/kg)
G=1.03 kg/m²s
qT=48.5%
Tj=19.1 °C
B=46.5 g/m²
TIe
TTe

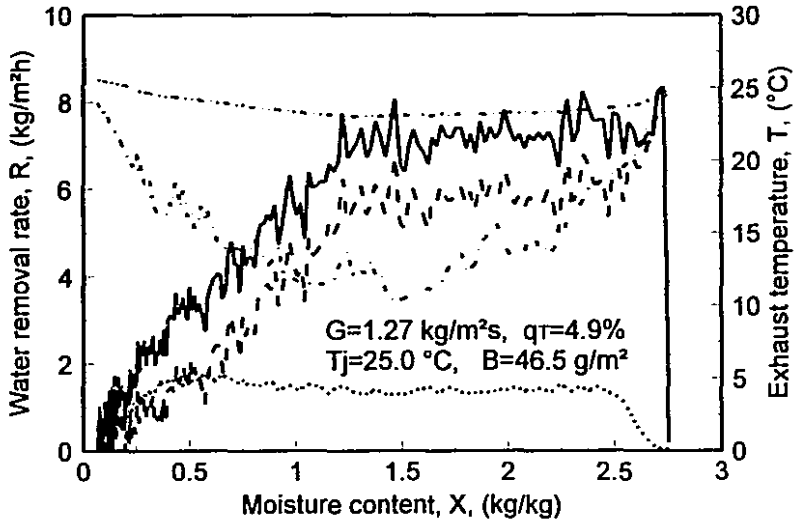
Water removal rate, R, (kg/m²h)
Exhaust temperature, T, (°C)
Moisture content, X, (kg/kg)
G=1.27 kg/m²s, qT=4.9%
Tj=25.0 °C, B=46.5 g/m²

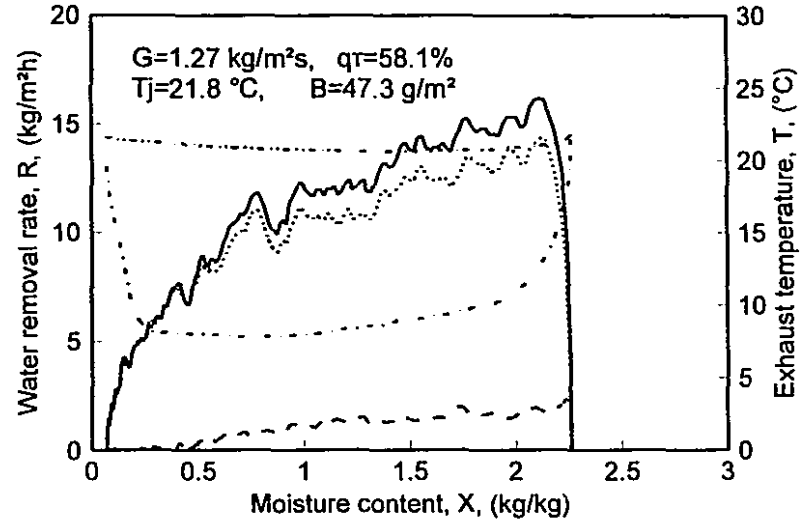
Water removal rate, R, (kg/m²h)
Exhaust temperature, T, (°C)
Moisture content, X, (kg/kg)
G=1.27 kg/m²s, qT=58.1%
Tj=21.8 °C, B=47.3 g/m²

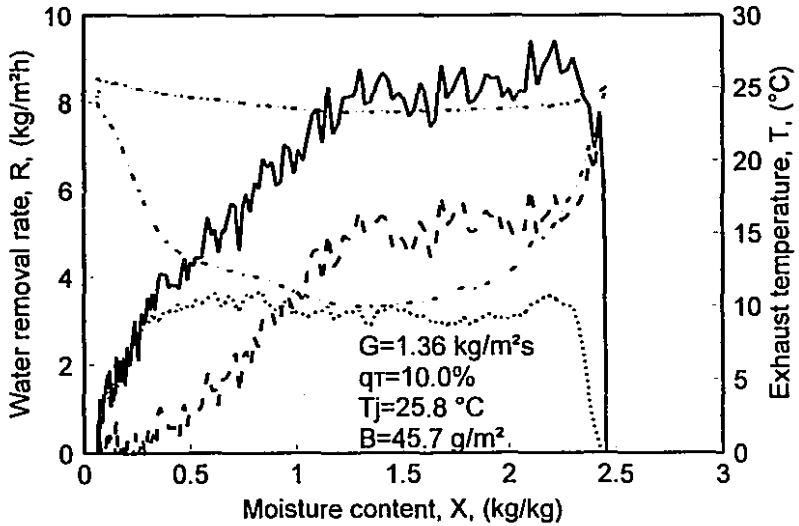
Water removal rate, R, (kg/m²h)
Exhaust temperature, T, (°C)
Moisture content, X, (kg/kg)
G=1.36 kg/m²s
qT=10.0%
Tj=25.8 °C
B=45.7 g/m²
R
RI
RT

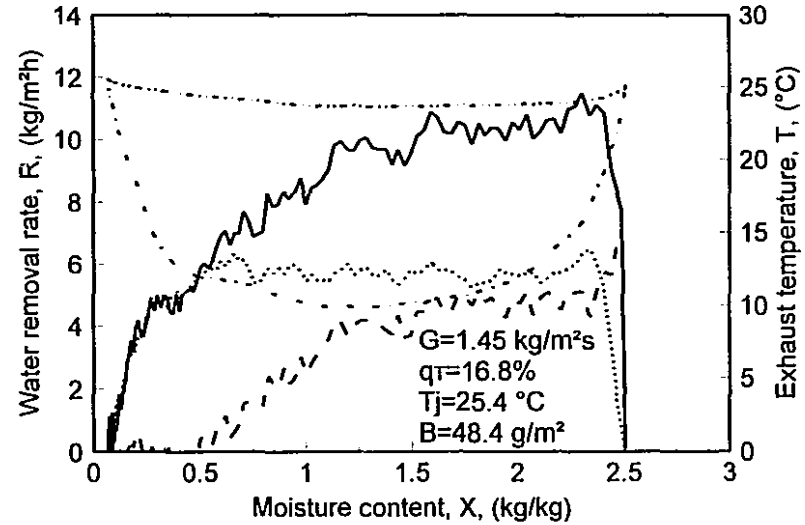
Water removal rate, R, (kg/m²h)
Exhaust temperature, T, (°C)
Moisture content, X, (kg/kg)
G=1.45 kg/m²s
qT=16.8%
Tj=25.4 °C
B=48.4 g/m²
TIe
TTe

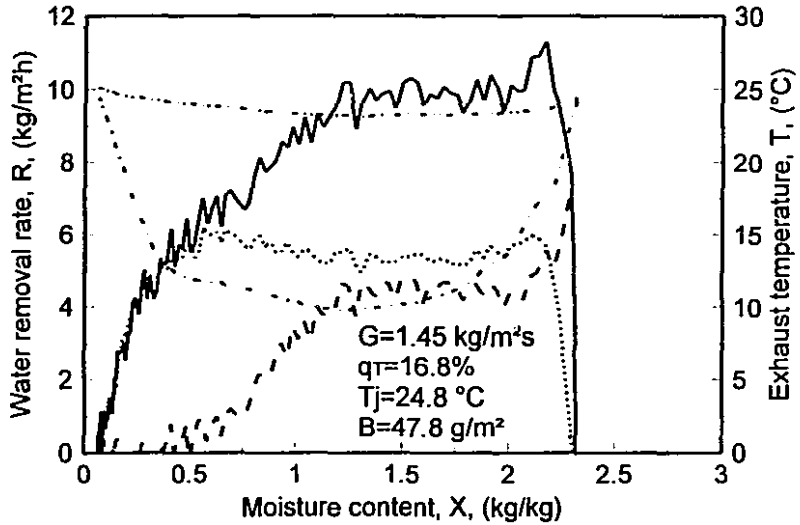
Water removal rate, R, (kg/m²h)
Exhaust temperature, T, (°C)
Moisture content, X, (kg/kg)
G=1.45 kg/m²s
qT=16.8%
Tj=24.8 °C
B=47.8 g/m²

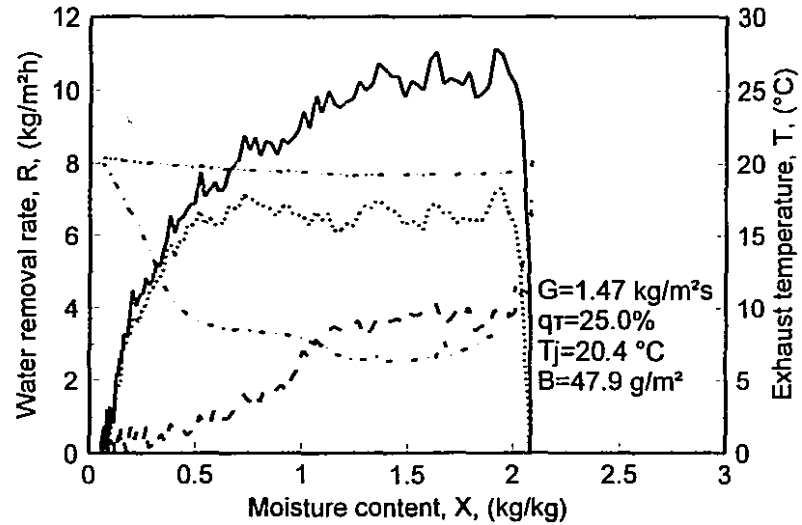
Water removal rate, R, (kg/m²h)
Exhaust temperature, T, (°C)
Moisture content, X, (kg/kg)
G=1.47 kg/m²s
qT=25.0%
Tj=20.4 °C
B=47.9 g/m²

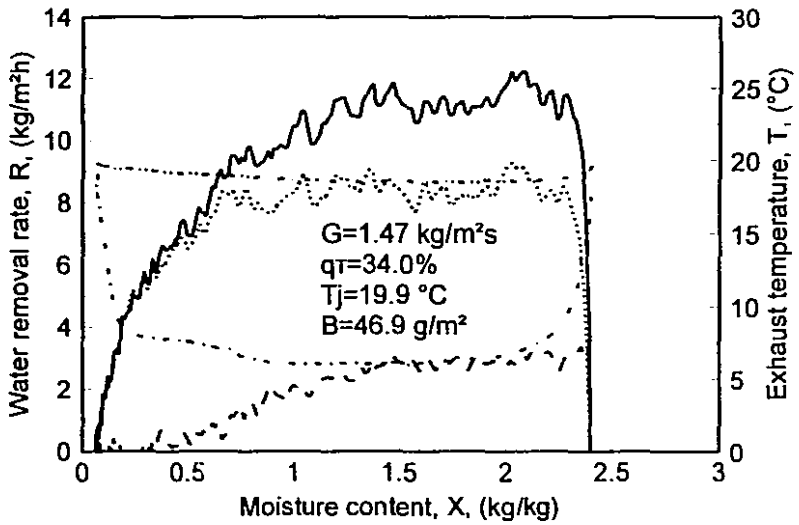
Water removal rate, R, (kg/m²h)
Exhaust temperature, T, (°C)
Moisture content, X, (kg/kg)
G=1.47 kg/m²s
qT=34.0%
Tj=19.9 °C
B=46.9 g/m²
R
RI
RT

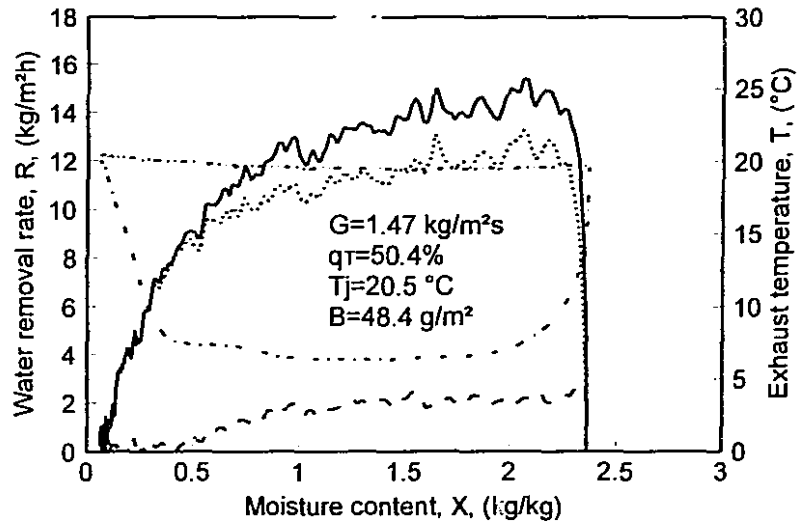
Water removal rate, R, (kg/m²h)
Exhaust temperature, T, (°C)
Moisture content, X, (kg/kg)
G=1.47 kg/m²s
qT=50.4%
Tj=20.5 °C
B=48.4 g/m²
TIe
TTe

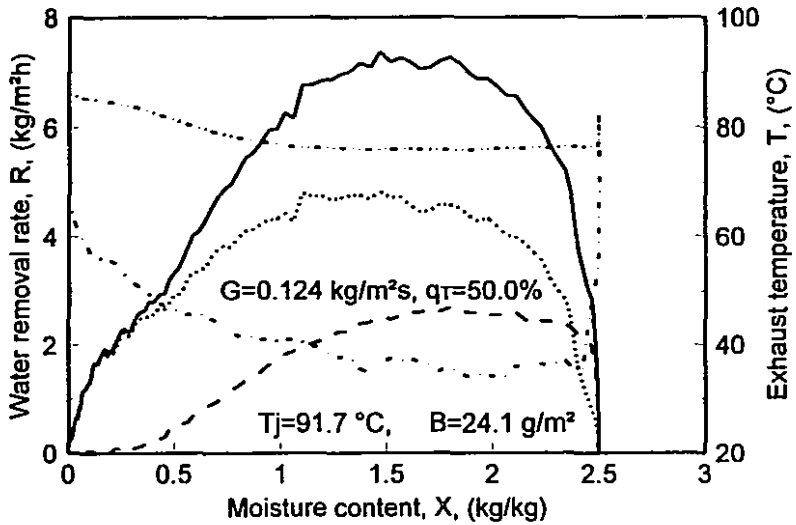
G=0.124 kg/m²s, qT=50.0%
Tj=91.7 °C, B=24.1 g/m²
Water removal rate, R, (kg/m²h)
Exhaust temperature, T, (°C)
Moisture content, X, (kg/kg)

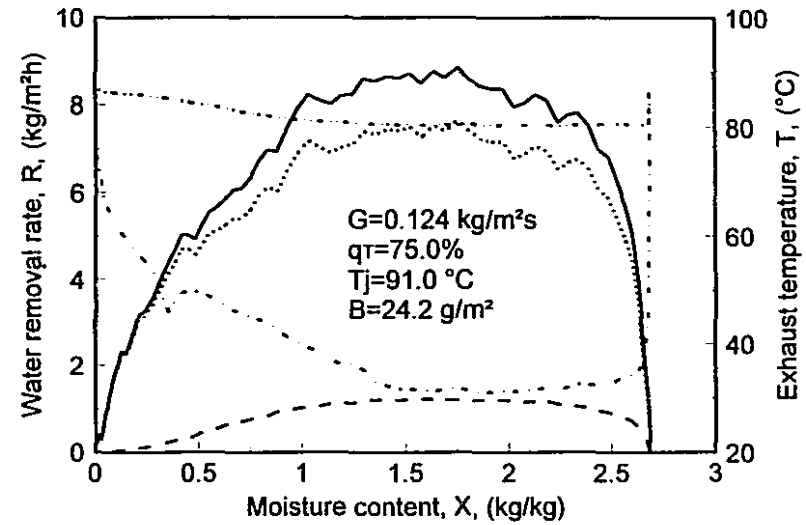
G=0.124 kg/m²s
qT=75.0%
Tj=91.0 °C
B=24.2 g/m²
Water removal rate, R, (kg/m²h)
Exhaust temperature, T, (°C)
Moisture content, X, (kg/kg)

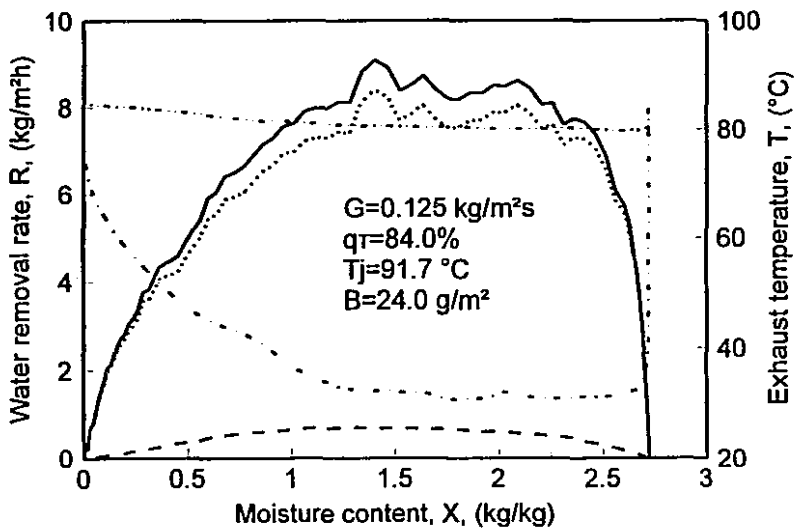
G=0.125 kg/m²s
qT=84.0%
Tj=91.7 °C
B=24.0 g/m²
Water removal rate, R, (kg/m²h)
Exhaust temperature, T, (°C)
Moisture content, X, (kg/kg)
R
RI
RT

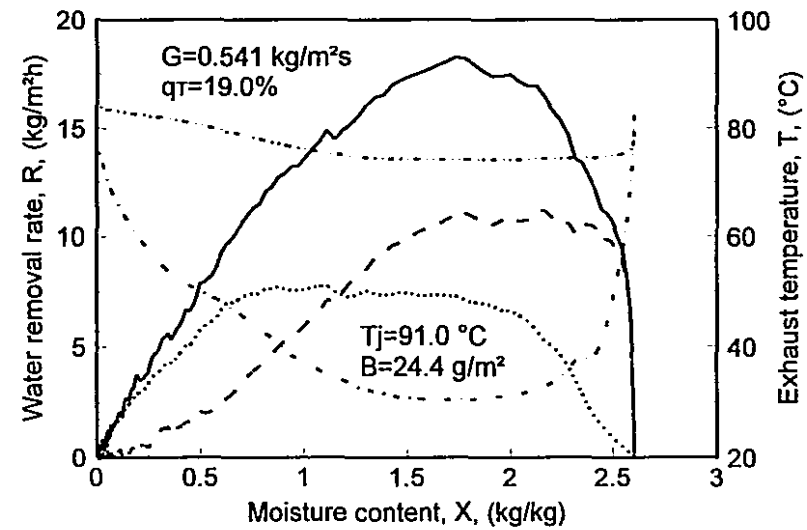
G=0.541 kg/m²s
qT=19.0%
Tj=91.0 °C
B=24.4 g/m²
Water removal rate, R, (kg/m²h)
Exhaust temperature, T, (°C)
Moisture content, X, (kg/kg)
TIe
TTe

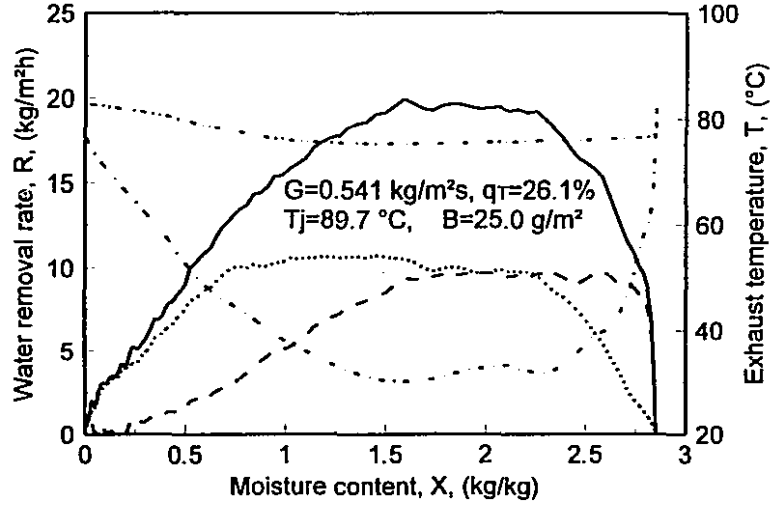
G=0.541 kg/m²s, qT=26.1%
Tj=89.7 °C, B=25.0 g/m²
Water removal rate, R, (kg/m²h)
Exhaust temperature, T, (°C)
Moisture content, X, (kg/kg)

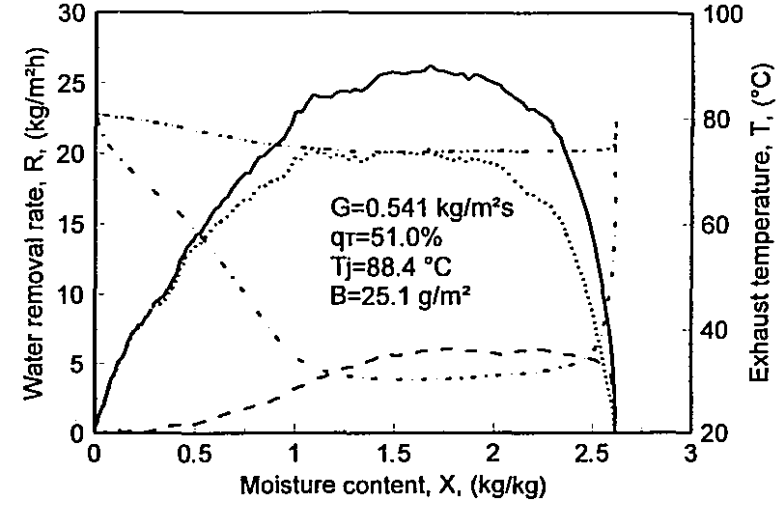
G=0.541 kg/m²s
qT=51.0%
Tj=88.4 °C
B=25.1 g/m²
Water removal rate, R, (kg/m²h)
Exhaust temperature, T, (°C)
Moisture content, X, (kg/kg)

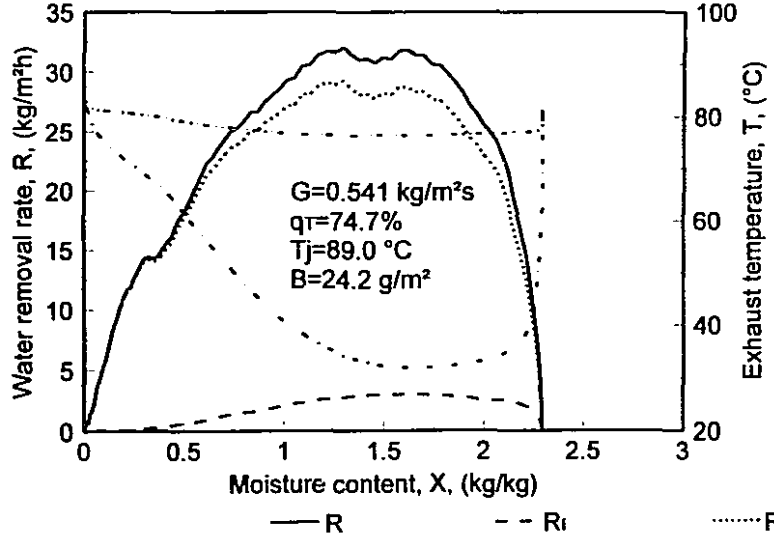
G=0.541 kg/m²s
qT=74.7%
Tj=89.0 °C
B=24.2 g/m²
Water removal rate, R, (kg/m²h)
Exhaust temperature, T, (°C)
Moisture content, X, (kg/kg)
R
RI
RT

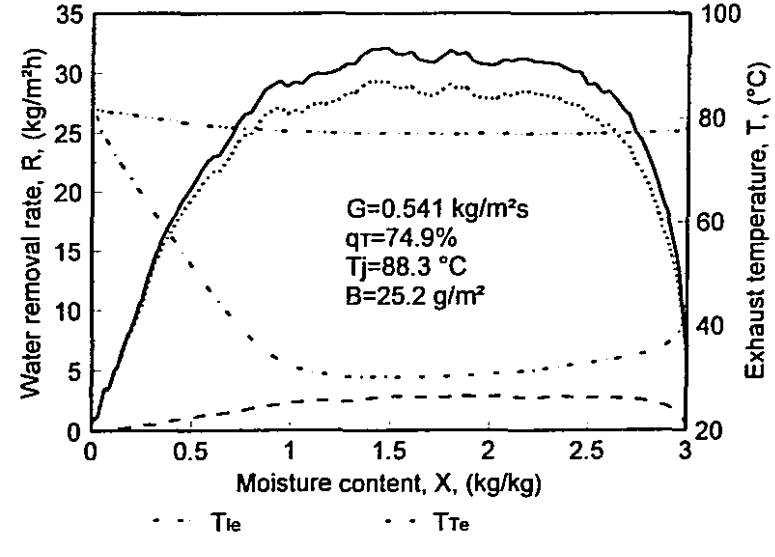
G=0.541 kg/m²s
qT=74.9%
Tj=88.3 °C
B=25.2 g/m²
Water removal rate, R, (kg/m²h)
Exhaust temperature, T, (°C)
Moisture content, X, (kg/kg)
TIe
TTe

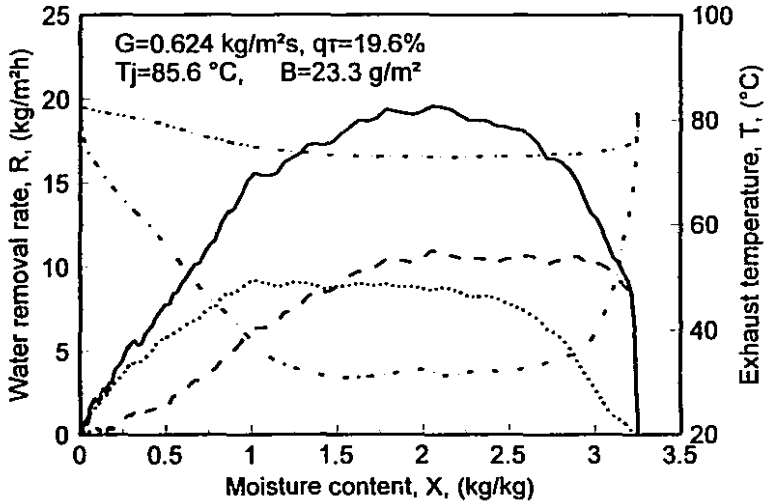
G=0.624 kg/m²s, qT=19.6%
Tj=85.6 °C, B=23.3 g/m²
Water removal rate, R, (kg/m²h)
Exhaust temperature, T, (°C)
Moisture content, X, (kg/kg)

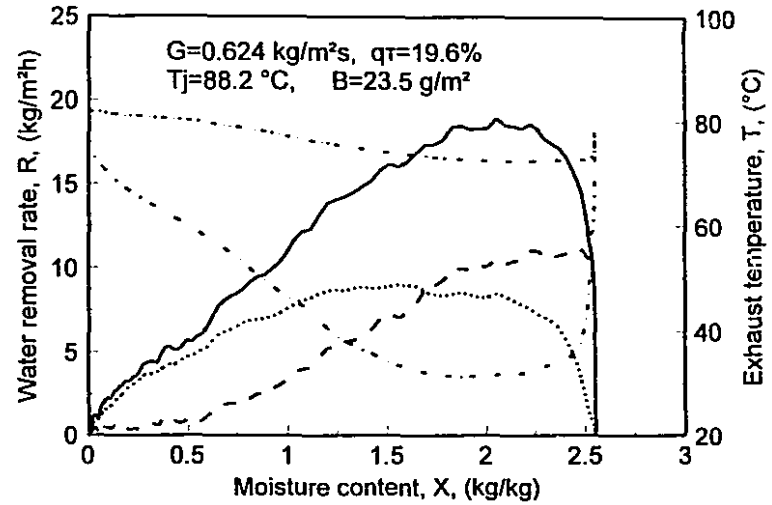
G=0.624 kg/m²s, qT=19.6%
Tj=88.2 °C, B=23.5 g/m²
Water removal rate, R, (kg/m²h)
Exhaust temperature, T, (°C)
Moisture content, X, (kg/kg)

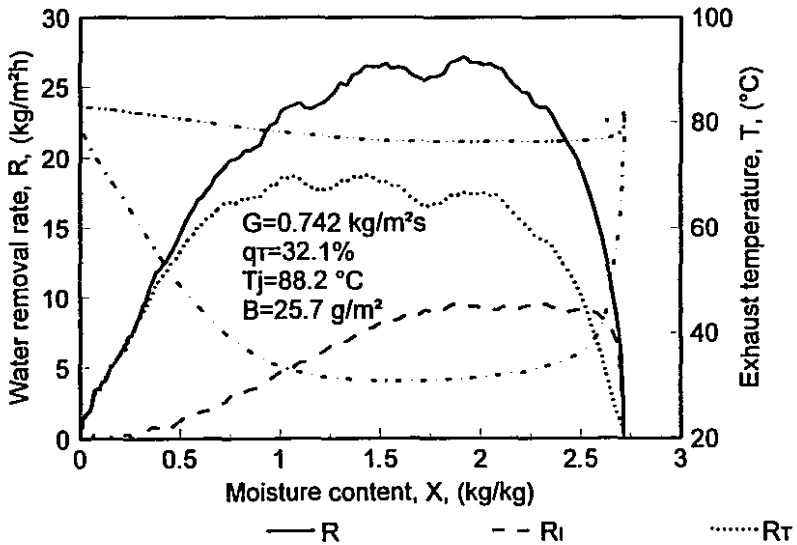
G=0.742 kg/m²s
qT=32.1%
Tj=88.2 °C
B=25.7 g/m²
Water removal rate, R, (kg/m²h)
Exhaust temperature, T, (°C)
Moisture content, X, (kg/kg)
R
RI
RT

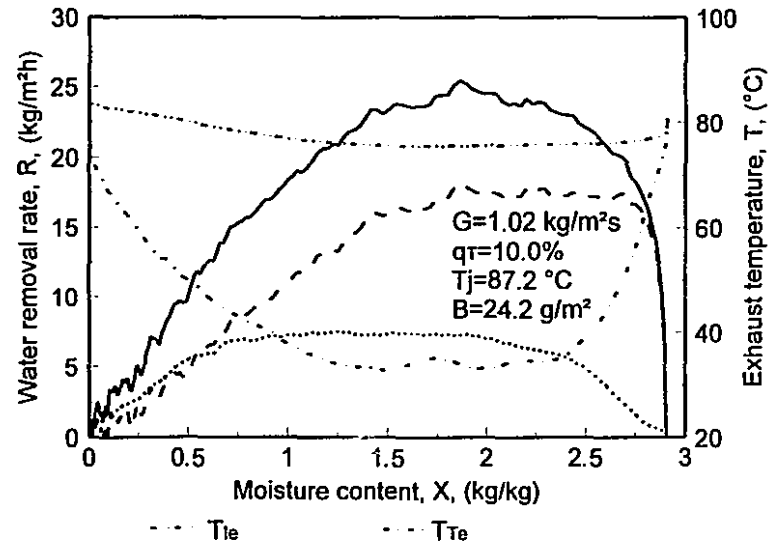
G=1.02 kg/m²s
qT=10.0%
Tj=87.2 °C
B=24.2 g/m²
Water removal rate, R, (kg/m²h)
Exhaust temperature, T, (°C)
Moisture content, X, (kg/kg)
TIe
TTe

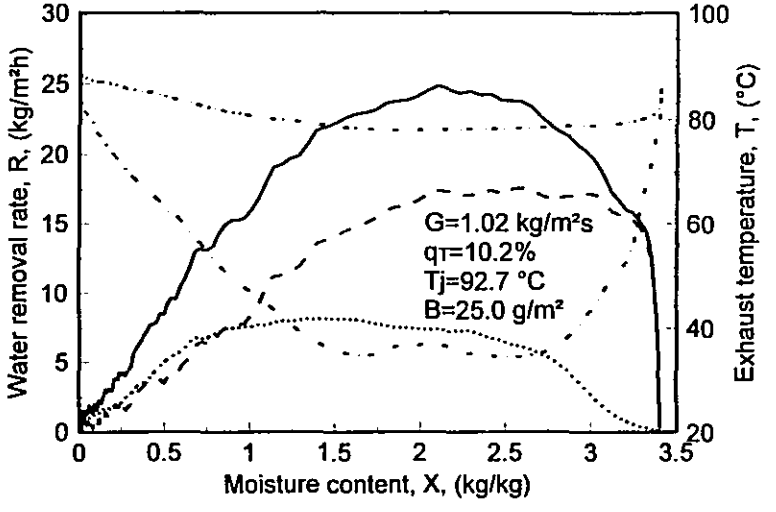
G=1.02 kg/m²s
qT=10.2%
Tj=92.7 °C
B=25.0 g/m²
Water removal rate, R, (kg/m²h)
Exhaust temperature, T, (°C)
Moisture content, X, (kg/kg)

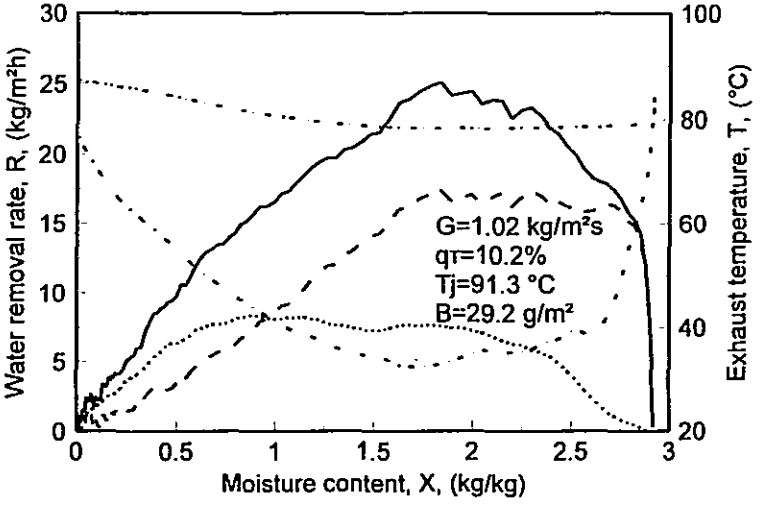
G=1.02 kg/m²s
qT=10.2%
Tj=91.3 °C
B=29.2 g/m²
Water removal rate, R, (kg/m²h)
Exhaust temperature, T, (°C)
Moisture content, X, (kg/kg)

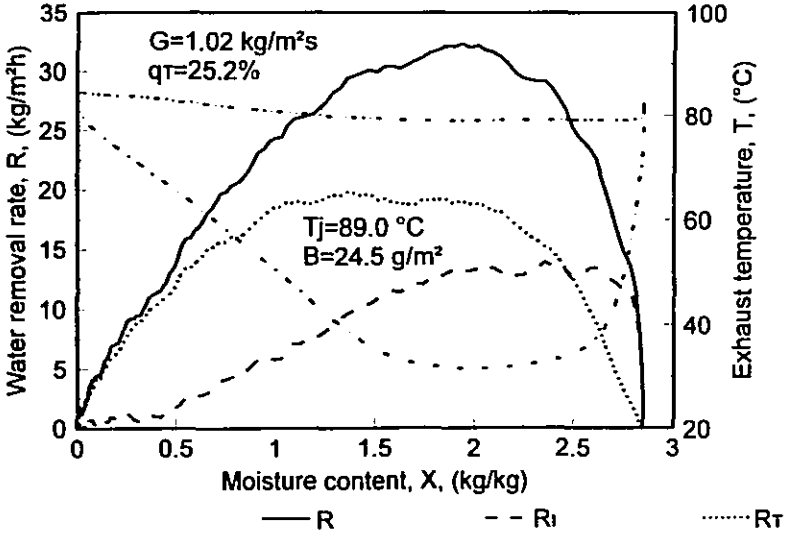
G=1.02 kg/m²s
qT=25.2%
Tj=89.0 °C
B=24.5 g/m²
Water removal rate, R, (kg/m²h)
Exhaust temperature, T, (°C)
Moisture content, X, (kg/kg)
R
RI
RT

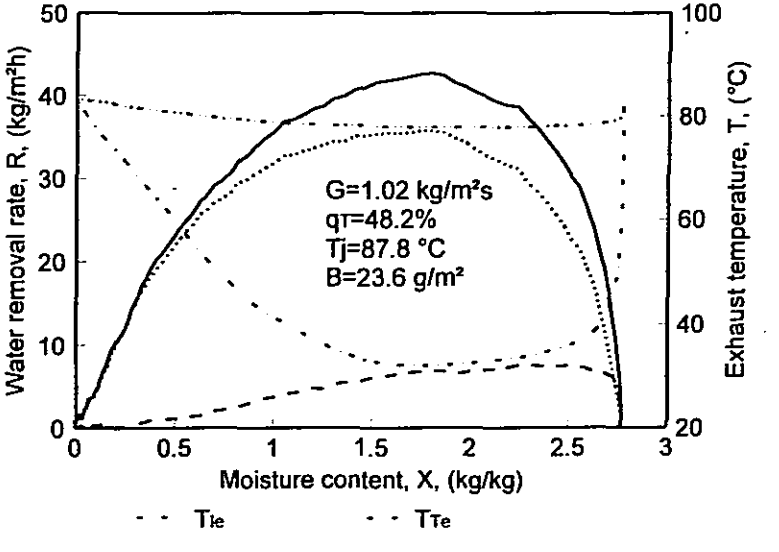
G=1.02 kg/m²s
qT=48.2%
Tj=87.8 °C
B=23.6 g/m²
Water removal rate, R, (kg/m²h)
Exhaust temperature, T, (°C)
Moisture content, X, (kg/kg)
TIe
TTe

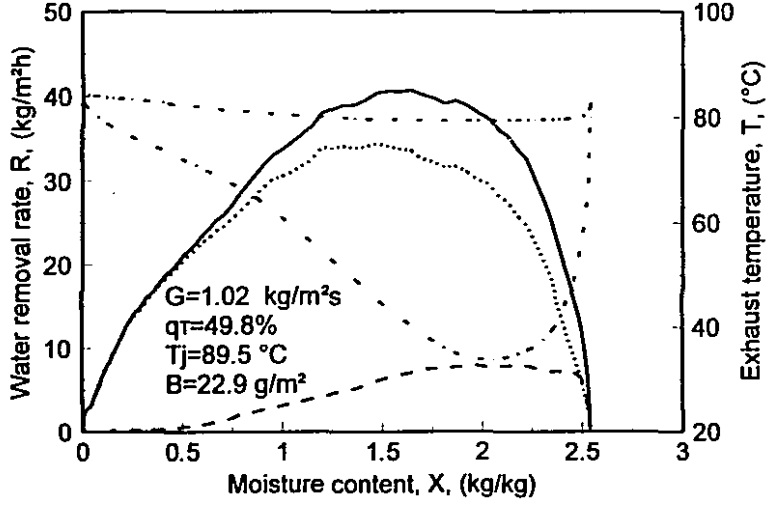
G=1.02 kg/m²s
qT=49.8%
Tj=89.5 °C
B=22.9 g/m²
Water removal rate, R, (kg/m²h)
Exhaust temperature, T, (°C)
Moisture content, X, (kg/kg)

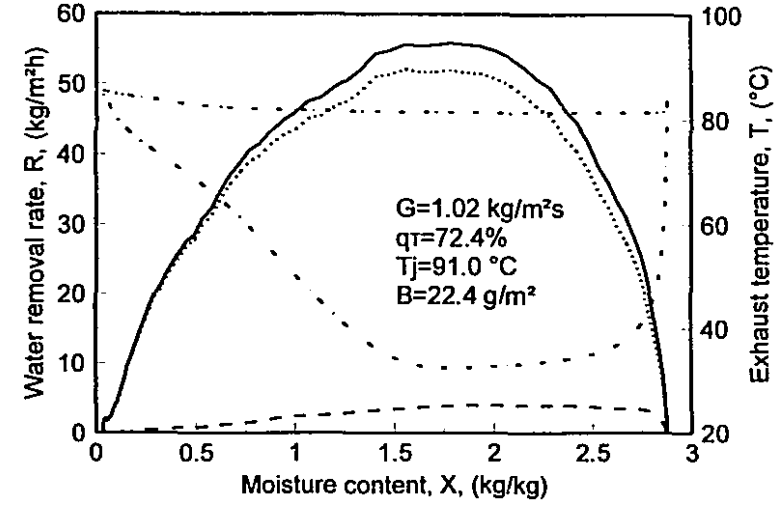
G=1.02 kg/m²s
qT=72.4%
Tj=91.0 °C
B=22.4 g/m²
Water removal rate, R, (kg/m²h)
Exhaust temperature, T, (°C)
Moisture content, X, (kg/kg)

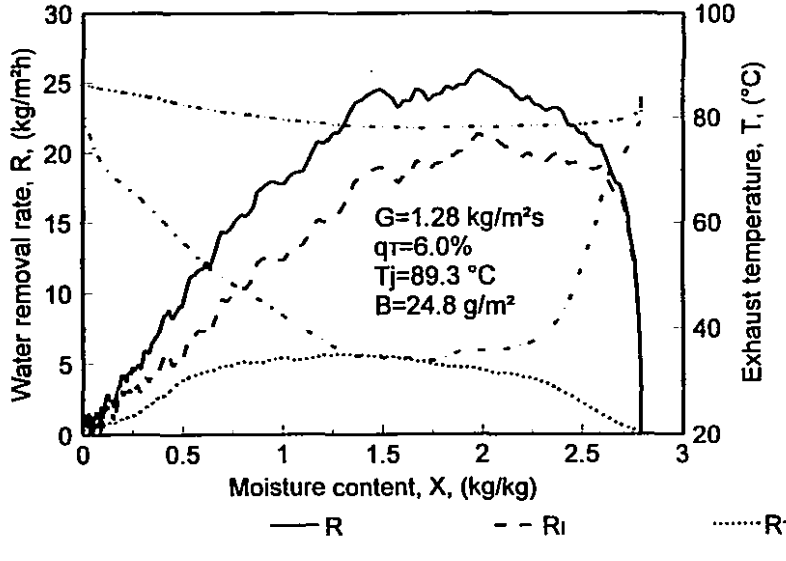
G=1.28 kg/m²s
qT=6.0%
Tj=89.3 °C
B=24.8 g/m²
Water removal rate, R, (kg/m²h)
Exhaust temperature, T, (°C)
Moisture content, X, (kg/kg)
R
RI
RT

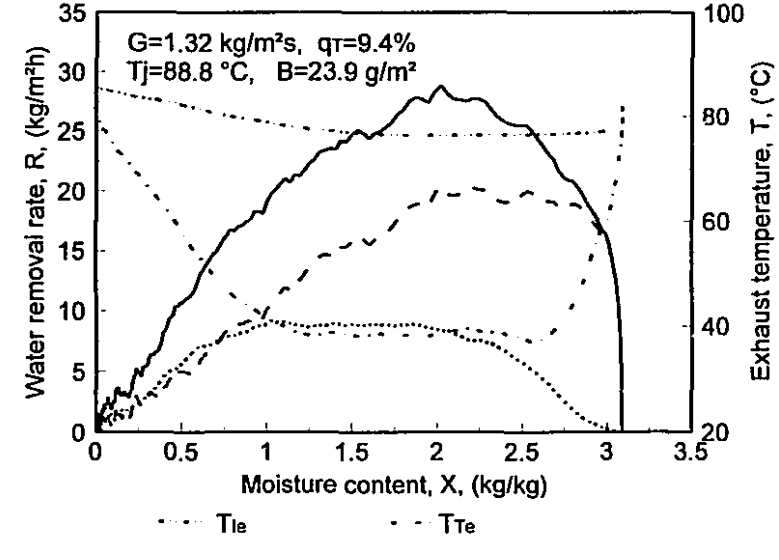
G=1.32 kg/m²s, qT=9.4%
Tj=88.8 °C, B=23.9 g/m²
Water removal rate, R, (kg/m²h)
Exhaust temperature, T, (°C)
Moisture content, X, (kg/kg)
TIe
TTe

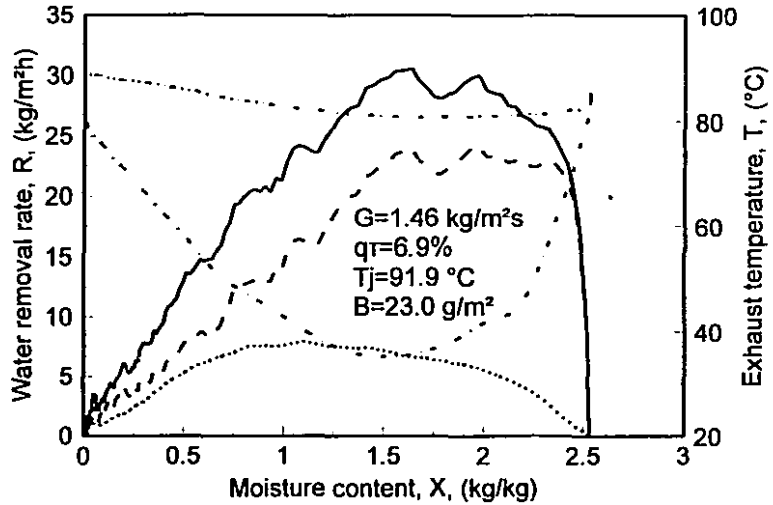
Water removal rate, R, (kg/m²h)
Exhaust temperature, T, (°C)
Moisture content, X, (kg/kg)
G=1.46 kg/m²s
qT=6.9%
Tj=91.9 °C
B=23.0 g/m²

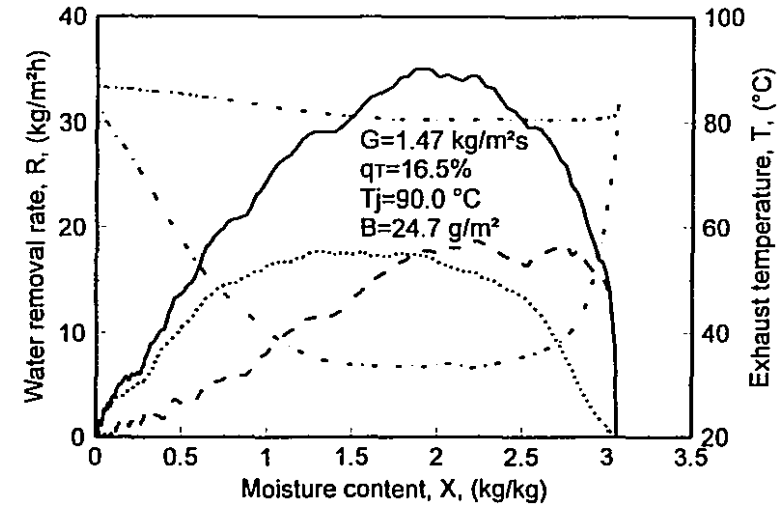
Water removal rate, R, (kg/m²h)
Exhaust temperature, T, (°C)
Moisture content, X, (kg/kg)
G=1.47 kg/m²s
qT=16.5%
Tj=90.0 °C
B=24.7 g/m²

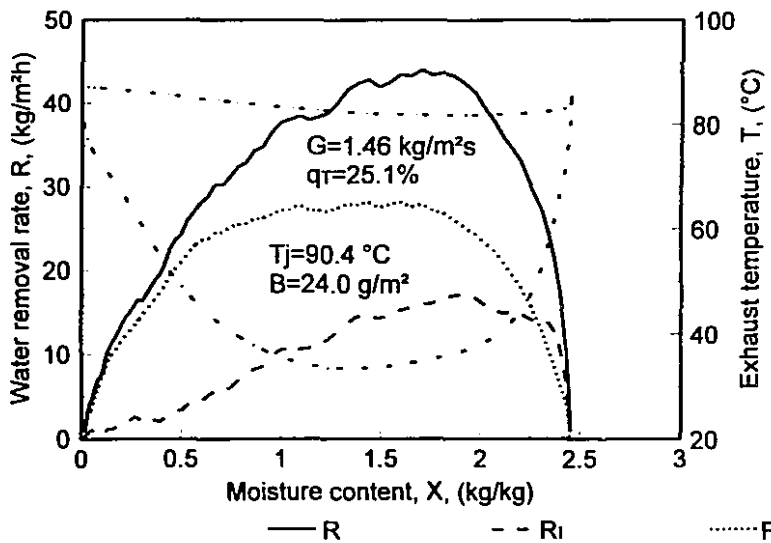
Water removal rate, R, (kg/m²h)
Exhaust temperature, T, (°C)
Moisture content, X, (kg/kg)
G=1.46 kg/m²s
qT=25.1%
Tj=90.4 °C
B=24.0 g/m²
R
RI
RT

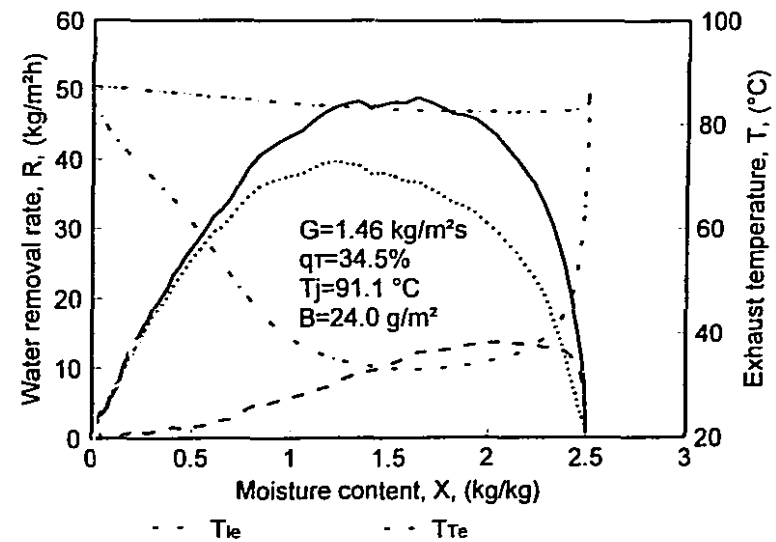
Water removal rate, R, (kg/m²h)
Exhaust temperature, T, (°C)
Moisture content, X, (kg/kg)
G=1.46 kg/m²s
qT=34.5%
Tj=91.1 °C
B=24.0 g/m²
TIe
TTe

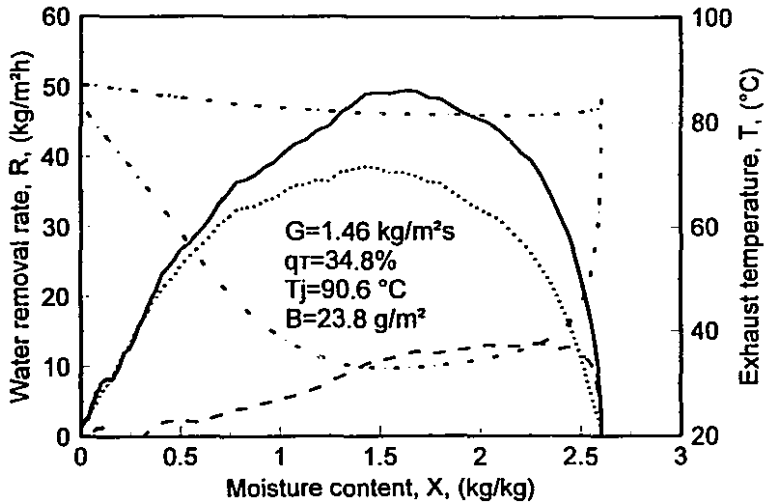
G=1.46 kg/m²s
qT=34.8%
Tj=90.6 °C
B=23.8 g/m²
Water removal rate, R, (kg/m²h)
Exhaust temperature, T, (°C)
Moisture content, X, (kg/kg)

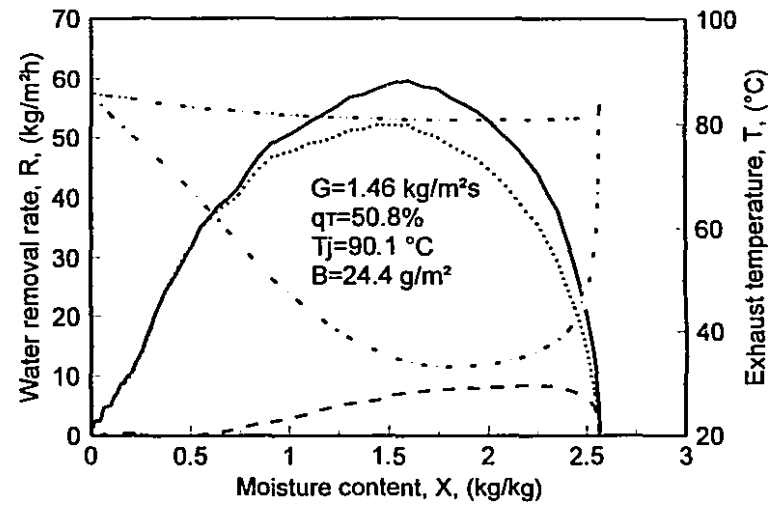
G=1.46 kg/m²s
qT=50.8%
Tj=90.1 °C
B=24.4 g/m²
Water removal rate, R, (kg/m²h)
Exhaust temperature, T, (°C)
Moisture content, X, (kg/kg)

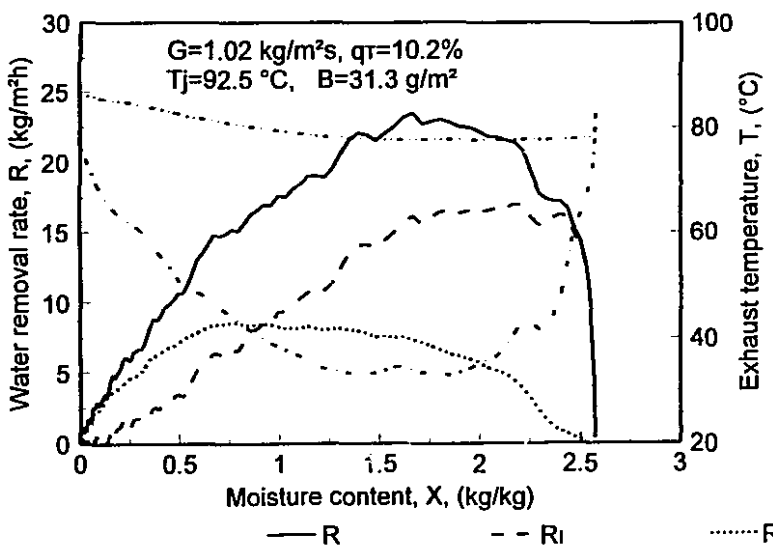
G=1.02 kg/m²s, qT=10.2%
Tj=92.5 °C, B=31.3 g/m²
Water removal rate, R, (kg/m²h)
Exhaust temperature, T, (°C)
Moisture content, X, (kg/kg)
R
RI
RT

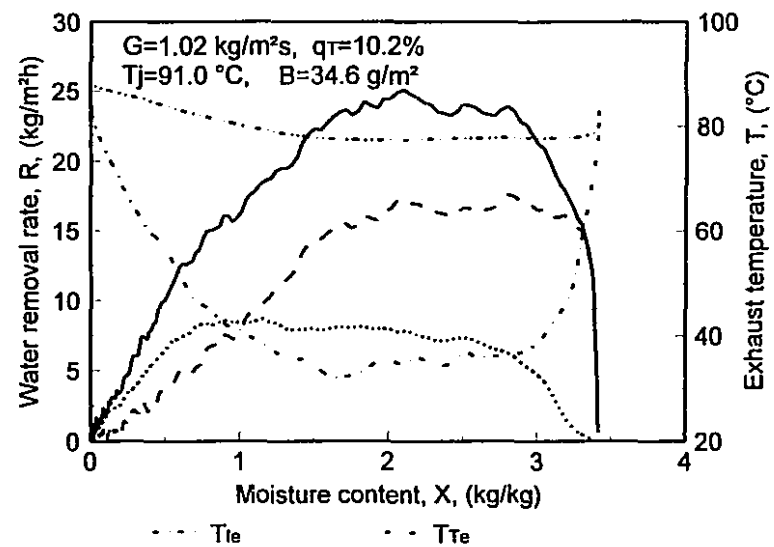
G=1.02 kg/m²s, qT=10.2%
Tj=91.0 °C, B=34.6 g/m²
Water removal rate, R, (kg/m²h)
Exhaust temperature, T, (°C)
Moisture content, X, (kg/kg)
TIe
TTe

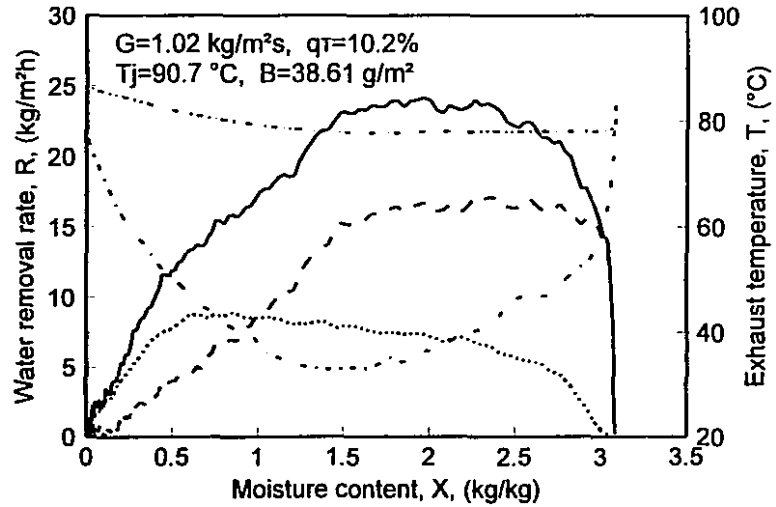
G=1.02 kg/m²s, qT=10.2%
Tj=90.7 °C, B=38.61 g/m²
Water removal rate, R, (kg/m²h)
Exhaust temperature, T, (°C)
Moisture content, X, (kg/kg)

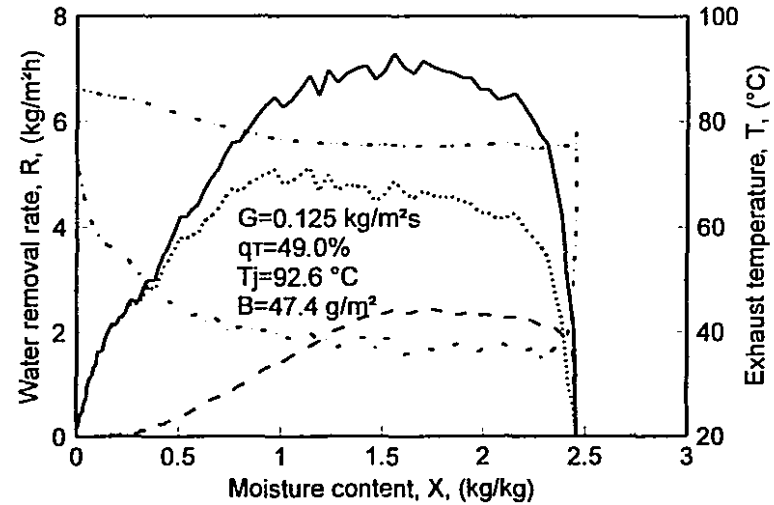
G=0.125 kg/m²s
qT=49.0%
Tj=92.6 °C
B=47.4 g/m²
Water removal rate, R, (kg/m²h)
Exhaust temperature, T, (°C)
Moisture content, X, (kg/kg)

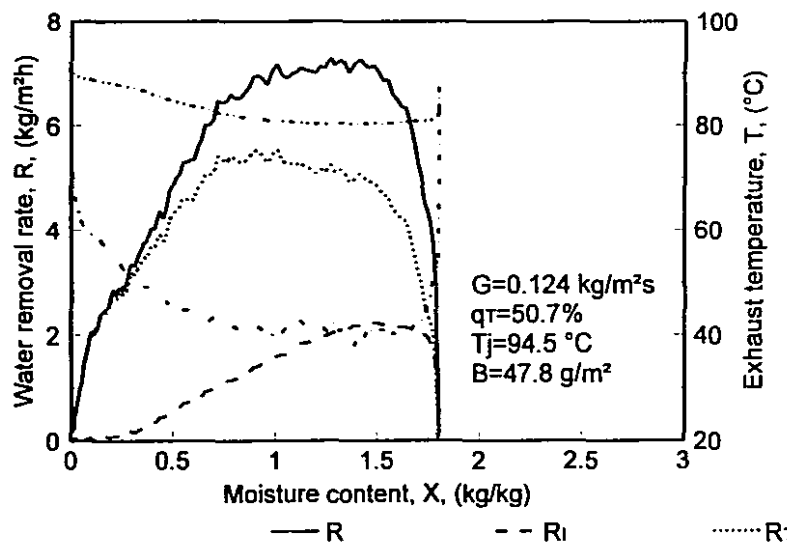
G=0.124 kg/m²s
qT=50.7%
Tj=94.5 °C
B=47.8 g/m²
Water removal rate, R, (kg/m²h)
Exhaust temperature, T, (°C)
Moisture content, X, (kg/kg)
R
RI
RT

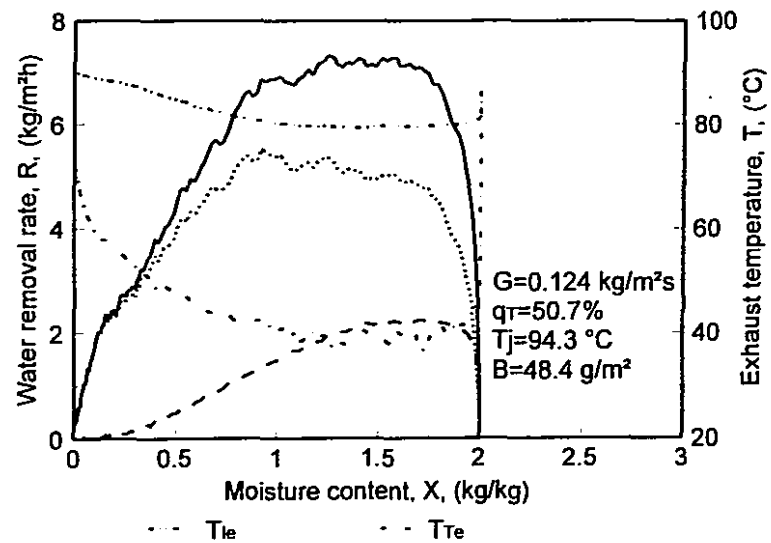
G=0.124 kg/m²s
qT=50.7%
Tj=94.3 °C
B=48.4 g/m²
Water removal rate, R, (kg/m²h)
Exhaust temperature, T, (°C)
Moisture content, X, (kg/kg)
TIe
TTe

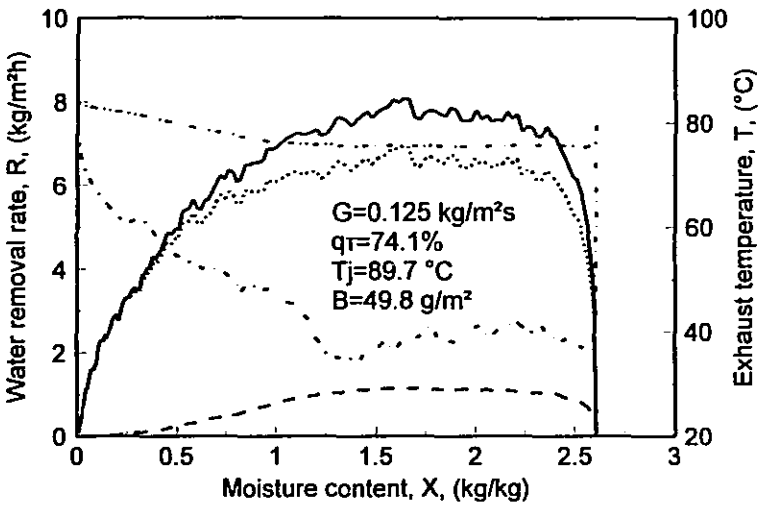
Water removal rate, R, (kg/m²h)
Exhaust temperature, T, (°C)
Moisture content, X, (kg/kg)
G=0.125 kg/m²s
qT=74.1%
Tj=89.7 °C
B=49.8 g/m²

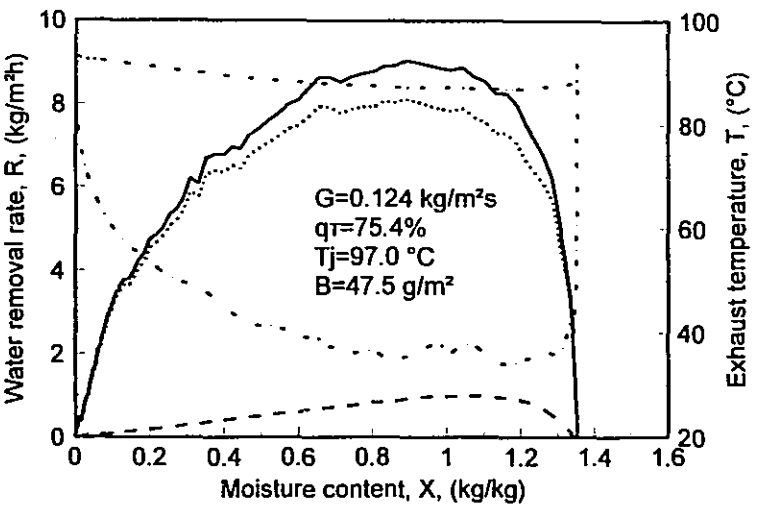
Water removal rate, R, (kg/m²h)
Exhaust temperature, T, (°C)
Moisture content, X, (kg/kg)
G=0.124 kg/m²s
qT=75.4%
Tj=97.0 °C
B=47.5 g/m²

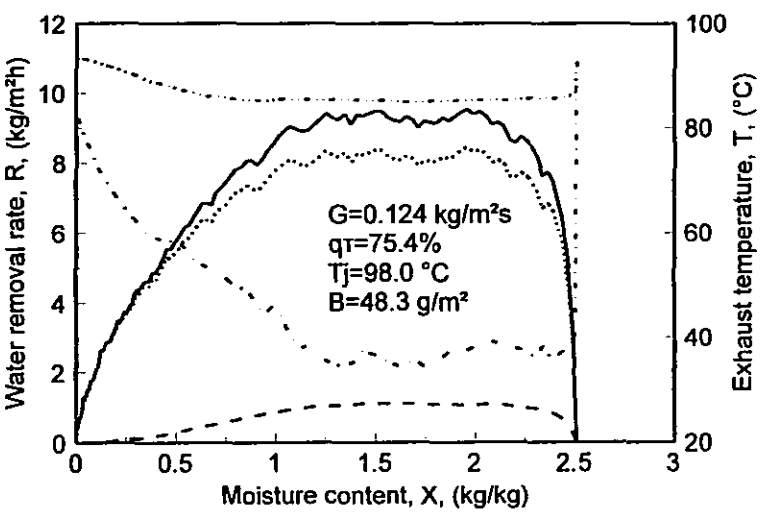
Water removal rate, R, (kg/m²h)
Exhaust temperature, T, (°C)
Moisture content, X, (kg/kg)
G=0.124 kg/m²s
qT=75.4%
Tj=98.0 °C
B=48.3 g/m²
R
RI
RT

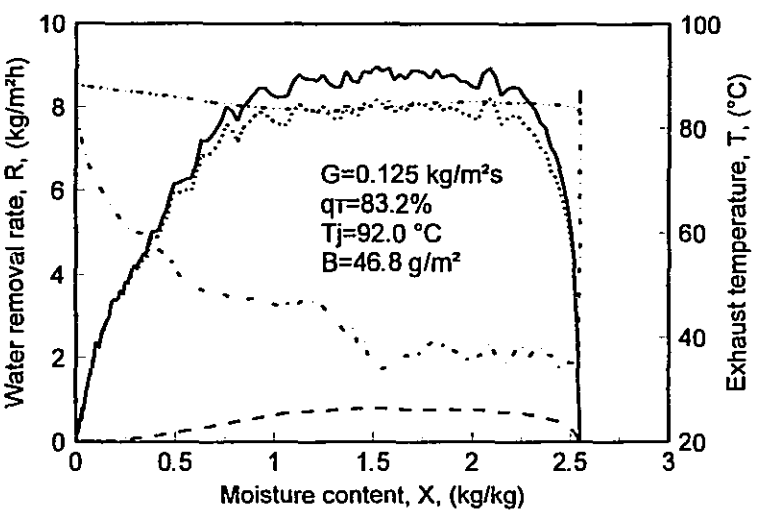
Water removal rate, R, (kg/m²h)
Exhaust temperature, T, (°C)
Moisture content, X, (kg/kg)
G=0.125 kg/m²s
qT=83.2%
Tj=92.0 °C
B=46.8 g/m²
TIe
TTe

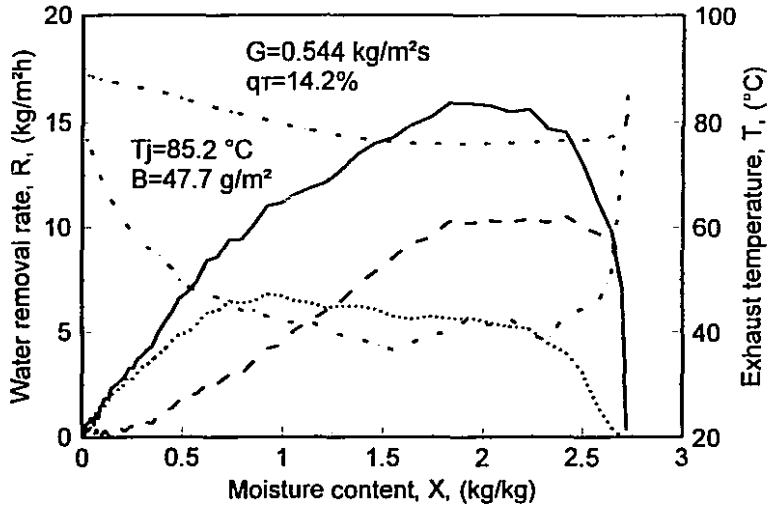
G=0.544 kg/m²s
qT=14.2%
Tj=85.2 °C
B=47.7 g/m²
Water removal rate, R, (kg/m²h)
Exhaust temperature, T, (°C)
Moisture content, X, (kg/kg)

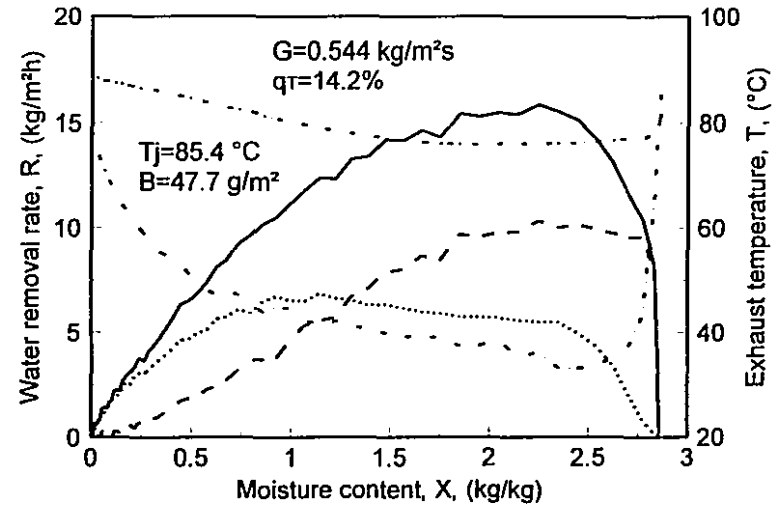
G=0.544 kg/m²s
qT=14.2%
Tj=85.4 °C
B=47.7 g/m²
Water removal rate, R, (kg/m²h)
Exhaust temperature, T, (°C)
Moisture content, X, (kg/kg)

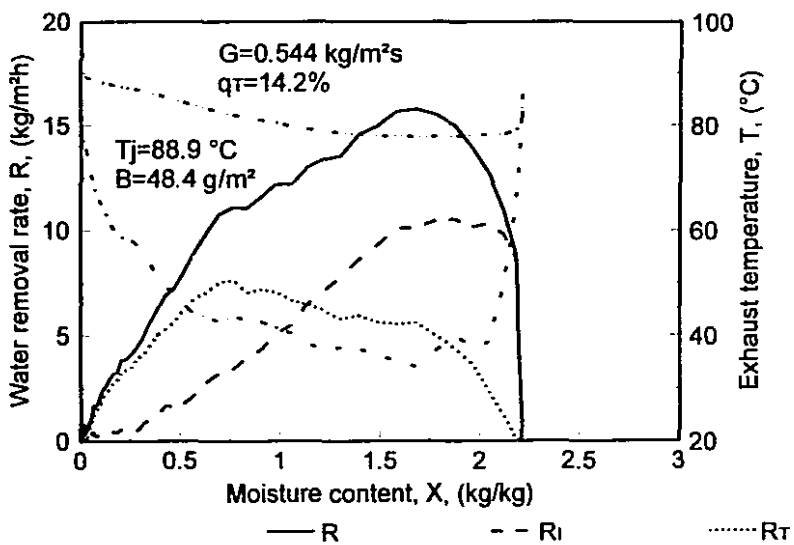
G=0.544 kg/m²s
qT=14.2%
Tj=88.9 °C
B=48.4 g/m²
Water removal rate, R, (kg/m²h)
Exhaust temperature, T, (°C)
Moisture content, X, (kg/kg)
R
RI
RT

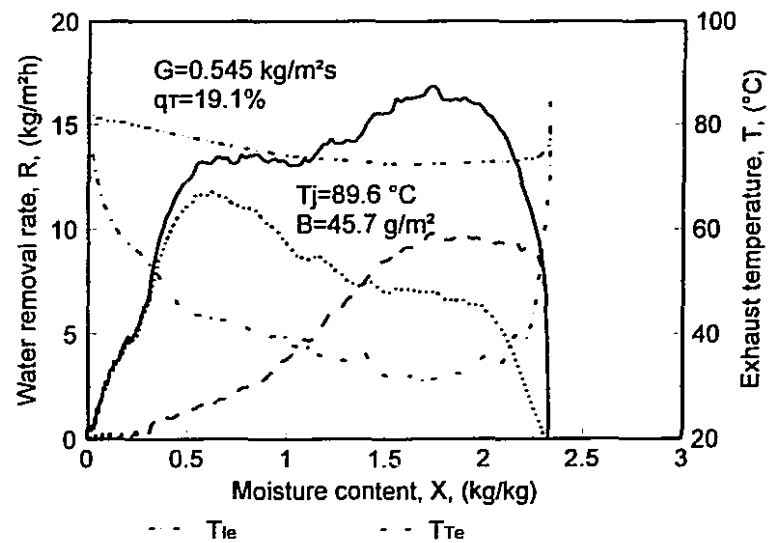
G=0.545 kg/m²s
qT=19.1%
Tj=89.6 °C
B=45.7 g/m²
Water removal rate, R, (kg/m²h)
Exhaust temperature, T, (°C)
Moisture content, X, (kg/kg)
TIe
TTe

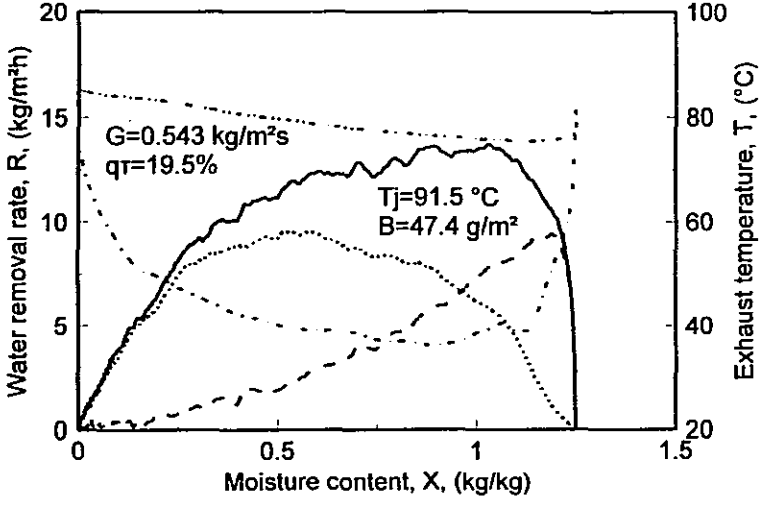
G=0.543 kg/m²s
qT=19.5%
Tj=91.5 °C
B=47.4 g/m²
Water removal rate, R, (kg/m²h)
Exhaust temperature, T, (°C)
Moisture content, X, (kg/kg)

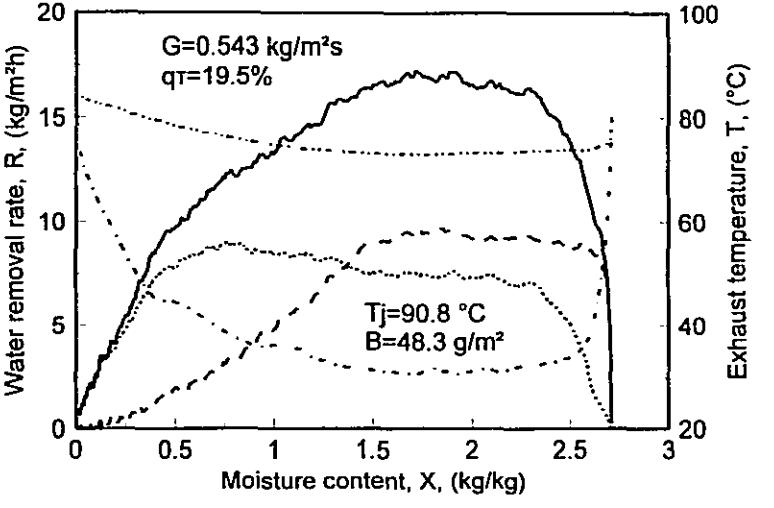
G=0.543 kg/m²s
qT=19.5%
Tj=90.8 °C
B=48.3 g/m²
Water removal rate, R, (kg/m²h)
Exhaust temperature, T, (°C)
Moisture content, X, (kg/kg)

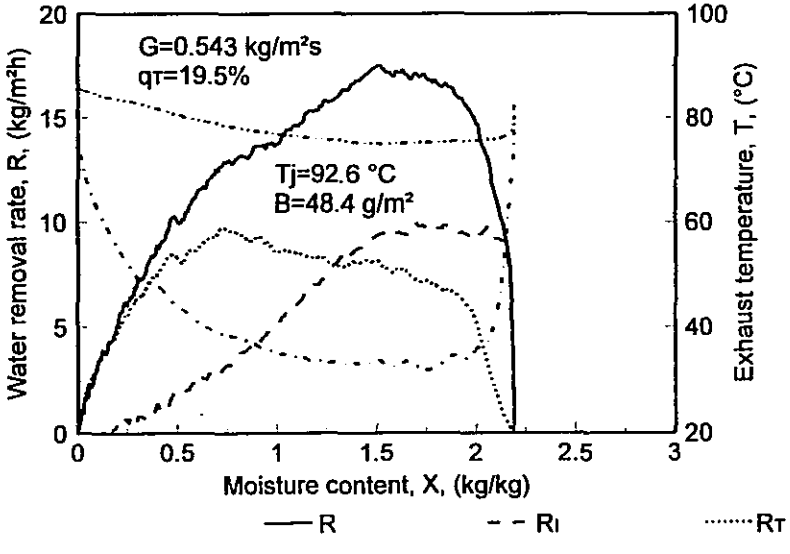
G=0.543 kg/m²s
qT=19.5%
Tj=92.6 °C
B=48.4 g/m²
Water removal rate, R, (kg/m²h)
Exhaust temperature, T, (°C)
Moisture content, X, (kg/kg)
R
RI
RT

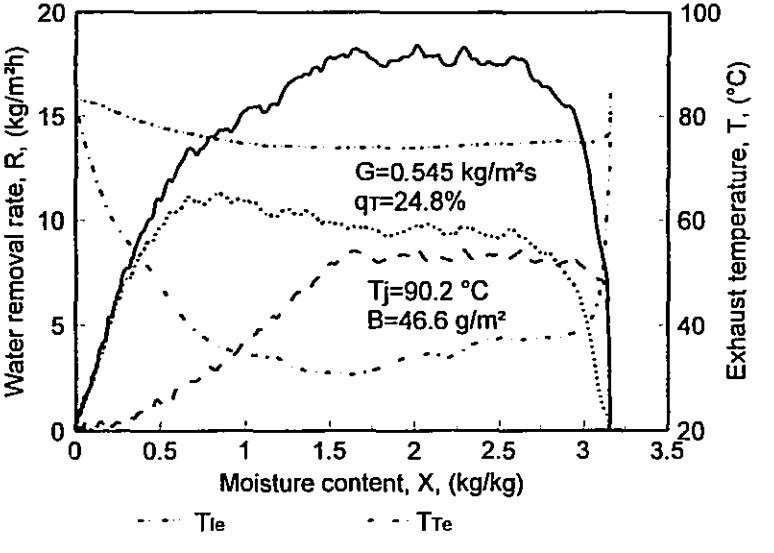
G=0.545 kg/m²s
qT=24.8%
Tj=90.2 °C
B=46.6 g/m²
Water removal rate, R, (kg/m²h)
Exhaust temperature, T, (°C)
Moisture content, X, (kg/kg)
TIe
TTe

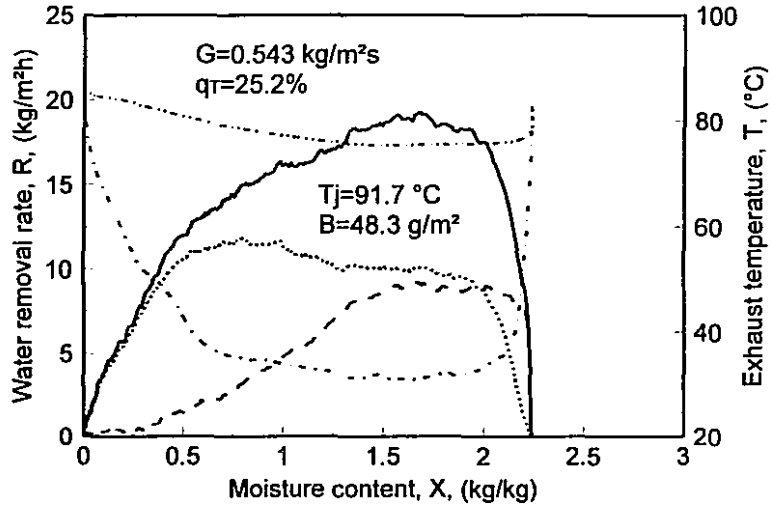
G=0.543 kg/m²s
qT=25.2%
Tj=91.7 °C
B=48.3 g/m²
Water removal rate, R, (kg/m²h)
Exhaust temperature, T, (°C)
Moisture content, X, (kg/kg)

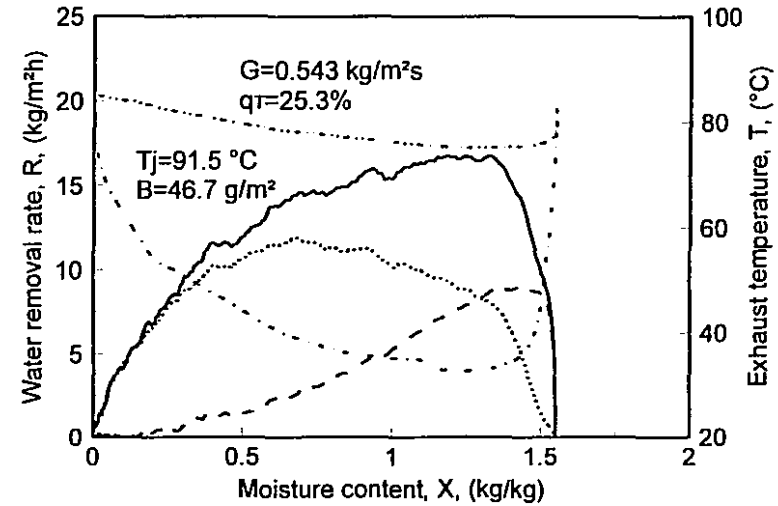
G=0.543 kg/m²s
qT=25.3%
Tj=91.5 °C
B=46.7 g/m²
Water removal rate, R, (kg/m²h)
Exhaust temperature, T, (°C)
Moisture content, X, (kg/kg)

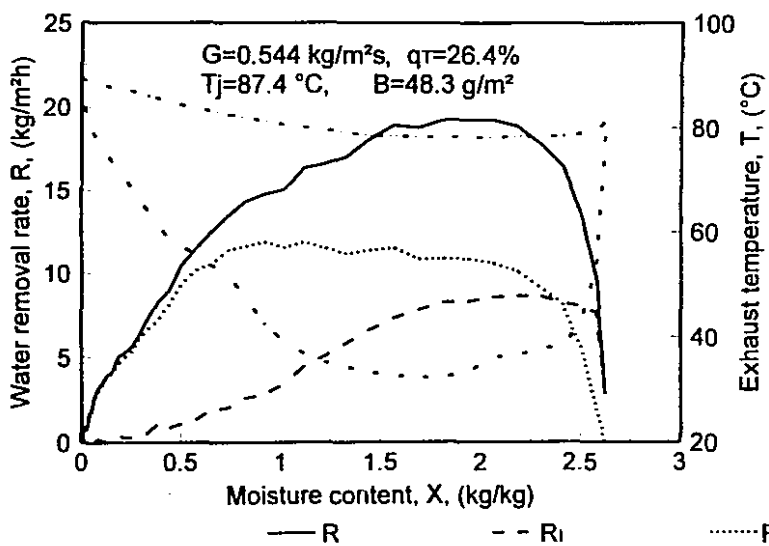
G=0.544 kg/m²s, qT=26.4%
Tj=87.4 °C, B=48.3 g/m²
Water removal rate, R, (kg/m²h)
Exhaust temperature, T, (°C)
Moisture content, X, (kg/kg)
R
RI
RT

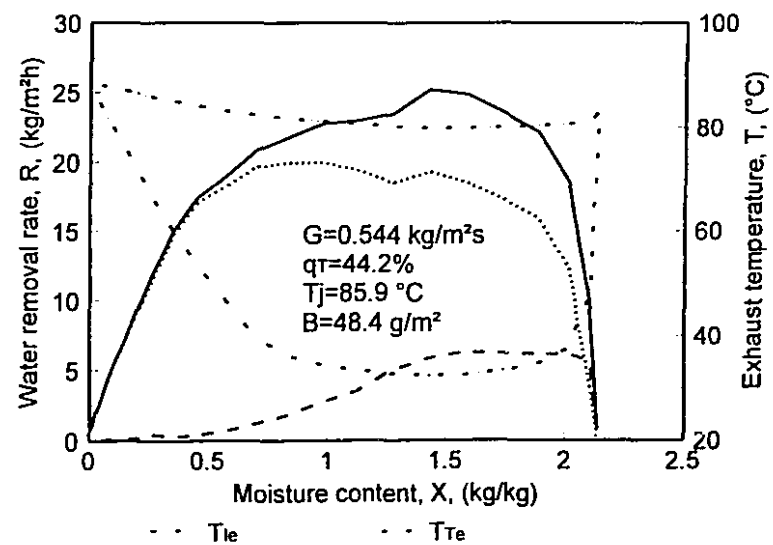
G=0.544 kg/m²s
qT=44.2%
Tj=85.9 °C
B=48.4 g/m²
Water removal rate, R, (kg/m²h)
Exhaust temperature, T, (°C)
Moisture content, X, (kg/kg)
TIe
TTe

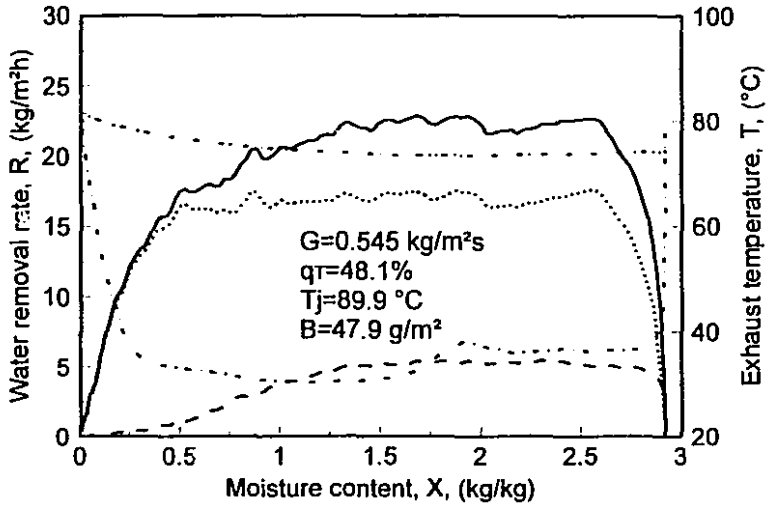
G=0.545 kg/m²s
qT=48.1%
Tj=89.9 °C
B=47.9 g/m²
Water removal rate, R, (kg/m²h)
Exhaust temperature, T, (°C)
Moisture content, X, (kg/kg)

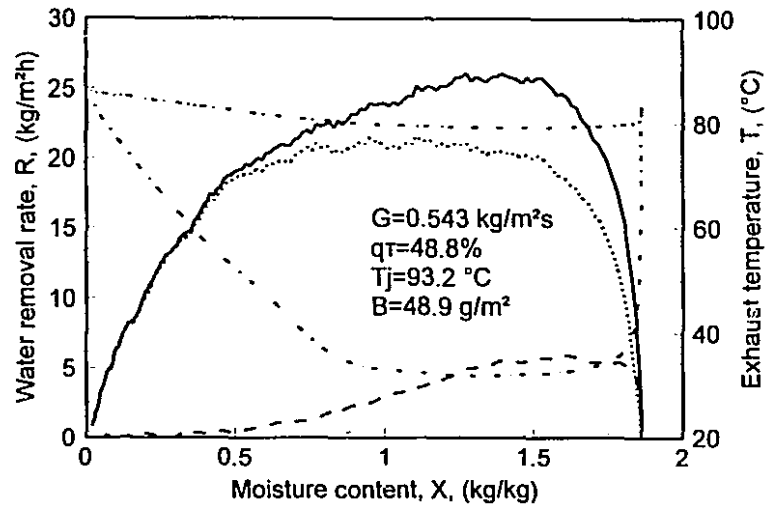
G=0.543 kg/m²s
qT=48.8%
Tj=93.2 °C
B=48.9 g/m²
Water removal rate, R, (kg/m²h)
Exhaust temperature, T, (°C)
Moisture content, X, (kg/kg)

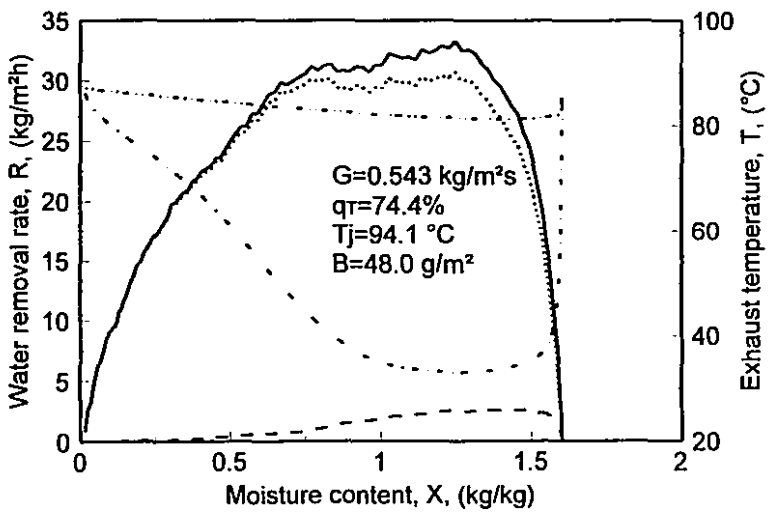
G=0.543 kg/m²s
qT=74.4%
Tj=94.1 °C
B=48.0 g/m²
Water removal rate, R, (kg/m²h)
Exhaust temperature, T, (°C)
Moisture content, X, (kg/kg)
R
RI
RT

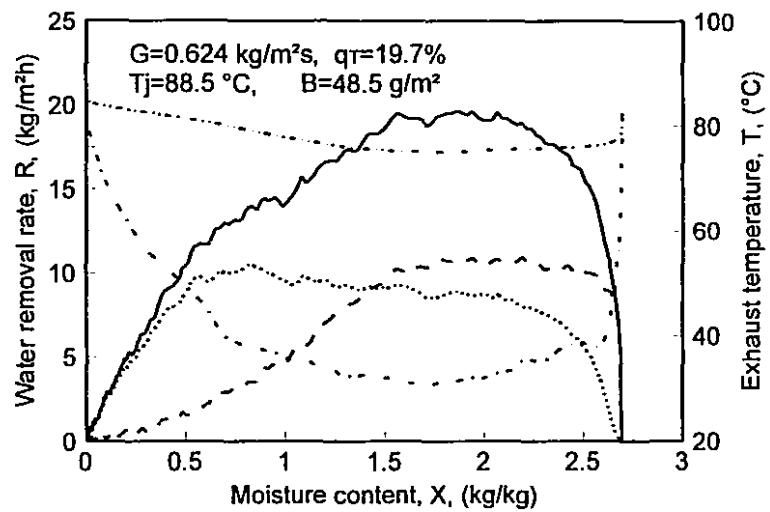
G=0.624 kg/m²s, qT=19.7%
Tj=88.5 °C, B=48.5 g/m²
Water removal rate, R, (kg/m²h)
Exhaust temperature, T, (°C)
Moisture content, X, (kg/kg)
TIe
TTe

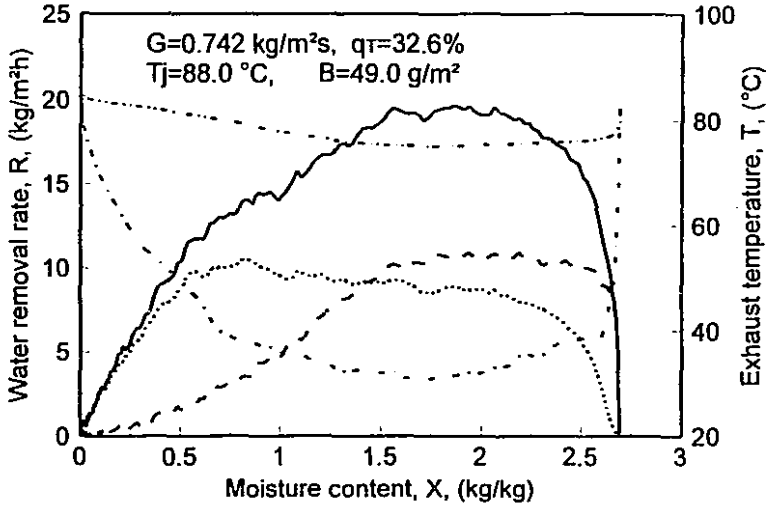
G=0.742 kg/m²s, qT=32.6%
Tj=88.0 °C, B=49.0 g/m²
Water removal rate, R, (kg/m²h)
Exhaust temperature, T, (°C)
Moisture content, X, (kg/kg)

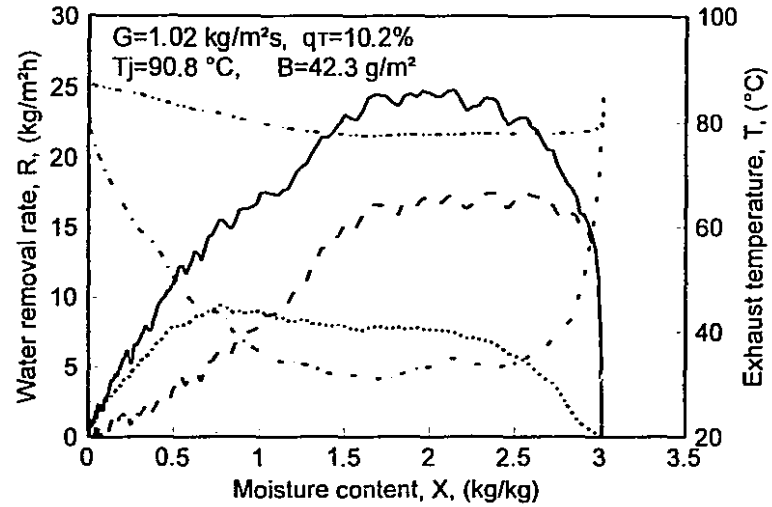
G=1.02 kg/m²s, qT=10.2%
Tj=90.8 °C, B=42.3 g/m²
Water removal rate, R, (kg/m²h)
Exhaust temperature, T, (°C)
Moisture content, X, (kg/kg)

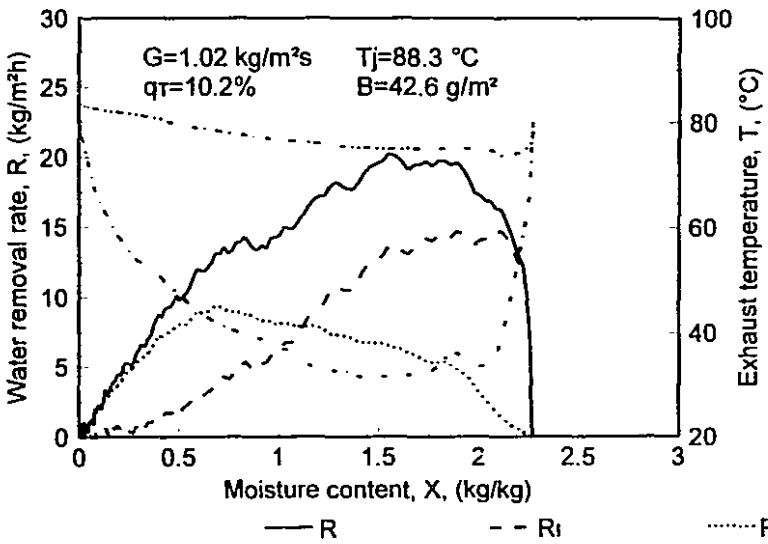
G=1.02 kg/m²s Tj=88.3 °C
qT=10.2% B=42.6 g/m²
Water removal rate, R, (kg/m²h)
Exhaust temperature, T, (°C)
Moisture content, X, (kg/kg)
R
RI
RT

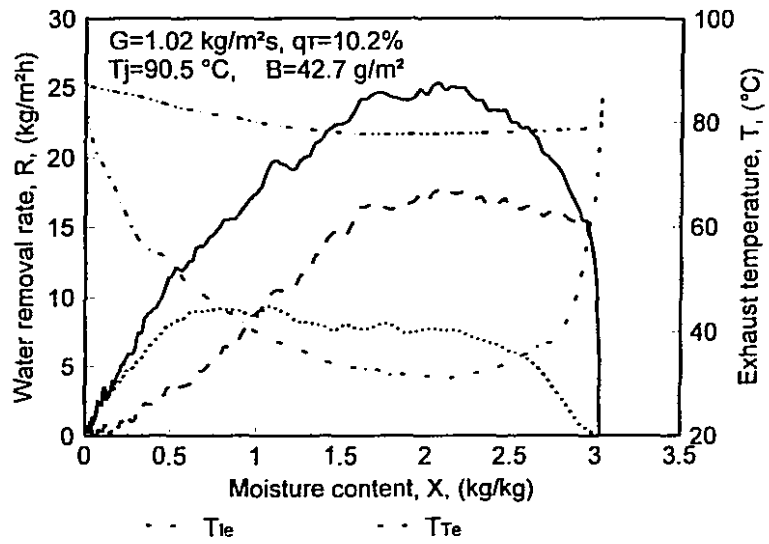
G=1.02 kg/m²s, qT=10.2%
Tj=90.5 °C, B=42.7 g/m²
Water removal rate, R, (kg/m²h)
Exhaust temperature, T, (°C)
Moisture content, X, (kg/kg)
TIe
TTe

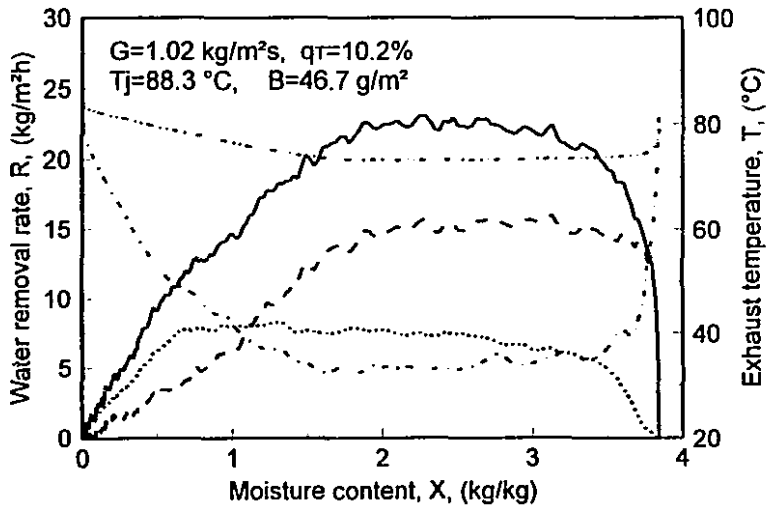
G=1.02 kg/m²s, qT=10.2%
Tj=88.3 °C, B=46.7 g/m²
Water removal rate, R, (kg/m²h)
Exhaust temperature, T, (°C)
Moisture content, X, (kg/kg)

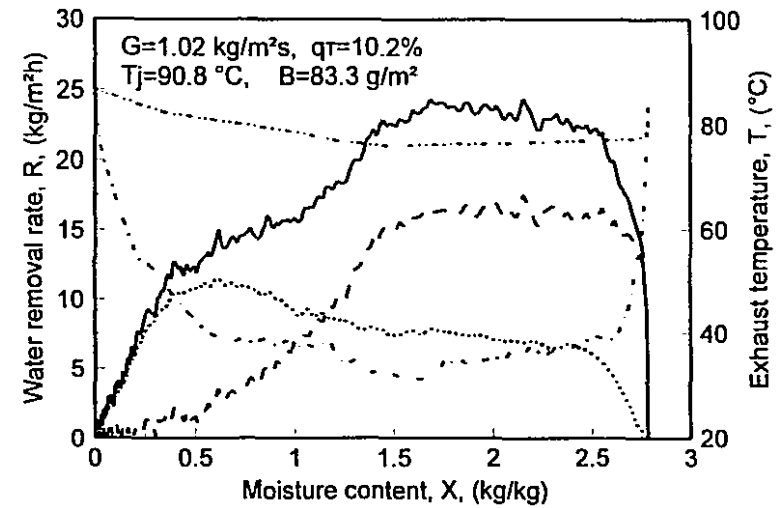
G=1.02 kg/m²s, qT=10.2%
Tj=90.8 °C, B=83.3 g/m²
Water removal rate, R, (kg/m²h)
Exhaust temperature, T, (°C)
Moisture content, X, (kg/kg)

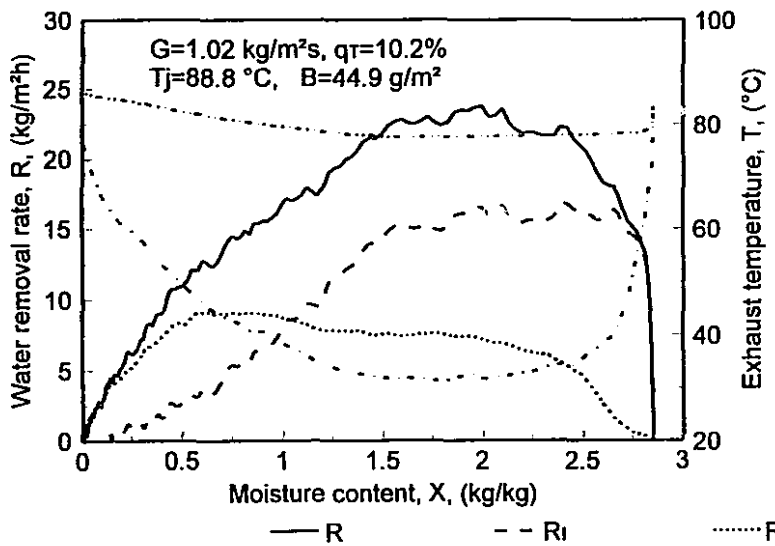
G=1.02 kg/m²s, qT=10.2%
Tj=88.8 °C, B=44.9 g/m²
Water removal rate, R, (kg/m²h)
Exhaust temperature, T, (°C)
Moisture content, X, (kg/kg)
R
RI
RT

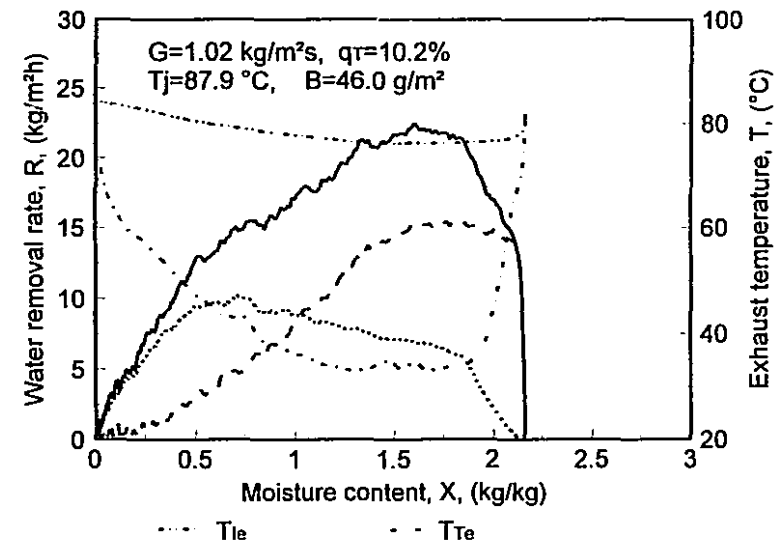
G=1.02 kg/m²s, qT=10.2%
Tj=87.9 °C, B=46.0 g/m²
Water removal rate, R, (kg/m²h)
Exhaust temperature, T, (°C)
Moisture content, X, (kg/kg)
TIe
TTe

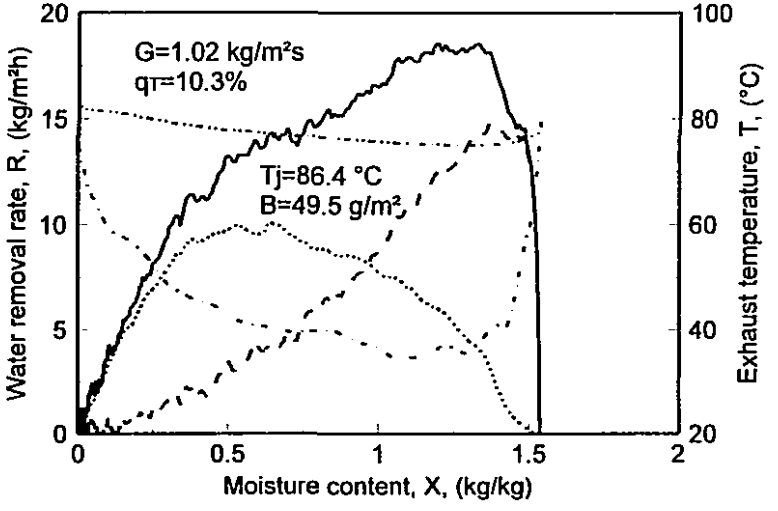
G=1.02 kg/m²s
qT=10.3%
Tj=86.4 °C
B=49.5 g/m²
Water removal rate, R, (kg/m²h)
Exhaust temperature, T, (°C)
Moisture content, X, (kg/kg)

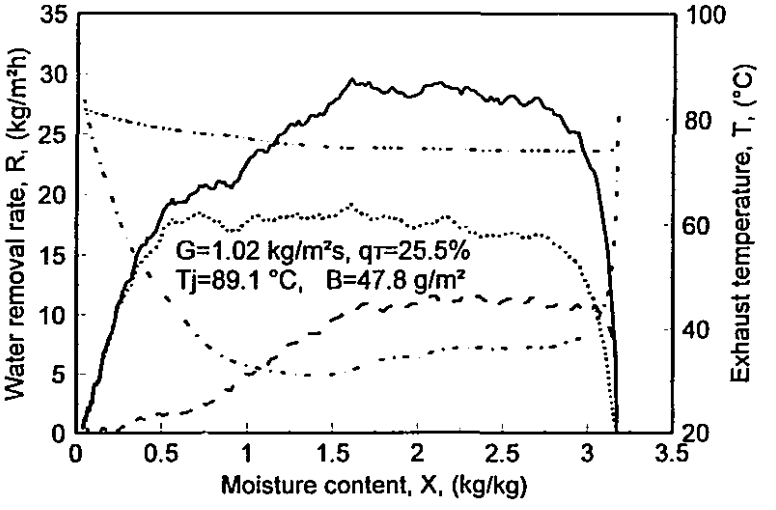
G=1.02 kg/m²s, qT=25.5%
Tj=89.1 °C, B=47.8 g/m²
Water removal rate, R, (kg/m²h)
Exhaust temperature, T, (°C)
Moisture content, X, (kg/kg)

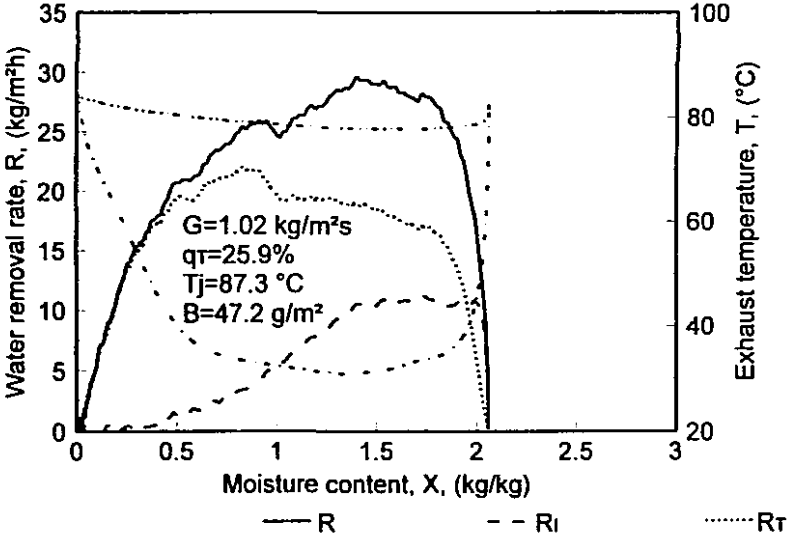
G=1.02 kg/m²s
qT=25.9%
Tj=87.3 °C
B=47.2 g/m²
Water removal rate, R, (kg/m²h)
Exhaust temperature, T, (°C)
Moisture content, X, (kg/kg)
R
RI
RT

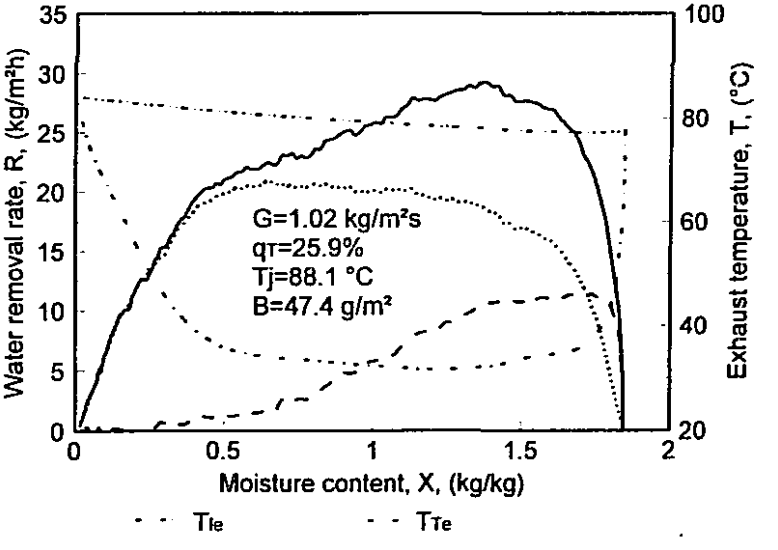
G=1.02 kg/m²s
qT=25.9%
Tj=88.1 °C
B=47.4 g/m²
Water removal rate, R, (kg/m²h)
Exhaust temperature, T, (°C)
Moisture content, X, (kg/kg)
TIe
TTe

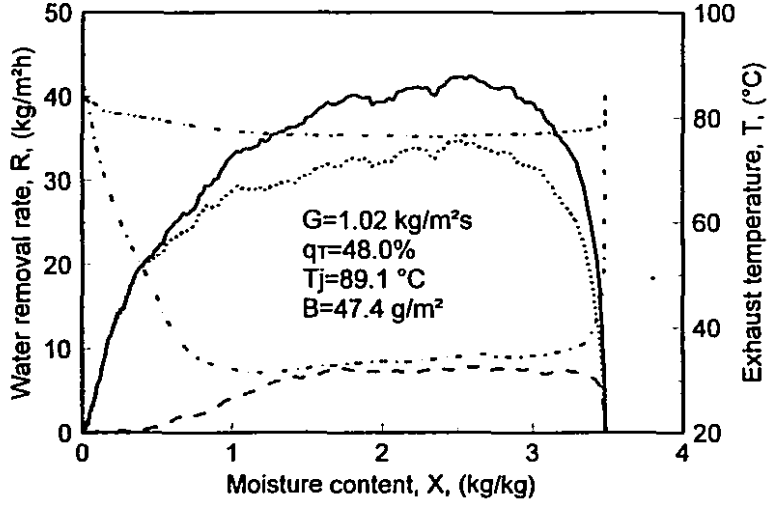
G=1.02 kg/m²s
qT=48.0%
Tj=89.1 °C
B=47.4 g/m²
Water removal rate, R, (kg/m²h)
Exhaust temperature, T, (°C)
Moisture content, X, (kg/kg)

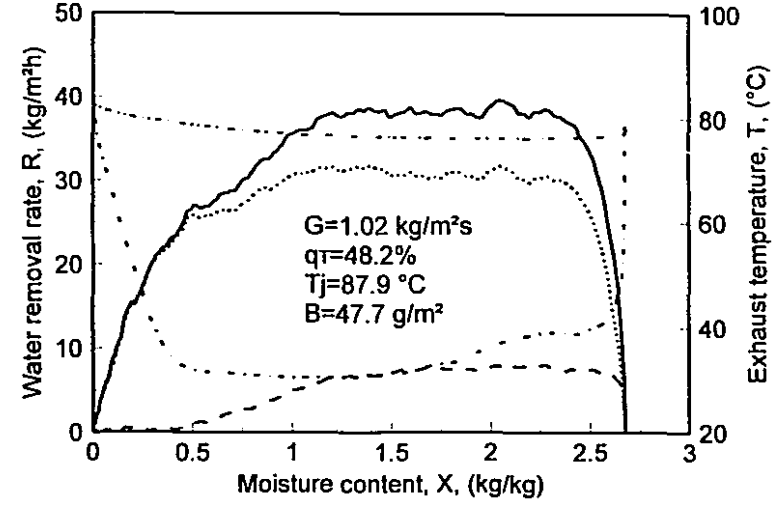
G=1.02 kg/m²s
qT=48.2%
Tj=87.9 °C
B=47.7 g/m²
Water removal rate, R, (kg/m²h)
Exhaust temperature, T, (°C)
Moisture content, X, (kg/kg)

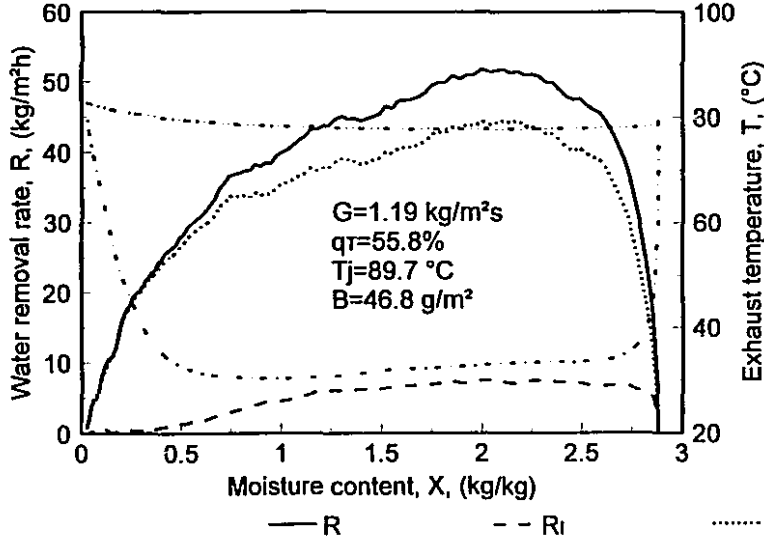
G=1.19 kg/m²s
qT=55.8%
Tj=89.7 °C
B=46.8 g/m²
Water removal rate, R, (kg/m²h)
Exhaust temperature, T, (°C)
Moisture content, X, (kg/kg)
R
RI
RT

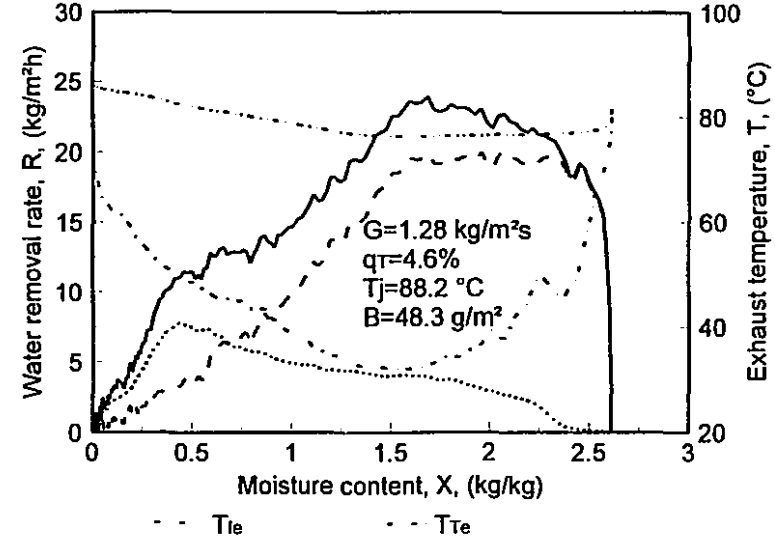
G=1.28 kg/m²s
qT=4.6%
Tj=88.2 °C
B=48.3 g/m²
Water removal rate, R, (kg/m²h)
Exhaust temperature, T, (°C)
Moisture content, X, (kg/kg)
TIe
TTe

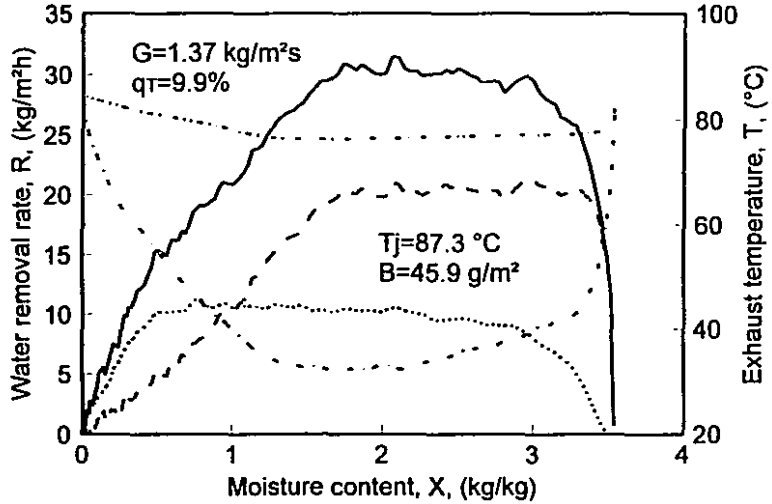
G=1.37 kg/m²s
qT=9.9%
Tj=87.3 °C
B=45.9 g/m²
Water removal rate, R, (kg/m²h)
Exhaust temperature, T, (°C)
Moisture content, X, (kg/kg)

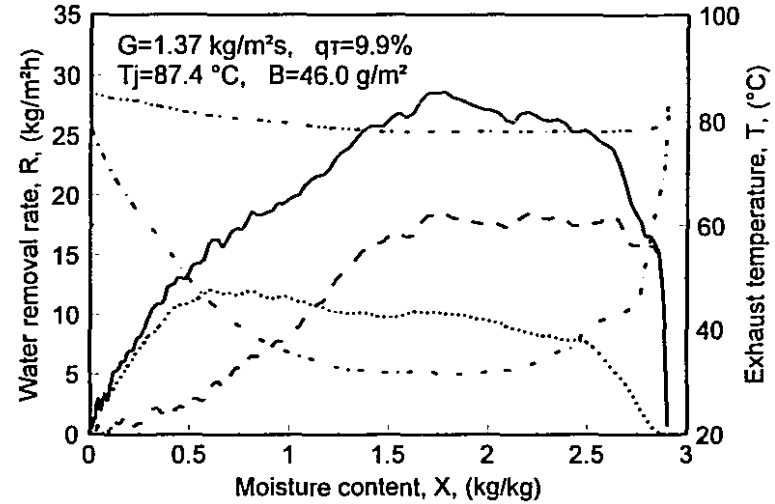
G=1.37 kg/m²s, qT=9.9%
Tj=87.4 °C, B=46.0 g/m²
Water removal rate, R, (kg/m²h)
Exhaust temperature, T, (°C)
Moisture content, X, (kg/kg)

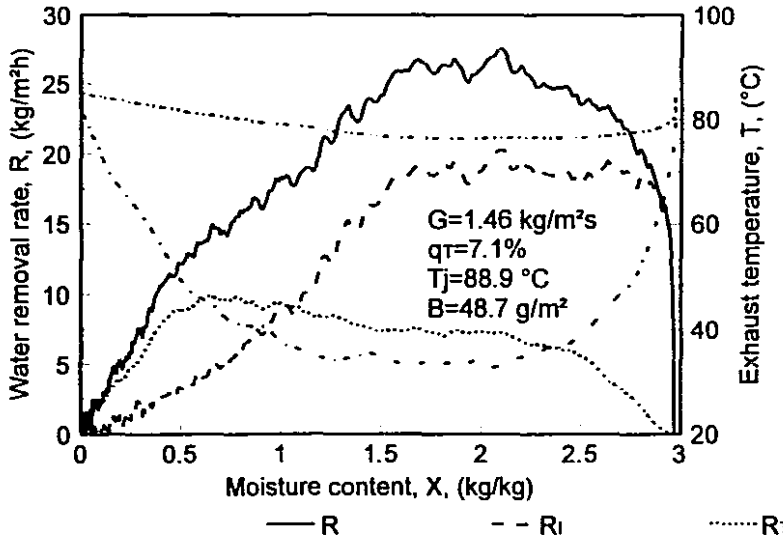
G=1.46 kg/m²s
qT=7.1%
Tj=88.9 °C
B=48.7 g/m²
Water removal rate, R, (kg/m²h)
Exhaust temperature, T, (°C)
Moisture content, X, (kg/kg)
R
RI
RT

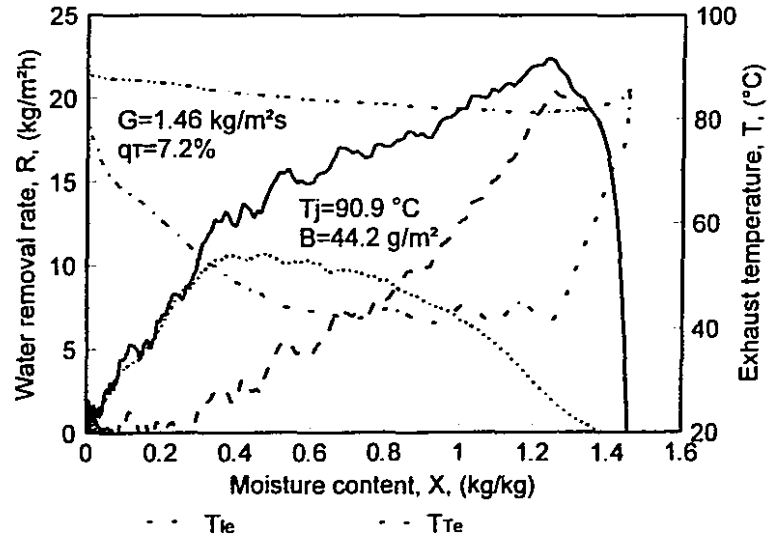
G=1.46 kg/m²s
qT=7.2%
Tj=90.9 °C
B=44.2 g/m²
Water removal rate, R, (kg/m²h)
Exhaust temperature, T, (°C)
Moisture content, X, (kg/kg)
TIe
TTe

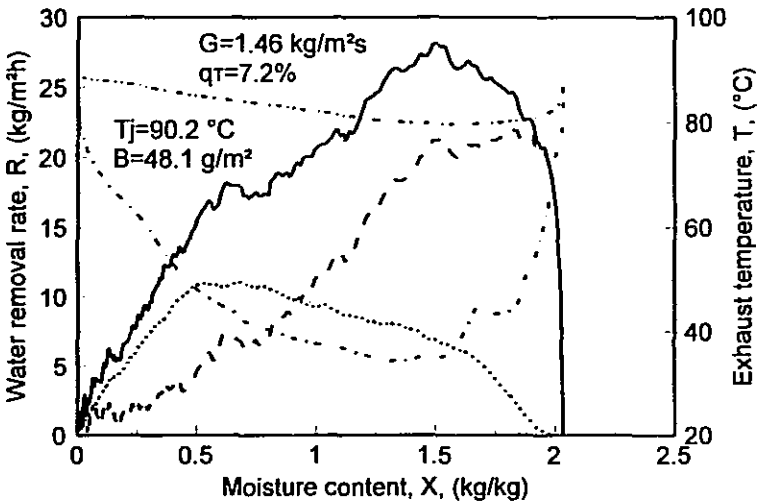
G=1.46 kg/m²s
qT=7.2%
Tj=90.2 °C
B=48.1 g/m²
Water removal rate, R, (kg/m²h)
Exhaust temperature, T, (°C)
Moisture content, X, (kg/kg)

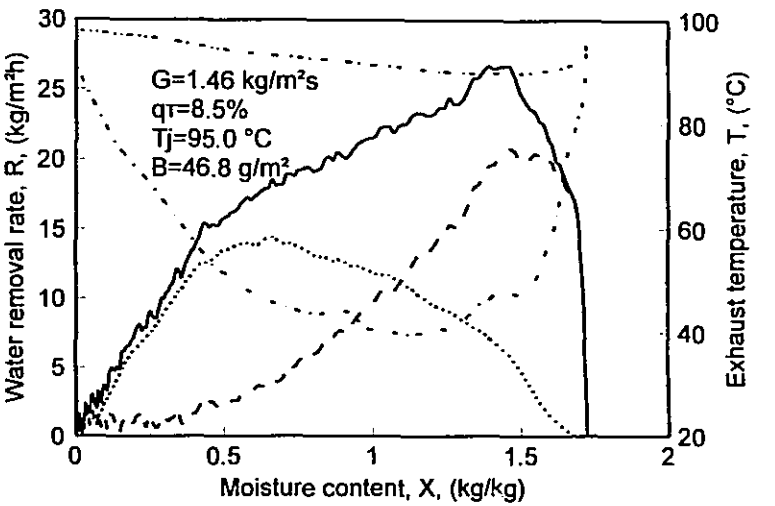
G=1.46 kg/m²s
qT=8.5%
Tj=95.0 °C
B=46.8 g/m²
Water removal rate, R, (kg/m²h)
Exhaust temperature, T, (°C)
Moisture content, X, (kg/kg)

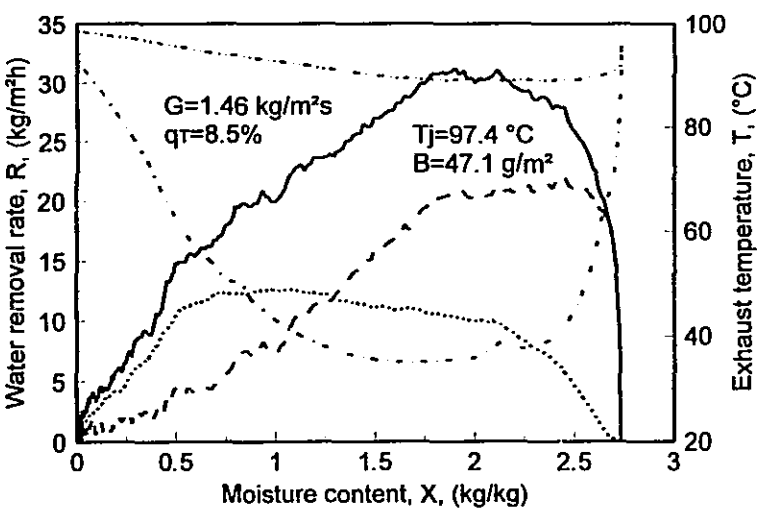
G=1.46 kg/m²s
qT=8.5%
Tj=97.4 °C
B=47.1 g/m²
Water removal rate, R, (kg/m²h)
Exhaust temperature, T, (°C)
Moisture content, X, (kg/kg)

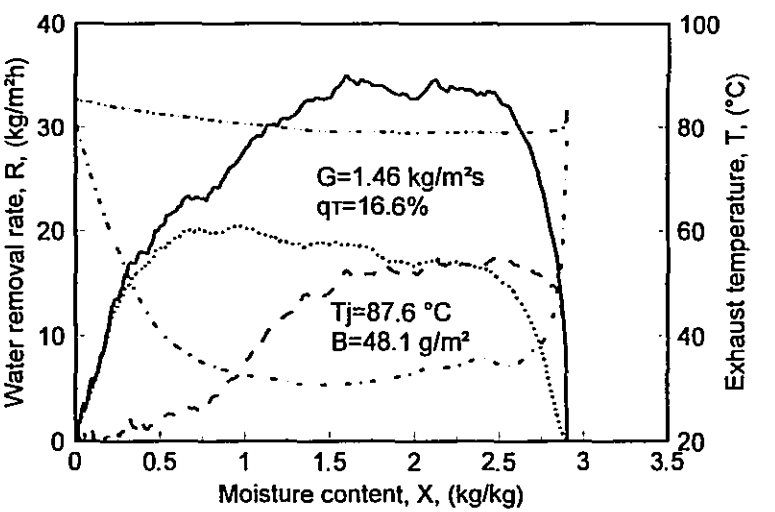
G=1.46 kg/m²s
qT=16.6%
Tj=87.6 °C
B=48.1 g/m²
Water removal rate, R, (kg/m²h)
Exhaust temperature, T, (°C)
Moisture content, X, (kg/kg)

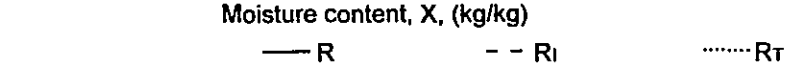
R
RI
RT

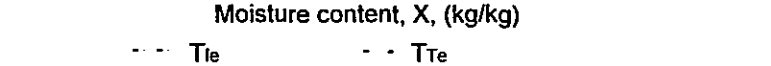
TIe
TTe

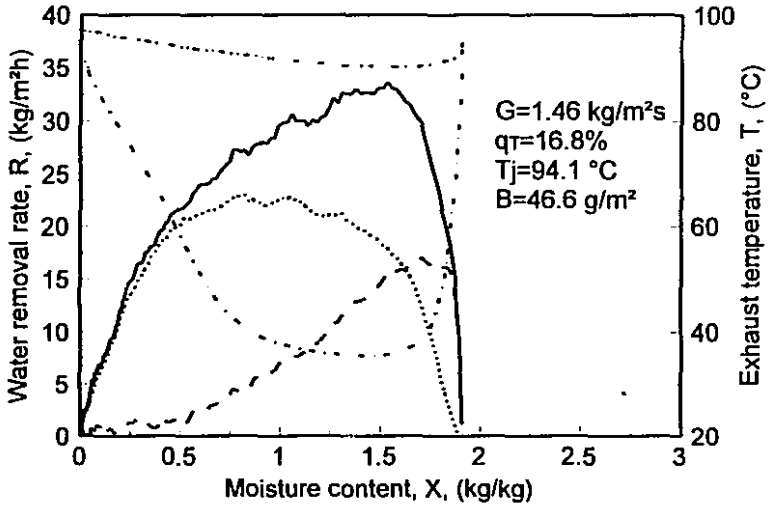
G=1.46 kg/m²s
qT=16.8%
Tj=94.1 °C
B=46.6 g/m²
Water removal rate, R, (kg/m²h)
Exhaust temperature, T, (°C)
Moisture content, X, (kg/kg)

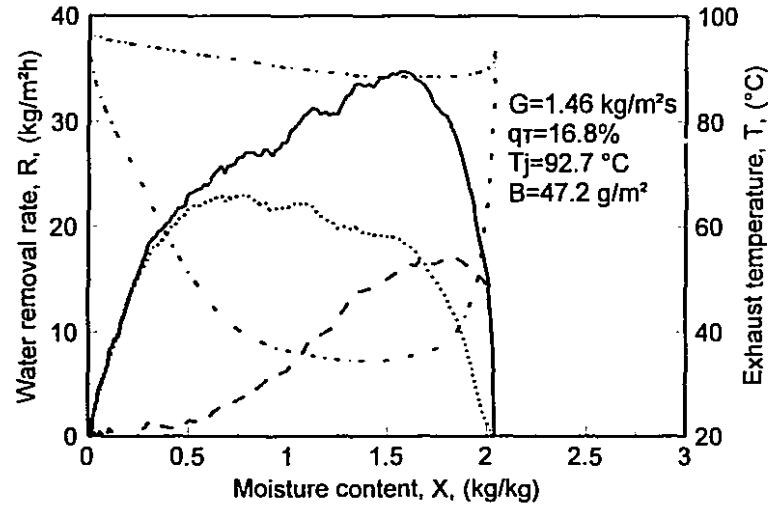
G=1.46 kg/m²s
qT=16.8%
Tj=92.7 °C
B=47.2 g/m²
Water removal rate, R, (kg/m²h)
Exhaust temperature, T, (°C)
Moisture content, X, (kg/kg)

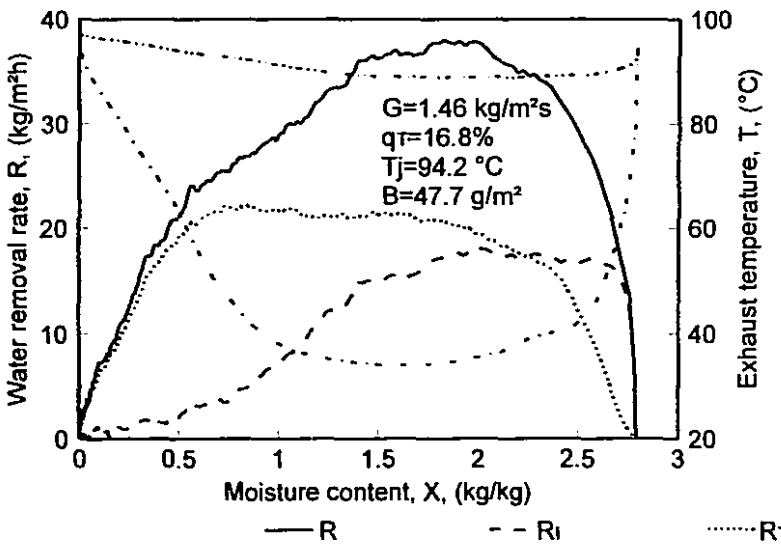
G=1.46 kg/m²s
qT=16.8%
Tj=94.2 °C
B=47.7 g/m²
Water removal rate, R, (kg/m²h)
Exhaust temperature, T, (°C)
Moisture content, X, (kg/kg)
R
RI
RT

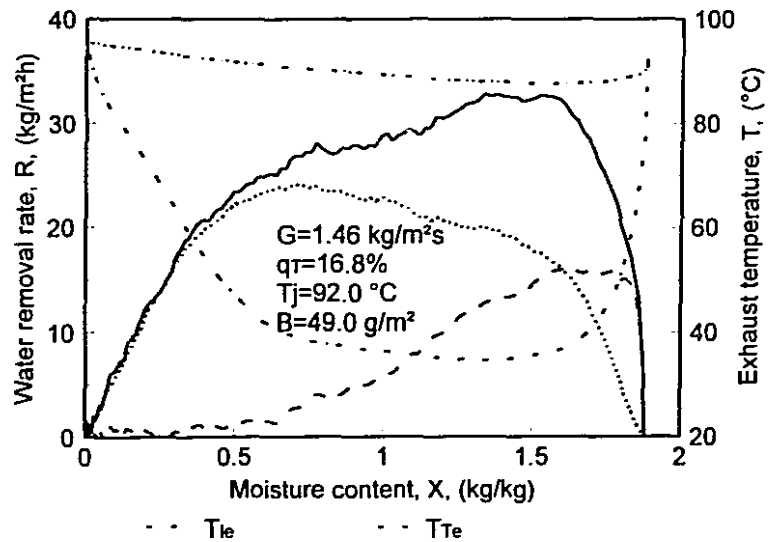
G=1.46 kg/m²s
qT=16.8%
Tj=92.0 °C
B=49.0 g/m²
Water removal rate, R, (kg/m²h)
Exhaust temperature, T, (°C)
Moisture content, X, (kg/kg)
TIe
TTe

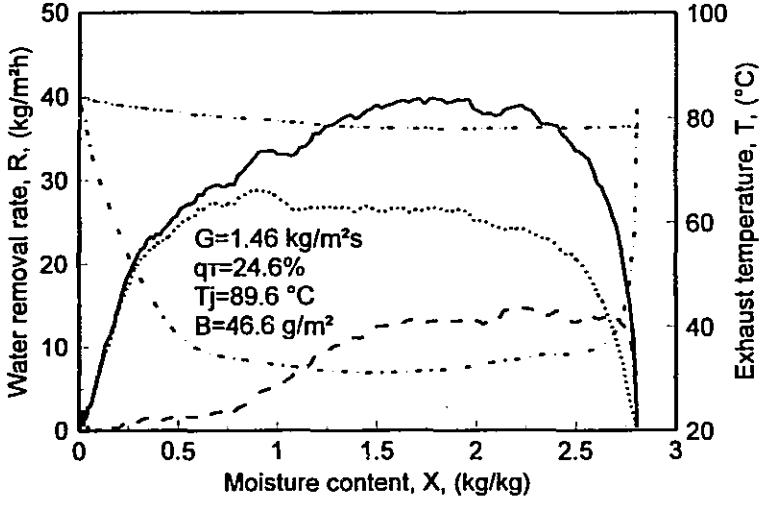
G=1.46 kg/m²s
qT=24.6%
Tj=89.6 °C
B=46.6 g/m²
Water removal rate, R, (kg/m²h)
Exhaust temperature, T, (°C)
Moisture content, X, (kg/kg)

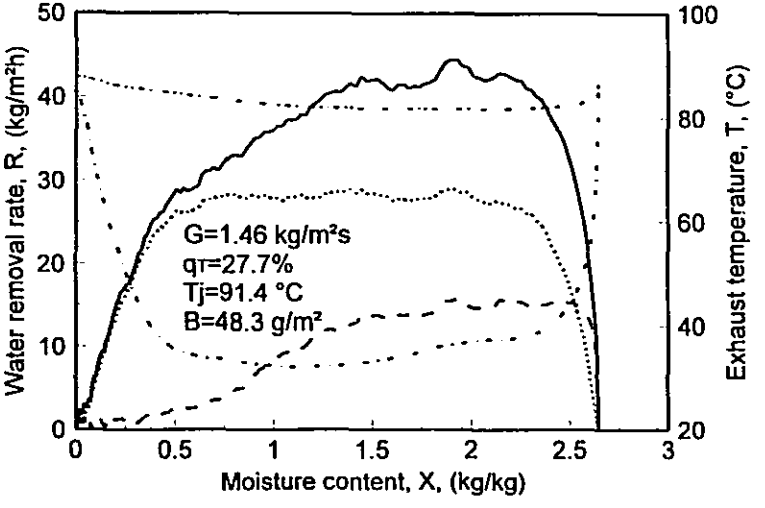
G=1.46 kg/m²s
qT=27.7%
Tj=91.4 °C
B=48.3 g/m²
Water removal rate, R, (kg/m²h)
Exhaust temperature, T, (°C)
Moisture content, X, (kg/kg)

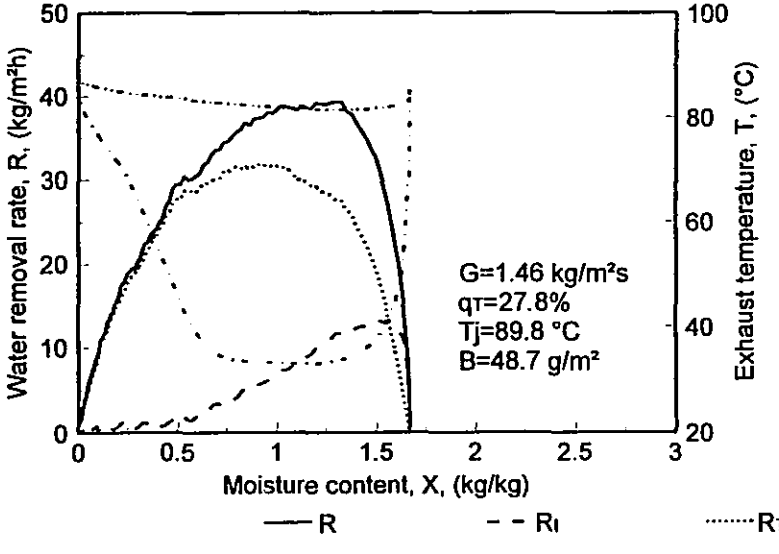
G=1.46 kg/m²s
qT=27.8%
Tj=89.8 °C
B=48.7 g/m²
Water removal rate, R, (kg/m²h)
Exhaust temperature, T, (°C)
Moisture content, X, (kg/kg)
R
RI
RT

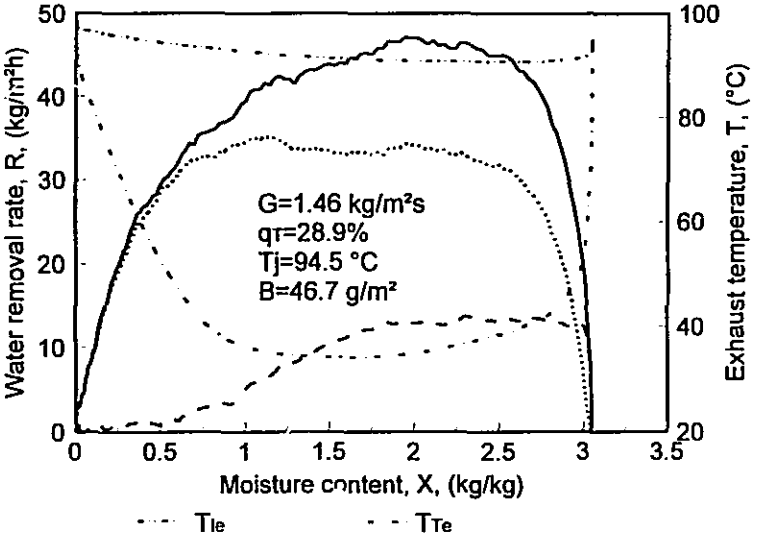
G=1.46 kg/m²s
qT=28.9%
Tj=94.5 °C
B=46.7 g/m²
Water removal rate, R, (kg/m²h)
Exhaust temperature, T, (°C)
Moisture content, X, (kg/kg)
TIe
TTe

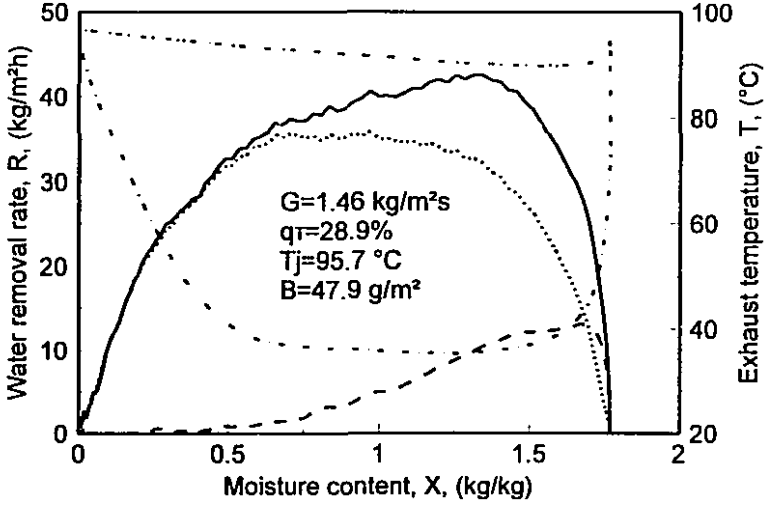
G=1.46 kg/m²s
qT=28.9%
Tj=95.7 °C
B=47.9 g/m²
Water removal rate, R, (kg/m²h)
Exhaust temperature, T, (°C)
Moisture content, X, (kg/kg)

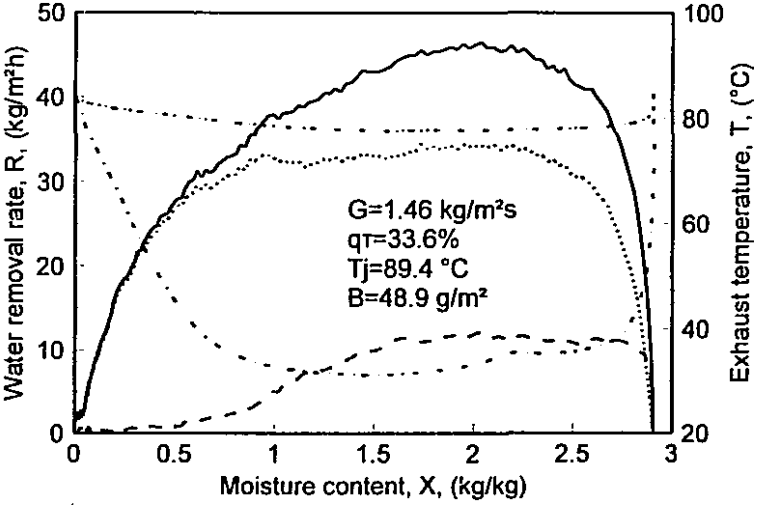
G=1.46 kg/m²s
qT=33.6%
Tj=89.4 °C
B=48.9 g/m²
Water removal rate, R, (kg/m²h)
Exhaust temperature, T, (°C)
Moisture content, X, (kg/kg)

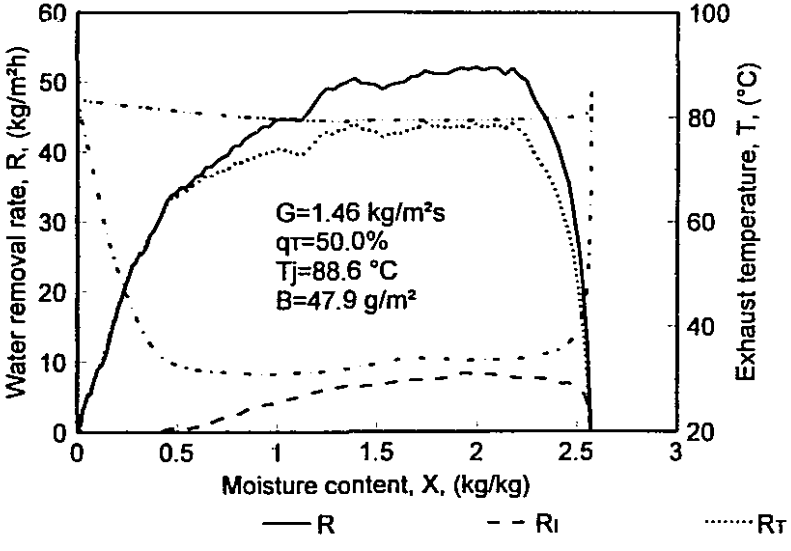
G=1.46 kg/m²s
qT=50.0%
Tj=88.6 °C
B=47.9 g/m²
Water removal rate, R, (kg/m²h)
Exhaust temperature, T, (°C)
Moisture content, X, (kg/kg)
R
RI
RT

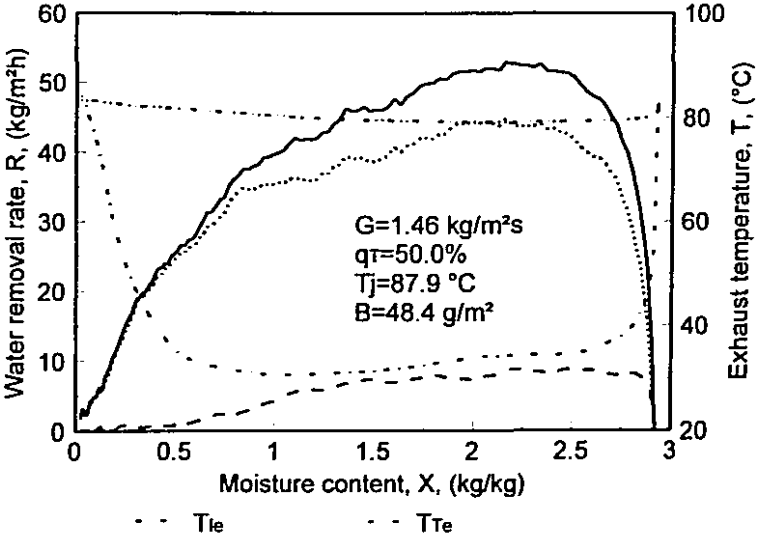
G=1.46 kg/m²s
qT=50.0%
Tj=87.9 °C
B=48.4 g/m²
Water removal rate, R, (kg/m²h)
Exhaust temperature, T, (°C)
Moisture content, X, (kg/kg)
TIe
TTe

Appendix F Characterization of the pulp

The freeness of the dry, unbleached standard laboratory kraft pulp (100% black spruce) and the physical properties of the handsheets are as follows:

Canadain standard freeness, ml	685
Grammage (Basis weight), g/m^2 (O.D.)	59.8
Bulking caliper, μm	120.1
Bulk, cm^3/g	2.01
Burst index, kPa m^2/g	1.96
Tear index, mN m^2/g	21.05
Breaking length, km	3.30
Stretch, %	1.77
Toughness index, mJ	37
Stress-strain factor, mJ/g	417
Zero-span breaking length, km (Pulmac)	16.84
Tensile index, N m/g	32.38
TEA, J/m^2	24.97